Università degli Studi di Palermo

AREA QUALITÀ, PROGRAMMAZIONE E SUPPORTO STRATEGICO
SETTORE STRATEGIA PER LA RICERCA
U. O. DOTTORATI

Dottorato di Ricerca Innovativo in Scienze Molecolari e Biomolecolari con Caratterizzazione Industriale (Internazionale) - XXXIV CICLO
Dipartimento di Scienze e Tecnologie Biologiche Chimiche e Farmaceutiche (STEBICEF)
Settore Scientifico Disciplinare CHIM/08

SYNTHESIS AND BIOLOGICAL EVALUATION OF NOVEL SMALL MOLECULES AS PROMISING ALTERNATIVE AGENTS TO COUNTERACT DRUG RESISTANCE IN CANCER AND MICROBIAL INFECTIONS

IL DOTTORE
Dott.ssa CAMILLA PECORARO

IL COORDINATORE
Chiar.ma Prof.ssa PATRIZIA DIANA

TUTOR
Chiar.ma Prof.ssa PATRIZIA DIANA

CO TUTOR
Chiar.ma Prof.ssa BARBARA PARRINO

Chiar.ma Prof.ssa ELISA GIOVANNETTI

Chiar.mo Prof.re GODEFRIDUS J. PETERS

CICLO XXXIV
ANNO CONSEGUIMENTO TITOLO 2022

Contents

Chapter 1

Introduction

Outline

Part I

Role of CDK-1 and GSK-3 β in driving key hallmarks of PDAC and preclinical evaluation of novel marine alkaloids analogs *(Chapter 2-6)*

Chapter 2

Wijnen, R.*, **Pecoraro, C.***, Carbone, D., Fiuji, H., Avan, A., Peters, G. J., Giovannetti, E., Diana, P.

Cyclin dependent kinase-1 (Cdk-1) inhibition as a novel therapeutic strategy against pancreatic ductal adenocarcinoma (pdac).

Cancers, (2021), *13*(17), 4389.

Chapter 3

Pecoraro, C.*, Faggion, B.*, Balboni, B., Carbone, D., Peters, G. J., Diana, P., Assaraf, Y. G., Giovannetti, E

GSK3β as a novel promising target to overcome chemoresistance in pancreatic cancer.

Drug Resistance Update, (2021), *58*, 100779.

Chapter 4

Pecoraro, C., Parrino, B., Cascioferro S., Puerta, A., Avan, A., Peters G.J., Diana P., Giovannetti, E., Carbone D.

A new oxadiazole-based topsentin derivative modulates CDK1 expression and exerts cytotoxic effects on PDAC cancer cells.

Molecules, (2021), *27*(1), 19.

Chapter 5

Carbone, D., Parrino, B., Cascioferro, S., **Pecoraro, C.**, Giovannetti, E., Di Sarno, V., Musella, S., Auriemma, G., Cirrincione, G., Diana, P.

1,2,4-Oxadiazole Topsentin Analogs with Antiproliferative Activity against Pancreatic Cancer Cells, Targeting GSK3β Kinase.

ChemMedChem (2021), *16*(3), 537-554.

Chapter 6

Pecoraro, C., Carbone, D., Aiello, D., Carbone, A.

Synthesis and cytotoxic activity of 3-[2-(1*H*-Indol-3-yl)-1,3-thiazol-4-yl]-1*H*-pyrrolo[3,2-c] pyridine hydrobromides, analogues of marine alkaloid nortopsentin.

Arkivoc (accepted), DOI: 10.24820/ark.5550190.p011.640

Part II

New therapeutic approaches against malignant mesothelioma *(chapters 7,8)*

Chapter 7

Anobile, D.P.*, Montenovo G.*, **Pecoraro, C.***, Franczak, M., Ait Iddouch, W., Peters G.J., Riganti, C., Giovannetti, E.

Splicing deregulation, microRNA and Notch aberrations: fighting the three-headed dog to overcome drug resistance in malignant mesothelioma.

Submitted to Expert Review of Clinical Pharmacology.

Chapter 8

Li Petri, G.*; **Pecoraro, C.***; Randazzo, O.*, Zoppi, S., Cascioferro, S., Parrino, B., Carbone, D., El Hassouni, B., Cavazzoni, A., Zaffaroni, N., Cirrincione, G., Diana, P., Peters, G.J., Giovannetti, E.

New imidazo[2,1-*b*][1,3,4]thiadiazole derivatives inhibit FAK phosphorylation and potentiate the antiproliferative effects of gemcitabine through modulation of the human equilibrative nucleoside transporter-1 in peritoneal mesothelioma.

Anticancer Research (2020), *40*(9), 4913-4919.

Part III

Biological evaluation of novel compounds analogues of the marine alkaloids topsentin and nortopsentin as bacterial biofilm inhibitors (*chapters 9-13*)

Chapter 9

Pecoraro, C.*, Carbone, D., Dongmei, D., Cascioferro, S., Diana, P.#, Giovannetti, E.#

Biofilm formation as valuable target to fight severe chronic infections.

Submitted to Current Medicinal Chemistry.

Chapter 10

Cascioferro, S., Carbone, D., Parrino, B., **Pecoraro, C.**, Giovannetti, E.,
Cirrincione, G., Diana, P.

Therapeutic Strategies to Counteract Antibiotic Resistance in MRSA Biofilm-Associated Infections.

ChemMedChem (2021), *16*(1), 65-80.

Chapter 11

Carbone, A., Cascioferro, S., Parrino, B., Carbone, D., **Pecoraro, C.**, Schillaci, D., Cusimano, M. G., Cirrincione, G., Diana, P.

Thiazole analogues of the marine alkaloid nortopsentin as inhibitors of bacterial biofilm formation.

Molecules (2021), *26*(1), 81.

Chapter 12

Parrino, B., Carbone, D., Cascioferro, S., **Pecoraro, C.**, Giovannetti, E., Deng, D., Di Sarno, V., Musella, S.; Auriemma, G., Cusimano, M. G., Schillaci, D., Cirrincione, G., Diana, P.

1,2,4-Oxadiazole topsentin analogs as staphylococcal biofilm inhibitors targeting the bacterial transpeptidase sortase A.

European Journal of Medicinal Chemistry (2021), *209*, 112892.

Chapter 13

Discussion and Conclusion

Chapter 14

Acknowledgements

Curriculum vitae

List of publication

Chapter 1

Introduction

Introduction

1. Novel insights on the development of FDA-approved small-molecule kinase inhibitors for the treatment of cancer
    - 1.1. Structure and Biological role of protein kinase
        - 1.1.1 Cyclin Dependent Kinase 1 (CDK1)
        - 1.1.2 Glycogen Synthase Kinase-3β (GSK-3β)

2. An overview on pancreatic cancer ductal adenocarcinoma (PDAC)
    - 2.1. Pancreas: anatomy and physiological function
    - 2.2. Pancreatic ductal adenocarcinoma (PDAC)
    - 2.3. Stages of PDAC
    - 2.4. Genetic abnormalities in PDAC

3. An overview of malignant mesotheliomas
    - 3.1. Malignant Pleural Mesothelioma (MPM): diagnosis and treatment
    - 3.2. Malignant Peritoneal Mesothelioma (MPeM): diagnosis and treatment

4. An overview on Biofilm formation and in antibiotic resistance

5. Outline of the PhD thesis

Chapter 1

Introduction

1.Novel insights on the development of FDA-approved small-molecule kinase inhibitors for the treatment of cancer

In recent years protein kinases emerged as one of the most promising pharmacological targets for the treatment of various diseases, due to their key role in controlling wide range of cellular activities such as: DNA replication, gene transcription, damage DNA reparation and energy metabolism (Figure 1). Deregulation of protein kinase has been demonstrated to play an important role not only in cancer, but also in neurodegenerative, cardiovascular, immunological, inflammatory, and infectious diseases [1].

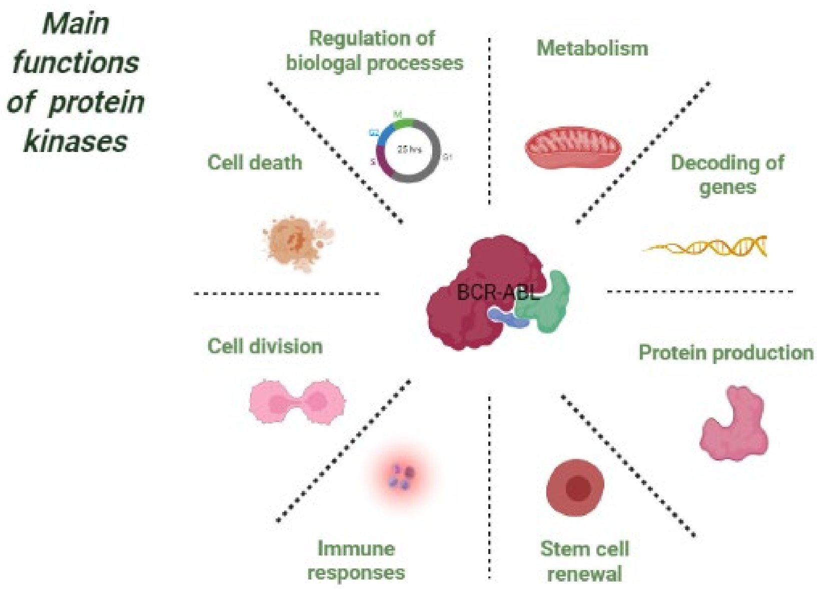
Main functions of protein kinases
Regulation of biologal processes
Metabolism
Cell death
Decoding of genes
BCR-ABL
Cell division
Protein production
Immune responses
Stem cell renewal

Figure 1 Protein kinases regulate fundamental cellular signaling pathway. Created with BioRender.com

The concept of protein kinase inhibition began in the 1950s and 1960s, when pioneering research was conducted on the role of protein kinases on the signaling cascade in the regulation of cellular homeostasis [2].

The strategy of developing compounds that can inhibit kinases originated in the late 1980s, when a study was conducted on the inhibition of epidermal growth factor receptor (EGFR) tyrosine kinase, which had been shown to be overexpressed in many cancer types and was associated with dismal prognosis [3].

Once established the therapeutical potential and the druggability of protein kinases, many inhibitors were developed by pharmaceutical companies, which have invested considerable resources in the design and synthesis of new small molecules kinase inhibitors (SMKIs).

In 2001 the first tyrosine kinase inhibitor was approved, imatinib (Gleevec), against Abelson (ABL) tyrosine kinase, that is expressed as a mutated fusion protein, called BCR-ABL, in nearly case of chronic myeloid leukemia (CML). The approval of imatinib was represented not only a breakthrough from the traditional chemotherapy but also the beginning of future research in the field [4].

Indeed, since 2001 when imatinib reached the market, until to date, approximately 70 molecules were approved by the Food and Drug Administration (FDA), of which most inhibit receptor tyrosine kinases, while a small number of inhibitors acts against non-receptor tyrosine kinases and serine-threonine kinases. Moreover, many other compounds are currently in clinical and preclinical studies to evaluate their potency against different protein kinases [5-11].

Therefore, it can be affirmed that in twenty years many steps forward have been made in this field, representing an incomparable result in the history of pharmaceutical chemistry. In particular, more than one million publications on protein kinases have been released, more than 5000 crystal structures of protein kinases with or without small molecules have been resolved, inhibition assays have been developed for many protein kinases and SMKIs have been identified for one fifth of the human kinome [12].

However, despite the huge number of synthesized protein kinase inhibitors and the abundance of structural features of SMKIs, there are still several issues to solve, especially regarding the selectivity and the side effects of the currently developed protein kinase inhibitors.

Firstly, all protein kinases have a highly conserved site called ATP binding pocket, which makes it nearly impossible to develop a compound that selectively inhibits one of the 518 protein kinases.

Secondly, the synthesis of a compound that has the power requirements necessary to compete with ATP, present in high concentration within the cells, seems to be something highly complicated to obtain.

On the other hand, since in most tumors multiple signaling pathways are involved in sustaining progression and resistance, it has been shown that the administration of multi-kinase inhibitors could represent an advantage for drug entry into the clinic, as they seem to be more effective than single targeted therapy [11,13].

A representative example of this mechanism is constituted by the cumulative antitumor efficacy shown by the simultaneous administration of a vascular endothelial growth factor receptor (VEGFR) inhibitor and a platelet derived growth factor receptor (PDGFR) inhibitor [14].

Remarkably, several cancer types have shown resistance caused by overexpression and/or mutation of the target kinase, in these cases, the inhibition of other kinases protein involved in the same signaling pathway of the primary kinase inhibited, could offer an additive efficacy.

In addition, pharmacokinetics (PK) determines the absorption, distribution, metabolism and excretion (ADME) of the drugs in human organisms and these processes are influenced by specific features of the inhibitors (i.e., molecular weight, hydrophilicity, hydrogen bonding and mechanisms of active transport), which affect the exact drug concentrations necessary to have inhibition of the target. According to these aspects multi kinase-inhibitors are preferred than to two single inhibitors.

Furthermore, the administration of more than one single inhibitor could lead to different problems associated to the simultaneous administration of two single inhibitors, considering that one drug could influence and interfere with the metabolism of the other.

Therefore, a single multi-kinase inhibitor seems to be better tolerated considering the pharmacokinetics properties.

Another aspect to consider in the choice between multiple or single kinase inhibitors is the toxicity of these compounds alone or in combination.

Each kinase inhibitor has specific toxicities, related to the primary kinase inhibited or to off-target effect caused by the inhibition of other kinase.

Therefore, the choice between a single or multi-kinase inhibitor is a tight balance and several aspects should be considered, including efficacy, toxicities, and metabolism.

Taking all the elements, the most effective way of cancer treatment by using kinase inhibitors is to consider the peculiar genetic constitution of the patient, the cancer type and the specific chemicals characteristic of the drugs.

1.1. Structure and Biological role of Protein Kinase

Protein kinases catalyze the transfer of the γ-phosphate group of adenosine triphosphate (ATP) to a specific target, with the aim to modulate the intrinsic activity of the latter. The phosphorylation regulates various cellular processes, including proliferation, survival, apoptosis, metabolism, transcription, differentiation and a wide range of other cellular activities. Deregulation of protein kinases can lead to the onset of numerous diseases, including neurological, cardiovascular, autoimmune diseases and cancer. For these reasons, kinases have proven to be promising targets of new drugs for the treatment of these malignancies.

The human genome encodes approximately for 538 different protein kinases which are divided into different families based on their selectivity for the various substrates. More specifically, the covalent bond of the phosphate group to a substrate requires the presence of a free hydroxyl group; in nature the amino acids serine (Ser), threonine (Thr) and tyrosine (Tyr) can provide for this; therefore, protein kinases that transfer phosphate groups to serine or threonine residues are called Ser/Thr kinases, while kinases that recognize tyrosine residues are called tyrosine kinases (Figure 2). These are the sites within proteins that can be phosphorylated and are located in common structural motifs called consensus sequences [15].

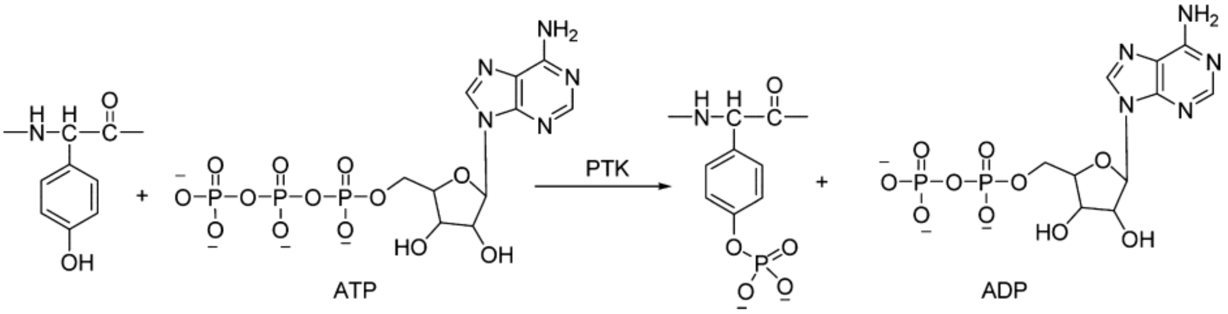

Figure 2 Phosphorylation of the hydroxyl group of tyrosine catalyzed by a generic protein kinase. *Created with ChemDraw*

Human protein kinases, although different in the primary amino acid sequence, show many similarities in their tertiary structure, especially at the level of the catalytic site where the ATP binding pocket is located. All kinases exhibit a two-lobed structure, an N-terminal lobe containing a β-sheet-rich structure and a lower C-terminal domain rich in α-helical structures, connected by a hinge region. ATP binds itself in the gap between the N-terminal domain and the C-terminal domain, and most of the protein kinase inhibitors interact with this region thus perturbing the binding of ATP to the catalytic site [8] (Figure 3).

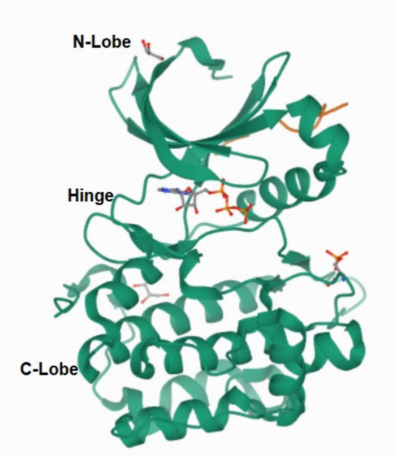

Figure 3 Co-crystal structure of Phosphoinositide-dependent kinase-1 (PDK1) with ATP (adenine and ribose in grey backbone, phosphate groups in orange). (PDB ID: 3HRC)

All protein kinases have a flexible activation loop, which is important in regulating kinase activity. In particular, the activation loop is marked by a conserved Asp-Phe-Gly (DFG) motif, located at the N-terminal lobe. The aspartate residue of DFG plays the role of coordinating Mg^{2+} in the active site, while the phenylalanine residue of the DFG pack into a hydrophobic pocket between N-lobe and C-lobe, thus generating a hydrophobic regulatory spine. This packing interaction is called "*DFG-in*" conformation.

Conversely, the protein kinase presented the "*DFG-out*" conformation when the phenylalanine moves out from the hydrophobic pocket, interrupting the orientation with the aspartate residue, which is no longer able to coordinate the Mg^{2+}, thus causing, in some case, the steric block within the ATP binding site (Figure 4) [16].

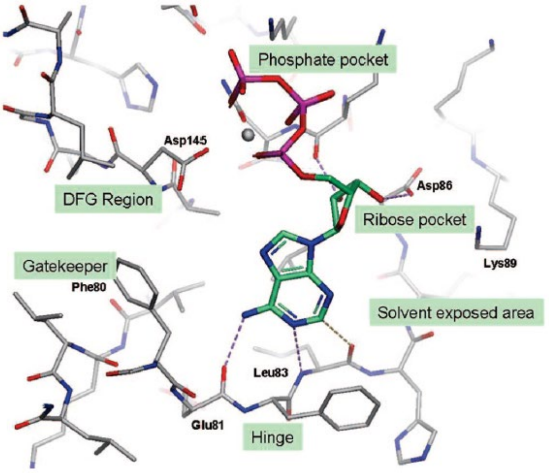

Figure 4 Structural elements around the ATP-binding site (J. Med. Chem. 2007, 50, 3, 409–424)

Protein kinases are fundamental enzymes responsible for the maintenance of cellular homeostasis, while a malfunction in their activity can lead to the onset of various diseases. Therefore, in the last decade, the scientific community has focused on the development of new molecules with the aim to modulate the activity of these enzymes.

Currently, the protein kinase inhibitors can be classified in two main categories:

1. Irreversible inhibitors, ATP non-competitive
2. Reversible inhibitors, ATP-competitive

The former covalently binds a reactive nucleophile cysteine residue adjacent to the ATP binding pocket, causing irreversible inhibition and the blockage of the ATP-active site. The latter according with the conformation of DFG can be divided in four subtypes (Figure 5):

1. *Type I inhibitors* that bind to the active conformation of the protein kinase with the aspartate residue of the DFG motif oriented towards the ATP binding site.
2. *Type II inhibitors* that bind the inactive form of the protein kinase with the aspartate of the DFG motif facing outward from the ATP binding site.
3. *Type III inhibitors* that bind in an allosteric site adjacent to the ATP binding site, without making interaction with ATP-binding pocket.
4. *Type IV inhibitors* that bind in an allosteric site remote to the ATP binding site.

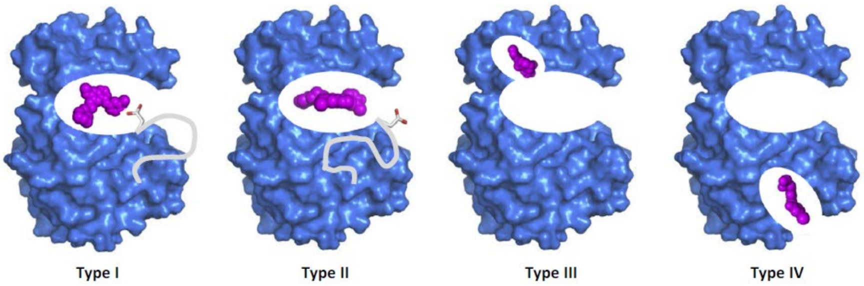

Figure 5 Representation of the different types of reversible kinase inhibitors. (Trends Pharmacol Sci. 2015 ;36(7):422-439).

Despite this classification, most of protein kinase inhibitors developed to date are ATP-competitive type I tyrosine kinase inhibitors [11].

1.1.1. Cyclin dependent kinase (CDK1)

Out of numerous protein kinases, cyclin-dependent kinase 1 (CDK1), a serine/threonine kinase which plays a crucial role in regulating the cell cycle, has emerged as a promising target for the treatment of several type of cancers. CDK1 regulates the transition from G2 phase to mitosis and a reduction in CDK1 activity results in a G2-M phase arrest. Normally, by binding to cyclin B, CDK1 allows the progression through mitosis. It was also reported that CDK1 is able to bind other cyclins that regulate the interphase, such as cyclin D and cyclin E and it was seen that mice *knockouted* for another CDK, but expressing CDK1, did not undergo to cell cycle arrest. CDK1 alone is able to promote cell cycle progression in mammalian cells and has been defined pluripotent protein kinase [17-19].

Moreover, CDK1 is strongly involved in maintaining a pluripotency state of cancer cells inside the tumor. It has been shown that its deregulation can lead to the development of cancer stem cells (CSCs) and lead to drug resistance. This is because of their ability to self-renewal, to produce new vessels, to trigger the process of epithelial mesenchymal transition (EMT), and being invisible to the immune system. It has been shown that CDK1 inhibition by RO3306, a CDK1 inhibitor, is able to reduce the expression of NANOG, OCT-4, SOX-2, transcription factors well known to be involved in stemness [20].

Considering the importance of CDK1 in maintaining the homeostasis of the cell cycle, its marked overexpression in almost all cancer types and its involvement in the maintenance of CSCs subpopulation, numerous efforts have been made to design new small molecule CDK1 inhibitors. Although to date there is no FDA approved molecule that has CDK1 as a target, there are 36 pan-CDK inhibitors under research and development [21-23] (Figure 6).

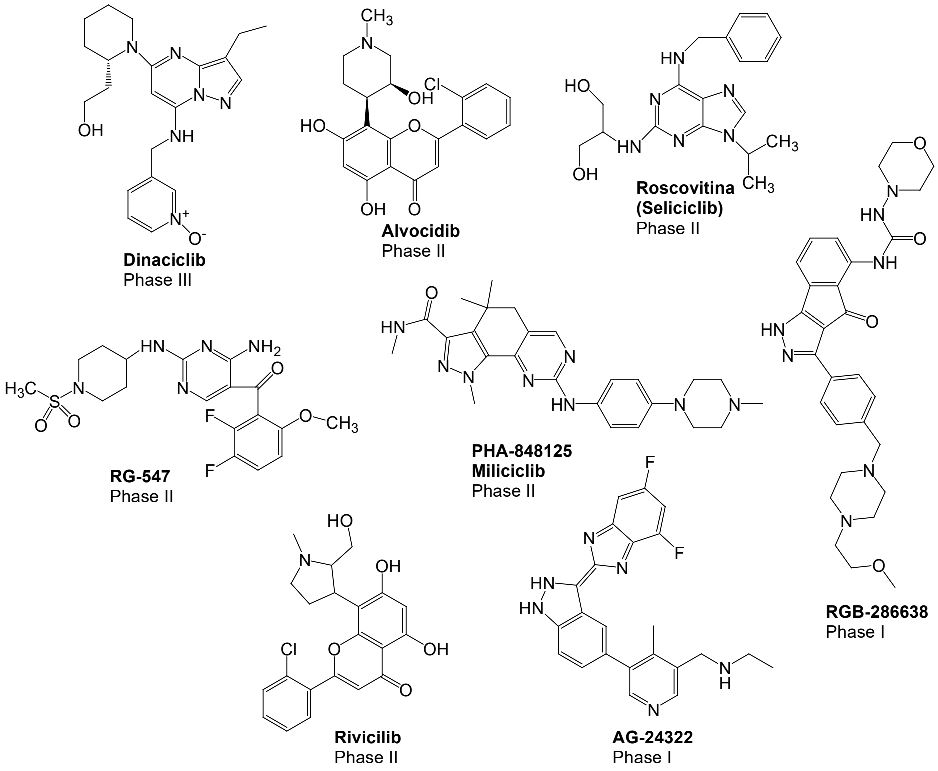
Dinaciclib
Phase III
Alvocidib
Phase II
Roscovitina
(Seliciclib)
Phase II
RG-547
Phase II
PHA-848125
Milliciclib
Phase II
RGB-286638
Phase I
Rivicilib
Phase II
AG-24322
Phase I

Figure 6 Representative pan-CDK inhibitors in clinical phase. Created with ChemDraw.

From a literature study of CDK1 inhibitors, most of the molecules are ATP competitive inhibitors, binding to the ATP-active site, showing hydrogen bond interactions in the hinge region with the leucine (Leu) 83 residue (donor-acceptor), but the strongest interaction occurs when leucine 83 behaves as a donor, with glutamate (Glu) 81 (acceptor) and a π- π interaction with phenylalanine (Phe) 80 (Figure 7).

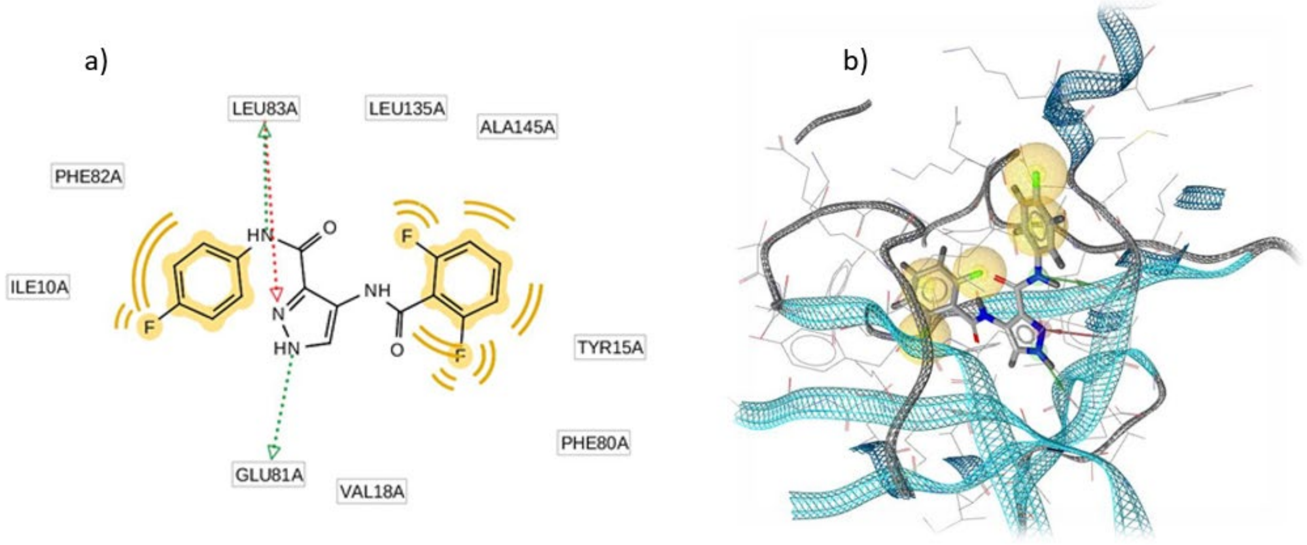

Figure 7 A) Chemical structure of AT7519 and its depicted binding mode with CDK1. B) Pharmacophoric models of AT7519 into CDK1. Created with Schrödinger.

1.1.2. Glycogen kinase synthase 3-β (GSK3β)

Glycogen synthase kinase-3 β (GSK-3β) is a ser/thr kinase, known to play a main role in the control of various cellular processes, acting on more than 40 substrates and is therefore defined as a multitasking kinase [24]. Regarding the catalytic activity of GSK-3β, it is possible to identify two main domains, the active site that catalyzes the phosphorylation of its substrates and the binding site for the activated substrate. More specifically, GSK-3β recognizes a specific amino acid sequence S/T-XXX-S/T(P) in its target, inducing a functional conformational change that assists the target positioning in the active catalytic domain of the kinase [25] (Figure 8).

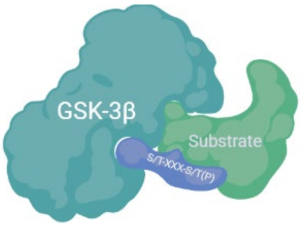

Figure 8 Schematic representation of primer substrate bound to GSK-3β. Created with BioRender.com

Unlike inducible protein kinases which require the activation, GSK-3β is a constitutively active protein within cells. Its activity is regulated by phosphorylation of specific Ser and Thr residues. The phosphorylation of Ser 9 (PSer9) determines its inactivation, because phosphorylated Ser9 occupies the binding site for the S/T(P) group of the recognition sequence, S/T-XXX-S/T(P), and acts as a pseudosubstrate hampering the interaction of the various proteins with the active site of the enzyme [26]. However, it was demonstrated that in presence of high concentrations of activated substrates, the latter will be able to overcome inhibition and be phosphorylated.

On the contrary, the phosphorylation of the tyrosine (Tyr) 216 residue is fundamental for GSK3-β activity and mutations in this residue that determine the presence of a Phe residue instead of Tyr or its dephosphorylation, lead to a drastic reduction of GSK-3β activity [27].

Although GSK3β has been recognized to act as a tumor suppressor against several pro-oncogenic factors such as EMT mediators, overexpression and dysregulation of this protein have been implicated in several pathological malignancies due to its master function in the regulation of multiple signal cascades that regulate cell homeostasis, cell survival, differentiation and stemness [28].

There is scientific evidence that GSK-3β is overexpressed in pancreatic cancer specimens with altered oncogenic *KRAS* status. Considering that *KRAS* is mutated in approximately 95% of pancreatic cancer, GSK-3β emerges as a promising new target in the war against pancreatic cancer aggressiveness [29].

Since the cation lithium, the first GSK-3β inhibitor approved by FDA in the early 1980s for the treatment of human bipolar depression [30,31], several GSK-3β ATP competitive inhibitor molecules have been developed. However, most of these inhibitors, can also exert inhibitory effects towards cyclin-dependent kinases (CDKs) including CDK1/CDK2, since these proteins share very similar ATP-binding pockets with GSK-3β [32]. Therefore, GSK-3β inhibitors may indirectly impact cell cycle regulation by CDK1-2 inhibition and enhance the antiproliferative outcome.

Aside from lithium, no other GSK-3β inhibitors have been approved by the FDA, however several small molecules, containing different heterocyclic rings are under investigation (Figure 9) [33].

Tideglusib, a non-ATP competitive inhibitor, has been tested in murine models of human glioblastoma, resulting in reduction of colony formation and consequently increase the number of glioblastoma cancer cells in phase G0/G1 [34]. Moreover, it can reduce the phosphorylation of tau protein in Alzheimer disease, increasing the level of proapoptotic proteins in murine models of human neuroblastoma [35].

Preclinical evaluation of tideglusib in AML mouse models also demonstrated its ability to increase the level of NK cytotoxic cells [36].

AR-A0-14418 is an ATP-competitive inhibitor and preclinical studies have demonstrated its ability to reduce the proliferation and increase the apoptosis in gastric cancer [37].

LY2090314, is an ATP-competitive inhibitor, which is able to inhibit both isoforms of GSK-3. Preclinical studies in breast cancer, non-small cell lung cancer and mesothelioma have been conducted and confirmed antitumor potential of LY2090314. Moreover, clinical studies for advanced metastatic solid tumor and leukemia demonstrated that LY2090314 is well tolerated when administrated with standard chemotherapeutic agents (i.e., gemcitabine and carboplatin), however no significant efficacy, when administered as single agent was detected [38,39].

The ATP competitive inhibitor 9-ING-41 has been studied as single agents or in combination with other drugs in different types of solid tumors including, neuroblastoma, pancreatic cancer, glioblastoma and bladder cancer, as well as in haematological malignancies such as, lymphoma.

Other GSK-3β inhibitors (e.g., CHIR99021, AR-A014418 and SB-732881-H) described in literature have been tested in cell and animal models to study their efficacy in several types of cancer, however different issues related to their pharmacokinetics were observed, therefore they withdrawn to advance as drug candidates in to the clinicals.

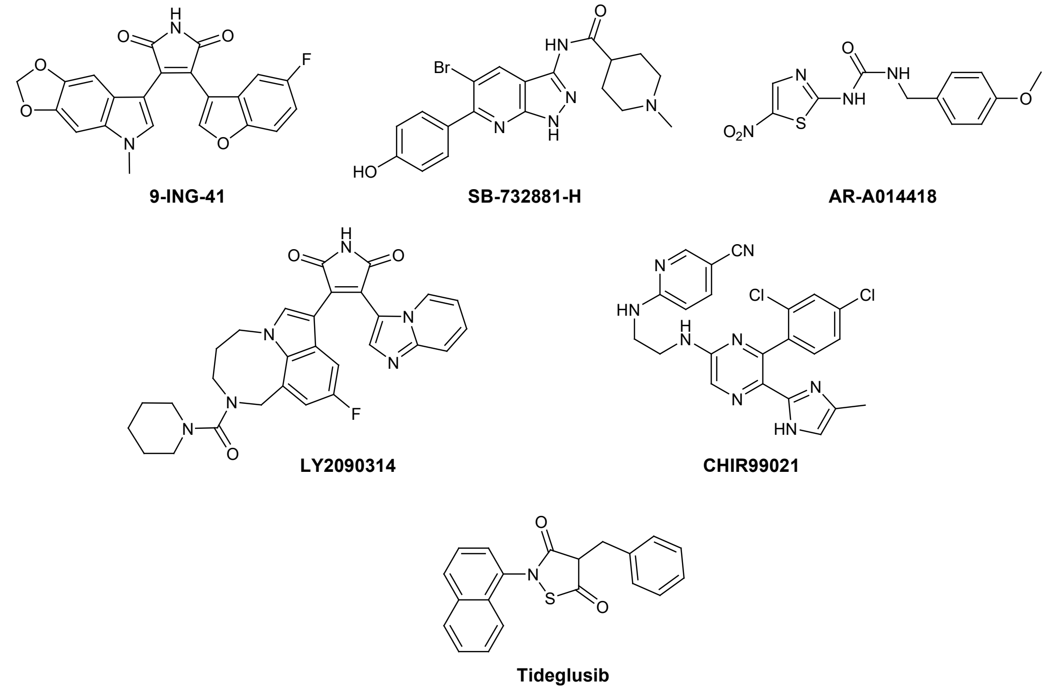

Figure 9 GSK-3β inhibitors in preclinical and clinical phase. Created with ChemDraw

2. An overview on pancreatic cancer ductal adenocarcinoma (PDAC)

2.1 Pancreas: anatomy and physiological function

The pancreas is a very blood-rich glandular organ of about 15 cm and 80 g with a flattened elongated shaped and a yellowish gray color. Is located behind the stomach and extends from the duodenum to the spleen. Four main regions can be identified in the pancreas, including: an enlarged head located in the loop formed by the duodenum; a thin neck, which constitutes the section between the head and the body of the gland; an elongated body that extends transversely towards the spleen and a short and blunt tail [40].

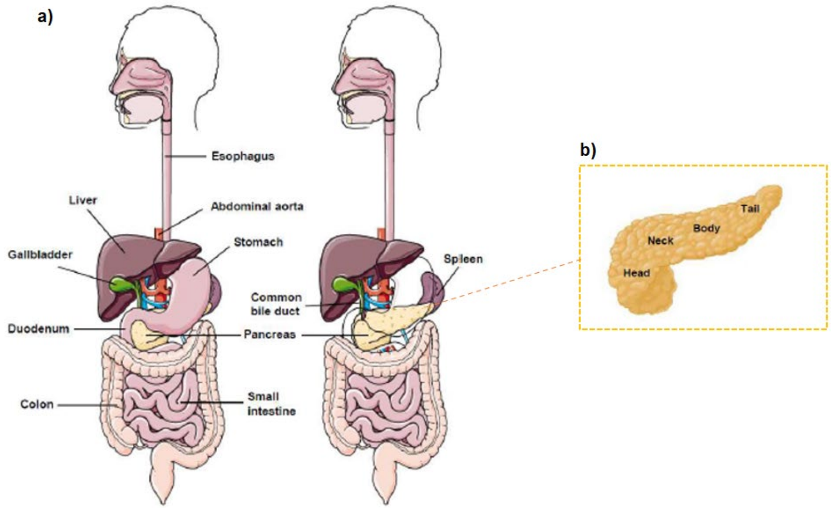
a)
Esophagus
Liver
Abdominal aorta
Stomach
Gallbladder
Spleen
Common bile duct
Duodenum
Pancreas
Colon
Small intestine
b)
Tail
Body
Neck
Head

Figure 10 a) Location and anatomical relationships between the pancreas and organs surrounding. b) Major anatomical regions of the pancreas. (Cancers, 13(16), 4173 2021).

The pancreas is mainly an exocrine gland that produces enzymes and digestive buffers, although it also performs an important endocrine function through the islets of Langerhans that secrete insulin and glucagon which regulate glucose metabolism (Figure 11). The large main pancreatic duct (duct of Wirsung) conveys exocrine pancreatic secretions towards the duodenal ampulla, while the accessory pancreatic duct (Duct of Santorini), not always present, can originate from the main pancreatic duct. This accessory pancreatic duct, when present, opens into the duodenum at the level of the minor pancreatic papilla, located a few centimeters above the major papilla [40].

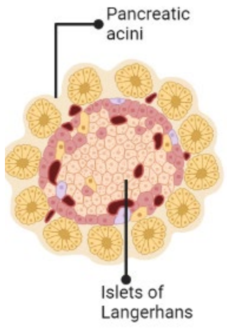
Pancreatic acini
Islets of Langerhans

Figure 11 Representation of pancreatic acinar cells responsible for the secretion of digestive enzymes and islets of Langerhans, endocrine cells that produce and release hormones (insulin and glucagon). Created with BioRender.com

2.2 Pancreatic ductal adenocarcinoma (PDAC)

Pancreatic cancer is a highly lethal form of cancer characterized by lack of specific symptoms and late diagnosis resulting in the seventh leading cause of cancer-related deaths worldwide [41]. Among pancreatic cancers, pancreatic ductal adenocarcinoma (PDAC) is the most common form of cancer, characterized by an incidence mortality rate nearly equivalent of 1:1. Moreover, PDAC has a long latency period between the onset of signs and symptoms resulting in poorly prognosis which has remained unchanged over the years. This disease is particularly difficult to treat due to its aggressive character and its tendency to form metastases.

In most cases, at the time of the diagnosis only 10-20% of patients are suitable for chirurgical resection, which is the only curative therapeutic option [42]. However, it has been found that even after surgical resection the survival rate remains almost stable at 5 years for the 10% of PDAC. The therapeutic options available to date for the treatment of PDAC include the use of FOLFIRINOX, a chemotherapeutic regimen consisting of the combination of folinic acid (Leucovorin), 5-fluorouracil 5-FU, irinotecan and oxaliplatin, representing the most effective option for the treatment of PDAC [43,44]. Another therapeutic option, which has been widely used for many years, include the use of gemcitabine, or gemcitabine plus nab-paclitaxel (Abraxane) [45]. These therapeutic options are characterized by high rate of toxicity (especially FOLFIRINOX) and showed only small benefits and are considered only palliative [46].

The reasons that make the diagnosis of PDAC particularly poor, can be summarized in the following points:

- lack of distinctive signs and symptoms necessary for early diagnosis;
- aggressive and metastatic nature of malignancy;
- low efficacy of therapeutic treatments;
- intrinsic and acquired chemoresistance of pancreatic cancer cells;
- genetic mutations of proteins involved in cellular homeostasis such as *TP53* and overexpression of oncogenes such as *KRAS* (Figure 12).

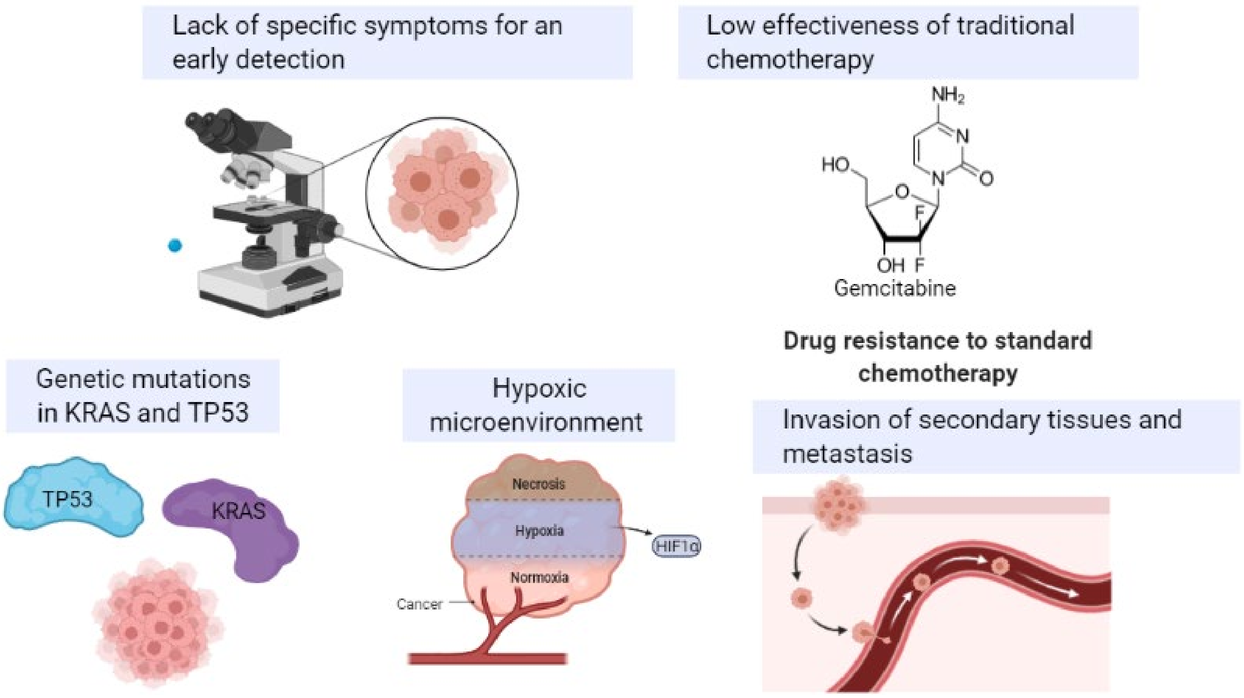
Lack of specific symptoms for an early detection
Low effectiveness of traditional chemotherapy
NH2
N
HO
O
N
O
F
OH F
Gemcitabine
Drug resistance to standard chemotherapy
Genetic mutations in KRAS and TP53
TP53
KRAS
Hypoxic microenvironment
Necrosis
Hypoxia
HIF1α
Normoxia
Cancer
Invasion of secondary tissues and metastasis

Figure 12 Major hallmarks in pancreatic cancer that affect chemotherapy efficacy and determine poor prognosis. Created with Biorender.com.

2.3 Stages of Pancreatic Cancer

To describe the level of progression of PDAC, its invasiveness and possible therapeutic options, four stages have been identified as follows:

Stage I: The tumor mass is limited to the pancreas and its size is between 2 and 4 cm.

Stage II: The tumor locally spreads in the pancreas, and its size is >4 cm.

The percentage of patients at the time of diagnosis that are in stage I and II, is around 10%.

Stage III: The tumor increases its level of spread by reaching blood vessels and nerves, without invading distant sites. The percentage of patients that at the time of diagnosis is in this stage, is around 35%.

Stage IV: The tumor has spread and metastasized to distant sites from the original organ. 50% of patients are in this stage at the time of diagnosis.

Patients in stage III and IV, at the time of the diagnosis cannot undergo surgical resection, showing an even lower survival rate [47].

2.3 Genetic abnormalities in PDAC

The major genetic mutation found in almost all PDACs involves the activating point mutation of the oncogene *KRAS*. The *KRAS* mutation is considered the initial genetic event for the onset of PDAC. Permanent activation of KRAS determines induction of Ras activated pathway, maintaining a high level of proliferation, transformation, invasiveness and survival of cancer cells. Other mutations that have been found in the tissues of PDAC patients involve the following proteins: tumor suppressor P53 (TP53) in 64% of cases, *SMAD4* in 21% of cases and finally *CDKN2A* in 17% of cases [48].

The mutations involving *KRAS* are point mutations and involve one of the following three amino acids: Glycine 12 (Gly 12), Glycine 13 (Gly 13) or Glutamine 61 (Glu 61). These mutations result in the binding of RAS to GTP, causing its permanent activation and the consequent stimulation of *KRAS*-activated pathways, involved in the development and onset of cancer. The therapeutic strategies developed to date to block the function of *KRAS* include the design of molecules active against protein kinase belonging to cellular signaling pathways activated by *KRAS* [49]. *KRAS* can also regulate other signaling pathways, such as PI3K-AKT, which is also known to be involved in cancer progression, EMT and metastasis [50].

Several clinical trials have tested the efficacy of active inhibitors against *KRAS* effector signaling proteins, such as mitogen-activated protein kinase (MEK) inhibitors and EGFR inhibitors, however, there was no significant increase in the overall survival rate in PDAC compared to the treatment with conventional chemotherapeutic agents [51]. For example, combination therapy of salumetinib (MEK inhibitor) and erlotinib (EGFR inhibitor) showed only a small increase in the overall survival rate, compared to the standard chemotherapy option (FOLFIRINOX) [52].

This clinical inefficacy of targeted therapies can be explained by an adaptive response from RAS effector signaling pathway and to the simultaneous activation of other pathways, which contribute to the sustainment of tumor cell growth and survival.

Another frequent mutation found in PDAC tissues involves *TP53*, mutated in 65% of PDAC patients [53]. *TP53* encodes for P53, which acts as a tumor suppressor gene, blocking the progression of cell cycle and cell proliferation in case of DNA damage or cellular stress. [54] *TP53* regulates the activity of CDK1 by p21. Under physiological conditions, CDK1 stimulates the progression of the cell cycle, however in case of DNA damage, *TP53* determines the inhibition of CDK1 activity resulting in cell cycle arrest and apoptosis [55]. Mutations inactivating *TP53* result in a lack of CDK1 inhibition and consequent progression of cell cycle and replication of cells with DNA damage.

3.0 An overview of malignant mesotheliomas

3.1 Malignant Pleural Mesothelioma: diagnosis and treatment

Malignant mesothelioma (MM) is a highly aggressive cancer arising from the mesothelium. It is characterized by poor prognosis due to the long latency period before clinical signs. MM can be classified into several subtypes including pleural, peritoneal, pericardial and testicular.

Malignant pleural mesothelioma (MPM) is a type of cancer that develops in the pleura, characterized by an average of survival rate around 12 months from the first diagnosis [56]. This low survival rate can also be attributed to the long latency period from the initial asbestos exposure to the diagnosis. The latency period has been estimated to be of about 30 years, ranging from 20 to 70 years and appears to be dose–dependent, however it is difficult to define an asbestos exposure threshold dose above there is a high probability to develop MPM [57,58]. The standard therapeutic approaches for the treatment of MPM include surgery, chemotherapy and radiation.

Surgical resection in combination with chemotherapy and or radiation represent the only attempt to eradicate the malignant tissue. It was found that surgery alone is better than radiation therapy in term of overall survival [59]. In patients with resectable MPM, a trimodality approach is recommended to show benefit in overall survival. The trimodality approach consists of the combination of extrapleural pneumonectomy (EPP), adjuvant chemotherapy and radiotherapy. Recent studies showed that radiation therapy after EPP reduces the progression of MPM and chemotherapy reduces risks of local recurrence and systemic metastases [60,61]. However, considering the latency period from the first symptoms and signs, most patients are diagnosed at a late stage, and are not eligible for resection.

For the MPM patients that are not candidate to undergo surgery, conventional chemotherapy represents a reasonable option, even though standard chemotherapeutic agents, such as gemcitabine or pemetrexed (always in combination with either cisplatin or carboplatin), provide only a small increase in the overall survival rate and are not able to eradicate MPM.

Radiation therapy represents another therapeutic option to treat MPM patients and performs its action by trying to counteract the spread of cancer cells along the pleura and the formation of small tumor cells called nodule. However, similar to chemotherapy, radiation can reduce the tumor spread and metastasis, but is not able to cure MPM [62].

Evidence supports the importance of developing new biomarkers for an earlier disease detection which might be useful to increase prognosis and overall survival of MPM. Among the several factors overexpressed in pleural mesothelioma tissues, increasing evidence demonstrated that Notch pathway seems to be involved in MPM cells survival [63]. Remarkably, previous studies reported that Notch receptors have an opposite role in mesothelioma progression, and it has been shown that Notch-1 upregulates the activity of the Phosphoinositide 3-kinase (PI3K)/AKT, pathway well known to be involved in cancer progression, by decreasing mRNA level of phosphatase and tensin homolog (PTEN) [64]. On the other hand, Notch-2 seems to have a suppressive role in the development and progression of MPM [65]. The explanation behind the Notch signaling pathway overexpression in malignant mesothelioma cells is related to the finding that the tumor microenvironment seems to profoundly affect the expression of Notch receptors.

More specifically, MPM is a form of tumor characterized by severe hypoxic condition [66]. Hypoxia activates the expression of Notch promoter hypoxia inducible factors (HIFs), stabilizing them from the degradation. Conversely, HIFs sustain the Notch transcriptional activity [67,68]. Moreover, it was also recognized that Notch expression is linked to cancer stem cells formation and self- renewal [69].

To conclude, MPM is characterized by a hypoxic microenvironment which further sustains the connection between Notch pathway overexpression and CSCs self-renewal [11], [70].

3.2 Malignant Peritoneal Mesothelioma (MPeM): diagnosis and treatment

Malignant peritoneal mesothelioma (MPeM) is a rare type of cancer with a poor prognosis, which spreads through the abdominal cavity and remains confined to the abdominal cavity during the duration of the disease, showing limited metastatic potential. [71]. Therapeutic options for the treatment of MPeM include: cytoreductive surgery (CRS) with hyperthermic intraperitoneal chemotherapy (HIPEC), where cisplatin or mitomycin are commonly used [72]. HIPEC is characterized by a pharmacokinetic advantage that maintains a high local concentration in the peritoneal cavity, but leads to a low systemic drug concentration in the plasma. For patients who cannot undergo surgical resection, systemic chemotherapy is an alternative treatment option.

Initially, the most widely used therapeutic agent for the treatment of MPeM was cisplatin as monotherapy, in 2004 the FDA approved the use of pemetrexed for the treatment of MPM and several studies also reported that pemetrexed may have some efficacy in the treatment of MPeM [73].

Gemcitabine plus pemetrexed was also evaluated in MPeM patients that are not eligible for chirurgical resection [74]. Currently the standard chemotherapeutic option is represented by cisplatin plus gemcitabine and the other therapeutic options are used for second-line therapy.

Despite HIPEC and standard chemotherapy, drug combinations for patient that cannot undergo surgery, have shown relatively good results. However, MPeM still shows a high mortality rate and still results in drug resistance and relapses.

For this reason, new strategies and therapeutic targets that could overcome chemoresistance and relapses are urgently needed. It was reported that focal adhesion kinase (FAK), is overexpressed in peritoneal mesothelioma cells [75]. FAK is a non-receptor protein-tyrosine kinase that plays a crucial role in regulating cell migration, adhesion, spreading, cell cycle progression, cell proliferation and apoptosis. There is some evidence that FAK regulates numerous signaling pathways involved in cancer progression and invasiveness such as PI3K/AKT signaling cascade, and MAP kinase signaling cascade [76]. Therefore, FAK inhibition could represent a new targeted therapeutic strategy for an earlier diagnosis and to overcome MPeM. drug resistance.

4. An overview on Biofilm formation and antibiotic resistance

Biofilm can be defined as "aggregates of microorganisms” in which cells are often incorporated into a self-produced matrix of extracellular polymeric substances (EPS), which are mainly formed by polysaccharides, proteins, lipids, extracellular DNA (e-DNA), and molecules originating from the host including mucus and DNA. This matrix provides protection from various stress conditions such as antimicrobial agents or immune response [77]. The term "aggregate" represents the fact that most cells in multi-layer biofilms experience cell-cell contact. In biofilm attached to the surface, only one layer of cells is in direct contact with the substrate. While non-attached biofilm or flakes are mobile biofilms, that form in the absence of surface. According to this classification, biofilms can be divided into two categories: aggregates adhering to a surface and flocculant bacterial aggregates not adhering to a surface [78].

Considering the interactions that occur between the individual bacteria and the bacteria and the matrix, the lifestyle of biofilm is clearly distinct from that of free-living bacteria. These peculiar biofilm’s characteristics allow bacteria to withstand harsh environmental conditions and makes them capable of causing a wide range of chronic diseases. Therefore, biofilms are the major cause of nosocomial infections in immunocompromised patients [79]. About 50% of nosocomial infections are restricted to patients by medical devices such as catheters, cardiac pacemakers, prostheses, dentures and contact lenses, foreign bodies that provide an ideal surface for bacterial cell attachment and biofilm formation [80].

In many cases, due to the toxicity of antibacterial drugs it is not possible to reach the minimum biofilm eradication concentration (MBEC), therefore, these agents can only reduce biofilm infections, but are not able to eradicate it entirely. The MBEC required to eradicate the biofilm is high to reach *in vivo* without causing toxicity; therefore, the antibiotics available to date are inadequate to counter biofilms [81,82]. In addition, the bacteria inside the biofilm possess implemented defense systems, such as the ability to inhibit the phagocytic response and the activation of a complement system, that protect bacteria from the responses by the immune system of the host organism [83].

The causes of biofilm drug resistance can be searched in the peculiar structure of the biofilm, including low availability of oxygen and nutrients, that renders biofilm particularly aggressive. The nature of biofilm can also contribute to resistance to antibiotics, for example it was reported that that *P. areuginosa* is particularly resistant to antibiotic therapy conducted with tobramicin due to the mucoid nature of the biofilm [84]. Another reason that determines drug resistance concerns the metabolism of biofilms; since the bacteria are in a state of nutrient deficiency, they may transform into a state of latency which determines resistance to antibiotic therapy, since the main antibiotics are active against cells characterized by high rate of cell division [85,86]. It has been confirmed that drug resistance is also due to the low availability of oxygen, which has been seen in *P. aeruginosa*, where antibiotic treatment was effective only in areas of the biofilm with high percentage of oxygen [87].

The low number of anti-biofilm therapies and the drug resistance that characterize biofilm infections, led to an increased interest to search for new agents able to overcome drug resistance, for new molecules able to block one or more mechanisms of formation or of maintenance of biofilms.

5. Outline

The subject of this dissertation is based on the study of new protein kinase involved in the development of drug resistance, major cause of failure of traditional chemotherapy. This dissertation consists in three parts: Part (1) *Role of CDK-1 and GSK-3 β in driving key hallmarks of PDAC and preclinical evaluation of novel marine alkaloids analogs*; for which **Chapter 2** describes the potential of CDK1 inhibition as a treatment for PDAC by outlining the molecular pathways influenced by CDK1 inhibition and new therapeutic strategies. **Chapter 3** summarizes the latest findings about GSK-3β biology and its role in the development and progression of pancreatic cancer. Moreover, in this chapter were reported therapeutic agents targeting GSK3β, which could represent novel strategies to surmount chemoresistance. **Chapter 4** describes the antitumor activity of novel 1,2,4-oxadiazole-based derivatives on a panel of PDAC cells (PATU-T, HPAF-II, Hs766t and PDAC3) and their ability to modulate CDK1 expression and induce the apoptosis.

Chapter 5 concerns the synthesis and antitumor activity of a series of novel 3-(1*H*-indol-3-yl)-1,2,4-oxadiazol-5-yl](1-methyl-1*H*-indol-3-yl) methanones against three PDAC cells, including SUIT-2, Capan-1, and Panc-1 cells. Moreover, their ability to induce apoptosis and inhibit GSK3β phosphorylation were reported.

Chapter 6 describes synthesis of new thiazoles nortopsentin derivatives and their cytotoxic activity against different human tumor cell lines of the NCI full panel.

Part (2) *New therapeutic approaches against malignant mesothelioma;* highlights the role of microRNA (miRNA) alterations, splicing and Notch signaling pathway deregulations in malignant mesothelioma progression and chemoresistance, as summarized in **Chapter 7** and the *in vitro* antitumor activity of new 2-(1*H*-indol-3-yl)-6-(thiophen-3-yl)imidazo[2,1-*b*][1,3,4]thiadiazole derivatives against two DMPM primary cell lines, MesoII and STO, as described in **Chapter 8**.

Part (3) *Biological evaluation of novel compounds analogues of the marine alkaloids topsentin and nortopsentin as bacterial biofilm inhibitors*, concerns the role of biofilm infections in antibiotic resistance, as summarized in **Chapter 9**. The involvement of methicillin-resistant *Staphylococcus aureus* (MRSA) as leading causes of persistent human infections and the latest finding about small molecules anti- biofilm, are summarized in **Chapter 10.**

Chapter 11, describes the antibiofilm properties of new thiazole nortopsentin analogues against Gram-positive bacterial (reference strains *Staphylococcus aureus* ATCC 25923, *Staphylococcus aureus* ATCC 6538) and Gram negative (strains Pseudomonas aeruginosa ATCC 15442).

Lastly, in **Chapter 12** is reported the anti-virulence activity of a series of new seventeen 1,2,4-oxadiazole derivatives and their potential ability to inhibit the bacterial transpeptidase sortase A.

References

1. Ardito, F., Giuliani, M., Perrone, D., Troiano, G., & Lo Muzio, L. (2017). The crucial role of protein phosphorylation in cell signaling and its use as targeted therapy (Review). International journal of molecular medicine, 40(2), 271–280.
2. Cohen P. (2002). The origins of protein phosphorylation. Nature cell biology, 4(5), E127–E130.
3. Yaish, P., Gazit, A., Gilon, C., & Levitzki, A. (1988). Blocking of EGF-dependent cell proliferation by EGF receptor kinase inhibitors. Science (New York, N.Y.), 242(4880), 933–935.
4. Cohen, P., Cross, D., & Jänne, P. A. (2021). Kinase drug discovery 20 years after imatinib: progress and future directions. Nature reviews. Drug discovery, 20(7), 551–569.
5. Attwood, M. M., Fabbro, D., Sokolov, A. V., Knapp, S., & Schiöth, H. B. (2021). Trends in kinase drug discovery: targets, indications and inhibitor design. Nature reviews. Drug discovery, 20(11), 839–861.
6. Roskoski R., Jr (2022). Properties of FDA-approved small molecule protein kinase inhibitors: A 2022 update. Pharmacological research, 175, 106037.
7. Roskoski R., Jr (2021). Properties of FDA-approved small molecule protein kinase inhibitors: A 2021 update. Pharmacological research, 165, 105463.
8. Roskoski R., (2019). Properties of FDA-approved small molecule protein kinase inhibitors: A 2020 update. Pharmacological Research, 152, 104609

9. Roskoski R. (2019). Properties of FDA-approved small molecule protein kinase inhibitors”, Pharmacological Research.
10. Wu P., Nielsen T. E., Clausen M. H., (2016). Small-molecule kinase inhibitors: an analysis of FDA-approved drugs. Drug Discovery Today, 21, 5-10.
11. Wu P., Nielsen T. E., Clausen M. H. (2015). FDA-approved small-molecule kinase inhibitors. Trends in Pharmacological Sciences, 36, 422-439.
12. Broekman, F., Giovannetti, E., & Peters, G. J. (2011). Tyrosine kinase inhibitors: Multi-targeted or single-targeted?. World journal of clinical oncology, 2(2), 80–93.
13. Cohen, P., & Alessi, D. R. (2013). Kinase drug discovery--what's next in the field?. ACS chemical biology, 8(1), 96–104.
14. Potapova, O., Laird, A. D., Nannini, M. A., Barone, A., Li, G., Moss, K. G., Cherrington, J. M., & Mendel, D. B. (2006). Contribution of individual targets to the antitumor efficacy of the multitargeted receptor tyrosine kinase inhibitor SU11248. Molecular cancer therapeutics, 5(5), 1280–1289.
15. Martin, J., Anamika, K., Srinivasan, N. (2010). Classification of protein kinases on the basis of both kinase and non-kinase regions. PloS one, 5(9), e12460.
16. Liao J. J. (2007). Molecular recognition of protein kinase binding pockets for design of potent and selective kinase inhibitors. Journal of medicinal chemistry, 50(3), 409–424.
17. Vermeulen, K., Van Bockstaele, D. R., & Berneman, Z. N. (2003). The cell cycle: a review of regulation, deregulation and therapeutic targets in cancer. Cell proliferation, 36(3), 131–149.
18. Santamaría, D., Barrière, C., Cerqueira, A., Hunt, S., Tardy, C., Newton, K., Cáceres, J. F., Dubus, P., Malumbres, M., & Barbacid, M. (2007). Cdk1 is sufficient to drive the mammalian cell cycle. Nature, 448(7155), 811–815.
19. Hu, X., & Moscinski, L. C. (2011). Cdc2: a monopotent or pluripotent CDK?. Cell proliferation, 44(3), 205–211.
20. Wu, C. X., Wang, X. Q., Chok, S. H., Man, K., Tsang, S., Chan, A., Ma, K. W., Xia, W., & Cheung, T. T. (2018). Blocking CDK1/PDK1/β-Catenin signaling by CDK1 inhibitor

RO3306 increased the efficacy of sorafenib treatment by targeting cancer stem cells in a preclinical model of hepatocellular carcinoma. Theranostics, 8(14), 3737–3750.

21. Asghar, U., Witkiewicz, A. K., Turner, N. C., & Knudsen, E. S. (2015). The history and future of targeting cyclin-dependent kinases in cancer therapy. Nature reviews. Drug discovery, 14(2), 130–146.
22. Ettl, T.; Schulz, D.; Bauer, R.J. (2022). The Renaissance of Cyclin Dependent Kinase Inhibitors. Cancers, 14, 293.
23. Zhang, M., Zhang, L., Hei, R., Li, X., Cai, H., Wu, X., Zheng, Q., & Cai, C. (2021). CDK inhibitors in cancer therapy, an overview of recent development. American journal of cancer research, 11(5), 1913-1935.
24. Cormier, K. W., & Woodgett, J. R. (2017). Recent advances in understanding the cellular roles of GSK-3. F1000Research, 6, F1000 Faculty Rev-167.
25. Frame, S., Cohen, P., & Biondi, R. M. (2001). A common phosphate binding site explains the unique substrate specificity of GSK3 and its inactivation by phosphorylation. Molecular cell, 7(6), 1321–1327.
26. Beurel, E., Grieco, S. F., & Jope, R. S. (2015). Glycogen synthase kinase-3 (GSK3): regulation, actions, and diseases. Pharmacology & therapeutics, 148, 114–131.
27. Kaidanovich-Beilin Oksana, Woodgett Jim. (2011). GSK-3: Functional Insights from Cell Biology and Animal Models. Frontiers in Molecular Neuroscience. 4, 40.
28. McCubrey, J. A., Davis, N. M., Abrams, S. L., Montalto, G., Cervello, M., Basecke, J., Libra, M., Nicoletti, F., Cocco, L., Martelli, A. M., & Steelman, L. S. (2014). Diverse roles of GSK-3: tumor promoter-tumor suppressor, target in cancer therapy. Advances in biological regulation, 54, 176–196.
29. Ding, L., & Billadeau, D. D. (2020). Glycogen synthase kinase-3β: a novel therapeutic target for pancreatic cancer. Expert opinion on therapeutic targets, 24(5), 417–426.
30. Freland, L., & Beaulieu, J. M. (2012). Inhibition of GSK3 by lithium, from single molecules to signaling networks. Frontiers in molecular neuroscience, 5, 14.
31. Bowden C. L. (2000). Efficacy of lithium in mania and maintenance therapy of bipolar disorder. The Journal of clinical psychiatry, 61 Suppl 9, 35–40.

32. Vulpetti, A., Crivori, P., Cameron, A., Bertrand, J., Brasca, M. G., D'Alessio, R., & Pevarello, P. (2005). Structure-based approaches to improve selectivity: CDK2-GSK3beta binding site analysis. Journal of chemical information and modeling, 45(5), 1282–1290.
33. Saraswati, A. P., Ali Hussaini, S. M., Krishna, N. H., Babu, B. N., & Kamal, A. (2018). Glycogen synthase kinase-3 and its inhibitors: Potential target for various therapeutic conditions. European journal of medicinal chemistry, 144, 843–858.
34. Mathuram, T. L., Ravikumar, V., Reece, L. M., Karthik, S., Sasikumar, C. S., & Cherian, K. M. (2016). Tideglusib induces apoptosis in human neuroblastoma IMR32 cells, provoking sub-G0/G1 accumulation and ROS generation. Environmental toxicology and pharmacology, 46, 194–205.
35. Serenó, L., Coma, M., Rodríguez, M., Sánchez-Ferrer, P., Sánchez, M. B., Gich, I., Agulló, J. M., Pérez, M., Avila, J., Guardia-Laguarta, C., Clarimón, J., Lleó, A., & Gómez-Isla, T. (2009). A novel GSK-3beta inhibitor reduces Alzheimer's pathology and rescues neuronal loss in vivo. Neurobiology of disease, 35(3), 359–367.
36. Parameswaran, R., Ramakrishnan, P., Moreton, S. A., Xia, Z., Hou, Y., Lee, D. A., Gupta, K., deLima, M., Beck, R. C., & Wald, D. N. (2016). Repression of GSK3 restores NK cell cytotoxicity in AML patients. Nature communications, 7, 11154.
37. Mai, W., Kawakami, K., Shakoori, A., Kyo, S., Miyashita, K., Yokoi, K., Jin, M., Shimasaki, T., Motoo, Y., & Minamoto, T. (2009). Deregulated GSK3{beta} sustains gastrointestinal cancer cells survival by modulating human telomerase reverse transcriptase and telomerase. Clinical cancer research: an official journal of the American Association for Cancer Research, 15(22), 6810–6819.
38. Gray, J. E., Infante, J. R., Brail, L. H., Simon, G. R., Cooksey, J. F., Jones, S. F., Farrington, D. L., Yeo, A., Jackson, K. A., Chow, K. H., Zamek-Gliszczynski, M. J., & Burris, H. A., 3rd (2015). A first-in-human phase I dose-escalation, pharmacokinetic, and pharmacodynamic evaluation of intravenous LY2090314, a glycogen synthase kinase 3 inhibitor, administered in combination with pemetrexed and carboplatin. Investigational new drugs, 33(6), 1187–1196.

39. Rizzieri, D. A., Cooley, S., Odenike, O., Moonan, L., Chow, K. H., Jackson, K., Wang, X., Brail, L., & Borthakur, G. (2016). An open-label phase 2 study of glycogen synthase kinase-3 inhibitor LY2090314 in patients with acute leukemia. Leukemia & lymphoma, 57(8), 1800–1806.
40. Talathi, S. S., Zimmerman, R., & Young, M. (2021). Anatomy, Abdomen and Pelvis, Pancreas. In StatPearls. StatPearls Publishing.
41. Sung, H., Ferlay, J., Siegel, R. L., Laversanne, M., Soerjomataram, I., Jemal, A., & Bray, F. (2021). Global Cancer Statistics 2020: GLOBOCAN Estimates of Incidence and Mortality Worldwide for 36 Cancers in 185 Countries. CA: a cancer journal for clinicians, 71(3), 209–249.
42. Ahrendt, S. A., & Pitt, H. A. (2002). Surgical management of pancreatic cancer. Oncology (Williston Park, N.Y.), 16(6), 725–743.
43. Caparello, C., Meijer, L. L., Garajova, I., Falcone, A., Le Large, T. Y., Funel, N., Kazemier, G., Peters, G. J., Vasile, E., & Giovannetti, E. (2016). FOLFIRINOX and translational studies: Towards personalized therapy in pancreatic cancer. World journal of gastroenterology, 22(31), 6987–7005.
44. Hruban, R. H., Goggins, M., Parsons, J., & Kern, S. E. (2000). Progression model for pancreatic cancer. Clinical cancer research, 6(8), 2969–2972.
45. Von Hoff, D. D., Ervin, T., Arena, F. P., Chiorean, E. G., Infante, J., Moore, M., Seay, T., Tjulandin, S. A., Ma, W. W., Saleh, M. N., Harris, M., Reni, M., Dowden, S., Laheru, D., Bahary, N., Ramanathan, R. K., Tabernero, J., Hidalgo, M., Goldstein, D., Van Cutsem, E., … Renschler, M. F. (2013). Increased survival in pancreatic cancer with nab-paclitaxel plus gemcitabine. The New England journal of medicine, 369(18), 1691–1703. https://doi.org/10.1056/NEJMoa1304369
46. Sciarrillo, R., Wojtuszkiewicz, A., Kooi, I. E., Gómez, V. E., Boggi, U., Jansen, G., Kaspers, G. J., Cloos, J., & Giovannetti, E. (2016). Using RNA-sequencing to Detect Novel Splice Variants Related to Drug Resistance in In Vitro Cancer Models. Journal of visualized experiments. JoVE, (118), 54714.

47. Kleeff, J., Korc, M., Apte, M., La Vecchia, C., Johnson, C. D., Biankin, A. V., Neale, R. E., Tempero, M., Tuveson, D. A., Hruban, R. H., & Neoptolemos, J. P. (2016). Pancreatic cancer. Nature reviews. 2, 16022.
48. Witkiewicz, A. K., McMillan, E. A., Balaji, U., Baek, G., Lin, W. C., Mansour, J., Mollaee, M., Wagner, K. U., Koduru, P., Yopp, A., Choti, M. A., Yeo, C. J., McCue, P., White, M. A., & Knudsen, E. S. (2015). Whole-exome sequencing of pancreatic cancer defines genetic diversity and therapeutic targets. Nature communications, 6, 6744.
49. Bamford, S., Dawson, E., Forbes, S., Clements, J., Pettett, R., Dogan, A., Flanagan, A., Teague, J., Futreal, P. A., Stratton, M. R., & Wooster, R. (2004). The COSMIC (Catalogue of Somatic Mutations in Cancer) database and website. British journal of cancer, 91(2), 355–358.
50. Cicenas, J., Tamosaitis, L., Kvederaviciute, K., Tarvydas, R., Staniute, G., Kalyan, K., Meskinyte-Kausiliene, E., Stankevicius, V., & Valius, M. (2017). KRAS, NRAS and BRAF mutations in colorectal cancer and melanoma. Medical oncology (Northwood, London, England), 34(2), 26.
51. Gillson, J., Ramaswamy, Y., Singh, G., Gorfe, A. A., Pavlakis, N., Samra, J., Mittal, A., & Sahni, S. (2020). Small Molecule KRAS Inhibitors: The Future for Targeted Pancreatic Cancer Therapy?. Cancers, 12(5), 1341.
52. Ko, A. H., Bekaii-Saab, T., Van Ziffle, J., Mirzoeva, O. M., Joseph, N. M., Talasaz, A., Kuhn, P., Tempero, M. A., Collisson, E. A., Kelley, R. K., Venook, A. P., Dito, E., Ong, A., Ziyeh, S., Courtin, R., Linetskaya, R., Tahiri, S., & Korn, W. M. (2016). A Multicenter, Open-Label Phase II Clinical Trial of Combined MEK plus EGFR Inhibition for Chemotherapy-Refractory Advanced Pancreatic Adenocarcinoma. Clinical cancer, 22(1), 61–68.
53. Notta, F., Chan-Seng-Yue, M., Lemire, M., Li, Y., Wilson, G. W., Connor, A. A., Denroche, R. E., Liang, S. B., Brown, A. M., Kim, J. C., Wang, T., Simpson, J. T., Beck, T., Borgida, A., Buchner, N., Chadwick, D., Hafezi-Bakhtiari, S., Dick, J. E., Heisler, L., Hollingsworth, M. A., Gallinger, S. (2016). A renewed model of pancreatic cancer evolution based on genomic rearrangement patterns. Nature, 538(7625), 378–382.

54. Aubrey, B. J., Strasser, A., & Kelly, G. L. (2016). Tumor-Suppressor Functions of the TP53 Pathway. Cold Spring Harbor perspectives in medicine, 6(5), a026062.
55. Benson, E. K., Mungamuri, S. K., Attie, O., Kracikova, M., Sachidanandam, R., Manfredi, J. J., & Aaronson, S. A. (2014). p53-dependent gene repression through p21 is mediated by recruitment of E2F4 repression complexes. Oncogene, 33(30), 3959–3969.
56. Carbone, M., Ly, B. H., Dodson, R. F., Pagano, I., Morris, P. T., Dogan, U. A., Gazdar, A. F., Pass, H. I., & Yang, H. (2012). Malignant mesothelioma: facts, myths, and hypotheses. Journal of cellular physiology, 227(1), 44–58.
57. Carbone, M., & Rdzanek, M. A. (2004). Pathogenesis of malignant mesothelioma. Clinical lung cancer, 5 Suppl 2, S46–S50.
58. van Meerbeeck, J. P., Scherpereel, A., Surmont, V. F., & Baas, P. (2011). Malignant pleural mesothelioma: the standard of care and challenges for future management. Critical reviews in oncology/hematology, 78(2), 92–111.
59. Taioli, E., Wolf, A. S., Camacho-Rivera, M., Kaufman, A., Lee, D. S., Nicastri, D., Rosenzweig, K., & Flores, R. M. (2015). Determinants of Survival in Malignant Pleural Mesothelioma: A Surveillance, Epidemiology, and End Results (SEER) Study of 14,228 Patients. PloS one, 10(12), e0145039.
60. Batirel, H. F., Metintas, M., Caglar, H. B., Yildizeli, B., Lacin, T., Bostanci, K., Akgul, A. G., Evman, S., & Yuksel, M. (2008). Trimodality treatment of malignant pleural mesothelioma. Journal of thoracic oncology: official publication of the International Association for the Study of Lung Cancer, 3(5), 499–504.
61. Van Schil, P. E., Baas, P., Gaafar, R., Maat, A. P., Van de Pol, M., Hasan, B., Klomp, H. M., Abdelrahman, A. M., Welch, J., van Meerbeeck, J. P., & European Organisation for Research and Treatment of Cancer (EORTC) Lung Cancer Group (2010). Trimodality therapy for malignant pleural mesothelioma: results from an EORTC phase II multicentre trial. The European respiratory journal, 36(6), 1362–1369.
62. Clive, A. O., Taylor, H., Dobson, L., Wilson, P., de Winton, E., Panakis, N., Pepperell, J., Howell, T., Stewart, S. A., Penz, E., Jordan, N., Morley, A. J., Zahan-Evans, N.,

Smith, S., Batchelor, T., Marchbank, A., Bishop, L., Ionescu, A. A., Bayne, M., Cooper, S., Maskell, N. A. (2016). Prophylactic radiotherapy for the prevention of procedure-tract metastases after surgical and large-bore pleural procedures in malignant pleural mesothelioma (SMART): a multicentre, open-label, phase 3, randomised controlled trial. The Lancet. Oncology, 17(8), 1094–1104.

63. Huang, Y., Lin, L., Shanker, A., Malhotra, A., Yang, L., Dikov, M. M., & Carbone, D. P. (2011). Resuscitating cancer immunosurveillance: selective stimulation of DLL1-Notch signaling in T cells rescues T-cell function and inhibits tumor growth. Cancer research, 71(19), 6122–6131.
64. Hales, E. C., Orr, S. M., Larson Gedman, A., Taub, J. W., & Matherly, L. H. (2013). Notch1 receptor regulates AKT protein activation loop (Thr308) dephosphorylation through modulation of the PP2A phosphatase in phosphatase and tensin homolog (PTEN)-null T-cell acute lymphoblastic leukemia cells. The Journal of biological chemistry, 288(31), 22836–22848.
65. Graziani, I., Eliasz, S., De Marco, M. A., Chen, Y., Pass, H. I., De May, R. M., Strack, P. R., Miele, L., & Bocchetta, M. (2008). Opposite effects of Notch-1 and Notch-2 on mesothelioma cell survival under hypoxia are exerted through the Akt pathway. Cancer research, 68(23), 9678–9685.
66. Klabatsa, A., Sheaff, M. T., Steele, J. P., Evans, M. T., Rudd, R. M., & Fennell, D. A. (2006). Expression and prognostic significance of hypoxia-inducible factor 1alpha (HIF-1alpha) in malignant pleural mesothelioma (MPM). Lung cancer (Amsterdam, Netherlands), 51(1), 53–59.
67. Zavadil, J., Cermak, L., Soto-Nieves, N., & Böttinger, E. P. (2004). Integration of TGF-beta/Smad and Jagged1/Notch signalling in epithelial-to-mesenchymal transition. The EMBO journal, 23(5), 1155–1165.
68. Miele L. (2006). Notch signaling. Clinical cancer research: an official journal of the American Association for Cancer Research, 12(4), 1074–1079.
69. Fazio, C., & Ricciardiello, L. (2016). Inflammation and Notch signaling: a crosstalk with opposite effects on tumorigenesis. Cell death & disease, 7(12), e2515.

70. Gustafsson, M. V., Zheng, X., Pereira, T., Gradin, K., Jin, S., Lundkvist, J., Ruas, J. L., Poellinger, L., Lendahl, U., & Bondesson, M. (2005). Hypoxia requires notch signaling to maintain the undifferentiated cell state. Developmental cell, 9(5), 617–628.
71. Feldman, A. L., Libutti, S. K., Pingpank, J. F., Bartlett, D. L., Beresnev, T. H., Mavroukakis, S. M., Steinberg, S. M., Liewehr, D. J., Kleiner, D. E., & Alexander, H. R. (2003). Analysis of factors associated with outcome in patients with malignant peritoneal mesothelioma undergoing surgical debulking and intraperitoneal chemotherapy. Journal of clinical oncology: official journal of the American Society of Clinical Oncology, 21(24), 4560–4567.
72. Sugarbaker, P. H., Welch, L. S., Mohamed, F., & Glehen, O. (2003). A review of peritoneal mesothelioma at the Washington Cancer Institute. Surgical oncology clinics of North America, 12(3), 605–xi.
73. Jänne, P. A., Wozniak, A. J., Belani, C. P., Keohan, M. L., Ross, H. J., Polikoff, J. A., Mintzer, D. M., Taylor, L., Ashland, J., Ye, Z., Monberg, M. J., & Obasaju, C. K. (2005). Open-label study of pemetrexed alone or in combination with cisplatin for the treatment of patients with peritoneal mesothelioma: outcomes of an expanded access program. Clinical lung cancer, 7(1), 40–46.
74. Simon, G. R., Verschraegen, C. F., Jänne, P. A., Langer, C. J., Dowlati, A., Gadgeel, S. M., Kelly, K., Kalemkerian, G. P., Traynor, A. M., Peng, G., Gill, J., Obasaju, C. K., & Kindler, H. L. (2008). Pemetrexed plus gemcitabine as first-line chemotherapy for patients with peritoneal mesothelioma: final report of a phase II trial. Journal of clinical oncology: official journal of the American Society of Clinical Oncology, 26(21), 3567–3572.
75. Kanteti, R., Mirzapoiazova, T., Riehm, J. J., Dhanasingh, I., Mambetsariev, B., Wang, J., Kulkarni, P., Kaushik, G., Seshacharyulu, P., Ponnusamy, M. P., Kindler, H. L., Nasser, M. W., Batra, S. K., & Salgia, R. (2018). Focal adhesion kinase a potential therapeutic target for pancreatic cancer and malignant pleural mesothelioma. Cancer biology & therapy, 19(4), 316–327.

76. . McLean, G., Carragher, N., Avizienyte, E. et al. The role of focal-adhesion kinase in cancer — a new therapeutic opportunity. Nat Rev Cancer 5, 505–515 (2005).
77. Flemming, HC., Wingender, J. (2010). The biofilm matrix. Nat Rev Microbiol **8,** 623–633.
78. Stoodley, P., Sauer, K., Davies, D. G., & Costerton, J. W. (2002). Biofilms as complex differentiated communities. Annual review of microbiology, 56, 187–209.
79. Davies D. Understanding biofilm resistance to antibacterial agents. Nat Rev Drug Discov 2003; 2:114-22
80. Singh PK, Schaefer AL, Parsek MR, Moninger TO, Welsh MJ, Greenberg EP. (2000) Quorum-sensing signals indicate that cystic fibrosis lungs are infected with bacterial biofilms. Nature; 407:762-4.
81. Høiby, N., Ciofu, O., Johansen, H. K., Song, Z. J., Moser, C., Jensen, P. Ø., Molin, S., Givskov, M., Tolker-Nielsen, T., & Bjarnsholt, T. (2011). The clinical impact of bacterial biofilms. International journal of oral science, 3(2), 55–65.
82. Wu, H., Moser, C., Wang, HZ. et al. (2015). Strategies for combating bacterial biofilm infections. Int J Oral Sci **7,** 1–7.
83. Götz F. (2002). Staphylococcus and biofilms. Molecular microbiology, 43(6), 1367–1378.
84. Ciofu O, Mandsberg LF, Wang H, Hoiby N. (2012). Phenotypes selected during chronic lung infection in cystic fibrosis patients: implications for the treatment of Pseudomonas aeruginosa biofilm infections.FEMS Immunol Medical Microbiol; 65:215-25; PMID:22540844.
85. Anderl JN, Zahller J, Roe F, Stewart PS. (2003). Role of nutrient limitation and stationary-phase existence in Klebsiella pneumoniae biofilm resistance to ampicillin and ciprofloxacin Antimicrobial Agents Chemotherapy; 47:1251-6.
86. Brown MR, Allison DG, Gilbert P. (1988). Resistance of bacterial biofilms to antibiotics: a growth-rate related effect? Antimicrobial Chemotherapy; 22:777-80.
87. Walters MC, Roe F, Bugnicourt A, Franklin MJ Stewart PS. (2003). Contributions of antibiotic penetration, oxygen limitation, and low metabolic activity to tolerance of

Pseudomonas aeruginosa biofilms to ciprofloxacin and tobramycin. Antimicrobial Agents Chemotherapy; 47:317-23.

Part I

Role of CDK-1 and GSK-3 β in driving key hallmarks of PDAC and preclinical evaluation of novel marine alkaloids analogs (*Chapter 2-6*)

Chapter 2

Cyclin dependent kinase-1 (Cdk-1) inhibition as a novel therapeutic strategy against pancreatic ductal adenocarcinoma (pdac).

Wijnen, R.*, **Pecoraro, C.***, Carbone, D., Fiuji, H., Avan, A., Peters, G. J., Giovannetti, E., & Diana, P.

Cancers (2021), *13*(17), 4389.

* These Authors contributed equally to this study.

cancers

Review

Cyclin Dependent Kinase-1 (CDK-1) Inhibition as a Novel Therapeutic Strategy against Pancreatic Ductal Adenocarcinoma (PDAC)

Rosa Wijnen [1,†], Camilla Pecoraro [1,2,†], Daniela Carbone [2], Hamid Fiuji [3], Amir Avan [4], Godefridus J. Peters [1,5], Elisa Giovannetti [1,6,*,‡] and Patrizia Diana [2,*,‡]

[1] Department of Medical Oncology, Cancer Center Amsterdam, Amsterdam UMC, VU University Medical Center (VUmc), 1081 HV Amsterdam, The Netherlands; rosavan2000@gmail.com (R.W.); camilla.pecoraro@unipa.it (C.P.); gj.peters@amsterdamumc.nl (G.J.P.)
[2] Dipartimento di Scienze e Tecnologie Biologiche Chimiche e Farmaceutiche (STEBICEF), Università degli Studi di Palermo, 90123 Palermo, Italy; daniela.carbone@unipa.it
[3] Department of Biochemistry, Payame-Noor University, Mashhad 19395-4697, Iran; hamid_fiuji@yahoo.com
[4] Metabolic Syndrome Research Center, Mashhad University of Medical Science, Mashhad 91886-17871, Iran; AvanA@mums.ac.ir
[5] Department of Biochemistry, Medical University of Gdansk, 80-210 Gdansk, Poland
[6] Cancer Pharmacology Lab, AIRC Start Up Unit, Fondazione Pisana per la Scienza, 56124 Pisa, Italy
* Correspondence: e.giovannetti@amsterdamumc.nl (E.G.); patrizia.diana@unipa.it (P.D.); Tel.: +31-2044-42633 (E.G.); +39-091-23896815 (P.D.)
† These authors contributed equally to this paper as first authors.
‡ These authors contributed equally to this paper as senior authors.

Citation: Wijnen, R.; Pecoraro, C.; Carbone, D.; Fiuji, H.; Avan, A.; Peters, G.J.; Giovannetti, E.; Diana, P. Cyclin Dependent Kinase-1 (CDK-1) Inhibition as a Novel Therapeutic Strategy against Pancreatic Ductal Adenocarcinoma (PDAC). *Cancers* **2021**, *13*, 4389. https://doi.org/10.3390/cancers13174389

Academic Editor: Louis Buscail

Received: 13 July 2021
Accepted: 27 August 2021
Published: 30 August 2021

Publisher's Note: MDPI stays neutral with regard to jurisdictional claims in published maps and institutional affiliations.

Copyright: © 2021 by the authors. Licensee MDPI, Basel, Switzerland. This article is an open access article distributed under the terms and conditions of the Creative Commons Attribution (CC BY) license (https://creativecommons.org/licenses/by/4.0/).

Simple Summary: Pancreatic ductal adenocarcinoma (PDAC) is one of the most lethal cancers in humans, due to late diagnosis and limited treatment possibilities. Improved treatment for PDAC patients is warranted. Cyclin-dependent kinase 1 (CDK1) is a stimulator of cell cycle progression and its activity is regularly enhanced in pancreatic cancer cells. Therefore, CDK1 has been proposed as a novel drug target to treat patients with PDAC. This review describes the potential of CDK1 inhibition as a treatment for PDAC by outlining the molecular pathways influenced by CDK1 inhibition and new therapeutic strategies.

Abstract: The role of CDK1 in PDAC onset and development is two-fold. Firstly, since CDK1 activity regulates the G2/M cell cycle checkpoint, overexpression of CDK1 can lead to progression into mitosis even in cells with DNA damage, a potentially tumorigenic process. Secondly, CDK1 overexpression leads to the stimulation of a range of proteins that induce stem cell properties, which can contribute to the development of cancer stem cells (CSCs). CSCs promote tumor-initiation and metastasis and play a crucial role in the development of PDAC. Targeting CDK1 showed promising results for PDAC treatment in different preclinical models, where CDK1 inhibition induced cell cycle arrest in the G2/M phase and led to induction of apoptosis. Next to this, PDAC CSCs are uniquely sensitive to CDK1 inhibition. In addition, targeting of CDK1 has shown potential for combination therapy with both ionizing radiation treatment and conventional chemotherapy, through sensitizing tumor cells and reducing resistance to these treatments. To conclude, CDK1 inhibition induces G2/M cell cycle arrest, stimulates apoptosis, and specifically targets CSCs, which makes it a promising treatment for PDAC. Screening of patients for CDK1 overexpression and further research into combination treatments is essential for optimizing this novel targeted therapy.

Keywords: pancreatic cancer; PDAC; CDK1 inhibition; cell cycle regulation; novel treatment

1. Introduction

With a 5-year survival rate of only 10 percent, pancreatic cancer is one of the most lethal cancers in humans [1]. The American Cancer Society estimates that in the United

States alone, 48,220 people will die as a result of pancreatic cancer in 2021 [2]. Currently pancreatic cancer is the seventh leading cause of global cancer deaths in both sexes, and is the most lethal of common malignancies, with incidence and mortality rates nearly equivalent [3]. Unlike most other forms of cancer, pancreatic cancer has seen only minor improvement in survival rates over the past 40 years [4]. These poor survival rates are largely attributable to a late diagnosis of the disease and limited treatment possibilities. Surgery represents the only curative treatment, but only 20 percent of pancreatic tumors are eligible for resection [5,6]. The current most commonly-used treatment options—FOLFIRINOX (folinic acid, fluorouracil, irinotecan, and oxaliplatin) and gemcitabine plus nab-paclitaxel—are highly toxic and not effective enough [7,8]. The detrimental impact of pancreatic cancer combined with the low availability of treatment options has caused the urgent need to develop novel therapeutic strategies.

Pancreatic ductal adenocarcinoma (PDAC) develops from differentiated pancreatic ductal cells and accounts for 90 percent of all pancreatic tumors. The disease advances in multiple stages, which are characterized by histopathological and molecular changes in the pancreatic duct cell lining. Through these stages, healthy epithelium transforms first into pancreatic intraepithelial neoplasia, followed by invasive carcinoma [9].

In 78% of the PDAC cases, mutations linked to cell cycle regulation occur [10]. Of these, tumor suppressor protein p53 (TP53) is one of the most frequent and relevant drivers of pancreatic tumorigenesis, as it is mutated in 70% of the PDAC cases. TP53 is a tumor suppressor gene that codes for p53, a molecule involved in cell cycle regulation [11]. Of note, loss of the TP53 appears to occur late (after KRAS and CDKN2A alterations) in the classical model of development of pancreatic neoplasia [7]. However, loss of heterozygosity at chromosome 17p (the location of the TP53 gene) as well as abnormalities of TP53 gene expression have all also been reported in pancreatic duct lesions, and a recent model suggests that PDAC progression is neither gradual nor follows the accepted mutation order because most tumors harbor complex rearrangement patterns associated with mitotic errors [8]. One of its downstream effects is cyclin-dependent kinase 1 (CDK1) inhibition, via p21 activation. This effect is lost when the TP53 gene is mutated, mutations fail to stimulate p21, thus CDK1 is no longer inhibited (Figure 1). CDK1 stimulates progression through the cell cycle [12]. When stress or DNA damage occurs, TP53 blocks CDK1 signaling, thus ultimately causing apoptosis. These properties of CDK1 suggest that in the opposite scenario, overexpression of the protein could result in replication of cells with faulty DNA, causing cancer cell proliferation. Indeed, scientists have identified sustained CDK1 activity as essential for tumorigenesis [13].

CDK1 genes are significantly overexpressed in tumor cells of PDAC patients [14], which is associated with more advanced stages of PDAC and is an indicator of poor survival rates for patients. Moreover, inhibition of CDC25, an activator of CDK1, leads to a reduction in growth of pancreatic cancer cell lines [15]. Together, these studies indicate the potential of CDK1 inhibition as a novel drug target to treat PDAC. In addition, several other studies indicate the potential of CDK1 inhibition for both cancer treatment in general [16,17], and specifically for PDAC [18,19].

However, there is only scarce clinical evidence for the concrete benefits of CDK1 inhibition [13]. Cytotoxic effects of CDK1 inhibitors on healthy cells indicate that the safety of CDK1 inhibition should be investigated [20]. Furthermore, there is limited research that thoroughly explains the molecular mechanisms through which CDK1 overexpression induces PDAC development and how CDK1 inhibition could combat this. Additionally, different PDAC subtypes may have different behaviors and targetability, but there are few studies focusing on these subtypes [21]. These questions should be explored further in order to reach a consensus on whether CDK1 inhibition is a good drug target to treat patients with PDAC, which is lacking in the existing literature. This literature review aims to assess the potential of CDK1 inhibition by outlining how enhanced activity of this kinase contributes to the development and progression of PDAC, and how a novel CDK1 inhibitor would influence the molecular pathways involved in PDAC to exert its proposed anticancer mechanism.

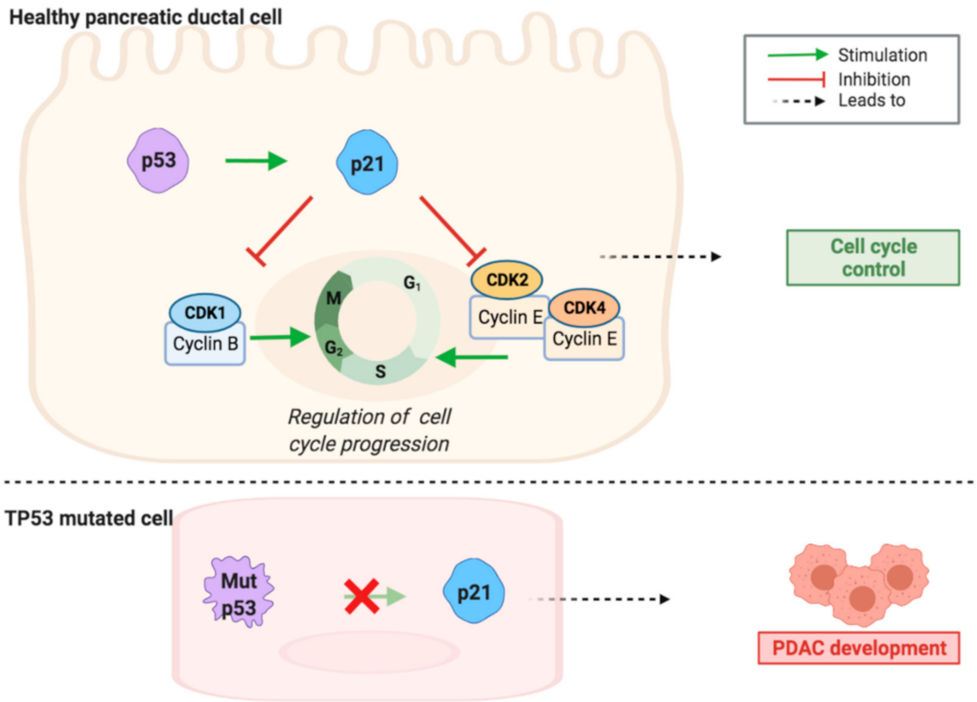

Figure 1. TP53 gene mutation contributes to loss of cell cycle regulation and PDAC formation and development. A healthy cell expresses normal p53, which influences cell cycle control via stimulation of p21, which can inhibit CDK/cyclin complexes. The CDK1/cyclin B complex promotes G2/M phase progression, whereas CDK2/cyclin E and CDK4/cyclin E complexes promote G1/S phase progression. Via loss of CDK/cyclin complexes inhibition, mutated p53 contributes to loss of cell cycle control, which can lead to PDAC development.

2. Tumorigenic Activity of CDK1 and Anticancer Mechanisms of CDK1 Inhibitors

2.1. CDK1 and Cell Cycle

Cyclin-dependent kinases (CDKs) are serine/threonine kinases which play a crucial role in regulating the cell cycle [12]. They depend on cyclins, separate protein subunits with which the kinases form CDK/cyclin complexes [22]. These complexes can control the cell cycle process by either stimulating or halting cell cycle progression. CDK activity is regulated by several factors, including the availability of their cyclin partners, the presence of inhibitory tyrosine phosphorylation, and the activity of CDK inhibitors [23]. There are currently more than 20 identified family members of CDKs, which share the catalytic domain formed by an ATP-binding pocket, the cyclin-binding domain, and the activation loop called T-loop motif [22]. CDK/cyclin complex formation induces a conformational change of the T-loop, which leads to the exposure and phosphorylation of the substrate-binding domain of the kinase. CDKs, besides the cell cycle, also influence other cellular and developmental processes [12]. These processes include stem cell self-renewal, transcription, epigenetic regulation, neuronal functions, and spermatogenesis.

CDK1—also known under the names of CDC2, CDC28A, cell division cycle 2 homolog A, p34 protein kinase, and p34—can form a complex with cyclins A, B, D, and E [13]. The kinase regulates G1/S and G2/M phase transition and promotes M phase progression [24]. It is regarded as the master regulator of the cell cycle, because its functions cannot be compensated by other CDKs, including the closely related CDK2 [25]. In contrast, CDK1 can compensate for the functions of other CDKs, and has been shown to drive mammalian cell cycle progression in the absence of other CDKs [26]. Although the main function of CDK1 is to regulate entry into and progression through mitosis, this protein can also form a complex with other cyclins, such as, D1, E, and A, to regulate G1 phase progression and G1/S transition [23]. During the late G2 phase of the cell cycle, increased levels of cyclin B allow stable CDK1/cyclin B complex formation [20]. This complex is kept inactive by Wee1- and Myt1-dependent inhibitory phosphorylation of the tyrosine 14 and 15 residues in the CDK1 subunit, which interfere with ATP alignment [23,27]. When CDC25 removes the inhibitory phosphates, the complex becomes activated, which induces G2/M phase transition. To exit the M phase, CDK1/cyclin B complex activity needs to be downregulated again, which is achieved through cyclin B proteolysis. The activated CDK1/cyclin B complex is capable of phosphorylating over 100 different proteins [20]. In addition to cell cycle-related targets, the complex has been shown to phosphorylate proteins involved in cell migration and cytoskeleton regulation [28]. Furthermore, CDK1 is emerging as a key regulator of self-renewal and differentiation of human embryonic stem cells (hESCs) and human induced pluripotent stem cells (hiPSCs) [25,29]. Although the knowledge on CDK1 has increased considerably over the last decade, not all processes in which CDK1 is involved in are already understood. CDK1 overexpression likely causes PDAC tumorigenesis by stimulation of checkpoint evasion and induction of stemness properties.

2.2. Bypassing the Cell Cycle Checkpoint

To ensure genomic integrity, several checkpoints regulate cell cycle progression, including the DNA structure checkpoint, also called the G2/M phase checkpoint [27]. Under normal conditions, CDK1 binds to cyclin B to mediate progression from the G2 to M phase of the cell cycle [12,13]. In a situation of cell stress or DNA damage, the activation of the CDK1/cyclin B complex is delayed by Chk1 and Chk2, which inhibit CDC25 and upregulate Wee1 and Myt1 [27]. This induces cell cycle arrest at the G2/M phase and DNA repair, after which the cell cycle can continue. In case of impaired DNA repair, the cell undergoes apoptosis to ensure that a cell with faulty DNA is not replicated. However, CDK1 overactivation might allow evasion of this checkpoint, even with DNA damage [30,31]. In a healthy cell, both of these pathways, regulated by (lack of) CDK1 activity, ensure that a cell with faulty DNA is not replicated (Figure 2). Since CDK1 activity promotes cell cycle progression through the G2/M cell cycle checkpoint, it is hypothesised that enhanced CDK1 activity allows cells with DNA damage to progress through this checkpoint, which can potentially be tumorigenic (Figure 2) [13]. In a physiological situation, multiple CDKs have the function of regulating progression through the different cell cycle checkpoints. However, in absence of other CDKs, CDK1 alone is sufficient to drive mammalian cell cycle progression [26]. This suggests that overexpression of CDK1 on its own is sufficient to drive cell cycle progression of cancer cells, without the need for other CDKs to be overexpressed.

2.3. Inducing G2/M Phase Cell Cycle Arrest

The first proposed anticancer mechanism of CDK1 inhibition is halting cell cycle progression of tumour cells at the DNA structure checkpoint, resulting in G2/M phase cell cycle arrest. Various studies described the effect of CDK1/cyclin B complex activity inhibition on cancer cell cycle proliferation.

Two compounds, RO-3306 and BA-j, specifically inhibit CDK1 without significantly affecting the activity of other CDKs [20,32]. The effect of these agents on PDAC cell lines was never investigated. They showed promising effects on other tumour cell lines, through induction of G2/M phase cell cycle arrest mediated by RO-3306 [20,33]. The structurally modified flavonoid BA-j inhibits CDK1 activity directly and indirectly, through inactivation of CDC25 [32]. Direct inhibition of CDK1 activity in PDAC cell lines has only been tested with CDK1 small interfering RNA (siRNA), which decreased survival of PDAC cell lines with a KRAS mutated form [34].

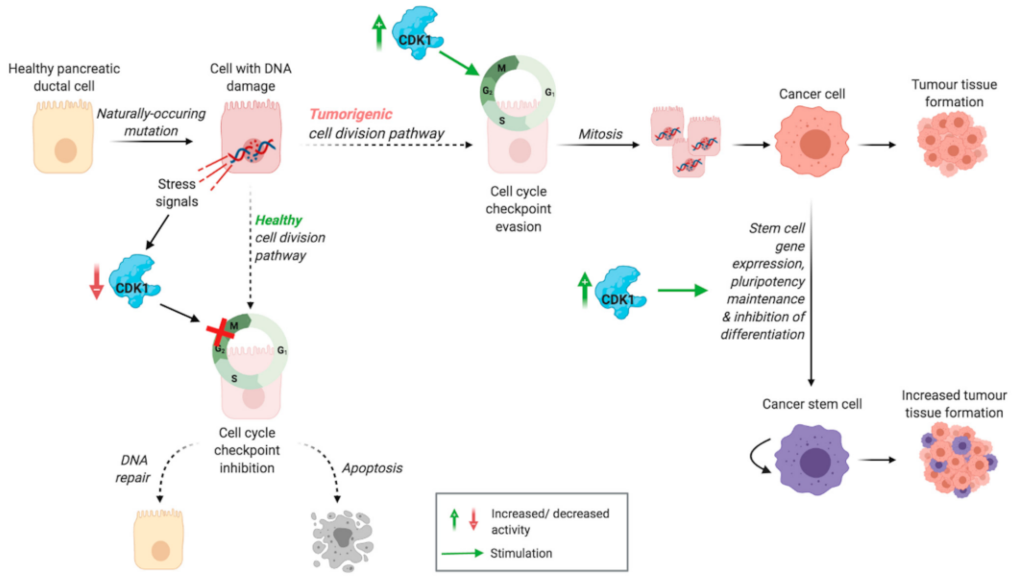
Healthy pancreatic ductal cell
Naturally-occuring mutation
Cell with DNA damage
Stress signals
Tumorigenic cell division pathway
CDK1
M
G2
G1
S
Cell cycle checkpoint evasion
Mitosis
Cancer cell
Tumour tissue formation
Healthy cell division pathway
CDK1
Stem cell gene exprression, pluripotency maintenance & inhibition of differentiation
CDK1
Cell cycle checkpoint inhibition
DNA repair
Apoptosis
Cancer stem cell
Increased tumour tissue formation
Increased/ decreased activity
Stimulation

Figure 2. Proposed tumorigenic activity of CDK1. Healthy cell division pathway: stress signals induced by DNA damage lead to inactivation of CDK, inhibiting the cell cycle checkpoint. This results in DNA repair or apoptosis, preventing replication of cells with DNA damage. Tumorigenic cell division pathway: CDK1 overexpression induces cell cycle checkpoint evasion, leading to proliferation of cells with DNA damage, which can eventually lead to tumour tissue formation. Pluripotency maintenance and stem cell gene expression, stimulated by CDK1 activity, contribute to the development of cancer stem cells, increasing tumour tissue formation.

Drugs which inhibit multiple CDKs have been tested more extensively. Huang [18] reported that dinaciclib, a CDK 1/2/5/9 inhibitor, induced G2/M phase cell cycle arrest in human PDAC cell lines. This evidence was confirmed by the study of Parry et al. [16] which investigated the effect of dinaciclib on tumour lines of diverse origins, including pancreatic cancer, reported that dinaciclib treatment induced cell cycle arrest, with a relatively high percentage of cells in G2/M phase, at the expense of S phase. In contrast, Khan et al. [19] found that treatment of human PDAC cell lines with dinaciclib generally resulted in an increased proportion of cells in the S phase, which is associated with the blockage of CDK2 activity. Since dinaciclib inhibits multiple CDKs, these results may suggest that the effect of the drug is dependent on the mutations present in the PDAC cell type used. This explanation is further confirmed by the observation variable results that were found for the different PDAC cell lines. In the Capan-1 cell line, the dinaciclib treatment did not induce S phase cell cycle arrest, and in the FA-6 cell line, the treatment did induce G2/M phase cell cycle arrest. The proportion of cells in the sub G1 phase was elevated in all cell lines tested, indicating that many cells were in an apoptotic state. Despite the different effect of dinaciclib in the PDAC cell lines, it is possible to say this drug significantly inhibited proliferation of PDAC cells and the drug was identified as a potent cytotoxic agent against PDAC [16,18,19].

Aside from direct targeting of CDK1 activity, there are multiple drugs for which the anticancer effect is proposed to be mediated at least partially through inhibition of CDK1. These drugs include 5MeOlndox, HDAC inhibitors, and flavonoids. 5MeOlndox has been shown to induce G2/M phase cell cycle arrest and reduce proliferation in both mouse and human PDAC cell lines [35]. The arrest of cells in G2/M phase was accompanied by a reduced level of CDK1 and cyclin B1, suggesting that the mechanism of tumour growth inhibition was mediated through reduced CDK1/cyclin B1 activity. Another study, examining the potential of treatment with silibinin and the HDAC inhibitor TSA, found that this combination effectively inhibited cell growth in human pancreatic cancer cell lines [36]. The treatment reduced the expression of cyclin A1, cyclin B1, and CDK1, and induced G2/M phase cell cycle arrest. This reduced expression of CDK1 and cyclin B1 suggests that the lack of activity of these proteins caused the cells to be arrested at the DNA structure checkpoint, resulting in G2/M phase cell cycle arrest. However, the expression of other CDKs and cyclins was not measured, which means it is not possible to assess the effect of (lack of) activity of other CDKs and cyclins.

2.4. Inducing Apoptosis

The existing literature on the effect of CDK1 inhibition on apoptosis reports some controversies. Under healthy conditions, it is assumed that CDK1 is required for the proper execution of apoptosis in the case of DNA damage or a condition of cell stress [13]. In cancer cells, the role of CDK1 in the apoptotic pathway is more complicated. CDK1 can phosphorylate both pro- and anti-apoptotic proteins, and the effect of this phosphorylation can be either activating or inhibitory [31,37]. Simultaneously, CDK1 can regulate transcription of proteins involved in apoptotic pathways, influencing the expression of these proteins.

There is substantial evidence that CDK1 activity phosphorylates the anti-apoptotic proteins Bcl-2 and Bcl-xL during mitosis [31,38,39]. When this phosphorylation is sustained, for example during mitotic arrest, this leads to inactivation of Bcl-2 and Bcl-xL and subsequently induces apoptosis [38]. This explains how, if cells are arrested in mitosis, CDK1 activity can switch mitotic arrest to apoptosis (Figure 3). This crucial role of CDK1 in inducing apoptosis helps to explain several studies reporting an association between absence of CDK1 expression in tumour tissue and decreased survival rates of patients.

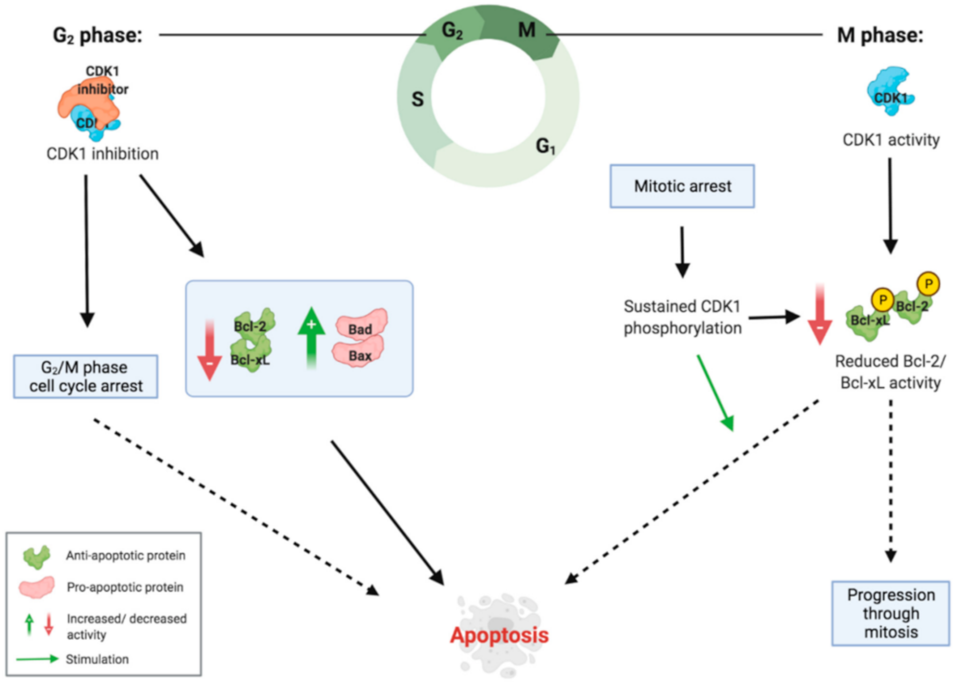
G₂ phase:
CDK1 inhibitor
CDK1
CDK1 inhibition
G₂
M
S
G₁
M phase:
CDK1
CDK1 activity
Mitotic arrest
Sustained CDK1 phosphorylation
P
P
Bcl-xL
Bcl-2
Reduced Bcl-2/ Bcl-xL activity
G₂/M phase cell cycle arrest
Bcl-2
Bcl-xL
Bad
Bax
Anti-apoptotic protein
Pro-apoptotic protein
Increased/ decreased activity
Stimulation
Apoptosis
Progression through mitosis

Figure 3. Role of CDK1 in apoptosis induction during the G2 and M phase. During the G2 phase, CDK1 inhibition leads to a decrease in anti-apoptotic proteins and an increase in pro-apoptotic proteins, stimulating the intrinsic apoptotic pathway. Furthermore, lack of CDK1 activity induces G2/M phase cell cycle arrest, which can also lead to apoptosis. During the M phase, CDK1 activity phosphorylates anti-apoptotic proteins in low amounts, inactivating them. In the situation of mitotic arrest, this phosphorylation is sustained, reaching high enough levels of inactivated anti-apoptotic proteins to induce apoptosis.

In contrast to this, there are also studies that indicate how the lack of CDK1 activity can stimulate apoptosis. Parry et al. [16] found that treating pancreatic cancer cells with dinaciclib resulted in detectable caspase activation in 11 of 15 cell lines tested. Similarly, treating human PDAC cell lines with dinaciclib was shown to induce caspase 3 activation, which is part of the intrinsic pathway of apoptosis [18]. In both studies, the treatment was also associated with G2/M phase cell cycle arrest, suggesting that the induction of apoptosis was mediated via the DNA structure checkpoint. Another study showed that treatment of human pancreatic cancer cell lines with the HDAC inhibitor TSA and the flavonoid silibinin led to a downregulation of Bcl-xL, which was accompanied by inhibition of CDK1 [36]. These results combined indicate that in the situation of G2/M phase cell cycle arrest, a lack of CDK1 activity contributes to the initiation of apoptotic pathways, whereas during mitotic arrest, CDK1 activity is necessary for inducing apoptosis (Figure 3).

2.5. Inducing and Maintaining Cancer Stem Cell Properties

CDK1 has been shown to play an important role in the maintenance of pluripotency in human pluripotent stem cells [25,40]. Next to this, high levels of CDK1 are associated with the pluripotency stage of embryonic stem cells [29]. Pluripotency and self-renewal are important properties of cancer stem cells (CSCs), which play a crucial role in the development and metastasis of PDAC [4]. The elevated ability of pancreatic cancer stem cells to self-renew contributes to enhanced tumour growth, which leads a to worse prognosis for patients (Figure 2). Moreover, the capability of CSCs to differentiate into heterogenous cancer cells contributes to tumour heterogeneity, which makes tumours more resistant to treatment [41].

There are several mechanisms through which CDK1 has the ability to induce pluripotency and inhibit differentiation in PDAC cells (Figure 4). Firstly, CDK1 is thought to directly influence the activity of pluripotency factors (Oct4, NANOG, and Sox2), while inhibiting differentiating factors (Cdx2) [42]. The CDK1/cyclin A complex can directly phosphorylate NANOG, promoting activity of the protein. Menon et al. [43] observed that CDK1 activity increased Sox2 phosphorylation and nuclear translocation, which induced the transcription of stem cell genes. Moreover, Sox2 is related to tumour initiation, therefore an excessive expression of CDK1 promotes the development of CSCs in the tumour microenvironment by Sox2 activity [43]. Multiple studies have shown that upon differentiation of embryonic stem cells, CDK1 mRNA and protein levels decreased following the same pattern as the pluripotency factors Oct4, NANOG, and Sox2 [25,29,43]. This further confirms the link between CDK1 activity, these pluripotency factors, and pluripotency maintenance.

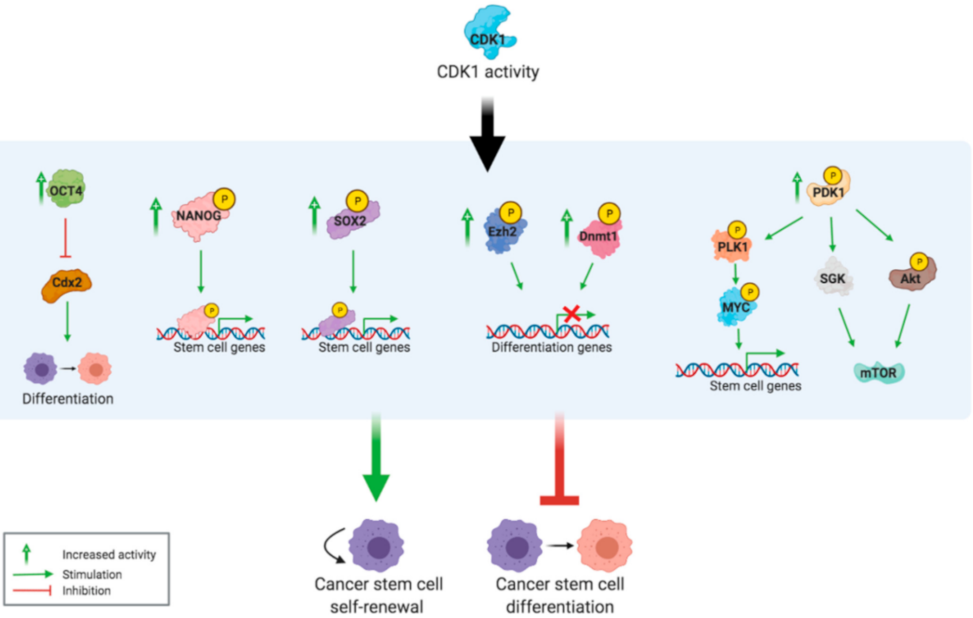

Figure 4. CDK1 overexpression induces cancer stem cell properties. The different mechanisms through which CDK1 overexpression contributes to the formation and maintenance of CSCs.

Moreover, CDK1 has the potential to influence epigenetic regulation via phosphorylation of DNA methyltransferase 1 (Dnmt1) and Enhancer of zeste homolog 2 (Ezh2), thus to contribute to the transcriptional induction of pluripotency [12].

Wang et al. [29] reported that 3′-phosphoinositide-dependent protein kinase-1 (PDK1) is a substrate of CDK1 and that CDK1 activity stimulates the PDK1/Akt/mTOR signalling pathway for self-renewal. Importantly, they noted that this process is unrelated to the effect of CDK1 on the cell cycle, because at a reduced level of CDK1 where the cell cycle was unaffected, pluripotency was already reduced. PDK1 also phosphorylates other targets, including the activation site of Akt [44]. Akt regulates many cellular processes like cell growth, cell proliferation, and survival through its effect on mTOR, and this pathway often acts as a drug and radiation resistance mechanism of cancer cells when the Akt signalling pathway is impaired [45]. Another tumorigenic effect of PDK1 is mediated through activity of the MYC protein, which is overexpressed in many human cancers and is considered a central oncogene in PDAC [46,47]. MYC has also been identified as one of the main driving forces behind the development of pancreatic CSCs, which show high metastatic potential [48]. PDK1 activity induces phosphorylation of PLK1, which phosphorylates and stabilizes the MYC protein. This leads to oncogenic transformation, partially through upregulation of cancer stem cell-like genes.

2.6. Targeting Cancer Stem Cells

Another mechanism through which CDK1 inhibition is proposed to work is by suppressing the effects of pluripotency maintenance induced by an enhanced CDK1 activity. Differentiation of cancer stem cells and loss of pluripotency could transform CSC into regular cancer cells, which may not replicate infinitely.

Menon et al. [43] showed that for melanoma cells, inhibition of CDK1 via AZD5438 decreased the tumour-initiating capacity, which is also a key characteristic of pancreatic CSCs [49]. This decrease in tumour-initiating capacity was mediated through reduced activation of Sox2, a key regulator of stem cell gene transcription. Casari et al. [50] showed that PDK1 inhibition impairs cell proliferation and colony formation of pancreatic cancer cell lines. Since CDK1 stimulates PDK1 activation, this indicated that CDK1 inhibition will impair cell proliferation and colony formation via reduced PDK1 activity, which induces differentiation of CSCs. This was further confirmed by another study, which showed that the silencing of CDK1 reduced tumour growth of hepatocellular carcinoma CSCs by inhibiting their clonogenic potential and self-renewal ability [41]. This anticancer effect was mediated through a downregulation of PDK1, β-Catenin, and Akt. Moreover, they established an interaction between both CDK1 and PDK1 and PDK1 and Akt.

Examination of the effects of CDK1 inhibition on embryonic stem cells (ESCs) can contribute to understanding the impact of this on CSCs. The effect of CDK1 inhibition on ESCs has been studied using both siRNAs and small molecule inhibitors. CDK1 inhibition results in an increased percentage of ESCs in the G2/M phase [25,51]. Neganova et al. [25] demonstrated that inducing CDK1 siRNA resulted in a loss of pluripotency in human ESCs. The loss of pluripotency was accompanied by a reduction in Oct4 and an increase in Cdx2. This suggests that CDK1 inhibition caused elevated Cdx2 activity via Oct4 downregulation, inducing differentiation. In contrast, Huskey, et al. [51] did not find evidence that CDK1 siRNAs promoted differentiation of mouse ESCs. This was explained by another study, showing that elongation of the ESC cell cycle does not induce differentiation [52], explaining that induction of G2/M phase cell cycle arrest via CDK1 inhibition does not have an effect on the pluripotency of ESCs. However, when CDK1 overexpression contributes to pluripotency maintenance of CSCs, inhibition of CDK1 can potentially still induce differentiation.

Thus, there is limited research suggesting that CDK1 inhibition induces differentiation of pancreatic cancer stem cells. However, the literature suggests that CSCs have increased sensitivity towards CDK1 inhibition compared to non-stem cells. This is promising for the application of CDK1 inhibitors to treat PDAC, because efficient and specific targeting of pancreatic CSCs has high therapeutic potential [49].

3. Therapeutic Potential

3.1. CDK1 Inhibitors

Since dysregulation and overexpression of protein kinases play an essential role in the prognosis of many types of cancer, including PDAC, in recent years many kinases inhibitor small molecules have been synthesized and advanced into clinical trials.

To date, the food and drug administration (FDA) has approved 62 small molecules protein kinase inhibitors. Among the 62 approved drugs, 35 small molecules are receptor protein-tyrosine kinase inhibitors, 13 small molecules target non receptor protein-kinase inhibitors, 10 small molecules are serine/threonine kinase antagonists, and 4 are dual protein kinase inhibitors (MEK1/2) [53].

During the last years, great progress has been made also in developing CDK inhibitors; however, among CDKs, the only FDA approved drugs work by inhibiting CDK4/CDK6 (abemaciclib, ribociclib, and palbociclib) and no CDK1 inhibitor has reached the market [53]. Moreover, the high degree of similarity shared between the ATP binding site of CDKs represented a challenge to generating selective compounds. Therefore, the first generation of CDK inhibitors developed showed activity across multiple CDKs and were defined as Pan-CDK inhibitors [54].

Flavopiridol, also known as Alvocidib, is a synthetic flavonoid based on the chromone alkaloid, rohitukine. It was one of the first CDKs inhibitors developed that exhibited potent inhibition of CDK 1, 2, 4, 6, 7, and 9, with IC_{50} values of 30, 20, 60, 10, 10 nM, respectively.

The X-ray crystal structure of CDK2 in complex with flavopiridol revealed the molecular structure features for the inhibition. In particular, the oxygen O4 and hydroxyl group at 5 position of flavones moiety bind with the hinge residues of leucine (Leu) 83 and glutamate (Glu) 81, whereas the piperidinyl group is exposed to the solvent region [55] (Figure 5A).

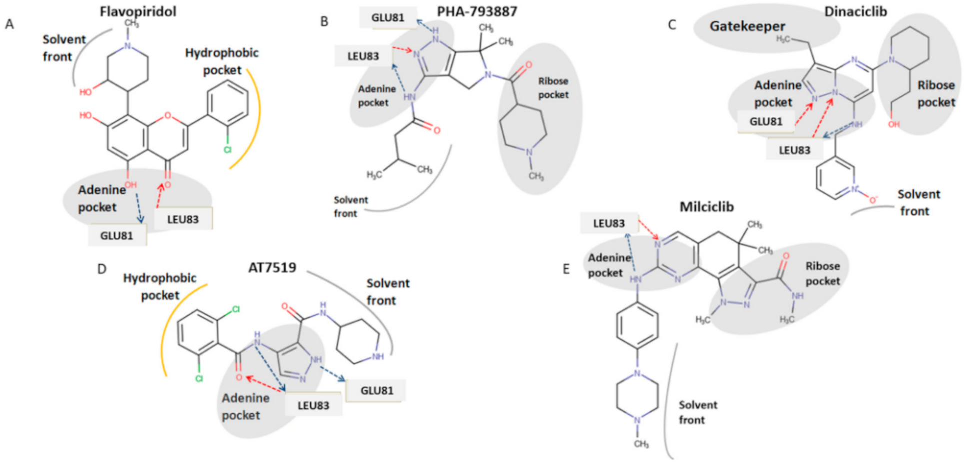
A
Flavopiridol
Solvent front
Hydrophobic pocket
Adenine pocket
LEU83
GLU81
B
GLU81
PHA-793887
LEU83
Adenine pocket
Ribose pocket
Solvent front
C
Gatekeeper
Dinaciclib
Adenine pocket
GLU81
LEU83
Ribose pocket
Solvent front
D
Hydrophobic pocket
AT7519
Solvent front
Adenine pocket
LEU83
GLU81
E
Milciclib
LEU83
Adenine pocket
Ribose pocket
Solvent front

Figure 5. Structures of CDKs inhibitors and proposed binding mode of these compounds binding with CDK1. (**A**) Chemical structure of flavopiridol and its depicted binding mode with CDK1. (**B**) Chemical structure of PHA-793887 and its depicted binding mode with CDK1. (**C**) Chemical structure of Dinaciclib and its depicted binding mode with CDK1. (**D**) Chemical structure of AT7519 and its depicted binding mode with CDK1 (**E**) Chemical structure of milciclib and its depicted binding mode with CDK1. Hydrogen bonds donor interactions are indicated by blue arrows, hydrogen bonds acceptor interactions are indicated by red arrows and amino acid residues that interact with inhibitors through hydrogen bonds are shown in grey backbone.

PHA-793887 is a pyrrolopyrazole derivative that mainly inhibits CDK2-cyclinA, CDK2-cyclinE, CDK5-p25, and CDK7-cyclinA, with IC_{50} values of 80, 80, 5, 10 nM, respectively. Moreover, PHA-793887 is able to inhibit CDK1-cyclin B, CDK4-cyclinD1, CDK9/cyclin

T1, and GSK3-β with IC_{50} values of 60, 62, 138, and 79 nM. Regarding the binding mode of PHA-793887 with CDK1, the pyrazole moiety occupies the adenine region of the ATP binding site. In particular, the amino group of burinamide forms a hydrogen bond with the backbone of Leu 83, while the nitrogen and amino group of the pyrazole makes two additional hydrogen bonds with the carbonyl oxygen of Glu 81 and with the amino group of Leu 83 at the hinge region, while the isobutyl group points toward the solvent accessible region [56] (Figure 5B).

Dinaciclib is a pyrazolopyrimidine derived inhibitor of CDK 1, 2, 5, and 9, with IC_{50} values of 3, 1, 1, 4 µM, respectively [16]. Dinaciclib is a type I inhibitor binding the ATP site through the pyrazolopyrimidine moiety that makes a hydrogen bond with Leu 81–83 of the hinge region. The 3-ethyl group of the pyrazolopyrimidine moiety establishes hydrophobic interactions with the gatekeeper residues of Phe 80. The pyridine oxide ring is exposed to the solvent region [57] (Figure 5C).

AT7519 was discovered through fragment-based screening approaches by Astex as CDK2 inhibitor with IC_{50} values of 47 nM, further studies demonstrated that this drug is also a potent on CDK 1, 4, 6, and 9 with IC_{50} values of 210, 100, 13, and 170 nM, respectively. The binding mode of AT7519 with CDK1 is that of a classic competitive inhibitor, with the carbonyl of 4-benzamide group that makes two hydrogen bonds with Leu 83 donor-acceptor. A further interaction occurs between the amino group of pyrazole ring and Glu 81 of the hinge region [58,59] (Figure 5D).

Milciclib (PHA-848125) is a multi-CDK inhibitor with IC_{50} values of 45, 160, 265, 363, 398, and 150 nM against CDK2-cyclinA, CDK4-cyclinD1, CDK5-p35, CDK2-cyclinE, CDK1-cyclinB, and CDK7-cyclinH, respectively. The proposed binding mode of this drug was confirmed by X-ray crystal structure of CDK1 in complex Milciclib. The pyrazoloquinazoline moiety of the molecule occupies the ATP binding site and makes hydrogen bonds with the backbone NH of Leu83, while the adjacent amino group binds to the carbonyl oxygen of Leu83 (Figure 5E) [60].

3.2. Preclinical Studies on CDK1 Inhibition

Multiple studies mentioned in the previous paragraphs demonstrated the efficacy of drugs targeting CDK1 inhibition on reducing PDAC cell growth in vitro [16,18,19,35,36]. In vivo mice experiments have also elicited promising results for CDK1-targeting drugs. Administration of dinaciclib, an inhibitor of CDKs 1/2/5/9, inhibited tumour growth in 10 out of 10 subcutaneous PDAC mouse models tested, with significant growth reduction (>40%) in 8 out of 10 [61]. Similarly, dinaciclib treatment delayed tumour progression and increased the overall survival from 31 to 57 days in a transgenic mouse model of PDAC [62]. Moreover, treatment induced apoptosis of tumour cells in vivo, next to inhibition of cell proliferation. Huang et al. [18] found that dinaciclib treatment in combination with immunotherapy improved survival rate and reduced tumour formation in subcutaneous, orthotopic, and transgenic PDAC mouse models. The treatment induced more effective tumour reduction than paclitaxel, a drug (as nab-paclitaxel) also used to treat PDAC patients. At half of the maximum tolerated dose for both drugs, paclitaxel showed a tumour growth inhibition of only 63 percent, compared to 90 percent for dinaciclib. Furthermore, dinaciclib prevented tumour formation and decreased the growth of established stem-cell derived tumours in mice [51]. The treatment selectively killed stem cell-derived tumour components, which shows potential for targeting CSCs via CDK1 inhibition. Together, these studies illustrate that the compound dinaciclib has the ability to significantly reduce PDAC cell growth in vivo.

Sano et al. [35] tested two other CDK1-inhibiting drugs, Indox and 5MeOIndox, on mice with subcutaneously transplanted PDAC cells. Both drugs inhibited tumour growth and reduced tumour weight, but only 5MeOIndox reduced CDK1/cyclin B1 complex levels. The authors concluded that treatment with 5MeOIndox was more promising to treat PDAC, because it induced early apoptosis as opposed to late apoptosis of Indox. Wu et al. [41] reported that in combination with sorafenib, RO 3306 CDK1 inhibitor decreased the population of CSCs both in vivo and in vitro, which was accompanied by a reduction in the stemness-related proteins Oct4, Sox2, and NANOG. Administration of the CDK 1/2/4/5 inhibitor purvalanol A was shown to specifically target Oct4 and NANOG-expressing cells and reduce tumour incidence in a population of subcutaneous teratoma xenograft mice [51]. Both studies suggest that CDK1 inhibition can effectively target CSCs in vivo.

When evaluating whether CDK1 suppression is a propitious drug target, it is crucial to assess the effect of CDK1 inhibition on healthy cells. Prevo et al. [20] investigated the effects of RO-3306 on both healthy and tumour cells. They found that RO-3306 can affect the survival of healthy cells, but only when they are proliferating. This implies a narrow therapeutic window. However, after a long 72 h of exposure to RO-3306, 40% of the cancer cells were in an apoptotic state but only 10 percent of normal cells, suggesting some selectivity of CDK1 [20]. Conversely, Sano et al. [35] found that 72 h of exposure to 5MeOIndox of both mouse and human PDAC cells led to a significantly impaired proliferation, while healthy mouse fibroblasts were unaffected. Moreover, in vivo, no significant weight loss was observed in any of the treated mice, suggesting a good tolerability of the drug. Additionally, in some other studies CDK1 inhibition was well-tolerated in vivo. For instance, BA-j caused no significant side effects when administered at a therapeutic dose range [32]. Similarly, dinaciclib was well tolerated in multiple in vivo studies [16,63,64]. Obviously, toxicity of CDK1 inhibition needs to be carefully investigated in additional preclinical trials before moving to the clinic.

3.3. Clinical Trials of CDK1 Inhibitors

Thus far, the promising results of the preclinical studies with CDK1 inhibitors have not yet been translated properly to the clinic as a novel potential treatment for PDAC. Table 1 gives an overview of completed clinical trials testing the efficacy and tolerability of different non-specific CDK1-inhibitors, since all drugs inhibit multiple CDKs. The most widely-tested drug is dinaciclib, a small molecule inhibitor of CDKs 1/2/5/9. This drug showed promising efficacy and good tolerability in phase II clinical trials for myeloma and phase III clinical trials for chronic lymphocytic leukaemia [65,66]. However, even though generally well-tolerated, dinaciclib was less effective in solid tumours, including pancreatic cancers [67–69]. In a combination treatment of dinaciclib with the Akt-inhibitor MK-2206, the best clinical result was stable disease in only four pancreatic cancer patients (10 percent) with a median survival rate of 2,2 months [68]. Similar poor results have been found for flavopiridol, an inhibitor of CDKs 1/2/4/6, in a phase II clinical trial on pancreatic cancer [70], since the combination treatment of flavopiridol and docetaxel generated no objective responses, and only three patients (33 percent) achieved stable disease, with a median survival rate of 4,2 months. Both the CDK 1/2/9 inhibitor AZD5438 and the CDK 1/2/4 inhibitor PHA-793887 showed no clinical benefit in phase I studies with patients with solid tumours [71,72], since in both clinical trials serious adverse effects were observed, leading to deaths.

However, the CDK1/2/4/5 inhibitor milciclib in combination with gemcitabine showed some clinical benefit in a phase I study on patients with refractory solid tumours [73]. Of the 16 patients, 43 percent showed stable disease, including long-term disease stabilisation for a pancreatic cancer patient of over 6 months. The combination treatment was well-tolerated with manageable toxicities. Comparable results have been found in a phase II study with hepatocellular carcinoma patients [74]. Furthermore, the CDK 1/2/4/5/7 inhibitor PHA-848125AC showed some efficacy (two partial responses in patients with thymic carcinoma) in a phase I clinical trial with patients with advanced solid tumours [75]. Interestingly, the pancreatic cancer patients showed, on average, stable disease for 10 months.

Table 1. Clinical trials testing different CDK1-inhibiting drugs.

Drug (Targeted CDKs)	Clinical Trial Phase	Disease (Number of Patients)	Efficacy	Tolerability	Observations	Reference
AZD5438 (1, 2, 9)	Phase I	Advanced solid tumours (64, 8 pancreatic)	−	− −		[71]
Dinaciclib (1, 2, 5, 9)	Phase I	Pancreatic cancer (39)	−	+	In combination with MK-2206 (Akt inhibitor)	[68]
		Advanced malignancies (61, 5 pancreatic)	− +	+		[67]
		Advanced malignancies(48, 4 pancreatic)	− +	− +		[69]
	Phase II	Advanced breast cancer (39)	− +	+	In comparison vs. capecitabine (similar but not superior anticancer activity)	[67]
		Refractory multiple myeloma (27)	++	+		[66]
	Phase III	Refractory chronic lymphocytic leukemia (42)	+ +	+	In comparison vs. ofatumumab (results suggest superior anticancer activity)	[65]
Flavopiridol (1, 2, 4, 6)	Phase II	Pancreatic cancer (10)	+ −	− −	In combination with docetaxel	[70]
Milciclib (1, 2, 4, 5)	Phase I	Refractory solid tumours (16, 13 pancreatic)	+	+ +	In combination with gemcitabine	[73]
	Phase II	Hepatocellular carcinoma (14)	+	+ +		[74]
PHA-848125AC (1, 2, 4, 5, 7)	Phase I	Advanced solid malignancies (37, 5 pancreatic)	+	− +		[75]
PHA-793887 (1, 2, 4)	Phase I	Solid tumours (19, 5 pancreatic)	−	− −		[72]

Hence, even though the preclinically promising drug dinaciclib has failed to show sufficient anticancer activity in clinical trials for PDAC, there is evidence suggesting that other CDK1-inhibiting drugs can contribute to improved treatment of this disease.

3.4. Importance of Screening Patients

The limited efficacy of the CDK inhibitors in clinical studies may be related to the lack of selection of patients. For any therapy, but especially for a therapy targeted against CDKs, it seems essential to screen patients in order to ensure that PDAC tumour cells are indeed overexpressing CDK1. This can be done in solid tumour tissue with immunohistochemistry staining for CDK1 [24,68]. Thus, CDK1 overexpression can be used as a biomarker to distinguish between different types of PDAC. Furthermore, siRNA-based screening might help to identify CDK1 as a target in tumour tissue [34,76], but this technique needs to be optimised further before being used to select PDAC patients likely to respond to CDK inhibition. In many clinical trials, patients are not screened for CDK1 overexpression [68,69,73]. Although Mita et al. [67] demonstrated that it is feasible to include skin and tumour biopsy immunohistochemistry staining in a clinical trial, they did not apply analysis of CDK1 expression in their study. In order to develop effective therapies targeting CDK1 inhibition, clinical trials should measure the CDK1 tumour expression of PDAC patients before and during treatment in order to keep track of how CDK1 expression is affected by the therapy.

3.5. Combination Therapy

Potentially, CDK1-targeted drugs can be combined with conventional chemotherapy, other forms of targeted therapy, or ionising radiation therapy. CDK1 inhibition can sensitise tumour cells to radiation [20]. Neganova et al. [25] showed increased apoptosis of human ESCs treated with a CDK1 inhibitor only when the drug was combined with radiation, which induced DNA damage. This might be related to the important role of CDK1 in DNA damage repair. The combination of inducing DNA damage through radiation and inhibition of the DNA damage repair through CDK1 inhibition could potentially be used to increase apoptosis in PDAC cells (Figure 6). Furthermore, cells are more susceptible to DNA damage induced by radiation during G2/M phase cell cycle arrest, which is a result of CDK1 inhibition [77]. Additionally, there is evidence that CDK1 overexpression can induce resistance to radiation therapy, which is reversed by knocking out CDK1 [78]. Taken together, these studies imply that CDK1 inhibitors can sensitise tumour cells for radiation therapy, increasing the efficacy of this therapy.

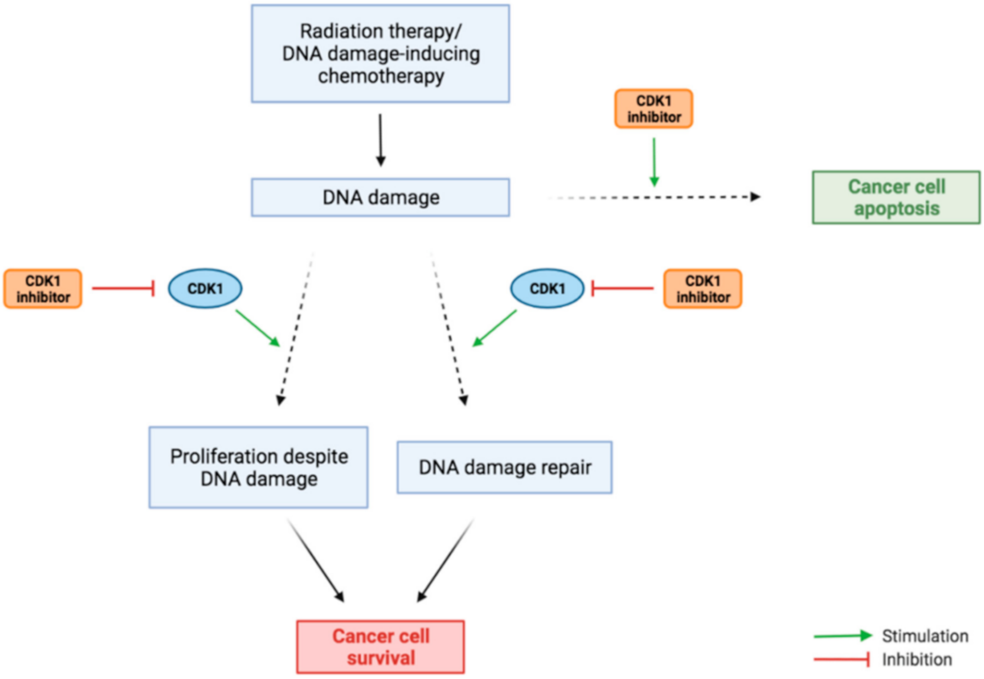

Figure 6. Interaction of CDK1 inhibitors in combination with radiation treatment and chemotherapy. CDK1 overactivity stimulates DNA damage repair and the proliferation of cells despite DNA damage (via cell cycle checkpoint evasion), leading to survival of cancer cells. CDK1 inhibitors combat this effect, stimulating the pathway from DNA damage which leads to apoptosis.

Regarding several forms of chemotherapy, the combination of existing treatments with CDK1-inhibiting drugs may have multiple potential benefits. Firstly, CDK inhibitors can prevent recovery of cells after DNA damage-inducing chemotherapy, enhancing the efficacy of the treatment [4], possibly via the same mechanism of inhibition of the DNA damage repair pathway as described for radiation therapy [77]. Specifically, CDK1 inhibition can sensitise cells to treatment with aphidicolin and cisplatin [79]. Secondly, CDK1 inhibition can sensitize specific cancer types that would be unsensitive by a specific form of chemotherapy alone, extending the therapeutic spectrum of these drugs. The PARP inhibitor olaparib, which is considered only effective against BRCA-mutated cells, showed enhanced cytotoxicity in BRCA-proficient cells in combination with RO-3306 [79]. Mayes et al. [80] showed that CDK1 sensitises cancer cells to TRAIL-induced apoptosis. These effects are mediated by the crucial role of CDK1 in survival of proliferating cells. The PARP inhibitor-induced DNA damage does not lead to apoptosis when enhanced CDK1 activity stimulates cell cycle progression, regardless of DNA damage. However, when this cell cycle checkpoint evasion is blocked by CDK1 inhibitors, the cancer cells are less likely to survive (Figure 6). This also explains studies demonstrating that CDK1 inhibition reduces gemcitabine- and 5-FU resistance in multiple different cancer types [73,80–82]. Another study showed that CDK1 inhibition enhanced the ability of the protein kinase inhibitor sorafenib to specifically kill stem cells of hepatocellular carcinoma [41]. This highlights the potential of this combination treatment to eliminate cancer stem cells in malignant solid tumours, which is beneficial for treating PDAC.

CDK1 inhibition will not work in combination with every treatment. For example, when combined with drugs that induce mitotic arrest, such as taxanes, CDK1 inhibition might have an adverse effect, due to its role in apoptosis initiation during mitosis. This illustrates the importance of carefully selecting a combination of therapies and focusing on the biochemical effects of their interaction.

4. Concluding Remarks

PDAC has a poor survival rate due to the lack of effective and tolerable treatment. Therefore, there is an urgent need to develop new therapies for this disease [4,13]. The overexpression of CDK1 genes suggests a role for this cyclin-dependent kinase in PDAC development and growth [14]. Hence, this literature review evaluated the potential of CDK1 inhibition for novel drug development to treat PDAC.

CDK1 overexpression exerts its tumorigenic effect predominantly via two mechanisms. Firstly, through stimulation of cell cycle progression at the G2/M phase checkpoint, leading to cell proliferation of cells with a potential tumorigenic mutation. Secondly, by inducing pluripotent characteristics in PDAC cells, leading to the development of CSCs. These CSCs promote tumour initiation, tumour growth, and heterogeneity of tumours, making them more challenging to treat [4,41]. Multiple studies showed the ability of CDK1 inhibitors to induce G2/M phase cell cycle arrest and apoptosis in tumour cells, both in vitro and in vivo. This effect was shown for many different cancer types, including PDAC. Furthermore, multiple studies suggest that CSCs might be especially sensitive toward CDK1-inhibiting drugs. The specificity of CDK1 inhibitors for pluripotent cells is beneficial when killing CSCs, but potentially very dangerous for healthy stem cells. Next to this, there are concerns about the potential toxic effect of CDK1 inhibition on healthy cells in general [20]. Thus, more research on the effects of CDK1 inhibition on healthy human (pluripotent) cells is needed.

An assessment of clinical trials revealed that CDK1 inhibitors failed to show sufficient response in patients with PDAC. The lack of efficacy of CDK1 inhibitors despite the strong preclinical data to support their use may be related to the poor pharmacokinetics of the drugs [67,69]. Another explanation for the lack of efficacy could be the rapidly progressive nature of PDAC. Additionally, clinical trials are usually performed on PDAC patients that failed to respond to other treatments. This often means that they are in an advanced stage of tumour progression and these patients might also be more resistant to therapy in general, reducing the chances that the treatment will be effective. To increase the potential of CDK1 inhibitors to reduce PDAC tumour growth, screening of patients for CDK1 overexpression is important for future clinical trials.

CDK1 inhibition might be best used in combination with other therapies. Promising results have been found for the combination of CDK1 inhibition with both ionising radiation therapy and DNA damaging chemotherapy. Reduction of CDK1 activity can both sensitise cancer cells to treatment and enlarge the therapeutic spectrum of existing therapies. This is promising for the use of CDK1 inhibition to overcome drug resistance, which is regarded as one of the main causes for the poor prognosis of PDAC patients [83]. However, inhibition of CDK1 will not work in combination with every treatment, and might even have adverse effects, for example when combined with drugs that induce mitotic arrest. The knowledge on molecular mechanisms of CDK1 inhibition can contribute to improve the selection of proper treatment combinations for different types of PDAC that needs further characterisation. This knowledge will also help to establish a lower minimal effective dose, which can limit the cytotoxic effects of the drugs on healthy cells.

In conclusion, CDK1 inhibition seems to be a propitious drug target for the treatment of PDAC. The anticancer mechanism is mediated through the induction of G2/M phase cell cycle arrest, induction of apoptosis, and specific targeting of cancer stem cells. At the moment, there are multiple clinical trials ongoing investigating the efficacy and tolerability of CDK1-inhibiting drugs, alone and in combination with other therapies. Next to this, screening possibilities for CDK1 overexpression need to be implemented to improve a personalized medicine approach that is essential to effectively apply these drugs.

Author Contributions: R.W. and C.P. were the principal investigators and take primary responsibility for the paper; E.G. and G.J.P. wrote additional paragraphs, D.C., H.F., A.A. provided essential material and participated in the research design; C.P., E.G. and P.D. checked the tables and figures the paper; G.J.P., E.G. and P.D. edited the paper. All authors have read and agreed to the published version of the manuscript.

Funding: This work was partially supported by the following grants: CCA Foundation 2012, 2015 and 2018 grants (Godefridus J Peters, Elisa Giovannetti), KWF Dutch Cancer Society grants (KWF project#19571, #13598, Elisa Giovannetti) and AIRC IG grant 24444 (Elisa Giovannetti); PRIN2017, Prot.No.2017E84AA4 (Patrizia Diana).

Data Availability Statement: Data related to the study are included in the article. Data are available from the corresponding authors (E.G. and P.D) upon reasonable request.

Acknowledgments: The Authors would like to thank Barbara Parrino for her support in the initial preparation of the manuscript.

Conflicts of Interest: The authors declare no conflict of interest.

References

1. Hill, A.; Chung, V. Pancreatic Cancer. In *Oncology in the Precision Medicine Era*; Salgia, R., Ed.; Springer: Cham, Germany, 2020; pp. 97–109.
2. American Cancer Society. Key Statistics for Pancreatic Cancer. *American Cancer Society*. Available online: https://www.cancer.org/cancer/pancreatic-cancer/about/key-statistics.html (accessed on 21 January 2021).
3. Sung, H.; Ferlay, J.; Siegel, R.L.; Laversanne, M.; Soerjomataram, I.; Jemal, A.; Bray, F. Global Cancer Statistics 2020: GLOBOCAN Estimates of Incidence and Mortality Worldwide for 36 Cancers in 185 Countries. *CA Cancer J. Clin.* **2021**, *71*, 209–249. [CrossRef] [PubMed]
4. Stoica, A.F.; Chang, C.H.; Pauklin, S. Molecular Therapeutics of Pancreatic Ductal Adenocarcinoma: Targeted Pathways and the Role of Cancer Stem Cells. *Trends Pharm. Sci.* **2020**, *41*, 977–993. [CrossRef]
5. Giovannetti, E.; van der Borden, C.L.; Frampton, A.E.; Ali, A.; Firuzi, O.; Peters, G.J. Never let it go: Stopping key mechanisms underlying metastasis to fight pancreatic cancer. *Sem. Cancer Biol.* **2017**, *44*, 43–59. [CrossRef]
6. Caparello, C.; Meijer, L.L.; Garajova, I.; Falcone, A.; Le Large, T.Y.; Funel, N.; Kazemier, G.; Peters, G.J.; Vasile, E.; Giovannetti, E. FOLFIRINOX and translational studies: Towards personalized therapy in pancreatic cancer. *World J. Gastroenterol.* **2016**, *22*, 6987–7005. [CrossRef] [PubMed]
7. Hruban, R.H.; Goggins, M.; Parsons, J.; Kern, S.E. Progression model for pancreatic cancer. *Clin. Cancer Res.* **2000**, *6*, 2969–2972. [PubMed]
8. Notta, F.; Chan-Seng-Yue, M.; Lemire, M.; Li, Y.; Wilson, G.W.; Connor, A.A.; Denroche, R.E.; Liang, S.B.; Brown, A.M.; Kim, J.C.; et al. A renewed model of pancreatic cancer evolution based on genomic rearrangement patterns. *Nature* **2016**, *538*, 378–382. [CrossRef] [PubMed]
9. Khan, M.A.; Azim, S.; Zubair, H.; Bhardwaj, A.; Patel, G.K.; Khushman, M.; Singh, S.; Singh, A.P. Molecular Drivers of Pancreatic Cancer Pathogenesis: Looking Inward to Move Forward. *Int. J. Mol. Sci.* **2017**, *18*, 779. [CrossRef]
10. Pelosi, E.; Castelli, G.; Testa, U. Pancreatic Cancer: Molecular Characterization, Clonal Evolution and Cancer Stem Cells. *Biomedicines* **2017**, *5*, 56. [CrossRef] [PubMed]
11. Da Costa, N.M.; Palumbo, A., Jr.; De Martino, M.; Fusco, A.; Pinto, L.F.R.; Nasciutti, L.E. Interplay between HMGA and TP53 in cell cycle control along tumor progression. *Cell Mol. Life Sci.* **2021**, *78*, 817–831. [CrossRef]
12. Lim, S.; Kaldis, P. Cdks, cyclins and CKIs: Roles beyond cell cycle regulation. *Development* **2013**, *140*, 3079–3093. [CrossRef]
13. García-Reyes, B.; Kretz, A.L.; Ruff, J.P.; von Karstedt, S.; Hillenbrand, A.; Knippschild, U.; Henne-Bruns, D.; Lemke, J. The Emerging Role of Cyclin-Dependent Kinases (CDKs) in Pancreatic Ductal Adenocarcinoma. *Int. J. Mol. Sci.* **2018**, *19*, 3219. [CrossRef] [PubMed]
14. Dong, S.; Huang, F.; Zhang, H.; Chen, Q. Overexpression of BUB1B, CCNA2, CDC20, and CDK1 in tumor tissues predicts poor survival in pancreatic ductal adenocarcinoma. *Biosci. Rep.* **2019**, *39*, 1–10. [CrossRef] [PubMed]
15. Guo, J.; Kleeff, J.; Li, J.; Ding, J.; Hammer, J.; Zhao, Y.; Giese, T.; Korc, M.; Büchler, M.W.; Friess, H. Expression and functional significance of CDC25B in human pancreatic ductal adenocarcinoma. *Oncogene* **2004**, *23*, 71–81. [CrossRef] [PubMed]
16. Parry, D.; Guzi, T.; Shanahan, F.; Davis, N.; Prabhavalkar, D.; Wiswell, D.; Seghezzi, W.; Paruch, K.; Dwyer, M.P.; Doll, R.; et al. Dinaciclib (SCH 727965), a Novel and Potent Cyclin-Dependent Kinase Inhibitor. *Mol. Cancer Ther.* **2010**, *9*, 2344–2353. [CrossRef] [PubMed]
17. Shendge, A.K.; Chaudhuri, D.; Mandal, N. The natural flavones, acacetin and apigenin, induce Cdk-Cyclin mediated G2/M phase arrest and trigger ROS-mediated apoptosis in glioblastoma cells. *Mol. Biol. Rep.* **2021**, *48*, 539–549. [CrossRef]
18. Huang, J.; Chen, P.; Liu, K.; Liu, J.; Zhou, B.; Wu, R.; Peng, Q.; Liu, Z.-X.; Li, C.; Kroemer, G.; et al. CDK1/2/5 inhibition overcomes IFNG-mediated adaptive immune resistance in pancreatic cancer. *Gut* **2020**, *70*, 890–899. [CrossRef] [PubMed]

19. Khan, T.; Seddon, A.M.; Dalgleish, A.G.; Khelwatty, S.; Ioannou, N.; Mudan, S.; Modjtahedi, H. Synergistic activity of agents targeting growth factor receptors, CDKs and downstream signaling molecules in a panel of pancreatic cancer cell lines and the identification of antagonistic combinations: Implications for future clinical trials in pancreatic. *Ongol. Rep.* **2020**, *44*, 2581–2594.
20. Prevo, R.; Pirovano, G.; Puliyadi, R.; Herbert, K.J.; Rodriguez-Berriguete, G.; O'Docherty, A.; Greaves, W.; McKenna, W.G.; Higgins, G.S. CDK1 inhibition sensitizes normal cells to DNA damage in a cell cycle dependent manner. *Cell Cycle* **2018**, *17*, 1513–1523. [CrossRef]
21. Mostafa, M.E.; Erbarut-Seven, I.; Pehlivanoglu, B.; Adsay, V. Pathologic classification of "pancreatic cancers": Current concepts and challenges. *Chin. Clin. Onc.* **2017**, *6*, 59. [CrossRef]
22. Malumbres, M. Cyclin-dependent kinases. *Genome Biol.* **2014**, *15*, 122. [CrossRef]
23. Novak, B.; Tyson, J.; Gyorffy, B.; Csikasz-Nagy, A. Irreversible cell-cycle transitions are due to systems-level feedback. *Nat. Cell Biol.* **2007**, *9*, 724–728. [CrossRef]
24. Sung, W.W.; Lin, Y.M.; Wu, P.R.; Yen, H.H.; Lai, H.W.; Su, T.C.; Huang, R.H.; Wen, C.K.; Chen, C.Y.; Chen, C.J.; et al. High nuclear/cytoplasmic ratio of Cdk1 expression predicts poor prognosis in colorectal cancer patients. *BMC Cancer* **2014**, *14*, 915. [CrossRef]
25. Neganova, I.; Tilgner, K.; Buskin, A.; Paraskevopoulou, I.; Atkinson, S.P.; Peberdy, D.; Passos, J.F.; Lako, M. CDK1 plays an important role in the maintenance of pluripotency and genomic stability in human pluripotent stem cells. *Cell Death Dis.* **2014**, *5*, 1508. [CrossRef]
26. Santamaría, D.; Barrière, C.; Cerqueira, A.; Hunt, S.; Tardy, C.; Newton, K.; Cáceres, J.F.; Dubus, P.; Malumbres, M.; Barbacid, M. Cdk1 is sufficient to drive the mammalian cell cycle. *Nature* **2009**, *488*, 811–816. [CrossRef] [PubMed]
27. Nigg, E.A. Mitotic Kinases as Regulators of Cell Division and its Checkpoints. *Nat. Rev. Mol. Cell Biol.* **2001**, *2*, 21–32. [CrossRef] [PubMed]
28. Bendris, N.; Lemmers, B.; Blanchard, J.M. Cell cycle, cytoskeleton dynamics and beyond: The many functions of cyclins and CDK inhibitors. *Cell Cycle* **2015**, *14*, 1786–1798. [CrossRef] [PubMed]
29. Wang, X.Q.; Lo, C.M.; Chen, L.; Ngan, E.S.; Xu, A.; Poon, R.Y. CDK1-PDK1-PI3K/Akt signaling pathway regulates embryonic and induced pluripotency. *Cell Death Differ.* **2017**, *24*, 38–48. [CrossRef]
30. Hsia, S.M.; Yu, C.C.; Shih, Y.H.; Yuanchien Chen, M.; Wang, T.H.; Huang, Y.T.; Shieh, T.M. Isoliquiritigenin as a cause of DNA damage and inhibitor of ataxia-telangiectasia mutated expression leading to G2/M phase arrest and apoptosis in oral squamous cell carcinoma. *Head Neck* **2016**, *38*, E360–E371. [CrossRef] [PubMed]
31. Choi, H.J.; Zhu, B.T. Upregulated cyclin B1/CDK1 mediates apoptosis following 2- methoxyestradiol-induced mitotic catastrophe: Role of Bcl-XL phosphorylation. *Steroids* **2019**, *150*, 108381. [CrossRef]
32. Zhang, S.; Bao, Y.; Ju, X.; Li, K.; Shang, H.; Ha, L.; Qian, Y.; Zou, L.; Sun, X.; Li, J.; et al. BA-j as a novel CDK1 inhibitor selectively induces apoptosis in cancer cells by regulating ROS. 1. *Sci. Rep.* **2015**, *5*, 13626. [CrossRef]
33. Vassilev, L.T.; Tovar, C.; Chen, S.; Knezevic, D.; Zhao, X.; Sun, H.; Heimbrook, D.C.; Chen, L. Selective small-molecule inhibitor reveals critical mitotic functions of human CDK1. *Proc. Natl. Acad. Sci. USA* **2006**, *103*, 10660–10665. [CrossRef]
34. Costa-Cabral, S.; Brough, R.; Konde, A.; Aarts, M.; Campbell, J.; Marinari, E.; Riffell, J.; Bardelli, A.; Torrance, C.; Lord, C.J.; et al. CDK1 Is a Synthetic Lethal Target for KRAS Mutant Tumours. *PLoS ONE.* **2016**, *11*, e0149099. [CrossRef]
35. Sano, M.; Ichimaru, Y.; Kurita, M.; Hayashi, E.; Homma, T.; Saito, H.; Masuda, S.; Nemoto, N.; Hemmi, A.; Suzuki, T.; et al. Induction of cell death in pancreatic ductal adenocarcinoma by indirubin 30-oxime and 5-methoxyindirubin 30-oxime in vitro and in vivo. *Cancer Lett.* **2017**, *397*, 72–82. [CrossRef] [PubMed]
36. Feng, W.; Cai, D.; Zhang, B.; Lou, G.; Zou, X. Combination of HDAC inhibitor TSA and silibinin induces cell cycle arrest and apoptosis by targeting survivin and cyclinB1/Cdk1 in pancreatic cancer cells. *Biomed Pharm.* **2015**, *74*, 257–264. [CrossRef]
37. Zhou, L.; Cai, X.; Han, X.; Xu, N.; Chang, D.C. CDK1 switches mitotic arrest to apoptosis by phosphorylating Bcl-2/Bax family proteins during treatment with microtubule interfering agents. *Cell Biol. Int.* **2014**, *38*, 737–746. [CrossRef]
38. Darweesh, O.; Al-Shehri, E.; Falquez, H.; Lauterwasser, J.; Edlich, F.; Patel, R. Identification of a novel Bax-Cdk1 signalling complex that links activation of the Mitotic Checkpoint to Apoptosis. *J. Cell Sci.* **2021**, *134*, 244152. [CrossRef] [PubMed]
39. Terrano, D.T.; Upreti, M.; Chambers, T.C. Cyclin-Dependent Kinase 1-Mediated Bcl-xL/Bcl-2 Phosphorylation Acts as a Functional Link Coupling Mitotic Arrest and Apoptosis. *Mol. Cell Biol.* **2010**, *30*, 640–656. [CrossRef]
40. Satyanarayana, A.; Kaldis, P. Mammalian cell-cycle regulation: Several Cdks, numerous cyclins and diverse compensatory mechanisms. *Oncogene* **2009**, *28*, 2925–2939. [CrossRef] [PubMed]
41. Wu, C.X.; Wang, X.Q.; Chok, S.H.; Man, K.; Tsang, S.H.Y.; Chan, A.C.Y.; Ma, K.W.; Xia, W.; Cheung, T.T. Blocking CDK1/PDK1/β-Catenin signaling by CDK1 inhibitor RO3306 increased the efficacy of sorafenib treatment by targeting cancer stem cells in a preclinical model of hepatocellular carcinoma. *Theranostics* **2018**, *8*, 3737–3750. [CrossRef]
42. Brumbaugh, J.; Russell, J.D.; Yu, P.; Westphall, M.S.; Coon, J.J.; Thomson, J.A. NANOG Is Multiply Phosphorylated and Directly Modified by ERK2 and CDK1 In Vitro. *Stem Cell Rep.* **2014**, *2*, 18–25. [CrossRef]
43. Menon, D.R.; Luo, Y.; Arcaroli, J.J.; Liu, S.; KrishnanKutty, L.N.; Osborne, D.G.; Li, Y.; Samson, J.M.; Bagby, S.; Tan, A.C.; et al. CDK1 Interacts with Sox2 and Promotes Tumor Initiation in Human Melanoma. *Cancer Res.* **2018**, *78*, 6561–6574. [CrossRef] [PubMed]
44. Lien, E.C.; Dibble, C.C.; Toker, A.A. P13K signaling in cancer: Beyond Akt. *Curr. Opin. Cell Bio.* **2017**, *45*, 62–71. [CrossRef]

45. Avan, A.; Narayan, R.; Giovannetti, E.; Peters, G.J. Role of Akt signaling in resistance to DNA-targeted therapy 5. *World J. Clin. Oncol.* **2016**, *7*, 352–369. [CrossRef]
46. Cunningham, J.T.; Ruggero, D. New Connections between Old Pathways: PDK1 Signaling Promotes Cellular Transformation through PLK1-Dependent MYC Stabilization. *Cancer Discov.* **2013**, *3*, 1099–1102. [CrossRef]
47. Hessmann, E.; Schneider, G.; Ellenrieder, V.; Siveke, J.T. MYC in pancreatic cancer: Novel mechanistic insights and their translation into therapeutic strategies. *Oncogene* **2016**, *35*, 1609–1618. [CrossRef] [PubMed]
48. Ischenko, I.; Petrenko, O.; Hayman, M.J. Analysis of the tumor-initiating and metastatic capacity of PDX1-positive cells from the adult pancreas. *Proc. Natl. Acad. Sci. USA* **2014**, *111*, 3466–3471. [CrossRef]
49. Hermann, P.C.; Mueller, M.T.; Heeschen, C. Pancreatic cancer stem Cells—Insights and perspectives. *Expert Opin. Biol. Ther.* **2009**, *9*, 1744–7682. [CrossRef]
50. Casari, I.; Domenichini, A.; Sestito, S.; Capone, E.; Sala, G.; Rapposelli, S.; Falasca, M. Dual PDK1/Aurora Kinase A Inhibitors Reduce Pancreatic Cancer Cell Proliferation and Colony Formation. *Cancers* **2019**, *11*, 1695. [CrossRef]
51. Huskey, N.E.; Guo, T.; Evason, K.J.; Momcilovic, O.; Pardo, D.; Creasman, K.J.; Judson, R.L.; Blelloch, R.; Oakes, S.A.; Hebrok, M.; et al. CDK1 Inhibition Targets the p53-NOXA-MCL1 Axis, Selectively Kills Embryonic Stem Cells, and Prevents Teratoma Formation. *Stem Cell Rep.* **2015**, *4*, 374–389. [CrossRef]
52. Li, V.C.; Ballabeni, A.; Kirschner, M.W. Gap 1 phase length and mouse embryonic stem cell self-renewal. *Proc. Natl. Acad. Sci. USA* **2012**, *109*, 12550–12555. [CrossRef] [PubMed]
53. Roskoski, R., Jr. Properties of FDA-approved small molecule protein kinase inhibitors. *Pharm. Res.* **2019**, *144*, 19–50. [CrossRef]
54. Mariaule, G.; Belmont, P. Cyclin-dependent kinase inhibitors as marketed anticancer drugs: Where are we now? A short survey. *Molecules* **2014**, *19*, 14366–14382. [CrossRef] [PubMed]
55. Kelland, L.R. Flavopiridol, the first cyclin-dependent kinase inhibitor to enter the clinic: Current status. *Expert Opin. Investig. Drugs* **2000**, *9*, 2903–2911. [CrossRef]
56. Brasca, M.G.; Albanese, C.; Alzani, R.; Amici, R.; Avanzi, N.; Ballinari, D.; Bischoff, J.; Borghi, D.; Casale, E.; Croci, V.; et al. Optimization of 6,6-dimethyl pyrrolo[3,4-c]pyrazoles: Identification of PHA-793887, a potent CDK inhibitor suitable for intravenous dosing. *Bioorg. Med. Chem.* **2010**, *18*, 1844–1853. [CrossRef]
57. Martin, M.P.; Olesen, S.H.; Georg, G.I.; Schönbrunn, E. Cyclin-dependent kinase inhibitor dinaciclib interacts with the acetyl-lysine recognition site of bromodomains. *ACS Chem. Biol.* **2013**, *8*, 2360–2365. [CrossRef] [PubMed]
58. Squires, M.S.; Feltell, R.E.; Wallis, N.G.; Lewis, E.J.; Smith, D.M.; Cross, D.M.; Lyons, J.F.; Thompson, N.T. Biological characterization of AT7519, a small-molecule inhibitor of cyclin-dependent kinases, in human tumor cell lines. *Mol. Cancer Ther.* **2009**, *8*, 324–332. [CrossRef] [PubMed]
59. Wyatt, P.G.; Woodhead, A.J.; Berdini, V.; Boulstridge, J.A.; Carr, M.G.; Cross, D.M.; Davis, D.J.; Devine, L.A.; Early, T.R.; Feltell, R.E.; et al. Identification of N-(4-Piperidinyl)-4-(2,6-dichlorobenzoylamino)-1H-pyrazole-3-carboxamide (AT7519), a Novel Cyclin Dependent Kinase Inhibitor Using Fragment-Based X-Ray Crystallography and Structure Based Drug Design. *J. Med. Chem.* **2008**, *51*, 4986–4999. [CrossRef]
60. Brasca, M.G.; Amboldi, N.; Ballinari, D.; Cameron, A.; Casale, E.; Cervi, G.; Colombo, M.; Colotta, F.; Croci, V.; D'Alessio, R.; et al. Identification of N,1,4,4-Tetramethyl-8-{[4-(4-methylpiperazin-1-yl)phenyl]amino}-4,5-dihydro1H-pyrazolo[4,3-h]quinazoline-3-carboxamide (PHA-848125), a Potent, Orally Available. *J. Med. Chem.* **2009**, *52*, 152–163. [CrossRef]
61. Feldmann, G.; Mishra, A.; Bisht, S.; Karikari, C.; Garrido-Laguna, I.; Rasheed, Z.; Ottenhof, N.A.; Dadon, T.; Alvarez, H.; Fendrich, V.; et al. Cyclin-dependent kinase inhibitor Dinaciclib (SCH727965) inhibits pancreatic cancer growth and progression in murine xenograft models. *Cancer Biol. Ther.* **2011**, *12*, 598–609. [CrossRef]
62. Yang, J.; Hu, S.; Shangguan, J.; Eresen, A.; Li, Y.; Ma, Q.; Yaghmai, V.; Benson, A.B., III; Zhang, Z. Dinaciclib prolongs survival in the LSL-KrasG12D/+; LSL-Trp53R172H/+; Pdx-1-Cre (KPC) transgenic murine models of pancreatic ductal adenocarcinoma. *Am. J. Transl. Res.* **2020**, *12*, 1031–1043. [PubMed]
63. Gregory, G.P.; Hogg, S.J.; Kats, L.M.; Vidacs, E.; Baker, A.J.; Gilan, O.; Lefebure, M.; Martin, B.P.; Dawson, M.A.; Johnstone, R.W.; et al. CDK9 inhibition by dinaciclib potently suppresses Mcl-1 to induce durable apoptotic responses in aggressive MYC-driven B-cell lymphoma in vivo. *Leukemia* **2015**, *29*, 1437–1441. [CrossRef]
64. Moharram, S.A.; Shah, K.; Khanum, F.; Marhäll, A.; Gazi, M.; Kazi, J.U. Efficacy of the CDK inhibitor dinaciclib in vitro and in vivo in T-cell acute lymphoblastic leukemia. *Cancer Lett.* **2017**, *405*, 73–78. [CrossRef] [PubMed]
65. Ghia, P.; Scarfò, L.; Perez, S.; Pathiraja, K.; Derosier, M.; Small, K.; McCrary Sisk, C.; Patton, N. Efficacy and safety of dinaciclib vs ofatumumab in patients with relapsed/refractory chronic lymphocytic leukemia. *Blood* **2017**, *129*, 1876–1878. [CrossRef] [PubMed]
66. Kumar, S.K.; LaPlant, B.; Chng, W.J.; Zonder, J.; Callander, N.; Fonseca, R.; Fruth, B.; Roy, V.; Erlichman, C.; Stewart, A.K. Mayo Phase 2 Consortium. Dinaciclib, a novel CDK inhibitor, demonstrates encouraging single-agent activity in patients with relapsed multiple myeloma. *Blood* **2015**, *125*, 443–448. [CrossRef] [PubMed]
67. Mita, M.M.; Mita, A.C.; Moseley, J.L.; Poon, J.; Small, K.A.; Jou, Y.M.; Kirschmeier, P.; Zhang, D.; Zhu, Y.; Statkevich, P.; et al. Phase 1 safety, pharmacokinetic and pharmacodynamic study of the cyclin-dependent kinase inhibitor dinaciclib administered every three weeks in patients with advanced malignancies. *Br. J. Cancer* **2017**, *117*, 1258–1268. [CrossRef] [PubMed]

68. Murphy, A.G.; Zahurak, M.; Shah, M.; Weekes, C.D.; Hansen, A.; Siu, L.L.; Spreafico, A.; LoConte, N.; Anders, N.M.; Miles, T.; et al. ETCTN-9231 Study Team. A Phase I Study of Dinaciclib in Combination With MK-2206 in Patients with Advanced Pancreatic Cancer. *Clin. Transl. Sci.* **2020**, *13*, 1178–1188. [CrossRef]
69. Nemunaitis, J.J.; Small, K.A.; Kirschmeier, P.; Zhang, D.; Zhu, Y.; Jou, Y.M.; Statkevich, P.; Yao, S.L.; Bannerji, R. A first-in-human, phase 1, dose-escalation study of dinaciclib, a novel cyclin-dependent kinase inhibitor, administered weekly in subjects with advanced malignancies. *J. Transl. Med.* **2013**, *11*, 259. [CrossRef]
70. Carvajal, R.D.; Tse, A.; Shah, M.A.; Lefkowitz, R.A.; Gonen, M.; Gilman-Rosen, L.; Kortmansky, J.; Kelsen, D.P.; Schwartz, G.K.; O'Reilly, E.M. A Phase II Study of Flavopiridol (Alvocidib) in Combination with Docetaxel in Refractory, Metastatic Pancreatic Cancer. *Pancreatology* **2009**, *9*, 404–409. [CrossRef]
71. Boss, D.S.; Schwartz, G.K.; Middleton, M.R.; Amakye, D.D.; Swaisland, H.; Midgley, R.S.; Ranson, M.; Danson, S.; Calvert, H.; Plummer, R.; et al. Safety, tolerability, pharmacokinetics and pharmacodynamics of the oral cyclin-dependent kinase inhibitor AZD5438 when administered at intermittent and continuous dosing schedules in patients with advanced solid tumours. *Ann. Oncol.* **2010**, *21*, 884–894. [CrossRef] [PubMed]
72. Massard, C.; Soria, J.C.; Anthoney, D.A.; Proctor, A.; Scaburri, A.; Pacciarini, M.A.; Laffranchi, B.; Pellizzoni, C.; Kroemer, G.; Armand, J.P.; et al. A first in man, phase I dose-escalation study of PHA-793887, an inhibitor of multiple cyclin-dependent kinases (CDK2, 1 and 4) reveals unexpected hepatotoxicity in patients with solid tumors. *Cell Cycle* **2011**, *10*, 963–970. [CrossRef]
73. Aspeslagh, S.; Shailubhai, K.; Bahleda, R.; Gazzah, A.; Varga, A.; Hollebecque, A.; Massard, C.; Spreafico, A.; Reni, M.; Soria, J.C. Phase I dose-escalation study of milciclib in combination with gemcitabine in patients with refractory solid tumors. *Cancer Chemother Pharm.* **2017**, *79*, 1257–1265. [CrossRef]
74. Villa, E.; Piscaglia, F.; Geva, R.; Dalecos, G.; Papatheodoridis, G.; Ciomei, M.; Davite, C.; Crivori, P.; Palejwala, V.; Jacob, J.; et al. Phase IIa safety and efficacy of milciclib, a pan-cyclin dependent kinase inhibitor, in unresectable, sorafenib-refractory or -intolerant hepatocellular carcinoma patients. *J. Clin. Oncol.* **2020**, *38*, e16711. [CrossRef]
75. Weiss, G.J.; Hidalgo, M.; Borad, M.J.; Laheru, D.; Tibes, R.; Ramanathan, R.K.; Blaydorn, L.; Jameson, G.; Jimeno, A.; Isaacs, J.D.; et al. Phase I study of the safety, tolerability and pharmacokinetics of PHA-848125AC, a dual tropomyosin receptor kinase A and cyclin-dependent kinase inhibitor, in patients with advanced solid malignancies. *Investig. New Drugs* **2012**, *30*, 2334–2343. [CrossRef]
76. Linton, A.; Cheng, Y.Y.; Griggs, K.; Schedlich, L.; Kirschner, M.B.; Gattani, S.; Srikaran, S.; Chuan-Hao Kao, S.; McCaughan, B.C.; Klebe, S.; et al. An RNAi-based screen reveals PLK1, CDK1 and NDC80 as potential therapeutic targets in malignant pleural mesothelioma. *Br. J. Cancer* **2018**, *118*, e13. [CrossRef]
77. Pawlik, T.M.; Keyomarsi, K. Role of cell cycle in mediating sensitivity to radiotherapy. *Int. J. Radiat. Oncol. Biol. Phys.* **2004**, *59*, 928–942. [CrossRef] [PubMed]
78. Deng, Y.R.; Chen, X.J.; Chen, W.; Wu, L.F.; Jiang, H.P.; Lin, D.; Wang, L.J.; Wang, W.; Guo, S.Q. Sp1 contributes to radioresistance of cervical cancer through targeting G2/M cell cycle checkpoint CDK1. *Cancer Manag. Res.* **2019**, *11*, 5835–5844. [CrossRef] [PubMed]
79. Liao, H.; Geng, X.; Xing, M.; Li, W.; Chen, Z.; Shen, H.; Ying, S. CDK1 promotes nascent DNA synthesis and induces resistance of cancer cells to DNA-damaging therapeutic agents. *Oncotarget* **2017**, *8*, 90662–90673. [CrossRef] [PubMed]
80. Mayes, P.A.; Dolloff, N.G.; Daniel, C.J.; Liu, J.J.; Hart, L.S.; Kuribayashi, K.; Allen, J.E.; Jee, D.I.; Dorsey, J.F.; Liu, Y.Y.; et al. Overcoming Hypoxia-Induced Apoptotic Resistance through Combinatorial Inhibition of GSK-3β and CDK1. *Cancer Res.* **2011**, *71*, 5265–5275. [CrossRef]
81. Zhang, P.; Kawakami, H.; Liu, W.; Zeng, X.; Strebhardt, K.; Tao, K.; Huang, S.; Sinicrope, F.A. Targeting CDK1 and MEK/ERK Overcomes Apoptotic Resistance in BRAF-Mutant Human Colorectal Cancer. *Mol. Cancer Res.* **2018**, *16*, 378–389. [CrossRef]
82. Zhu, Y.; Li, K.; Zhang, J.; Wang, L.; Sheng, L.; Yan, L. Inhibition of CDK1 Reverses the Resistance of 5-Fu in Colorectal Cancer. *Cancer Manag. Res.* **2020**, *12*, 11271–11283. [CrossRef]
83. Chand, S.; O'Hayer, K.; Blanco, F.F.; Winter, J.M.; Brody, J.R. The Landscape of Pancreatic Cancer Therapeutic Resistance Mechanisms. *Int. J. Biol. Sci.* **2016**, *12*, 273–282. [CrossRef]

Chapter 3

GSK3β as a novel promising target to overcome chemoresistance in pancreatic cancer.

Pecoraro, C.*, Faggion, B.*, Balboni, B., Carbone, D., Peters, G. J., Diana, P., Assaraf, Y. G., & Giovannetti, E.

Drug Res. Upd. (2021), *58*, 100779.

* These Authors contributed equally to this study.

Drug Resistance Updates 58 (2021) 100779

Contents lists available at ScienceDirect

Drug Resistance Updates

journal homepage: www.elsevier.com/locate/drup

GSK3β as a novel promising target to overcome chemoresistance in pancreatic cancer

Camilla Pecoraro [a,b,1], Beatrice Faggion [a,1], Beatrice Balboni [a,c], Daniela Carbone [b], Godefridus J. Peters [a,d], Patrizia Diana [b], Yehuda G. Assaraf [e], Elisa Giovannetti [a,f,*]

[a] *Department of Medical Oncology, Amsterdam University Medical Center, VU University, 1081 HV Amsterdam, the Netherlands*
[b] *Department of Biological, Chemical and Pharmaceutical Sciences and Technologies (STEBICEF), University of Palermo, Palermo, Italy*
[c] *Computational and Chemical Biology, Istituto Italiano di Tecnologia, Via Morego 30, 16163 Genoa, Italy, and Department of Pharmacy and Biotechnology, University of Bologna, Via Belmeloro 6, 40126 Bologna, Italy*
[d] *Department of Biochemistry, Medical University of Gdansk, Poland*
[e] *The Fred Wyszkowski Cancer Research Laboratory, Department of Biology, Technion-Israel Institute of Technology, Haifa, 3200003, Israel*
[f] *Cancer Pharmacology Lab, Fondazione Pisana per la Scienza, Via Ferruccio Giovannini 13, 56017 San Giuliano Terme (Pisa), Italy*

ARTICLE INFO

Keywords:
GSK3β
Pancreatic cancer
Chemoresistance
Tumor chromatin profiling
Anticancer drug combinations

ABSTRACT

Pancreatic cancer is an aggressive malignancy with increasing incidence and poor prognosis due to its late diagnosis and intrinsic chemoresistance. Most pancreatic cancer patients present with locally advanced or metastatic disease characterized by inherent resistance to chemotherapy. These features pose a series of therapeutic challenges and new targets are urgently needed.

Glycogen synthase kinase 3 beta (GSK3β) is a conserved serine/threonine kinase, which regulates key cellular processes including cell proliferation, DNA repair, cell cycle progression, signaling and metabolic pathways. GSK3β is implicated in non-malignant and malignant diseases including inflammation, neurodegenerative diseases, diabetes and cancer. GSK3β recently emerged among the key factors involved in the onset and progression of pancreatic cancer, as well as in the acquisition of chemoresistance. Intensive research has been conducted on key oncogenic functions of GSK3β and its potential as a druggable target; currently developed GSK3β inhibitors display promising results in preclinical models of distinct tumor types, including pancreatic cancer.

Here, we review the latest findings about GSK-3β biology and its role in the development and progression of pancreatic cancer. Moreover, we discuss therapeutic agents targeting GSK3β that could be administered as monotherapy or in combination with other drugs to surmount chemoresistance. Several studies are also defining potential gene signatures to identify patients who might benefit from GSK3β-based therapeutic intervention. This detailed overview emphasizes the urgent need of additional molecular studies on the impact of GSK3β inhibition as well as structural analysis of novel compounds and omics studies of predictive biomarkers.

1. Introduction

Pancreatic cancer is currently the third most common cancer in Western countries, with an increasing incidence and poor outcome and constitutes one of the most lethal of the common malignancies with a poor five-year survival rate below 10 % (Hill and Chung, 2020; Siegel et al., 2021; Rahib et al., 2014; Coppola et al., 2017; Binenbaum et al., 2015)

Pancreatic ductal adenocarcinoma (PDAC) accounts for approximately 90 % of pancreatic tumors (Sarantis et al., 2020). This malignancy is among one of most inadequately understood human disorders, posing a significant diagnostic and therapeutic challenge. The lack of specific symptoms and reliable biomarkers for early detection screening of asymptomatic PDAC patients, results in a most dismal prognosis (Kaur et al., 2017; Zhou et al., 2017). In this respect, approximately 52 % of PDAC patients are diagnosed with an advanced-stage or metastatic disease, for which the 5-year survival trend is as low as 3% (Giovannetti et al., 2017; Supadmanaba et al., 2021).

The aggressive nature and the early metastatic behavior of PDAC are

---

[*] Corresponding author at: Department of Medical Oncology, Amsterdam University Medical Center, VU University, 1081HV Amsterdam, the Netherlands.
E-mail address: elisa.giovannetti@gmail.com (E. Giovannetti).

[1] Co-first authors.

https://doi.org/10.1016/j.drup.2021.100779
Received 7 July 2021; Received in revised form 2 August 2021; Accepted 9 August 2021
Available online 12 August 2021
1368-7646/© 2021 The Authors. Published by Elsevier Ltd. This is an open access article under the CC BY license (http://creativecommons.org/licenses/by/4.0/).

not the only responsible factors for the poor prognosis of this disorder, but also for its insensitivity to most therapies, such as chemotherapy, radiotherapy and immunotherapy. Among all clinical intervention, surgical resection remains the mainstay chance for cure. However, less than 20 % of patients are good candidates for pancreatectomy due to the usually diagnosed metastatic state of PDAC (Giovannetti et al., 2017). Additionally, chemotherapeutic and radiotherapeutic regimens are often palliative and their high toxicity provides a very marginal improvement in the survival rate of patients with advanced disease (Zeng et al., 2019). This poor treatment efficacy is accompanied by either intrinsic resistance or rapid acquisition of chemoresistance (Arora et al., 2013; Caparello et al., 2016). Thus, despite the advances in the use of combination chemotherapeutic regimens, survival remains dismal, highlighting the tremendous urgency for the design and development of novel therapeutic strategies to overcome the chemoresistant nature of this lethal disease.

In recent years, GSK3β has emerged as a new potential target in PDAC due to its involvement in promoting neoplastic transformation, tumor cell survival and chemoresistance (Cormier and Woodgett, 2017; Ding and Billadeau, 2020; Uehara et al., 2020). Clinical trials are currently testing several GSK3β inhibitors either as monotherapy or in combination with chemotherapeutic agents with the aim of developing promising PDAC therapeutic interventions that suppress PDAC growth and prevent disease progression (Garcia-Sampedro et al., 2021; Abrams et al., 2021).

The purpose of the current review is to determine whether or not GSK3β might be considered a good therapeutic target in advanced PDAC and which patient signatures might be prognostic of good therapy response. Furthermore, it will focus on GSK3β inhibitors that are currently approved or are undergoing clinical trials. We also discuss possible drug combinations that might prevent tumor recurrence and therapy resistance.

2. Glycogen synthase kinase 3 (GSK3)

2.1. GSK3β biology in normal cells

Glycogen synthase kinase 3 (GSK3) is a family of serine-threonine kinases which encompasses two highly conserved isoforms, GSK3α and GSK3β, sharing approximately 85 % overall sequence homology (Woodgett, 1990). Even if functional redundancy has been observed within the two isoforms, most studies in the oncology field focused on GSK3β activity, mainly due to its known enigmatic effects on many physiological and pathological processes. By phosphorylating serine and threonine residues of a broad range of functional and structural proteins, GSK3β regulates many fundamental biological processes in cells such as glycogen metabolism, Wnt/β-catenin signaling, G-protein-coupled signal transduction and maintenance of stem cell identity (Cormier and Woodgett, 2017; Doble and Woodgett, 2003; Gao et al., 2013; Xu et al., 2009; Wu and Pan, 2010; Riobó et al., 2006). The large number of GSK3β substrates explains its emblematic function as tumor promoter or tumor suppressor. Those roles have already been extensively summarized in many recent review articles (Sutherland, 2011; McCubrey et al., 2016; Duda et al., 2020; Xie and Wang, 2017).

The most common targets of GSK3β are primed substrates harboring a pre-phosphorylated sequence S/T-X-X-X-S/T(P). Specifically, this provides the binding site for GSK3β, inducing a functional conformation change that assists the target positioning in the active catalytic domain of the kinase (Fig. 1) (ter Haar et al., 2001; Dajani et al., 2003). Hence, the kinase activity of GSK3β leads to either suppression and proteasomal degradation or enhanced activation and protein stabilization of target substrates.

Notably, GSK3β has the unconventional characteristic for a kinase of being normally active in cells under resting conditions. This is mainly correlated with phosphorylation of its tyrosine (Y)216 residue, which induces a conformational change that allows the interaction and phosphorylation of protein targets (Hughes et al., 1993; Kaidanovich-Beilin and Woodgett, 2011). On the other hand, extracellular signals, negatively regulate GSK3β kinase activity *via* N-terminal phosphorylation of the serine (S)9 residue which is required for the maintenance of normal cell homeostasis (Sutherland, 2011; Frame et al., 2001). Crystal structure analysis revealed that phosphorylation of the inhibitory serine-9 residue causes the self-association of the GSK3β N-terminal tail to its substrate binding pocket, thus hampering the interaction with target substrates (Frame et al., 2001; Stamos et al., 2014).

While there are multiple mechanisms that modulate GSK3β activity, they have not been yet completely elucidated due to the highly complex interconnections with several molecular signaling cascades. Interestingly, consistent experimental evidence reported that various regulatory protein kinases such as Akt, cyclic adenosine monophosphate (cAMP)-dependent, protein kinase A (PKA), p70 S6 kinase (p70S6K), p90RSK and Notch3, increase the inhibitory GSK3β serine-9 phosphorylation in response to extracellular signals (Fig. 1) (Kaidanovich-Beilin and Woodgett, 2011; Fang et al., 2000; Foltz et al., 2002). In addition, growth factors such as EGF, PDGF and insulin inhibit GSK3 activity *via* induction of the phosphatidylinositol-3-kinase (PI3K)/MAPK pathway. Other mechanisms that alter the inhibitory phosphorylation status of GSK3β are represented by elevated intracellular cAMP levels mediated by PKA and amino acid deprivation caused by mTOR signaling (Fig. 1) (Krause et al., 2002; Li et al., 2000).

Next to the phosphorylation status of GSK3β, which dynamically oscillates in response to extracellular signals and substrate availability, other varying and controversial mechanisms regulate GSK3β kinase activity such as GSK3β localization and protein-complex formation

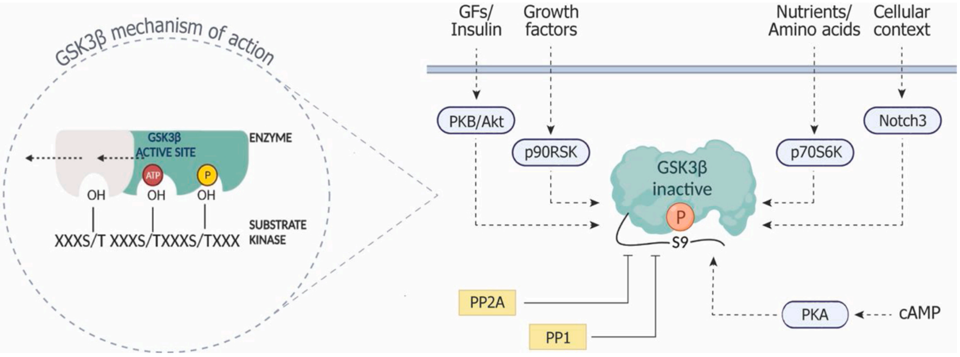

Fig. 1. Mechanism of action of GSK3β with a special focus on mechanisms regulating GSK3β activity by phosphorylation of N-terminal Serine-9. A. GSK3β recognizes a specific amino acid sequence motif S / T-XXX-S / T (P), in which S represents a serine, T a threonine, X a generic amino acid and P indicates the presence of a phosphate group previously bound by another protein kinase which is called kinase primer. The presence of the phosphorylated residue in the recognition sequence allows the substrate to position itself at the active site, thus placing the S/T residue of the target sequence near the kinase site, allowing its phosphorylation. B. Extracellular signals lead to the activation of transduction cascades that result in the phosphorylation of the serine-9 (S9) residue which blocks the target substrate binding and inactivate the kinase activity of GSK3β. Kinase phosphorylating S9 residues are represented with blue ovals and dashed lines. Protein phosphatases PP2A and PP1 restore GSK3β catalytic activity.

(Kaidanovich-Beilin and Woodgett, 2011; Beurel et al., 2015).

Although the exact mechanisms that govern GSK3β trafficking are not fully understood, GSK3β is mainly considered a cytoplasmic protein, with active kinase form more likely found in the nucleus and mitochondria in response to cell cycle stimuli (Bijur and Jope, 2003). GSK3β function in the cytoplasm is primarily related to its recruitment in pre-assembled or signal-induced protein complexes. A classic example is the β-catenin destruction complex in the Wnt signaling cascade among resting conditions, where GSK3β mediates its tumor suppressor action (Wu and Pan, 2010; Komiya and Habas, 2008). Within this complex, GSK3β phosphorylation on Thr41, Ser37 and Ser33 of β-catenin after casein kinase 1 (CK1) priming phosphorylation, results in β-catenin recognition and subsequent ubiquitin-mediated proteasomal degradation, thus modulating the transcriptional activation of target genes (Komiya and Habas, 2008).

Dysregulation of GSK3β has been implicated in diverse pathological entities due to its master function as molecular hub orchestrating the crossroad of multiple essential signals cascades that regulate cell homeostasis, cell survival, differentiation, stemness and epithelial to mesenchymal transition (EMT).

2.2. *The tumor-promoting properties of aberrant GSK3β in pancreatic cancer cells*

Although GSK3β has been recognized to act as a tumor suppressor against several pro-oncogenic molecules and mediators of EMT, aberrant overexpression of GSK3β is implicated in many human malignancies including PDAC (McCubrey et al., 2014) (Fig. 2). Ubiquitous expression and activity of GSK3β have been described to participate in tumor cell survival, apoptosis suppression, cell proliferation and invasion, cancer stemness induction as well as in promotion of chemotherapy resistance (Kockeritz et al., 2006; Ougolkov et al., 2006). Clinical evidence reported that GSK3β-overexpressing PDAC with low Ser9 phosphorylation, inflict a negative prognosis due to sustained tumor promoting signals (Garcea et al., 2007).

The mechanisms leading to tumorigenesis and increased GSK3β in PDAC were investigated by Ding and colleagues. They observed a progressive increase in GSK3β expression in tumor specimens of PDAC patients, correlating with altered oncogenic KRas status (Garcea et al., 2007; Eser et al., 2014; Waters and Channing, 2018; Kazi et al., 2018). Indeed, overexpression of constitutively active Ras isoforms has been registered in approximately 95 % of PDAC patients. Therefore, the subsequent induction of Ras-driven MAPK signaling, in turn, enhances GSK3β expression and alters cancer cell plasticity (Zhang et al., 2011).

In PDAC cell lines, aberrant GSK3β expression and phosphorylation status are also accompanied by a subsequently enhanced nuclear accumulation of active GSK3β, further suggesting the involvement of GSK3β activity in PDAC pathogenesis and progression (Ougolkov et al., 2006). Specifically, deregulated GSK3β expression and activity in PDAC cells result in many pro-survival signals, mainly mediated by NF-kB, JNK, Rb, Notch, TFEB, C-Myc, TP53, WNT/β-catenin signaling pathways (Fig. 3) (Nagini et al., 2019).

Among all, the pro-carcinogenesis role of NF-kB has been extensively described in different cancers, due to its fundamental activity in sustaining tumor cell survival and growth, as well as in modulating cancer cell metabolism and inflammatory microenvironment (Xia et al., 2014; Kaltschmidt et al., 2018). In PDAC, active GSK3β positively regulates NF-kB transcriptional activity at a pathway site, downstream of the IκB kinase complex, thus sustaining NF-kB mediated pro-survival gene expression (Ougolkov et al., 2006; Wilson and Baldwin, 2008; Ougolkov et al., 2005).

Sustained cell survival also appears to be maintained by GSK3β-dependent negative regulation of apoptotic stimuli induced by tumor necrosis factor (TNF)-related apoptosis-inducing ligand (TRAIL), mainly through promotion of the expression of the pro-survival molecules Bcl-XL, Bcl-2 and Mcl-1. These observations were confirmed by experimental inhibition of GSK3β which resulted in PDAC cell sensitization to TRAIL-induced apoptosis (Zhang et al., 2014; Mamaghani et al., 2012).

The intricate link between GSK3β and the PI3K/PTEN/Akt/mTOR signaling axis may further promote PDAC cell proliferation and tumor progression. AKT, the central node of PI3K transduction cascade regulates GSK3 activity, influencing the inhibitoryS9 phosphorylation (Hermida et al., 2017). Thus, sustained Akt activity and consequent GSK3β inhibitory phosphorylation, lead to increased cyclin D1 and promotes G1/S cell cycle progression (Liang and Slingerland, 2003). However, other studies reported that in pancreatic cells, some pools of GSK3β maintain their functional kinase activity irrespective of AKT activation and consequent inhibition of GSK3β. This evidence further highlights the complex interplay within GSK3 and this mitogenic signaling cascade (Ougolkov et al., 2005).

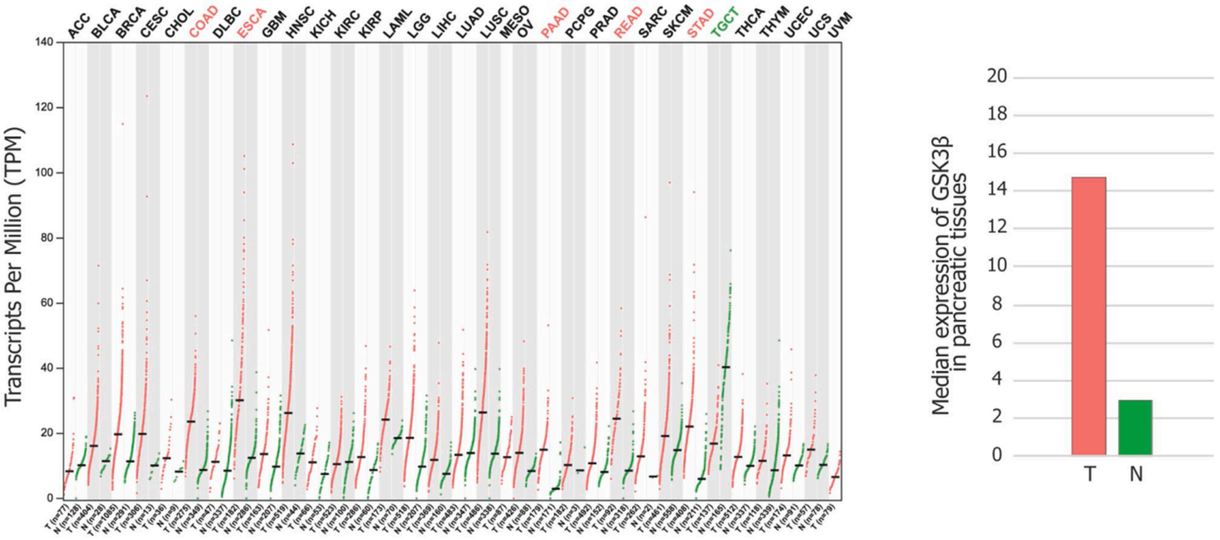

Fig. 2. Studies evaluating GSK3β gene expression levels in tumor samples and paired normal tissues. GSK3β is overexpressed in different tumor types, including pancreatic cancer (PAAD) resulting from the analysis of RNA sequencing expression data of 179 pancreatic tumors and 171 normal pancreatic samples from the TCGA and GTEx projects (http://gepia.cancer-pku.cn/detail.php?gene=GSK3b). Each dot on panel A represents GSK3β expression in tissue samples. Accordingly, the height of bars in panel B represent the median expression of GSK3β in pancreatic tumors (14,97) or pancreatic normal tissues (2,97).

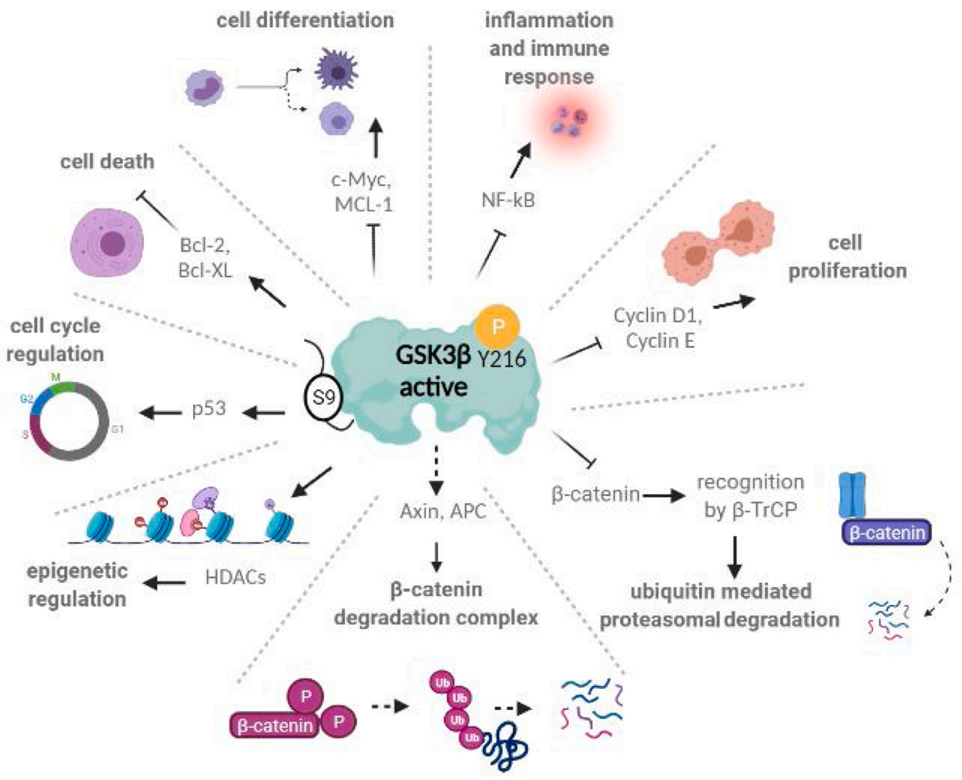

Fig. 3. Multiple roles of GSKβ and its target substrates in key biological processes for cancer cells. GSK3β modulates the activity of many cellular substrates involved in cell cycle progression, cell proliferation and differentiation (p53, c-Myc, MCL-1, Cyclin D1, Cyclin E). GSK3β regulates NF-kB and CREB (not shown) transcription factors affecting inflammatory and immune responses. In the absence of Wnt ligands, the Axin-APC-CK1-GSK3β-β-catenin destruction complex allows GSK3β to phosphorylate β-catenin (residues 41, 37, and 33). This phosphorylation leads to the release of β-catenin from the complex and targets it for proteasomal degradation. GSK3β phosphorylates several histone deacetylases (HDACs) modulating their regulatory epigenetic functions. GSK3β-mediated phosphorylation of some molecules of the anti-apoptotic Bcl-2 family results in their stabilization and increased anti-apoptotic effects.

Additionally, recent findings showed that GSK3 cooperates with mTOR to regulate the activity of p70 ribosomal protein S6 kinase 1 (S6K1), which is a pivotal regulator of extracellular signals supporting cell growth (Shin et al., 2011). Other outstanding mechanisms sustaining cancer cell survival and proliferation involve modulation of c-Myc signaling, Hedgehog (Hh) signaling and STAT3 cascade, but further research is required in the context of PDAC (Baumgart et al., 2016; Singh et al., 1995).

Moreover, the WNT/β-catenin signaling pathway plays an important role in the modulation of apoptosis, differentiation, invasion and epithelial to mesenchymal transition, all critical hallmarks for cancer metastasis (Doble and Woodgett, 2007). GSK3β is a well-established regulator of β-catenin subcellular localization and deregulated GSK3β activity may severely impact the tumor-suppressive and tumor-promoting roles of the WNT/β-catenin signaling cascade (Domoto et al., 2016). Consistently, pharmacologic inhibition of GSK3β was shown to upregulate β-catenin and c-Myc levels, as well as suppress tumor growth in KRas-mutant PDAC and non-small lung cancer models (Kazi et al., 2018).

Interestingly, it has been recently observed that GSK3β plays a key role in modulating cell cycle progression at different regulatory levels. In pancreatic cancer models, GSK3β was observed to directly support the phosphorylation status of many cell cycle modulators such as cyclin D1, p53 and various transcription factors (Kitano et al., 2013; McCubrey et al., 2016). The growth promoting function of GSK3β in this tumor type is supported by both *in vitro* and in tumor xenograft experiments *in vivo*: specifically, pharmacological inhibition of GSK3β activity was reported to promote apoptosis by suppressing Cyclin D1 expression, as well as impairing the transcriptional activity of E2F transcription factor and consequent phosphorylation of the Rb protein (Kitano et al., 2013). Furthermore, Yoshino and colleagues observed that apoptosis-resistant PDAC cells treated with GSK3β inhibitors, exhibited biodynamic cell mechanisms typical of mitotic catastrophe (Yoshino and Ishioka, 2015). This study provided the first proof of fundamental role of GSK3β in controlling mitotic processes in PDAC cells. Similar observations were also recently made in colorectal cancer cells (Yoshino and Ishioka, 2015; Dewi et al., 2018).

Overall, within the complexity of the GSK3β signaling cascades in pancreatic tumorigenesis and tumor progression, cumulative evidence renders GSK3β a promising therapeutic target in order to improve the survival of PDAC patient and enhance the therapeutic responses.

2.3. *Chemoresistance in advanced or metastatic pancreatic cancer*

Surgical resection of PDAC remains the curative treatment choice for achieving long-term survival. However, more than 85 % of PDAC patients are diagnosed with advanced-stage or metastatic disease which is not generally amenable to pancreatectomy (Meijer et al., 2020).

The standard-of-care intervention in those tumors with aggressive-stages mainly include chemotherapeutic agents, such as gemcitabine, 5-fluorouracil, oxaliplatin, irinotecan and nab-paclitaxel (El Hassouni et al., 2019). However, after a good initial response of sensitive tumors, overt chemoresistance eventually develops within weeks, thus severely limiting the effectiveness of those therapeutic interventions (Zeng et al., 2019).

Particularly, PDAC cells showed stronger intrinsic or acquired insensitivity to gemcitabine. Recent phase III clinical trials reported superior overall survival in patients with advanced or metastatic PDAC receiving nab-paclitaxel plus gemcitabine or FOLFIRINOX compared to gemcitabine alone (Caparello et al., 2016). However, although these treatments achieved a longer survival rate than gemcitabine use alone, combinations of chemotherapeutic agents generally show higher frequency of toxicity and patients still become resistant after short times (Pusceddu et al., 2019).

Therefore, gaining insights into tumor intrinsic or acquired strategies responsible for chemotherapy resistance are of urgent need in order to develop novel targeted therapeutic approaches that improve patient overall survival, lower toxicity profile and overcome chemoresistance in advanced or metastatic PDAC (Zeng et al., 2019).

2.3.1. *GSK3 β and chemoresistance*

Even though the underlying mechanisms which trigger chemoresistance remain controversial, defective pharmacodynamics of biochemical mechanisms, together with perturbations on several cellular signaling cascades, were found in gemcitabine-resistant PDAC cells. These mainly involve nucleoside transport and metabolism, reactivation of EMT and developmental pathways, such as WNT/β-catenin, Hh and Notch, and growth factor signaling (El Hassouni et al., 2019; Randazzo et al., 2020; Saiki et al., 2012; Ireland et al., 2016; Shukla et al., 2017).

As previously described, mounting evidences report that aberrant activation of NF-kB plays a crucial role in uncontrolled cell proliferation, tumorigenesis, metastasis, angiogenesis, inflammation and chemotherapy resistance in PDAC (Arlt et al., 2003; Okamoto et al., 2007; Liptay et al., 2003; Holcomb et al., 2008; Mamaghani et al., 2009). Specifically, a strong correlation was observed between basal level of NF-kB activity and gemcitabine resistance. Indeed, in resistant PDAC cell lines (PancTu-1, Capan-1 and BxPc-3 cells) a strong activation of NF-kB was detected when compared to sensitive T3M4 and PT45-P1 PDAC cell lines (Arlt et al., 2003).

NF-kB contribution to chemoresistance was further confirmed by pharmacologic inhibition and by targeting IkBα super-repressor or GSK3β, which resulted in increased sensitivity to gemcitabine in non-responsive PDAC cell lines (Arlt et al., 2003). Mechanistically, GSK3β has been shown to positively regulate NF-kB maintaining high NF-kB activity, thus evidencing GSK3β contribution to chemoresistance onset in PDAC (Ougolkov et al., 2006, 2005; Walz et al., 2017).

PI3K/Akt-mediated signal transduction is another important anti-apoptotic signaling cascade that has been related to chemoresistance of PDAC. Akt is the primary mediator of PI3k-initiated signaling cascade and is specifically involved in the phosphorylation and subsequent inactivation of pro-apoptotic molecules such as Bad, IKb (Ikk β) kinase, caspase-9, the forehead family of transcription factors (FKHR/AFX/FOX), CREB, Raf, p21, as well as GSK3 (Massihnia et al., 2017). A recent study reported that activation of Akt and inhibition of GSK3β through Akt-mediated Serine 9 phosphorylation resulted in the upregulation of Snail1 expression through increased protein stability, promoting EMT-like phenotype and gemcitabine tolerance (Namba et al., 2015).

In order to define the stepwise processes triggering gemcitabine resistance in the clinic, Uehara and colleagues developed a gemcitabine-resistant systemic model derived from the gemcitabine-sensitive human PDAC cell line BxPC-3 (Uehara et al., 2020). Through their work, they demonstrated that GSK3β facilitates the capacity of PDAC to tolerate chemotherapy by interfering with Rb protein function and E2 transcription factor (E2F)1-mediated transcription. Specifically, gemcitabine-resistant clones were characterized by high expression of ribonucleotide reductase M1 (RRM1), a well-known transcriptional target of the pro-oncogenic E2F1 (Uehara et al., 2020; Yoneyama et al., 2015). Additionally, pharmacological inhibition of GSK3β was proved to re-sensitize resistant cells to gemcitabine by restoring the functional Rb-mediated regulation of E2F1, attenuating E2F1 transcriptional activity and consequently decreasing RRM1 expression (Uehara et al., 2020; Kitano et al., 2013).

In summary, GSK3β seems to be involved in many different processes that promote resistance of PDAC cells to gemcitabine and other drugs by sustaining the invasive capacity and stemness phenotype of pancreatic malignant cells.

2.4. *Targeting GSK3β in pancreatic cancer*

GSK3β regulation of several molecular promoters of neoplastic transformation, together with the shorter survival of PDAC patients harboring high GSK3β expression, strongly sustain the hypothesis of GSK3β central involvement in PDAC onset and progression (McCubrey et al., 2016). Thus, accumulating evidence on GSK3β functions has proven the rationale for the clinical development of novel therapeutic strategies targeting GSK3β in advanced PDAC (Cormier and Woodgett, 2017; Baumgart et al., 2016; Walz et al., 2017; Hoeflich et al., 2000).

The therapeutic and antitumor effects achieved by GSK3β inhibition have been described in different cancer types, as reviewed recently by Domoto and colleagues (Domoto et al., 2020). Notably, some evidence reveals that GSK3β inhibition leads to induction of apoptosis in PDAC cells, whereas normal pancreatic epithelial cells seem to be protected from the inhibitory effects associated with the targeted treatment (Marchand et al., 2012). This might find an explanation in the intrinsic biological nature of PDAC cells which present high levels of active GSK3β aberrantly accumulated in the nucleus (Ougolkov et al., 2006; Walz et al., 2017). Thus, PDAC may become more sensitive to the proteasome-dependent GSK3β loss from the nucleus that is induced by the treatment with GSK3 inhibitors (Marchand et al., 2012, 2015).

Inhibition of GSK3β may therefore be a promising precision medicine strategy in PDAC treatment (Domoto et al., 2020; Baudino, 2015). Through cancer cell death promoting effects, this approach may restrict tumor recurrence and metastasis as well as spare harmful consequences on healthy cells and tissues, frequently associated with conventional cytotoxic therapies.

2.4.1. *GSK3 β inhibitors*

Multiple GSK3β inhibitors have been developed and many others are now under investigation (Table 1), as previously reviewed by Saraswati AP et al., and Eldar-Finkelman H et al. (Saraswati et al., 2018; Eldar-Finkelman and Martinez, 2011). In the early 1980s, the cation lithium was the first GSK3β inhibitor being described and then approved by the Food and Drug Administration (FDA) for the treatment of human bipolar depression (Johnson and Amdisen, 1983; Freland and Beaulieu, 2012; Bowden, 2000).

Studies on the mechanism of action of lithium showed that it disrupts the catalytic function of GSK3β by competing for the binding of magnesium (Mg^{2+}) cofactor, but not for ATP or the substrate (Ryves and Harwood, 2001; Phiel and Klein, 2001; Pasquali et al., 2010). Additionally, lithium indirectly increased the N-terminal inhibitory phosphorylation of GSK3β either by enhancing the activity of Akt, through the regulation/dissociation of the Akt:β-arrestin 2 (βArr2): protein phosphatase 2A (PP2A) signaling complex, or by blocking the dephosphorylation of PKB (Pasquali et al., 2010; Zhang et al., 2003; Mora et al., 2002; De Sarno et al., 2002).

Experimental studies on PDAC cells reported reduced tumorigenic potential and cell proliferation, as well as increased apoptosis among lithium treatment (Peng et al., 2013). This outcome was associated with the enhanced ubiquitin-dependent proteasome degradation of the glioma-associated oncogene-1 (GLI1), a crucial downstream component of the Hh signaling pathway, following GSK3β inhibition (Peng et al., 2013; Zhu and Lo, 2010).

The ATP-binding pocket is an essential site for the catalytic action of GSK3β; thus, various GSK3β inhibitors competing with ATP molecules have been developed in order to block the kinase activation. However, one has to note that, whereas those agents might selectively target GSK3β, they can also exert inhibitory effects towards cyclin-dependent kinases (CDKs) since some of them including CDK2, share very similar ATP-binding pockets with GSK3β (Vulpetti et al., 2005). Therefore, the dual inhibitory function of ATP-competitive GSK3β inhibitors may directly impact cell cycle regulation and enhance the antiproliferative outcome.

Gaisina and colleagues designed a preliminary library of benzofuran-3-yl-(indol-3-yl) maleimides, including some selective and potent ATP competitive inhibitors of GSK3β. *In vitro* evaluation of the therapeutic potency of these maleimides showed that compounds **1a-e** exhibited promising antiproliferative effects against a panel of PDAC cell lines (MiaPaCa-2, HupT3 and BXPC2) (Table 1) (Gaisina et al., 2009). Among all, treatment with compounds **1a** and **1e** resulted in pronounced inhibition of GSK3β activity, which correlated with reduced NF-kB-mediated expression of the antiapoptotic X-linked inhibitor of apoptosis protein (XIAP).

Recently, **1e** (9-ING-41), maleimide-based ATP-competitive GSK3β

Table 1
GSK3β Inhibitors in pancreatic cancer preclinical and clinical studies.

Category	Inhibitor	Structure	Pharmacologic activity	GSK3β inhibitory effects	Ref/Clinical trial
ATP competitive	benzofuran-3-yl-(indol-3-yl) maleimides	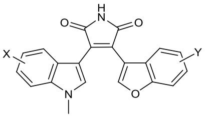	Potent ATP competitor	Apoptosis induction, reduced NF-kB-mediated expression of XIAP	Gaisina IN et al., 2009
	9-ING-41	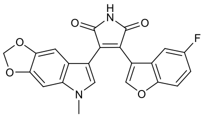	Potent ATP competitor	Cell cycle arrest, reduced expression of anti-apoptotic molecules Bcl-2 and XIAP	Ding L et al., 2017 NCT03678883, 1801 pase 1/2 study
	SB-732881-H	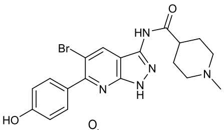	Potent ATP competitor	Apoptosis induction, increased expression of the Bcl-2 protein family	Marchand B et al., 2012
	AR-A014418	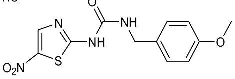	Potent ATP competitor	Lowers cytoplasmic β-catenin levels and abrogates NF-kB transcriptional activation	Bhat et al. (2003) Mamaghani S et al., 2009
	BIO	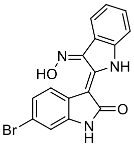	Reduced inhibitory S9 phosphorylation	Enhanced apoptosis via JNK-dependent mechanism	Meijer L. et al., 2003 Kazi A et al., 2018
	CHIR99021	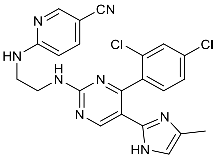	Potent ATP competitor	Apoptosis induction	Marchand B et al., 2012
	LY2090314	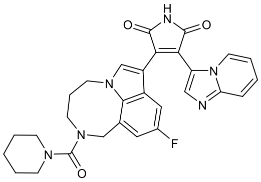	Increased inhibitory phosphorylation	Suppressed pro-survival signals	NCT01287520, 2018 NCT01632306, 2019
	AZD-1080	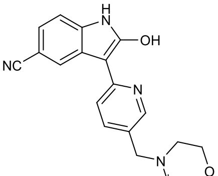	Potent ATP competitor	Reduced cell cycle progression related genes	Kazi A et al., 2018
	Library of synthetic topsentin analogs	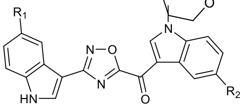	Docked in the ATP binding site	Pro-apoptotic signals induction, reduced expression of EMT markers	Carbone D et al., 2021
Non-ATP competitive	Tideglusib	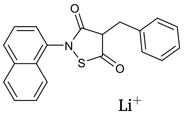	Binding site not yet defined	Cell cycle arrest, impaired phosphorylation of β-catenin and c-Myc	Kazi A et al., 2018 ; Domínguez JM et al., 2012
	Lithium	Li^+	Compete for Mg^{2+} cofactor binding	Suppressed hedgehog signaling pathway	Peng Z et al., 2013
Dual inhibitor	Metavert	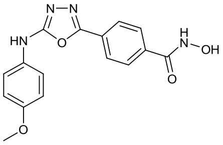	Inhibition of GSK3β and HDAC-2	Cell cycle arrest, reduced expression of EMT markers	Edderkaoui M et al., 2018

inhibitor, showed cytostatic effects in PDAC models and is now under investigation in a phase I/II clinical trial (NCT03678883) in patients with advanced solid tumors (Ding and Billadeau, 2020; NCT03678883, 2021; Carneiro et al., 2020). Even if available results reported a good 9-ING-41 monotherapy tolerance and antitumor efficiency more promising therapeutic effects were obtained under combination chemotherapeutic regimens in patients with refractory PDAC (Carneiro et al., 2020; Ding et al., 2019).

Increased sensitivity to chemotherapy or chemoresistance regression upon treatment with 9-ING-41 have been newly discovered to be related to GSK3β regulation of the gemcitabine-induced TopBP1/ATR/Chk1 DNA damage response pathway, as will be discussed later (Ding et al., 2019).

SB-732881-H (SB), a dual inhibitor of both GSK3 isoforms, selectively suppressed the viability of mutant KRas-dependent tumor cells (Kazi et al., 2018; Fleming et al., 2005). *In vitro* studies on human PDAC cellss MiaPaCa2 harboring aberrant KRas, revealed high sensitivity to SB treatment (IC_{50} of 0.4 μM), resulting in caspase-3 activation and induction of PARP cleavage (Kazi et al., 2018; Demarchi et al., 2003). Furthermore, additional reproducible data suggested that the antitumor effect of SB on KRas-mutant PDAC is supported by apoptosis induction in a c-Myc- and β-catenin-dependent manner (Kazi et al., 2018). In contrast, pharmacologic activity of SB did not affect the viability of non-malignant pancreatic epithelial cells. Overall, these findings are consistent with the pro-survival function of GSK3 in PDAC and further support the assumption that mutant KRas tumors are dependent on GSK3α/β signalling for cancer cell survival and tumor growth (Kazi et al., 2018; Saiki et al., 2012; Fleming et al., 2005; Demarchi et al., 2003; Bang et al., 2013).

AR-A014418, another dual GSK3 inhibitor, induced a strong dose-dependent growth reduction in various pancreatic tumor models (Bhat et al., 2003; Kunnimalaiyaan et al., 2015). By selectively competing for the ATP-binding pocket of GSK3β, AR-A014418 lowered the cytoplasmic β-catenin levels and abrogated NF-kB activation, thus reducing the expression of NF-kB target genes cyclin D1, XIAP and Bcl-XL (Mamaghani et al., 2009; Bhat et al., 2003). Moreover, a recent *in vitro* study reported that AR-A014418 inhibition of GSK3α phosphorylation decreased the expression of Notch pathway members, thus attenuating tumor cell survival (Kunnimalaiyaan et al., 2015).

6-bromoindirubin-3′-oxime (BIO), a synthetic analog of natural indirubins, has been studied in the context of drug resistance in many different cancer types for its indirubin-related property to concomitantly inhibit CDKs and GSK3β (Zhang et al., 2017; Liu et al., 2017; Li et al., 2018;), *via* interaction with the ATP-binding pocket of both kinases (Meijer et al., 2003).

Studies on beneficial effects of BIO have been conducted in the context of anti-aging properties, where treatment with 6-bromoindirubin-3′-oxime reported ameliorated lipid metabolism and positive modulation of autophagy, inflammation and oxidative stress (Guo et al., 2019).

In PDAC cells, treatment with BIO directly inhibited GSK3β *via* suppression of Tyr216 phosphorylation and enhanced apoptosis through JNK-dependent mechanisms (Marchand et al., 2015). However, Marchand and colleagues observed that BIO-GSK3β inhibition augmented the activation of the autophagy/lysosomal network which was elicited through enhanced nuclear localization of the transcription factor EB (TFEB), a master regulator of autophagy and lysosomal biogenesis (Marchand et al., 2015; Zhitomirsky and Assaraf, 2016; Zhitomirsky et al., 2018; Zhitomirsky and Assaraf, 2015). Although the autophagy effects on cancer cells are not well defined, it has been reported that sustained autophagy in PDAC cells elicits cell proliferation by overcoming death signals and favoring oxidative phosphorylation (Yang and Kimmelman, 2011). This metabolic switch provides a proper bioenergetic metabolism and pivotal survival signals to malignant cells under restrictive growth conditions, thus supporting cancer cell growth and tumor progression. Overall, these undesired modulatory effects exerted by BIO, hampered its progression into clinical trials.

Comparably to BIO, the aminopyrimidine derived GSK3 inhibitor CHIR99021 exhibited both apoptosis induction and concomitant increased autophagic response *via* LC3B II expression in PDAC cell models (Tran and Zheng, 2017). Pharmacologic depletion of vacuolar H^+ ATPase with bafilomycin A1, prevented autophagy by disrupting lysosomal acidification, thus forcing PDAC cells to preferentially respond to the death signals mediated by CHIR99021. Indeed, this study supported the hypothesis of addressing autophagy induction as a promising mechanism of escape to the antiproliferative effects of GSK3 inhibitors in the setting of PDAC treatment.

Conversely, LY2090314, an ATP-competitive and highly selective GSK3 inhibitor, is currently under clinical evaluation for cancer treatment (clinical trials: NCT01632306 Phase I/II, NCT01287520 Phase I). *In vitro* and *in vivo* studies showed that treatment with LY2090314 in PDAC models increased the inhibitory phosphorylation of GSK3 and significantly suppressed the expression and pro-survival activity of TGFβ-activated kinase 1 (TAK1), a crucial mediator of cellular signals that sustain PDAC aggressiveness and chemoresistance (Bang et al., 2013; Melisi et al., 2011; Giovannetti et al., 2014). Moreover, Santoro and co-workers demonstrated that reduced TAK1 expression induced by pharmacologic inhibition of GSK3 impacts the YAP/TAZ functions in PDAC cells, thus affecting their contribution to the progression and drug insensitivity of this malignancy (Santoro et al., 2020; Lin et al., 2015).

The GSK3 inhibitors AZD-1080 and Tideglusib were first designed and tested for the treatment of Alzheimer's disease (AD). Notably, they are currently under investigation in the context of cancer therapy (Lovestone et al., 2015). Ovarian carcinoma cells exposed to AZD-1080 showed a significant downregulation of GSK3β, as well as cell cycle progression related genes at both the transcript and protein levels (Chen et al., 2016). The high selectivity and remarkable suppression of cancer cell proliferation following AZD-1080 treatment has been recently confirmed in PDAC cell lines.

As BIO and AZD-1080, Tideglusib showed selective inhibitory activity on GSK3β, impairing the phosphorylation of many GSK3 targets, including β-catenin and c-Myc in refractory PDAC cells and models harboring mutated KRas (Kazi et al., 2018; Domínguez et al., 2012). Mechanistically, Tideglusib differs from the ATP-competitive hallmark of AZD-1080, eliciting an irreversible inhibition of GSK3β *via* a non-competitive mode, although the exact binding site of this molecule has not been elucidated yet (Domínguez et al., 2012).

Interestingly, Edderkaoui and colleagues observed that even though the treatment with Tideglusib in PDAC cells (HPDE6, Bx-PC3, MIA PaCa-2 and HPAF-II) promoted the expression of the EMT marker vimentin, the combinatorial inhibition of histone deacetylases (HDAC) class I-II and GSK3β reduced cancer cell survival and the levels of EMT markers (Edderkaoui et al., 2018).

Based on this observational study, they developed Metavert, a novel synthetic molecule designed by combining Tideglusib and suberoylanilide hydroxamic acid (SAHA) active pharmacophores. SAHA (Vorinostat) is an FDA approved inhibitor of HDAC classI-II currently used for the treatment of cutaneous T cell lymphoma. By inhibiting both GSK3β and HDAC-2, Metavert synergistically impaired *in vitro* PDAC cell proliferation and prevented drug resistance as well as the expression of migration-, EMT- and stemness–associated markers. Furthermore, it significantly reduced tumor cell growth, preventing metastasis and improving overall survival in aggressive PDAC mouse models (Edderkaoui et al., 2018)

Recently, a new library of synthetic topsentin analogs with a central replaced 1,2,4-oxadiazole ring reported promising 50 % growth inhibition values against a panel of different human cancer cell lines [49]. Specifically, five of these newly synthetized agents (**2a-e**) effectively reduced cancer cell viability in PDAC cells (Panc-1, SUIT-2 and Capan-1), with compound **2a** displaying the highest cytotoxic activity (IC_{50} range 0.40–1.19 μM) (Supplemental Table 1) (Carbone et al., 2021). Compounds **2a** and **2e** significantly reduce GSK3β phosphorylation in Panc-1 cells, potentially impacting cancer cell survival and tumor progression. Overall, *in vitro* studies revealed that the antiproliferative effects of these novel topsentin derivatives correlated with apoptosis induction, reduced cell migration and expression of the EMT markers SNAIL-2 and metalloproteinase-9, thus paving the way for new promising studies for the treatment of PDAC with GSK3 inhibitors (Carbone et al., 2021).

2.4.2. Combined therapy with GSK-3β inhibitors

Limited second line therapy approaches are currently available for the management of refractory PDAC. Multiple studies in cancer models reported that certain GSK3β inhibitors enhance tumor sensitivity to chemotherapeutic agents (Abrams et al., 2021; Miyashita et al., 2009; Shimasaki et al., 2012). Therefore, in the past decade various GSK3β inhibitors have been experimentally and clinically tested in the context of refractory and advanced metastatic PDAC with the purpose of developing effective therapeutic strategies that could prevent or overcome drug resistance, while lowering chemotherapy-associated untoward toxicity (Table 2). *In vitro* and *in vivo* research showed that, as gemcitabine cytotoxicity is dependent on cell cycle regulatory processes, pharmacologic inhibition of GSK3β can prevent DNA damage repair inflicted by gemcitabine and induced apoptosis in chemoresistant PDAC cells (Ding et al., 2019; Shimasaki et al., 2012). For example, 9-ING-41 ameliorates the antitumor effects of gemcitabine through modulating the ATR-Chk1 DNA damage response (Ding et al., 2019). In fact, observational studies reported that pharmacologic inhibition of GSK3β in PDAC cells triggers topoisomerase IIβ binding protein (TopBP1) degradation and impairs ATR activation, consequently reducing gemcitabine-mediated Chk1 phosphorylation (Ding et al., 2019). Additionally, in contrast to results obtained by Mamaghani and colleagues, novel experimental evidence reported that AR-A014418 not only suppressed proliferation of PDAC cells and impaired tumor growth, but also synergistically sensitized tumor cells to gemcitabine treatment. Indeed, transcriptome profiling revealed that inhibition of GSK3β counteracts the gemcitabine-induced expression of DNA repair, cell death and autophagy–related genes, such as the tumor protein 53-induced nuclear protein 1 (TP53INP1) (Mamaghani et al., 2009; Shimasaki et al., 2012).

Further research revealed that LY2090314 synergistically interacts with clinically relevant chemotherapeutic agents gemcitabine, oxaliplatin, nab-paclitaxel and SN-38, the active metabolite of irinotecan (Santoro et al., 2020; Lin et al., 2015), by modulating the intrinsic chemoresistance of PDAC cells. Interestingly, while treatment with drug combinations decreased PDAC cell viability, mice treated with LY2090314 and nab-paclitaxel exerted improved overall survival with reduced cytotoxic effects on non-malignant pancreatic cells (Santoro et al., 2020; Zamek-Gliszczynski et al., 2013).

Moreover, the pioneer GSK3β inhibitor lithium has been observed to synergistically improve the antitumor effect of gemcitabine mainly by perturbing the Hh-GLI cascade and enhancing the proteasome-degradation of GLI (Peng et al., 2013). Next to that, Elmaci and Altinoz suggested that the triple-agent regimen comprising already-in-use drugs metformin, pioglitazone and lithium may synergistically target cancer cell metabolism by activating AMPK and PPAR-γ and perturbing GSK3β, respectively (Elmaci and Altinoz, 2016). In *in vitro* as well as in animal model studies, this triple drug combination increased the intrinsic sensitivity of PDAC cells to apoptosis, potentially providing a novel beneficial adjuvant therapy for refractory PDAC.

Furthermore, Metavert, the dual GSK3β/HDAC inhibitor, when used in combination with irradiation and chemotherapeutic agents paclitaxel or gemcitabine, it reduced tumor growth compared to monotherapy and significantly prolonged the survival rate of mice harboring drug-resistant PDAC (Edderkaoui et al., 2018).

Overall, the combination of GSK3β inhibitors and other chemotherapeutic agents appears to synergistically reduce tumor cell growth and increase survival in different models, revealing encouraging therapeutic effects towards the overcoming of chemoresistance in refractory PDAC and paving the way for future clinical studies.

2.4.3. Clinical studies on drug combination regimens including GSK-3β inhibitors

At present, different drug combinations have been explored in preclinical and early-phase clinical studies in order to meet the urgent demand for efficient strategies in the therapeutic management of advanced and metastatic PDAC. However, none of them has already been approved.

Cumulative preclinical evidence provided the rationale to clinically test 9-ING-41 (phase I/II, NCT03678883) in combination with the standard chemotherapeutic agents gemcitabine, nab-paclitaxel, carboplatin, paclitaxel, doxorubicin, lomustine or irinotecan in patients with advanced or refractory solid tumors, including PDAC (NCT03678883, 2021; Carneiro et al., 2020). Furthermore, the promising preclinical outcome of LY2090314 and platinum combination in xenograft models have prompted the clinical evaluation of LY2090314 plus carboplatin and pemetrexed in patients with advanced or metastatic cancer (phase I, NCT01287520) (NCT01287520, 2018). Although establishing the efficiency of LY2090314 combined with carboplatin and pemetrexed requires further interventional confirmations, LY2090314 safety profile, pharmacokinetic parameters and optimal drug doses were established (NCT01287520, 2018; Gray et al., 2015). A parallel study conducted on patients with acute leukemia showed that LY2090314 was well tolerated and reported good antitumor activity when combined with chemotherapeutics, while minimal clinical benefits were observed if administered as monotherapy (Gray et al., 2015; Rizzieri et al., 2016). Additionally, phase I/II trial (NCT01632306, 2019) assessing the combination regimen of LY2090314 and different chemotherapies (FOLFOX, gemcitabine and nab-paclitaxel) in patients with metastatic PDAC was recently terminated due to slow enrollment procedure (NCT01632306, 2019).

Currently, combination treatment with lithium, cimetidine, olanzapine and valproate regimen (CLOVA cocktail) is under clinical investigation with simultaneous usage of gemcitabine in advanced PDAC patients (UMIN000005095), but no data are available yet.

Various phase II clinical trials on diverse pathologies are actually evaluating possible therapeutic regimens with the GSK3β inhibitor tideglusib (NCT01350362, NCT02586935, NCT02858908), providing potential curative possibilities to be tested in the near future also in

Table 2
Drug combination: with GSK3β inhibitors in PDAC.

Drug Combinations with GSK3β inhibitors in PDAC

Treatment	GSK3βi effect	Pharmacological interaction	Tumor stage	Ref/Clinical trial ID
AR-A014418 and Gemcitabine	Impaired DNA repair gene regulation and expression. Inhibition of Notch1 expression.	Synergistic	Preclinical models	Kunnimalaiyaan et al., 2015
9-ING-41 and Gemcitabine	Modulation of ATR-Chk1 DNA damage response	Synergistic	Refractory	NCT03678883 Ding et al., 2019
LY2090314 and Gemcitabine, FOLFOX or Gemcitabine + Nab-paclitaxel	CDK-dependent RRM1/2 downregulation and increased DNA damage	Synergistic	Advanced or metastatic	NCT01632306, 2019 Phase I/II NCT01287520, 2018
Metavert and Gemcitabine	Impaired metabolic profile, cell migration capability and cancer stemness. Altered tumor microenvironment.	Synergistic	Locally advanced	Edderkaoui et al., 2018
Lithium and Gemcitabine	Impaired Hh-GLI signaling	Additive	Preclinical models	Peng et al., 2013

patients with PDAC (Lovestone et al., 2015; Horrigan et al., 2020). Nevertheless, it is important to consider that currently available clinical data provide limited information regarding the overall administration-related adverse events of these combination therapeutic regimens. Indeed, the complexity of cellular GSK3β interconnections, the small number of ongoing clinical trial and the fact that none of the GSK3β inhibitors has been approved for clinical use to date, excluding lithium, further complicate the prediction of beneficial or adverse effects in patients. Therefore, additional studies are required before proposing GSK3β inhibitors-based interventions as therapeutic alternatives in the clinical management of advanced and metastatic PDAC.

2.5. *Resistance to GSK-3 inhibitors*

Experimental studies revealed that various gene programs are activated upon GSK3β inhibition, mainly involving metabolic reprogramming, compensatory pro-survival signaling cascades, hyper-activation of NF-kB and WNT signaling, as well as increased autophagy/lysosomal network activity (Ougolkov et al., 2005; Marchand et al., 2015; Seino et al., 2018; Webster et al., 2000; Sun et al., 2016; Bruton et al., 2020).

Despite the general consensus regarding the antineoplastic activity of GSK3β inhibitors, a more comprehensive analysis on the downstream effects of GSK3β inhibition uncovered the potential induction of escape signals mediated by increased autophagic response (Marchand et al., 2015). Although PDAC cells harbor elevated levels of basal autophagy, whether autophagy displays a tumor suppressor role or a potential resistance mechanism to anticancer therapy, remains elusive (Yang et al., 2011; Galluzzi et al., 2015).

A recent study demonstrated that pharmacologic inhibition of GSK3β in PDAC cells enhanced the transcriptional activity of TFEB, thus positively modulating the autophagic flux (Marchand et al., 2015). Moreover, experimental inhibition of the autophagy cascade with bafilomycin A1 and/or CHIR99021 ameliorated the sensitivity of human PDAC cells to apoptosis triggered upon concomitant treatment with GSK3 inhibitor (Marchand et al., 2015). Similar outcomes were observed in prostate and bladder cancer cells, further sustaining the hypothesis that autophagy exerts a potential mechanism of resistance to GSK3β inhibition and that a combination drug treatment targeting both GSK3β and the autophagy/lysosomal network might prevent this issue (Marchand et al., 2015; Kuroki et al., 2019). Furthermore, autonomous production of stromal WNT ligands, sustaining constitutive Wnt signaling, as well as hyper-activated NF-kB transcriptional activity, have been described in various subsets of PDAC cells (Ougolkov et al., 2005; Seino et al., 2018; Webster et al., 2000; Bruton et al., 2020). Therefore, in light of the molecular interconnections between GSK3β and these signaling pathways, it would not be surprising if these processes might constitute intrinsic mechanisms of resistance to GSK3β inhibition in pancreatic tumor cells.

In this regard, several analyses distinguished two PDAC subtypes, the classical and squamous lineages, which are characterized by distinct transcriptomic and proteomic profiles, as well as prognosis (Collisson et al., 2019; Bailey et al., 2016; Le Large et al., 2020). Specifically, while the classical subtype expresses differentiated endoderm cell markers and mostly experiences favorable clinical outcome, the squamous phenotype harbors altered epigenetic landscape, affecting the expression of duct cell markers and leading to a rapid metabolic reprogramming often leading to a worse prognosis (Bailey et al., 2016; Lomberk et al., 2018; Le Large et al., 2017). This was corroborated by Brunton and colleagues, who reported that a subset of squamous pancreatic cell lines rapidly acquired drug resistance upon treatment with GSK3β inhibitors (Brunton et al., 2020). Specifically, these cancer cells encountered a metabolic adaptation under persistent suppression of glycolysis mediated by pharmacologic inhibition of GSK3β. Furthermore, this was accompanied by an increased dependency on autophagy and activation of a unique gene transcription program resulting in the self-production of WNT ligands, and ultimately leading to drug resistance.

Overall, sustained autophagy flux and activation of compensatory cascades appear to rapidly induce acquired resistance to GSK3β inhibition in PDAC cells. Therefore, further studies are warranted to unravel the complexity of autophagy: potential therapeutic applications in PDAC (Gomez Mellado et al., 2015). However, in-depth analysis of unique chromatin landscape signatures and mutation profiles of PDAC cells might improve our understanding of the dynamics of emergence of drug resistance mechanisms, thus supporting the design of more effective therapeutic approaches.

2.6. *Tumor chromatin profiling may predict patients with pancreatic tumors sensitive to GSK3B-targeted therapy*

The lack of defined biomarkers and the high disease heterogeneity characterizing PDAC are representative of the difficulties in predicting and determining which patients might respond to targeted therapies.

To date observational data highlighted the link between mutant KRas PDAC and GSK3β overexpression (Zhang et al., 2011; Fleming et al., 2015; Fitzgerald et al., 2015). In fact, oncogenic KRas signaling, positively regulates GSK3β expression and activity, thus favoring cell proliferation, survival and tumor dedifferentiation. Pharmacologic inhibition of GSK3β in KRas-dependent tumors was found to impair cancer cell growth and induce apoptosis, partly mediated by c-Myc- and β-catenin-dependent mechanisms (Kazi et al., 2018; Kim et al., 2000). However, the intrinsic plasticity and aggressiveness of KRas-dependent tumors may rapidly lead to the acquisition of drug resistance conclusively discouraging clinical intervention with targeted therapies such as GSK3β inhibitors (Marchand et al., 2015; Downward, 2015; Cox et al., 2014).

Novel epigenetic and transcriptomic studies allowed the classification of PDAC into two main subtypes according to their gene expression profiles, hence providing a prediction of chemoresistance as well as the prognosis (Chan-Seng-Yue et al., 2020). As mentioned above, concomitant inhibition of HDAC and GSK3β may prevent the emergence of drug resistance (Edderkaoui et al., 2018). More recently, new analyses were performed to define chromatin accessibility regions to identify epigenetics hallmarks of tumors sensitive to GSK3 inhibition; they reported that increased access to intronic and distal promoters regulating WNT cascade genes, as well as enrichment in transcription factor motifs, may result in WNT cascade amplification and drug resistance (Bruton et al., 2020). These findings, combined with early results from the prospective COMPASS study (NCT02750657), confirmed that chromatin profiling in advanced PDAC may help define tumors that could benefit from target therapies (Chan-Seng-Yue et al., 2020; Aung et al., 2018).

Specifically, Bruton and colleagues suggested that pancreatic tumors with high mutational burden and chromatin instability are more prone to develop drug resistance. Moreover, those tumors harboring loss of hepatocyte nuclear factor 4-α (HNF4α), an important regulator of endodermal lineage differentiation, more likely maintain sensitivity to GSK3β inhibitors, due to GSK3β upregulation and consequent increased tumor dependency (Bruton et al., 2020). Furthermore, ATAC-seq analysis on sensitive pancreatic tumors revealed mutations on chromatin modulators, possibly KFM6A, SETD2, MLL3, ARID1A and SETBP1, that favor distal promoter usage and alterations in either the AMPK signaling activator LKB1, or in WNT canonical pathway transducer LRP6. This proves their crucial role in the maintenance of cancer cell response to GSK3β-targeted monotherapy.

Many studies clearly showed the complex heterogeneity of pancreatic tumors and their microenvironment aiming to link the tumor genetic mapping with the prediction of patients' response to tailored treatment approaches (Bailey et al., 2016; Boyd et al., 2021). Determining the constellation of tumor genetic and transcriptional alterations not only helps the definition of specific cancer subtypes, but might also have implications to the development of targeted therapeutic strategies specifically designed to address the patient tumor profiles as well as to circumvent or surmount drug resistance.

3. Discussion and conclusions

Pancreatic cancer is a growing global health concern with an increasing incidence-to-mortality ratio. To date, it is the third most common cancer and, due to its frequent dismal prognosis, it will probably become the second-leading cause of cancer-related death in Western countries by 2030 (Rahib et al., 2014). The high genomic complexity and heterogeneity of pancreatic cancer, as well as its intrinsic metastatic behavior, represent an important barrier for the successful treatment of this lethal disease (Boyd et al., 2021). Surgical resection constitutes the only modest chance of cure, while actually standard-of-care therapeutic options are often palliative and offer an average of 5-years survival with most of patients developing drug resistance during the course of the treatment (Zeng et al., 2019). The poor outcomes are mainly related to late diagnosis and the strong aggressive nature of this malignant disease, highlighting the demand for discovering novel tumor vulnerabilities and effective therapies.

Despite dismal statistics, significant progress has been made to elucidate the molecular mechanisms involved in pancreatic cancer progression and chemoresistance. Among all, the glycogen synthase kinase-3 β, a highly conserved isoform of serine-threonine kinase GSK-3 family, has been recently found as an important determinant of PDAC onset and progression (Ougolkov et al., 2006; Zhang et al., 2011;). Initially described as a crucial modulator of glycogen synthesis, GSK3β is now confirmed to be involved in many fundamental cellular processes. Indeed, aberrant GSK3β activity has been implicated in different human disorders including bipolar depression, neurodegenerative disorders, acute myeloid leukemia, as well as many other malignancies (Walz et al., 2017; Hooper et al., 2008; Martelli et al., 2021).

Pre-clinical studies showed that pharmacologic inhibition or genetic depletion of GSK3β drastically reduced cell proliferation and cell survival of multiple human tumor types, further highlighting GSK3β as an attractive pharmacological target for therapeutic interventions against cancer (Rizzieri et al., 2016; Kotliarova et al., 2008; Korur et al., 2009; Song et al., 2010; Cohen et al., 1998; Carter et al., 2014; Kroon et al., 2014). Moreover, several studies on drug combination in patients with refractory solid tumors have shown that inhibition of GSK3β sensitizes resistant cancer cells to standard chemotherapeutic agents such as gemcitabine, nab-paclitaxel, doxorubicin, and FOLFIRINOX (Bhat et al., 2003; Kunnimalaiyaan et al., 2015; Shimasaki et al., 2012;). Thus, multiple evidence suggested that targeting GSK3β may reverse chemoresistance and highlighted its key role in many intracellular signaling pathways. These brought GSK3β to the attention of many researchers which are currently attempting to better understand the role of this this enigmatic kinase in the cellular dynamics of pancreas tumorigenesis and drug resistance.

Although GSK3β has been previously described as a tumor suppressor regulating the activity of numerous pro-oncogenic molecules such as c-Myc, β-catenin, cyclin D and c-Jun, a series of consistent observational studies reported that GSK3β is strongly upregulated in PDAC cells and could sustain pancreatic tumorigenesis (Kockeritz et al., 2006; Nagini et al., 2019; Walz et al., 2017). Notably, mutant KRas pancreatic cancers, accounting for 91 % of overall PDAC patients, present the overexpression and nuclear accumulation of active GSK3β which often correlate with poorly differentiated tumor state and poor outcomes (Christenson et al., 2016).

Tumors expressing mutated Ras usually harbor enhanced activation of mitogenic PI3k signaling and perturbed PTEN phosphatase activity, providing crucial signals driving tumor formation and maintenance (McCubrey et al., 2012a, 2012b; Fitzgerald et al., 2015; Waters and Channing, 2018). However, the intricate role of KRas in sustaining multiple mitogenic signaling pathways, such as activation of Akt, HER2 and EGFR, may explain the lack of success in developing KRas targeted therapies, despite decades of intense research efforts. More intriguing, GSK3β seems to be fundamental for the survival and growth of KRas-driven PDAC. Pharmacologic inhibition of GSK3β with SB, Tideglusib, AZD1080 and BIO, selectively reduced the proliferation of PDAC with dependency on mutant KRas, further evidencing the pro-survival effect of GSK3β in these tumors.

The controversial anti-tumorigenic or pro-tumorigenic role of GSK3β in PDAC is finely regulated by diverse mechanisms, including post-translational modifications, cellular localization and trafficking, formation of protein complexes, and substrate priming. All these processes have been extensively studied in order to understand the dynamics governing GSK3β activation and disruption.

Among all, phosphorylation of tyrosine 216, located within the conserved activation loop, is responsible for the full activation and kinase function of GSK3β, while serine 9 residue in the N-terminal lobe inhibits GSK3β activity when phosphorylated by other kinases (Cormier and Woodgett, 2017; Sutherland, 2011; Frame et al., 2001). However, considering pGSK3β-S9 as the inactive and pGSK3β-Y216 as the active form is probably over simplistic. In fact, GSK3β undergoes a dynamic equilibrium within those and others recently identified phosphorylation status in concert with stimulatory signaling molecules and primed substrate concentration. Additionally, serine 9 phosphorylation does not completely abrogate the catalytic activity of this kinase, as proven by the pGSK3β-S9-mediated phosphorylation of Gli3 within the Hh signaling pathway (Fitzgerald et al., 2015).

These observations might explain why many ATP-competitive GSK3β inhibitors interacting with the N-terminal lobe exert high concentration IC_{50} values and low kinase selectivity when compared to covalent inhibitors or non-ATP competitors. In fact, the ATP-binding domain is structurally conserved among most of kinases and, therefore, it is not surprising that some ATP competitive GSK3β inhibitors target also CDKs and other kinases which share a good degree of homology. Moreover, ATP-competitors increasing the inhibitory phosphorylation on serine-9 might not be optimal to abrogate GSK3β activity since phosphorylation of this residue, located within the binding pocket for primed-substrates recognition, might still result in GSK3β-mediated regulation of non-pre-phosphorylated targets.

On the other hand, covalent- or non-ATP-competitive inhibitors of GSK3β such as tideglusib, display moderate-to-weak binding but improved selectivity and low drug concentrations are required to attain therapeutic effects. Overall, these factors might determine the choice of using these classes of GSK3β inhibitors in clinical practice, but further studies on GSK-3 protein-substrate are required for future development of portent GSK3β inhibitors.

The promising therapeutic results expected from GSK3β targeting in PDAC found a solid base in the progressive increase of GSK3β expression which, in turn, strongly regulates NF-kB transcriptional activity (Ougolkov et al., 2006; Demarchi et al., 2003; Ben-Josef et al., 2015). This consequently triggered the stimulation of pathways involved in cell survival, proliferation and a pro-invasive transformation of pancreatic cancer cells, as well as in the promotion of Bim family proteins expression (Marchand et al., 2012).

Moreover, GSK3β appears to have a negative regulatory role on apoptosis, through phosphorylation and subsequent inactivation of pro-apoptotic molecules such as Bad, Ikk β and caspase 9, further sustaining a pro-survival phenotype (Cervello et al., 2012; Meng et al., 2018). GSK3β also modulates Wnt/β-catenin signaling: active GSK3β phosphorylates β-catenin, targeting it for ubiquitin-mediated proteasomal degradation (McCubrey et al., 2016) mediating Wnt cascade activation. This leads to inhibition of GSK3β activity, β-catenin accumulation and translocation into the nucleus, causing the expression of proto-oncogenes such as c-Myc and cyclin D1, along with genes promoting cell invasion and migration. In this regard, whether GSK3β action is dependent or not on β-catenin perturbation is still controversial, sustained WNT cascade activity was observed to drive drug resistance in PDAC models treated with GSK3β inhibitors (Freland and Beaulieu, 2012; Zhang et al., 2003; Yu et al., 2012).

To date, further mechanisms of drug resistance have been identified to be provoked by treatment with GSK3β inhibitors, mainly involving the activation of autophagy/lysosomal network (Marchand et al., 2015). Although coexistence of both apoptosis and autophagic responses have been observed in many *in vitro* studies testing different GSK3β inhibitors, additional molecular studies reported that the transcription factor EB provided pro-survival autophagic signals by enhancing autophagy/lysosomal activity. Concomitantly, TFEB-depleted PDAC cells exhibited enhanced sensitivity to cell death upon GSK3β inhibition, further proving the protective role of autophagy in pancreatic cancer cells under GSK3β disruption. Similar results were observed in prostate cancer models, where GSK3β depletion enhanced AMP/ATP ratio, eliciting AMPK signals and autophagy activation (Sun et al., 2016). Even if combinatorial inhibition of GSK3β and TFED has not been investigated yet, assessing GSK3β-mediated regulation of autophagic responses might be a future achievement in the development of PDAC treatment.

To prevent the onset of drug resistance, novel advances in understanding escape pathways and chromatin landscape in GSK3β inhibition have been elucidated in experimental settings. Epigenetic analysis revealed that histone deacetylases are highly expressed in PDAC cells, coordinating cell cycle progression, differentiation and apoptosis. Enhanced HDACs activity, resulting from GSK3β-mediated activation of Zeb1 transcription factors, consequently induced the repression of E-cadherin expression and lead to a poorer prognosis (Aghdassi et al., 2012). Indeed, concomitant inhibition of GSK3β and HDACs with the synthetic agent Metavert caused synergistic anti-proliferative effects on PDAC cells and prevented EMT-associated gene expression (Edderkaoui et al., 2018).

Furthermore, chromatin profiling among advanced pancreatic cancer suggests that tumors harboring high mutational burden and chromatin instability are more prone to present drug resistance, and patients with loss of the hepatocyte nuclear factor 4-α and enhanced GSK3β expression were more likely to respond to treatment with GSK3β inhibitors (Bruton et al., 2020).

A general optimism is increasing nowadays when combining chemotherapy with novel agents, targeting specific features of different tumors. Indeed, it is overall admitted that drugs targeting various tumor-survival signaling cascades might exert therapeutic advantages compared to single agent treatment approaches. Therefore, considerable advances have been achieved in the development of targeted drugs with reduced toxicities, improved survival benefits and potentiality to overcome or prevent chemoresistance.

However, approved targeted therapies for pancreatic cancer treatment include only olaparib (Lynparza), and erlotinib (Tarceva). Recent preclinical studies underlined the potential of new inhibitors of the focal adhesion kinase (Le Large et al., 2021) or c-Met (Firuzi et al., 2019). Similarly, a few studies showed that administration of GSK3β inhibitors reduced pancreatic cancer cell proliferation, but more interestingly, it resensitized drug resistant cells to standard of care chemotherapy within combinatorial regimens. Indeed, disruption of GSK3β has been described to modulate the TAK1-YAP/TAZ axis and the ATR-mediated DNA damage response pathway, thus driving the restoration of effective cytotoxic response (Ding et al., 2019; Lin et al., 2015).

On the other hand, GSK3β is a fundamental crossroad for multiple anti-oncogenic pathways, by promoting tumor suppressor signaling cascades and this feature has raised a general mistrust in approving such agents for therapeutic interventions against cancer. Thus, the evaluation of GSK3β inhibitors in clinical trials has been hampered by the concern that inhibition of GSK3β may stimulate malignant transformation. However, future promising perspectives for GSK3β inhibitors clinical management of cancer has been recently achieved from observational studies reporting that long-term use of the only approved GSK3 inhibitor, lithium, is not associated with increased risk of cancer in patients with bipolar disorder (Martinsson et al., 2016)

Overall, developing the medical treatment of choice for tumors, such as PDAC, that manifests high recurrence and persistent invasion capacity, metastasis and development of drug tolerance, remains a challenge for current clinical interventions. Chemotherapeutic interventions, radiation and immunotherapy have indeed minimal effect on patient's survival, highlighting the burning need for additional mechanistic studies exploiting cellular vulnerabilities of advanced and metastatic PDAC. In this respect, additional studies are required to extensively understand the consequence and dynamics regulating aberrant GSK3β activity. Furthermore, a specific focus should also be directed to GSK-3α, the other isoform of GSK3, which presents distinctive cellular functions. Since these kinases are differentially expressed within tissues and the majority of cancer studies has focused on GSK3β, it is questionable if targeting GSK3α together with GSK3β has a major effect than single GSK-3β inhibition.

In conclusion, the combination of GSK3β inhibitors with chemotherapy is strategically poised to be a promising approach to overcome the emergence of early drug resistance or to overcome chemoresistance in advanced and metastatic pancreatic tumors. Further understanding of the dynamics governing PDAC tumorigenesis and cancer progression involving GSK3β, might help the achievement of clinical strategies aimed at ameliorating survival benefits and to convert this deadly tumor into a more manageable chronic malignancy.

Acknowledgements

This work was supported by Associazione Italiana per la Ricerca sul Cancro (AIRC) IG2020-24444 (P.I. Elisa Giovannetti), Dutch Cancer Society KWF grant#11957 and 13598 (P.I. Elisa Giovannetti), European Union 2014-2020 PON Dottorati in Ricerca e Innovazione grant from the Italian Ministry of Education, University and Research (P.I. Patrizia Diana and Elisa Giovannetti).

Appendix A. Supplementary data

Supplementary material related to this article can be found, in the online version, at doi:https://doi.org/10.1016/j.drup.2021.100779.

References

Abrams, S.L., Akula, S.M., Meher, A.K., Steelman, L.S., Gizak, A., Duda, P., Rakus, D., Martelli, A.M., Ratti, S., Cocco, L., Montalto, G., Cervello, M., Ruvolo, P., Libra, M., Falzone, L., Candido, S., McCubrey, J.A., 2021. GSK-3β can regulate the sensitivity of MIA-PaCa-2 pancreatic and MCF-7 breast cancer cells to chemotherapeutic drugs, targeted therapeutics and nutraceuticals. Cells 10 (4), 816. https://doi.org/10.3390/cells10040816.

Aghdassi, A., Sendler, M., Guenther, A., Mayerle, J., Behn, C.O., Heidecke, C.D., Friess, H., Büchler, M., Evert, M., Lerch, M.M., Weiss, F.U., 2012. Recruitment of histone deacetylases HDAC1 and HDAC2 by the transcriptional repressor ZEB1 downregulates E-cadherin expression in pancreatic cancer. Gut 61, 439–448.

Arlt, A., Gehrz, A., Müerköster, S., Vorndamm, J., Kruse, M.L., Fölsch, U.R., Schäfer, H., 2003. Role of NF-kappaB and Akt/PI3K in the resistance of pancreatic carcinoma cell lines against gemcitabine-induced cell death. Oncogene 22, 3243–3251.

Arora, S., Bhardwaj, A., Singh, S., Srivastava, S.K., McClellan, S., Nirodi, C.S., Piazza, G. A., Grizzle, W.E., Owen, L.B., Singh, A.P., 2013. An undesired effect of chemotherapy: gemcitabine promotes pancreatic cancer cell invasiveness through reactive oxygen species-dependent, nuclear factor κB- and hypoxia-inducible factor 1α-mediated up-regulation of CXCR4. J. Biol. Chem. 288, 21197–21207.

Aung, K.L., Fischer, S.E., Denroche, R.E., Jang, G.H., Dodd, A., Creighton, S., Southwood, B., Liang, S.B., Chadwick, D., Zhang, A., O'Kane, G.M., Albaba, H., Moura, S., Grant, R.C., Miller, J.K., Mbabaali, F., Pasternack, D., Lungu, I.M., Bartlett, J.M.S., Ghai, S., Lemire, M., Holter, S., Connor, A.A., Moffitt, R.A., Yeh, J.J., Timms, L., Krzyzanowski, P.M., Dhani, N., Hedley, D., Notta, F., Wilson, J.M., Moore, M.J., Gallinger, S., Knox, J.J., 2018. Genomics-driven precision medicine for advanced pancreatic cancer: early results from the COMPASS trial. Clin. Cancer Res. 24, 1344–1354.

Bailey, P., Chang, D., Nones, K., et al., 2016. Genomic analyses identify molecular subtypes of pancreatic cancer. Nature 531, 47–52.

Bang, D., Wilson, W., Ryan, M., Yeh, J.J., Baldwin, A.S., 2013. GSK-3α promotes oncogenic KRAS function in pancreatic cancer via TAK1-TAB stabilization and regulation of noncanonical NF-κB. Cancer Discov. 3, 690–703.

Baudino, T.A., 2015. Targeted cancer therapy: the next generation of cancer treatment. Curr. Drug Discov. Technol. 12, 3–20.

Baumgart, S., Chen, N.M., Zhang, J.S., Billadeau, D.D., Gaisina, I.N., Kozikowski, A.P., Singh, S.K., Fink, D., Ströbel, P., Klindt, C., Zhang, L., Bamlet, W.R., Koenig, A., Hessmann, E., Gress, T.M., Ellenrieder, V., Neesse, A., 2016. GSK-3β governs inflammation-induced NFATc2 signaling hubs to promote pancreatic cancer progression. Mol. Cancer Ther. 15, 491–502.

Ben-Josef, George, A., Regine, W.F., Abrams, R., Morgan, M., Thomas, D., Schaefer, P.L., DiPetrillo, T.A., Fromm, M., Small Jr., W., Narayan, S., Winter, K., Griffith, K.A., Guha, C., T.M, 2015. Williams Glycogen synthase kinase 3 beta predicts survival in resected adenocarcinoma of the pancreas. Clin. Cancer Res. 21, 5612–5618.

Beurel, E., Grieco, S.F., Jope, R.S., 2015. Glycogen synthase kinase-3 (GSK3): regulation, actions, and diseases. Pharmacol. Ther. 0, 114–131.

Bhat, R., Xue, Y., Berg, S., Hellberg, S., Ormö, M., Nilsson, Y., Radesäter, A.C., Jerning, E., Markgren, P.O., Borgegård, T., Nylöf, M., Giménez-Cassina, A., Hernández, F., Lucas, J.J., Díaz-Nido, J., Avila, J., 2003. Structural insights and biological effects of glycogen synthase kinase 3-specific inhibitor AR-A014418. J. Biol. Chem. 278, 45937–45945.

Bijur, G.N., Jope, R.S., 2003. Glycogen synthase kinase-3 beta is highly activated in nuclei and mitochondria. Neuroreport 14, 2415–2419.

Binenbaum, Y., Na'ara, S., Gil, Z., 2015. Gemcitabine resistance in pancreatic ductal adenocarcinoma. Drug Resist. Updat. 23, 55–68.

Bowden, C.L., 2000. Efficacy of lithium in mania and maintenance therapy of bipolar disorder. J. Clin. Psychiatry 61 (Suppl. 9), 35–40.

Boyd, L.N.C., Andini, K.D., Peters, G.J., Kazemier, G., Giovannetti, E., 2021. Heterogeneity and plasticity of cancer-associated fibroblasts in the pancreatic tumor microenvironment. Semin. Cancer Biol. 15. S1044-579X(21)00056-0.

Brunton, H., Caligiuri, G., Cunningham, R., et al., 2020. HNF4A and GATA6 loss reveals therapeutically actionable subtypes in pancreatic cancer. Cell Rep. 31 (6), 107625. https://doi.org/10.1016/j.celrep.2020.107625.

Caparello, C., Meijer, L.L., Garajova, I., Falcone, A., Le Large, T.Y., Funel, N., Kazemier, G., Peters, G.J., Vasile, E., Giovannetti, E., 2016. FOLFIRINOX and translational studies: towards personalized therapy in pancreatic cancer. World J. Gastroenterol. 22, 6987–7005.

Carbone, D., Parrino, B., Cascioferro, S., Pecoraro, C., Giovannetti, E., Di Sarno, V., Musella, S., Auriemma, G., Cirrincione, G., Diana, P., 2021. 1,2,4-oxadiazole topsentin analogs with antiproliferative activity against pancreatic cancer cells, targeting GSK3β kinase. ChemMedChem 16, 537–554.

Carneiro, B.A., Anraku, T., Kazama, A., Bilim, V., Tasaki, M., Schmitt, D., Mazar, A.P., Giles, F.J., Ugolkov, A., Tomita, Y., 2020. Phase I study of 9-ing-41, a small molecule selective glycogen synthase kinase-3 beta (GSK-3β) inhibitor, as a single agent and combined with chemotherapy, in patients with refractory tumors. J. Clin. Oncol. 38, 3507.

Carter, Y.M., Kunnimalaiyaan, S., Chen, H., Gamblin, T.C., Kunnimalaiyaan, M., 2014. Specific glycogen synthase kinase-3 inhibition reduces neuroendocrine markers and suppresses neuroblastoma cell growth. Cancer Biol. Ther. 15, 510–515.

Cervello, M., McCubrey, J.A., Cusimano, A., Lampiasi, N., Azzolina, A., Montalto, G., 2012. Targeted therapy for epatocellular carcinoma: novel agents on the horizon. Oncotarget 3, 236–260.

Chan-Seng-Yue, M., Kim, J.C., Wilson, G.W., et al., 2020. Transcription phenotypes of pancreatic cancer are driven by genomic events during tumor evolution. Nat. Genet. 52, 231–240.

Chen, S., Sun, K.X., Feng, M.X., Sang, X.B., Liu, B.L., Zhao, Y., 2016. Role of glycogen synthase kinase-3β inhibitor AZD1080 in ovarian cancer. Drug Des. Devel. Ther. 10, 1225–1232.

Christenson, E.S., Jaffee, E., Azad, N.S., 2016. Current and emerging therapies for patients with advanced pancreatic ductal adenocarcinoma: a bright future. Lancet Oncol. 21 (3), e135–e145.

Cohen, Y., Chetrit, A., Cohen, Y., Sirota, P., Modan, B., 1998. Cancer morbidity in psychiatric patients: influence of lithium carbonate treatment. Med. Oncol. Northwood Lond. Engl. 15, 32–36.

Collisson, E.A., Bailey, P., Chang, D.K., Biankin, A.V., 2019. Molecular subtypes of pancreatic cancer. Nat. Rev. Gastroenterol. Hepatol. 16, 207–220.

Coppola, S., Carnevale, I., Danen, E.H.J., Peters, G.J., Schmidt, T., Assaraf, Y.G., Giovannetti, E., 2017. A mechanopharmacology approach to overcome chemoresistance in pancreatic cancer. Drug Resist. Update 31, 43–51.

Cormier, K.W., Woodgett, J.R., 2017. Recent advances in understanding the cellular roles of GSK-3. F1000Research 6.

Cox, A.D., Fesik, S.W., Kimmelman, A.C., Luo, J., Der, C.J., 2014. Drugging the undruggable Ras: mission possible? Nat. Rev. Drug Discov. 13, 828–851.

Dajani, R., Fraser, E., Roe, S.M., Yeo, M., Good, V.M., Thompson, V., Dale, T.C., Pearl, L. H., 2003. Structural basis for recruitment of glycogen synthase kinase 3beta to the axin-APC scaffold complex. EMBO J. 22, 494–501.

De Sarno, P., Li, X., Jope, R.S., 2002. Regulation of Akt and glycogen synthase kinase-3 beta phosphorylation by sodium valproate and lithium. Neuropharmacology 43, 1158–1164.

Demarchi, F., Bertoli, C., Sandy, P., Schneider, C., 2003. Glycogen synthase kinase-3 beta regulates NF-kappa B1/p105 stability. J. Biol. Chem. 278, 39583–39590.

Dewi, F.R.P., Domoto, T., Hazawa, M., Kobayashi, A., Douwaki, T., Minamoto, T., Wong, R.W., 2018. Colorectal cancer cells require glycogen synthase kinase-3β for sustaining mitosis via translocated promoter region (TPR)-dynein interaction. Oncotarget 9, 13337–13352.

Ding, L., Billadeau, D.D., 2020. Glycogen synthase kinase-3β: a novel therapeutic target for pancreatic cancer. Expert Opin. Ther. Targets 24, 417–426.

Ding, L., Liou, G.Y., Schmitt, D.M., Storz, P., Zhang, J.S., Billadeau, D.D., 2017. Glycogen synthase kinase-3β ablation limits pancreatitis-induced acinar-to-ductal metaplasia. J. Pathol. 243, 65–77. https://doi.org/10.1002/path.4928.

Ding, L., Madamsetty, V.S., Kiers, S., Alekhina, O., Ugolkov, A., Dube, J., Zhang, Y., Zhang, J.S., Wang, E., Dutta, S.K., Schmitt, D.M., Giles, F.J., Kozikowski, A.P., Mazar, A.P., Mukhopadhyay, D., Billadeau, D.D., 2019. Glycogen synthase kinase-3 inhibition sensitizes pancreatic cancer cells to chemotherapy by abrogating the TopBP1/ATR-mediated DNA damage response. Clin. Cancer Res. Off. J. Am. Assoc. Cancer Res. 25, 6452–6462.

Doble, B.W., Woodgett, J.R., 2003. GSK-3: tricks of the trade for a multi-tasking kinase. J. Cell. Sci. 116, 1175–1186.

Doble, B.W., Woodgett, J.R., 2007. Role of glycogen synthase kinase-3 in cell fate and epithelial-mesenchymal transitions. Cells Tissues Organs (Print) 185, 73–84.

Domínguez, J.M., Fuertes, A., Orozco, L., del Monte-Millán, M., Delgado, E., Medina, M., 2012. Evidence for irreversible inhibition of glycogen synthase kinase-3β by tideglusib. J. Biol. Chem. 287, 893–904. https://doi.org/10.1074/jbc.M111.306472.

Domoto, T., Pyko, I.V., Furuta, T., Miyashita, K., Uehara, M., Shimasaki, T., Nakada, M., Minamoto, T., 2016. Glycogen synthase kinase-3β is a pivotal mediator of cancer invasion and resistance to therapy. Cancer Sci. 107, 1363–1372.

Domoto, T., Uehara, M., Bolidong, D., Minamoto, T., 2020. Glycogen synthase kinase 3β in cancer biology and treatment. Cells 9.

Downward, J., 2015. RAS synthetic lethal screens revisited: still seeking the elusive prize? Clin. Cancer Res. Off. J. Am. Assoc. Cancer Res. 21, 1802–1809.

Duda, P., Akula, S.M., Abrams, S.L., Steelman, L.S., Martelli, A.M., Cocco, L., Ratti, S., Candido, S., Libra, M., Montalto, G., Cervello, M., Gizak, A., Rakus, D., McCubrey, J. A., 2020. Targeting GSK3 and associated signaling pathways involved in cancer. Cells 9.

Edderkaoui, M., Chheda, C., Soufi, B., Zayou, F., Hu, R.W., Ramanujan, V.K., Pan, X., Boros, L.G., Tajbakhsh, J., Madhav, A., Bhowmick, N.A., Wang, Q., Lewis, M., Tuli, R., Habtezion, A., Murali, R., Pandol, S.J., 2018. An inhibitor of GSK3B and HDACs kills pancreatic cancer cells and slows pancreatic tumor growth and metastasis in mice. Gastroenterology 155. https://doi.org/10.1053/j.gastro.2018.08.028, 1985-1998.e5.

El Hassouni, B., Li Petri, G., Liu, D., Cascioferro, S., Parrino, B., Hassan, W., Diana, P., Ali, A., Frampton, A.E., Giovannetti, E., 2019. Pharmacogenetics of treatments for pancreatic cancer. Expert Opin. Drug Metab. Toxicol. 15, 437–447.

Eldar-Finkelman, H., Martinez, A., 2011. GSK-3 inhibitors: preclinical and clinical focus on CNS. Front. Mol. Neurosci. 4.

Elmaci, İ., Altinoz, M.A., 2016. A metabolic inhibitory cocktail for grave cancers: metformin, pioglitazone and Lithium combination in treatment of pancreatic cancer and glioblastoma multiforme. Biochem. Genet. 54, 573–618.

Eser, S., Schnieke, A., Schneider, G., Saur, D., 2014. Oncogenic KRAS signalling in pancreatic cancer. Br. J. Cancer 111, 817–822.

Fang, X., Yu, S.X., Lu, Y., Bast Jr, R.C., Woodgett, J.R., Mills, G.B., 2000. Phosphorylation and inactivation of glycogen synthase kinase 3 by protein kinase A. Proc. Natl. Acad. Sci. U. S. A. 97, 11960–11965.

Firuzi, O., Che, P.P., El Hassouni, B., Buijs, M., Coppola, S., Löhr, M., Funel, N., Heuchel, R., Carnevale, I., Schmidt, T., Mantini, G., Avan, A., Saso, L., Peters, G.J., Giovannetti, E., 2019. Role of c-MET inhibitors in overcoming drug resistance in spheroid models of primary human pancreatic cancer and stellate cells. Cancers (Basel) 11 (5), 638.

Fitzgerald, T.L., Lertpiriyapong, K., Cocco, L., Martelli, A.M., Libra, M., Candido, S., Montalto, G., Cervello, M., Steelman, L., Abrams, S.L., et al., 2015. Roles of EGFR and KRAS and their downstream signaling pathways in pancreatic cancer and pancreatic cancer stem cells. Adv. Biol. Regul. 59, 65–81.

Fleming, J.B., Shen, G.-L., Holloway, S.E., Davis, M., Brekken, R.A., 2005. Molecular consequences of silencing mutant K-ras in pancreatic cancer cells: justification for K-ras-directed therapy. Mol. Cancer Res. MCR 3, 413–423. https://doi.org/10.1158/1541-7786.MCR-04-0206.

Foltz, D.R., Santiago, M.C., Berechid, B.E., Nye, J.S., 2002. Glycogen synthase kinase-3beta modulates notch signaling and stability. Curr. Biol. CB 12, 1006–1011.

Frame, S., Cohen, P., Biondi, R.M., 2001. A common phosphate binding site explains the unique substrate specificity of GSK3 and its inactivation by phosphorylation. Mol. Cell 7, 1321–1327.

Freland, L., Beaulieu, J.-M., 2012. Inhibition of GSK3 by lithium, from single molecules to signaling networks. Front. Mol. Neurosci. 5.

Gaisina, I.N., Gallier, F., Ougolkov, A.V., Kim, K.H., Kurome, T., Guo, S., Holzle, D., Luchini, D.N., Blond, S.Y., Billadeau, D.D., Kozikowski, A.P., 2009. From a natural product lead to the identification of potent and selective benzofuran-3-yl-(indol-3-yl) maleimides as glycogen synthase kinase 3beta inhibitors that suppress proliferation and survival of pancreatic cancer cells. J. Med. Chem. 52, 1853–1863.

Galluzzi, L., Pietrocola, F., Bravo-San Pedro, J.M., Amaravadi, R.K., Baehrecke, E.H., Cecconi, F., Codogno, P., Debnath, J., Gewirtz, D.A., Karantza, V., Kimmelman, A., Kumar, S., Levine, B., Maiuri, M.C., Martin, S.J., Penninger, J., Piacentini, M., Rubinsztein, D.C., Simon, H.U., Simonsen, A., Thorburn, A.M., Velasco, G., Ryan, K. M., Kroemer, G., 2015. Autophagy in malignant transformation and cancer progression. EMBO J. 34, 856–880.

Gao, X., Wang, J.-Y., Gao, L.-M., Yin, X.-F., Liu, L., 2013. Identification and analysis of glycogen synthase kinase 3 beta1 interactome. Cell Biol. Int. 37, 768–779.

Garcea, G., Manson, M.M., Neal, C.P., Pattenden, C.J., Sutton, C.D., Dennison, A.R., Berry, D.P., 2007. Glycogen synthase kinase-3 beta; a new target in pancreatic cancer. Curr. Cancer Drug Targets 7, 209–215. https://doi.org/10.2174/156800907780618266.

Garcia-Sampedro, A., Gaggia, G., Ney, A., Mahamed, I., Acedo, P., 2021. The state-of-the-Art of phase II/III clinical trials for targeted pancreatic cancer therapies. J. Clin. Med. 10, 566.

Giovannetti, E., Wang, Q., Avan, A., Funel, N., Lagerweij, T., Lee, J.H., Caretti, V., van der Velde, A., Boggi, U., Wang, Y., Vasile, E., Peters, G.J., Wurdinger, T., Giaccone, G., 2014. CYB5A role in pancreatic cancer prognosis and autophagy modulation. JNCI – J. Natl. Cancer Inst. 106, djt346.

Giovannetti, E., van der Borden, C.L., Frampton, A.E., Ali, A., Firuzi, O., Peters, G.J., 2017. Never let it go: stopping key mechanisms underlying metastasis to fight pancreatic cancer. Semin. Cancer Biol. 44, 43–59.

Gomez Mellado, V., Giovannetti, E., Peters, G.J., 2015. Unraveling the complexity of autophagy: potential therapeutic applications in Pancreatic Ductal Adenocarcinoma. Sem Cancer Biol. 35, 11–19.

Gray, J.E., Infante, J.R., Brail, L.H., Simon, G.R., Cooksey, J.F., Jones, S.F., Farrington, D. L., Yeo, A., Jackson, K.A., Chow, K.H., Zamek-Gliszczynski, M.J., Burris, H.A., 2015. A first-in-human phase I dose-escalation, pharmacokinetic, and pharmacodynamic evaluation of intravenous LY2090314, a glycogen synthase kinase 3 inhibitor, administered in combination with pemetrexed and carboplatin. Invest. New Drugs 33, 1187–1196.

Guo, D., Shen, Y., Li, W., Li, Q., Zhao, Y., Pan, C., Chen, B., Zhong, Y., Miao, Y., 2019. 6-bromoindirubin-3′-Oxime (6BIO) suppresses the mTOR pathway, promotes autophagy, and exerts anti-aging effects in rodent liver. Front. Pharmacol. 10.

Hermida, M.A., Dinesh Kumar, J., Leslie, N.R., 2017. GSK3 and its interactions with the PI3K/AKT/mTOR signalling network. Adv. Biol. Regul. 65, 5–15.

Hill, A., Chung, V., 2020. Pancreatic cancer. In: Salgia, R. (Ed.), Oncology in the Precision Medicine Era. Springer, Cham.

Hoeflich, K.P., Luo, J., Rubie, E.A., Tsao, M.S., Jin, O., Woodgett, J.R., 2000. Requirement for glycogen synthase kinase-3beta in cell survival and NF-kappaB activation. Nature 406, 86–90. https://doi.org/10.1038/35017574.

Holcomb, B., Yip-Schneider, M., Schmidt, C.M., 2008. The role of nuclear factor kappaB in pancreatic cancer and the clinical applications of targeted therapy. Pancreas 36, 225–235.

Hooper, C., Killick, R., Lovestone, S., 2008. The GSK3 hypothesis of Alzheimer's disease. J. Neurochem. 104, 1433–1439.

Horrigan, J., Gomes, T.B., Snape, M., Nikolenko, N., McMorn, A., Evans, S., Yaroshinsky, A., Della Pasqua, O., Oosterholt, S., Lochmüller, H., 2020. A phase 2 study of AMO-02 (Tideglusib) in congenital and childhood-onset myotonic dystrophy type 1 (DM1). Pediatr. Neurol. 112, 84–93.

Hughes, K., Nikolakaki, E., Plyte, S.E., Totty, N.F., Woodgett, J.R., 1993. Modulation of the glycogen synthase kinase-3 family by tyrosine phosphorylation. EMBO J. 12, 803–808.

Ireland, L., Santos, A., Ahmed, M.S., Rainer, C., Nielsen, S.R., Quaranta, V., Weyer-Czernilofsky, U., Engle, D.D., Perez-Mancera, P.A., Coupland, S.E., Taktak, A., Bogenrieder, T., Tuveson, D.A., Campbell, F., Schmid, M.C., Mielgo, A., 2016. Chemoresistance in pancreatic cancer is driven by stroma-derived insulin-like growth factors. Cancer Res. 76, 6851–6863.

Johnson, F.N., Amdisen, A., 1983. The first era of lithium in medicine. An historical note. Pharmacopsychiatria 16, 61–63.

Kaidanovich-Beilin, O., Woodgett, J.R., 2011. GSK-3: functional insights from cell biology and animal models. Front. Mol. Neurosci. 4.

Kaltschmidt, B., Greiner, J.F.W., Kadhim, H.M., Kaltschmidt, C., 2018. Subunit-specific role of NF-κB in cancer. Biomedicines 6, 44.

Kaur, S., Smith, L.M., Patel, A., Menning, M., Watley, D.C., Malik, S.S., Krishn, S.R., Mallya, K., Aithal, A., Sasson, A.R., Johansson, S.L., Jain, M., Singh, S., Guha, S., Are, C., Raimondo, M., Hollingsworth, M.A., Brand, R.E., Batra, S.K., 2017. A combination of MUC5AC and CA19-9 improves the diagnosis of pancreatic cancer: a multicenter study. Am. J. Gastroenterol. 112, 172–183.

Kazi, A., Xiang, S., Yang, H., Delitto, D., Trevino, J., Jiang, R.H.Y., Ayaz, M., Lawrence, H.R., Kennedy, P., Sebti, S.M., 2018. GSK3 suppression upregulates β-catenin and c-Myc to abrogate KRas-dependent tumors. Nat. Commun. 9, 5154.

Kim, K., Pang, K.M., Evans, M., Hay, E.D., 2000. Overexpression of beta-catenin induces apoptosis independent of its transactivation function with LEF-1 or the involvement of major G1 cell cycle regulators. Mol. Biol. Cell 11, 3509–3523.

Kitano, A., Shimasaki, T., Chikano, Y., Nakada, M., Hirose, M., Higashi, T., Ishigaki, Y., Endo, Y., Takino, T., Sato, H., Sai, Y., Miyamoto, K., Motoo, Y., Kawakami, K., Minamoto, T., 2013. Aberrant glycogen synthase kinase 3β is involved in pancreatic Cancer cell invasion and resistance to therapy. PLoS One 8.

Kockeritz, L., Doble, B., Patel, S., Woodgett, J.R., 2006. Glycogen synthase kinase-3–an overview of an over-achieving protein kinase. Curr. Drug Targets 7, 1377–1388.

Komiya, Y., Habas, R., 2008. Wnt signal transduction pathways. Organogenesis 4, 68–75. https://doi.org/10.4161/org.4.2.5851.

Korur, S., Huber, R.M., Sivasankaran, B., Petrich, M., Morin Jr., P., Hemmings, B.A., Merlo, A., Lino, M.M., 2009. GSK3beta regulates differentiation and growth arrest in glioblastoma. PLoS One 4, e7443.

Kotliarova, S., Pastorino, S., Kovell, L.C., Kotliarov, Y., Song, H., Zhang, W., Bailey, R., Maric, D., Zenklusen, J.C., Lee, J., Fine, H.A., 2008. Glycogen synthase kinase 3 inhibition induces glioma cell death through c-MYC, NF-κB and glucose regulation. Cancer Res. 68, 6643–6651.

Krause, U., Bertrand, L., Maisin, L., Rosa, M., Hue, L., 2002. Signalling pathways and combinatory effects of insulin and amino acids in isolated rat hepatocytes. Eur. J. Biochem. 269, 3742–3750.

Kroon, J., in' t Veld, L.S., Buijs, J.T., Cheung, H., van der Horst, G., van der Pluijm, G., 2014. Glycogen synthase kinase-3β inhibition depletes the population of prostate cancer stem/progenitor-like cells and attenuates metastatic growth. Oncotarget 5, 8986–8994.

Kunnimalaiyaan, S., Gamblin, T.C., Kunnimalaiyaan, M., 2015. Glycogen synthase kinase-3 inhibitor AR-A014418 suppresses pancreatic cancer cell growth via inhibition of GSK-3-mediated Notch1 expression. HPB 17, 770–776.

Kuroki, H., Anraku, T., Kazama, A., Bilim, V., Tasaki, M., Schmitt, D., Mazar, A.P., Giles, F.J., Ugolkov, A., Tomita, Y., 2019. 9-ING-41, a small molecule inhibitor of GSK-3beta, potentiates the effects of anticancer therapeutics in bladder cancer. Sci. Rep. 9, 19977.

Le Large, T.Y., Bijlsma, M.F., Kazemier, G., van Laarhoven, H.M., Giovannetti, E., Jimenez, C.R., 2017. Key biological processes driving metastatic spread of pancreatic cancer as identified by multi-omics studies. Semin. Cancer Biol. 44, 153–169.

Le Large, T.Y., Mantini, G., Meijer, L.L., Pham, T.V., Funel, N., van Grieken, N.C., Kok, B., Knol, J., van Laarhoven, H.W., Piersma, S.R., Jimenez, C.R., Kazemier, G., Giovannetti, E., Bijlsma, M.F., 2020. Microdissected pancreatic cancer proteomes reveal tumor heterogeneity and therapeutic targets. JCI Insight 5, 138290.

Le Large, T.Y.S., Bijlsma, M.F., El Hassouni, B., Mantini, G., Lagerweij, T., Henneman, A. A., Funel, N., Kok, B., Pham, T.V., de Haas, R., Morelli, L., Knol, J.C., Piersma, S.R., Kazemier, G., van Laarhoven, H.W.M., Giovannetti, E., Jimenez, C.R., 2021. Focal adhesion kinase inhibition synergizes with nab-paclitaxel to target pancreatic ductal adenocarcinoma. J. Exp. Clin. Cancer Res. 40, 91.

Li, M., Wang, X., Meintzer, M.K., Laessig, T., Birnbaum, M.J., Heidenreich, K.A., 2000. Cyclic AMP promotes neuronal survival by phosphorylation of glycogen synthase kinase 3beta. Mol. Cell. Biol. 20, 9356–9363.

Li, J., Gong, X., Jiang, R., Lin, D., Zhou, T., Zhang, A., Li, H., Zhang, X., Wan, J., Kuang, G., Li, H., 2018. Fisetin inhibited growth and metastasis of triple-negative breast cancer by reversing epithelial-to-mesenchymal transition via PTEN/Akt/GSK3β signal pathway. Front. Pharmacol. 9.

Liang, J., Slingerland, J.M., 2003. Multiple roles of the PI3K/PKB (Akt) pathway in cell cycle progression. Cell Cycle Georget. Tex 2, 339–345.

Lin, L., Sabnis, A.J., Chan, E., Olivas, V., Cade, L., Pazarentzos, E., Asthana, S., Neel, D., Yan, J.J., Lu, X., Pham, L., Wang, M.M., Karachaliou, N., Cao, M.G., Manzano, J.L., Ramirez, J.L., Torres, J.M., Buttitta, F., Rudin, C.M., Collisson, E.A., Algazi, A., Robinson, E., Osman, I., Muñoz-Couselo, E., Cortes, J., Frederick, D.T., Cooper, Z.A., McMahon, M., Marchetti, A., Rosell, R., Flaherty, K.T., Wargo, J.A., Bivona, T.G., 2015. The Hippo effector YAP promotes resistance to RAF- and MEK-targeted cancer therapies. Nat. Genet. 47, 250–256.

Liptay, S., Weber, C.K., Ludwig, L., Wagner, M., Adler, G., Schmid, R.M., 2003. Mitogenic and antiapoptotic role of constitutive NF-kappaB/Rel activity in pancreatic cancer. Int. J. Cancer 105, 735–746.

Liu, K., Li, J., Wu, X., Chen, M., Luo, F., Li, J., 2017. GSK-3β inhibitor 6-bromo-indirubin-3'-oxime promotes both adhesive activity and drug resistance in colorectal cancer cells. Int. J. Oncol. 51, 1821–1830.

Lomberk, G., Blum, Y., Nicolle, R., et al., 2018. Distinct epigenetic landscapes underlie the pathobiology of pancreatic cancer subtypes. Nat. Commun. 9, 1978.

Lovestone, S., Boada, M., Dubois, B., Hüll, M., Rinne, J.O., Huppertz, H.J., Calero, M., Andrés, M.V.-, Gómez-Carrillo, B., León, T., del Ser, T., 2015. A phase II trial of tideglusib in Alzheimer's disease. J. Alzheimers Dis. JAD 45, 75–88.

Mamaghani, S., Patel, S., Hedley, D.W., 2009. Glycogen synthase kinase-3 inhibition disrupts nuclear factor-kappaB activity in pancreatic cancer, but fails to sensitize to gemcitabine chemotherapy. BMC Cancer 9, 132.

Mamaghani, S., Simpson, C.D., Cao, P.M., Cheung, M., Chow, S., Bandarchi, B., Schimmer, A.D., Hedley, D.W., 2012. Glycogen synthase kinase-3 inhibition sensitizes pancreatic cancer cells to TRAIL-induced apoptosis. PLoS One 7, e41102.

Marchand, B., Tremblay, I., Cagnol, S., Boucher, M.-J., 2012. Inhibition of glycogen synthase kinase-3 activity triggers an apoptotic response in pancreatic cancer cells through JNK-dependent mechanisms. Carcinogenesis 33, 529–537.

Marchand, B., Arsenault, D., Raymond-Fleury, A., Boisvert, F.-M., Boucher, M.-J., 2015. Glycogen synthase Kinase-3 (GSK3) inhibition induces prosurvival autophagic signals in human pancreatic cancer cells*. J. Biol. Chem. 290, 5592–5605.

Martelli, A.M., Evangelisti, C., Paganelli, F., Chiarini, F., McCubrey, J.A., 2021. GSK-3: a multifaceted player in acute leukemias. Leukemia 1–14.

Martinsson, L., Westman, J., Hällgren, J., Ösby, U., Backlund, L., 2016. Lithium treatment and cancer incidence in bipolar disorder. Bipolar Disord. 18 (1), 33–40.

Massihnia, D., Avan, A., Funel, N., Maftouh, M., van Krieken, A., Granchi, C., Raktoe, R., Boggi, U., Aicher, B., Minutolo, F., Russo, A., Leon, L.G., Peters, G.J., Giovannetti, E., 2017. Phospho-Akt overexpression is prognostic and can be used to tailor the synergistic interaction of Akt inhibitors with gemcitabine in pancreatic cancer. J. Hematol. Oncol. 10, 9.

McCubrey, J.A., Steelman, L.S., Chappell, W.H., Abrams, S.L., Franklin, R.A., Montalto, G., Cervello, M., Libra, M., Candido, S., Malaponte, G., et al., 2012a. Ras/Raf/MEK/ERK and PI3K/PTEN/Akt/mTOR cascade inhibitors: how mutations can result in therapy resistance and how to overcome resistance. Oncotarget 3, 1068–1111.

McCubrey, J.A., Steelman, L.S., Chappell, W.H., Abrams, S.L., Franklin, R.A., Montalto, G., Cervello, M., Libra, M., Candido, S., Malaponte, G., et al., 2012b. Mutations and deregulation of Ras/Raf/MEK/ERK and PI3K/PTEN/Akt/mTOR cascades which alter therapy response. Oncotarget 3, 954–987.

McCubrey, J.A., Davis, N.M., Abrams, S.L., Montalto, G., Cervello, M., Basecke, J., Libra, M., Nicoletti, F., Cocco, L., Martelli, A.M., Steelman, L.S., 2014. Diverse roles of GSK-3: tumor promoter-tumor suppressor, target in cancer therapy. Adv. Biol. Regul. 54, 176–196.

McCubrey, J.A., Rakus, D., Gizak, A., Steelman, L.S., Abrams, S.L., Lertpiriyapong, K., Fitzgerald, T.L., Yang, L.V., Montalto, G., Cervello, M., Libra, M., Nicoletti, F., Scalisi, A., Torino, F., Fenga, C., Neri, L.M., Marmiroli, S., Cocco, L., Martelli, A.M., 2016. Effects of mutations in Wnt/β-catenin, hedgehog, Notch and PI3K pathways on GSK-3 activity-Diverse effects on cell growth, metabolism and cancer. Biochim. Biophys. Acta 1863, 2942–2976.

Meijer, L., Skaltsounis, A.L., Magiatis, P., Polychronopoulos, P., Knockaert, M., Leost, M., Ryan, X.P., Vonica, C.A., Brivanlou, A., Dajani, R., Crovace, C., Tarricone, C., Musacchio, A., Roe, S.M., Pearl, L., Greengard, P., 2003. GSK-3-selective inhibitors derived from Tyrian purple indirubins. Chem. Biol. 10, 1255–1266.

Meijer, L.L., Garajova, I., Caparello, C., Le Large, T.Y., Frampton, A., Vasile, E., Funel, N., Kazemier, G., Giovannetti, E., 2020. Plasma miR-181a-5p down-regulation predicts response and improved survival after FOLFIRINOX in pancreatic ductal adenocarcinoma. Ann Surgery. 271, 1137–1147.

Melisi, D., Xia, Q., Paradiso, G., Ling, J., Moccia, T., Carbone, C., Budillon, A., Abbruzzese, J.L., Chiao, P.J., 2011. Modulation of pancreatic cancer chemoresistance by inhibition of TAK1. J. Natl. Cancer Inst. 103, 1190–1204.

Meng, Q., Shi, S., Liang, C., et al., 2018. Abrogation of glutathione peroxidase-1 drives EMT and chemoresistance in pancreatic cancer by activating ROS-mediated Akt/GSK3β/Snail signaling. Oncogene 37, 5843–5857.

Miyashita, K., Nakada, M., Shakoori, A., Ishigaki, Y., Shimasaki, T., Motoo, Y., Kawakami, K., Minamoto, T., 2009. An emerging strategy for cancer treatment targeting aberrant glycogen synthase kinase 3 beta. Anticancer Agents Med. Chem. 9, 1114–1122.

Mora, A., Sabio, G., Risco, A.M., Cuenda, A., Alonso, J.C., Soler, G., Centeno, F., 2002. Lithium blocks the PKB and GSK3 dephosphorylation induced by ceramide through protein phosphatase-2A. Cell. Signal. 14, 557–562.

Nagini, S., Sophia, J., Mishra, R., 2019. Glycogen synthase kinases: moonlighting proteins with theranostic potential in cancer. Semin. Cancer Biol. 56, 25–36.

Namba, T., Kodama, R., Moritomo, S., Hoshino, T., Mizushima, T., 2015. Zidovudine, an anti-viral drug, resensitizes gemcitabine-resistant pancreatic cancer cells to gemcitabine by inhibition of the Akt-GSK3β-Snail pathway. Cell Death Dis. 6, e1795.

NCT01287520, 2018. Eli Lilly and Company. Phase 1 Dose Escalation Study of LY2090314 in Patients With Advanced or Metastatic Cancer in Combination With Pemetrexed and Carboplatin. https://clinicaltrials.gov/ct2/show/NCT01287520.

NCT01632306, 2019. Eli Lilly and Company. Phase I/II Study of LY2090314 and Chemotherapy in Metastatic Pancreatic Cancer Patients With Metastases Amenable to Biopsy. https://clinicaltrials.gov/ct2/show/NCT01632306.

NCT03678883, 2021. Actuate Therapeutics Inc. Phase 1/2 Study of 9-ING-41, a Glycogen Synthase Kinase-3 Beta (GSK-3β) Inhibitor, as a Single Agent and Combined With Chemotherapy, in Patients With Refractory Hematologic Malignancies or Solid Tumors. https://clinicaltrials.gov/ct2/show/NCT03678883.

Okamoto, T., Sanda, T., Asamitsu, K., 2007. NF-kappa B signaling and carcinogenesis. Curr. Pharm. Des. 13, 447–462.

Ougolkov, A.V., Fernandez-Zapico, M.E., Savoy, D.N., Urrutia, R.A., Billadeau, D.D., 2005. Glycogen synthase kinase-3beta participates in nuclear factor kappaB-mediated gene transcription and cell survival in pancreatic cancer cells. Cancer Res. 65, 2076–2081.

Ougolkov, A.V., Fernandez-Zapico, M.E., Bilim, V.N., Smyrk, T.C., Chari, S.T., Billadeau, D.D., 2006. Aberrant nuclear accumulation of glycogen synthase kinase-3beta in human pancreatic cancer: association with kinase activity and tumor dedifferentiation. Clin. Cancer Res. 12, 5074–5081.

Pasquali, L., Busceti, C.L., Fulceri, F., Paparelli, A., Fornai, F., 2010. Intracellular pathways underlying the effects of lithium. Behav. Pharmacol. 21, 473–492.

Peng, Z., Ji, Z., Mei, F., Lu, M., Ou, Y., Cheng, X., 2013. Lithium inhibits tumorigenic potential of PDA cells through targeting Hedgehog-GLI signaling pathway. PLoS One 8, e61457.

Phiel, C.J., Klein, P.S., 2001. Molecular targets of lithium action. Annu. Rev. Pharmacol. Toxicol. 41, 789–813.

Pusceddu, S., Ghidini, M., Torchio, M., Corti, F., Tomasello, G., Niger, M., Prinzi, N., Nichetti, F., Coinu, A., Di Bartolomeo, M., Cabiddu, M., Passalacqua, R., de Braud, F., Petrelli, F., 2019. Comparative effectiveness of gemcitabine plus nab-paclitaxel and FOLFIRINOX in the first-line setting of metastatic pancreatic cancer: a systematic review and meta-analysis. Cancers 11.

Rahib, L., Smith, B.D., Aizenberg, R., Rosenzweig, A.B., Fleshman, J.M., Matrisian, L.M., 2014. Projecting cancer incidence and deaths to 2030: the unexpected burden of thyroid, liver, and pancreas cancers in the United States. Cancer Res. 74, 2913–2921.

Randazzo, O., Papini, F., Mantini, G., Gregori, A., Parrino, B., Liu, D.S.K., Cascioferro, S., Carbone, D., Peters, G.J., Frampton, A.E., Garajova, I., Giovannetti, E., 2020. "Open Sesame?": impact of biomarker role and molecular mechanisms influencing the human equilibrative nucleoside transporter-1 in the uptake and cytotoxicity of gemcitabine in pancreatic cancer. Cancers 12, 3206.

Riobó, N.A., Lu, K., Ai, X., Haines, G.M., Emerson, C.P., 2006. Phosphoinositide 3-kinase and Akt are essential for Sonic Hedgehog signaling. Proc. Natl. Acad. Sci. U. S. A. 103, 4505–4510.

Rizzieri, D.A., Cooley, S., Odenike, O., Moonan, L., Chow, K.H., Jackson, K., Wang, X., Brail, L., Borthakur, G., 2016. An open-label phase 2 study of glycogen synthase kinase-3 inhibitor LY2090314 in patients with acute leukemia. Leuk. Lymphoma 57, 1800–1806.

Ryves, W.J., Harwood, A.J., 2001. Lithium inhibits glycogen synthase kinase-3 by competition for magnesium. Biochem. Biophys. Res. Commun. 280, 720–725.

Saiki, Y., Yoshino, Y., Fujimura, H., Manabe, T., Kudo, Y., Shimada, M., Mano, N., Nakano, T., Lee, Y., Shimizu, S., Oba, S., Fujiwara, S., Shimizu, H., Chen, N., Nezhad, Z.K., Jin, G., Fukushige, S., Sunamura, M., Ishida, M., Motoi, F., Egawa, S., Unno, M., Horii, A., 2012. DCK is frequently inactivated in acquired gemcitabine-resistant human cancer cells. Biochem. Biophys. Res. Commun. 421, 98–104.

Santoro, R., Zanotto, M., Simionato, F., Zecchetto, C., Merz, V., Cavallini, C., Piro, G., Sabbadini, F., Boschi, F., Scarpa, A., Melisi, D., 2020. Modulating TAK1 expression inhibits YAP and TAZ oncogenic functions in pancreatic cancer. Mol. Cancer Ther. 19, 247–257.

Sarantis, P., Koustas, E., Papadimitropoulou, A., Papavassiliou, A.G., Karamouzis, M.V., 2020. Pancreatic ductal adenocarcinoma: treatment hurdles, tumor microenvironment and immunotherapy. World J. Gastrointest. Oncol. 12, 173–181.

Saraswati, A.P., Ali Hussaini, S.M., Krishna, N.H., Babu, B.N., Kamal, A., 2018. Glycogen synthase kinase-3 and its inhibitors: potential target for various therapeutic conditions. Eur. J. Med. Chem. 144, 843–858.

Seino, T., Kawasaki, S., Shimokawa, M., Tamagawa, H., Toshimitsu, K., Fujii, M., Ohta, Y., Matano, M., Nanki, K., Kawasaki, K., Takahashi, S., Sugimoto, S., Iwasaki, E., Takagi, J., Itoi, T., Kitago, M., Kitagawa, Y., Kanai, T., Sato, T., 2018. Human pancreatic tumor organoids reveal loss of stem cell niche factor dependence during disease progression. Cell Stem Cell 22, 454-467.e6.

Shimasaki, T., Ishigaki, Y., Nakamura, Y., Takata, T., Nakaya, N., Nakajima, H., Sato, I., Zhao, X., Kitano, A., Kawakami, K., Tanaka, T., Takegami, T., Tomosugi, N., Minamoto, T., Motoo, Y., 2012. Glycogen synthase kinase 3β inhibition sensitizes pancreatic cancer cells to gemcitabine. J. Gastroenterol. 47, 321–333.

Shin, S., Wolgamott, L., Yu, Y., Blenis, J., Yoon, S.-O., 2011. Glycogen synthase kinase (GSK)-3 promotes p70 ribosomal protein S6 kinase (p70S6K) activity and cell proliferation. Proc. Natl. Acad. Sci. U. S. A. 108, E1204–1213.

Shukla, S.K., Purohit, V., Mehla, K., Gunda, V., Chaika, N.V., Vernucci, E., King, R.J., Abrego, J., Goode, G.D., Dasgupta, A., Illies, A.L., Gebregiworgis, T., Dai, B., Augustine, J.J., Murthy, D., Attri, K.S., Mashadova, O., Grandgenett, P.M., Powers, R., Ly, Q.P., Lazenby, A.J., Grem, J.L., Yu, F., Matés, J.M., Asara, J.M., Kim, J.W., Hankins, J.H., Weekes, C., Hollingsworth, M.A., Serkova, N.J., Sasson, A. R., Fleming, J.B., Oliveto, J.M., Lyssiotis, C.A., Cantley, L.C., Berim, L., Singh, P.K., 2017. MUC1 and HIF-1alpha signaling crosstalk induces anabolic glucose metabolism to impart gemcitabine resistance to pancreatic cancer. Cancer Cell 32, 71-87.e7.

Siegel, R.L., Miller, K.D., Fuchs, H.E., Jemal, A., 2021. Cancer statistics, 2021. CA Cancer J. Clin. 71, 7–33.

Singh, T.J., Zaidi, T., Grundke-Iqbal, I., Iqbal, K., 1995. Modulation of GSK-3-catalyzed phosphorylation of microtubule-associated protein tau by non-proline-dependent protein kinases. FEBS Lett. 358, 4–8.

Song, E.Y., Palladinetti, P., Klamer, G., Ko, K.H., Lindeman, R., O'Brien, T.A., Dolnikov, A., 2010. Glycogen synthase kinase–3β inhibitors suppress leukemia cell growth. Exp. Hematol. 38 (908-921) e1.

Stamos, J.L., Chu, M.L.-H., Enos, M.D., Shah, N., Weis, W.I., 2014. Structural basis of GSK-3 inhibition by N-terminal phosphorylation and by the Wnt receptor LRP6. eLife 3, e01998.

Sun, A., Li, C., Chen, R., Huang, Y., Chen, Q., Cui, X., Liu, H., Thrasher, J.B., Li, B., 2016. GSK-3β controls autophagy by modulating LKB1-AMPK pathway in prostate cancer cells. Prostate 76, 172–183.

Supadmanaba, I.G.P., Comandatore, A., Morelli, L., Giovannetti, E., Lagerweij, T., 2021. Organotypic-liver slide culture systems to explore the role of extracellular vesicles in pancreatic cancer metastatic behavior and guide new therapeutic approaches. Expert Opin. Drug Metab. Toxicol. 21, 1–10.

Sutherland, C., 2011. What are the bona fide GSK3 substrates? Int. J. Alzheimers Dis. 2011, 505607.

ter Haar, E., Coll, J.T., Austen, D.A., Hsiao, H.M., Swenson, L., Jain, J., 2001. Structure of GSK3beta reveals a primed phosphorylation mechanism. Nat. Struct. Biol. 8, 593–596.

Tran, F.H., Zheng, J.J., 2017. Modulating the wnt signaling pathway with small molecules. Protein Sci. Publ. Protein Soc. 26, 650–661.

Uehara, M., Domoto, T., Takenaka, S., Bolidong, D., Takeuchi, O., Miyashita, T., Minamoto, T., 2020. Glycogen synthase kinase-3β participates in acquired resistance to gemcitabine in pancreatic cancer. Cancer Sci. 111, 4405–4416.

Vulpetti, A., Crivori, P., Cameron, A., Bertrand, J., Brasca, M.G., D'Alessio, R., Pevarello, P., 2005. Structure-based approaches to improve selectivity: CDK2-GSK3beta binding site analysis. J. Chem. Inf. Model. 45, 1282–1290.

Walz, A., Ugolkov, A., Chandra, S., Kozikowski, A., Carneiro, B.A., O'Halloran, T.V., Giles, F.J., Billadeau, D.D., Mazar, A.P., 2017. Molecular pathways: revisiting glycogen synthase Kinase-3β as a target for the treatment of cancer. Clin. Cancer Res. Off. J. Am. Assoc. Cancer Res. 23, 1891–1897.

Waters, A.M., Channing, D.J., 2018. KRAS: the critical driver and therapeutic target for pancreatic cancer. Cold SpringHarb. Perspect. Med. 8, a031435.

Webster, M.T., Rozycka, M., Sara, E., Davis, E., Smalley, M., Young, N., Dale, T.C., Wooster, R., 2000. Sequence variants of the axin gene in breast, colon, and other cancers: an analysis of mutations that interfere with GSK3 binding. Genes Chromosomes Cancer 28, 443–453.

Wilson, W., Baldwin, A.S., 2008. Maintenance of constitutive IkappaB kinase activity by glycogen synthase kinase-3alpha/beta in pancreatic cancer. Cancer Res. 68, 8156–8163.

Woodgett, J.R., 1990. Molecular cloning and expression of glycogen synthase kinase-3/factor A. EMBO J. 9, 2431–2438.

Wu, D., Pan, W., 2010. GSK3: a multifaceted kinase in Wnt signaling. Trends Biochem. Sci. 35, 161–168.

Xia, Y., Shen, S., Verma, I.M., 2014. NF-κB, an active player in human cancers. Cancer Immunol. Res. 2, 823–830.

Xie, S., Wang, C., 2017. GSK-3 inhibition suppresses lung cancer cell survival, metastasis and proliferation through down-regulation the phosphorylation sites of CAP1. Eur. Respir. J. 50.

Xu, C., Kim, N.-G., Gumbiner, B.M., 2009. Regulation of protein stability by GSK3 mediated phosphorylation. Cell Cycle Georget. Tex 8, 4032–4039.

Yang, S., Kimmelman, A.C., 2011. A critical role for autophagy in pancreatic cancer. Autophagy 7, 912–913.

Yang, S., Wang, X., Contino, G., Liesa, M., Sahin, E., Ying, H., Bause, A., Li, Y., Stommel, J.M., Dell'antonio, G., Mautner, J., Tonon, G., Haigis, M., Shirihai, O.S., Doglioni, C., Bardeesy, N., Kimmelman, A.C., 2011. Pancreatic cancers require autophagy for tumor growth. Genes Dev. 25, 717–729.

Yoneyama, H., Takizawa-Hashimoto, A., Takeuchi, O., Watanabe, Y., Atsuda, K., Asanuma, F., Yamada, Y., Suzuki, Y., 2015. Acquired resistance to gemcitabine and cross-resistance in human pancreatic cancer clones. Anticancer Drugs 26, 90–100.

Yoshino, Y., Ishioka, C., 2015. Inhibition of glycogen synthase kinase-3 beta induces apoptosis and mitotic catastrophe by disrupting centrosome regulation in cancer cells. Sci. Rep. 5, 13249.

Yu, M., Ting, D.T., Stott, S.L., et al., 2012. RNA sequencing of pancreatic circulating tumour cells implicates WNT signalling in metastasis. Nature 487, 510–513.

Zamek-Gliszczynski, M.J., Abraham, T.L., Alberts, J.J., Kulanthaivel, P., Jackson, K.A., Chow, K.H., McCann, D.J., Hu, H., Anderson, S., Furr, N.A., Barbuch, R.J., Cassidy, K.C., 2013. Pharmacokinetics, metabolism, and excretion of the glycogen synthase kinase-3 inhibitor LY2090314 in rats, dogs, and humans: a case study in rapid clearance by extensive metabolism with low circulating metabolite exposure. Drug Metab. Dispos. Biol. Fate Chem. 41, 714–726.

Zeng, S., Pöttler, M., Lan, B., Grützmann, R., Pilarsky, C., Yang, H., 2019. Chemoresistance in pancreatic cancer. Int. J. Mol. Sci. 20.

Zhang, F., Phiel, C.J., Spece, L., Gurvich, N., Klein, P.S., 2003. Inhibitory phosphorylation of glycogen synthase kinase-3 (GSK-3) in response to lithium. Evidence for autoregulation of GSK-3. J. Biol. Chem. 278, 33067–33077.

Zhang, J.-S., Koenig, A., Harrison, A., Ugolkov, A.V., Fernandez-Zapico, M.E., Couch, F. J., Billadeau, D.D., 2011. Mutant K-Ras increases GSK-3β gene expression via an ETS-p300 transcriptional complex in pancreatic cancer. Oncogene 30, 3705–3715.

Zhang, J.-S., Herreros-Villanueva, M., Koenig, A., de Narvajas, A.A., Gomez, T.S., Meng, X., Bujanda, L., Ellenrieder, V., Li, X.K., Kaufmann, S.H., Billadeau, D.D., 2014. Differential activity of GSK-3 isoforms regulates NF-κB and TRAIL- or TNFα induced apoptosis in pancreatic cancer cells. Cell Death Dis. 5, e1142.

Zhang, X., Castanotto, D., Nam, S., Horne, D., Stein, C., 2017. 6BIO enhances oligonucleotide activity in cells: a potential combinatorial anti-androgen receptor therapy in prostate cancer cells. Mol. Ther. 25, 79–91.

Zhitomirsky, B., Assaraf, Y.G., 2015. Lysosomal sequestration of hydrophobic weak base chemotherapeutics triggers lysosomal biogenesis and lysosome-dependent cancer multidrug resistance. Oncotarget 6 (January (2)), 1143–1156. https://doi.org/10.18632/oncotarget.2732.

Zhitomirsky, B., Assaraf, Y.G., 2016. Lysosomes as mediators of drug resistance in cancer. Drug Resist. Updat. 24 (January), 23–33.

Zhitomirsky, B., Yunaev, A., Kreiserman, R., Kaplan, A., Stark, M., Assaraf, Y.G., 2018. Lysosomotropic drugs activate TFEB via lysosomal membrane fluidization and consequent inhibition of mTORC1 activity. Cell Death Dis. 9 (December (12)), 1191.

Zhou, B., Xu, J.W., Cheng, Y.G., Gao, J.Y., Hu, S.Y., Wang, L., Zhan, H.X., 2017. Early detection of pancreatic cancer: where are we now and where are we going? Int. J. Cancer 141, 231–241.

Zhu, H., Lo, H.-W., 2010. The human glioma-associated oncogene homolog 1 (GLI1) family of transcription factors in gene regulation and diseases. Curr. Genomics 11, 238–245.

Chapter 4

A new oxadiazole-based topsentin derivative modulates CDK1 expression and exerts cytotoxic effects on PDAC cancer cells

Pecoraro, C., Parrino, B., Cascioferro, S., Puerta, A., Avan, A., Peters, G.J., Diana, P., Giovannetti, E., Carbone D.

Molecules 2021, 27(1):19

molecules

MDPI

Article

A New Oxadiazole-Based Topsentin Derivative Modulates Cyclin-Dependent Kinase 1 Expression and Exerts Cytotoxic Effects on Pancreatic Cancer Cells

Camilla Pecoraro [1,2], Barbara Parrino [1], Stella Cascioferro [1], Adrian Puerta [2,3], Amir Avan [2,4], Godefridus J. Peters [2,5], Patrizia Diana [1], Elisa Giovannetti [2,6,*] and Daniela Carbone [1,*]

[1] Dipartimento di Scienze e Tecnologie Biologiche Chimiche e Farmaceutiche (STEBICEF), Università degli Studi di Palermo, Via Archirafi 32, 90123 Palermo, Italy; camilla.pecoraro@unipa.it (C.P.); barbara.parrino@unipa.it (B.P.); stellamaria.cascioferro@unipa.it (S.C.); patrizia.diana@unipa.it (P.D.)
[2] Department of Medical Oncology, Cancer Center Amsterdam, Amsterdam UMC, VU University Medical Center (VUmc), De Boelelaan 1117, 1081 HV Amsterdam, The Netherlands; apuertaa@ull.edu.es (A.P.); AvanA@mums.ac.ir (A.A.); gj.peters@amsterdamumc.nl (G.J.P.)
[3] BioLab, Instituto Universitario de Bio-Orgánica "Antonio González" (IUBO-AG), Universidad de La Laguna, c/Astrofísico Francisco Sánchez 2, 38206 La Laguna, Spain
[4] Metabolic Syndrome Research Center, Mashhad University of Medical Science, Mashhad 91886-17871, Iran
[5] Department of Biochemistry, Medical University of Gdansk, 80-210 Gdansk, Poland
[6] Cancer Pharmacology Laboratory, Fondazione Pisana per la Scienza, Via Ferruccio Giovannini 13, San Giuliano Terme, 56017 Pisa, Italy
* Correspondence: e.giovannetti@amsterdamumc.nl (E.G.); daniela.carbone@unipa.it (D.C.)

check for updates

Citation: Pecoraro, C.; Parrino, B.; Cascioferro, S.; Puerta, A.; Avan, A.; Peters, G.J.; Diana, P.; Giovannetti, E.; Carbone, D. A New Oxadiazole-Based Topsentin Derivative Modulates Cyclin-Dependent Kinase 1 Expression and Exerts Cytotoxic Effects on Pancreatic Cancer Cells. *Molecules* **2022**, *27*, 19. https://doi.org/10.3390/molecules27010019

Academic Editors: Diego Muñoz-Torrero, Simona Rapposelli, Michael Gütschow, Maria João Matos, Maria Emília de Sousa and Luciano Saso

Received: 14 November 2021
Accepted: 14 December 2021
Published: 21 December 2021

Publisher's Note: MDPI stays neutral with regard to jurisdictional claims in published maps and institutional affiliations.

Copyright: © 2021 by the authors. Licensee MDPI, Basel, Switzerland. This article is an open access article distributed under the terms and conditions of the Creative Commons Attribution (CC BY) license (https://creativecommons.org/licenses/by/4.0/).

Abstract: Pancreatic ductal adenocarcinoma (PDAC) is a highly lethal form of cancer characterized by drug resistance, urging new therapeutic strategies. In recent years, protein kinases have emerged as promising pharmacological targets for the treatment of several solid and hematological tumors. Interestingly, cyclin-dependent kinase 1 (CDK1) is overexpressed in PDAC tissues and has been correlated to the aggressive nature of these tumors because of its key role in cell cycle progression and resistance to the induction of apoptosis. For these reasons, CDK1 is one of the main causes of chemoresistance, representing a promising pharmacological target. In this study, we report the synthesis of new 1,2,4-oxadiazole compounds and evaluate their ability to inhibit the cell growth of PATU-T, Hs766T, and HPAF-II cell lines and a primary PDAC cell culture (PDAC3). Compound **6b** was the most active compound, with IC_{50} values ranging from 5.7 to 10.7 μM. Molecular docking of **6b** into the active site of CDK1 showed the ability of the compound to interact effectively with the adenosine triphosphate binding pocket. Therefore, we assessed its ability to induce apoptosis (which increased 1.5- and 2-fold in PATU-T and PDAC3 cells, respectively) and to inhibit CDK1 expression, which was reduced to 45% in Hs766T. Lastly, compound **6b** passed the ADME prediction, showing good pharmacokinetic parameters. These data demonstrate that **6b** displays cytotoxic activity, induces apoptosis, and targets CDK1, supporting further studies for the development of similar compounds against PDAC.

Keywords: 1,2,4-oxadiazole; marine alkaloids; topsentin; CDK1 inhibitor; pancreatic cancer; PDAC; antiproliferative; apoptosis

1. Introduction

Pancreatic ductal adenocarcinoma (PDAC), the most common type of pancreatic cancer, is a highly lethal form of cancer, for which surgery is the only curative treatment [1]. However, only a small percentage of PDACs are eligible for resection. Polychemotherapy regimens, such as FOLFIRINOX (folinic acid, fluorouracil, irinotecan, and oxaliplatin) or gemcitabine plus nab-paclitaxel, are the standard therapies for most PDAC patients but are characterized by a high rate of toxicity and modest survival benefit, since almost all PDAC patients become or are already drug resistant [2–4]. The causes of such drug resistance are many, and recent omics studies, including phosphoproteomics, have shown aberrations in key functional signaling that could hopefully be used to identify new therapeutic strategies [5].

In recent years, particular attention has been paid to protein kinases, which emerged as promising pharmacological targets given their role in regulating fundamental cellular processes. Since the first kinase inhibitor, imatinib, was approved for the treatment of chronic myeloid leukemia in 2001, the Food and Drug Administration has approved more than 50 small-molecule kinase inhibitors, of which the majority are tyrosine kinase inhibitors, while some are serine/threonine kinase inhibitors [6–9].

Cyclin-dependent kinase 1 (CDK1) is a serine/threonine kinase which plays a crucial role in regulating the cell cycle and has recently emerged as a promising target for the treatment of PDAC. Indeed, CDK1 overexpression was correlated with the progression of this type of cancer [10,11]. Under physiological conditions, CDK1 tightly regulates the progression of the cell cycle. However, abnormal expression of CDK1 determines cell replication even in case of DNA damage, resulting in the proliferation of cancer cells. Moreover, the activity of CDK1 is strongly regulated by the gene *TP53*, which is mutated in 70% of PDAC [12]. Together, these observations suggest the potential of CDK1 inhibition as a novel promising strategy to treat PDAC. They prompted us to synthesize new bioactive compounds against this target.

Considering the importance of marine microenvironments as an important resource of bioactive molecules containing different heterocyclic rings and different heteroatoms, our research group synthesized a number of small molecules obtained through the structural manipulation of nortopsentins **1**, natural bis-indolyl alkaloids isolated from deep-sea sponges (*Spongsorites ruetzleri*), which are characterized by significant antiproliferative activity against the P388 murine leukemia cell line [13]. In particular, we produced many derivatives in which the modification of nortopsentin involved the central imidazole ring, which was replaced by several five-membered heterocycles, while an indole moiety was substituted with an azaindole portion. These compounds had a significantly improved antiproliferative activity against a wide range of tumor cell lines, with half of the maximal inhibitory concentration (IC_{50}) in the micro-submicromolar range [14,15]. In particular, thiazole nortopsentin derivatives **2**, determined CDK1 inhibition with IC_{50} values of 0.64–0.89 μM, which is comparable to the values reported for roscovitine and purvalanol A, two well-known CDK1 inhibitors. Moreover, a more recently synthesized indolyl-7-azaindolyl thiazole compound demonstrated its ability to reduce colorectal cancer stem cells (CR-CSCs), showing a synergistic effect with standard chemotherapy, such as oxaliplatin and 5-fluorouracil, as well as the ability of eradicating CR-CSCs when combined with the CHK1 inhibitor Rabusertinib [16]. Considering that, among nitrogen heterocycles, indole and oxadiazole rings are found in many molecules with significant biological activity, and especially antitumor activity [17–19], we also synthesized new 1,2,4-oxadiazole nortopsentin analogs **3**, which were screened for their antiproliferative activity [14]. Then, we further investigated the bis-indolyl marine alkaloid topsentin **4**, characterized by the presence of a carbonyl spacer group, which gives greater flexibility to the molecule to better adapt to the ATP-binding site of CDK1 and represents a hydrogen bonding acceptor, which could interact with the amino acid residues of the active site of CDK1. Topsentin was extracted from the sponge *Topsentia genitrix* and showed in vitro cytotoxic activity against P-388 murine tumor cells, with an IC_{50} of 8.8 μM, as well as at micromolar concentrations against several human cancer cell lines. Lastly, considering the promising results shown by [3-(1*H*-Indol-3-yl)-[1,2,4]oxadiazol-5-yl]-(1-methyl-1*H*-pyrrolo[2,3-*b*]pyridin-3-yl)-methanones **5** on PDAC cancer cell lines [20], we decided to synthesize a new series of topsentin analogs of the type **6** shown in Scheme 1, in which the imidazole central ring was replaced by 1,2,4-oxadiazole moiety, and one indole portion was converted into 7-azaindole ring (Scheme 1). In the present study, we also report the cytotoxic activity of these new derivatives against PDAC cells as well as their capability to inhibit CDK1 and to induce apoptosis.

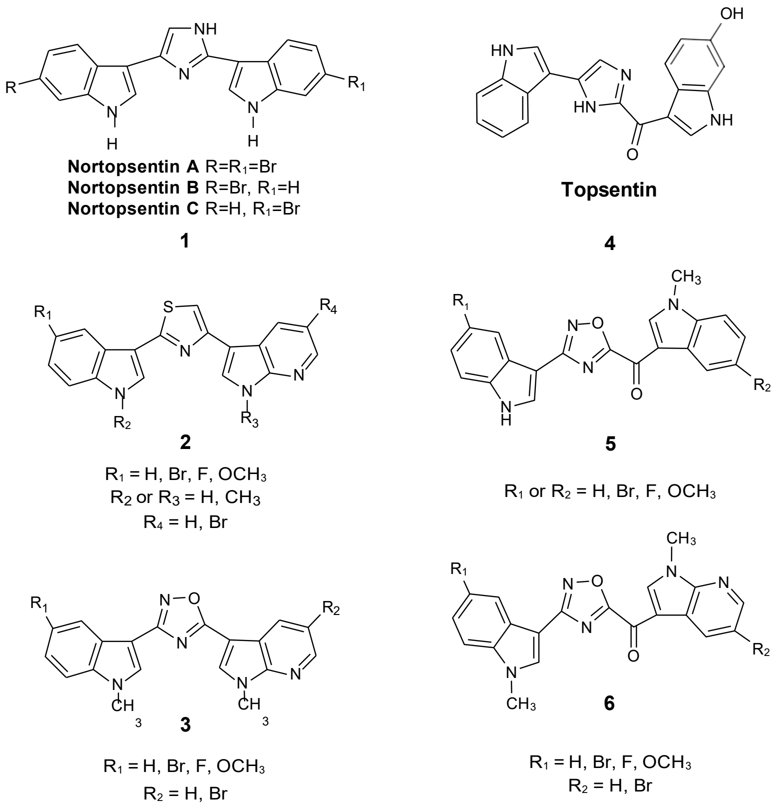
Nortopsentin A R=R$_1$=Br
Nortopsentin B R=Br, R$_1$=H
Nortopsentin C R=H, R$_1$=Br
1
Topsentin
4
2
R$_1$ = H, Br, F, OCH$_3$
R$_2$ or R$_3$ = H, CH$_3$
R$_4$ = H, Br
5
R$_1$ or R$_2$ = H, Br, F, OCH$_3$
3
R$_1$ = H, Br, F, OCH$_3$
R$_2$ = H, Br
6
R$_1$ = H, Br, F, OCH$_3$
R$_2$ = H, Br

Scheme 1. Chemical structures of nortopsentin **1** and topsentin **4** alkaloids and their derivatives **2**,**3** and **5**,**6**.

2. Results and Discussion

2.1. Chemistry

A new series of new 7-azaindolyl oxadiazole compounds **6a–f** was efficiently synthesized as described in Scheme 2.

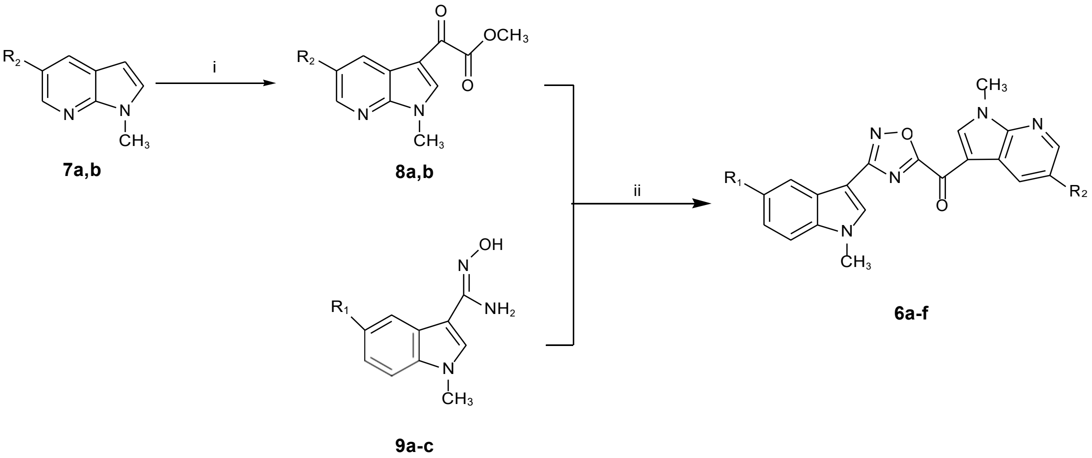
i
ii
7a,b
8a,b
9a-c
6a-f

Scheme 2. Synthesis of (1-methyl-1*H*-pyrrolo[2,3-*b*]pyridin-3-yl)-[3-(1-methyl-1*H*-indol-3-yl)-[1,2,4]oxadiazol-5-yl]-methanones (**6a–f**). Reagents and conditions: (i) oxalyl chloride, diethyl ether, r.t., overnight, then −65 °C, sodium methoxide solution 25 wt. % in methanol, r.t., 2 h, 62–73%; (ii) dimethylsulfoxide, r.t., 30 min. 60–85%.

The key intermediates, (1-methyl-1*H*-pyrrolo[2,3-*b*]pyridine-3-yl)-oxo-acetic acid methyl esters **8a**,**b**, were prepared in good yield (62% and 73%, respectively) by keeping the corresponding methylindole precursor of the type **7a**,**b**, synthesized as previously described [14], with an excess of oxalyl chloride. The resulting non-isolated acetyl chloride intermediate was then converted in situ into methyl esters **8a,b** using a sodium methoxide solution 25 wt. % in methanol.

The latter compounds were subjected to a coupling reaction with carboxamidines **9a–c**, synthesized in turn from the corresponding 1-methyl-1*H*-indoles, converted to their carbonitriles, and had a successive reaction with hydroxylamine hydrochloride, as previously reported [21].

The azaindole substituent of the original oxo-acetic acid methyl ester is in position C(5), and the oxadiazole ring is obtained by means of the [4+1] synthetic route, as previously explained [21]. The coupling reaction, performed in anhydrous dimethylsulfoxide (DMSO) at r.t. for 30 min, proceeded without the isolation of an acylamidoxime intermediate, yielding, after purification by chromatography, the desired 7-azaindolyl oxadiazoles **6a–f** (Scheme 2) in yields ranging from 60% to 85% (Table 1).

Table 1. Yields of the synthesis of **6a–f**; (1-Methyl-1*H*-pyrrolo[2,3-*b*]pyridin-3-yl)-[3-(1-methyl-1*H*-indol-3-yl)-[1,2,4]oxadiazol-5-yl]-methanones.

Compound	R_1	R_2	Yield (%)
6a	H	Br	60%
6b	F	Br	67%
6c	OCH_3	Br	85%
6d	H	H	77%
6e	F	H	68%
6f	OCH_3	H	80%

2.2. *Biological Studies*

2.2.1. Antiproliferative Activity of the New 1,2,4-Oxadiazole Compounds **6a–f** against PDAC3, PATU-T, Hs766T, and HPAF-II PDAC Cells

The in vitro antiproliferative activity of the new 7-azaindolyl oxadiazole compounds **6a–f** was initially evaluated by the sulforhodamine-B assay (SRB) against PATU-T immortalized PDAC cell line. All compounds were tested at three different concentrations of 50.0, 5.0, and 0.5 μM.

Among the tested compounds, derivative **6b** showed the highest potency, exhibiting an IC_{50} value of 10.7 μM, while other compounds showed minimal cytotoxic effect with IC_{50s} > 20 μM. In order to extend the antiproliferative evaluation of compound **6b** towards other pancreatic cells, we assessed the inhibition of cell growth in primary pancreatic cell lines including both the immortalized HPAF-II and Hs766T cancer cell lines and the primary culture PDAC3. Interestingly, compound **6b** was active against all these PDAC cells. The best result was observed against Hs766T, with an IC_{50} value of 5.7 μM. However, the compound **6b** was also able to inhibit the viability of PDAC3 and HPAF-II with IC_{50} values of 6.9 and 9.8 μM, respectively (Table 2). A representative curve of cell growth inhibition of **6b** in PDAC3 is reported in Figure 1. In parallel experiments we also evaluated the IC_{50} of the conventional anticancer drug gemcitabine, which was used as positive control and presented IC_{50} value below 1 μM. This result was in agreement with previous studies [22–24].

Table 2. IC_{50s} of **6b** against Hs766T, HPAF-II, PDAC3, and PATU-T cells.

IC_{50} [a] (μM) ± SEM		
Compound	**Cell Line**	**IC_{50} ± SEM**
6b	Hs766T	5.7 ± 0.60
	PDAC3	6.9 ± 0.25
	HPAF-II	9.8 ± 0.70
	PATU-T	10.7 ± 0.16

[a] Values (in μM) are reported as means ± SEM (Standard Error of the Mean) of three separate experiments.

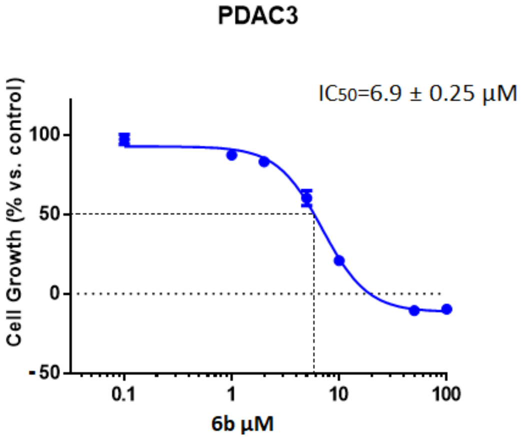

Figure 1. Representative growth inhibition curve of PDAC3 PDAC primary cells, treated for 72 h with the compound **6b**. Points: mean values obtained from three independent experiments; bars: SEM.

From structure activity relationship (SAR) analysis on compounds of type **5** and **6** (Scheme 1), we observed that the introduction of a nitrogen atom at position 7 of the indole moiety does not significantly improve the antiproliferative activity, as well as the presence of a methyl group at the indole N-atom. Conversely, in accordance with previous results concerning [3-(1*H*-indol-3-yl)-1,2,4-oxadiazol-5-yl](1-methyl-1*H*-indol-3-yl) methanones **5** [20], in type **6** derivatives the presence of a halogen atom, e.g., fluorine or bromine, at 5 position of the indole or 7-azaindole ring seems to be essential for the cytotoxic activity.

2.2.2. Modulation of CDK1 Expression by ELISA

Considering the promising results obtained with compound **6b**, further studies were carried out to investigate its mechanism of action. In order to evaluate whether compound **6b** was able to reduce CDK1 expression, a specific ELISA assay was performed in the three immortalized PDAC cell lines, i.e., Hs766T, HPAF-II, and PATU-T, as well as in the PDAC3 cells. These cell models were treated with 10 μM **6b**. As shown in Figure 2, we observed a reduction of CDK1 expression compared to control cells, supporting the potential role of the inhibition of CDK1 in the mechanism of action of this compound.

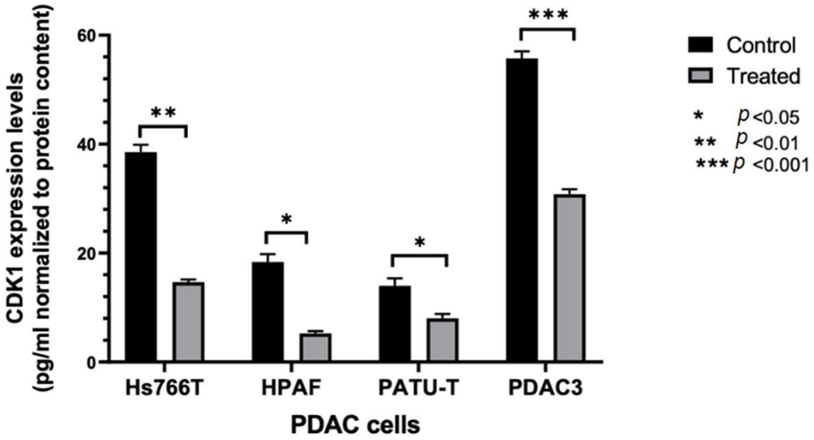

Figure 2. ELISA-based quantitation of CDK1 expression in PDAC cells following a 24 h exposure to DMSO (control) or to 10 μM of compound **6b**. CDK1 expression was quantified using Human cyclin-dependent kinase 1 (CDK1) ELISA Kit according to the manufacturer's instructions. Columns: mean; bars: SEM (n = 3). *: $p < 0.05$, **: $p < 0.01$, ***: $p < 0.001$, significantly different compared with control.

2.2.3. Induction of Apoptosis

Considering that a number of previous studies reported that the inhibition of CDK1 activity contributes to the initiation of apoptotic process [25–27], we then evaluated the effect of **6b** on the induction of apoptosis in pancreatic cancer cells. For this purpose, we measured the externalization of the plasma membrane phosphatidylserine, a reliable marker of cell apoptosis, which was quantified by measurement of fluorescence of annexin V by spectrophotometric and microscopy assays.

These experiments were performed on the most sensitive and most resistant models, i.e., Hs766T and PATU-T cells. After 24 h of treatment with 2*IC_{50} of **6b**, a significant increase in the portion of apoptotic cells was observed. In particular, we noticed that the percentages of apoptotic Hs766T and PATU-T cells were comparable to the number of cells that underwent apoptosis after treatment with gemcitabine (at 2*IC_{50}), which is a standard drug for the treatment of PDAC (Figure 3).

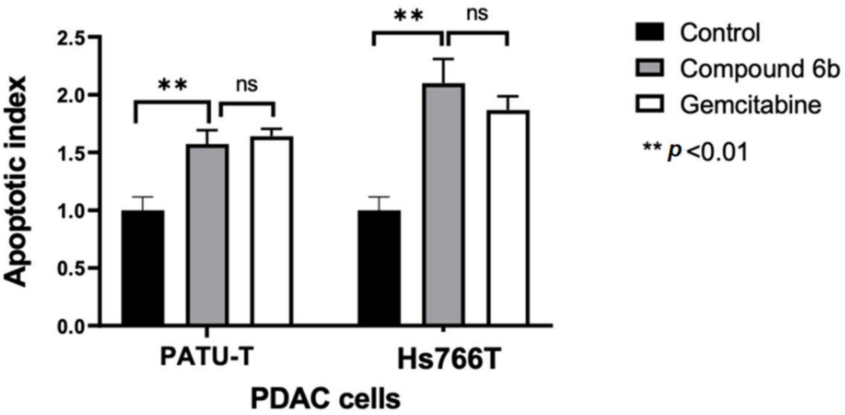

Figure 3. Effects of compound **6b** on apoptosis induction in PATU-T and Hs766T pancreatic cancer cells. The apoptotic index was calculated by evaluating the annexin V-FITC fold change compared with control cells after 24 h treatment. Gemcitabine was used as a positive control. Columns: mean; bars: SEM (*n* = 3). **: $p < 0.01$, significantly different compared with control; ns: not significant.

2.2.4. Molecular Modeling

A potential binding mode for the most active compound **6b** within the ATP binding site of CDK1 (PDB ID: 4YC6) is depicted in Figure 4. **6b** is placed in a nucleotide pocket, establishing a hydrogen bond through the carbonyl group with the backbone of Gly11 residue.

Moreover, the nitrogen group of 7-azaindole moiety accepts a hydrogen bond from a water molecule interacting with Gln132, a residue well known to constitute the DFG motif and to establish water-mediated interaction with H-bond acceptors of CDK1 inhibitors (Figure 4) [28].

The molecular docking scores of compound **6b** was found to be - 6.999 Kcal/mol, indicating efficient binding to the active site of CDK1.

2.2.5. ADME Prediction

In order to evaluate and predict the fate of compound **6b** within the human body, ADME and pharmacokinetic predictions were carried out using a freely available in silico ADME software [29]. Compound **6b**, as shown in Table 3, displayed promising physicochemical and pharmacokinetic parameters in ADME prediction studies, showing 3 H-bond acceptors, 0 H-bond donors, 3 rotatable bonds, and log $p < 5$. Moreover, our compound respects the Lipinski rule of 5, a feature making it a promising hit compound in the drug discovery field. Compound **6b** displayed a high gastrointestinal (GI) absorbance score but is not predicted to cross the blood brain barrier (BBB).

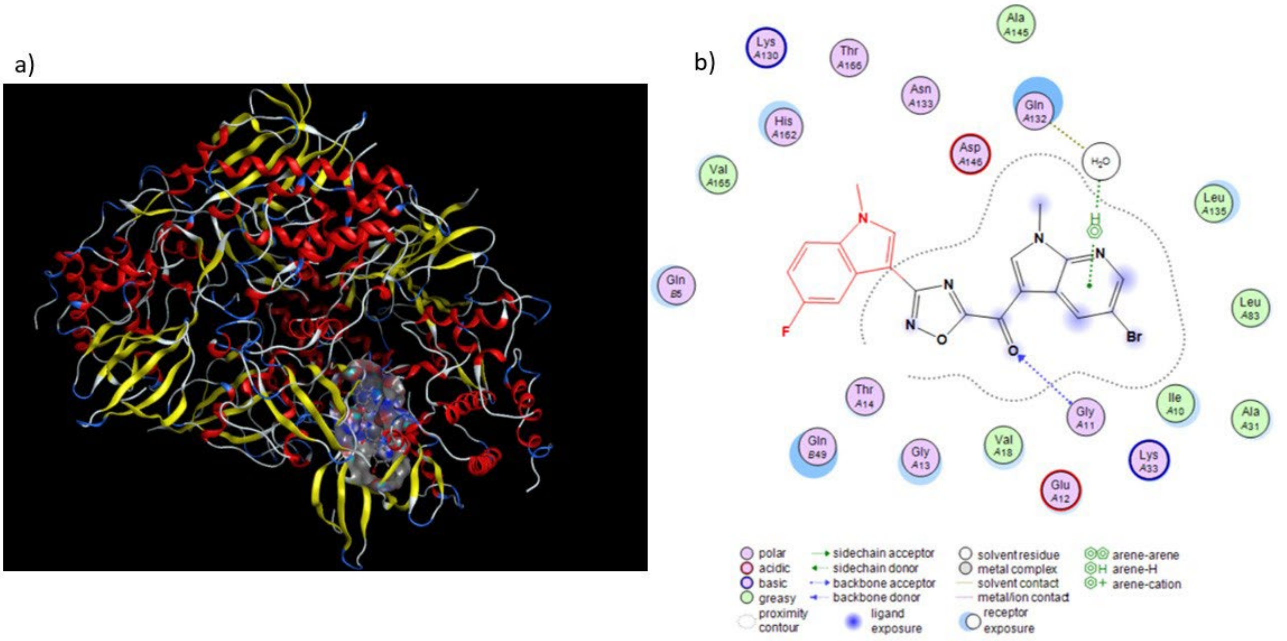
a)
b)
Lys A130
Thr A166
Ala A145
Asn A133
Gln A132
His A162
Asp A146
H₂O
Val A165
Leu A135
Gln B5
Leu A83
N
F
N
N
O
O
N
H
N
Br
Thr A14
Ile A10
Ala A31
Gly A11
Gln B49
Gly A13
Val A18
Lys A33
Glu A12
polar
acidic
basic
greasy
proximity contour
sidechain acceptor
sidechain donor
backbone acceptor
backbone donor
ligand exposure
solvent residue
metal complex
solvent contact
metal/ion contact
receptor exposure
arene-arene
arene-H
arene-cation

Figure 4. Proposed binding mode of compounds **6b** with CDK1 (PDB ID: 4YC6). (**a**) Surface representation of **6b** in CDK1 binding pocket. (**b**) H-bonds between the carbonyl group of our compound with the peptide nitrogen of Gly11 residue is shown with blue dashed arrow, while the water-mediated interaction between the nitrogen atom of the 7-azaindole portion adjacent to the oxadiazole ring and the Gln132 residue is depicted with green dashed lines.

Table 3. ADME predictions of compound **6b**.

Parameters	Score
n. H-bond acceptor	6
n. H-bond donor	0
n. rotable bonds	3
LogPo/w(iLOGP)	3.67
Lipinski's rule violation	No
Bioavailability score	0.55
GI absorption	High
BBB permeation	no

3. Materials and Methods

3.1. Chemistry

All melting points were taken on a Buchi-Tottoly capillary apparatus and were uncorrected. IR spectra were determined in bromoform using a Shimadzu FT/IR 8400S spectrophotometer. ^{1}H and ^{13}C NMR spectra were measured at 200 and 50 MHz, respectively, in DMSO-d_6 solution, using a Bruker Avance II series 200 MHz spectrometer. Chromatography was performed with a MERK silica gel 230–400 mesh ASTM column or a FLASH40i Biotage or with a Buchi Sepacore chromatography module (prepacked cartridge reference). Elementary analyses (C, H, N) were within ± 0.4% of the theoretical values.

3.1.1. Synthesis of 1-methyl-1*H*-pyrrolo[2,3-*b*]pyridines (**7a**,**b**)

t-BuOK (0.38 g, 3.4 mmol) and TDA-1 (1 or 2 drops) were added to a cold solution of appropriate commercial 7-azaindoles (2.5 mmol) in anhydrous toluene (25 mL), at 0 °C. The reaction mixture was stirred at room temperature for 3 h, and then methyl iodide (2.5 mmol, 0.2 mL) was added at 0 °C. TLC analysis (cyclohexane/ethyl acetate 7:3) revealed that methylation was complete after 1 h. The solvent was evaporated under reduced pressure. The residue was treated with water, extracted with DCM (3 × 20 mL), dried (Na_2SO_4), evaporated, and purified by column chromatography using DCM/ethyl acetate (9/1) as the eluent, to give the desired product.

For 5-Bromo-1-methyl-1*H*-pyrrolo[2,3-*b*]pyridine (**7a**) and 1-Methyl-1*H*-pyrrolo[2,3-*b*]pyridine (**7b**), analytical and spectroscopic data were in accordance to those reported in literature [14].

3.1.2. Synthesis of (1-methyl-1*H*-pyrrolo[2,3-*b*]pyridin-3-yl)-oxo-acetic Acid Methyl Esters (**8a,b**)

Oxalyl chloride (0.42 mL, 4.8 mmol) was added dropwise to a solution of appropriate 1-methyl-1*H*-pyrrolo[2,3-*b*]pyridine **7a,b** (1 g, 4.8 mmol) in dry diethyl ether (8.5 mL) under a nitrogen atmosphere at 0 °C. The reaction mixture was stirred overnight at room temperature. The solution was cooled to −65 °C using an acetone bath with an immersion cooler, before adding a sodium methoxide solution, 25 wt. % in methanol (11 mL, 10.8 mmol, 2.3 eq.) dropwise. The reaction mixture was heated up to room temperature and stirred for 2 h. The reaction was quenched with brine (1 mL) and water (1 mL), and the obtained precipitate was filtered off. Upon filtering, the isolated solid was dried under high vacuum overnight.

(5-Bromo-1-methyl-1H-pyrrolo[2,3-b]pyridin-3-yl)-oxo-acetic acid methyl ester (**8a**) Yield: 62%; light yellow solid; mp: 140.5–141.5 °C; IR (cm^{-1}): 1731 (CO), 1653 (CO); ^{1}H-NMR (200 MHz, DMSO-*d*$_6$) δ: 3.91 (3H, s, CH_3), 3.92 (3H, s, OCH_3), 8.54 (1H, d, *J* = 2.2 Hz, H-4), 8.57 (1H, d, *J* = 2.2 Hz, H-6), 8.80 (1H, s, H-2); ^{13}C NMR (50 MHz, DMSO-*d*$_6$) δ: 32.0 (q), 52.8 (q), 109.2 (s), 114.7 (s), 131.4 (d), 143.0 (d), 145.1 (d), 146.6 (s), 162.6 (s), 176.8 (s), 177.6 (s); *Anal.* calculated for $C_{11}H_9BrN_2O_3$ (MW: 297.10): C, 44.47; H, 3.05; N, 9.43%. Found: C, 44.58; H, 3.24; N, 9.65%.

(1-Methyl-1H-pyrrolo[2,3-b]pyridin-3-yl)-oxo-acetic acid methyl ester (**8b**) Yield: 73%; white solid; mp: 97.8–98.8 °C; IR (cm^{-1}): 1729 (CO), 1650 (CO); $^{1H-NMR}$ (200 MHz, DMSO-*d*$_6$) δ: 3.91 (3H, s, CH_3), 3.93 (3H, s, OCH_3), 7.38 (1H, dd, *J* = 7.8, 4.8 Hz, H-4), 8.44–8.51 (2H, m, H-5 and H-6), 8.74 (1H, s, H-2); ^{13}C NMR (50 MHz, DMSO-*d*$_6$) δ: 31.8 (q), 52.7 (q), 109.7 (s), 118.3 (s), 119.3 (d), 129.8 (d), 141.8 (d), 144.9 (d) 148.1 (s), 163.1 (s), 176.8 (s), 178.0 (s); *Anal.* calculated for $C_{11}H_{10}N_2O_3$ (MW: 218.21): C, 60.55; H, 4.62; N, 12.84%. Found: C, 60.38; H, 4.78; N, 12.72%.

3.1.3. Synthesis of (1-methyl-1*H*-pyrrolo[2,3-*b*]pyridine-3-yl)-[3-(1-methyl-1*H*-indol-3-yl)-[1,2,4]oxadiazol-5-yl]-methanones (**6a–f**)

A fine powder of sodium hydroxide (60 mg, 1.5 mmol) was quickly added to a solution of appropriate (1-methyl-1*H*-pyrrolo[2,3-*b*]pyridine-3-yl)-oxo-acetic acid methyl ester **8a,b** (446 mg, 1.5 mmol) and a suitable carboxamidine **9a–c** (190 mg, 1.0 mmol) in dry dimethylsulfoxide (DMSO) (2 mL). The resulting solution was allowed to stir at room temperature for 30 min. Then, water and ice were slowly added, and the obtained precipitate was filtered off. The residue was purified by column chromatography using cyclohexane/ethyl acetate (1/1) as the eluent.

(5-Bromo-1-methyl-1H-pyrrolo[2,3-b]pyridin-3-yl)-[3-(1-methyl-1H-indol-3-yl)-[1,2,4]oxadiazol-5-yl]-methanone (**6a**) Yield: 60%; yellow solid; mp: 258 °C (dec); IR (cm^{-1}): 1630 (CO); ^{1}H-NMR (200 MHz, DMSO-*d*$_6$) δ: 3.90 (3H, s, CH_3), 3.98 (3H, s, CH_3), 7.21–7.33 (2H, m, H-5 and H-6), 7.56–7.60 (1H, m, H-7), 7.99–8.06 (1H, m, H-4), 8.37 (1H, s, H-2), 8.56 (1H, d, *J* = 2.2 Hz, H-4), 8.68 (1H, d, *J* = 2.2 Hz, H-6), 9.24 (1H, s, H-2); *Anal.* calculated for $C_{20}H_{14}BrN_5O_2$ (MW: 436.26): C, 55.06; H, 3.23; N, 16.05%. Found: C, 55.18; H, 3.04; N, 15.89%.

(5-Bromo-1-methyl-1H-pyrrolo[2,3-b]pyridin-3-yl)-[3-(5-fluoro-1-methyl-1H-indol-3-yl)-[1,2,4]oxadiazol-5-yl]-methanone (**6b**) Yield: 67%; yellow solid; mp: 246 °C (dec); IR (cm^{-1}): 1635 (CO); ^{1}H-NMR (200 MHz, DMSO-*d*$_6$) δ: 3.97 (3H, s, CH_3), 4.04 (3H, s, CH_3), 7.17–7.28 (1H, m, H-6), 7.65–7.78 (2H, m, H-7 and H-4), 8.50 (1H, s, H-2), 8.61 (1H, d, *J* = 1.8 Hz,

H-4), 8.73 (1H, d, *J* = 1.8 Hz, H-6), 9.30 (1H, s, H-2); *Anal.* calculated for $C_{20}H_{13}BrFN_5O_2$ (MW: 454.25): C, 52.88; H, 2.88; N, 15.42%. Found: C, 55.80; H, 3.00; N, 15.55%.

(5-Bromo-1-methyl-1H-pyrrolo[2,3-b]pyridin-3-yl)-[3-(5-methoxy-1-methyl-1H-indol-3-yl)-[1,2,4] oxadiazol-5-yl]-methanone (**6c**) Yield: 85%; yellow solid; mp: 288 °C (dec); IR (cm^{-1}): 1637 (CO); ^{1}H-NMR (200 MHz, DMSO-d_6) δ: 3.86 (3H, s, CH_3), 3.92 (3H, s, CH_3), 4.02 (3H, s, OCH_3), 6.95–7.08 (1H, m, H-6), 7.54–7.55 (2H, m, H-7 and H-4), 8.35 (1H, s, H-2), 8.60 (1H, s, H-4), 8.72 (1H, s, H-6), 9.29 (1H, s, H-2); *Anal.* calculated for $C_{21}H_{16}BrN_5O_3$ (MW: 466.29): C, 54.09; H, 3.46; N, 15.02%. Found: C, 54.28; H, 3.30; N, 15.15%.

(1-Methyl-1H-pyrrolo[2,3-b]pyridin-3-yl)-[3-(1-methyl-1H-indol-3-yl)-[1,2,4]oxadiazol-5-yl] -methanone (**6d**) Yield: 77%; yellow solid; mp: 230 °C (dec); IR (cm^{-1}): 1620 (CO); ^{1}H-NMR (200 MHz, DMSO-d_6) δ: 3.97 (3H, s, CH_3), 4.05 (3H, s, CH_3), 7.28–7.40 (2H, m, H-5 and H-6), 7.46 (1H, dd, *J* = 9.9, 4.8 Hz, H-4), 7.65 (1H, dd, *J* = 6.5, 2.1 Hz, H-7), 8.11 (1H, dd, *J* = 6.2, 2.4 Hz, H-4), 8.44 (1H, s, H-2), 8.51 (1H, dd, *J* = 4.7, 1.3 Hz, H-6), 8.64 (1H, dd, *J* = 7.9, 1.3 Hz, H-5), 9.27 (1H, s, H-2); *Anal.* calculated for $C_{20}H_{15}N_5O_2$ (MW: 357.37): C, 67.22; H, 4.23; N, 19.60%. Found: C, 67.08; H, 4.04; N, 19.78%.

(1-Methyl-1H-pyrrolo[2,3-b]pyridin-3-yl)-[3-(5-fluoro-1-methyl-1H-indol-3-yl)-[1,2,4]oxadiazol-5-yl]-methanone (**6e**) Yield: 68%; yellow solid; mp: 257 °C (dec); IR (cm^{-1}): 1638 (CO); ^{1}H-NMR (200 MHz, DMSO-d_6) δ: 3.98 (3H, s, CH_3), 4.05 (3H, s, CH_3), 7.18–7.28 (1H, m, H-6), 7.42–7.50 (1H, m, H-4), 7.66–7.79 (2H, m, H-7 and H-4), 8.50 (1H, s, H-2), 8.52–8.67 (2H, m, H-5 and H-6), 9.26 (1H, s, H-2); *Anal.* calculated for $C_{20}H_{14}FN_5O_2$ (MW: 375.36): C, 64.00; H, 3.76; N, 18.66%. Found: C, 64.20; H, 3.64; N, 18.50%.

(1-Methyl-1H-pyrrolo[2,3-b]pyridin-3-yl)-[3-(5-methoxy-1-methyl-1H-indol-3-yl)-[1,2,4]oxadiazol- 5-yl]-methanone (**6f**) Yield: 80%; yellow solid; mp: 231 °C (dec); IR (cm^{-1}): 1623 (CO); ^{1}H-NMR (200 MHz, DMSO-d_6) δ: 3.87 (3H, s, CH_3), 3.92 (3H, s, CH_3), 4.04 (3H, s, OCH_3), 6.95–7.08 (1H, m, H-6), 7.40–7.63 (3H, m, H-7 , H-4 and H-4), 8.31–8.67 (3H, m, H-2 , H-5 and H-6), 9.29 (1H, s, H-2); *Anal.* calculated for $C_{21}H_{17}N_5O_3$ (MW: 387.39): C, 65.11; H, 4.42; N, 18.08%. Found: C, 65.28; H, 4.60; N, 18.25%.

3.2. Biology

3.2.1. Drugs and Chemicals

The 1,2,4-oxadiazole compounds **6a–f** were synthesized at the Department of Pharmacy, University of Palermo (Palermo, Italy). The drugs were dissolved in DMSO. The medium, fetal bovine serum (FBS), penicillin (50 IU mL^{-1}), and streptomycin (50 μg mL^{-1}) were from Gibco (Gaithersburg, MD, USA). All other chemicals were from Sigma (Zwijndrecht, the Netherlands).

3.2.2. Cell Cultures

HPAF-II, Hs766T, and PATU-T cell lines were purchased from the ATCC (American Type Culture Collection) (Manassas, VA, USA). The cell lines were tested for their authentication by STR–PCR (Short Tandem Repeat-Polymerase Chain Reaction). The primary cell line, PDAC3, was obtained from a patient undergoing pancreaticoduodenectomy, as described previously [30]. Additionally, all these cells were routinely tested for mycoplasma using PCR.

The cells were cultured in RPMI-1640 (Roswell Park Memorial Institute 1640) supplemented with 10% heat-inactivated FBS and 1% penicillin/streptomycin or in DMEM (Dulbecco's Modified Eagle's Medium), supplemented with 10% heat-inactivated FBS and 1% HEPES (4-(2-hydroxyethyl)-1-piperazineethanesulfonic acid). The cells were kept in a humidified atmosphere of 5% CO_2 and 95% air at 37 °C and harvested with trypsin-EDTA (Ethylenediaminetetraacetic acid).

3.2.3. Inhibition of Cell Growth

To evaluate the inhibitory effects of the 1,2,4-oxadiazole compounds **6a–f** on cell growth, we performed a Sulforhodamine-B (SRB) assay, as previously described [31,32]. Cells were seeded into 96-well flat-bottom plates in triplicate at a density of 3 10^3 cells/well. Cells were incubated at 37 °C for 24 h to create a confluent monolayer, and then they were treated with 100 μL of increasing concentrations of the compounds dissolved in DMSO. After 72 h of treatment, the cells were fixed with 25 μL of 50% cold trichloroacetic acid and kept for at least 60 min at 4 °C. Then, the plates were washed gently with deionized water, dried at r.t. overnight, and stained with 50 μL of 0.4% SRB solution in 1% acetic acid for 15 min at r.t. The excess SRB stain was removed on dried tissues, and the plates were washed with 1% acetic acid and left to dry at r.t. overnight. The SRB was dissolved in 150 μL of tris(hydroxymethyl)aminomethane solution (pH = 8.8 (TRIS base)), and the optical density (OD) was detected at a wavelength of 490 nm and 540 nm. Cell growth inhibition was calculated as the percentage versus vehicle-treated cells ("negative control"), OD (corrected for OD before drug addiction). Finally, the half maximal inhibitory concentration (IC_{50}) was calculated using a non-linear least squares curve fitting (GraphPad Prism 7, Intuitive Software for Science, San Diego, CA, USA).

3.2.4. Enzyme-Linked Immunosorbent Assay (ELISA) for CDK1 Expression

The expression of CDK1 was detected and quantified using an Enzyme-Linked Immunosorbent Assay (ELISA, Human cyclin-dependent kinase 1 (CDK1) ELISA Kit, Catalog Number: MBS707090) according to the manufacturer's protocol and our previous studies [33]. Volumes of 100 μL of the standard and the sample were added for each well, and the plates were incubated for 2 h at 37 °C. Then, the liquid was removed, and 100 μL of Biotin-antibody was added to each well, the plates were then incubated for 1 h at 37 °C. The medium was removed, and the plates were washed with Wash Buffer (200 μL). Subsequently, 100 μL of HRP-avidin was added to each well, and the plates were incubated for 1 h at 37 °C. The washing process was repeated five times. At the end, 90 μL of TMB Substrate was added to each well, and the plates were incubated for 30 min at 37 °C in the dark. Finally, 50 μL of stop solution was added to each well. The optical density of each well was determined using a microplate reader set to 450 nm.

3.2.5. Apoptosis

Cells were seeded in 96-well plates (5×10^3 cells/well) and, after one day, treated with drugs at the indicated concentrations for 24 h. At the end of the treatments, cells were fixed with 4% paraformaldehyde in PBS at r.t. for 30 min, then washed twice with PBS and stained with annexin V-FITC in a binding buffer (10 mM HEPES/NaOH pH 7.4, 140 mM NaCl, and 2.5 mM $CaCl_2$) for 10 min at r.t. in the dark. Finally, cells were washed with binding buffer solution and fluorescence was measured using a multimode plate reader with excitation and emission filters at 485 nm and 535 nm, respectively. Parallel studies using the same method, counted the cells at the fluorescence microscopy and evaluated the apoptotic index. The values were normalized on cell proliferation using a crystal violet assay.

3.2.6. Statistical Analysis

All the SRB and ELISA assays were carried out in triplicate and repeated at least three times, whereas the percentages of apoptotic cells were calculated taking into account three biological replicates. The data were evaluated using a GraphPad Prism (GraphPad Software, San Diego, CA, USA). Data were expressed as mean values ± SEM and analyzed using a Student's *t*-test.

3.3. In Silico Studies

3.3.1. Molecular Modelling and Docking

The molecular docking into CDK1 was performed for the compound **6b**. The CDK1 (PDB: 4YC6) X-ray crystal structure with a resolution of 2.60 Å, R-value 0.227 (observed), was obtained from the protein data bank [34]. The ligand **6b** was saved as a mol file, and the docking was performed using the Molecular Operating Environment (MOE) 2015.10.

3.3.2. ADME Studies

The ADME predictions were performed using SwissADME prediction software. The number of H-bond donors, H-bond acceptors, and rotatable bonds, as well as the bioavailability, GI absorption, and BBB permeation were evaluated.

4. Conclusions

In the present study we efficiently synthesized a new series of 1,2,4-oxadiazole derivatives **6a–f** that showed promising antiproliferative activities in vitro against a series of PDAC cells.

PDAC is one of the most lethal forms of cancer, characterized by poor survival rates of 5 years, late diagnosis, and lack of effective treatment. The American Cancer Society estimated that 48,220 people will die of pancreatic cancer in the United States (US) in 2021 [35]. Due to the lack of specific symptoms, most patients are diagnosed at an advanced stage and cannot undergo surgical resection. The currently available therapeutic regimens include combinations of standard chemotherapy drugs, such as FOLFIRINOX [33,34]. However, PDACs are typically resistant to these treatments, and new therapeutic strategies are urgently needed.

Most PDACs harbor mutations linked to cell-cycle regulation [36], and *TP53* is one of the most frequent and relevant driver genes of pancreatic tumorigenesis. When the *TP53* gene is mutated, CDK1 is no longer inhibited and stimulates progression through the cell cycle [10]. In addition, recent studies have shown that CDK1 overexpression is associated with more advanced stages of significantly shorter survival of PDAC patients [37]. Thus, CDK1 inhibition seems a promising strategy for the treatment of PDAC, and there are multiple preclinical studies and clinical trials investigating the efficacy and tolerability of CDK1-inhibiting drugs.

Because of the key role of CDK1 in the regulation of apoptosis, we assessed the ability of compound **6b** to induce apoptosis, which proved to be comparable to that observed for gemcitabine. As one of the major hallmarks of PDAC is its resistance to apoptosis induction by gemcitabine [38], these results support future investigation of this compound as an excellent candidate for combination with gemcitabine.

In addition, ADME predictions demonstrated that compound **6b** possessed good pharmacokinetic properties, followed the Lipinski rule of five, and had a high level of gastrointestinal absorption, indicating that our compound could be formulated as an oral drug.

Overall, the results of cytotoxicity, modulation of CDK1 expression, and apoptosis obtained with compound **6b** support its role as an interesting hit compound for further chemical modification and biological analysis in order to discover new compounds for the treatment of patients with PDAC.

Author Contributions: C.P., B.P. and S.C. performed chemical research and analyzed the data. C.P., A.P. and A.A. performed biological research and analyzed the data. P.D., G.J.P., E.G. and D.C. participated in the design of the research and the writing of the manuscript. All authors have read and agreed to the published version of the manuscript.

Funding: This work was partially supported by the following grants: CCA Foundation 2015 and 2018 grants (to E.G.), KWF Dutch Cancer Society grants (KWF project#19571, #13598) (to E.G.), and AIRC IG grant 24444 (to E.G.); PRIN2017, Prot.No.2017E84AA4 (to P.D.) and European Union 2014–2020 PON Ricerca e Innovazione grant from the Italian Ministry of Education, University and Research, entitled "PROGEMA-Processi Green per l'Estrazione di Principi Attivi e la Depurazione di Matrici di Scarto e Non" (ARS01_00432) (to P.D.). EU Social Fund (FSE) and the Canary Islands ACIISI for a predoctoral grant TESIS2020010055 and a short internship grant EST2021010019 cofinanced 85% (to A.P.).

Data Availability Statement: Not applicable.

Conflicts of Interest: The authors declare no conflict of interest.

References

1. Sung, H.; Ferlay, J.; Siegel, R.L.; Laversanne, M.; Soerjomataram, I.; Jemal, A.; Bray, F. Global Cancer Statistics 2020: GLOBOCAN Estimates of Incidence and Mortality Worldwide for 36 Cancers in 185 Countries. *CA Cancer J. Clin.* **2021**, *71*, 209–249. [CrossRef] [PubMed]
2. Conroy, T.; Desseigne, F.; Ychou, M.; Bouché, O.; Guimbaud, R.; Bécouarn, Y.; Adenis, A.; Raoul, J.L.; Gourgou-Bourgade, S.; de la Fouchardière, C.; et al. FOLFIRINOX versus gemcitabine for metastatic pancreatic cancer. *N. Engl. J. Med.* **2011**, *364*, 1817–1825. [CrossRef] [PubMed]
3. Caparello, C.; Meijer, L.L.; Garajova, I.; Falcone, A.; Le Large, T.Y.; Funel, N.; Kazemier, G.; Peters, G.J.; Vasile, E.; Giovannetti, E. FOLFIRINOX and translational studies: Towards personalized therapy in pancreatic cancer. *World J. Gastroenterol.* **2016**, *22*, 6987–7005. [CrossRef]
4. Von Hoff, D.D.; Ervin, T.; Arena, F.P.; Chiorean, E.G.; Infante, J.; Moore, M.; Seay, T.; Tjulandin, S.A.; Ma, W.W.; Saleh, M.N.; et al. Increased survival in pancreatic cancer with nab-paclitaxel plus gemcitabine. *N. Engl. J. Med.* **2013**, *369*, 1691–1703. [CrossRef] [PubMed]
5. Le Large, T.Y.S.; Bijlsma, M.F.; El Hassouni, B.; Mantini, G.; Lagerweij, T.; Henneman, A.A.; Funel, N.; Kok, B.; Pham, T.V.; de Haas, R.; et al. Focal adhesion kinase inhibition synergizes with nab-paclitaxel to target pancreatic ductal adenocarcinoma. *J. Exp. Clin. Cancer Res.* **2021**, *40*, 91. [CrossRef]
6. Roskoski, R., Jr. Properties of FDA-approved small molecule protein kinase inhibitors: A 2020 update. *Pharmacol. Res.* **2019**, *152*, 104609. [CrossRef] [PubMed]
7. Roskoski, R., Jr. Properties of FDA-approved small molecule protein kinase inhibitors. *Pharmacol. Res.* **2019**, *144*, 19–50. [CrossRef]
8. Wu, P.; Nielsen, T.E.; Clausen, M.H. Small-molecule kinase inhibitors: An analysis of FDA-approved drugs. *Drug Discov. Today* **2016**, *21*, 5–10. [CrossRef]
9. Wu, P.; Nielsen, T.E.; Clausen, M.H. FDA-approved small-molecule kinase inhibitors. *Trends Pharmacol. Sci.* **2015**, *36*, 422–439. [CrossRef]
10. Lim, S.; Kaldis, P. Cdks, cyclins and CKIs: Roles beyond cell cycle regulation. *Development* **2013**, *140*, 3079–3093. [CrossRef] [PubMed]
11. Wijnen, R.; Pecoraro, C.; Carbone, D.; Fiuji, H.; Avan, A.; Peters, G.J.; Giovannetti, E.; Diana, P. Cyclin Dependent Kinase-1 (CDK-1) Inhibition as a Novel Therapeutic Strategy against Pancreatic Ductal Adenocarcinoma (PDAC). *Cancers* **2021**, *13*, 4389. [CrossRef] [PubMed]
12. Pelosi, E.; Castelli, G.; Testa, U. Pancreatic Cancer: Molecular Characterization, Clonal Evolution and Cancer Stem Cells. *Biomedicines* **2017**, *5*, 65. [CrossRef] [PubMed]
13. Sakemi, S.; Sun, H.H. Nortopsentins A, B, and C. Cytotoxic and antifungal imidazolediylbis[indoles] from the sponge Spongosorites ruetzleri. *J. Org. Chem.* **1991**, *56*, 4304–4307. [CrossRef]
14. Cascioferro, S.; Attanzio, A.; Di Sarno, V.; Musella, S.; Tesoriere, L.; Cirrincione, G.; Diana, P.; Parrino, B. New 1,2,4-Oxadiazole Nortopsentin Derivatives with Cytotoxic Activity. *Mar. Drugs* **2019**, *17*, 35. [CrossRef]
15. Pecoraro, C.; Carbone, D.; Aiello, D.; Carbone, A. Synthesis and cytotoxic activity of 3-[2-(1*H*-Indol-3-yl)-1,3-thiazol-4-yl]-1*H*-pyrrolo[3,2-c]pyridine hydrobromides, analogues of marine alkaloid nortopsentin. *Arkivoc* **2021**. [CrossRef]
16. Di Franco, S.; Parrino, B.; Gaggianesi, M.; Pantina, V.D.; Bianca, P.; Nicotra, A.; Mangiapane, L.R.; Lo Iacono, M.; Ganduscio, G.; Veschi, V.; et al. CHK1 inhibitor sensitizes resistant colorectal cancer stem cells to nortopsentin. *iScience* **2021**, *24*, 102664. [CrossRef]
17. Li Petri, G.; Cascioferro, S.; El Hassouni, B.; Carbone, D.; Parrino, B.; Cirrincione, G.; Peters, G.J.; Diana, P.; Giovannetti, E. Biological Evaluation of the Antiproliferative and Anti-migratory Activity of a Series of 3-(6-Phenylimidazo[2,1-b][1,3,4]thiadiazol- 2-yl)-1H-indole Derivatives against Pancreatic Cancer Cells. *Anticancer Res.* **2019**, *39*, 3615–3620. [CrossRef]
18. Cascioferro, S.; Li Petri, G.; Parrino, B.; El Hassouni, B.; Carbone, D.; Arizza, V.; Perricone, U.; Padova, A.; Funel, N.; Peters, G.J.; et al. 3-(6-Phenylimidazo [2,1-b][1,3,4]thiadiazol-2-yl)-1H-Indole Derivatives as New Anticancer Agents in the Treatment of Pancreatic Ductal Adenocarcinoma. *Molecules* **2020**, *25*, 329. [CrossRef] [PubMed]
19. Vitaku, E.; Smith, D.T.; Njardarson, J.T. Analysis of the Structural Diversity, Substitution Patterns, and Frequency of Nitrogen Heterocycles among U.S. FDA Approved Pharmaceuticals. *J. Med. Chem.* **2014**, *57*, 10257–10274. [CrossRef]
20. Carbone, D.; Parrino, B.; Cascioferro, S.; Pecoraro, C.; Giovannetti, E.; Di Sarno, V.; Musella, S.; Auriemma, G.; Cirrincione, G.; Diana, P. 1,2,4-Oxadiazole Topsentin Analogs with Antiproliferative Activity against Pancreatic Cancer Cells, Targeting GSK3β Kinase. *ChemMedChem* **2021**, *16*, 537–554. [CrossRef]
21. Parrino, B.; Carbone, D.; Cascioferro, S.; Pecoraro, C.; Giovannetti, E.; Deng, D.; Di Sarno, V.; Musella, S.; Auriemma, G.; Cusimano, M.G.; et al. 1,2,4-Oxadiazole topsentin analogs as staphylococcal biofilm inhibitors targeting the bacterial transpeptidase sortase A. *Eur. J. Med. Chem.* **2021**, *209*, 112892. [CrossRef]
22. Avan, A.; Caretti, V.; Funel, N.; Galvani, E.; Maftouh, M.; Honeywell, R.J.; Lagerweij, T.; Van Tellingen, O.; Campani, D.; Fuchs, D.; et al. Crizotinib inhibits metabolic inactivation of gemcitabine in c-Met-driven pancreatic carcinoma. *Cancer Res.* **2013**, *73*, 6745–6756. [CrossRef]
23. Maftouh, M.; Belo, A.I.; Avan, A.; Funel, N.; Peters, G.J.; Giovannetti, E.; Van Die, I. Galectin-4 expression is associated with reduced lymph node metastasis and modulation of Wnt/β-catenin signalling in pancreatic adenocarcinoma. *Oncotarget* **2014**, *5*, 5335–5349. [CrossRef]

24. Le Large, T.Y.; Mantini, G.; Meijer, L.L.; Pham, T.V.; Funel, N.; van Grieken, N.C.; Kok, B.; Knol, J.; van Laarhoven, H.W.; Piersma, S.R.; et al. Microdissected pancreatic cancer proteomes reveal tumor heterogeneity and therapeutic targets. *JCI Insight* **2021**, *5*, e138290. [CrossRef] [PubMed]
25. Parry, D.; Guzi, T.; Shanahan, F.; Davis, N.; Prabhavalkar, D.; Wiswell, D.; Seghezzi, W.; Paruch, K.; Dwyer, M.P.; Doll, R.; et al. Dinaciclib (SCH 727965), a Novel and Potent Cyclin-Dependent Kinase Inhibitor. *Mol. Cancer Ther.* **2010**, *9*, 2344–2353. [CrossRef] [PubMed]
26. Shendge, A.K.; Chaudhuri, D.; Mandal, N. The natural flavones, acacetin and apigenin, induce Cdk-Cyclin mediated G2/M phase arrest and trigger ROS-mediated apoptosis in glioblastoma cells. *Mol. Biol. Rep.* **2021**, *48*, 539–549. [CrossRef] [PubMed]
27. Huang, J.; Chen, P.; Liu, K.; Liu, J.; Zhou, B.; Wu, R.; Peng, Q.; Liu, Z.-X.; Li, C.; Kroemer, G.; et al. CDK1/2/5 inhibition overcomes IFNG-mediated adaptive immune resistance in pancreatic cancer. *Gut* **2020**, *70*, 890–899. [CrossRef]
28. Navarro-Retamal, C.; Caballero, J. Flavonoids as CDK1 Inhibitors: Insights in Their Binding Orientations and Structure-Activity Relationship. *PLoS ONE* **2016**, *11*, e0161111. [CrossRef] [PubMed]
29. SwissADME: A free web tool to evaluate pharmacokinetics, drug-likeness and medicinal chemistry friendliness of small molecules. *Sci. Rep.* **2017**, *7*, 42717. [CrossRef]
30. Rovithi, M.; Avan, A.; Funel, N.; Leon, L.G.; Gomez, V.E.; Wurdinger, T.; Griffioen, A.W.; Verheul, H.M.; Giovannetti, E. Development of bioluminescent chick chorioallantoic membrane (CAM) models for primary pancreatic cancer cells: A platform for drug testing. *Sci. Rep.* **2017**, *7*, 44686. [CrossRef]
31. Sciarrillo, R.; Wojtuszkiewicz, A.; Kooi, I.E.; Gómez, V.E.; Boggi, U.; Jansen, G.; Kaspers, G.J.; Cloos, J.; Giovannetti, E. Using RNA-sequencing to Detect Novel Splice Variants Related to Drug Resistance in In Vitro Cancer Models. *J. Vis. Exp.* **2016**, *118*, 54714. [CrossRef]
32. Massihnia, D.; Avan, A.; Funel, N.; Maftouh, M.; van Krieken, A.; Granchi, C.; Raktoe, R.; Boggi, U.; Aicher, B.; Minutolo, F.; et al. Phospho-Akt overexpression is prognostic and can be used to tailor the synergistic interaction of Akt inhibitors with gemcitabine in pancreatic cancer. *J. Hematol. Oncol.* **2017**, *10*, 9. [CrossRef]
33. Bianco, C.; Giovannetti, E.; Ciardiello, F.; Mey, V.; Nannizzi, S.; Tortora, G.; Troiani, T.; Pasqualetti, F.; Eckhardt, G.; de Liguoro, M.; et al. Synergistic antitumor activity of ZD6474, an inhibitor of vascular endothelial growth factor receptor and epidermal growth factor receptor signaling, with gemcitabine and ionizing radiation against pancreatic cancer. *Clin. Cancer Res.* **2006**, *12*, 7099–7107. [CrossRef]
34. Brown, N.R.; Korolchuk, S.; Martin, M.P.; Stanley, W.A.; Moukhametzianov, R.; Noble, M.; Endicott, J.A. CDK1 structures reveal conserved and unique features of the essential cell cycle CDK. *Nat. Commun.* **2015**, *6*, 6769. [CrossRef] [PubMed]
35. American Cancer Society. Key Statistics for Pancreatic Cancer. Available online: https://www.cancer.org/cancer/pancreatic-cancer/about/key-statistics.html (accessed on 2 November 2021).
36. Le Large, T.Y.S.; Bijlsma, M.F.; Kazemier, G.; van Laarhoven, H.W.M.; Giovannetti, E.; Jimenez, C.R. Key biological processes driving metastatic spread of pancreatic cancer as identified by multi-omics studies. *Semin. Cancer Biol.* **2017**, *44*, 153–169. [CrossRef] [PubMed]
37. Dong, S.; Huang, F.; Zhang, H.; Chen, Q. Overexpression of BUB1B, CCNA2, CDC20, and CDK1 in tumor tissues predicts poor survival in pancreatic ductal adenocarcinoma. *Biosci. Rep.* **2019**, *39*, BSR20182306. [CrossRef] [PubMed]
38. Elnaggar, M.; Giovannetti, E.; Peters, G.J. Molecular targets of gemcitabine action: Rationale for development of novel drugs and drug combinations. *Curr. Pharm. Des.* **2012**, *18*, 2811–2829. [CrossRef] [PubMed]

Chapter 5

1,2,4-Oxadiazole Topsentin Analogs with Antiproliferative Activity against Pancreatic Cancer Cells, Targeting GSK3β Kinase.

Carbone, D.; Parrino, B.; Cascioferro, S.; **Pecoraro, C.**; Giovannetti, E.; Di Sarno, V.; Musella, S.; Auriemma, G.; Cirrincione, G.; Diana, P.

ChemMedChem (2021), 16(3), 537-554.

Special Collection

1,2,4-Oxadiazole Topsentin Analogs with Antiproliferative Activity against Pancreatic Cancer Cells, Targeting GSK3β Kinase

Daniela Carbone+,[a, b] Barbara Parrino+,[a] Stella Cascioferro,[a] Camilla Pecoraro,[a, b] Elisa Giovannetti,[b, c] Veronica Di Sarno,[d] Simona Musella,[d] Giulia Auriemma,[d] Girolamo Cirrincione,[a] and Patrizia Diana*[a]

A new series of topsentin analogs, in which the central imidazole ring of the natural lead was replaced by a 1,2,4-oxadiazole moiety, was efficiently synthesized. All derivatives were pre-screened for antiproliferative activity against the National Cancer Institute (NCI-60) cell lines panel. The five most potent compounds were further investigated in various pancreatic ductal adenocarcinoma (PDAC) cell lines, including SUIT-2, Capan-1, and Panc-1 cells, eliciting EC_{50} values in the micromolar and sub-micromolar range, associated with significant reduction of cell migration. These remarkable results might be explained by the effects of these new topsentin analogues on epithelial-to-mesenchymal transition markers, including SNAIL-1/2 and metalloproteinase-9. Moreover, flow cytometric analysis after Annexin V-FITC and propidium iodide staining demonstrated that these derivatives enhanced apoptosis of PDAC cells. Keeping with these data, the PathScan intracellular signaling and ELISA array revealed cleavage of caspase-3 and PARP and a significant inhibition of GSK3β phosphorylation, suggesting this kinase as a potential downstream target of our novel compounds. This was further supported by a specific assay for the evaluation of GSK3β activity, showing IC_{50} values for the most active compounds against this enzyme in the micromolar range.

1. Introduction

A huge number of new compounds used in drug regimens for the treatment of different cancer types, have been obtained directly or indirectly from natural sources, modifying the molecular structure of natural compounds or synthesizing new derivatives using their structures as models. Among the small-molecule approved drugs for all diseases in the last 30 years, only the 17% are considered as merely synthetic, being the 83% natural products *per se* or mimicked natural products.[1]

Different anticancer agents have been isolated from marine sources that offered unique secondary metabolites with significant biological activities. In particular, more than half of the new marine natural products discovered from 1985 to 2012 showed anticancer properties and among these, several molecules were approved or tested in clinical trials.[2] Examples of marine-derived approved drugs are represented by trabectedin, a tetrahydroisoquinoline alkaloid first isolated from the ascidian *Ecteinascidia* approved by the European Union (EU) in 2007 and by the Food and Drug Administration (FDA, US) in 2015 for the treatment of adult patients with advanced soft tissue sarcoma, and eribulin mesylate, a synthetic analog of halichondrin B isolated from marine sponges, that was approved by the FDA in 2010 and by the EU in 2011 for patients with locally advanced or metastatic breast cancer.[2]

Considering the success gained by molecules derived from the marine environment, our research group synthesized a library of compounds obtained through the structure manipulation of nortopsentin, a natural bis-indolyl alkaloid isolated from deep-sea sponge *Spongsorites ruetzleri* which is characterized by significant antiproliferative activity against the P388 murine leukemia cell line.[3] In particular, we produced many derivatives in which the central imidazole ring was replaced by several five-membered heterocycles.[4–7]

Successively, structural manipulation of nortopsentins involved an indole moiety, which was modified into an azaindole portion and many derivatives showed significant antiprolifer-

---

[a] *Dr. D. Carbone,+ Dr. B. Parrino,+ Dr. S. Cascioferro, C. Pecoraro,*
Prof. G. Cirrincione, Prof. P. Diana
Department of Biological, Chemical and Pharmaceutical Sciences and Technologies (STEBICEF)
University of Palermo
Via Archirafi 32
90123, Palermo (Italy)
E-mail: patrizia.diana@unipa.it
[b] *Dr. D. Carbone,+ C. Pecoraro, Prof. E. Giovannetti*
Department of Medical Oncology
VU University Medical Center (VUmc)
De Boelelaan 1117
1081HV, Amsterdam (The Netherlands)
[c] *Prof. E. Giovannetti*
Cancer Pharmacology Lab, AIRC Start Up
Fondazione Pisana per la Scienza
Via Ferruccio Giovannini 13
56017 San Giuliano Terme, Pisa (Italy)
[d] *Dr. V. Di Sarno, Dr. S. Musella, Dr. G. Auriemma*
Department of Pharmacy
University of Salerno
Via G. Paolo II 132
84084 Fisciano (Italy)

[+] *These authors contributed equally to this work.*

Supporting information for this article is available on the WWW under https://doi.org/10.1002/cmdc.202000752

This article belongs to the Special Collection "NMMC 2019: DCF-SCI 40th Anniversary"

© 2020 Wiley-VCH GmbH

ative activity in a wide range of human tumor cell lines.[8–10] Some of them acted as CDK1 inhibitors,[11–12] and the most active derivatives determined a significant reduction of tumor volume with two complete responses at well-tolerated doses in mesothelioma mouse models.[13]

These promising results prompted us to perform additional studies, focusing our attention on the bis-indolyl alkaloid topsentins, characterized by the presence of a carbonyl group that differentiates their skeleton from that of the nortopsentin, as linker between one of the two indolyl portion and the position 2 of the central imidazole ring. Topsentin and bromotopsentin (Figure 1) were extracted from the sponge *Topsentia genitrix*. Topsentin showed *in vitro* cytotoxic activity against P-388 murine tumor cells, with IC$_{50}$ value of 8.8 μM and against several human tumor cells, including HCT-8, A-549, T47D. In addition, it exhibited *in vivo* activity against P-388 (T/C 137 %, 150 mg/kg) and B16 melanoma (T/C 144 %, 37.5 mg/kg). Bromotopsentin was found to be active against human non-small-cell bronchopulmonary cancer cells NSCLC–N6 and P-388, with IC$_{50}$ values of 28.5 μM and 16.6 μM, respectively.[14,15]

Deoxytopsentin, bromodeoxytopsentin and isobromodeoxytopsentin (Figure 1) are also belonging to the topsentin class, and were isolated from *Hexadella sp.* and *Spongosorites genitrix* sponges, respectively. The unsubstituted deoxytopsentin was found to be active against human lung cancer (NSCLC-N6), breast cancer (BC) and hepatoma (HepG2) cells, reporting IC$_{50}$ values of 19.3, 32.8 and 10.1 μM, respectively. Bromodeoxytopsentin and isobromodeoxytopsentin showed cytotoxicity against the human leukemia cell-line K-562, with LC$_{50}$ values of 1.5 and 5.2 μM, respectively.[16,17]

On the other hand, nitrogen heterocycles constitute the pharmacophore moiety of several molecules with different biological activities,[18–20] including antitumor activity.[21–24] These compounds are able to improve the interaction with target proteins, enzymes and receptors through the formation of hydrogen bonds, dipole-dipole and hydrophobic interactions, van der Waals forces and π-stacking interactions. Moreover, the presence of the nitrogen atom allows to improve solubility.[25] Among nitrogen heterocycles, the 1,2,4-oxadiazole ring is found in many molecules with significant biological activity, especially antitumor[26–29] and being a bioisostere of amides and esters is able to improve bioavailability and physiochemical properties of compounds bearing it.

Considering the interesting antiproliferative activity of topsentins, as well as the important features and properties of the 1,2,4-oxadiazole ring, herein we report the synthesis of the new 1,2,4-oxadiazole topsentin analogs **1** (Figure 1). The biological activity of the synthesized compound was investigated against the NCI-60 panel and on cell lines of pancreatic ductal adenocarcinoma, one of the most aggressive solid malignancies characterized by poor response to current treatments and extremely poor prognosis.

2. Results and Discussion

2.1. Chemistry

We successfully synthesized the new 1,2,4-oxadiazoles of type **1** following a multistep sequence described in Scheme 1. The retrosynthetic analysis of the title ring system suggested N-hydroxy-1*H*-indole-3-carboxamidine **2**, and (1-methyl-1*H*-indol-3-yl)-oxo-acetic acid **3** as suitable building blocks.

The N-hydroxy-1*H*-indole-3-carboxamidines **2 a**–**d** (75-85 %) were synthesized from 1*H*-indole-3-carbonitriles **4 a**–**d**, prepared from the corresponding indoles **5 a**–**d**, as previously reported,[30,31] through reaction with hydroxylamine hydrochloride in ethanol (EtOH), in the presence of diisopripylenethylamide (DIPEA).

The (1-methyl-1*H*-indol-3-yl)-oxo-acetic acids (**3 a**–**d**) were prepared from the commercially available 1*H*-indoles **5** which were subjected to methylation, providing the corresponding methyl derivatives **6**.[7,12,32] Their subsequent acylation using an excess of oxalyl chloride in diethyl ether, at 0 °C and under nitrogen atmosphere, gave **7 a**–**d** in excellent yields (89–96 %).

In the attempt to obtain 1,2,4-oxadiazoles **1**, compounds **7** were first reacted with carboxamidines of type **2**. In spite of several reaction conditions employed, in no case, the expected compounds were isolated in acceptable yields, due to the extreme reactivity of the indolyl-oxo-acetyl chlorides in the complex reaction mixture. Thus, acyl chlorides were converted into oxo-acetic acids **3 a**–**d** (78–95 %), using a solution of sodium

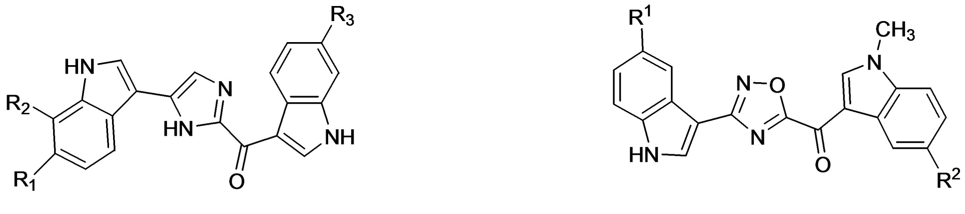

Topsentin, R_1=R_2=H, R_3=OH
Bromotopsentin, R_1=Br, R_2=H, R_3=OH
Deoxytopsentin, R_1=R_2=R_3=H
Bromodeoxytopsentin, R_1=Br, R_2=R_3=H
Isobromodeoxytopsentin, R_1=R_2=H, R_3=Br

1

Figure 1. Structures of topsentins and new topsentin analogs **1**.

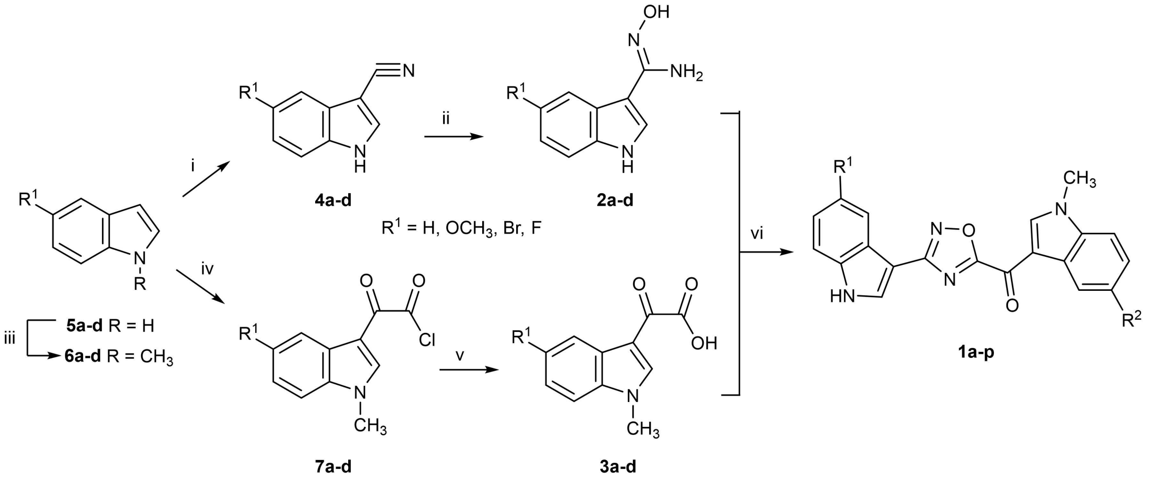

Scheme 1. Synthesis of [3-(1*H*-Indol-3-yl)-1,2,4-oxadiazol-5-yl](1-methyl-1*H*-indol-3-yl)methanone **1 a**–**p**. Reagents and conditions: (i) (a) CSI, MeCN, 0 °C, 2 h; (b) DMF, 0 °C, 1 h, 90–98 %; (ii) NH_2NH_2 HCl, DIPEA, EtOH, reflux, 4 h, 75–85 %; (iii) *t*-BuOK, TDA-1, toluene, RT, 1–24 h, then CH_3I, RT, 1–2 h, 97–99 %; (iv) oxalyl chloride, diethyl ether, 0 °C, 3 h, then 24 °C, 1 h, 89–96 %; (v) NaOH 2 M, THF, RT, 12 h, 78–95 %; (vi) EDC, HOBt, DMF, 0 °C, 15 min, then 100 °C, 15 min, 45–78 %.

hydroxide (NaOH) at room temperature. The reaction between the two key building blocks **2 a**–**d** and **3 a**–**d** was performed in DMF and in the presence of N-(3-dimethylaminopropyl)-N′-ethylcarbodiimide hydrochloride (EDC) and hydroxybenzotriazole (HOBt) as the coupling reagents, inducing the formation of an amide bond by previous activation of the carboxylic acid group.[33] Subsequent in situ temperature-catalyzed cyclodehydration, performed warming the reaction mixture at 100 °C, gave the desired oxadiazole derivatives **1 a**–**p** in yields ranging from 45–78 %.

2.2. Biology

2.2.1. Antiproliferative activity

According to the NCI protocol, all the newly synthesized oxadiazoles **1 a**–**p** were screened for *in vitro* antiproliferative activity in a panel of 60 human tumor cell lines derived from 9 human cancer cell types, grouped in disease sub-panels (supporting information, Table S1). The growth percentages were calculated and the "One-dose" (10 μM) data was reported as a mean graph of the percent growth of treated cells. Among all submitted oxadiazoles, the compounds **1 b**, **1 c** and **1 l** showed the best mean growth percentages, with growth inhibition values, against several cancer cell lines, lower than 10%. In particular, the compound **1 b** showed a high level of tumor selectivity, exhibiting pronounced lethality toward cell lines derived from melanoma (MDA-MB-435, −19.13 %) and leukemia (HL-60, −6.73 %). The cell lines OVCAR-3 (ovarian cancer), HT29 (colon cancer) and NCI–H522 (non-small cell lung cancer) were also highly sensitive to the antiproliferative effects of this drug (growth values, 0.72 %, 8.80 % and 2.36 %, respectively) (Table S1). For the compound **1 c**, the strongest activity was detected toward melanoma MDA-MB-435 (7.96 %), as well as against breast MDA-MB-468 (-4.38 %) cells (Table S1). The same data mining approach from the NCI-60 panel demonstrated that the most sensitive cell lines for the compound **1 l** were SR (included in the leukemia subpanel), SW-620 (colorectal cancer), OVCAR-4 (ovarian cancer) and DU-145 (prostate cancer), with growth percent values of 6.41 %, −2.17 %, −0.34 and 3.08 %, respectively (Table S1).

Since the NCI panel do not include PDAC cell lines, we decided to evaluate the *in vitro* antiproliferative activity of these compounds on a panel of immortalized PDAC cells, including SUIT-2, Capan-1 and Panc-1, by Sulforhodamine-B (SRB) assay. These analyses allowed us to get further insight about the drug activity of our compounds against additional cancer cell models. Furthermore, the search for novel effective drugs is extremely important in PDAC, a devastating type of cancer with poor survival rates due to very limited therapeutic options.

An initial screening was performed using three concentrations (0.1 μM, 1 μM, 10 μM). Below, data of compounds **1 b**, **1 c**, **1 i**, **1 j** and **1 l**, which showed significant cytotoxic activity, were reported (Figure 2).

In particular, the compounds **1 b** and **1 c** were more active against the SUIT-2 pancreatic cells, if compared to the other cells, with mean growth percent values of 18.97 % and 27.09 %, respectively (Figure 2a,b). Conversely, the compounds **1 i** and **1 j** had highest antiproliferative/cytotoxic effects against CAPAN-1 cells, for which we observed growth percent values of −5.62 % and 19.63 %, respectively (Figure 2c,d). However, the compound **1 l** at concentration of 10 μM inhibited the viability of all the three cell lines, with effects ranging from −0.04 to 34.31 percent of growth (Figure 2e).

To assess the potential toxicity effects of the new compounds **1 b**, **1 c**, **1 i**, **1 j** and **1 l**, *in vitro* cell viability of immortalized human pancreatic normal ductal cells HPNE was measured after treatment with three different concentrations of each compound (0.1, 1 and 10 μM). As shown in the Figure 2f, all derivatives did not cause cytotoxic effects on non-tumor pancreatic cells. We found only 10–20 % growth inhibition after

© 2020 Wiley-VCH GmbH

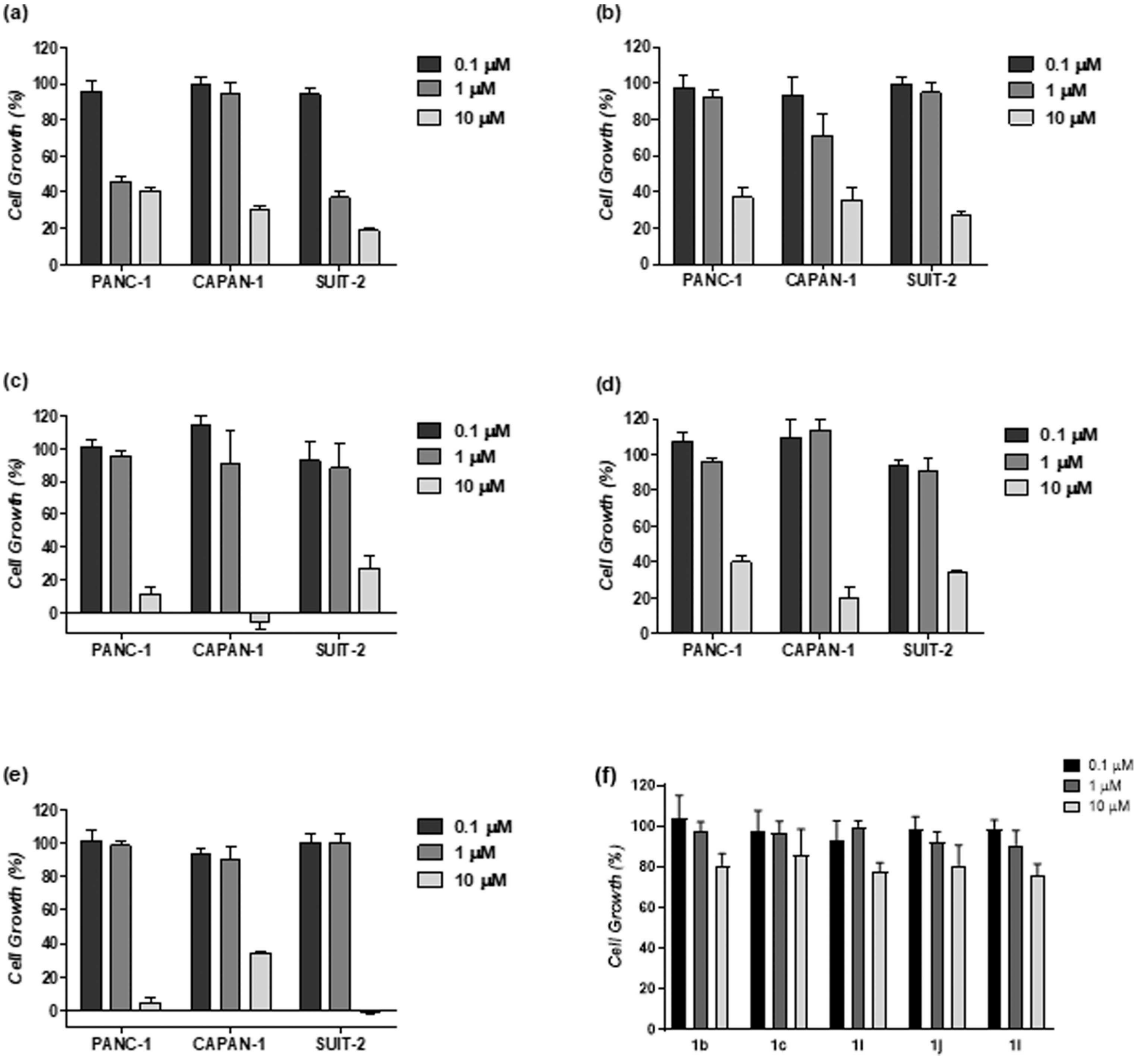

Figure 2. Cell growth data after 72 h exposure to the compounds **1 b** (a), **1 c** (b), **1 i** (c), **1 j** (d) and **1 l** (e) using a panel of pancreatic cancer cell lines, as assessed by the SRB assay. In the panel (f), assessment of toxicity of compounds **1 b**, **1 c**, **1 i**, **1 j** and **1 l** at three different concentrations against HPNE human normal pancreatic cells. The results are expressed as percentage of cell growth compared to untreated control cells. Columns, mean values obtained from three independent experiments; bars, SEM.

72 h of HPNE cells treated with the highest concentration tested (10 μM). The other concentrations tested (0.1 and 1 μM) did not impair the viability of HPNE cells. The results of these experiments allowed us to consider these new compounds highly cancer selective compared to the non-tumor pancreatic cells HPNE.

In order to better determine the concentration achieving a 50% inhibition (EC_{50}) of cell growth, the PDAC cells were then exposed to nine increasing concentrations (from 0.1 μM to 40 μM) of each compound for 72 hours. These studies revealed (Figure 3a,b) that SUIT-2 cells were the most sensitive cells to **1 b**, with an EC_{50} value below 0.50 μM (0.40 μM). This compound showed antitumor activity also against Panc-1 and Capan-1 cells, but with slightly higher EC_{50} values (0.8 and 1.2 μM, respectively). Conversely the compound **1 c** showed a lower anti-proliferative potency in SUIT-2 cells (EC_{50} = 3.2 μM, Table 1),

Table 1. Summary of the antiproliferative activity of oxadiazole derivatives in pancreatic cancer cells.

Compound	EC_{50} [μM][a] Panc-1	Capan-1	SUIT-2
1 b	0.8	1.2	0.40
1 c	1.6	1.3	3.2
1 i	2.8	2.8	7.1
1 j	6.8	2.6	5.9
1 l	1.5	1.4	1.9
Gemcitabine	0.10	0.020	0.010
5-Fluorouracil	4.3	0.50	0.91

[a] Data are reported as EC_{50} values (the molar concentration of a compound where 50% of its maximal effect is observed) determined by the SRB assay after 72 hours exposure to each compound. Gemcitabine and 5-fluorouracil were reported as reference drugs. Data represent mean values from at least 3 independent experiments.

© 2020 Wiley-VCH GmbH

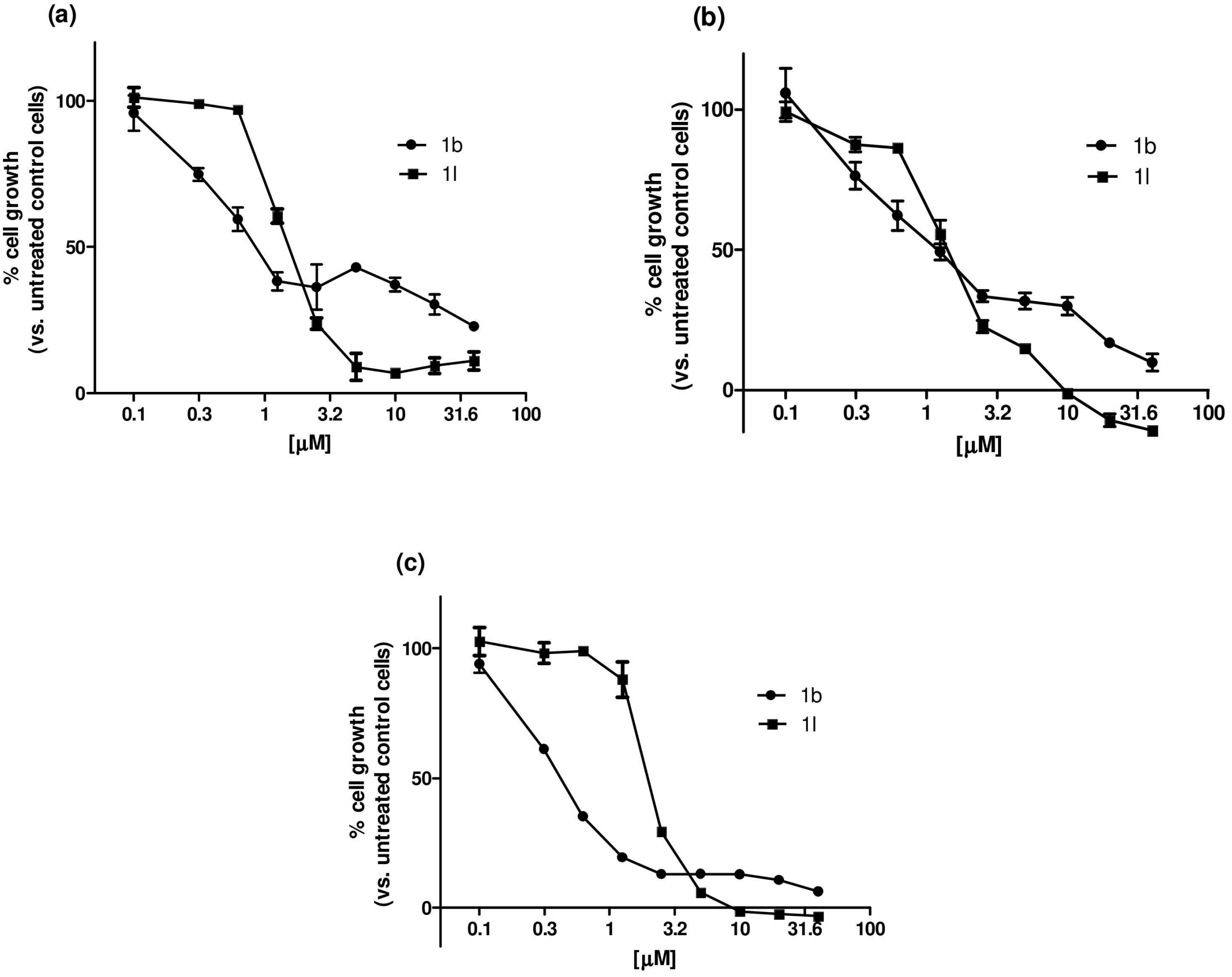

Figure 3. Effects of most active compounds **1 b** and **1 l** on the viability of Panc-1 (a), Capan-1 (b) and SUIT-2 (c) PDAC cell lines. Cells were treated with nine different concentrations of the compound and cell survival was measured after 72 h by SRB assay in comparison to untreated control cells. Values are reported as the mean ± SEM of three separate experiments, performed in triplicate.

inhibiting the growth of Panc-1 and Capan-1 with IC_{50} values of 1.6 and 1.3 μM, respectively. Similarly, the compound **1 i** was more active against Panc-1 and Capan-1 cancer cell lines, with the same EC_{50} values of 2.8 μM; while a weak antiproliferative activity was observed against SUIT-2 cell line (Table 1). The compound **1 j** had EC_{50} values at higher micromolar levels, ranging from 2.6 μM to 6.8 μM (Table 1). However, the compound **1 l** showed comparable antiproliferative activity against Panc-1, Capan-1 and SUIT-2 cells, with EC_{50} values of 1.5 μM, 1.4 μM and 1.9 μM, respectively (Figure 3a-c).

Overall, it is clear that all derivatives resulted active from nanomolar to micromolar concentrations, against all of tested cell lines, as it has been confirmed by the range of EC_{50} values, from 0.40 to 7.1 μM (Table 1).

2.2.2. Effects on cell-cycle modulation

Alterations in the cell cycle caused by **1 b**, **1 c** and **1 l** were evaluated in the SUIT-2 cell line, which was selected because of the faster doubling time. Cell cycle progression was analyzed by cytofluorimetry, using propidium iodide (3,8-diamino-5-[3-(diethylmethylammonio)propyl]-6phenyl- diiodide, PI) staining solution.

In SUIT-2 cells, the compound **1 b**, at concentration of 2 μM and 5 μM, decreased the G0/G1 phase from 50.6 % to 37.9 % and 33.5 %, respectively, as well as the S phase from 24.5 % to 17.3 % and 15.5 %. In contrast, the G_2/M phase increased from 24.9 % to 44.8 % and 51.0 %. This could be due to the triggering, in at least some cell subpopulations, of different cell survival mechanisms in response to the antiproliferative effect of this compound, eventually leading to an increase in the number of mitosis events. The cells treated with **1 l**, at both 5 and 10 μM, gave results comparable to the ones obtained from the control samples, while all the samples treated with the compound **1 c**

© 2020 Wiley-VCH GmbH

at 2 μM and at 5 μM, showed a reduction in the percentages of G0/G1 cells to 32.6% and 30.4%, respectively. Conversely, the percentages of cells in the S-phase increased till 30.8% and 33.6%, respectively, while the G_2/M phase increased to 36.6% after treatment with the compound **1c** at both 5 and 10 μM (Figure 4).

2.2.3. Effects on induction of apoptosis

To prove the pro-apoptotic nature of new oxadiazole compounds against pancreatic cancer cells, an evaluation of externalization of plasma membrane phosphatidylserine, a reliable marker of cell apoptosis, was performed by flow cytometry analysis of annexin V-FITC and 7-Amino-Actinomycin D (7-AAD) stained cancer cells.

As shown in Figure 5a, the highest levels of apoptosis features were detectable after SUIT-2 cells were treated with 5 μM or 10 μM of **1l** for 24 hours. The apoptotic rates of SUIT-2 cells were increased in a concentration-dependent manner. In particular, the percentages of apoptotic SUIT-2 cells were 12.6% and 15.9% when compared to the control group (5.4%), when treated with 5 μM and 10 μM of the compound **1l**, respectively. The compound **1c** did also increase apoptotic death to 8.5% and 10.6% at 5 μM and 10 μM, respectively.

Induction of apoptotic death following treatment with **1c** and **1l** suggests that these compounds may orchestrate a potential modulation of the pathways that induce apoptosis, and we performed further studies in the Panc-1, which are mesenchymal pancreatic cancer cells. Compared to control cells (6.2%), the compound **1c**, at 5 μM and 10 μM, increased the apoptotic rate to 19.2% and 19.7%, respectively. The same effect was observed after treatment with **1l**, that increased the apoptotic rate to 18.2 and 19.0% at concentration of 5 and 10 μM (Figure 5). Of note, the compound **1b** did not appreciably induce apoptotic death in both SUIT-2 and Panc-1 cells (data not shown).

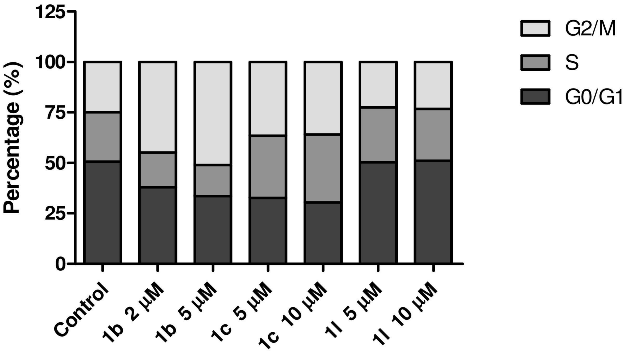

Figure 4. Effects of the oxadiazole compounds **1b**, **1c** and **1l** on cell cycle modulation. SUIT-2 cells were exposed for 24 hours and columns show the mean percentages of cells at various stages of cell cycle, G0/G1 (black), S (dark gray), and G_2/M (light gray) phase, in untreated control and after treatment with the compounds.

2.2.4. Anti-migratory activity

In order to evaluate the impact of the compounds **1b**, **1c**, **1i**, **1j**, and **1l** on cell migration, which constitutes an important step in the metastatic process, the *in vitro* scratch wound healing assay has been performed on Capan-1, Panc-1 and SUIT-2 PDAC cell lines. The Panc-1 cell line was chosen for anti-migration study due to previous studies showing its highly aggressive and strongly metastatic properties.[34] However, further studies were performed in Capan-1 and SUIT-2 which are both derived from liver metastases of PDAC.

The compound **1b**, tested at concentrations of 2 μM and 5 μM, determined a slight inhibition of the migration rate of SUIT-2 and Panc-1 cells compared with untreated cells, 20 hours after the treatment (Table 2). On the other hand, the same

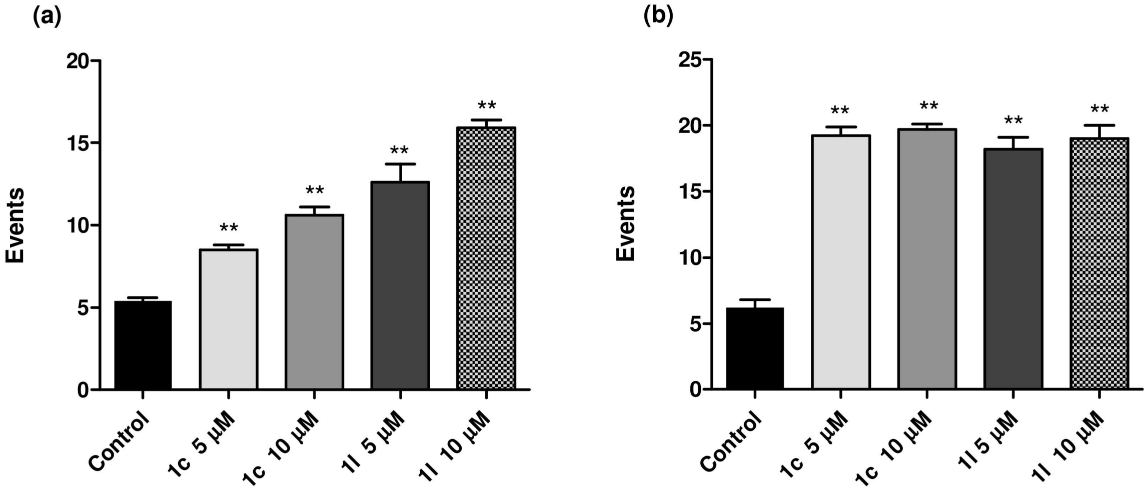

Figure 5. Effects of compounds **1c**, and **1l** on apoptosis induction in SUIT-2 (a) and Panc-1 (b) pancreatic cancer cells. The percentage of cells with apoptotic features was assessed by FACS analysis of annexin V after 24-hour treatment. Columns, mean values obtained from three independent measurements; bars, SEM; **$P < 0.001$ compared to control/untreated cells.

© 2020 Wiley-VCH GmbH

Table 2. Percentages of migration monitored over time (0, 4, 8, 20 and 24 h) of Capan-1, Panc-1 and SUIT-2 cells treated with the compounds **1 b**, **1 c**, **1 i**, **1 j** and **1 l**.

	Percentages of migration [%]											
	Capan-1 hours				Panc-1 hours				SUIT-2 hours			
	4	**8**	**20**	**24**	**4**	**8**	**20**	**24**	**4**	**8**	**20**	**24**
Control	34	43	87	95	29	34	86	95	4	8	17	20
1 b 2 μM	34	35	56	62	28	36	66	77	4	12	13	16
1 b 5 μM	34	36	49	56	25	29	73	81	3	8	12	13
Control	24	37	90	93	56	80	85	75	49	49	58	58
1 c 5 μM	26	34	68	80	40	61	65	77	51	49	62	62
1 c 10 μM	28	29	45	43	45	54	65	61	41	34	60	60
Control	30	5	95	100	20	35	57	67	32	47	51	57
1 i 2 μM	35	63	100	100	30	50	74	130	18	25	51	48
1 i 5 μM	38	71	100	100	40	42	71	133	24	31	54	48
Control	22	44	100	100	50	54	55	52	37	41	54	52
1 j 5 μM	35	57	100	100	50	67	66	56	41	41	53	60
1 j 10 μM	39	56	100	100	60	63	66	56	18	27	52	54
Control	34	34	100	100	20	32	91	96	4	6	7	20
1 l 5 μM	30	32	92	99	18	30	91	93	7	9	17	21
1 l 10 μM	27	31	86	94	14	27	84	92	7	9	14	16

compound, at both above-mentioned concentrations, showed strong inhibitory effects on the migration of Capan-1 cells (Figure 6). These effects were already detectable after 8 hours, as shown by the representative images in the Figure 6c, demonstrating that the cell density in the scratch area was reduced after treatment as reflected by a higher scratch area in treated wells (Figure 6b), compared to untreated/control wells. As reported in the Figure 6a, after 24 hours, the compound **1 b**, reduced the cell migration to 33% and 39%; at the concentration of 2 μM and 5 μM, respectively. The compound **1 c** had minimal effects on SUIT-2, while a 20% decrease of migration was observed in Panc-1 cells between 8 and 20 hours after treatment (Table 2). However, this compound showed the best results in inhibiting the migration of Capan-1 cells, as reflected by a significantly higher scratch area in treated wells. In particular, after 20 h exposure, an average of 90% of the scratches was closed in the untreated wells, whereas after treatment at 5 μM, only 45% of the scratches were closed (Table 2).

The compound **1 i** did not exhibit considerable inhibitory effect on cell migration. Conversely, the wound closure rate of SUIT-2 cells was notably decreased when treated with 10 μM of compound **1 j** at 4 h (18%) and 8 h (27%), compared with untreated/control SUIT-2 cells (37% and 41%, respectively). However, no significant differences in the levels of cell migration were identified for the cells treated with the compound **1 j** at 5 μM. The treatment of Panc-1 and Capan-1 cells with the same compound did not significantly modify the percentages of cell migration with respect to control (Table 2). Similarly, the treatment with the compound **1 l** at two concentrations (5 μM and 10 μM) in the assays performed on SUIT-2, Panc-1 and Capan-1 cells was not able to stop the cells from healing the scratch wound.

2.2.5. Gene expression profiling of key factors in epithelial-mesenchymal transition and evaluation of MMP9 activity

Epithelial-mesenchymal transition (EMT) has been proposed as the critical mechanism for the acquisition of malignant phenotypes by epithelial cancer cells, resulting in tumour invasion and induction of the metastasis process.[35,36]

During EMT, primary site epithelial cells acquire the motile and invasive characteristics of mesenchymal cells, such as motility, invasiveness, and resistance to apoptosis, resulting in secondary tumor formation at another site.[37] Thus, controlling of EMT is considered a promising approach for the inhibition of metastasis.

In order to evaluate the capability of the most promising antitumor compounds (**1 b** and **1 l**) to modulate EMT, we firstly evaluated the effects on EMT critical determinants, such as SNAIL1, SNAL2 and MMP9. To this goal, a specific Real-Time PCR analysis has been performed on the total mRNA extracted from the Panc-1 and Capan-1 PDAC cell lines.

Output data of the Real-Time PCR experiment (Figure 7) have been normalized by a standard curve of the housekeeping gene β-actin, in order to obtain quantitative information about gene expression levels, in Panc-1 and Capan-1 cells treated with the compounds **1 b** and **1 l**, at concentrations of 2 μM and 5 μM, compared to untreated control cells

Our correlation analysis indicated an interesting potential influence of the new topsentin analogues treatment on EMT pathways. In Panc-1 cells, both compounds **1 b** and **1 l** induced over-expression of SNAIL2 and MMP9 and down-regulation of SNAIL1 (Figure 7a). Similarly, in Capan-1 cells, the compounds **1 b** and **1 l** induced over-expression of SNAIL2 and MMP9. However, SNAIL1 expression was up-regulated under **1 b** treat-

© 2020 Wiley-VCH GmbH

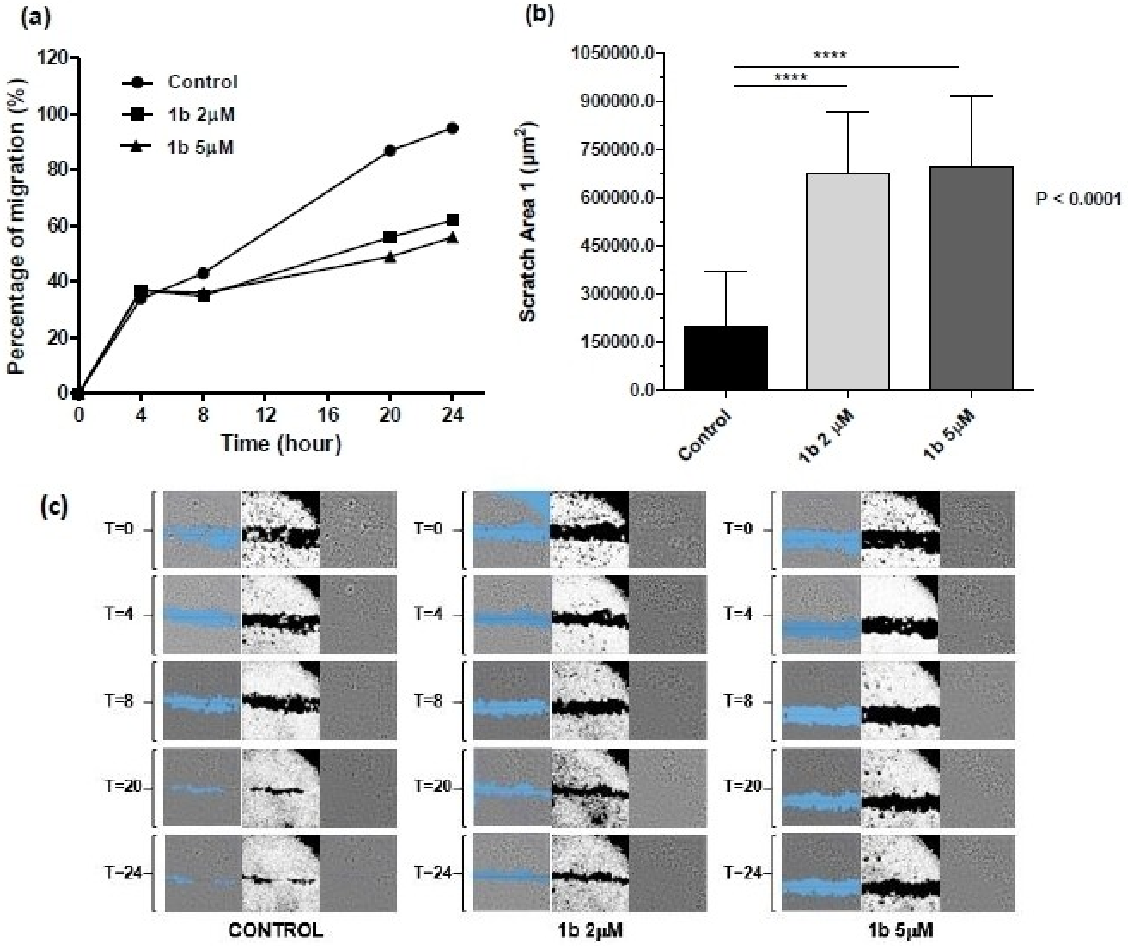

Figure 6. Evaluation of cell migration using the wound healing scratch assay. (a) The percentages of migration were calculated for untreated cells (control, circles), cells treated with **1 b** at concentration of 2 μM (squares) and cells treated with **1 b** at concentration of 5 μM (triangles). (b) Scratch area values and comparison of the areas of the scratches in Capan-1, calculated 20 hours after scratch and treatment with the compound **1 b**. Columns, mean values; bars, SEM; *****P* < 0.0001 compared to control/untreated cells (c) Representative images from wound healing assay of Capan-1 cell cultures treated with or without the compound **1 b** at concentration of 2 μM and 5 μM.

ment. Conversely this expression was down-regulated under **1 l** treatment at 2 μM and up-regulated at 5 μM (Figure 7b).

These studies indicated that, regardless of cell phenotype, SNAIL2 mRNA was significantly over-expressed after treatment with our analogues. As reported in previous studies, we hypothesized the existence of a negative feed-back control by the protein SNAIL2, which might be a potential downstream molecular target of these compounds, and then could provide cells with the capability of buffering, meaning to stabilize SNAIL2 levels in spite of small perturbations.[38] Similarly, the gene of MMP-9 was over-expressed after treatment in both cell lines, suggesting a negative feed-back mechanism that controls MMP-9 mRNA expression. Through a specific gelatine zymography assay we indeed observed a decrease in the activity of MMP-9 protein levels (Figure 8), supporting the anti-migration activity induced by these compounds. In particular, our studies showed a significant decrease of the activity of MMP-9 isolated from Panc-1 and Capan-1 cells, which decreased by about 40% after 24 hours exposure to both compounds at 5 μM.

2.2.6. Modulation of key oncogenic signaling by protein phosphorylation array and ELISA

A protein phosphorylation array was performed on lysates of Panc-1 cells treated with the selected compounds (**1 b** and **1 l**) to assess the phosphorylation or cleavage of an array of important proteins in oncogenic intracellular signaling (Figure 9a). The relative fluorescent units (RFU) were compared between the treatment conditions. We observed a significant decreased phosphorylation in the following proteins and phosphorylation sites: ERK1/2 Thr202/204, Bad Ser112 and GSK3β Ser9. Besides phosphorylation, we also assessed cleavage of caspase-3 and PARP which were associated with the induction of apoptosis, as described above. In order to validate whether our compounds could reduce GSK3β phosphorylation at serine residue 9 as well as at tyrosine 216, which are essential for the kinase activity of this protein we then performed specific ELISA assays. These assays were carried out on Panc-1 cells treated with compounds at concentrations of 5 μM for 24 hours.

© 2020 Wiley-VCH GmbH

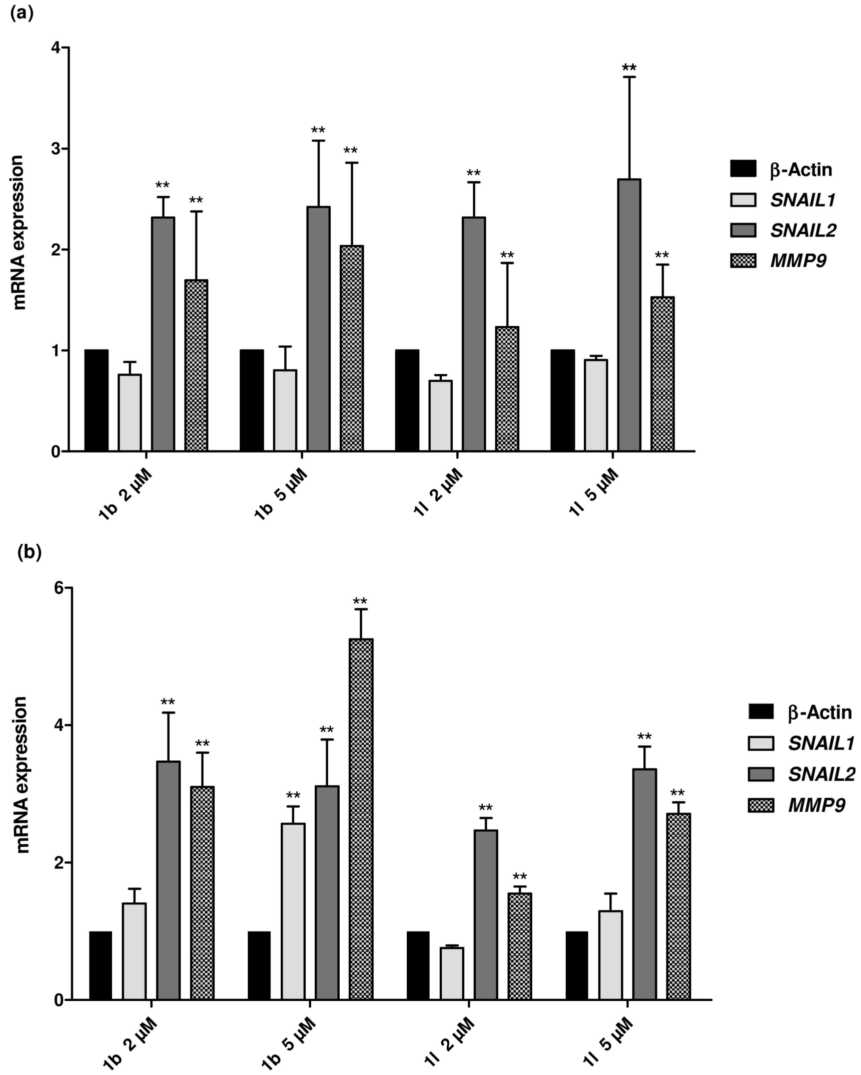

Figure 7. Analysis of the relative levels of SNAIL1, SNAIL2, and MMP9 gene expression by real-time quantitative PCR in Panc-1 (a) and Capan-1 (b) pancreatic cancer cells treated with the compounds **1 b** and **1 l**, at concentration of 2 μM or 5 μM, for 24 hours. Normalized gene expression levels were given as the ratio between the mean value for the target gene and that of the housekeeping genes β-actin in each sample, compared to untreated/control cells whose expression values were set at 1; Columns, mean values; bars, SEM; $^{**}P<0.001$ compared to control/untreated cells.

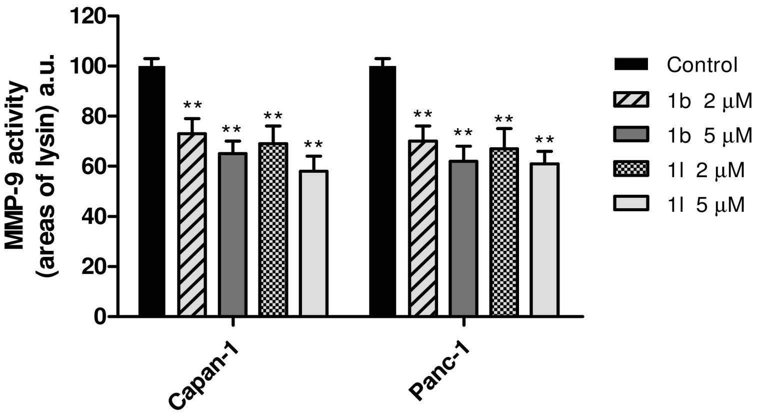

Figure 8. Gelatine zymography analysis of media from Capan-1 and Panc-1 cells incubated with serum-free medium for 24 hours. The enzymatic activity of MMP9 was determined by densitometric analysis. The cells were treated with the compounds **1 b** and **1 l** at concentration IC_{50} and 2x IC_{50} values for 24 hours. Columns, mean values; bars, SEM; $^{**}P<0.001$ compared to control/untreated cells.

© 2020 Wiley-VCH GmbH

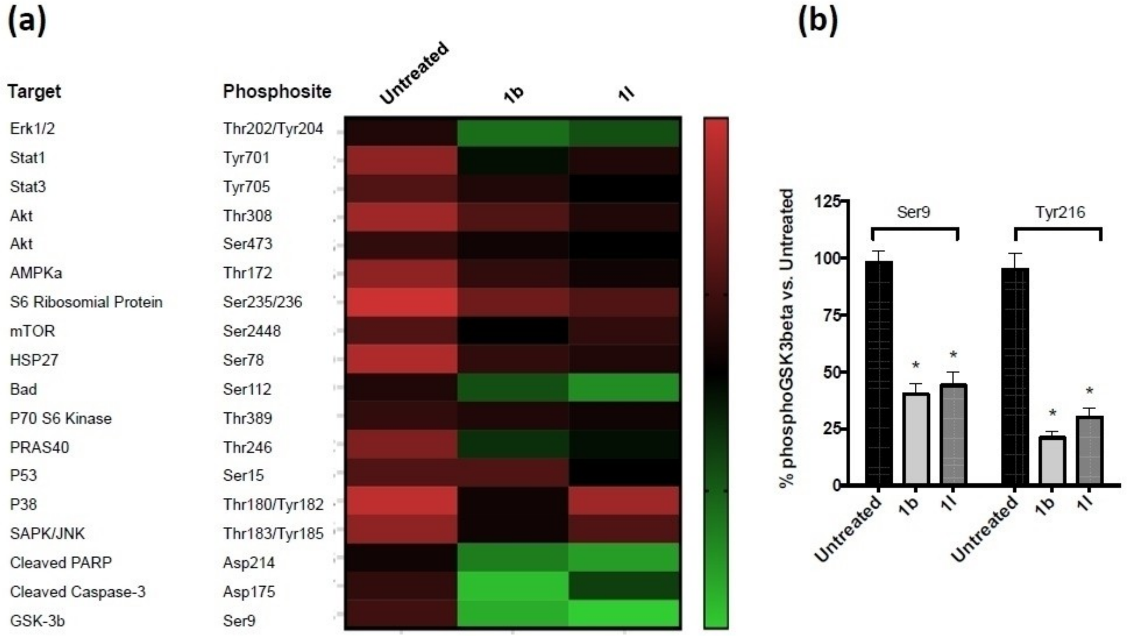

Figure 9. Modulation of key oncogenic signaling by protein phosphorylation array and ELISA. (a) Modulation of the phosphorylation or cleavage of an array of important proteins in oncogenic intracellular signaling. Red signals indicate higher phosphorylation levels, and green signals indicate lower phosphorylation levels. (b) Inhibition of GSK3β phosphorylation by compounds **1 b** and **1 l**. Modulation of phosphorylated-GSK3β (pGSK3β) at serine residue 9 and at tyrosine residue 216 by compounds **1 b** and **1 l** on Panc-1 cells. Columns, mean values; bars, SEM; $^*P < 0.05$.

As shown in the Figure 9b, we observed a reduction of phospho-GSK3β at serine residue 9 ranging from 40% to 50%, while the inhibition of phospho-GSK3β at tyrosine residue 216 ranged between 70 and 80%. Similar results were observed using the known inhibitor enzastaurin (data not shown). These results suggest that GSK3β is a target of our compounds and might explain how they can then suppress GSK3β-driven proliferation, anti-apoptotic and migration activities.

2.2.7. Kinase activity assays and molecular modelling

To further investigate whether our compounds could modulate the activity of GSK-3β, a specific ADP-Glo™ activity assay was employed. As shown in Figure 10a, the novel 1,2,4-oxadiazole compounds exhibited inhibition on GSK-3β in a dose-dependent manner. The concentrations leading to a loss of 50% enzyme activity (IC_{50}) for the two most active compounds (**1 b** and **1 l**) were 0.62 and 0.81 μM, respectively. The other compounds (**1 c**, **1 l** and **1 j**) inhibited GSK3β, with a slightly

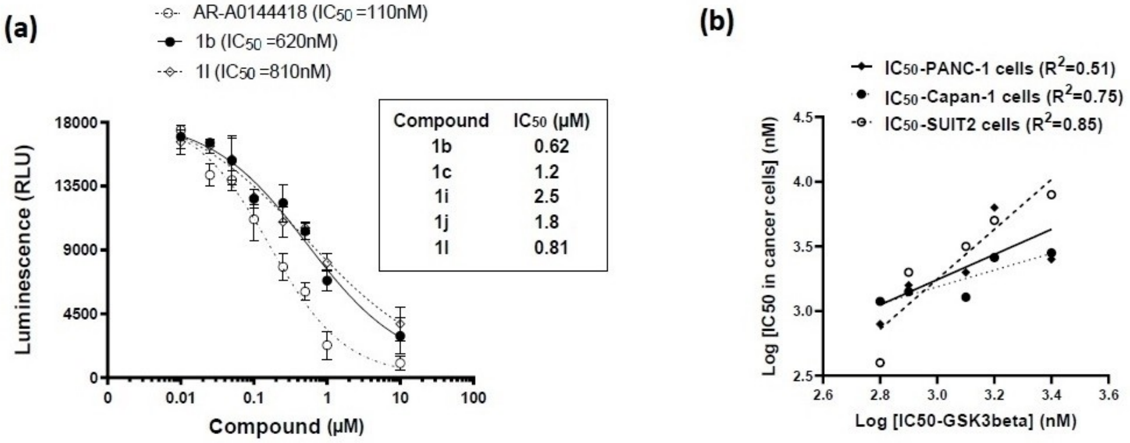

Compound	IC50 (μM)
1b	0.62
1c	1.2
1i	2.5
1j	1.8
1l	0.81

Figure 10. Effects of most active compounds **1 b**, **1 c**, **1 i**, **1 j** and **1 l** on the *in vitro* GSK-3β kinase activity. (a) Determination of IC_{50} values of inhibitors using ADP-Glo™ assay. (b) Linear regression analyses to determine relationships between concentration achieving a 50% inhibition (IC_{50}) of PDAC cell growth and half- maximal inhibitory concentration (IC_{50}) in inhibiting the GSK-3β kinase activity.

© 2020 Wiley-VCH GmbH

lower potency (IC_{50} values in the range of 1.2–2.5 μM). In order to verify the accuracy of this method, AR-A0144418, a specific GSK-3β inhibitor, was used as positive control and its IC_{50} value was 0.11 μM, in agreement with previous data from literature (0.104 μM).[39] These results indicate that our novel oxadiazole compounds are direct GSK-3β inhibitors *in vitro*. Despite the low number of data points, the anti-GSK3β activity seems to correlate with the IC_{50} values obtained in the antiproliferative assays, as reported in Figure 10b, with R^2 values ranging from 0.51 to 0.85 and *P* values <0.05 at the Sperman analyses. A potential binding mode for the most active compounds **1 b** and **1 c** within the ATP binding site of GSK-3β is depicted in Figure 11. Both compounds were docked in the ATP binding site of GSK3β (PDB 1UV5)[40] showing similar interactions to the co-crystalized ligand 6-bromoindirubin, a known potent and selective bis-indolyl inhibitor of the enzyme. Compounds **1 b** and **1 l** are located into the same narrow hydrophobic pocket of the co-crystallized ligand, establishing a hydrogen bond through their indole nitrogen with the peptide carbonyl oxygen of Val135 residue. Moreover, their carbonyl group accepts a hydrogen bond from a water molecule interacting with Lys85, a residue that has been successfully targeted by carbonyl groups of potent inhibitors by direct or water-mediated interactions.[41,42]

3. Conclusion

A new series of sixteen topsentin analogues, characterized by a central 1,2,4-oxadiazole ring, was efficiently synthesized. Five of these new topsentin derivatives exhibited good antiproliferative activity against a panel of PDAC cells, namely SUIT-2, Capan-1 and Panc-1, with EC_{50} values ranging from micromolar to sub-micromolar level. A particular efficacy was observed for the compound **1 b** against all PDAC preclinical models, showing EC_{50} values in the range of 0.40–1.19 μM. The mechanism of the anti-proliferative effect of these derivatives was pro-apoptotic, being associated with externalization of plasma membrane phosphatidylserine, a reliable marker of cell apoptosis. Through wound-healing assays we found remarkably reduction of cell migration in the metastatic Capan-1 PDAC preclinical model when treated with the most promising compound **1 b**. These effects might be explained by interesting influence of the new topsentin analogues treatment on EMT determinants such as SNAIL-2 and metalloproteinase-9. Moreover, PathScan intracellular signaling and ELISA assays in Panc-1 cells revealed a significant inhibition of GSK3β phosphorylation, suggesting this kinase as a potential downstream target of our novel compounds. This was further supported by data from *in vitro* assay for GSK3β activity and molecular modelling. Future studies should investigate the kinase profiling data of our compounds against a wide range of kinases.

Experimental Section

Chemistry

Analytical thin layer chromatography (TLC) was performed on silica gel 60 F254 plates (0.25 mm thickness) and the develop plates were examined under ultraviolet (UV) light. All melting points were taken on a Buchi-Tottoly capillary apparatus and were uncorrected. IR spectra were determined in bromoform with a Shimadzu FT / IR 8400S spectrophotometer and peaks were reported in wavenumber (cm^{-1}). ^1H and ^{13}C NMR spectra were measured at 200 and 50 MHz, respectively, on [D_6]DMSO solution, using a Bruker Avance II series 200 MHz spectrometer. Chromatography column was performed with MERK silica gel 230–400 mesh ASTM or FLASH40i Biotage chromatography or with Buchi Sepacore chromatography module (prepacked cartridge reference). Elementary analyses (C, H, N) were within ±0.4% of the theoretical values and were performed with a VARIO EL III elemental analyzer (Elementar, Langenselbold, Germany). The HRMS have been obtained on a Thermo Q-Exactive system.

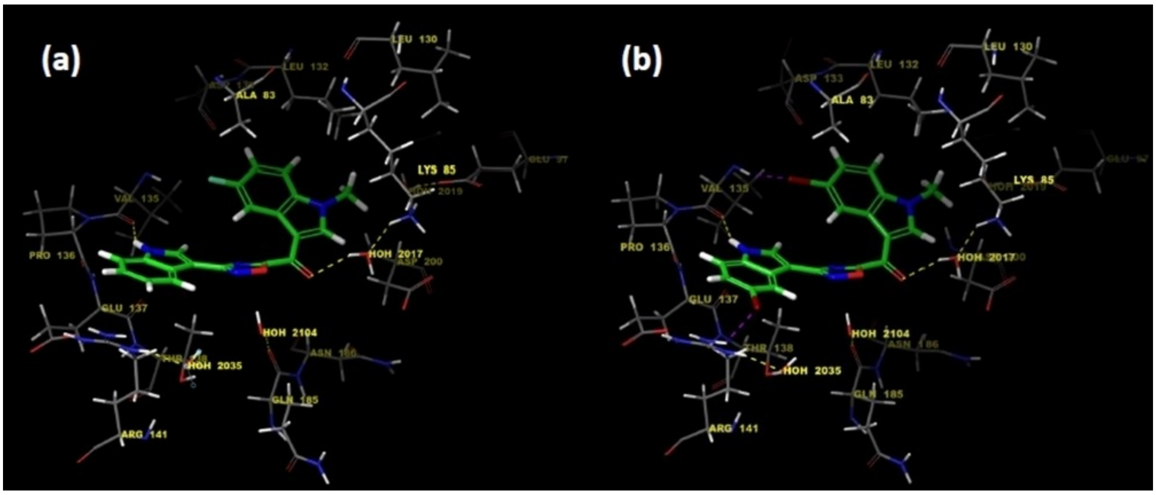

Figure 11. Proposed binding mode of compounds **1 b** (a) and **1 l** (b) with GSK3β (PDB ID: 1UV5). H-bonds between the indole nitrogen of our compounds with the peptide carbonyl oxygen of Val135 residue, as well as the water-mediated interaction between the carbonyl group adjacent to oxadiazole ring and the Lys85 residue are shown with yellow dashed lines.

© 2020 Wiley-VCH GmbH

General procedure for the synthesis of *N*-hydroxy-1*H*-indole-3-carboxamidines (2 a-d)

To a solution of the appropriate indole carbonitrile **4 a**–**d** (2.88 mmol) in anhydrous ethanol (50 mL), *N,N*-diisopropylethylamine (DIPEA) (1.08 mL) and hydroxylamine hydrochloride ($NH_2OH{\cdot}HCl$) (530 mg, 7.63 mmol) were added in portions. The reaction mixture was heated to vigorous reflux for 4 hours. The solvent was removed under reduced pressure and the residue was treated with a saturated aqueous solution of sodium hydrogen carbonate ($NaHCO_3$) (10 mL) and then extracted with ethyl acetate (3×20 mL), dried (Na_2SO_4), filtered and concentrated under *vacuum*. The product was purified by column chromatography using dichloromethane/ethyl acetate (DCM/EtOAc) or EtOAc as eluent.

*5-Bromo-N′-hydroxy-1H-indole-3-carboxamidine (**2 a**).* Eluent: DCM/EtOAc 75:25 (v/v); $R_f = 0.42$ (EtOAc); white solid; yield: 85%; mp: 167.6-168.6 °C; ^1H NMR (200 MHz, [D_6]DMSO) δ: 5.70 (s, 2H, NH_2), 7.22 (dd, $J = 8.6$, 2.6 Hz, 1H, H-6), 7.36 (d, $J = 8.6$ Hz, 1H, H-7), 7.84 (d, $J = 2.6$ Hz, 1H, H-4), 8.27 (d, $J = 1.9$ Hz, 1H, H-2), 9.34 (s, 1H, OH), 11.47 (s, 1H, NH); ^{13}C NMR (50 MHz, [D_6]DMSO) δ: 108.6 (s), 112.0 (s), 113.4 (d), 123.9 (d), 124.3 (d), 126.0 (d), 126.2 (s), 135.0 (s), 148.8 (s); IR (KBr): $\tilde{\nu} = 3476$ (OH), 3382 (NH_2), 3310 (NH), 1653 cm^{-1} (C=N); elemental analysis calcd (%) for $C_9H_8BrN_3O$ (MW: 254.08): C, 42.54; H, 3.17; N, 16.54; found: C, 42.70; H, 3.38; N, 16.32.

*5-Fluoro-N′-hydroxy-1H-indole-3-carboxamidine (**2 b**).* Eluent: EtOAc; $R_f = 0.38$ (EtOAc); white solid; yield: 78%; mp: 142.7-143.7 °C; ^1H NMR (200 MHz, [D_6]DMSO) δ: 5.64 (s, 2H, NH_2), 6.96 (td, $J = 9.1$, 9.1, 2.7 Hz, 1H, H-6), 7.37 (dd, $J = 9.1$, 4.7 Hz, 1H, H-7), 7.73-7.86 (m, 2H, H-4 and H-2), 9.25 (s, 1H, OH), 11.36 (s, 1H, NH); ^{13}C NMR (50 MHz, [D_6]DMSO) δ: 106.5 (d, $J_{C4\text{-}F} = 24.4$ Hz), 109.1 (d, $J_{C7a\text{-}F} = 4.7$ Hz), 109.7 (d, $J_{C6\text{-}F} = 26.1$ Hz), 112.4 (d, $J_{C7\text{-}F} = 9.6$ Hz), 124.7 (d, $J_{C3a\text{-}F} = 11.0$ Hz), 126.4 (d), 133.0 (s), 149.1 (s), 157.1 (d, $J_{C5\text{-}F} = 231.9$ Hz); IR (KBr): $\tilde{\nu} = 3467$ (OH), 3359 (NH_2), 3200 (NH), 1630 cm^{-1} (C=N); elemental analysis calcd (%) for $C_9H_8FN_3O$ (MW: 193.18): C, 55.96; H, 4.17; N, 21.75; found: C, 56.02; H, 4.38; N, 21.52.

*N′-Hydroxy-1H-indole-3-carboxamidine (**2 c**).* Eluent: DCM/EtOAc 55:45 (v/v); $R_f = 0.33$ (EtOAc); white solid; yield: 75%; mp: 147–148 °C; spectroscopic data in accordance with those reported in literature.[43]

*5-Metoxy-N′-hydroxy-1H-indole-3-carboxamidine (**2 d**).* Eluent: EtOAc; $R_f = 0.44$ (EtOAc); white solid; yield: 80%; mp: 113.2-114.2 °C; ^1H NMR (200 MHz, [D_6]DMSO) δ: 3.74 (s, 3H, OCH_3), 5.59 (s, 2H, NH_2), 6.75 (dd, $J = 8.8$, 2.5 Hz, 1H, H-6), 7.27 (d, $J = 8.8$ Hz, 1H, H-7), 7.58 (d, $J = 2.5$ Hz, 1H, H-4), 7.73 (s, 1H, H-2), 9.23 (s, 1H, OH), 11.11 (s, 1H, NH); ^{13}C NMR (50 MHz, [D_6]DMSO) δ: 55.2 (q), 103.5 (d), 108.7 (s), 111.8 (d), 112.0 (d), 124.9 (s), 125.1 (d), 131.4 (s), 149.6 (s), 153.6 (s); IR (KBr): $\tilde{\nu} = 3467$ (OH), 3364 (NH_2), 3279 (NH), 1634 cm^{-1} (C=N); elemental analysis calcd (%) for $C_{10}H_{11}N_3O_2$ (MW: 205.21): C, 58.53; H, 5.40; N, 20.48; found: C, 58.84; H, 5.21; N, 20.22.

*General procedure for the synthesis of (1-methyl-1*H*-indol-3-yl)-oxo-acetyl chlorides (7 a–d)*

To a solution of the opportune methyl-indole of the type **6** (10 mmol) in anhydrous diethyl ether (20 mL), oxalyl chloride (11.16 mmol, 0.95 mL) was added dropwise at 0 ° C. The reaction mixture was left to stir at 0 ° C for 3 hours and then brought to room temperature for 1 hour. The resulting solid product was collected by *vacuum* filtration and recrystallized from diethyl ether.

*(5-Bromo-1-methyl-1H-indol-3-yl)-oxo-acetyl chloride (**7 a**).* $R_f = 0.68$ (CH_2Cl_2/MeOH 6:4); yellow solid; yield: 91%; mp: 134.4-135.4 °C; ^1H NMR (200 MHz, [D_6]DMSO) δ: 3.92 (s, 3H, CH_3), 7.50 (dd, $J = 8.7$, 1.9 Hz, 1H, H-6), 7.61 (d, $J = 8.7$ Hz, 1H, H-7), 8.31 (d, $J = 1.9$ Hz, 1H, H-4) 8.55 (s, 1H, H-2); ^{13}C NMR (50 MHz, [D_6]DMSO) δ: 33.6 (q), 110.6 (s), 113.4 (d), 115.9 (s), 123.3 (d), 126.2 (d), 127.7 (s), 136.2 (s), 142.2 (d), 164.6 (s), 179.9 (s); IR (KBr): $\tilde{\nu} = 1772$ (CO), 1613 cm^{-1} (CO); elemental analysis calcd (%) for $C_{11}H_7BrClNO_2$ (MW: 300.54): C, 43.96; H, 2.35; N, 4.66; found: C, 44.14; H, 2.29; N, 4.78.

*(5-Fluoro-1-methyl-1H-indol-3-yl)-oxo-acetyl chloride (**7 b**).* $R_f = 0.75$ (CH_2Cl_2/MeOH 6:4); yellow solid; yield: 96%, mp: 148.6-149.6 °C; ^1H NMR (200 MHz, [D_6]DMSO) δ: 3.93 (s, 3H, CH_3), 7.22 (td, $J = 9.6$, 9.2, 2.6 Hz, 1H, H-6), 7.64 (dd, $J = 9.2$, 4.4 Hz, 1H, H-7), 7.86 (dd, $J = 9.6$, 2.6 Hz, 1H, H-4), 8.55 (s, 1H, H-2); ^{13}C NMR (50 MHz, [D_6]DMSO) δ: 33.7 (q), 106.2 (d, $J_{C4\text{-}F} = 24.8$ Hz), 111.1 (d, $J_{C7a\text{-}F} = 4.4$ Hz), 111.7 (d, $J_{C6\text{-}F} = 25.7$ Hz), 112.7 (d, $J_{C7\text{-}F} = 9.8$ Hz), 126.7 (d, $J_{C3a\text{–}F} = 11.2$ Hz), 134.0 (s), 142.4 (d), 159.3 (d, $J_{C5\text{-}F} = 234.3$ Hz), 166.4 (s), 181.2 (s); IR (KBr): $\tilde{\nu} = 1743$ (CO), 1642 cm^{-1} (CO); elemental analysis calcd (%) for $C_{11}H_7ClFNO_2$ (MW: 239.63): C, 55.13; H, 2.94; N, 5.85; found: C, 54.98; H, 3.01; N, 5.69.

*(1-Methyl-1H-indol-3-yl)-oxo-acetyl chloride (**7 c**).* $R_f = 0.66$ (CH_2Cl_2/MeOH 6:4); yellow solid; yield: 89%, mp: 156.4-157.4 °C; ^1H NMR (200 MHz, [D_6]DMSO) δ: 3.93 (s, 3H, CH_3), 7.28-7.41 (m, 2H, H-5 and H-6), 7.59-7.64 (m, 1H, H-7), 8.18-8.23 (m, 1H, H-4), 8.50 (s, 1H, H-2); ^{13}C NMR (50 MHz, [D_6]DMSO) δ: 33.4 (q), 111.1 (s), 111.2 (d), 121.2 (d), 123.1 (d), 123.7 (d), 126.0 (s), 137.35 (s), 141.3 (d), 165.1 (s), 180.0 (s); IR (KBr): $\tilde{\nu} = 1735$ (CO); 1604 cm^{-1} (CO); elemental analysis calcd (%) for $C_{11}H_8ClNO_2$ (MW: 221.64): C, 59.61; H, 3.64; N, 6.32; found: C, 59.69; H, 3.70; N, 6.18.

*(5-Methoxy-1-methyl-1H-indol-3-yl)-oxo-acetyl chloride (**7 d**).* $R_f = 0.60$ (CH_2Cl_2/MeOH 6:4); orange solid; yield: 90%, mp: 132.2-133.2 °C; ^1H NMR (200 MHz, [D_6]DMSO) δ: 3.82 (s, 3H, CH_3), 3.89 (s, 3H, OCH_3), 6.98 (dd, $J = 8.9$, 2.5 Hz, 1H, H-6), 7.52 (d, $J = 8.9$ Hz, 1H, H-7), 7.70 (d, $J = 2.5$ Hz, 1H, H-4), 8.42 (s, 1H, H-2); ^{13}C NMR (50 MHz, [D_6]DMSO) δ: 33.5 (q), 55.3 (q), 103.2 (d), 110.9 (s), 112.0 (d), 113.1 (d), 127.0 (s), 132.2 (s), 141.0 (d), 156.4 (s), 165.3 (s), 180.0 (s); IR (KBr): $\tilde{\nu} = 1779$ (CO); 1625 cm^{-1} (CO); elemental analysis calcd (%) for $C_{12}H_{10}ClNO_3$ (MW: 251.67): C, 57.27; H, 4.01; N, 5.57%; found: C, 57.19; H, 4.12; N, 5.37.

*General procedure for the synthesis of (1-methyl-1*H*-indol-3-yl)-oxo-acetic acids (3 a-d)*

To a solution of the suitable acyl chloride of the type **7** (10 mmol) in anhydrous tetrahydrofuran (THF) (20 mL), a solution of sodium hydroxide (NaOH) 2 M (15 mL) was added dropwise, until complete alkalization, reaching a pH of 14. The reaction mixture was stirred at room temperature overnight. A solution of hydrochloric acid (HCl) 6 M (10 mL) was added up to pH = 1. The resulting solid precipitate was collected by *vacuum* filtration, washed with water and dried under *vacuum* for 24 hours and purified by column chromatography using ethyl acetate as eluent to give desired oxo-acetic acids **3 a**-**d**.

*(5-Bromo-1-methyl-1H-indol-3-yl)-oxo-acetic acid (**3 a**).* $R_f = 0.20$ (CH_2Cl_2/MeOH 8:2); yellow solid; yield: 87%; mp: 256.6 °C; ^1H NMR (200 MHz, [D_6]DMSO) δ: 3.93 (s, 3H, CH_3), 7.50 (dd, $J = 8.7$, 1.5 Hz, 1H, H-6), 7.62 (d, $J = 8.7$ Hz, 1H, H-7), 8.31 (d, $J = 1.5$ Hz, 1H, H-4), 8.55 (s, 1H, H-2), 14.03 (s, 1H, OH); ^{13}C NMR (50 MHz, [D_6]DMSO) δ: 33.6 (q), 110.6 (s), 113.4 (d), 116.0 (s), 123.3 (d), 126.2 (d), 127.7 (s), 136.2 (s), 142.2 (d), 164.7 (s), 180.0 (s); IR (KBr): $\tilde{\nu} = 3273$ (OH), 1760 (CO), 1628 cm^{-1} (CO); elemental analysis calcd (%) for $C_{11}H_8BrNO_3$ (MW: 282.09): C, 46.84; H, 2.86; N, 4.97; found: C, 46.54; H, 2.98; N, 5.04%.

*(5-Fluoro-1-methyl-1H-indol-3-yl)-oxo-acetic acid (**3 b**).* $R_f = 0.16$ (CH_2Cl_2/MeOH 8:2); yellow solid; yield: 95%; mp: 194.5 °C; ^1H NMR (200 MHz, [D_6]DMSO) δ: 3.93 (s, 3H, CH_3), 7.23 (td, $J = 9.2$, 9.1, 2.6 Hz, 1H, H-6), 7.66 (dd, $J = 9.1$, 4.5 Hz, 1H, H-7), 7.86 (dd, $J = 9.2$, 2.6 Hz,

1H, H-4), 8.56 (s, 1H, H-2), 13.94 (s, 1H, OH); ^{13}C NMR (50 MHz, [D$_6$]DMSO) δ: 33.7 (q), 106.2 (d, J_{C4-F} = 24.8 Hz), 111.1 (d, J_{C7a-F} = 4.4 Hz), 111.7 (d, J_{C6-F} = 25.7 Hz), 112.8 (d, J_{C7-F} = 9.8 Hz,) 126.8 (d, J_{C3a-F} = 11.2 Hz), 134.0 (s) 142.4 (d) 159.3 (d, J_{C5-F} = 234.3 Hz), 164.8 (s), 179.9 (s); IR (KBr): $\tilde{\nu}$ = 3216 (OH), 1760 (CO), 1623 cm^{-1} (CO); elemental analysis calcd (%) for $C_{11}H_8FNO_3$ (MW: 221.18): C, 59.73; H, 3.65; N, 6.33; found: C, 59.84; H, 3.71; N, 6.83.

*(1-Methyl-1H-indol-3-yl)-oxo-acetic acid (**3 c**).* R_f = 0.24 (CH_2Cl_2/MeOH 8:2); yellow solid; yield: 78%; mp: 150.6 °C; ^{1}H NMR (200 MHz, [D$_6$]DMSO) δ: 3.93 (s, 3H, CH$_3$), 7.28-7.41 (m, 2H, H-5 and H-6), 7.62 (m, 1H, H-7), 8.20 (m, 1H, H-4), 8.49 (s, 1H, H-2), 13.88 (s, 1H, OH); ^{13}C NMR (50 MHz, [D$_6$]DMSO) δ: 33.4 (q), 111.1 (s), 111.2 (d), 121.2 (d), 123.1 (d), 123.7 (d), 126.0 (s), 137.3 (s), 141.3 (d), 165.2 (s), 180.2 (s); IR (KBr): $\tilde{\nu}$ = 3261 (OH), 1748 (CO), 1623 cm^{-1} (CO); elemental analysis calcd (%) for $C_{11}H_9NO_3$ (MW: 203.19): C, 65.02; H, 4.46; N, 6.89; Found: C, 65.18; H, 4.36; N, 6.99.

*(5-Methoxy-1-methyl-1H-indol-3-yl)-oxo-acetic acid (**3 d**).* R_f = 0.22 (CH_2Cl_2/MeOH 8:2); yellow solid; yield: 86%; mp: 196.2 °C; ^{1}H NMR (200 MHz, [D$_6$]DMSO) δ: 3.82 (s, 3H, CH$_3$), 3.89 (s, 3H, OCH$_3$), 6.98 (dd, J = 8.9, 2.5 Hz, 1H, H-6), 7.52 (d, J = 8.9 Hz, 1H, H-7), 7.7 (d, J = 2.5 Hz, 1H, H-4), 8.41 (s, 1H, H-2), 13.89 (s, 1H, OH); ^{13}C NMR (50 MHz, [D$_6$]DMSO) δ: 33.5 (q), 55.3 (q) 103.2 (d), 110.9 (s), 112.0 (d), 113.1 (d), 127.0 (s), 132.2 (s), 141.0 (d), 156.4 (s), 165.3 (s), 180.0 (s); IR (KBr): $\tilde{\nu}$ = 3216 (OH), 1765 (CO), 1628 cm^{-1} (CO); elemental analysis calcd (%) for $C_{12}H_{11}NO_4$ (MW: 233.22): C, 61.80; H, 4.75; N, 6.01; found: C, 61.60; H, 4.55; N, 6.21.

General procedure for the synthesis of [3-(1H-indol-3-yl)-1,2,4-oxadiazol-5-yl](1-methyl-1H-indol-3-yl) methanones (1 a-p)

To a solution of the proper (1-methyl-1*H*-indol-3-yl)-oxo-acetic acid **3 a-d** (1.42 mmol) and 1-hydroxybenzotriazole hydrate (HOBt) (230 mg, 1.7 mmol) in anhydrous dimethylformamide (DMF) (2 mL) at 0 °C, *N*-ethyl-*N′*-(3-dimethylaminopropyl)carbodiimide hydrochloride (EDC·HCl) (326 mg, 1.7 mmol) was added in portions. After 15 min, a DMF (1 mL) solution of triethylamine (Et_3N) (0.2 mL, 1.42 mmol) and appropriate carboxamidine **2 a-d** (0.71 mmol) was added dropwise at 0 °C. The reaction mixture was stirred at 0 °C for 15 minutes. After bringing the reaction mixture to room temperature, it was heated at 100 °C for 15 minutes. After cooling, the mixture was poured into water and ice; the obtained precipitate was filtered off and dried under high *vacuum*. The crude was purified on flash chromatography, using dichloromethane as eluent, to obtain the desired products **1 a-p.**

*(5-Bromo-1-methyl-1H-indol-3-yl)[3-(1H-indol-3-yl)-1,2,4-oxadiazol-5-yl]methanone (**1 a**).* R_f = 0.78 (CH_2Cl_2/EtOAc 7:3); yellow solid; yield: 45%; mp: 255 °C (dec.); ^{1}H NMR (200 MHz, [D$_6$]DMSO) δ: 4.04 (s, 3H, CH$_3$), 7.22–7.32 (m, 2H, H-5′ and H-6′), 7.54–7.72 (m, 3H, H-6, H-7′ and H-7), 8.07- 8.11 (m, 1H, H-4′), 8.43–8.46 (m, 2H, H-4 and H-2′), 9.16 (s, 1H, H-2), 12.07 (s, 1H, NH); ^{13}C NMR (50 MHz, [D$_6$]DMSO) δ: 33.9 (q), 101.9 (s), 112.0 (s), 112.4 (d), 113.7 (d), 116.4 (s), 120.5 (d), 121.1 (d), 122.7 (d), 123.6 (d), 124.2 (s), 126.6 (d), 128.1 (s), 129.9 (d), 136.4 (s), 136.8 (s), 143.2 (d), 165.4 (s), 169.2 (s), 170.4 (s); IR (KBr): $\tilde{\nu}$ = 3280 (NH), 1623 cm^{-1} (CO); elemental analysis calcd (%) for $C_{20}H_{13}BrN_4O_2$ (MW: 421.25): C, 57.02; H, 3.11; N, 13.30; found: C, 57.10; H, 3.21; N, 13.24.

*(5-Fluoro-1-methyl-1H-indol-3-yl)[3-(1H-indol-3-yl)-1,2,4-oxadiazol-5-yl]methanone (**1 b**).* R_f = 0.77 (CH_2Cl_2/EtOAc 7:3); yellow solid; yield: 46%; mp: 248 °C (dec.); ^{1}H NMR (200 MHz, [D$_6$]DMSO) δ: 4.05 (s, 3H, CH$_3$), 7.25–7.32 (m, 3H, H-5′, H-6′ and H-6), 7.55–7.59 (m, 1H, H-7′), 7.74 (dd, J = 8.9, 2.4 Hz, 1H, H-7), 7.98–8.12 (m, 2H, H-4′ and H-4), 8.43 (d, J = 2.8 Hz, 1H, H-2′), 9.17 (s, 1H, H-2), 12.06 (s, 1H, NH); ^{13}C NMR (50 MHz, [D$_6$]DMSO) δ: 34.0 (q), 99.5 (d), 101.9 (s), 106.6 (d, J_{C4-F} = 25.4 Hz), 112.1 (d, J_{C6-F} = 29.2 Hz), 112.6 (d, J_{C7a-F} = 4.0 Hz), 113.1 (d, J_{C7-F} = 9.7 Hz), 120.5 (d), 121.1 (d), 122.7 (d), 124.2 (s), 127.2 (d, J_{C3a-F} = 10.9 Hz), 129.9 (d), 134.2 (s), 136.8 (s), 143.5 (d), 159.6 (d, J_{C5-F} = 237.3 Hz), 165.4 (s), 169.3 (s), 170.3 (s); IR (KBr): $\tilde{\nu}$ = 3281 (NH), 1617 cm^{-1} (CO); elemental analysis calcd (%) for $C_{20}H_{13}FN_4O_2$ (MW: 360.34): C, 66.66; H, 3.64; N, 15.55; found: C, 66.78; H, 3.51; N, 15.34; HRMS: *m/z* = 361.11 [M + H]$^+$; t_R = 3.57 min (> 98 % purity).

*[3-(1H-Indol-3-yl)-1,2,4-oxadiazol-5-yl](1-methyl-1H-indol-3-yl) methanone (**1 c**).* R_f = 0.83 (CH_2Cl_2/EtOAc 7:3); yellow solid; yield: 50%; mp: 230 °C (dec.); ^{1}H NMR (200 MHz, [D$_6$]DMSO) δ: 4.04 (s, 3H, CH$_3$), 7.23-7.33 (m, 2H, H-5 and H-5′), 7.40-7.47 (m, 2H, H-6 and H-6′), 7.55- 7.60 (m, 1H, H-7′), 7.68-7.72 (m, 1H, H-7), 8.07-8.13 (m, 1H, H-4′), 8.33-8.37 (m, 1H, H-4), 8.43 (d, J = 2.8 Hz, 1H, H-2′), 9.13 (s, 1H, H-2), 12.07 (s, 1H, NH); ^{13}C NMR (50 MHz, [D$_6$]DMSO) δ: 33.7 (q), 102.0 (s), 111.4 (d), 112.4 (d), 112.7 (s), 120.5 (d), 121.1 (d), 121.5 (d), 122.7 (d), 123.6 (d), 124.1 (d), 124.2 (s), 126.4 (s), 129.8 (d), 136.8 (s), 137.5 (s), 142.5 (d), 165.3 (s), 169.6 (s), 170.4 (s); IR (KBr): $\tilde{\nu}$ = 3393 (NH), 1617 cm^{-1} (CO); elemental analysis calcd (%) for $C_{20}H_{14}N_4O_2$ (MW: 342.35): C, 70.17; H, 4.12; N, 16.37; found: C, 70.30; H, 4.30; N, 16.14; HRMS: *m/z* = 343.12 [M + H]$^+$; t_R = 3.52 min (> 98 % purity).

*[3-(1H-Indol-3-yl)-1,2,4-oxadiazol-5-yl](5-methoxy-1-methyl-1H-indol-3-yl)methanone (**1 d**).* R_f = 0.78 (CH_2Cl_2/EtOAc 7:3); yellow solid; yield: 48%; mp: 258 °C (dec.); ^{1}H NMR (200 MHz, [D$_6$]DMSO) δ: 3.86 (s, 3H, CH$_3$), 4.01 (s, 3H, OCH$_3$), 7.04 (dd, J = 8.9, 2.4 Hz, 1H, H-6′), 7.23-7.33 (m, 2H, H-5 and H-6), 7.55-7.62 (m, 2H, H-7′ and H-7), 7.85 (d, J = 2.4 Hz, 1H, H-4′), 8.08-8.13 (m, 1H, H-4), 8.42 (d, J = 2.4 Hz, 1H, H-2′), 9.04 (s, 1H, H-2), 12.05 (s, 1H, NH); ^{13}C NMR (50 MHz, [D$_6$]DMSO) δ: 33.9 (q), 55.4 (q), 102.0 (s), 103.5 (d), 112.4 (d), 113.4 (d), 120.5 (d), 121.1 (d), 122.7 (d), 124.2 (s), 127.4 (s), 129.6 (d), 129.8 (d), 132.4 (s), 133.5 (s), 136.8 (s), 142.2 (d), 156.8 (s), 165.3 (s), 169.6 (s), 170.2 (s); IR (KBr): $\tilde{\nu}$ = 3228 (NH), 1617 cm^{-1} (CO); elemental analysis calcd (%) for $C_{21}H_{16}N_4O_3$ (MW: 372.38): C, 67.73; H, 4.33; N, 15.05; found: C, 67.92; H, 4.12; N, 15.14.

*(5-Fluoro-1-methyl-1H-indol-3-yl)[3-(5-methoxy-1H-indol-3-yl)-1,2,4-oxadiazol-5-yl]methanone (**1 e**).* R_f = 0.72 (CH_2Cl_2/EtOAc 7:3); Yellow solid; yield: 60%; mp: 262 °C (dec.); ^{1}H NMR (200 MHz, [D$_6$]DMSO) δ: 3.85 (s, 3H, CH$_3$), 4.04 (s, 3H, OCH$_3$), 6.92 (dd, J = 8.8, 2.4 Hz, 1H, H-6′), 7.29 (td, J = 9.2, 9.2, 2.6 Hz, 1H, H-6), 7.46 (d, J = 8.8 Hz, 1H, H-7′), 7.56 (d, J = 2.4 Hz, 1H, H-4′), 7.74 (dd, J = 9.2, 4.4 Hz, 1H, H-7), 8.01 (dd, J = 9.6, 2.6 Hz, 1H, H-4), 8.36 (d, J = 2.9 Hz, 1H, H-2′), 9.17 (s, 1H, H-2), 11.94 (s, 1H, NH); ^{13}C NMR (50 MHz, [D$_6$]DMSO) δ: 34.0 (q), 55.2 (q), 101.7 (s), 102.0 (d), 106.6 (d, J_{C4-F} = 25.5 Hz), 112.1 (d, J_{C6-F} = 25.7 Hz), 112.6 (d, J_{C7a}F = 4.8 Hz), 112.8 (d), 113.1 (d, J_{C7-F} = 10.2 Hz), 113.2 (d), 124.8 (s), 127.2 (d, J_{C3a-F} = 11.4 Hz), 130.0 (d), 131.7 (s), 134.2 (s), 143.4 (d), 154.8 (s), 159.6 (d, J_{C5-F} = 237.0 Hz), 165.4 (s), 169.3 (s), 170.3 (s); IR (KBr): $\tilde{\nu}$ = 3267 (NH), 1623 cm^{-1} (CO); elemental analysis calcd (%) for $C_{21}H_{15}FN_4O_3$ (MW: 390.37): C, 64.61; H, 3.87; N, 14.35; found: C, 64.70; H, 3.61; N, 14.24.

*[3-(5-Methoxy-1H-indol-3-yl)-1,2,4-oxadiazol-5-yl](5-methoxy-1-methyl-1H-indol-3-yl)methanone (**1 f**).* R_f = 0.74 (CH_2Cl_2/EtOAc 7:3); yellow solid; yield: 62%; mp: 244 °C (dec.); ^{1}H NMR (200 MHz, [D$_6$]DMSO) δ: 3.86 (bs, 6H, CH$_3$ and OCH$_3$), 4.00 (s, 3H, OCH$_3$), 6.92 (dd, J = 8.9, 2.3 Hz, 1H, H-6′), 7.03 (dd, J = 8.9, 2.3 Hz, 1H, H-6), 7.46 (d, J = 8.9 Hz, 1H, H-7), 7.56-7.62 (m, 2H, H-7 and H-4), 7.85 (d, J = 2.3 Hz, 1H, H-4), 8.34 (d, J = 2.7 Hz, 1H, H-2′), 9.03 (s, 1H, H-2), 11.93 (s, 1H, NH); ^{13}C NMR (50 MHz, [D$_6$]DMSO) δ: 33.83 (q), 55.3 (q), 55.4 (q), 101.7 (s), 102.0 (d), 103.6 (d), 112.3 (d), 112.5 (s), 112.8 (d), 113.2 (d), 113.4 (d), 124.8 (s), 127.4 (s), 129.9 (d), 131.7 (s), 132.4 (s), 142.2 (d), 154.8 (s), 156.8 (s), 165.3 (s), 169.6 (s), 170.2 (s); IR (KBr): $\tilde{\nu}$ = 3290 (NH), 1627 cm^{-1} (CO); elemental analysis calcd (%) for $C_{22}H_{18}N_4O_4$ (MW: 402.40): C, 65.66; H, 4.51; N, 13.92; found: C, 65.76; H, 4.61; N, 14.04.

*(5-Bromo-1-methyl-1H-indol-3-yl)[3-(5-methoxy-1H-indol-3-yl)-1,2,4-oxadiazol-5yl]methanone (**1 g**).* R_f = 0.76 (CH_2Cl_2/EtOAc 7:3); yellow

solid; yield: 52 %; mp: 274 °C (dec.); ^{1}H NMR (200 MHz, [D$_6$]DMSO) δ: 3.85 (s, 3H, CH$_3$), 4.03 (s, 3H, OCH$_3$), 6.92 (dd, J = 8.9, 2.4 Hz, 1H, H-6′), 7.46 (d, J = 8.9 Hz, 1H, H-7′), 7.55- 7.60 (m, 2H, H-6 and H-4′), 7.70 (d, J = 8.7 Hz, 1H, H-7), 8.35 (d, J = 2.8 Hz, 1H, H-2′), 8.46 (d, J = 1.6 Hz, 1H, H-4), 9.16 (s, 1H, H-2), 11.93 (s, 1H, NH); ^{13}C NMR (50 MHz, [D$_6$]DMSO) δ: 33.9 (q), 55.2 (q), 101.7 (s), 102.0 (d), 112.0 (s), 112.8 (d), 113.2 (d), 113.6 (d), 116.4 (s), 123.6 (d), 124.8 (s), 126.6 (d), 128.1 (s), 130.0 (d), 131.7 (s), 136.3 (s), 143.2 (d), 154.8 (s), 165.4 (s), 169.2 (s), 170.3 (s); IR (KBr): $\tilde{\nu}$ = 3312 (NH), 1623 cm^{-1} (CO); elemental analysis calcd (%) for $C_{21}H_{15}$ BrN_4O_3 (MW: 451.27): C, 55.89; H, 3.35; N, 12.42; found: C, 56.02; H, 3.61; N, 12.08.

*[3-(5-Methoxy-1H-indol-3-yl)-1,2,4-oxadiazol-5-yl](1-methyl-1H-indol-3-yl)methanone (**1 h**).* R_f = 0.79 (CH$_2$Cl$_2$/EtOAc 7 : 3); yellow solid; yield: 56 %; mp: 247 °C (dec.); ^{1}H NMR (200 MHz, [D$_6$]DMSO) δ: 3.86 (s, 3H, CH$_3$), 4.04 (s, 3H, OCH$_3$), 6.92 (dd, J = 8.9, 2.3 Hz, 1H, H-6′), 7.36 – 7.49 (m, 3H, H-5, H-6 and H-7′), 7.56 (d, J = 2.3 Hz, 1H, H-4′), 7.67-7.71 (m, 1H, H-7), 8.33 – 8.37 (m, 2H, H-4 and H-2′), 9.12 (s, 1H, H-2), 11.94 (s, 1H, NH); ^{13}C NMR (50 MHz, [D$_6$]DMSO) δ: 34.1 (q), 55.8 (q), 102.2 (s + d), 102.6 (s), 111.3 (s), 111.9 (d), 113.7 (d), 122.0 (d), 124.0 (d), 124.6 (d), 125.4 (s), 126.9 (d), 130.4 (d), 132.2 (s), 138.0 (s), 142.9 (d), 155.3 (s), 165.9 (s), 170.1 (s), 170.9 (s); IR (KBr): $\tilde{\nu}$ = 3302 (NH), 1616 cm^{-1} (CO); elemental analysis calcd (%) for $C_{21}H_{16}N_4O_3$ (MW: 372.38): C, 67.73; H, 4.33; N, 15.05; found: C, 67.70; H, 4.51; N, 15.20.

*[3-(5-Bromo-1H-indol-3-yl)-1,2,4-oxadiazol-5-yl](5-methoxy-1-methyl-1H-indol-3-yl)methanone (**1 i**).* R_f = 0.69 (CH$_2$Cl$_2$/EtOAc 7 : 3); yellow solid; yield: 78 %; mp: 258 °C (dec.); ^{1}H NMR (200 MHz, [D$_6$]DMSO) δ: 3.85 (s, 3H, CH$_3$), 4.00 (s, 3H, OCH$_3$), 7.03 (dd, J = 8.9, 2.5 Hz, 1H, H-6), 7.41 (dd, J = 8.6, 1.9 Hz, 1H, H-6′), 7.53–7.61 (m, 2H, H-7 and H-7′), 7.83 (d, J = 2.5 Hz, 1H, H-4), 8.21 (d, J = 1.9 Hz, 1H, H-4′), 8.47 (d, J = 2.8 Hz, 1H, H-2′), 9.02 (s, 1H, H-2), 12.27 (s, 1H, NH); ^{13}C NMR (50 MHz, [D$_6$]DMSO) δ: 33.9 (q), 55.4 (q), 101.6 (s), 103.5 (d), 112.4 (d), 112.5 (s), 113.4 (d), 113.6 (s), 114.5 (d), 122.6 (d), 125.3 (d), 125.9 (s), 127.4 (s), 131.1 (d), 132.3 (s), 135.6 (s), 142.2 (d), 156.8 (s), 164.9 (s), 169.8 (s), 170.0 (s); IR (KBr): $\tilde{\nu}$ = 3302 (NH), 1610 cm^{-1} (CO); elemental analysis calcd (%) for $C_{21}H_{15}BrN_4O_3$ (MW: 451.27): C, 55.89; H, 3.35; N, 12.42; found: C, 55.70; H, 3.51; N, 12.24; HRMS: m/z = 451.04 [M + H]$^+$; t_R = 3.65 min (> 99 % purity).

*[3-(5-Bromo-1H-indol-3-yl)-1,2,4-oxadiazol-5-yl](1-methyl-1H-indol-3-yl)methanone (**1 j**).* R_f = 0.75 (CH$_2$Cl$_2$/EtOAc 7 : 3); yellow solid; yield: 46 %; mp: 271 °C (dec.); ^{1}H NMR (200 MHz, [D$_6$]DMSO) δ: 4.04 (s, 3H, CH$_3$), 7.36-7.47 (m, 3H, H-5, H-6 and H-6′), 7.56 (d, J = 8.6 Hz, 1H, H-7′), 7.67- 7.72 (m, 1H, H-7), 8.22 (d, J = 1.8 Hz, 1H, H-4′), 8.32-8.37 (m, 1H, H-4), 8.48 (d, J = 2.8 Hz, 1H, H-2′), 9.11 (s, 1H, H-2), 12.27 (s, 1H, NH); ^{13}C NMR (50 MHz, [D$_6$]DMSO) δ: 33.7 (q), 101.6 (s), 111.4 (d), 112.7 (s), 113.7 (s), 114.6 (d), 121.5 (d), 122.6 (d), 123.6 (d), 124.1 (d), 125.3 (d), 125.9 (s), 126.4 (s), 131.1 (d), 135.6 (s), 137.5 (s), 142.5 (d), 164.9 (s), 169.8 (s), 170.2 (s); IR (KBr): $\tilde{\nu}$ = 3376 (NH), 1618 cm^{-1} (CO); elemental analysis calcd (%) for $C_{20}H_{13}BrN_4O_2$ (MW: 421.25): C, 57.02; H, 3.11; N, 13.30; found: C, 56.92; H, 3.02; N, 13.14; HRMS: m/z = 421.03 [M + H]$^+$; t_R = 3.68 min (> 99 % purity).

*[3-(5-Bromo-1H-indol-3-yl)-1,2,4-oxadiazol-5-yl](5-fluoro-1-methyl-1H-indol-3-yl)methanone (**1 k**).* R_f = 0.70 (CH$_2$Cl$_2$/EtOAc 7 : 3); yellow solid; yield: 58 %; mp: 277 °C (dec.); ^{1}H NMR (200 MHz, [D$_6$]DMSO) δ: 4.04 (s, 3H, CH$_3$), 7.29 (td, J = 9.2, 9.2, 2.6 Hz, 1H, H-6), 7.41 (dd, J = 8.7, 1.9 Hz, 1H, H-6′), 7.55 (d, J = 8.7 Hz, 1H, H-7′), 7.73 (dd, J = 9.2, 4.4 Hz, 1H, H-7), 8.00 (dd, J = 9.5, 2.6 Hz, 1H, H-4), 8.20 (d, J = 1.9 Hz, 1H, H-4′), 8.48 (d, J = 2.1 Hz, 1H, H-2′), 9.16 (s, 1H, H-2), 12.27 (s, 1H, NH); ^{13}C NMR (50 MHz, [D$_6$]DMSO) δ: 34.0 (q), 101.54 (s), 106.6 (d, J_{C4-F} = 24.9 Hz), 112.1 (d, J_{C6-F} = 26.4 Hz), 112.5 (d, J_{C7a-F} = 4.2 Hz), 113.1 (d, J_{C7-F} = 10.2 Hz), 113.7 (s), 114.6 (d), 122.6 (d), 125.3 (d), 125.9 (s), 127.2 (d, J_{C3a-F} = 11.3 Hz), 131.1 (d), 134.1 (s), 135.6 (s), 143.6 (d), 159.6 (d, J_{C5-F} = 236.0 Hz), 164.9 (s), 169.5 (s), 170.1 (s); IR (KBr): $\tilde{\nu}$ = 3267 (NH), 1615 cm^{-1} (CO); elemental analysis calcd (%) for $C_{20}H_{12}BrFN_4O_2$ (MW: 439.24): C, 54.69; H, 2.75; N, 12.76; found: C, 54.55; H, 2.60; N, 13.00.

*[3-(5-Bromo-1H-indol-3-yl)-1,2,4-oxadiazol-5-yl](5-bromo-1-methyl-1H-indol-3-yl)methanone (**1 l**).* R_f = 0.66 (CH$_2$Cl$_2$/EtOAc 7 : 3); yellow solid; yield: 73 %; mp: 294 °C (dec.); ^{1}H NMR (200 MHz, [D$_6$]DMSO) δ: 4.04 (s, 3H, CH$_3$), 7.42 (dd, J = 8.6, 1.8 Hz, 1H, H-6′), 7.54-7.60 (m, 2H, H-6 and H-7), 7.70 (d, J = 8.6 Hz, 1H, H-7′), 8.21 (d, J = 1.8 Hz, 1H, H-4′), 8.46 (d, J = 1.6 Hz, 1H, H-4), 8.49 (s, 1H, H-2′), 9.16 (s, 1H, H-2), 12.28 (s, 1H, NH); ^{13}C NMR (50 MHz, [D$_6$]DMSO) δ: 33.9 (q), 101.5 (s), 112.0 (s), 113.7 (d), 114.5 (d), 116.4 (s), 122.6 (d), 123.5 (d), 125.3 (d), 125.9 (s), 126.6 (d), 128.1 (s), 131.2 (d), 135.6 (s), 136.3 (s), 143.2 (d), 158.7 (s), 164.9 (s), 169.4 (s), 170.1 (s); IR (KBr): $\tilde{\nu}$ = 3341 (NH), 1617 cm^{-1} (CO); elemental analysis calcd (%) for $C_{20}H_{12}Br_2N_4O_2$ (MW: 500.14): C, 48.03; H, 2.42; N, 11.20; found: C, 48.12; H, 2.60; N, 11.05; HRMS: m/z = 498.94 [M + H]$^+$; t_R = 3.84 min (> 99 % purity).

*[3-(5-Fluoro-1H-indol-3-yl)-1,2,4-oxadiazol-5-yl](1-methyl-1H-indol-3-yl)methanone (**1 m**).* R_f = 0.71 (CH$_2$Cl$_2$/EtOAc 7 : 3); yellow solid; yield: 59 %; mp: 261 °C (dec.); ^{1}H NMR (200 MHz, [D$_6$]DMSO) δ: 4.04 (s, 3H, CH$_3$), 7.15 (td, J = 9.4, 9.1, 2.4 Hz, 1H, H-6′), 7.39-7.43 (m, 2H, H-5 and H-6), 7.59 (dd, J = 9.1, 4.5 Hz, 1H, H-7′), 7.67-7.78 (m, 2H, H-7 and H-4′), 8.32-8.36 (m, 1H, H-4), 8.49 (s, 1H, H-2′), 9.11 (s, 1H, H-2), 12.18 (s, 1H, NH); ^{13}C NMR (50 MHz, [D$_6$]DMSO) δ: 33.7 (q), 102.1 (d, J_{C7a-F} = 4.5 Hz), 105.2 (d, J_{C4-F} = 23.6 Hz), 111.0 (d, J_{C6-F} = 26.0 Hz), 111.4 (d), 112.7 (s), 113.7 (d, J_{C7-F} = 12.0 Hz), 121.5 (d), 123.6 (d), 124.1 (d), 124.6 (d, J_{C3a-F} = 11.2 Hz), 126.4 (s), 131.5 (d), 133.5 (s), 137.5 (s), 142.5 (d), 158.0 (d, J_{C5-F} = 234.6 Hz), 165.0 (s), 169.7 (s), 170.3 (s); IR (KBr): $\tilde{\nu}$ = 3284 (NH), 1623 cm^{-1} (CO); elemental analysis calcd (%) for $C_{20}H_{13}FN_4O_2$ (MW: 360.34): C, 66.66; H, 3.64; N, 15.55; found: C, 66.70; H, 3.60; N, 15.22.

*[3-(5-Fluoro-1H-indol-3-yl)-1,2,4-oxadiazol-5-yl](5-fluoro-1-methyl-1H-indol-3-yl)methanone (**1 n**).* R_f = 0.65 (CH$_2$Cl$_2$/EtOAc 7 : 3); yellow solid; yield: 63 %; mp: 265 °C (dec.); ^{1}H NMR (200 MHz, [D$_6$]DMSO) δ: 4.03 (s, 3H, CH$_3$), 7.15 (td, J = 9.2, 9.1, 2.6 Hz, 1H, H-6′), 7.30 (td, J = 9.2, 9.1, 2.6 Hz, 1H, H-6), 7.60 (dd, J = 9.1, 4.6 Hz, 1H, H-7′), 7.71- 7.77 (m, 2H, H-7 and H-4′), 8.01 (dd, J = 9.6, 2.6 Hz, 1H, H-4), 8.50 (d, J = 2.9 Hz, 1H, H-2′), 9.16 (s, 1H, H-2), 12.19 (s, 1H, NH); ^{13}C NMR (50 MHz, [D$_6$]DMSO) δ: 34.0 (q), 102.1 (d, $J_{C7'a-F}$ = 4.3 Hz), 105.2 (d, $J_{C4'-F}$ = 25.1 Hz), 106.6 (d, J_{C4-F} = 24.9 Hz), 111.0 (d, $J_{C6'-F}$ = 26.4 Hz), 112.1 (d, J_{C6-F} = 25.7 Hz), 112.5 (d, J_{C7a-F} = 4.2 Hz), 113.1 (d, J_{C7-F} = 9.5 Hz), 113.7 (d, $J_{C7'-F}$ = 9.7 Hz), 124.6 (d, $J_{C3'a-F}$ = 11.2 Hz), 127.2 (d, J_{C3a-F} = 11.1 Hz), 131.5 (d), 133.4 (s), 134.2 (s), 143.5 (d), 158.0 (d, $J_{C5'-F}$ = 234.1 Hz), 159.6 (d, J_{C5-F} = 235.3 Hz), 165.0 (s), 169.4 (s), 170.1 (s); IR (KBr): $\tilde{\nu}$ = 3267 (NH), 1615 cm^{-1} (CO); elemental analysis calcd (%) for $C_{20}H_{12}F_2N_4O_2$ (MW: 378.33): C, 63.49; H, 3.20; N, 14.81; found: C, 63.60; H, 3.32; N, 15.00.

*[3-(5-Fluoro-1H-indol-3-yl)-1,2,4-oxadiazol-5-yl](5-methoxy-1-methyl-1H-indol-3-yl)methanone (**1 o**).* R_f = 0.66 (CH$_2$Cl$_2$/EtOAc 7 : 3); yellow solid; yield: 62 %; mp: 218 °C (dec.); ^{1}H NMR (200 MHz, [D$_6$]DMSO) δ: 3.86 (s, 3H, CH$_3$), 4.00 (s, 3H, OCH$_3$), 7.04 (dd, J = 8.9, 2.5 Hz, 1H, H-6), 7.15 (td, J = 9.2, 9.1, 2.6 Hz, 1H, H-6′), 7.55-7.62 (m, 2H, H-7 and H-7′), 7.74 (dd, J = 9.7, 2.6 Hz, 1H, H-4′), 7.84 (d, J = 2.5 Hz, 1H, H-4), 8.48 (d, J = 2.7 Hz, 1H, H-2′), 9.03 (s, 1H, H-2), 12.18 (s, 1H, NH); ^{13}C NMR (50 MHz, [D$_6$]DMSO) δ: 33.9 (q), 55.4 (q), 102.1 (d, J_{C7a-F} = 4.5 Hz), 103.5 (d), 105.2 (d, J_{C4-F} = 24.7 Hz), 111.0 (d, J_{C6-F} = 26.1 Hz), 112.4 (d), 112.5 (s), 113.4 (d), 113.7 (d, J_{C7-F} = 9.5 Hz), 124.6 (d, J_{C3a-F} = 11.1 Hz), 127.4 (s), 131.5 (d), 132.3 (s), 133.4 (s), 142.2 (d), 156.8 (s), 158.0 (d, J_{C5-F} = 234.4 Hz), 165.0 (s), 169.8 (s), 170.0 (s); IR (KBr): $\tilde{\nu}$ = 3244 (NH), 1618 cm^{-1} (CO); elemental analysis calcd (%) for $C_{21}H_{15}FN_4O_3$ (MW: 390.37): C, 64.61; H, 3.87; N, 14.35; found: C, 64.70; H, 3.70; N, 14.10.

(5-Bromo-1-methyl-1H-indol-3-yl)[3-(5-fluoro-1H-indol-3-yl)-1,2,4-oxadiazol-5-yl]methanone (**1 p**). R_f = 0.67 (CH$_2$Cl$_2$/EtOAc 7 : 3); yellow solid; yield: 59 %; mp: 280 °C (dec.); ^{1}H NMR (200 MHz, [D$_6$]DMSO) δ:

4.03 (s, 3H, CH$_3$), 7.14 (td, J=9.1, 9.1, 2.6 Hz, 1H, H-6′), 7.53-7.76 (m, 4H, H-6, H-7, H-7′ and H-4′), 8.44-8.49 (m, 2H, H-4 and H-2′), 9.13 (s, 1H, H-2), 12.18 (s, 1H, NH); ^{13}C NMR (50 MHz, [D$_6$]DMSO) δ: 33.9 (q), 99.5 (d), 102.1 (d, $J_{C7a\text{-}F}$ = 4.5 Hz), 105.2 (d, $J_{C4\text{-}F}$ = 25.1 Hz), 111.0 (d, $J_{C6\text{-}F}$ = 26.6 Hz), 112.0 (s), 113.7 (d, $J_{C7\text{-}F}$=9.2 Hz), 116.4 (s), 123.6 (d), 124.6 (d, $J_{C3a\text{-}F}$ = 11.1 Hz), 126.6 (d), 128.1 (s), 131.6 (d), 133.5 (s), 136.3 (s), 143.2 (d), 158.0 (d, $J_{C5\text{-}F}$ = 234.4 Hz), 165.1 (s), 169.3 (s), 170.2 (s); IR (KBr): $\tilde{\nu}$=3310 (NH), 1592 cm^{-1} (CO); elemental analysis calcd (%) for $C_{20}H_{12}BrFN_4O_2$ (MW: 439.24): C, 54.69; H, 2.75; N, 12.76; found: C, 54.80; H, 2.81; N, 12.60.

Biology

Drugs and Chemicals

Each compound was initially dissolved in dimethyl sulfoxide (DMSO), in order to obtain 10 mM stock solution, stored at +4 °C, which was then diluted in complete culture medium immediately before use at the appropriate concentration. The medium, Foetal Bovine Serum (FBS), penicillin and streptomycin were from Gibco (Gaithersburg, MD, USA).

Cell culture

For the in vitro experiments in PDAC cell lines, we selected three models which are representative of primary (Panc-1) and metastatic (SUIT-2 and Capan-1) PDAC as well as of epithelial (SUIT-2 and Capan-1) and mesenchymal (Panc-1) phenotypes.

SUIT-2 is a cell line derived from a metastatic liver tumour of human pancreatic carcinoma. SUIT-2 cell line produces and releases at least two tumour markers, carcinoembryonic antigen and carbohydrate antigen 19–9.[44] Cells were cultured in Roswell Park Memorial Institute (RPMI) supplemented with 10% FBS and 1% Pen/Strep in T-75 flasks.

Capan-1 cells are adherent epithelial-like cells derived from a liver metastasis of a pancreatic adenocarcinoma that grown in tissue culture appeared as large epithelial-like mucin-producing cells.[45,46] Cells were cultured in Dulbecco's Modified Eagle Medium (DMEM) supplemented with 10% foetal bovine serum and 20 mM (1%) HEPES in T-75 flasks.

Panc-1 is an epithelioid carcinoma attached cell line, that is commonly used as an *in vitro* model to study pancreatic ductal adenocarcinoma carcinogenesis and tumour therapies, especially in light of the presence of the SSTR2 receptors, which have been proposed as potential prognostic markers in pancreatic cancer.[47,48] Panc-1 cells were cultured in Dulbecco's Modified Eagle Medium (DMEM) supplemented with 10% fetal bovine serum and 20 mM (1%) HEPES in T-75 flasks.

hTERT-HPNE is a human pancreatic duct epithelial-like cell line. Cells were obtained from the American Type Culture Collection (ATCC, Manassas, VA) and cultured in RPMI-1640, supplemented with 10% heat-inactivated-FBS,10 ng/ml human recombinant EGF and 1% streptomycin/penicillin at 37 °C, in T-75 flasks.

The cell lines were routinely tested for Mycoplasma, while their authentication was performed by short tandem repeat-polymerase chain reaction at BaseClear (Leiden, the Netherlands).

Viability assay in vitro

Cytotoxic activity of the topsentin derivatives **1 b**, **1 c**, **1 i**, **1 j** and **1 l** on pancreatic cancer cells (SUIT-2, Capan-1 and Panc-1) and on non-neoplastic pancreatic cells (HPNE) was determined by the sulforhodamine B (SRB) chemosensitivity assay, as described previously.[49]

Cells were plated in 96-well flat-bottom plates at final concentrations ranging from 3000–5000 cells/well in 100 μL of medium. After a 24 hours pre-incubation period, cells were treated with the compounds at nine screening concentrations (from 0.1 μM to 40 μM) in triplicate and incubated at 37 °C for 72 hours. After the treatment, cells were fixed with 25 μL of cold 50% trichloroacetic acid (TCA) for each well and incubated at 4 °C for 1 hour. Afterwards plates were washed five times with demi-water and air dried overnight. Then, the plates were stained with 50 μL of 0.4% SRB solution in 1% acetic acid for 15 minutes. The excess stain was rinsed off by placing the plates under running 1% acetic acid and allowed to dry at room temperature for overnight. SRB staining was rinsed with 150 μL tris(hydroxymethyl)aminomethane solution pH= 8.8 (TRIS-base), and the optical density (OD) was read at 492 nm. Each assay was performed in triplicate and assays were repeated at least three times. The comparison of the average optical density of the growth in control wells with that in the sample wells allowed estimating the percentage of cell growth, using the following equation:

$$\%\ \text{Cell Growth} = (\text{mean OD}_{\text{compound}}\text{-mean OD}_{\text{day zero plate}})/$$
$$(\text{mean OD}_{\text{cells}}\text{-mean OD}_{\text{day zero plate}}) \times 100$$

The results obtained were adjusted by the day zero plate (wells containing cells growing for only 24 hours) and normalized by the control cells (wells with untreated cells) to obtain the rate of viable cells.

Cell cycle analysis

Cell cycle modulation was analyzed by flow cytometry, as described previously.[49] Cells (2.5×10^5 cells/flask) were seeded in T25 cell flasks. After overnight incubation at 37 °C, the cells were treated with the compounds **1 b, 1 c, 1 l**, at two concentrations (i.e., 2 μM and 5 μM for **1 b** and 5 μM and 10 μM for **1 c** and **1 l**), and incubated for 24 hours. Drug concentrations were chosen on the basis of the respective EC$_{50}$ values. After treatment, the cells were harvested by trypsinization (0.5 mL/flask of trypsin-EDTA), incubated until the cells detached from the bottom of the flask and collected using the same medium used for the culture. The samples were then centrifuged in order to form a pellet (5 minutes at 1200 rpm). Finally, these pellets were fixed in ice-cold 70% ethanol, washed twice with phosphate-buffered saline (PBS) and incubated for 30 minutes at 37 °C with 50 μL of RNase (100 μg/mL) followed by incubation with 200 μL of propidium iodide solution (PI, 50 μg/mL). The cycle analysis was performed on the FACS Calibur instrument (Becton Dickinson, San José, CA). Data analysis was carried out with FACSdiva software (Becton Dickinson), while cell cycle distribution was determined using Modfit software (Verity-Software, Topsham, ME).

Cell apoptosis analysis

Apoptosis induction was evaluated with by detection of the externalization of phosphatidylserine to the cell surface using the double staining with annexin V/7-AAD. To perform this assay, cells (2.0 x 10^5 cells/flask) were seeded in T25 flasks. After overnight incubation at 37 °C, the cells were treated with compounds **1 b, 1 c, 1 l** at two concentrations (i.e. 2 μM and 5 μM for **1 b**, and 5 μM and 10 μM for **1 c** as well as for **1 l**) and incubated for another 24 hours. Cells recovered from cultures were trypsinized and resuspended in fresh medium. Cells were then stained by the addition of 7AAD and annexin V. In particular, a volume of 2.5 μL of 7-AAD (Calbiochem, San Diego, CA) was added to 100 μL of cell suspension. The samples were incubated in the dark at room temperature for 15 minutes. Each sample was washed in 3 mL of PBS, supplemented with 0.1% HSA and azide, and pelleted by centrifugation. Staining of the apoptotic cells was performed by incubating the cells with annexin V-FITC in annexin buffer (1:1000) for 15 minutes on ice. The samples were analyzed with a FACScan and data analysis was carried out with FACSdiva software (Becton Dickinson).

Wound healing assay

Cell migration was assessed using a wound healing assay, as described previously.[50] A total of 5 x 10^4 cells/well were seeded in a 96-well plate, to form confluent monolayer. Gaps or scratch were created in confluent cell layers using the sterile scratch tool (Figure 6c). The detached cell following scratch induction were removed and new medium was added to the wells. Cells were next treated with two concentrations of each compound (i.e. 2 μM and 5 μM for **1 b** and 5 μM and 10 μM for **1 c** and **1 l**). Cells growing in complete medium were maintained at 37 °C with a supply of 5% CO_2/95% air atmosphere and 100% relative humidity. The wound closure was monitored by phase-contrast microscopy and photographed at the 0th, 4th, 8th, 20th and 24th hour. Pictures of the plates were taken using the Universal Grab 6.3 software (DCILabs) from a computer connected to a Leica microscope with a JAI TMC-1327 camera.

The percentage of migration was calculated using the following equation:

$$\%\ \text{Migration} = (\text{Wound width at } t = 0\text{-Wound width at } t = X)/$$
$$(\text{Wound width at } t = 0) \times 100$$

Gene expression analysis

In order to evaluate the capability of epithelial to mesenchymal transition (EMT) modulation by the new most active oxadiazole compounds **1 b** and **1 l**, we determined the gene expression of key EMT determinants by Real-Time PCR analysis in Panc-1 and Capan-1 cells.

Cells (3 x 10^5 cells/well) were seeded in a 6-well plate and treated with compounds for 24 hours. Cells were then harvested by 250 μL of Trizol reagent and collected in a new eppendorf tube. Total RNA was extracted by adding 50 μL chloroform to each sample, shaking vigorously and spinning 10 minutes at 12000 RPM at 4 °C, after 3 minutes of incubation at room temperature. After obtaining a lysate from each sample, the upper aqueous phase containing RNA was collected and washed with isopropanol and 70% ethanol. The pellet was resuspended in nuclease free water and the amount of nucleic acid was determined through NanoDrop technology.

Afterwards, reverse transcription (RT) reactions to produce cDNA from RNA for RT-PCR were conducted using M–MuLV RNAse H^+ reverse transcriptase enzyme, Reverse Transcription buffer 2X, including dNTP mix and $MgCl_2$, and random hexamers primer (DyNAmo™ cDNA Synthesis Kit). cDNA was synthesised from 7 μL of RNA at concentration of 143 ng/mL in a 13 μL reaction volume (10 μL of RT buffer, 1 μL of random hexamer primer and 2 μL of Reverse Transcriptase). The cDNA synthesis reactions were initiated with a primer extension step at 25 °C for 10 minutes, followed by cDNA synthesis at 37 °C for 30 minutes, termination at 85 °C for 5 minutes and sample cooling at 4 °C.

Finally, RT-PCR reactions were performed using the commercial kit TaqMan® Universal PCR Master Mix. Amplification mixtures, set up in a final volume of 25 μL, contained 12.5 μL of Universal Master Mix 2X (AmpliTaq Gold DNA Polymerase, dNTPs with dUTP, passive reference, and optimized buffer components), 1 μL of Primers and TaqMan® probe, 6.5 μL of H_2O and 5 μL of cDNA sample. RT-PCR assays were carried out in a GeneAmp 5700 Sequence Detection System programmed to hold at 50 °C for 30 minutes, to hold at 95 °C for 10 minutes, and to complete 45 cycles of 95 °C for 15 minutes and 50 °C for 1 minute. The gene expression profiling was determined using the Sequence Detection System (SDS) software, as described previously.[51]

Analysis of the activity of MMP9 by gelatine zymography

The activity of MMP9 was evaluated by gelatine zymography, as described.[52] Panc-1 and Capan-1 cells (10^6) were seeded in Petri dishes and incubated with serum-free medium for 24 hours, with or without the most promising compounds **1 b** and **1 l** at 2 and 5 μM. Medium was harvested and centrifuged in order to remove cellular debris. The media were then mixed with SDS-PAGE buffer 4X without reducing agent and underwent electrophoresis in 10% polyacrylamide gel containing 1 mg/mL gelatine. After 1 hour, the gel was exposed to renaturing buffer and finally incubated with developing buffer. The staining was then performed using 0.25% Coomassie Brilliant Blue R-250 solution and the areas of protease activity were detected as clear bands and the activity of MMP9 was assessed by using ImageJ software (National Institutes of Health, Bethesda, MD, US).

PathScan intracellular signaling array

The fluorescent PathScan sandwich ELISA was purchased from Cell Signaling Technology (Leiden, Netherlands) and used according to manufacturer's instructions, as described previously.[53] The Panc-1 cells were seeded and treated for 24 hours and lysed in lysis buffer with 1 mM PMSF. The glass slide was blocked and the lysate was added to the wells. The slide was washed thoroughly and incubated with the detection antibody cocktail. The fluorescent signal was determined using the ArrayVision software, which measured the pixel intensity.

Enzyme-linked immunosorbent assay (ELISA) for phosphorylated GSK3β kinase

The phospho-GSK3β levels at serine residue 9 and at tyrosine residue 216 were detected and quantified using Enzyme-Linked Immunosorbent Assay (ELISA, Invitrogen™ phospho-GSK3 beta (Ser9) InstantOne Kit, Catalog Number: 85–86172 and Biomatik Phospho-GSK3 (Tyr216) kit, Cat#EKA50974) according to the manufacturer's protocols. Supernatants from Panc-1, cells were evaluated after 24 hours from the treatment with the selected compounds **1 b** and **1 l** at 5 μM concentration. The absorbance was read at 450 nm. We performed a parallel ELISA test using the inhibitor enzastaurin (5 μM), as described previously.[54] This drug reduced the phosphorylation of 65%, supporting the use of this method in order to check the inhibition of phospho-*GSK3beta.*

GSK3β kinase assay

The inhibitory activity on GSK3β was evaluated by using the ADP-Glo™ Kinase Assay kit from Promega (Promega Corporation, Madison, WI 53711, USA). The assay was performed in non-treated 384-well plates as previously describe,[55] using a volume of 2 μl of recombinant human GSK3β and 2 μL of substrate/ATP mix, in presence of serial dilutions of each compound (**1 b**, **1 c**, **1 i**, **1 j** and **1 l**). Kinase was incubated with the test compounds for 10 min at rt and the reaction was then started with the addition of substrate/ATP and run for 60 min at rt. After the addition of ADP-Glo™ reagent (5μL, for 40 minutes incubation) and kinase detection reagent (10μL, for 30 minutes incubation), the luminescence was measured with an integration time of 0.5-1 second. Raw data were normalized to the values of control wells and plotted using GraphPad Prism 8.

Molecular modeling

The X-ray crystal structure of GSK-3β (PDB ID 1UV5)[40] was retrieved from the RCSB Protein Data Bank (http://www.rcsb.org). Schrödinger's Protein Preparation Wizard of the Prime module was used for protein structure refinements (Prime, Schrödinger, LLC, New York, NY, 2017). In the pre-process phase, hydrogen atoms were added and bond orders were assigned, missing loops were filled according to the amino acid sequence. In the refinement phase the hydrogen bond network was restored using the H-bond assignment option, which was followed by a restrained minimization (converged heavy atoms to RMSD: 0.3 Å) with OPLS_2003 force field.

Schrödinger's Maestro was used to visualize interactions between binding site and inhibitors (Maestro, 11.1 version, Schrödinger, LLC, New York, NY, 2017). Structures of compounds **1 b** and **1 l** were drawn manually, 2D structures were optimized with Schrödinger's LigPrep module with standard settings using the OPLS_2003 forcefield (LigPrep, Schrödinger, LLC, New York, NY, 2017). Compounds were docked with Schrödinger's Glide software package (Glide, Schrödinger, LLC, New York, NY, 2017). In the grid generation phase, the position of the grid box was determined by the co-crystallized ligand: the center of the docking box was fixed on the center of the inhibitor. The size of the box was 20×20×20 Å (the inner box was 10×10×10 Å). The standard precision mode (SP) and standard settings (Van der Waals Radius and Charge Scaling) were used for calculations. Moreover, the crystallized ligand 6-bromoindirubin was redocked with the aim to evaluate the ability of SP protocol to reproduce the experimental conformation.

Statistics

All the SRB, PCR, zymography and ELISA assays were carried out in triplicate and repeated at least three times, whereas the percentages of cell migration were calculated taking into account at least six scratch areas. The data was evaluated using the GraphPad Prism v. 5 software (GraphPad Software, San Diego, CA). Data was expressed as mean values ± SEM and analyzed by the Student t test. *P* values < 0.05 were considered significant (*).

Acknowledgements

This work was partially supported by the following grants: CCA Foundation 2015 and 2018 grants, KWF Dutch Cancer Society grants (KWF project#11957), AIRC/Start-Up grant (to E.G.), PRIN2017, Prot.No.2017E84AA4 and European Union 2014-2020 PON Ricerca e Innovazione grant from the Italian Ministry of Education, University and Research, entitled "PROGEMA-Processi Green per l'Estrazione di Principi Attivi e la Depurazione di Matrici di Scarto e Non" (ARS01_00432) to P.D. The Authors would like to thank Professor A Griffioen (Angiogenesis group, Department Medical Oncology, VUmc, Amsterdam VUmc, Amsterdam) for the migration station used to perform wound healing assays, and the members of the Drug Discovery Committee of the EORTC-PAMM group for the useful discussion and support.

Conflict of Interest

The authors declare no conflict of interest.

Keywords: 1,2,4-oxadiazole topsentin analogs · inhibition of migration · GSK3β kinase · PDAC antiproliferative activity · proapoptotic activity

[1] D. J. Newman, G. M. Cragg, *J. Nat. Prod.* **2016**, *79* (3), 629–661.
[2] U. Lindequist, *Biomol. Ther. (Seoul).* **2016**, *24* (6), 561–571.
[3] S. Sakemi, H. H. Sun, *J. Org. Chem.* **1991**, *56*, 4304–4307.
[4] A. Carbone, B. Parrino, P. Barraja, V. Spanò, G. Cirrincione, P. Diana, A. Maier, G. Kelter, H. H. Fiebig, *Mar. Drugs* **2013**, *11* (3), 643–654.
[5] P. Diana, A. Carbone, P. Barraja, A. Martorana, O. Gia, L. DallaVia, G. Cirrincione, *Bioorg. Med. Chem. Lett.* **2007**, *17* (22), 6134–6137.
[6] P. Diana, A. Carbone, P. Barraja, A. Montalbano, A. Martorana, G. Dattolo, L. DallaVia, G. Cirrincione, *Bioorg. Med. Chem. Lett.* **2007**, *17*, 2342–2346.
[7] P. Diana, A. Carbone, P. Barraja, G. Kelter, H.-H. Fiebig, G. Cirrincione, *Bioorg. Med. Chem.* **2010**, *18*, 4524–4529.
[8] V. Spanò, A. Attanzio, S. Cascioferro, A. Carbone, A. Montalbano, P. Barraja, L. Tesoriere, G. Cirrincione, P. Diana, B. Parrino, *Mar. Drugs* **2016**, *14*, 226.
[9] B. Parrino, A. Carbone, G. Di Vita, C. Ciancimino, A. Attanzio, A. Montalbano, P. Barraja, L. Tesoriere, M. A. Livrea, P. Diana, G. Cirrincione, *Mar. Drugs* **2015**, *13*, 1901–1924.
[10] A. Carbone, B. Parrino, G. Di Vita, A. Attanzio, V. Spanò, A. Montalbano, P. Barraja, L. Tesoriere, M. A. Livrea, P. Diana, G. Cirrincione, *Mar. Drugs* **2015**, *13*, 460–492.
[11] A. Carbone, M. Pennati, P. Barraja, A. Montalbano, B. Parrino, V. Spano, A. Lopergolo, S. Sbarra, V. Doldi, N Zaffaroni, G. Cirrincione, P. Diana, *Curr. Med. Chem.* **2014**, *21* (14), 1654.
[12] P. Diana, A. Carbone, P. Barraja, A. Montalbano, B. Parrino, A. Lopergolo, M. Pennati, N. Zaffaroni, *ChemMedChem* **2011**, *6*, 1300–1309.
[13] A. Carbone, M. Pennati, B. Parrino, A. Lopergolo, P. Barraja, A. Montalbano, V. Spanò, S. Sbarra, V. Doldi, M. De Cesare, G. Cirrincione, P. Diana, N. Zaffaroni, *J. Med. Chem.* **2013**, *56* (17), 7060–7072.
[14] B. Bao, Q. Sun, X. Yao, J. Hong, C. O. Lee, C. J. Sim, K. S. Im, J. H. Jung, *J. Nat. Prod.* **2005**, *68* (5), 711–715.
[15] S. Tsujii, K. L. Rinehart, S. P. Gunasekera, S. S. Cross, M. S. Lui, S. A. Pomponi, M. Cristina Diaz, Y. Kashman, *J. Org. Chem.* **1988**, *53* (23), 5446–5453.
[16] K.-B. Oh, W. Mar, S. Kim, J.-Y. Kim, T.-H. Lee, J.-G. Kim, D. Shin, C. J. Sim, J. Shin, *Biol. Pharm. Bull.* **2006**, *29* (3), 570–573.
[17] J. Shin, Y. Seo, K. W. Cho, J. R. Rho, C. J. Sim, *J. Nat. Prod.* **1999**, *62* (4), 647–649.
[18] B. Parrino, D. Schillaci, I. Carnevale, E. Giovannetti, P. Diana, G. Cirrincione, S. Cascioferro, *Eur. J. Med. Chem.* **2019**, *161*, 154–178.
[19] P. Diana, A. Stagno, P. Barraja, A. Montalbano, A. Carbone, B. Parrino, G. Cirrincione, *Tetrahedron* **2011**, *67* (19), 3374–3379.
[20] S. Cascioferro, B. Parrino, G. Li Petri, M. G. Cusimano, D. Schillaci, V. Di Sarno, S. Musella, E. Giovannetti, G. Cirrincione, P. Diana, *Eur. J. Med. Chem.* **2019**, *167*, 200–210.
[21] S. Cascioferro, G. Li Petri, B. Parrino, B. El Hassouni, D. Carbone, V. Arizza, U. Perricone, A. Padova, N. Funel, G. J. Peters, G. Cirrincione, E. Giovannetti, P. Diana, *Molecules* **2020**, *25*, 329.
[22] G. Li Petri, S. Cascioferro, B. El Hassouni, D. Carbone, B. Parrino, G. Cirrincione, G. J. Peters, P. Diana, E. Giovannetti, *Anticancer Res.* **2019**, *39*, 3615–3620.
[23] B. Parrino, A. Carbone, V. Spanò, A. Montalbano, D. Giallombardo, P. Barraja, A. Attanzio, L. Tesoriere, C. Sissi, M. Palumbo, G. Cirrincione, P. Diana, *Eur. J. Med. Chem.* **2015**, *94*, 367–377.

© 2020 Wiley-VCH GmbH

[24] B. Parrino, A. Carbone, C. Ciancimino, V. Spanò, A. Montalbano, P. Barraja, G. Cirrincione, P. Diana, C. Sissi, M. Palumbo, O. Pinato, M. Pennati, G. Beretta, M. Folini, P. Matyus, B. Balogh, N. Zaffaroni, *Eur. J. Med. Chem.* **2015**, *94*, 149–162.
[25] N. Kerru, L. Gummidi, S. Maddila, K. K. Gangu, S. B. Jonnalagadda, *Molecules* **2020**, *25* (8).
[26] D. Kumar, G. Patel, A. K. Chavers, K.-H. Chang, K. Shah, *Eur. J. Med. Chem.* **2011**, *46* (7), 3085–3092.
[27] H.-Z Zhang, S. Kasibhatla, J. Kuemmerle, W. Kemnitzer, K. Ollis-Mason, L. Qiu, C. Crogan-Grundy, B. Tseng, J. Drewe, S. X. Cai, *J. Med. Chem.* **2005**, *48* (16), 5215–5223.
[28] M. Krasavin, A. V. Sosnov, R. Karapetian, I. Konstantinov, O. Soldatkina, E. Godovykh, F. Zubkov, R. Bai, E. Hamel, A. A. Gakh, *Bioorg. Med. Chem. Lett.* **2014**, *24* (18), 4477–4481.
[29] S. Cascioferro, A. Attanzio, V. Di Sarno, S. Musella, L. Tesoriere, G. Cirrincione, P. Diana, B. Parrino, *Mar. Drugs* **2019**, *17*, 35.
[30] A. Carbone, B. Parrino, M. G. Cusimano, V. Spanò, A. Montalbano, P. Barraja, D. Schillaci, G. Cirrincione, P. Diana, S. Cascioferro, *Mar. Drugs* **2018**, *16* (8), 274–289.
[31] L. Zhang, Q. Wen, J. Jin, C. Wang, P. Lu, Y. Wang, *Tetrahedron* **2013**, *69* (21), 4236–4240.
[32] B. Parrino, A. Attanzio, V. Spanò, S. Cascioferro, A. Montalbano, P. Barraja, L. Tesoriere, P. Diana, G. Cirrincione, A. Carbone, *Eur. J. Med. Chem.* **2017**, *138*, 371–383.
[33] E. Valeur, M. Bradley, *Chem. Soc. Rev.* **2009**, *38* (2), 606–631.
[34] V. J. Bhagwandin, J. M. Bishop, W. E. Wright, J. W. Shay, *PLoS One* **2016**, *11* (2), 1–16.
[35] G. A. Lee, K. A. Hwang, *Toxin Rev.* **2016**, 8 (6), 1–17.
[36] N. Gavert, A. Ben-Ze'ev, *Trends Mol. Med.* **2008**, *14* (5), 199–209.
[37] H. Hugo, M. L. Ackland, T. Blick, M. G. Lawrence, J. A. Clements, E. D. Williams, E. W. Thompson, *J. Cell. Physiol.* **2007**, *213*, 374–383.
[38] S. Peirò, M. Escriva, I. Puig, M. J. Barberà, N. Dave, N. Herranz, M. J. Larriba, M. Takkunen, C. Francı, A. Munoz, I. Virtanen, J. Baulida, A. G. Herreros, *Nucleic Acids Res.* **2006**, *34* (7), 2077–2084.
[39] R. Bhat, Y. Xue, S. Berg, S. Hellberg, M. Ormo, Y. Nilsson, A.-C Radesater, E. Jerning, P.-O Markgren, T. Borgegård, M. Nylof, A. Gimenez-Cassina, F. Hernandez, J. J. Lucas, J. Dıaz-Nido, J. Avila, *J. Biol. Chem.* **2003**, *278*, 45937–45945.
[40] L. Meijer, A.-L Skaltsounis, P. Magiatis, P. Polychronopoulos, M. Knockaert, M. Leost, X. P. Ryan, C. A. Vonica, A. Brivanlou, R. Dajani, C. Crovace, C. Tarricone, A. Musacchio, S. M. Roe, L. Pearl, P. Greengard, *Chem. Biol.* **2003**, *10* (12), 1255–1266.
[41] F. Heider, T. Pantsar, M. Kudolo, F. Ansideri, A. De Simone, L. Pruccoli, T. Schneider, M. I. Goettert, A. Tarozzi, V. Andrisano, S. A. Laufer, P. Koch, *ACS Med. Chem. Lett.* **2019**, *10* (10), 1407–1414.
[42] H. Park, Y. Shin, J. Kim, S. Hong, *J. Med. Chem.* **2016**, *59* (19), 9018–9034.
[43] K. Lynch, W. Santos, WO 2016054261, **2016**; *Chem. Abstr.* **2016**, 164, 472549.
[44] Y. Ikeda, M. Ezakv, I. Hayashv, D. Yasuda, K. Nakayama , *Jpn. J. Cancer Res.* **1990**, *81*, 987–993.
[45] P. Skehan, S. J. Friedman, *Vitr. Cell. Dev. Biol.* **2014**, *21* (5), 288–290.
[46] M. Lieber, J. Mazzetta, W. Nelson-Rees, M. Kaplan, G. Todaro, *Int. J. Cancer* **1975**, *15* (5), 741–747.
[47] R. Gradiz, H. C. Silv, L. Carvalho, M. F. Botelho, *Sci. Rep.* **2016**, *No. February*, 1–14.
[48] M. Pilichowska, N. Kimura, M. Schindler, M. Kobari, *Endocr. Pathol.* **2001**, *12* (2), 147–155.
[49] R. Sciarrillo, A. Wojtuszkiewicz, I.E. Kooi, V. E. Gómez, U. Boggi, G. Jansen, G. J. Kaspers, J. Cloos, E. Giovannetti, *J. Visualization* **2016**, *118*, e54714.
[50] E. Giovannetti, Q. Wang, A. Avan, N. Funel, T. Lagerweij, J.-H. Lee, V. Caretti, A. van der Velde, U. Boggi, Y. Wang, E. Vasile, G. J. Peters, T. Wurdinger, G. Giaccone, *J. Natl. Cancer Inst.* **2014**, *106* (1), djt346.
[51] E. Giovannetti, P. A. Zucali, Y. G. Assaraf, L. G. Leon, K. Smid, C. Alecci, F. Giancola, A. Destro, L. Gianoncelli, E. Lorenzi, M. Roncelli, A. Santoro, G. J. Peters, *Br. J. Cancer* **2011**, *105* (10), 1542–1553.
[52] S. Cascioferro, G. Li Petri, B. Parrino, D. Carbone, N. Funel, C. Bergonzini, G. Mantini, H. Dekker, D. Geerke, G. J. Peters, G. Cirrincione, E. Giovannetti, P. Diana, *Eur. J. Med. Chem.* **2020**, *189*, 112088.
[53] N. Van Der Steen, A. Leonetti, K. Keller, H. Dekker, N. Funel, F. Lardon, R. Ruijtenbeek, M. Tiseo, C. Rolfo, P. Pauwels, G. J. Peters, *E. Biochem. Pharmacol.* **2019**, *166*, 128–138.
[54] E. Giovannetti, R. Honeywell, A. R. Hanauske, C. Tekle, B. Kuenen, J. Sigmond, G. Giaccone, G. J. Peters, *Curr. Drug Targets* **2010**, *11* (1), 12–28.
[55] F. Heider, F. Ansideri, R. Tesch, T. Pantsar, U. Haun, E. Doring, M. Kudolo, A. Poso, W. Albrecht, S. A. Laufer, P. Koch, *Eur. J. Med. Chem.* **2019**, *175*, 309–329.

Manuscript received: September 21, 2020
Version of record online: November 3, 2020

ChemMedChem

Supporting Information

1,2,4-Oxadiazole Topsentin Analogs with Antiproliferative Activity against Pancreatic Cancer Cells, Targeting GSK3β Kinase

Daniela Carbone[+], Barbara Parrino[+], Stella Cascioferro, Camilla Pecoraro, Elisa Giovannetti, Veronica Di Sarno, Simona Musella, Giulia Auriemma, Girolamo Cirrincione, and Patrizia Diana*

Table S1. Growth Percent of treated cells with the compounds **1b**, **1c** and **1l**.[a]

	Growth Percent				Growth Percent		
Panel/Cell line	**1b**	**1c**	**1l**	**Panel/Cell line**	**1b**	**1c**	**1l**
Leukemia				**Melanoma**			
CCRF-CEM	23.89	86.71	45.62	SK-MEL-2	26.94	65.30	108.99
HL-60(TB)	-6.73	58.54	82.91	SK-MEL-5	25.32	16.84	83.36
K-562	16.72	37.87	37.69	UACC-257	51.17	83.93	109.10
SR	11.18	44.12	6.41	UACC-62	31.73	60.32	86.14
Non-Small Cell Lung Cancer				**Ovarian Cancer**			
A549/ATCC	40.55	73.65	32.13	IGROV1	32.52	25.69	69.49
EKVX	57.51	50.50	60.48	OVCAR-3	0.72	12.83	92.67
HOP-62	30.52	78.89	78.41	OVCAR-4	69.77	57.28	-0.34
HOP-92	43.62	63.76	83.91	OVCAR-8	49.32	91.09	48.61
NCI-H460	14.14	35.19	12.46	NCI/ADR-RES	36.47	64.23	56.06
NCI-H522	2.36	56.49	84.18	SK-OV-3	43.28	69.77	87.70
Colon Cancer				**Renal Cancer**			
COLO 205	34.67	56.00	93.27	786-0	5.55	98.42	99.42
HCT-116	19.54	47.08	63.47	A498	25.28	95.90	105.58
HCT-15	33.24	25.60	56.10	ACHN	49.61	86.37	80.87
HT29	8.80	35.79	43.97	CAKI-1	32.88	56.93	67.43
KM12	26.75	21.9	55.24	RXF 393	89.88	90.10	96.41
SW-620	23.22	56.80	-2.17	SN12C	59.50	91.27	80.10
CSN Cancer				TK-10	57.58	68.15	99.88
SF-268	54.89	92.09	55.94	UO-31	42.44	61.58	66.96
SF-295	20.74	68.49	88.41	**Prostate Cancer**			
SF-539	30.04	91.67	88.71	PC-3	41.87	-	39.34
SNB-19	38.77	91.79	86.24	DU-145	72.52	101.68	3.08
SNB-75	27.39	55.64	73.67	**Breast Cancer**			
U251	28.52	92.44	51.97	MCF7	19.16	19.98	38.85
Melanoma				MDA-MB-231/ATCC	57.10	69.77	45.86
LOX IMVI	39.48	83.95	78.25	HS 578T	44.81	56.21	80.32
MALME-3M	37.34	58.42	43.65	BT-549	47.96	69.67	78.95
M14	33.02	64.51	47.01	T-47D	37.84	44.36	71.82
MDA-MB-435	-19.13	7.96	63.30	MDA-MB-468	62.99	-4.38	66.07

[a] Data obtained from the NCI *in vitro* disease-oriented human tumor cell line screen.

Figure S1. ^{1}H NMR of compound **1a**

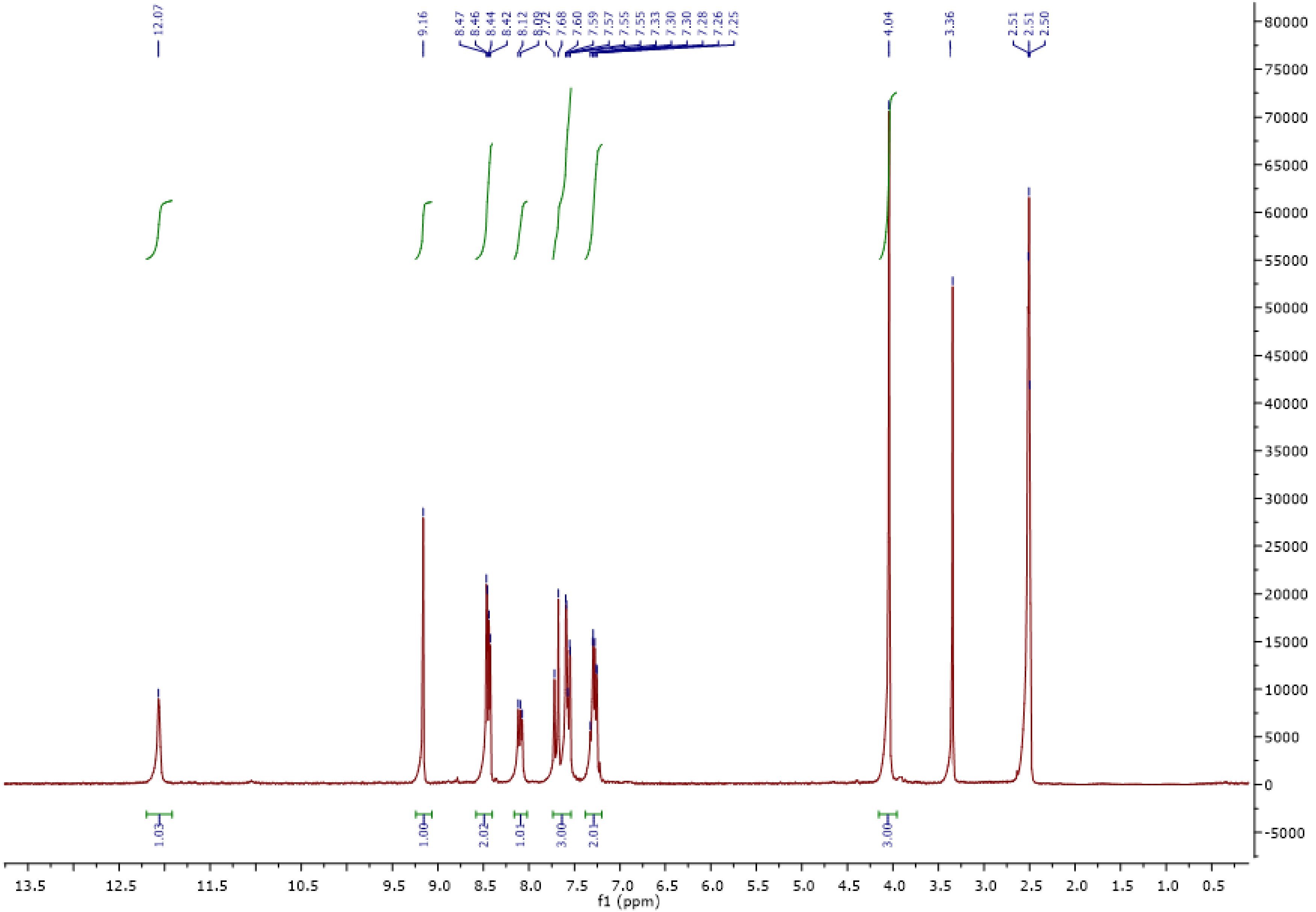

Figure S2. ^{13}C NMR of compound **1a**

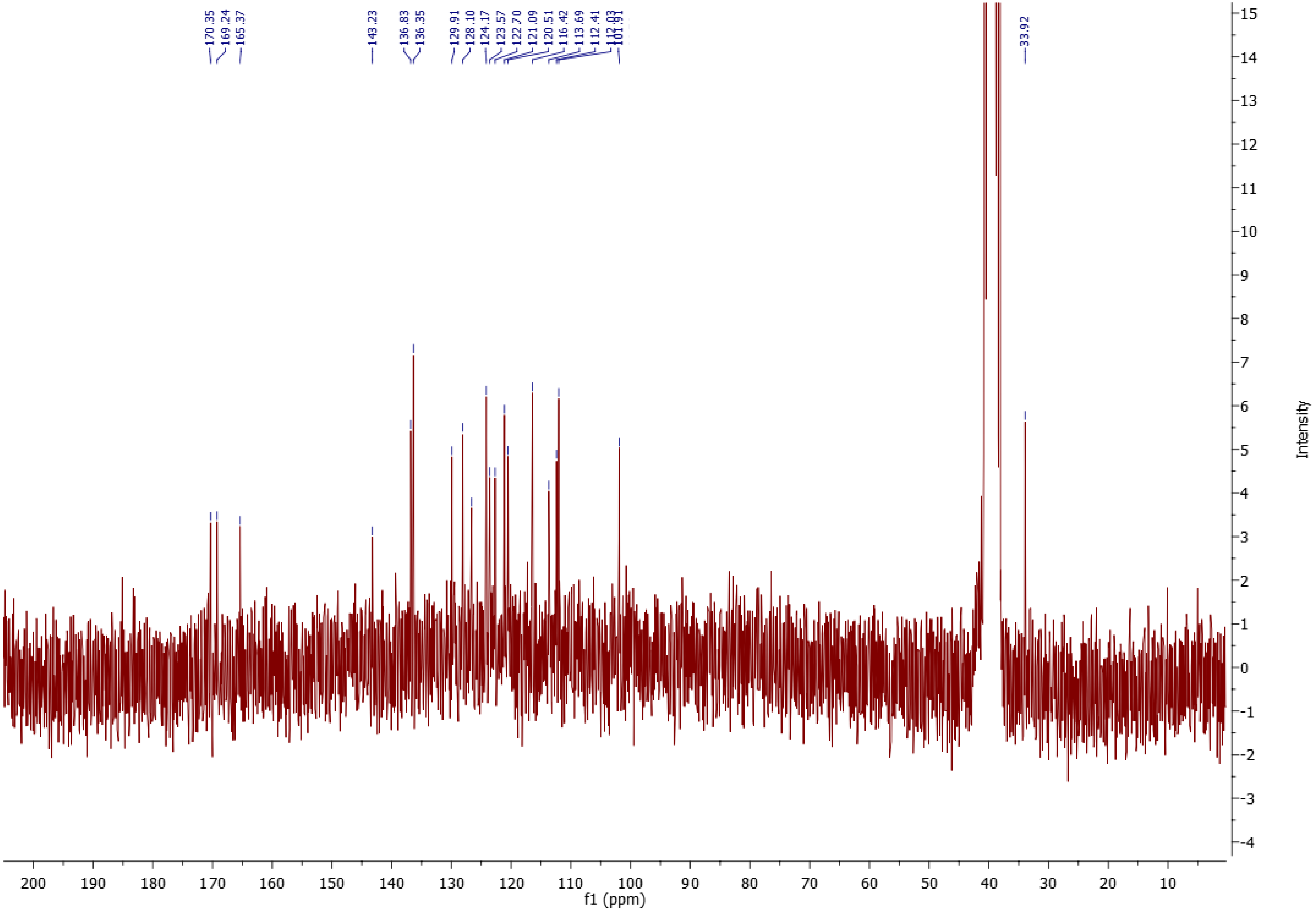

Figure S3. ^{1}H NMR of compound **1b**

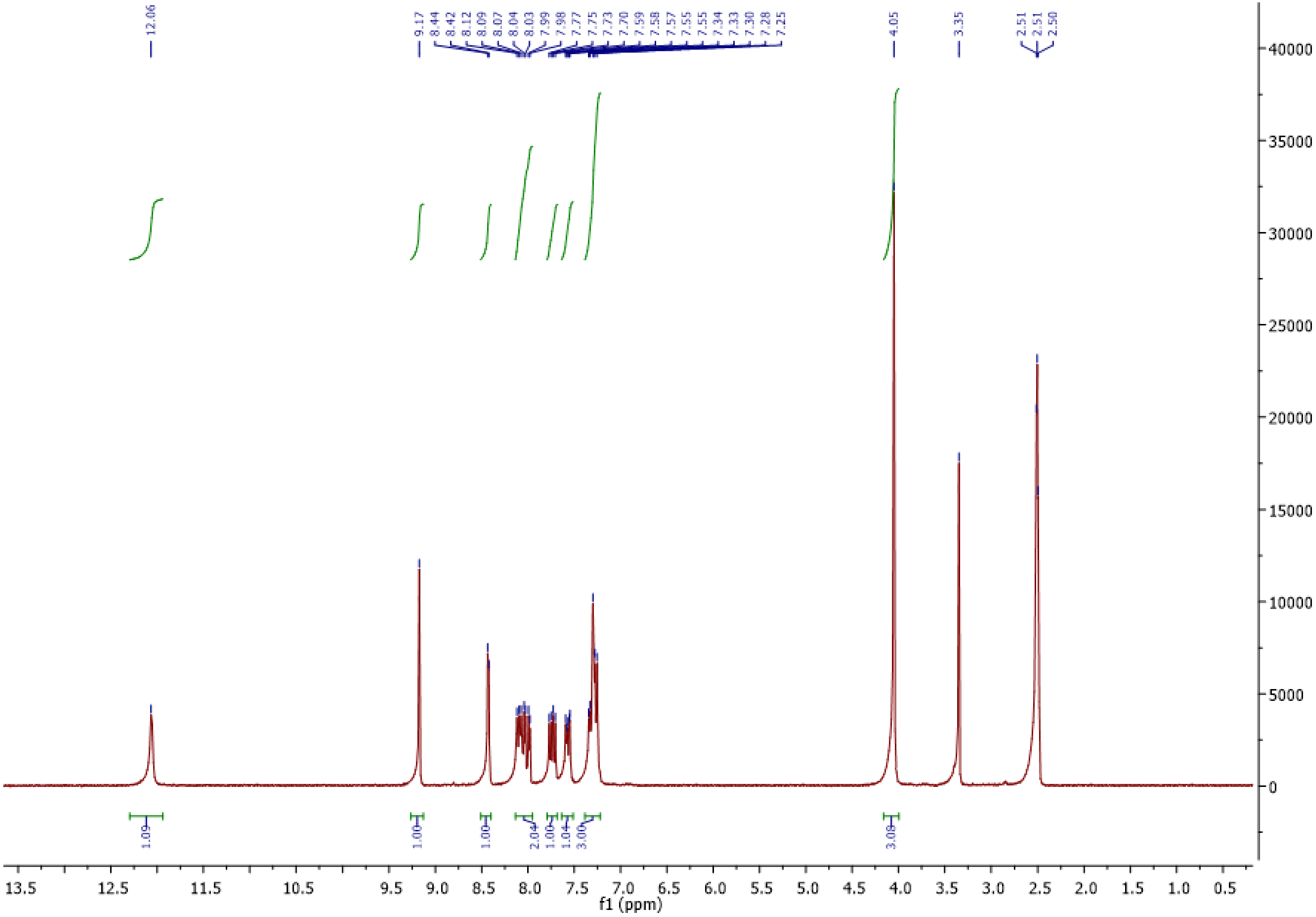

Figure S4. ^{13}C NMR of compound **1b**

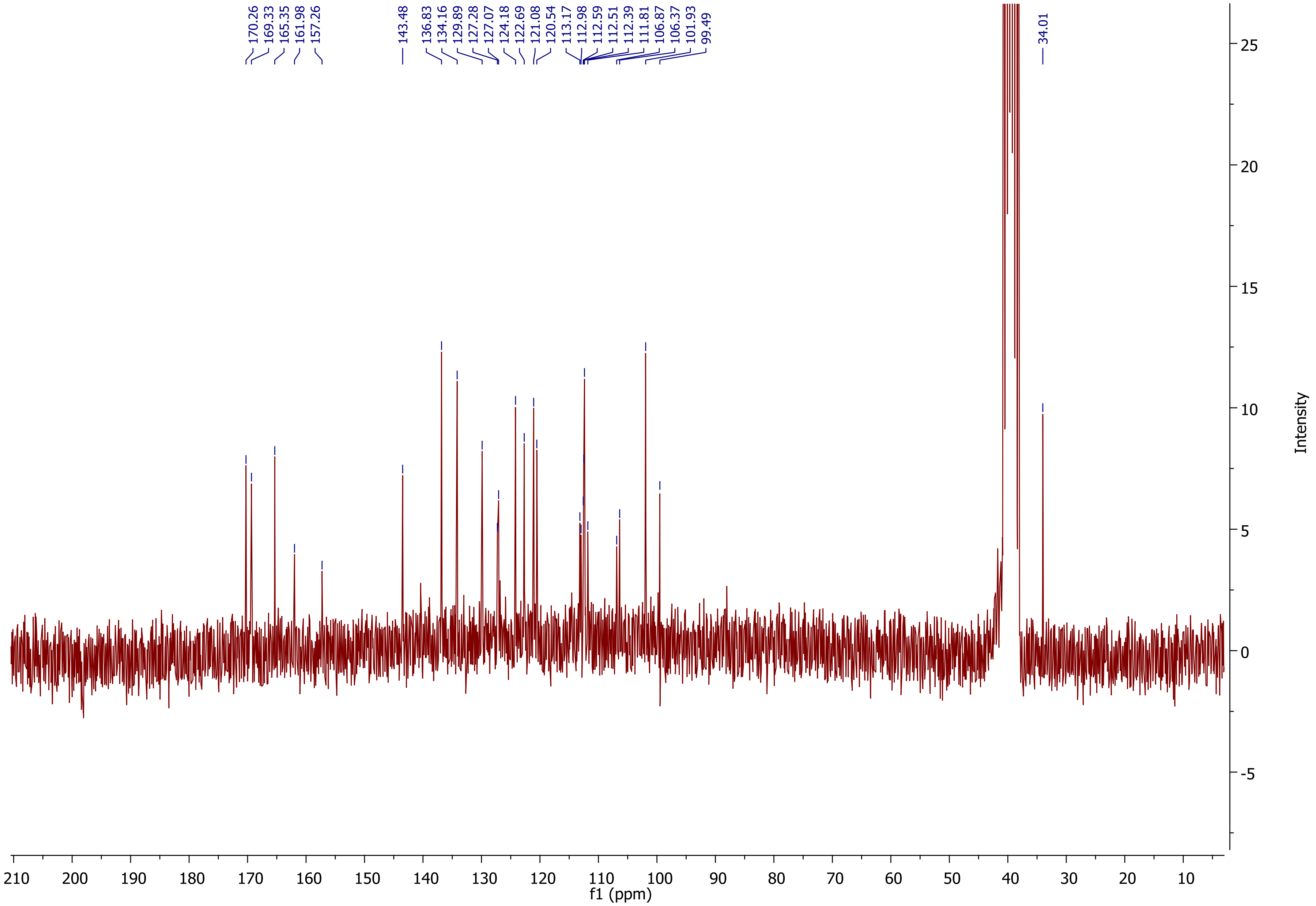

Figure S5. ^{1}H NMR of compound **1c**

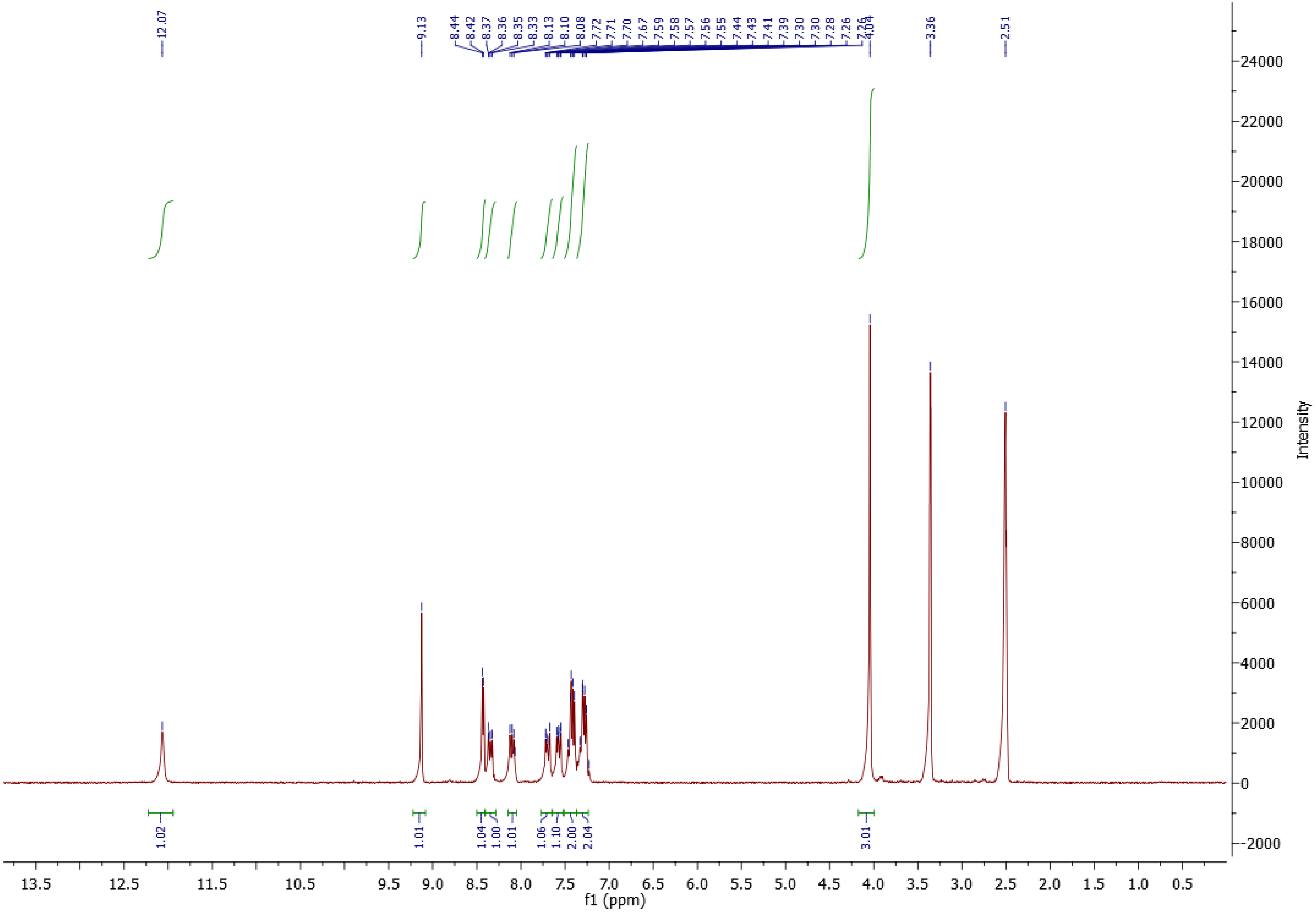

Figure S6. ^{13}C NMR of compound **1c**

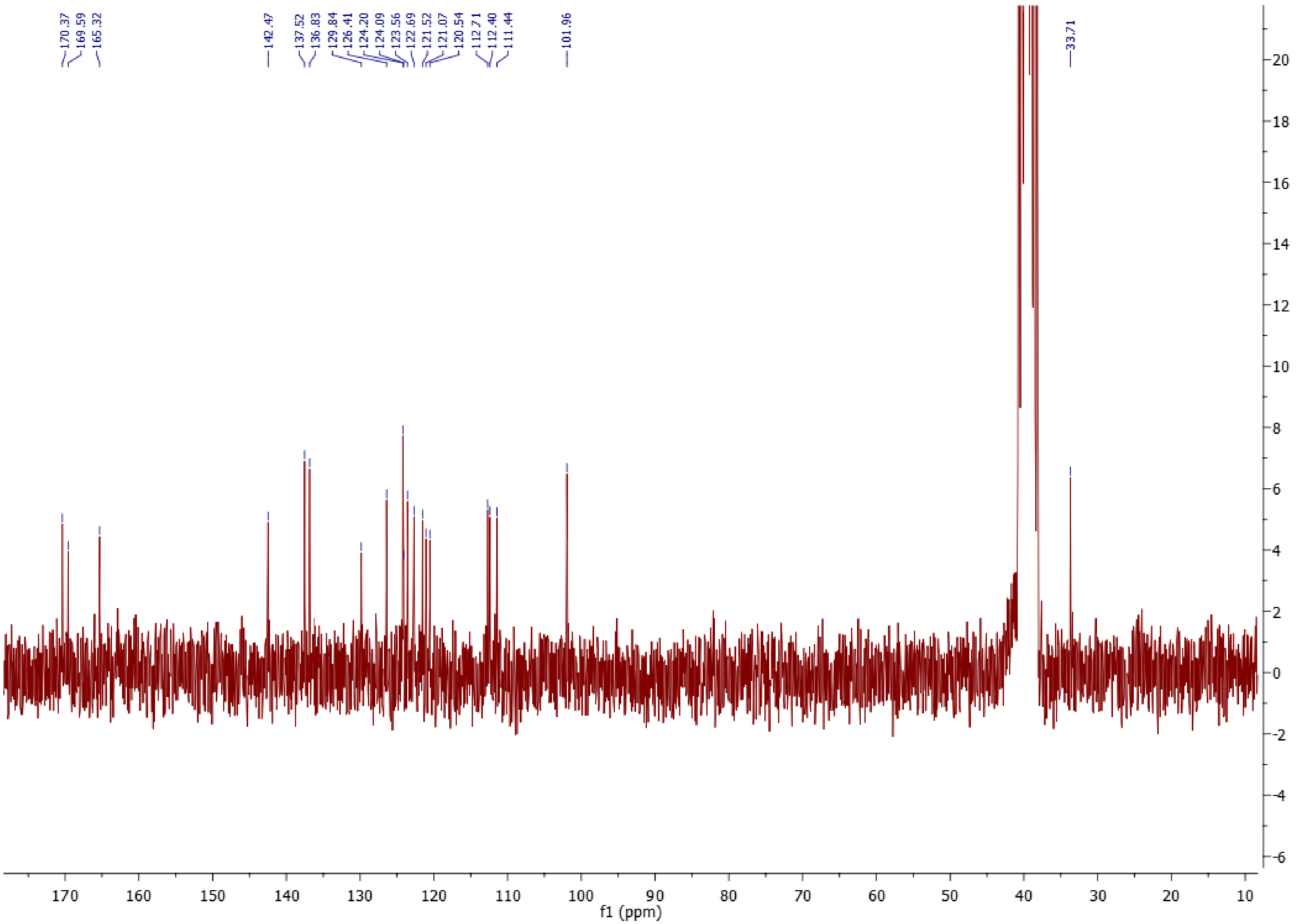

Figure S7. ^{1}H NMR of compound **1d**

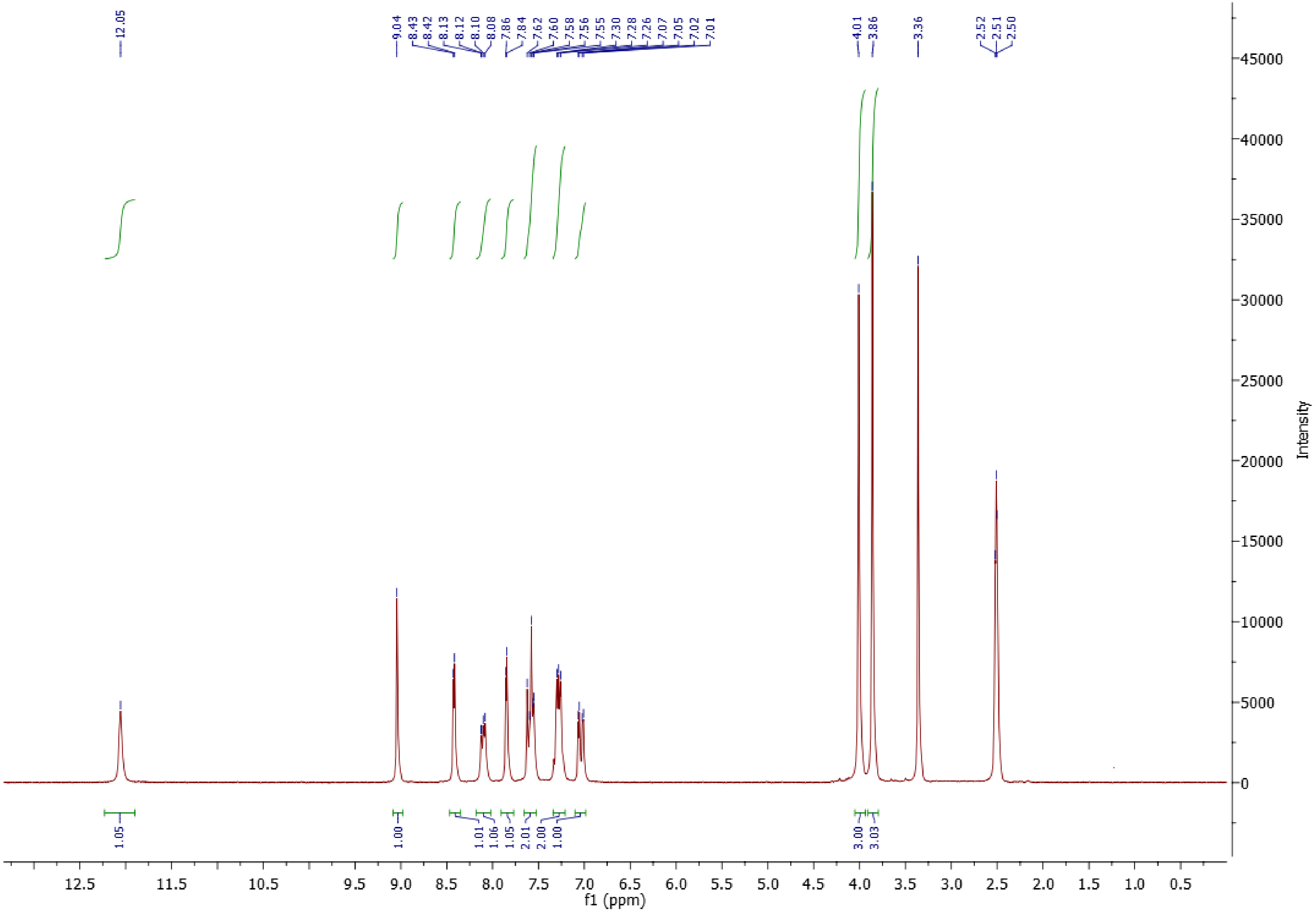

Figure S8. ^{13}C NMR of compound **1d**

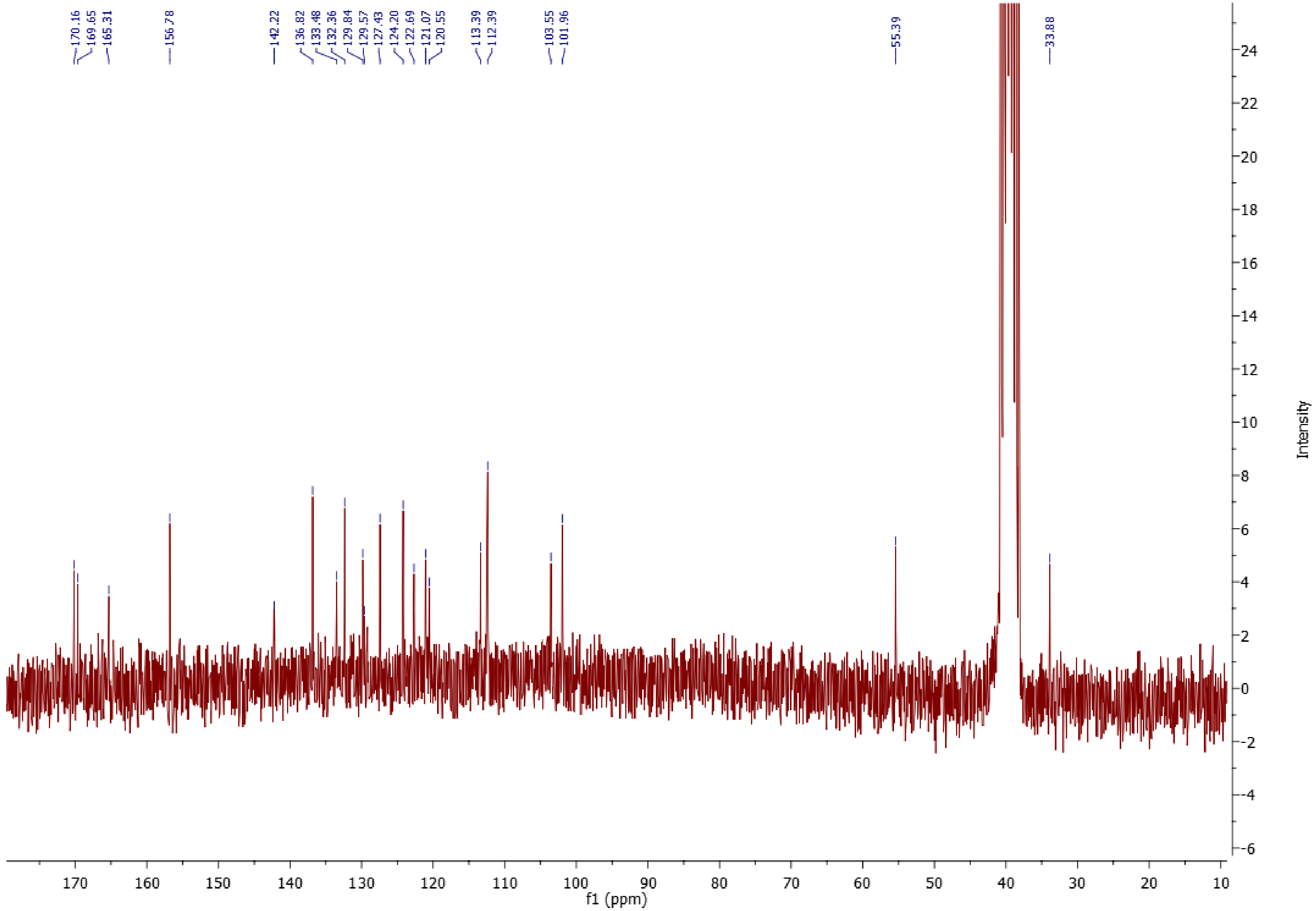

Figure S9. ^{1}H NMR of compound **1e**

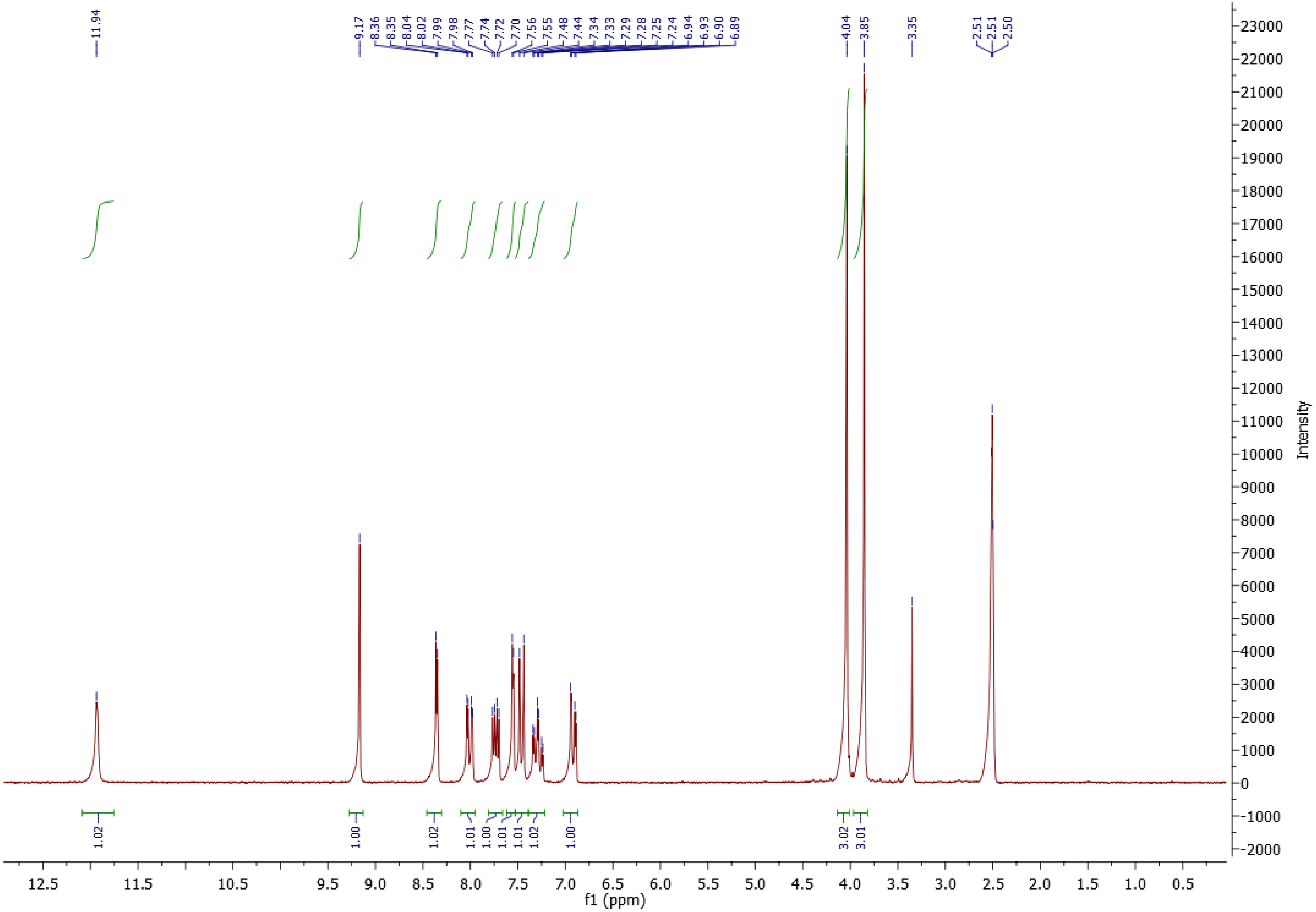

Figure S10. ^{13}C NMR of compound **1e**

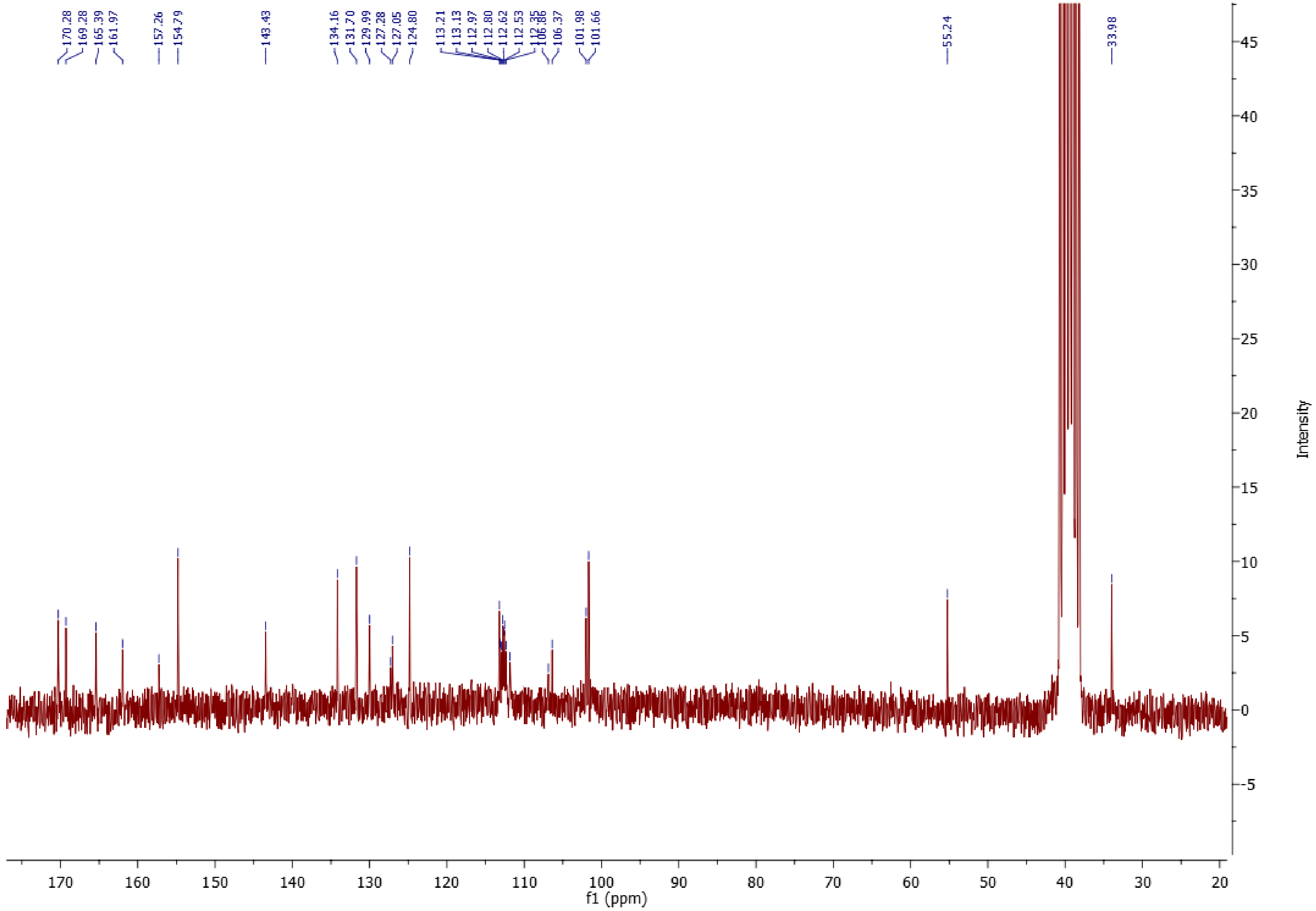

Figure S11. ^{1}H NMR of compound **1f**

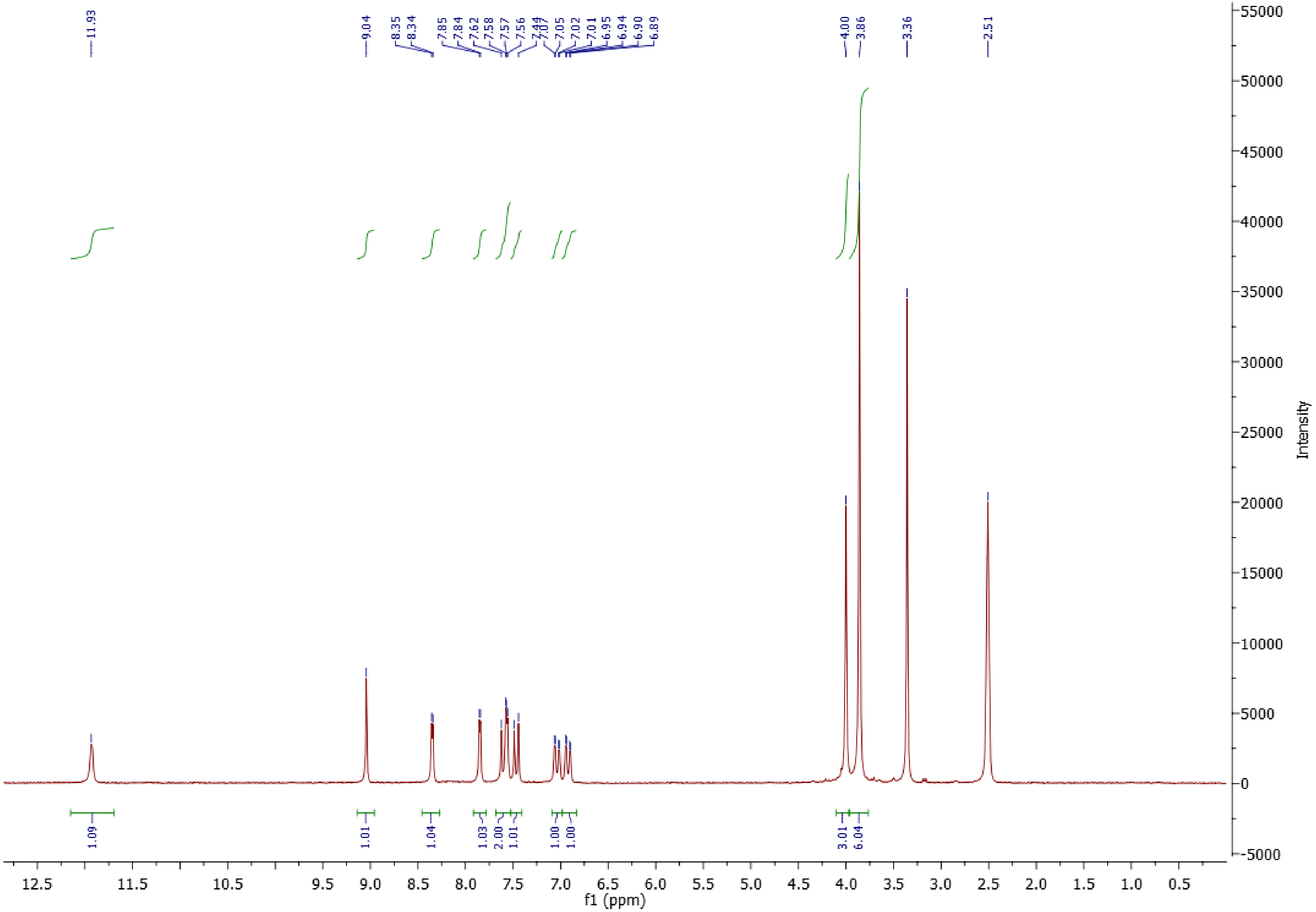

Figure S12. ^{13}C NMR of compound **1f**

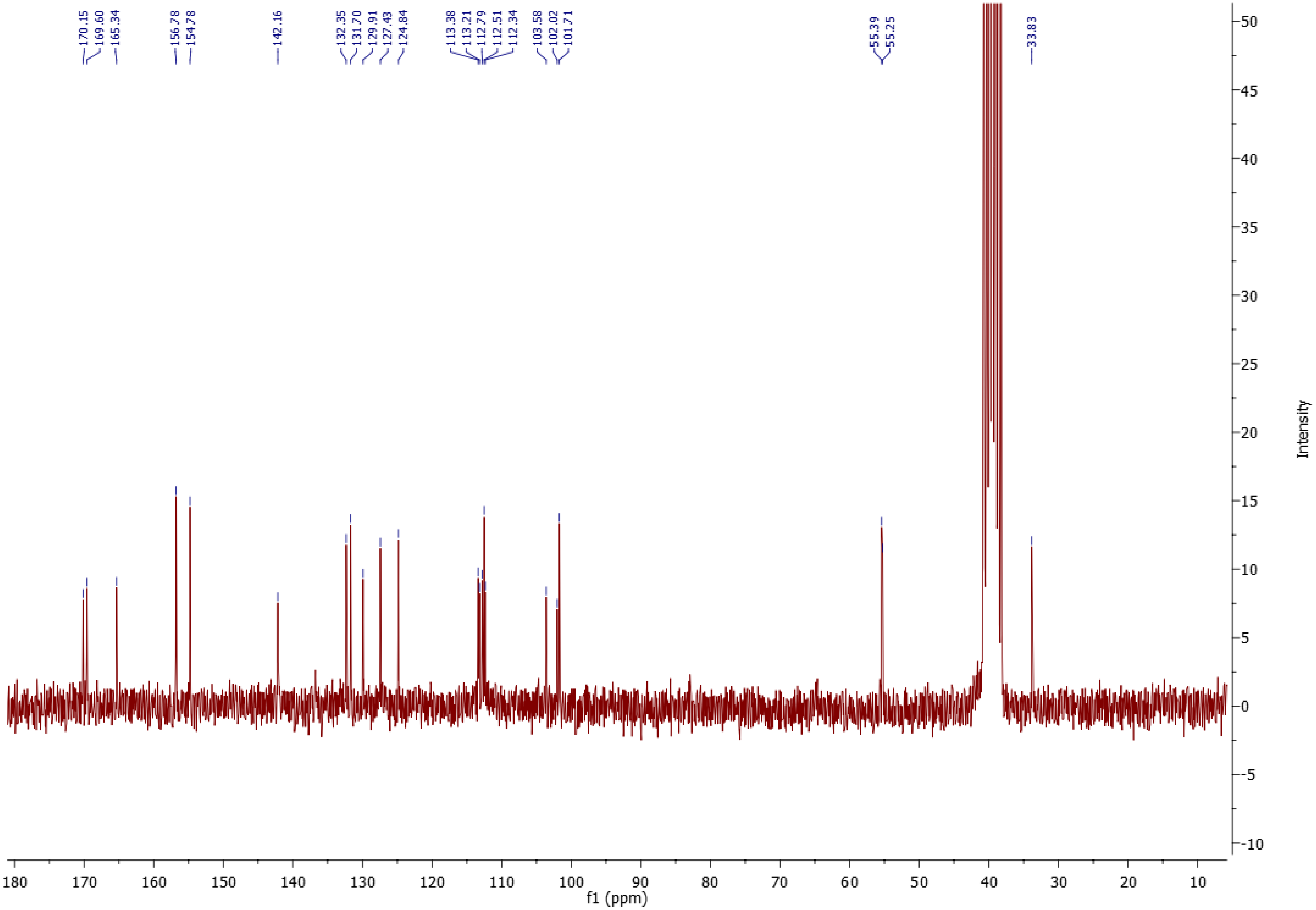

Figure S13. ^{1}H NMR of compound **1g**

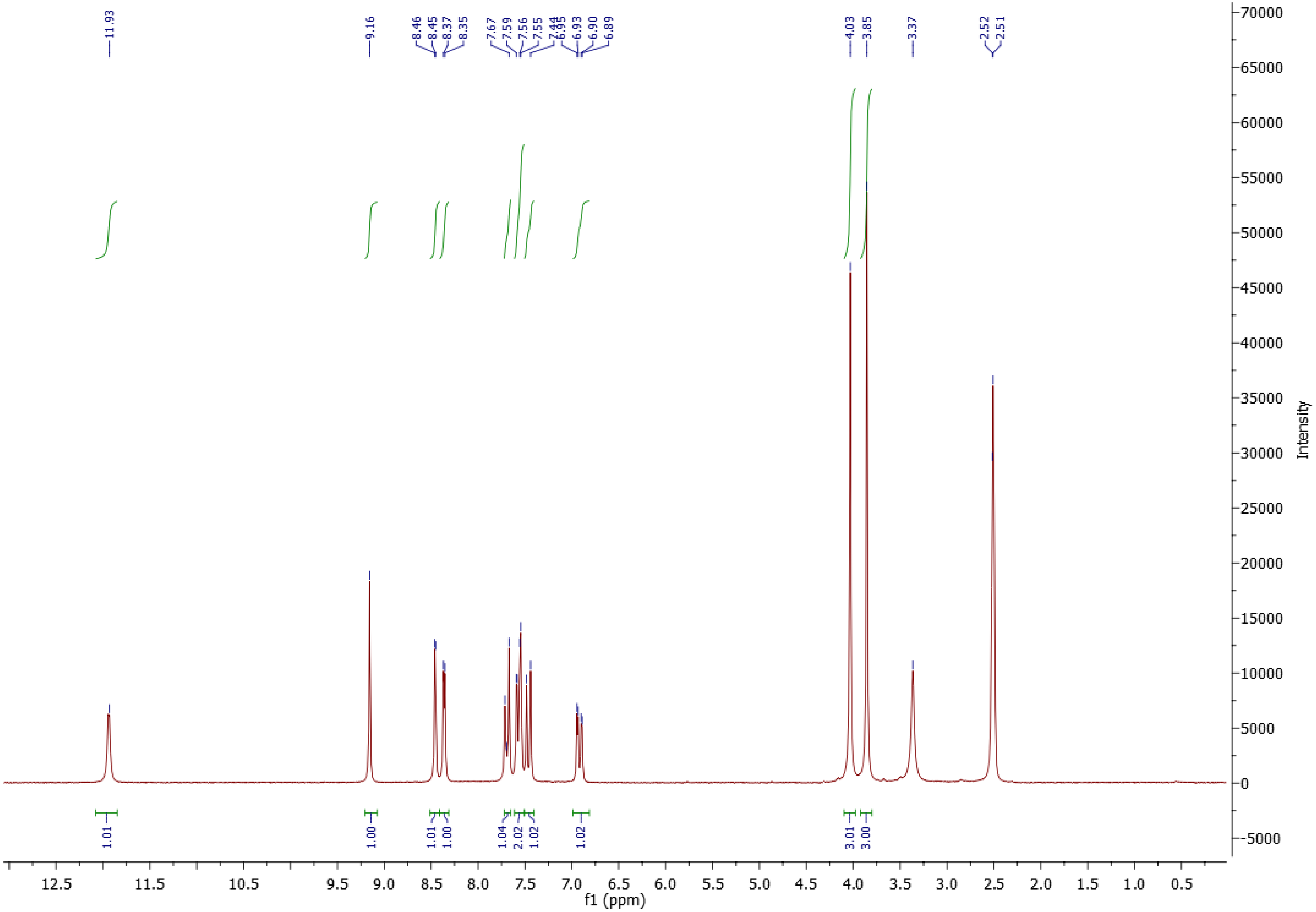

Figure S14. ^{13}C NMR of compound **1g**

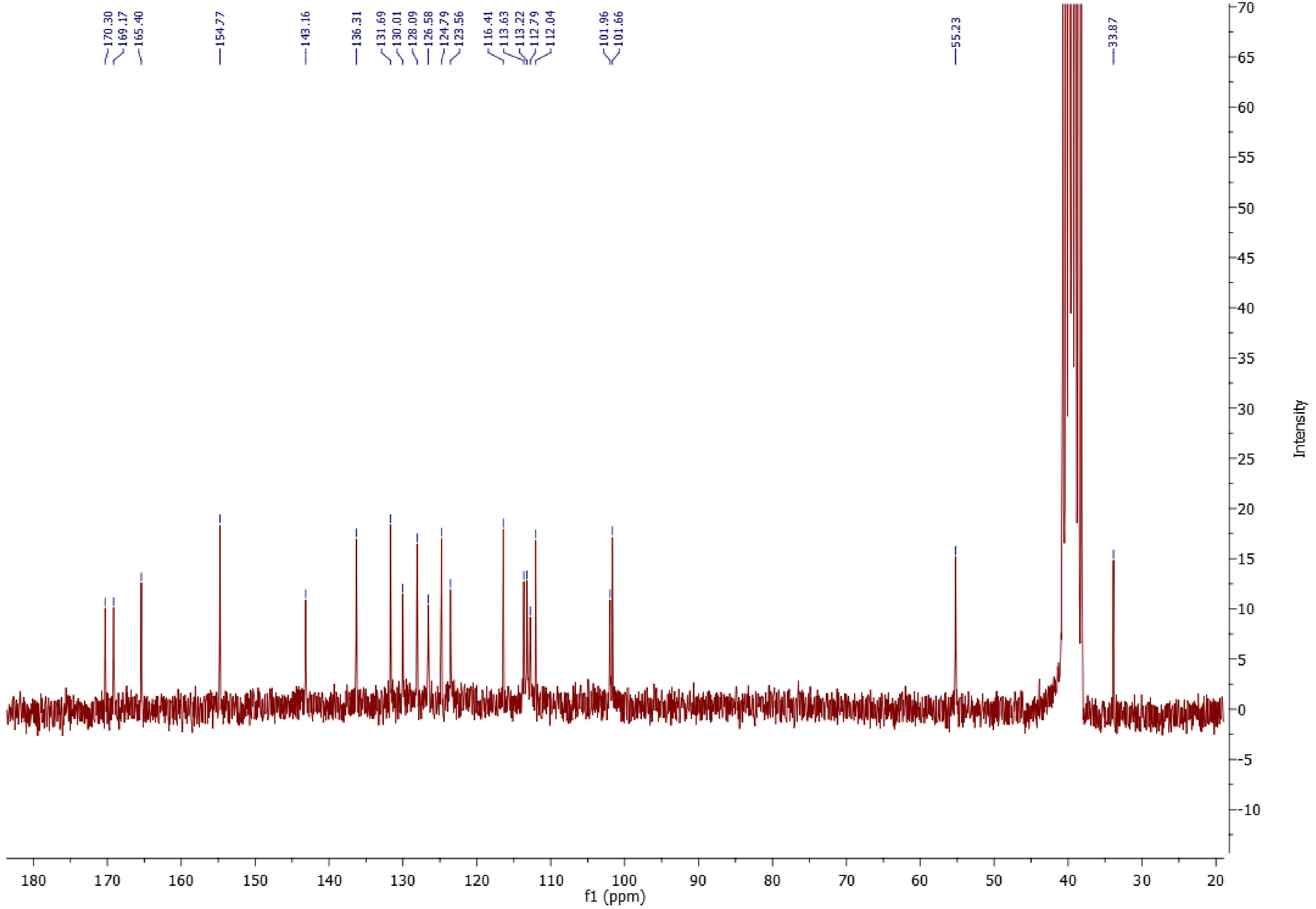

Figure S15. ^{1}H NMR of compound **1h**

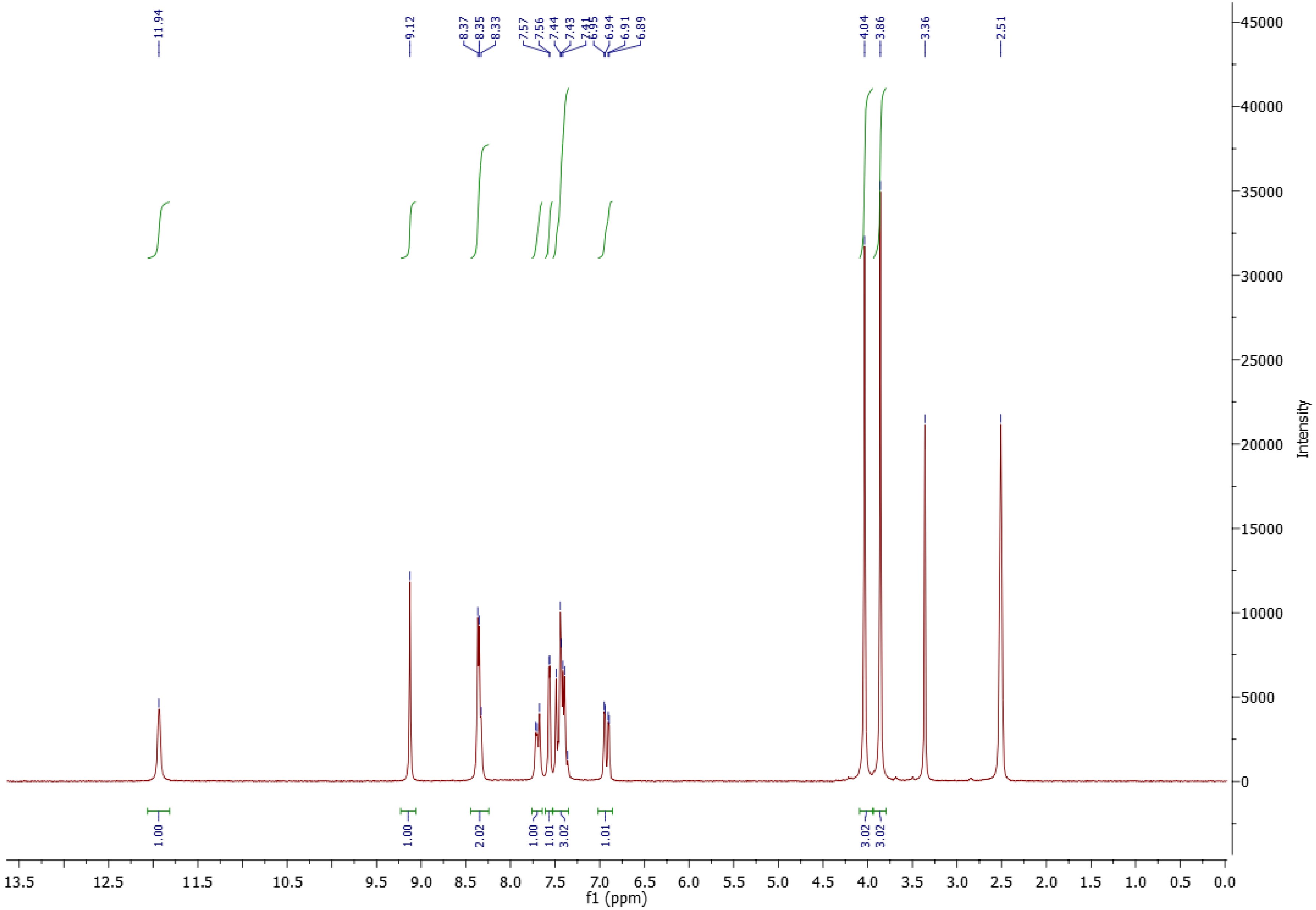

Figure S16. ^{13}C NMR of compound **1h**

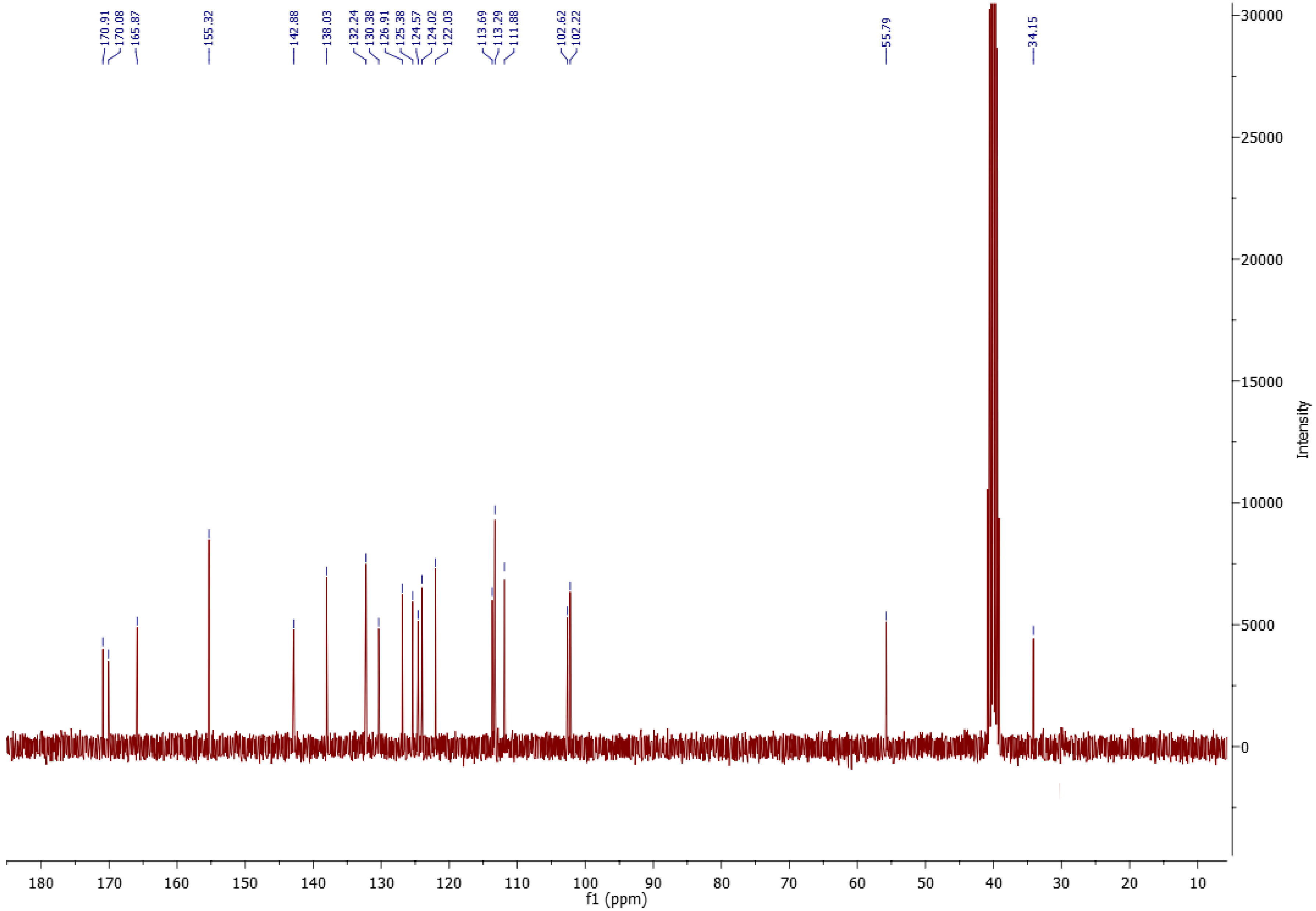

Figure S17. ^{1}H NMR of compound **1i**

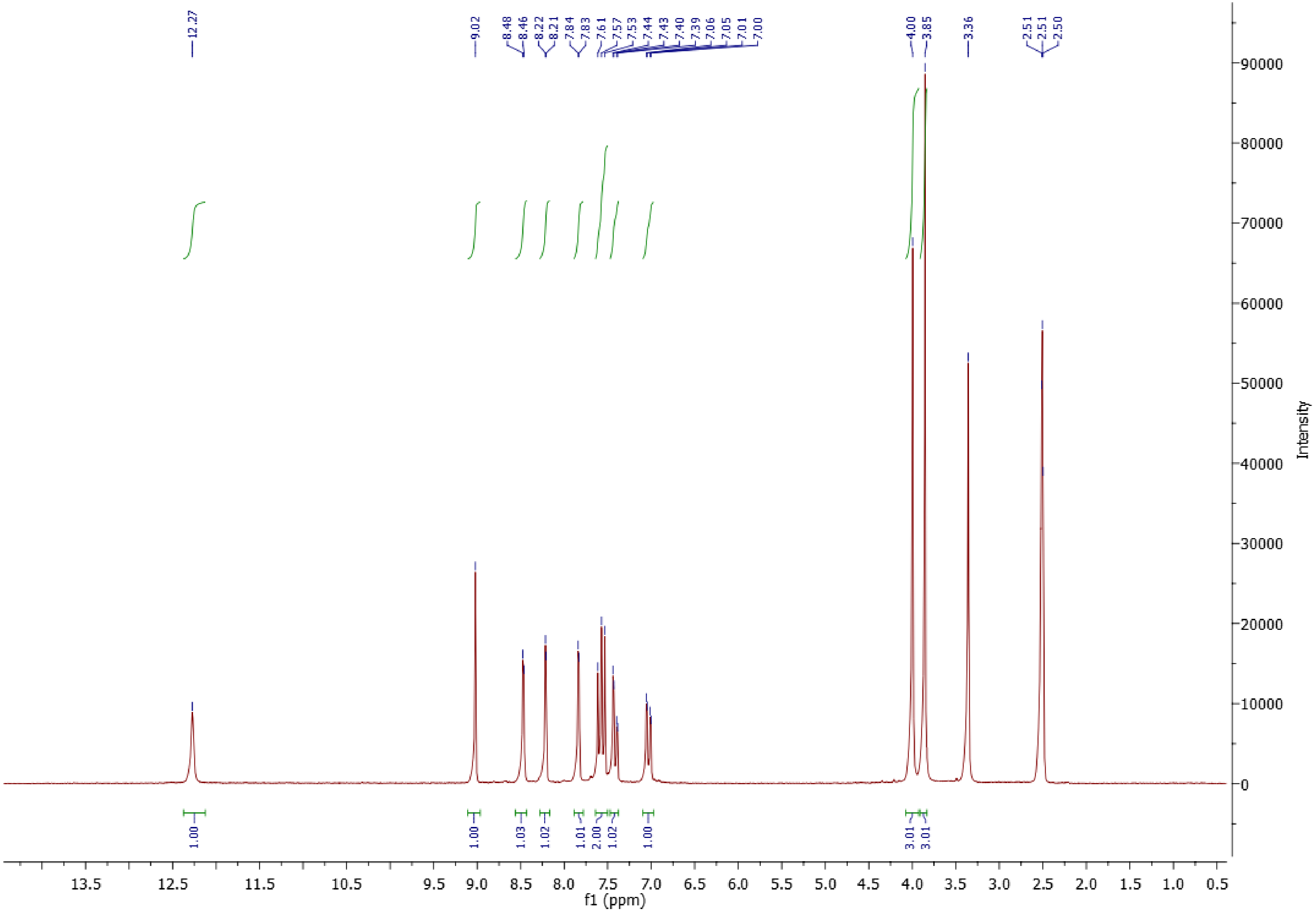

Figure S18. ^{13}C NMR of compound **1i**

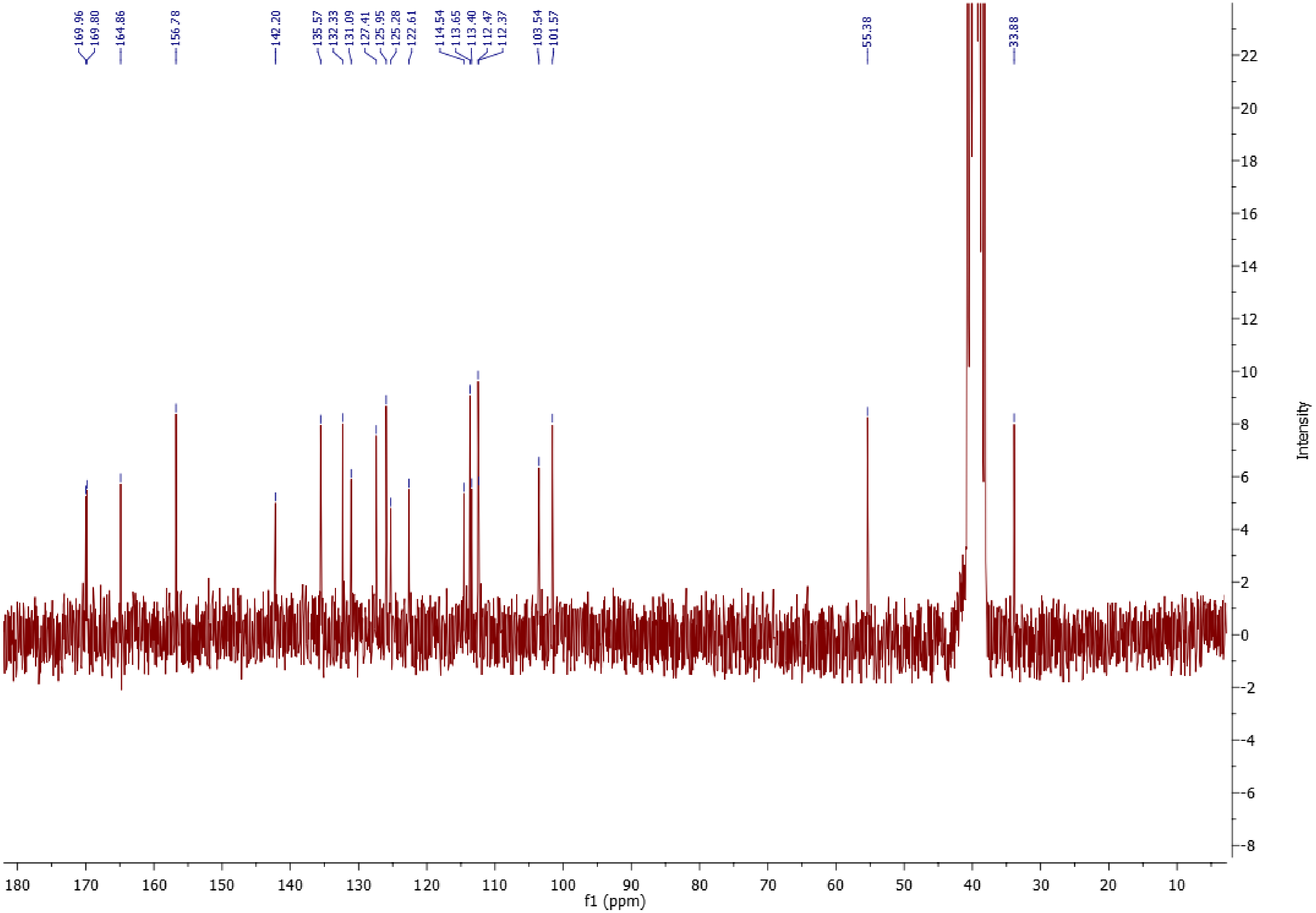

Figure S19. ^{1}H NMR of compound **1j**

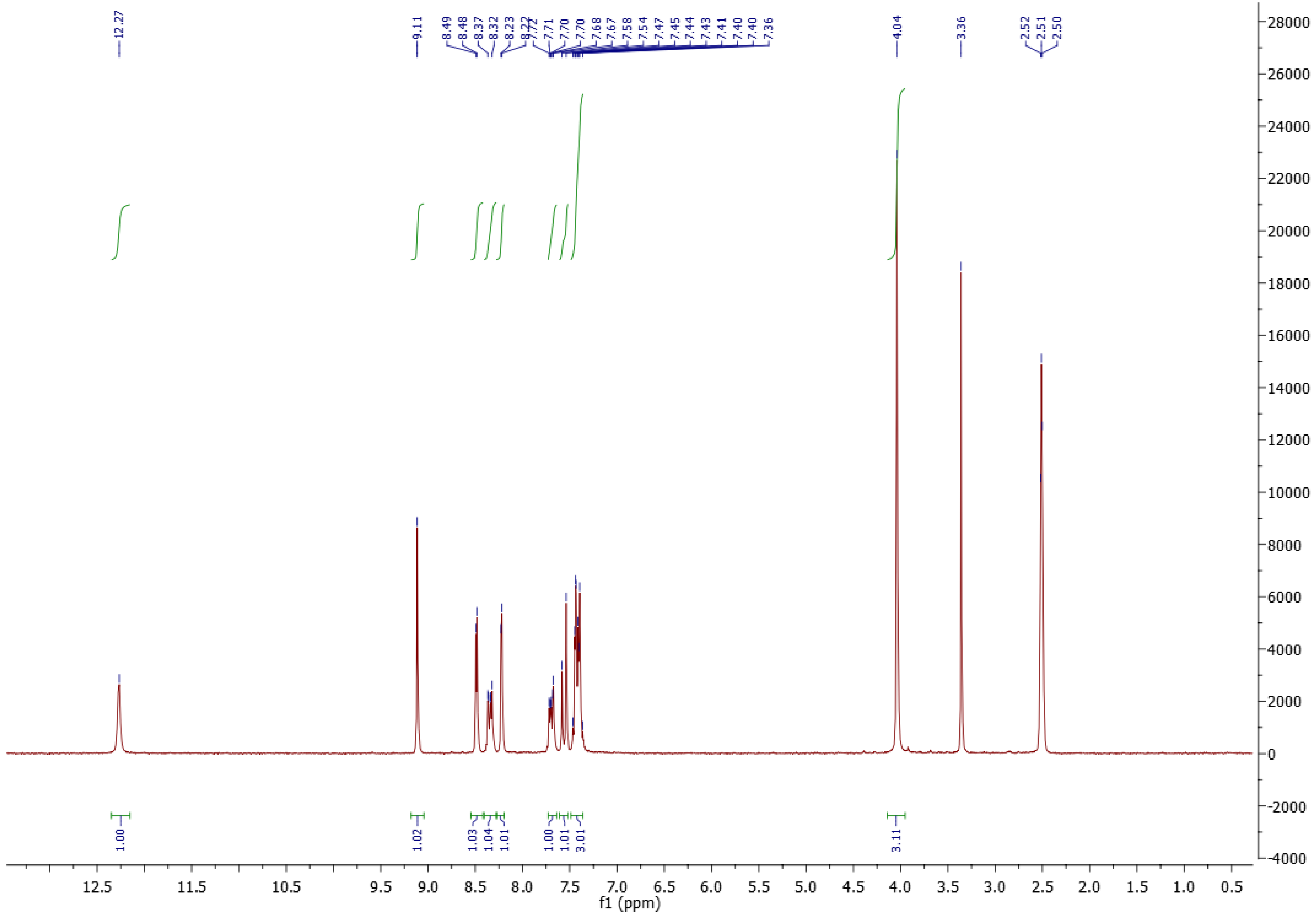

Figure S20. ^{13}C NMR of compound **1j**

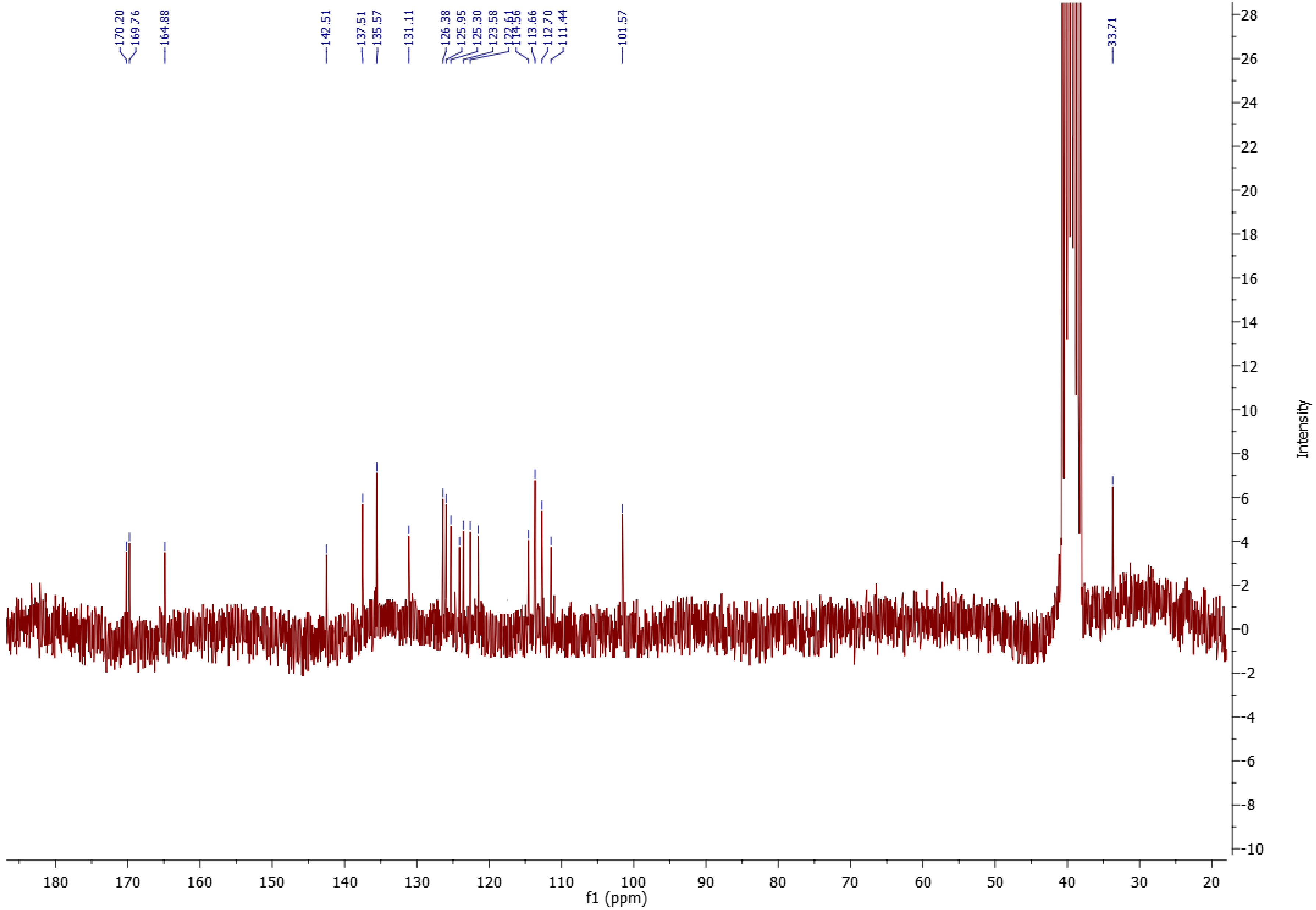

Figure S21. ^{1}H NMR of compound **1k**

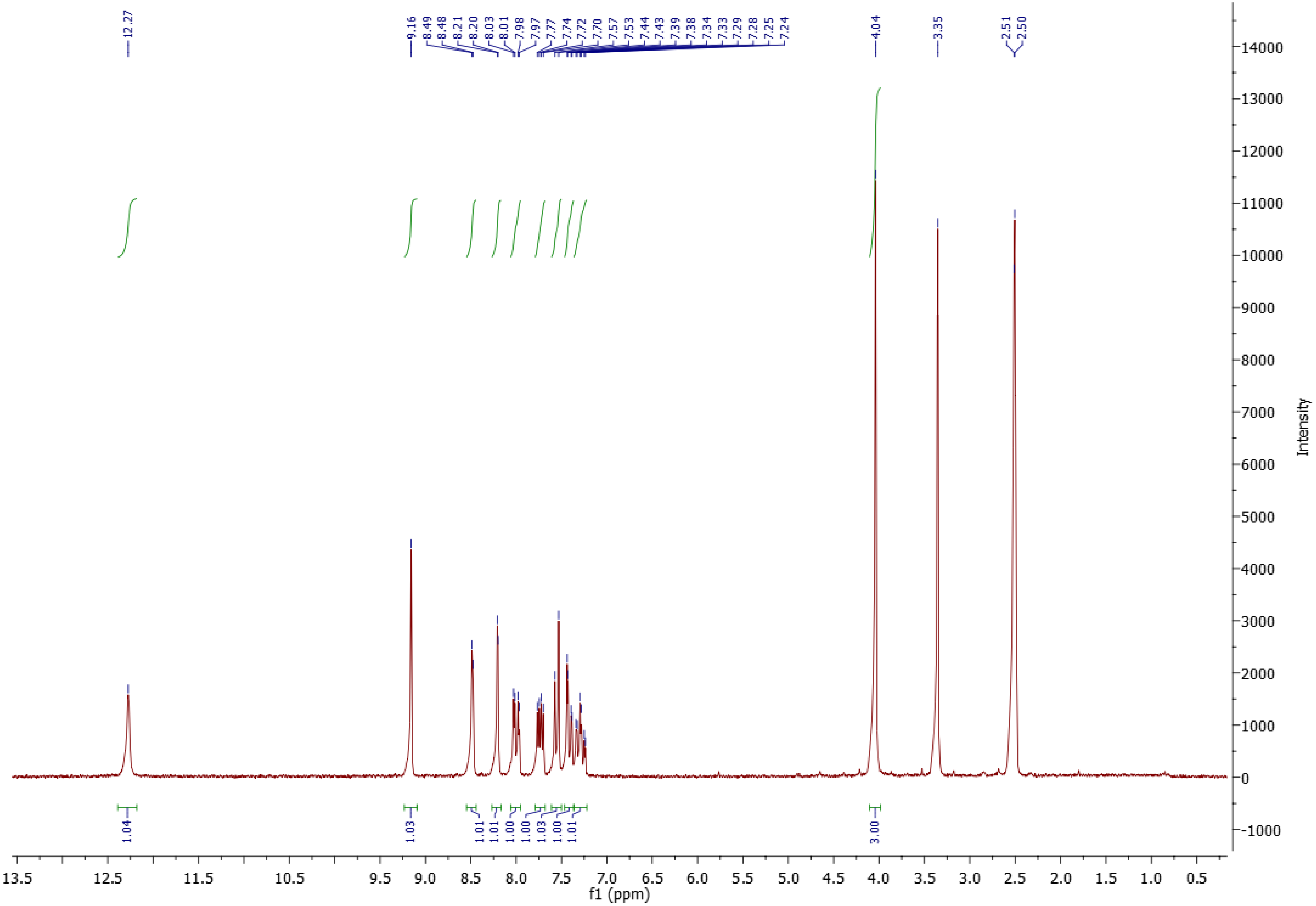

Figure S22. ^{13}C NMR of compound **1k**

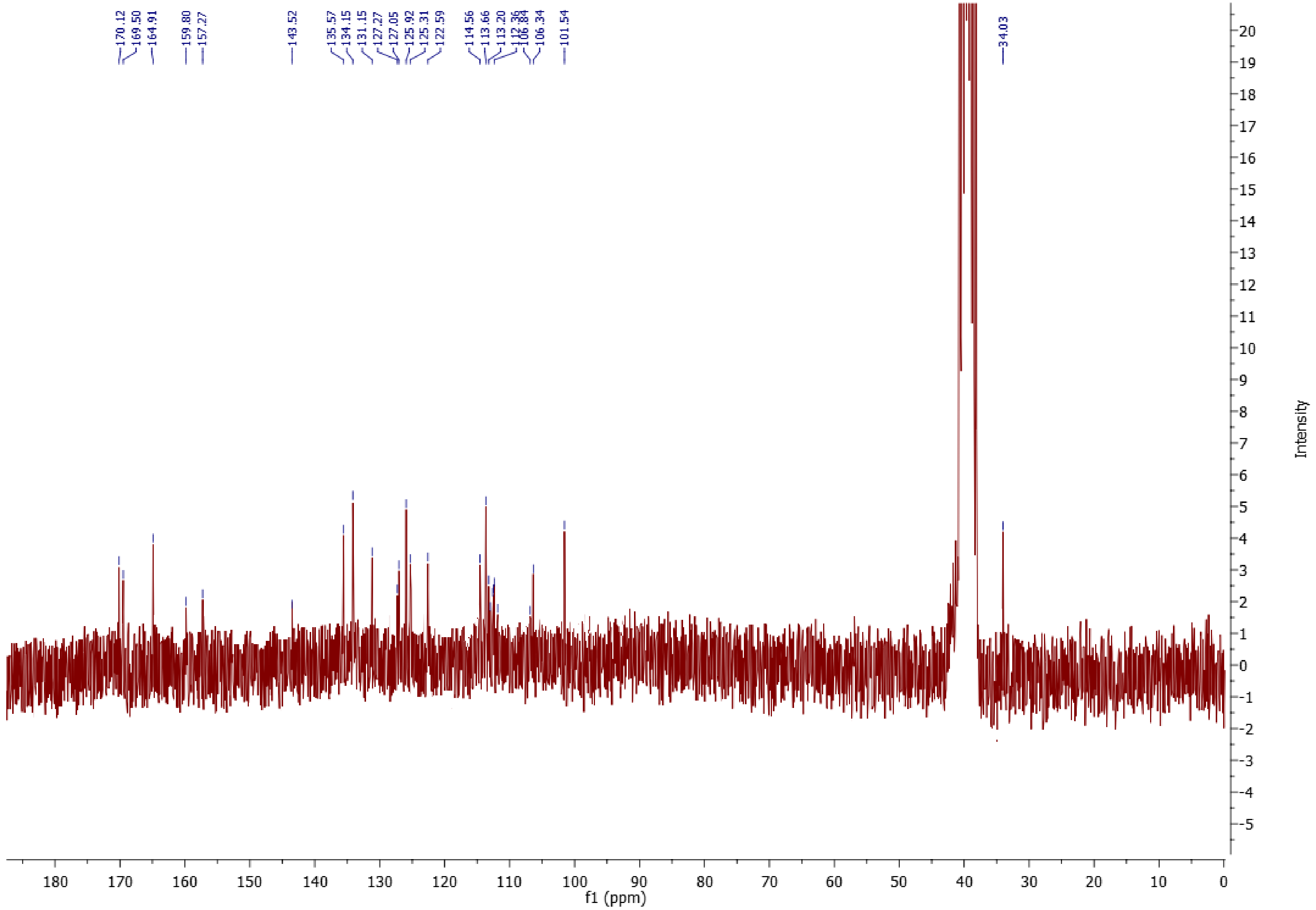

Figure S23. ^{1}H NMR of compound **1l**

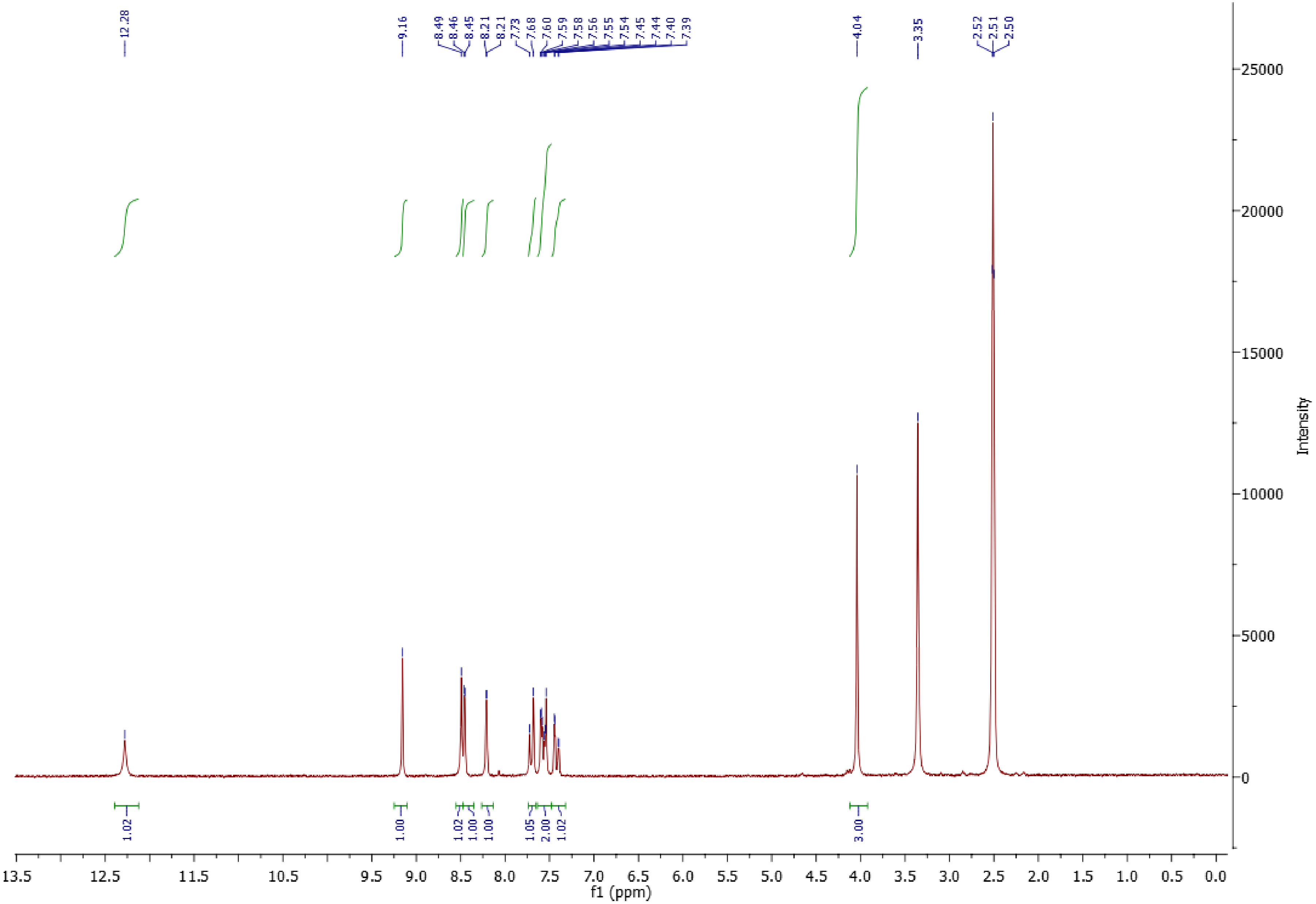

Figure S24. ^{13}C NMR of compound **1l**

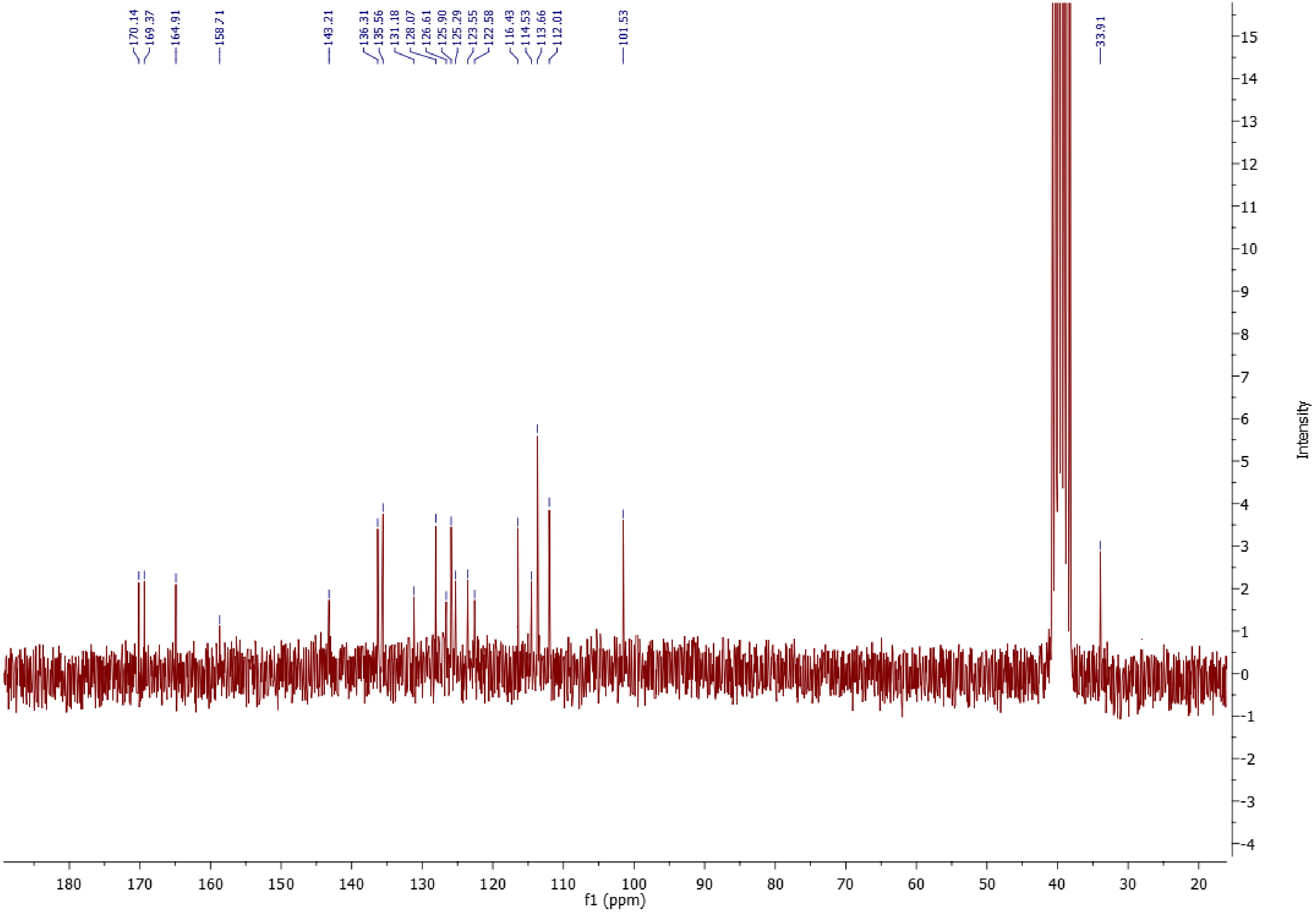

Figure S25. ^{1}H NMR of compound **1m**

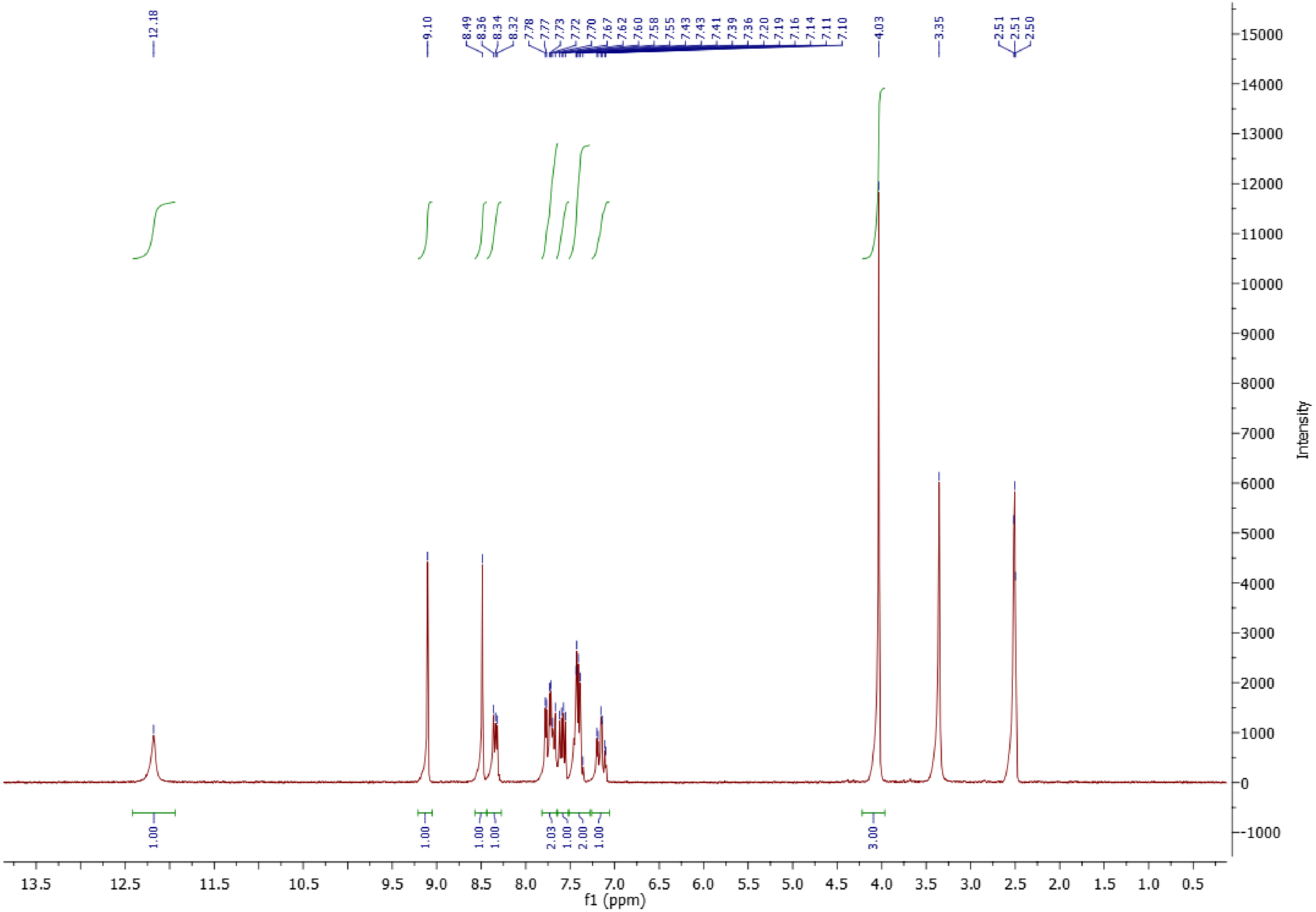

Figure S26. ^{13}C NMR of compound **1m**

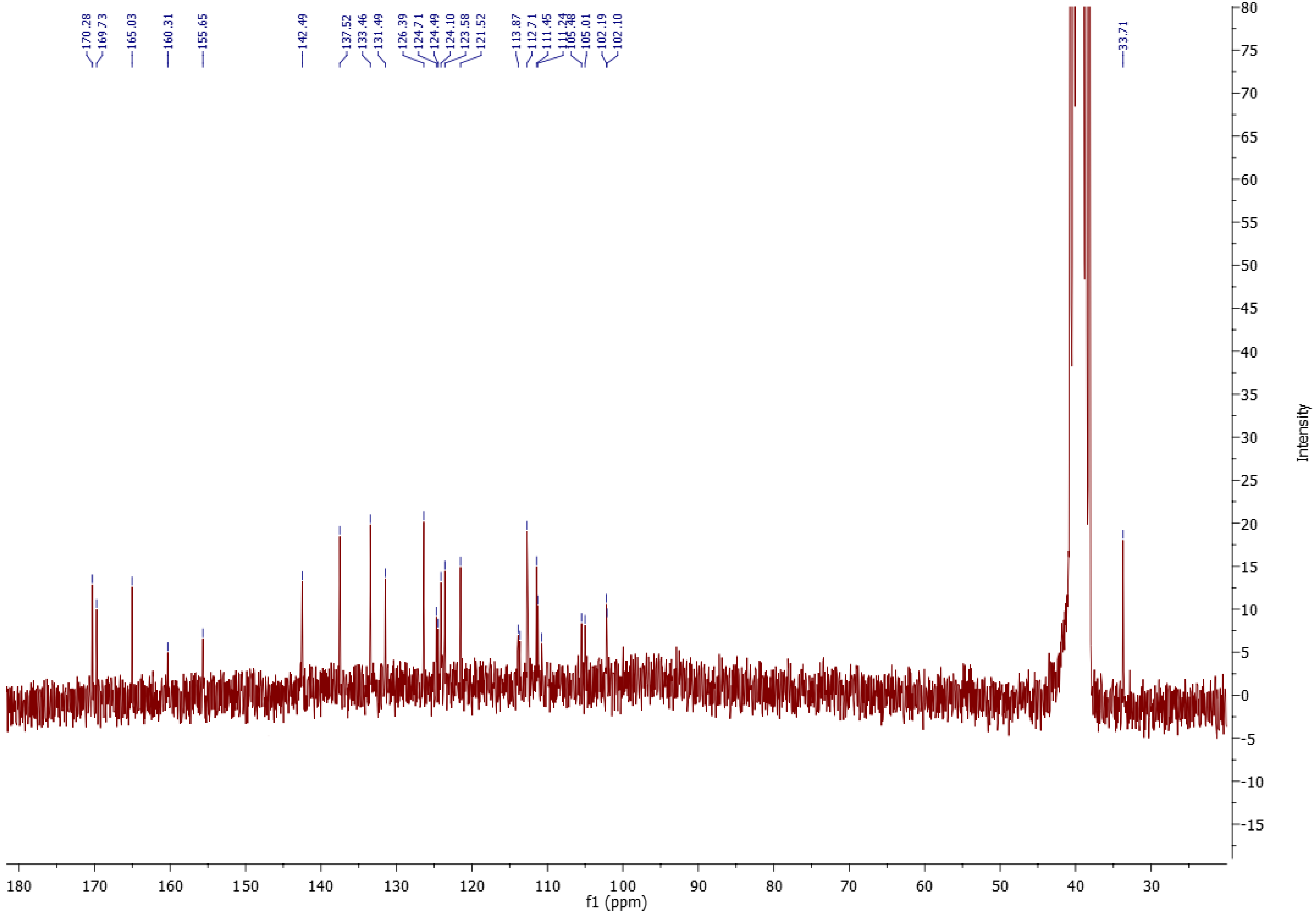

Figure S27. ^{1}H NMR of compound **1m**

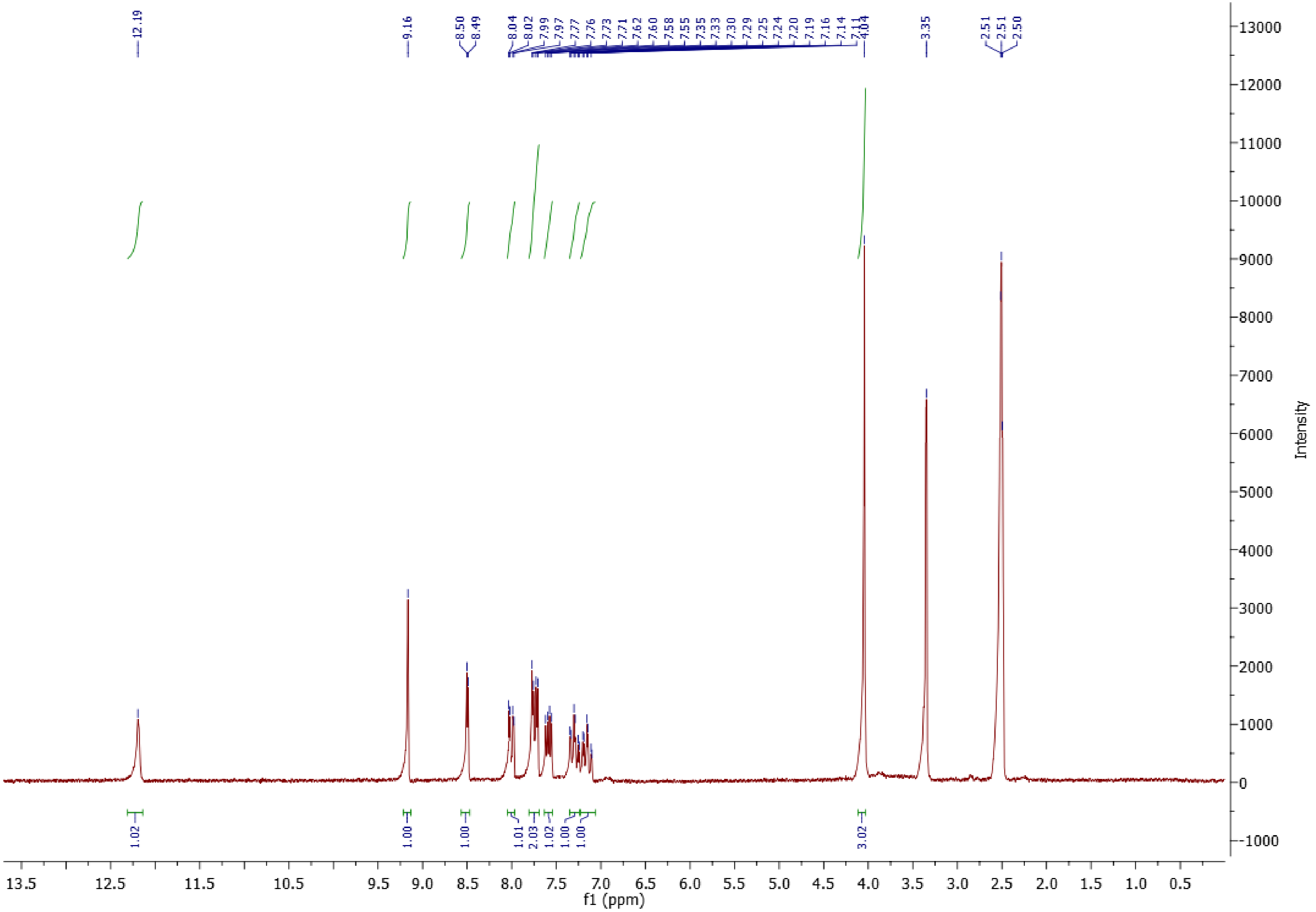

Figure S28. ^{13}C NMR of compound **1n**

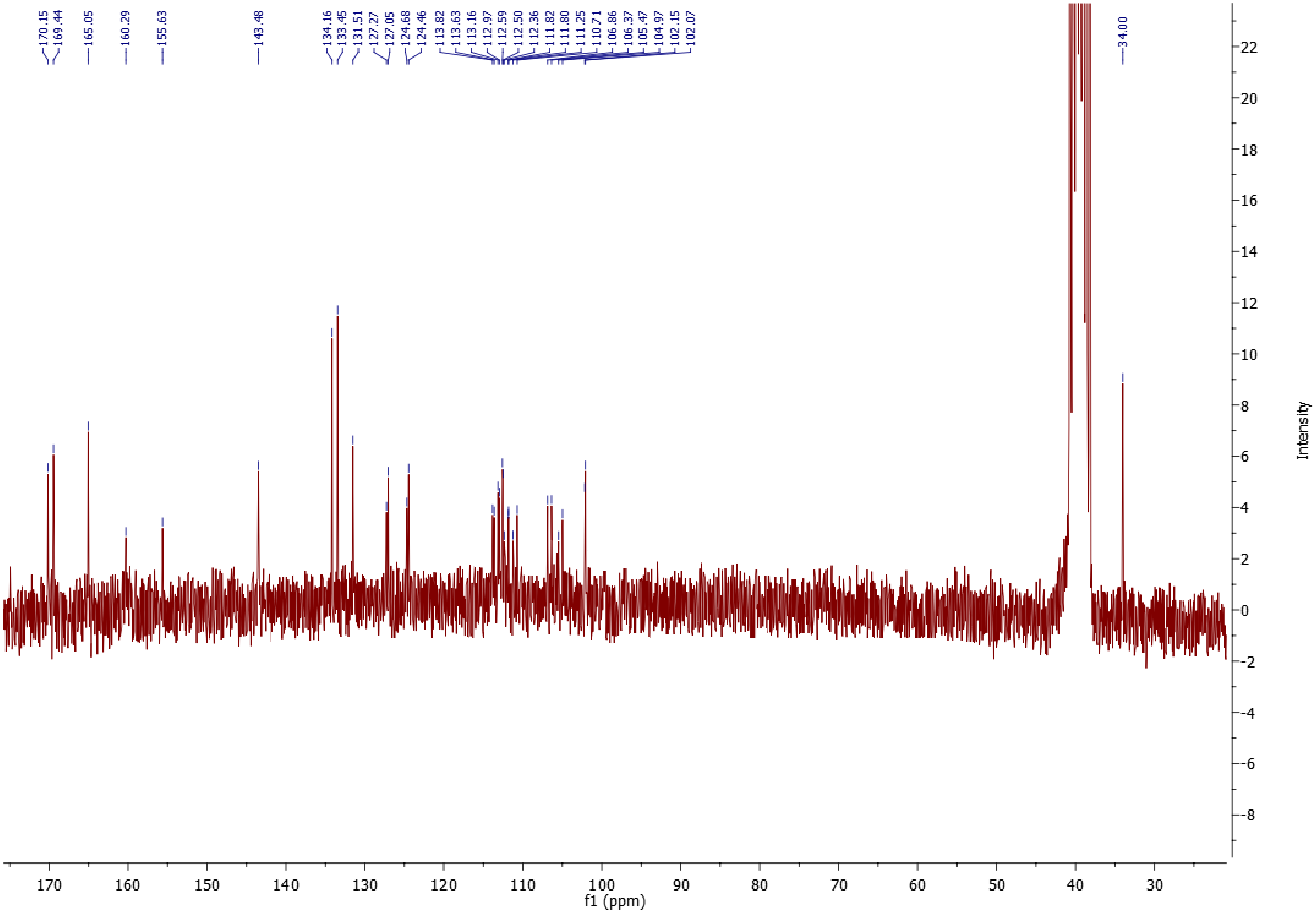

Figure S29. ^{1}H NMR of compound **1o**

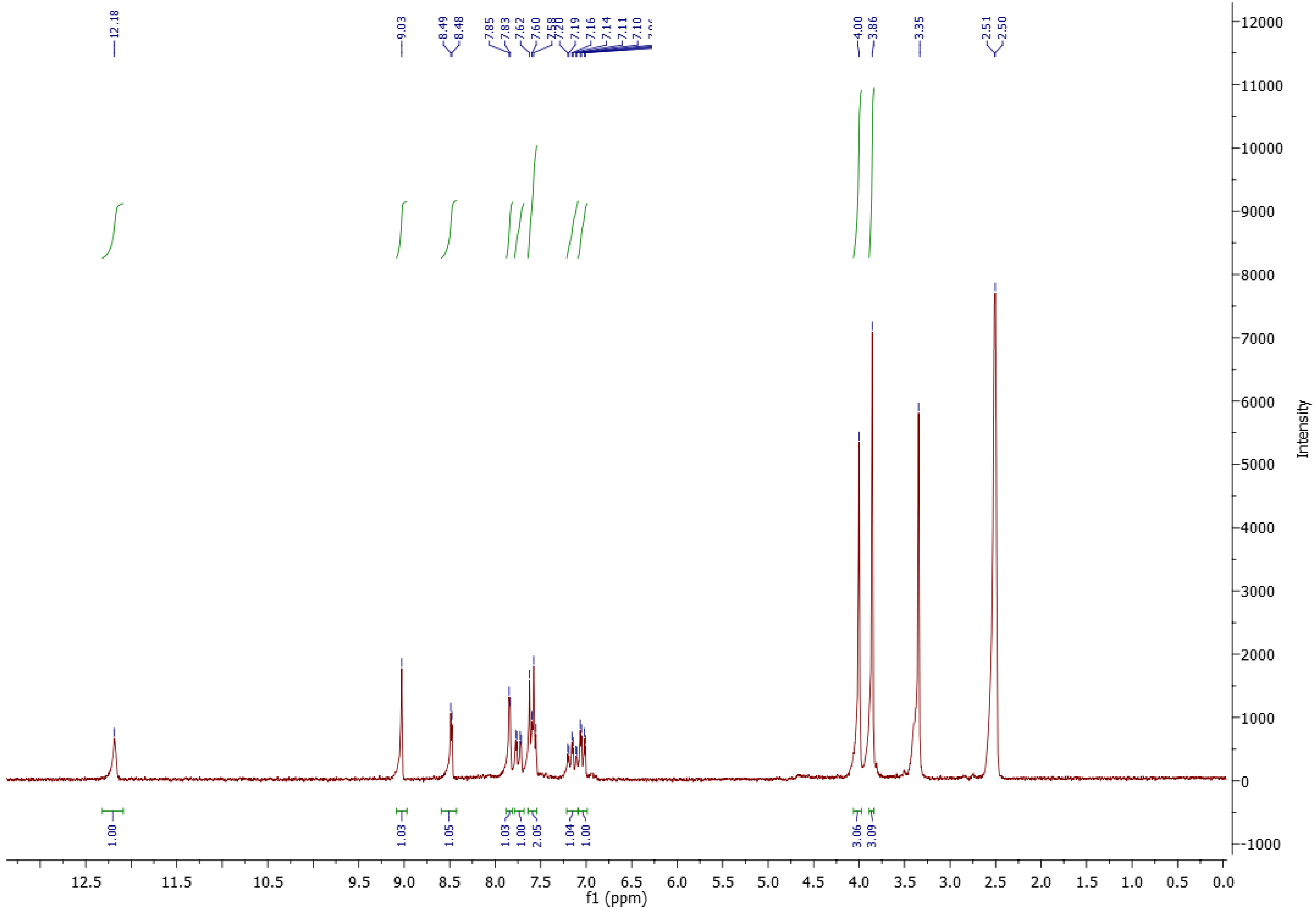

Figure S30. ^{13}C NMR of compound **1o**

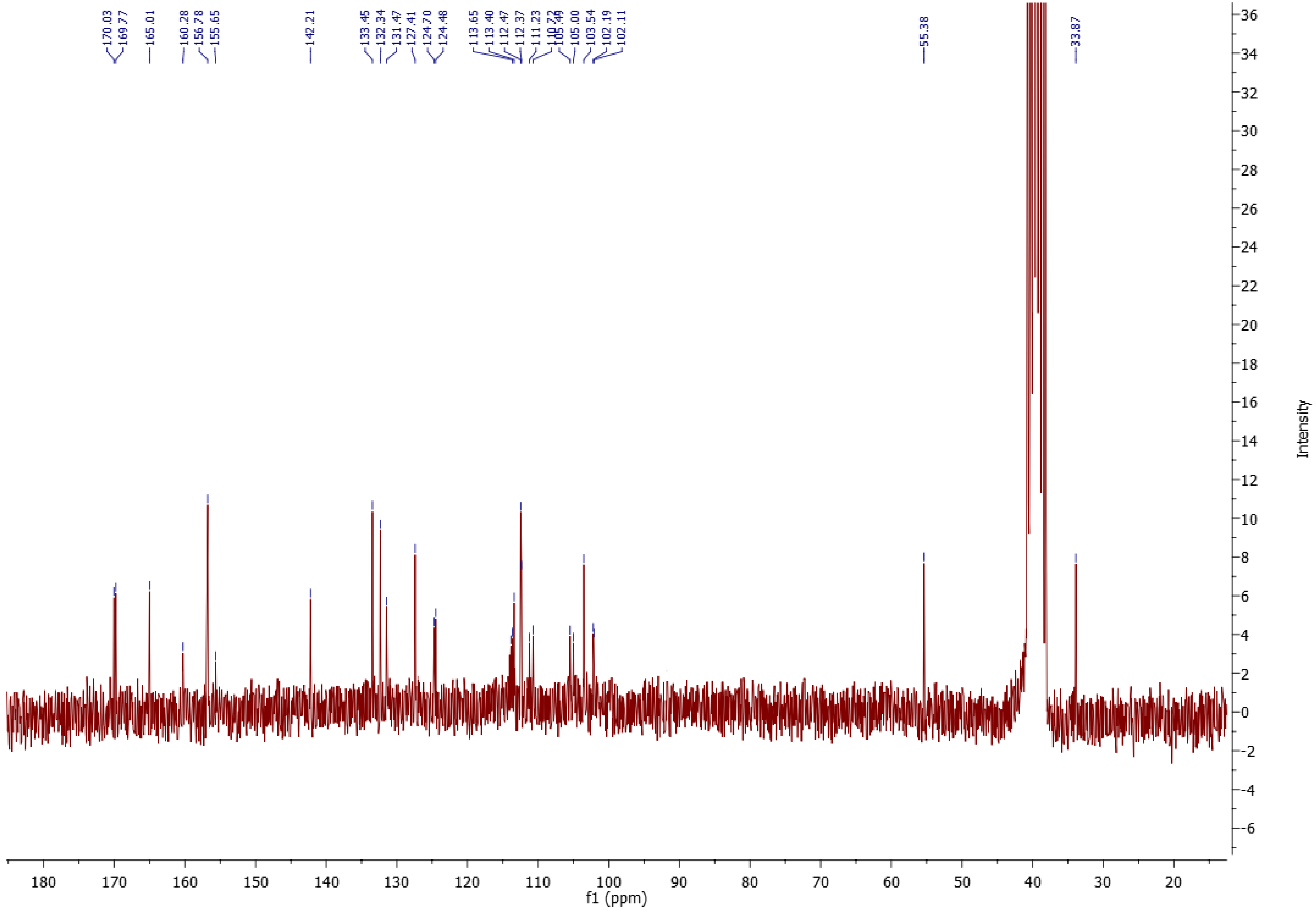

Figure S31. ^{1}H NMR of compound **1p**

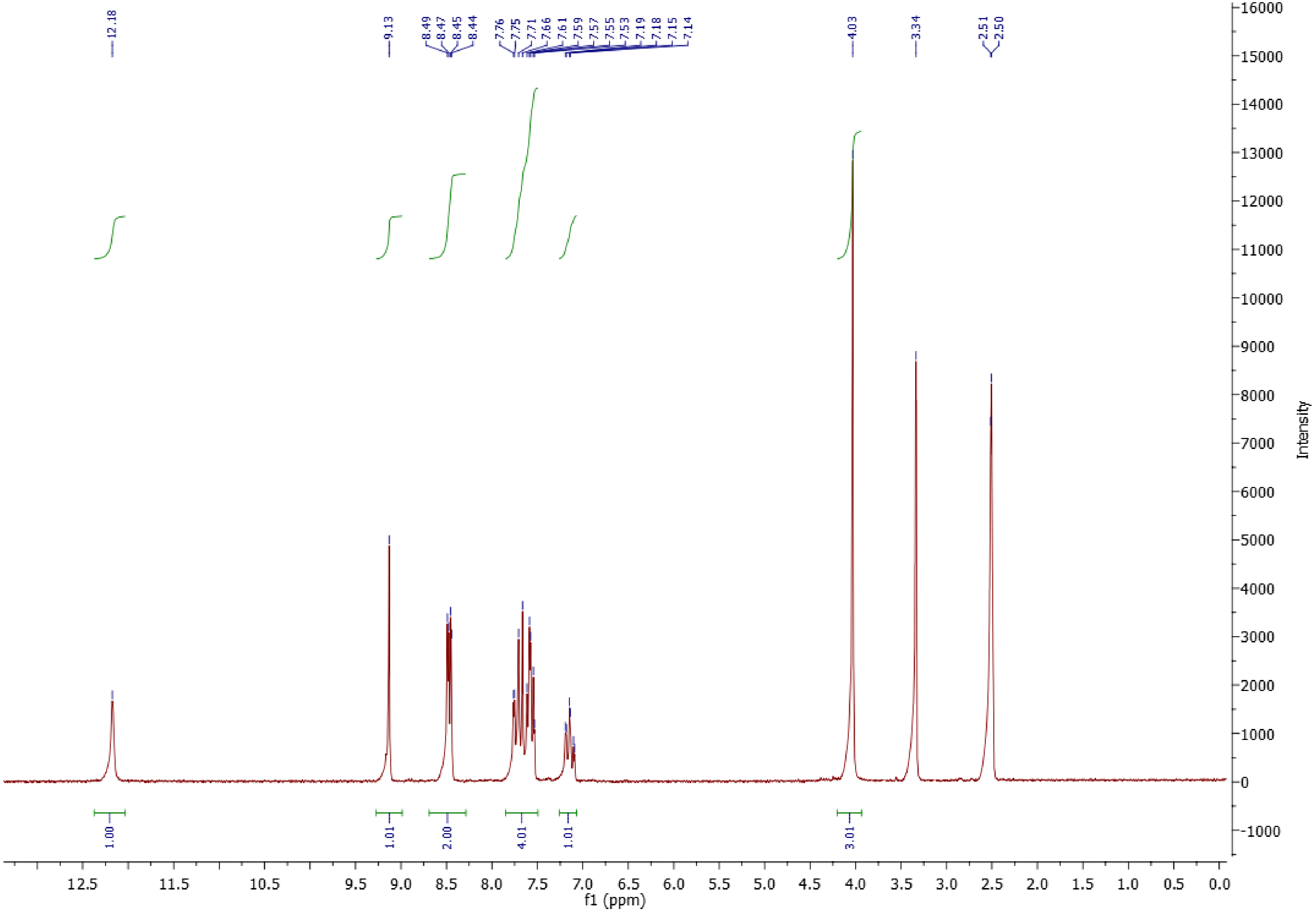

Figure S32. ^{13}C NMR of compound **1o**

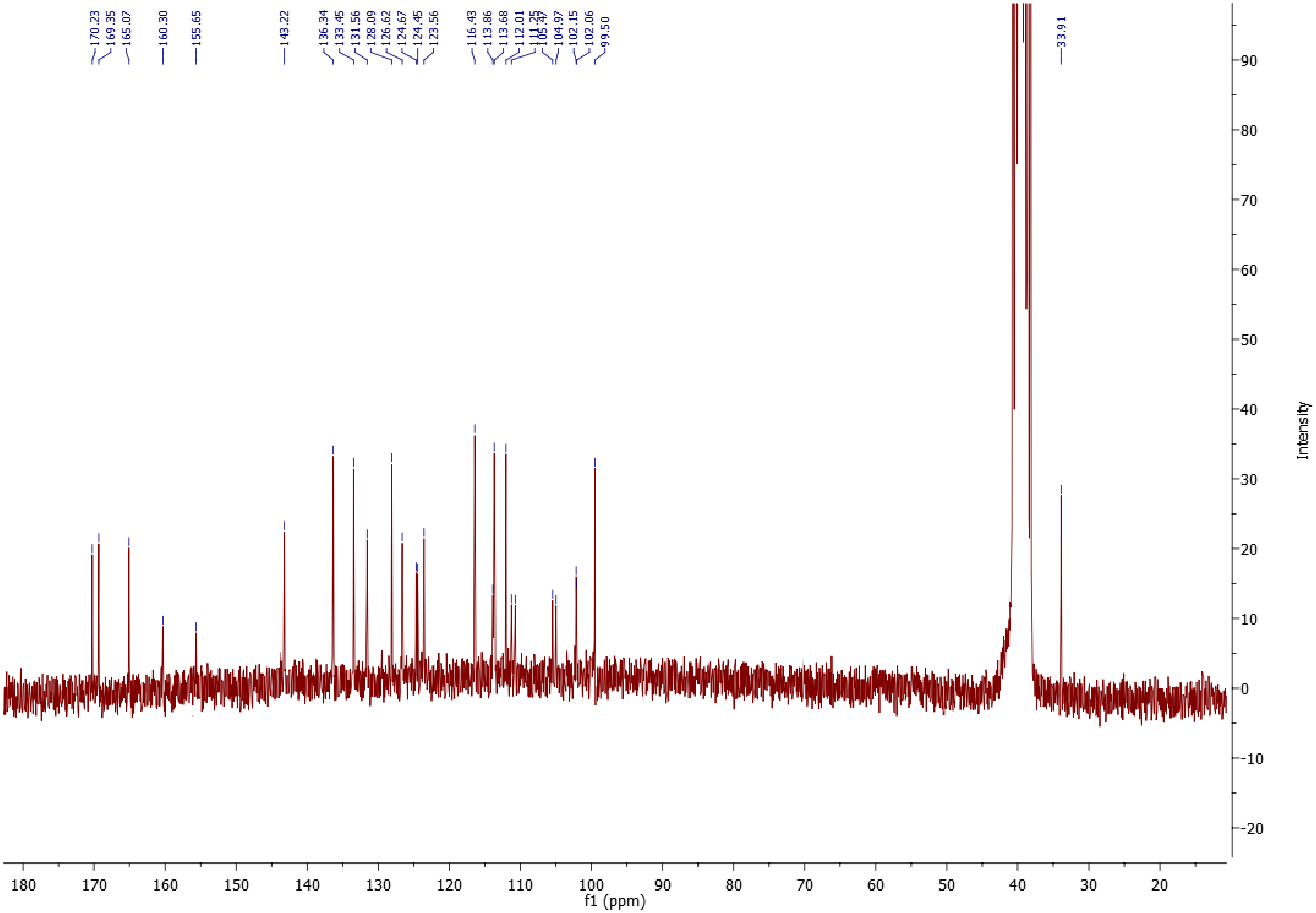

Figure S33. HSMR of compound **1b**

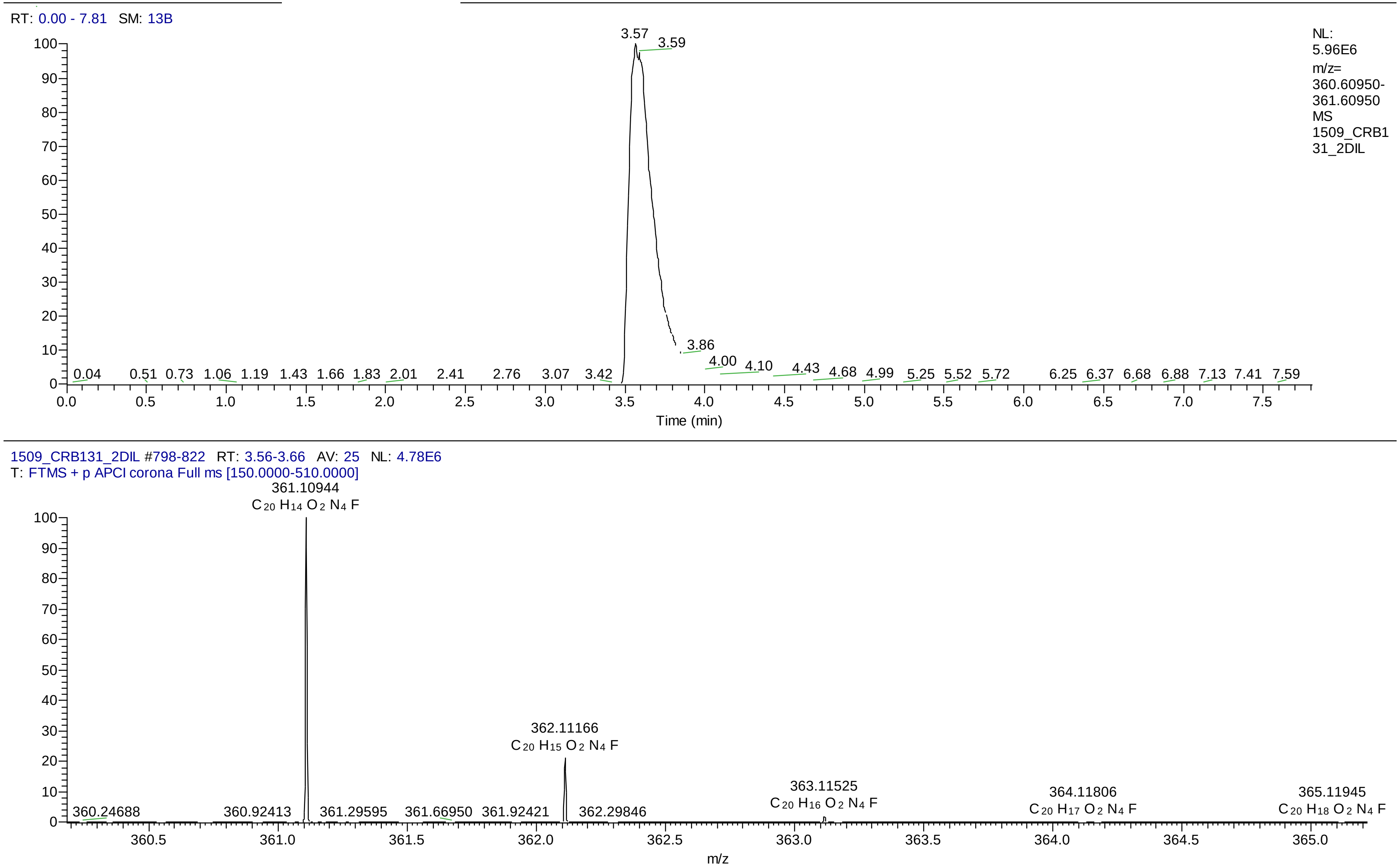

Figure S34. HSMR of compound **1c**

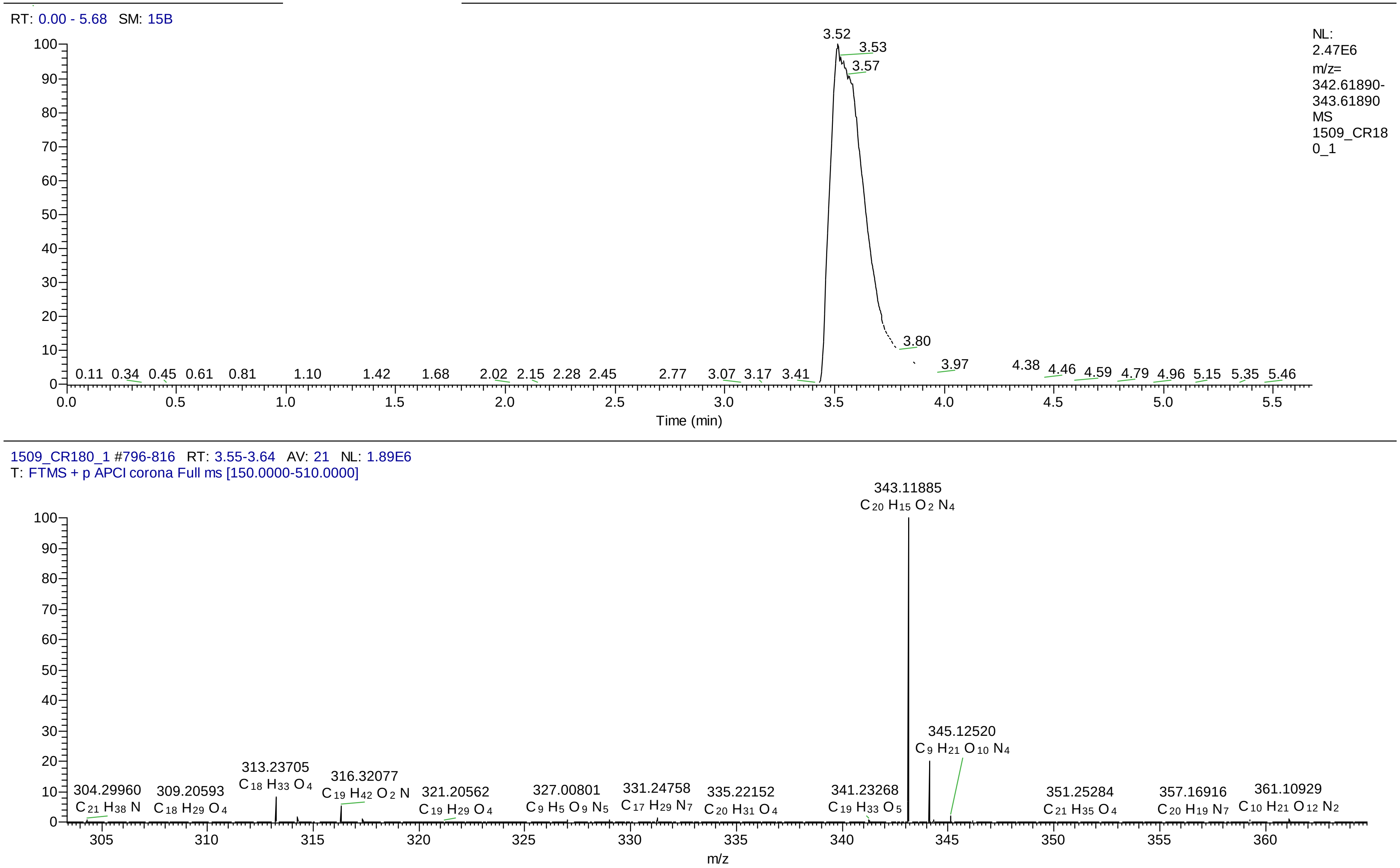

Figure S35. HSMR of compound **1i**

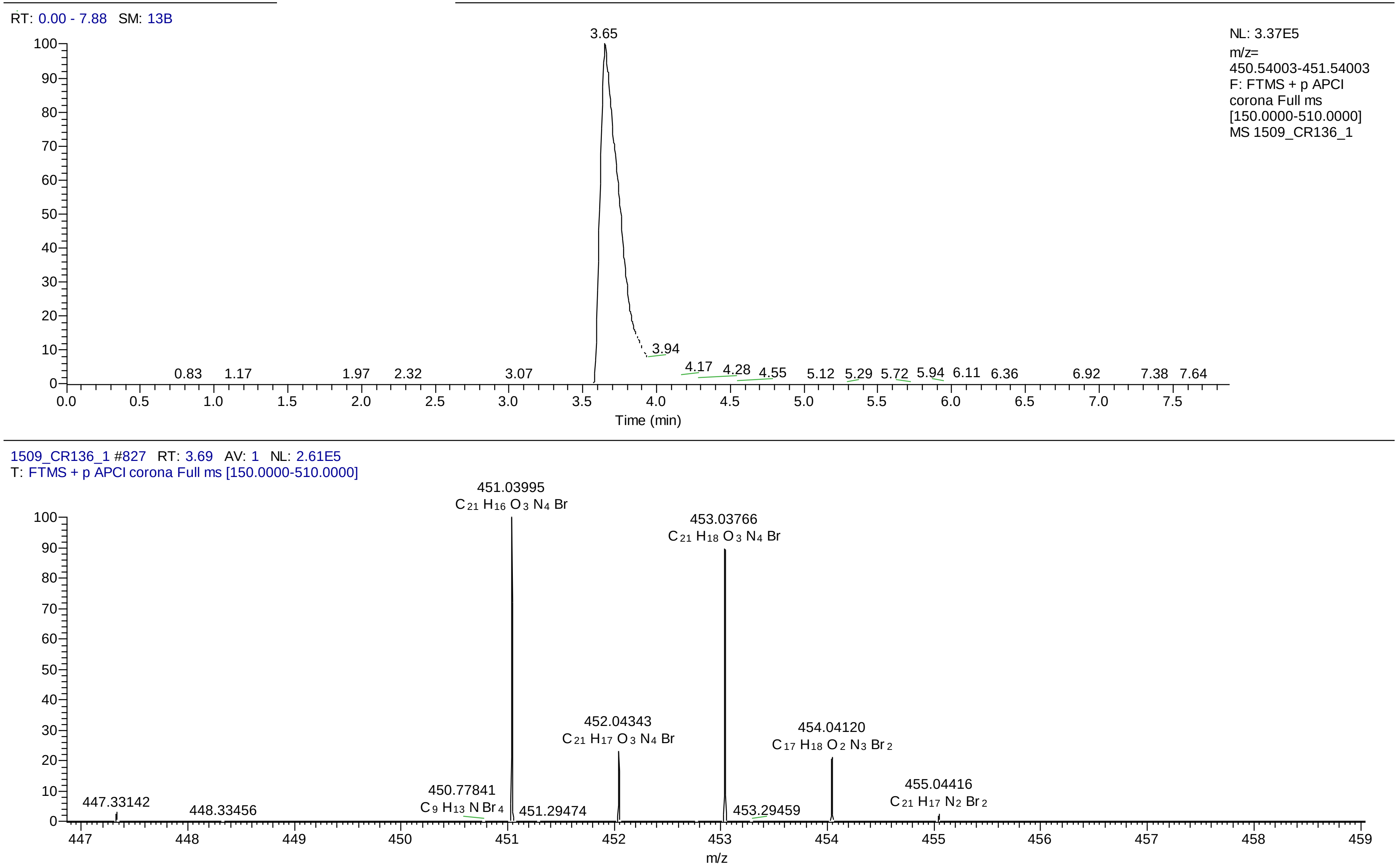

Figure S36. HSMR of compound **1j**

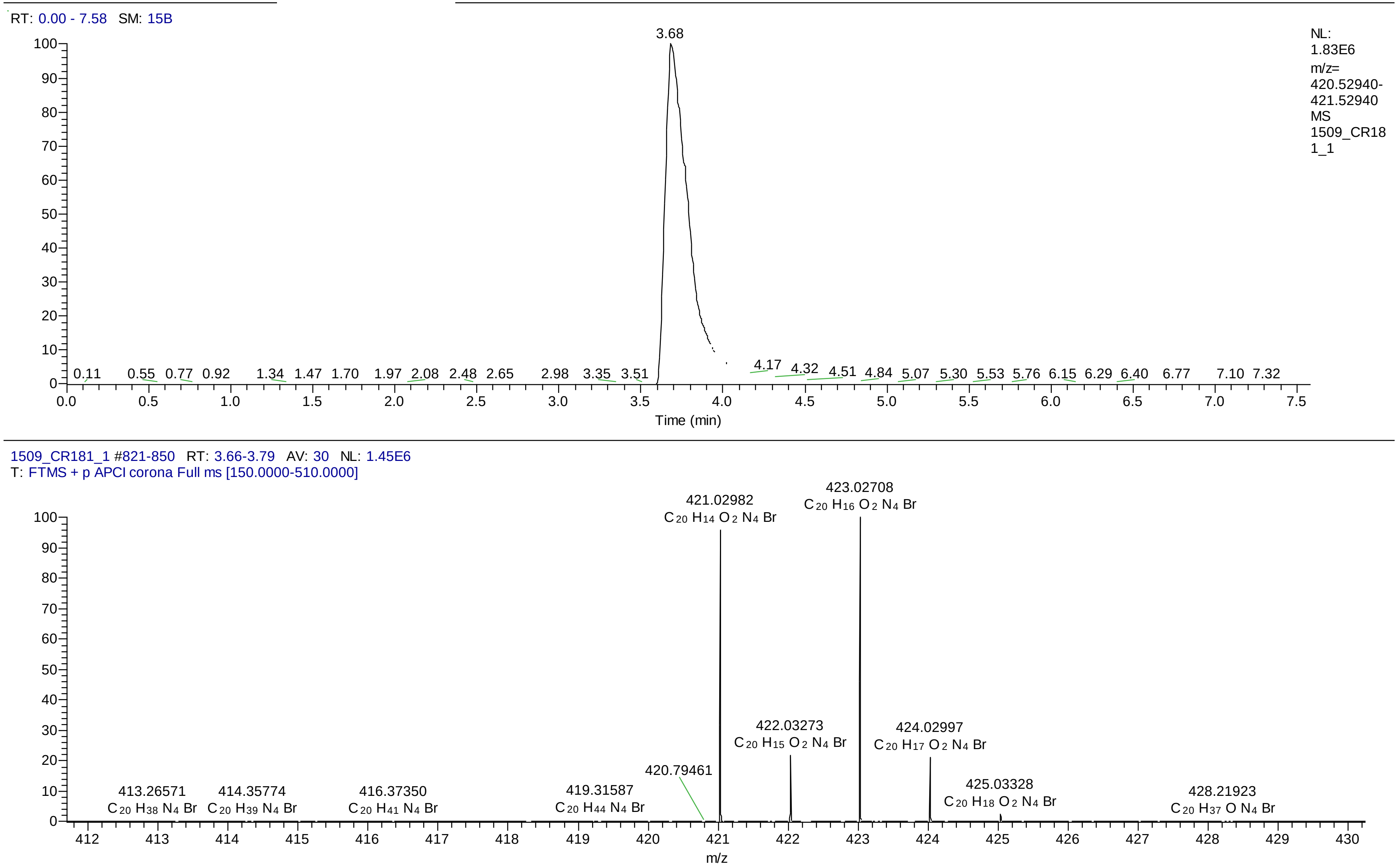

Figure S37. HSMR of compound **1l**

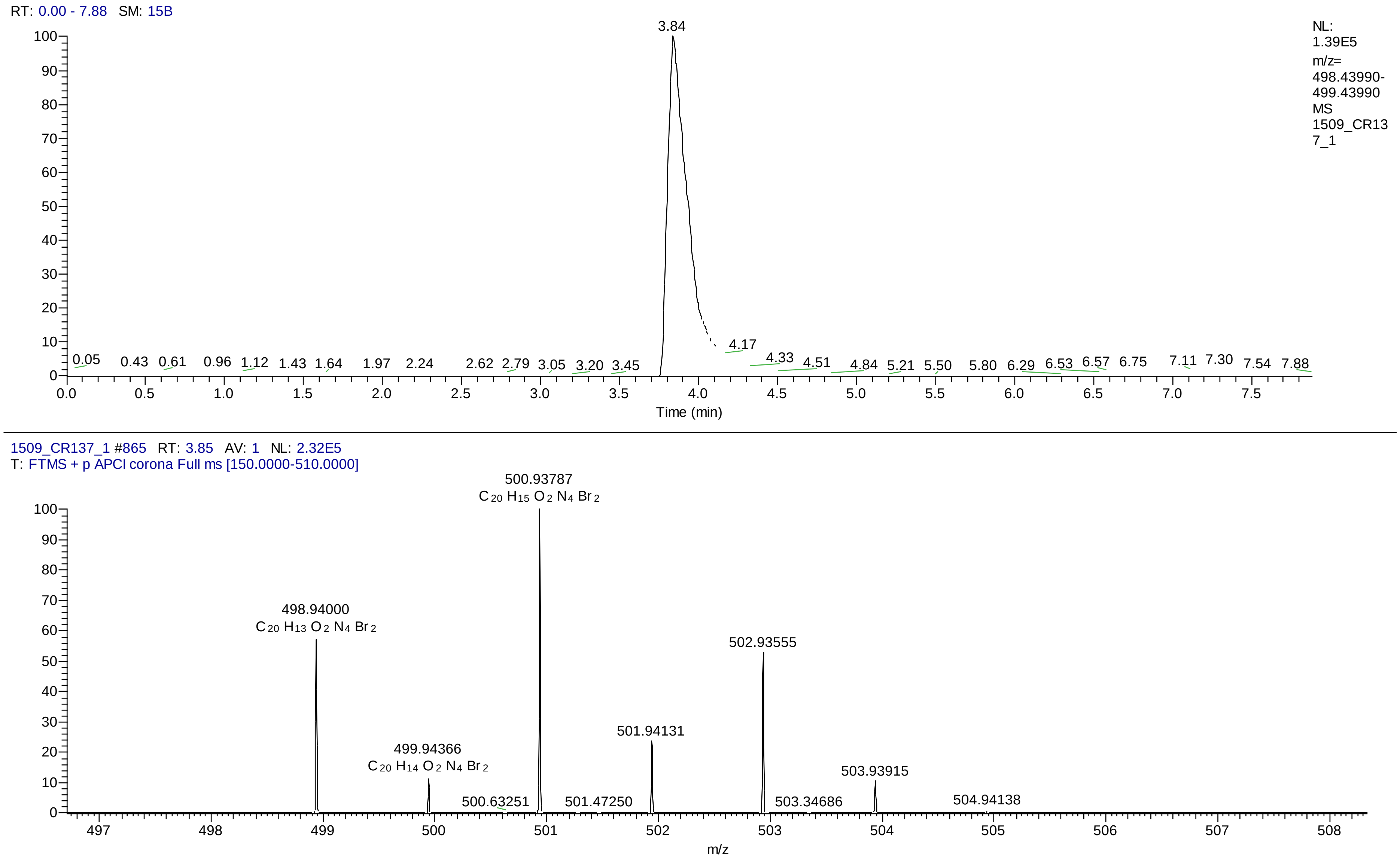

Chapter 6

Synthesis and cytotoxic activity of 3-[2-(1*H*-Indol-3-yl)-1,3-thiazol-4-yl]-1*H*pyrrolo[3,2-c]pyridine hydrobromides, analogues of the marine alkaloid nortopsentin

Pecoraro, C., Carbone, D., Aiello, D.,Carbone, A.

(2022) ARKIVOC, 11640, 30-42

A Platinum Open Access Journal
for Organic Chemistry

Paper

Free to Authors and Readers

DOAJ Seal

Arkivoc **2022**, part ii, 0-0
to be inserted by editorial office

Synthesis and cytotoxic activity of 3-[2-(1*H*-Indol-3-yl)-1,3-thiazol-4-yl]-1*H*-pyrrolo[3,2-*c*]pyridine hydrobromides, analogues of the marine alkaloid nortopsentin

Camilla Pecoraro,[a] Daniela Carbone,[a] Daniele Aiello,[a] and Anna Carbone*[a,b]

[a]Dipartimento di Scienze e Tecnologie Biologiche Chimiche e Farmaceutiche (STEBICEF), Università degli Studi di Palermo, Via Archirafi 32, 90123 Palermo, Italy
[b]Dipartimento di Farmacia, Università degli Studi di Genova, Viale Benedetto XV 3, 16132 Genova, Italy
Email: carbone@difar.unige.it

Dedicated to Professor Girolamo Cirrincione on the occasion of his retirement

Received 09-10-2021 **Accepted Manuscript** 11-01-2021 **Published on line** 11-10-2021

Abstract

A new series of thiazole nortopsentin analogues with a 5-azaindole moiety was conveniently synthesized in good to excellent yields by an Hantzsch reaction between thioamides and α-bromoacetyl compounds. The cytotoxic activity of the new derivatives was tested against different human tumor cell lines of the NCI full panel. All tested compounds were active against all of the investigated cell lines showing GI_{50} values from micro to submicromolar levels. Some of the new analogues exhibited good selectivities against different NCI sub-panels.

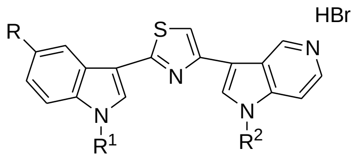

Indolyl-thiazolyl-5-azaindoles

GI_{50} 0.18-26.3 µM

Keywords: Marine bis-indolyl alkaloids, nortopsentin analogues, antitumor activity, 5-azaindole, thiazole

Introduction

The marine environment covers approximately 70% of the earth's surface and represents a rich source of compounds with a wide range of biological activities.[1] For this reason several efforts have been made aiming to exploit the enormous potential of marine natural products, developing their total synthesis in laboratory or synthesizing derived molecules using their scaffolds as leads. Up to 2019, the clinical marine pharmaceutical pipeline consisted of 31 marine-derived compounds in active clinical trials and 9 approved marine-derived compounds.[2] Among the approved drugs, many compounds found application as anticancer drugs such as cytarabine used for the therapy of malignant acute myeloid, lymphocytic and myelogenous leukemia, trabectedin for tissue sarcoma, midostaurine for the acute myeloid leukemia, eribulin mesylate for breast cancer and liposarcoma.[3] Marine alkaloids constitute one of the most attractive class of natural products [4] and in particular bis-indolyl alkaloids, characterized by two indole units connected to a spacer through their 3 position, constitute a group of deep-sea sponge metabolites with very interesting pharmacological activities such as antiproliferative,[5] antiinflammatory,[6] antimicrobial,[7] and antiviral.[8] Nortopsentins A-C (Chart 1), isolated from the Halichondride sponge *Spongosorites ruetzleri* from deep water in the Bahamas, are the only family of bis-indolyl alkaloids bearing an imidazolediylbis[indole] skeleton. They exhibited *in vitro* cytotoxicity against P388 leukemia cells (IC_{50}, 4.5− 20.7 μM) and inhibited the growth of *Bacillus subtilis* and *Candida albicans.* Their methylated derivatives (Figure 1) showed a significant improvement in cytotoxicity against P388 cells compared to that of the parent compounds (IC_{50}, 0.8−2.1 μM).[9] Furthermore, nortopsentin C inhibited neural nitric oxide synthase (bNOS) and calcineurin activities, suggesting its probable action against calmodulin, a common co-factor of these two enzymes.[6] More recently, the antiviral activity against tobacco mosaic virus (TMV) and anti-phytopathogenic-fungus property of nortopsentins A-C and their analogues were also reported.[10]

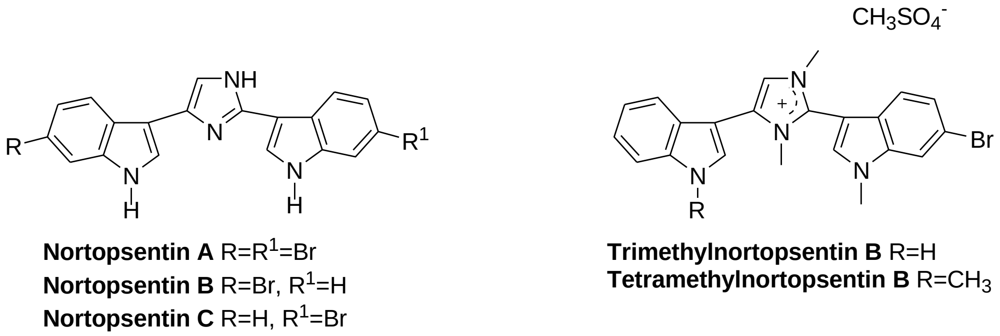
NH
N
R
R1
N
H
N
H
CH3SO4-
N
+
N
Br
N
R
N
Nortopsentin A R=R1=Br
Nortopsentin B R=Br, R1=H
Nortopsentin C R=H, R1=Br
Trimethylnortopsentin B R=H
Tetramethylnortopsentin B R=CH3

Figure 1. Structures of nortopsentins A-C and their methylated derivatives.

With the aim to search new bioactive nortopsentin analogues, the central imidazole ring of the marine alkaloid was replaced by different five-membered heterocycles and/or the indole moiety by other rings.[11-17]
In this effort, our research group synthesized a large library of analogues in which the imidazole moiety of nortopsentins A-C was replaced by a thiazole core and one indole portion by an azaindole ring, leading to compounds that showed antiproliferative activity against a wide range of human tumor cell lines with GI_{50} values in the micro-submicromolar range. Among of them, the indolyl-7-azaindolyl thiazoles (Figure 2)
the most active derivatives, exhibiting antiproliferative activity in the micro-submicromolar range, CDK1 inhibition (IC_{50} 0.64-0.89 μM) and significant tumor volume inhibition in mouse xenograft models.[18]

A recent study demonstrated that the treatment of colorectal cancer stem cells (CR-CSCs) with indolyl-7-azaindolyl thiazoles induces reduction of CSCs viability, making them sensitive to conventional chemotherapy drugs, such as oxaliplatin and 5FU. Moreover, the combination therapy of these derivatives with CHK1 inhibitor Rabusertinib showed a synergistic effect, abrogating CR-CSCs proliferative and clonogenic potential.[19]

In addition to the frequently used 7-azaindoles, the 5-azaindole ring is a promising pharmacophore moiety found in different antitumor molecules, despite its uncommon presence in marine natural products.[20,21] Thus, continuing our studies on bioactive nitrogen heterocyclic systems[22,23] and to complete the structure-activity relationship (SAR) analysis of the nortopsentin azaindole analogues, herein we report a new series of indolyl-5-azaindolyl thiazoles of type **1** (Figure 2). We also describe the NCI's *in vitro* disease-oriented antitumor screen of the new synthesized analogues.

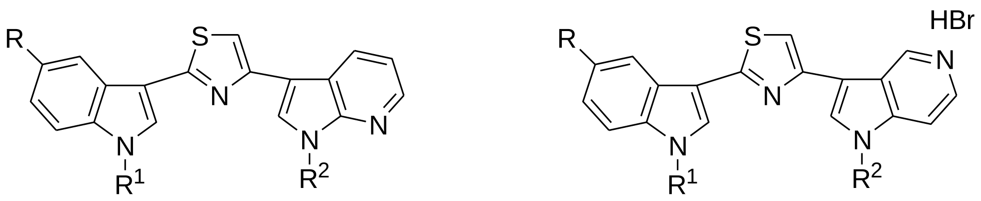

indolyl-7-azaindolyl thiazoles

1

Figure 2. Azaindole derivatives of thiazole nortopsentin analogues.

Results and Discussion

The synthesis of new indolyl- 5-azaindolyl thiazoles **1a-v** (Scheme 1) was conveniently carried out through a Hantzsch reaction between thioamides of type **5-7** and α-bromoacetyl compounds **9a,b**. In detail, indole-3-carbothioamides **5d,6a-d,7a-c** (Scheme 1) were obtained from the corresponding carboxamides **2d, 3a-d** and **4a-c** using Lawesson's reagent under reflux in toluene or benzene as previously reported.[18] The 2-bromo-ethanones **9a,b** were efficiently synthesized (90-93%) by acylation of suitable 5-azaindoles **8a,b** with bromoacetyl bromide in the presence of aluminium chloride in anhydrous dichloromethane. The commercially available 5-azaindole **8a** was converted into the corresponding *N*-methyl derivative **8b** by reaction with potassium *tert*-butoxide, tris[2-(2-methoxyethoxy)ethyl]amine (TDA-1) as a catalyst and iodomethane in anhydrous toluene (Scheme 1).

The reaction between thioamides **5d,6a-d** and α-bromoacetyl compounds **9a,b** in ethanol under reflux gave the desired 3-[2-(1*H*-indol-3-yl)-1,3-thiazol-4-yl]-1*H*-5-azaindoles **1c,d,g,h,k-p** as hydrobromide salts (58-84%) (Table 1). The reaction of thioamides **7a-c** with ethanones **9a,b** gave very unstable thiazoles **1a,b,e,f,i,j** that were used in the next step without purification. In particular, the subsequent deprotection of *N*-*tert*-butylcarboxylate derivatives **1a,b,e,f,i,j** using trifluoroacetic acid in dichloromethane under reflux afforded the corresponding thiazoles **1q-v** in good to excellent yields (62-93%) (Table 1).

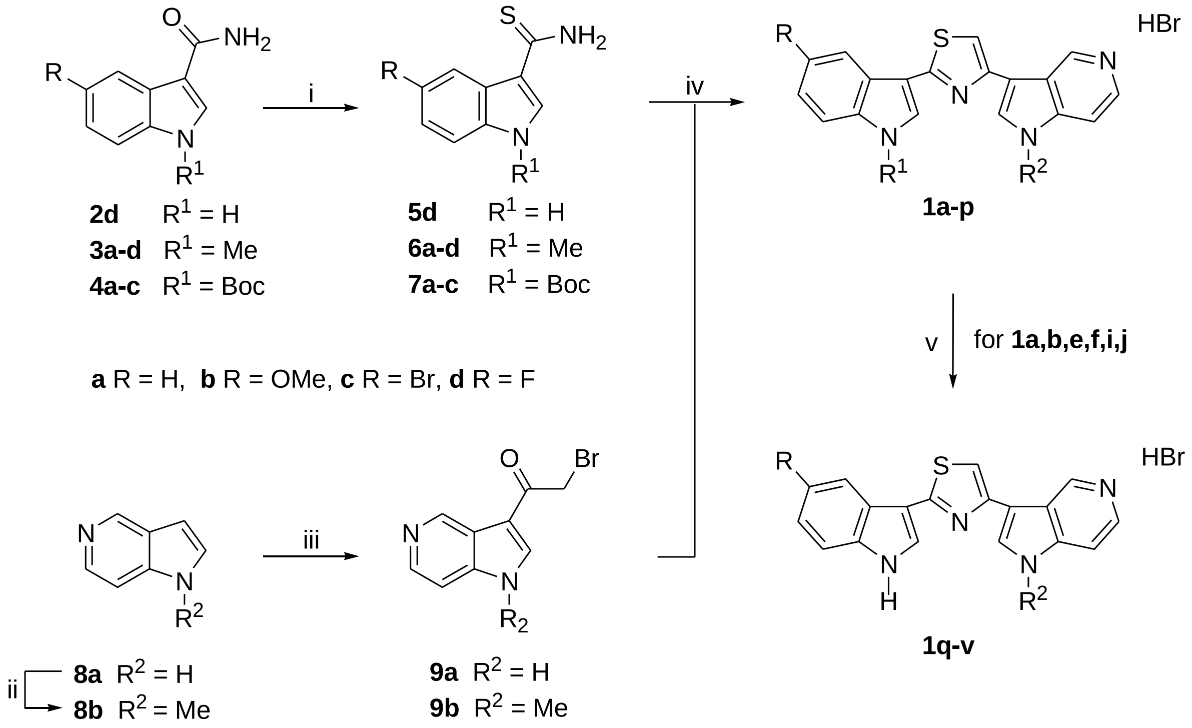
R
NH2
O
N
R1
i
S
iv
HBr
2d R1 = H
3a-d R1 = Me
4a-c R1 = Boc
5d R1 = H
6a-d R1 = Me
7a-c R1 = Boc
1a-p
v
for 1a,b,e,f,i,j
a R = H, b R = OMe, c R = Br, d R = F
Br
iii
R2
R2
H
1q-v
ii
8a R2 = H
8b R2 = Me
9a R2 = H
9b R2 = Me

Scheme 1. Synthesis of indolyl-5-azaindolyl thiazole hydrobromides **1a-v.** Reagents and conditions: (i) Lawesson's reagent, toluene or benzene, reflux, 0.5-24 h, 90-98%; (ii) *t*-BuOK, toluene, TDA-1, rt, 4 h; then MeI, rt, 16 h, 60%; (iii) $AlCl_3$, DCM, $BrCOCH_2Br$, reflux, 40 min (for derivative **9a**) or 15 min (for derivative **9b**), 90-93%; (iv) EtOH, reflux, 1 h, 58-84%; (v) TFA, DCM, reflux, 24 h, 62-93%.

Table 1. Substituted 3-[2-(1*H*-indol-3-yl)-1,3-thiazol-4-yl]-1*H*-5-azaindole hydrobromides **1a-v**

	R	R^1	R^2	Yield%	Compd.	R	R^1	R^2	Yield%
1a	H	Boc	H	ND[a]	**1l**	Br	Me	Me	66[b]
1b	H	Boc	Me	ND[a]	**1m**	F	Me	H	56[b]
1c	H	Me	H	84[b]	**1n**	F	Me	Me	70[b]
1d	H	Me	Me	52[b]	**1o**	F	H	H	58[b]
1e	OMe	Boc	H	ND[a]	**1p**	F	H	Me	67[b]
1f	OMe	Boc	Me	ND[a]	**1q**	H	H	H	55[c]
1g	OMe	Me	H	70[b]	**1r**	H	H	Me	69[c]
1h	OMe	Me	Me	53[b]	**1s**	OMe	H	H	88[c]
1i	Br	Boc	H	ND[a]	**1t**	OMe	H	Me	72[c]
1j	Br	Boc	Me	ND[a]	**1u**	Br	H	H	62[c]
1k	Br	Me	H	80[b]	**1v**	Br	H	Me	93[c]

[a] ND: not determined. The crude was used in the step v without further purification.

[b] Calculated over the step iv.

[c] Calculated over the two steps iv and v.

The isolated thiazoles **1c,d,g,h,k-v** were submitted to the National Cancer Institute (NCI; Bethesda, MD), and were prescreened according to the NCI protocol at a 10^{-5} M dose (data not shown) on the full panel of approximately 55 human cancer cell lines derived from 9 human cancer cell types that have been grouped into disease subpanels including leukemia, non-small cell lung, colon, central nervous system, melanoma, ovarian, renal, prostate, and breast tumor cell lines. All tested thiazoles satisfied the criteria set by the NCI for activity in this assay and were selected for further screenings at five concentrations at 10-fold dilution (10^{-4}–10^{-8} M) on the full panel. The growth inhibition activity of compounds was defined in terms of the GI$_{50}$ value (which represents the molar concentration of the compound that inhibits 50% net cell growth).

The thiazoles **1c,d,g,h,k-v** were active against the total number of cell lines investigated, showing antitumor activity in the micromolar - submicromolar range (GI$_{50}$ 0.18-26.3 µM) (Table2).

All derivatives were efficacious against the leukemia sub-panel (Table 2), with particularly selectivity towards K-562 cell line, eliciting GI$_{50}$s in the range 0.24-2.09 µM. In addition, compounds **1l** and **1v** also exhibited good selectivity against CCRF-CEM cells of the same sub-panel, with GI$_{50}$ values of 0.36 µM and 0.42 µM, respectively (Table 2).

Moreover, all compounds also proved to be active towards MDA-MB-468 and MCF7 cell lines of breast cancer sub-panel, for which thiazoles **1c** and **1d** were the most potent compounds, with GI$_{50}$ values lower than or equal to 0.4 µM (Table 2). Regarding MDA-MB-468 cell line, also thiazoles **1g** and **1q** exhibited good GI$_{50}$ values (0.44 µM and 0.23 µM, respectively).

Likewise, towards HCT-116 cell line of the colon cancer sub-panel, the GI$_{50}$s were registered in the low micromolar range, with values of 0.93 µM and 0.18 µM for the most active compounds **1d** and **1l,** respectively.

Table 2. *In vitro* inhibition of cancer cell lines growth by thiazoles **1c,d,g,h,k-v**

Cell lines	**GI$_{50}$[a]**															
	1c	**1d**	**1g**	**1h**	**1k**	**1l**	**1m**	**1n**	**1o**	**1p**	**1q**	**1r**	**1s**	**1t**	**1u**	**1v**
Leukemia																
CCRF-CEM	2.02	1.78	1.83	2.15	1.30	0.36	1.74	1.96	1.89	1.75	1.44	2.40	2.45	2.33	2.24	0.42
HL-60(TB)	2.03	1.94	1.68	1.96	1.71	1.48	1.76	1.93	2.07	2.19	2.02	2.17	1.51	1.90	2.09	2.11
K-562	1.76	2.09	0.72	1.90	0.24	0.24	0.46	1.70	0.37	1.48	2.05	1.85	1.72	1.78	0.98	0.35
RPMI-8226	2.00	1.76	1.83	1.84	1.58	1.57	1.77	1.98	1.77	1.86	1.25	2.14	2.08	2.02	2.48	2.13
Non-Small Cell Lung Cancer																
A549/ATCC	1.83	2.38	1.87	1.93	1.78	1.83	1.85	1.67	1.87	1.83	2.45	2.47	2.35	1.79	1.90	2.81
EKVX	1.64	1.56	1.76	1.77	1.54	1.86	1.72	1.87	1.66	1.62	1.78	1.92	1.99	1.92	1.73	2.50
HOP-62	1.48	1.67	1.81	1.90	1.61	1.90	1.73	1.92	1.53	1.54	1.71	1.79	2.08	1.92	1.65	3.17
HOP-92	1.51	1.35	1.64	1.96	1.77	1.52	1.65	1.64	1.38	1.49	1.44	1.52	1.79	1.90	1.72	2.98
NCI-H226	1.75	1.82	1.88	1.83	1.69	2.02	1.92	2.05	1.76	1.88	3.24	17.1	2.36	18.3	1.87	2.34
NCI-H23	1.65	1.64	1.81	1.81	1.65	1.93	1.72	1.94	1.58	1.62	1.85	1.77	1.76	2.12	1.64	2.73
NCI-H322M	1.67	1.63	1.69	1.78	1.82	1.77	1.65	1.81	1.52	1.79	2.05	2.53	1.85	1.87	1.75	3.64
NCI-H460	1.90	1.79	1.73	1.94	1.73	1.87	1.77	1.97	1.78	1.99	1.76	1.85	1.84	1.97	1.95	1.92
NCI-H522	1.73	2.00	1.65	1.77	1.84	1.76	1.67	1.77	1.68	1.79	1.92	2.02	1.81	1.74	1.79	2.05

Table 2. Continued

Cell lines	GI$_{50}$[a]															
	1c	**1d**		**1h**	**1k**	**1l**	**1m**	**1n**	**1o**	**1p**	**1q**	**1r**	**1s**	**1t**	**1u**	**1v**
Colon Cancer																
HCC-2998	1.22	1.26	1.85	1.89	1.76	1.90	1.64	1.86	1.92	1.95	1.87	2.01	1.87	1.88	1.98	2.10
HCT-116	1.61	0.93	1.69	1.90	1.21	0.18	1.63	1.66	1.61	1.22	1.71	1.73	1.77	1.77	1.66	1.56
HCT-15	1.37	1.51	1.25	1.54	1.35	1.75	1.33	1.68	1.33	1.67	1.56	1.79	1.95	1.88	1.65	1.38
HT29	1.82	1.98	1.20	1.43	1.59	1.60	1.44	1.47	1.35	1.69	2.07	2.01	2.23	1.53	1.71	1.57
KM12	1.11	1.00	1.73	1.84	1.71	1.97	1.63	1.79	1.67	1.83	2.02	1.65	1.76	1.87	1.91	2.33
SW-620	2.03	1.85	1.75	1.96	1.52	1.85	1.65	1.88	1.88	2.12	1.73	1.98	1.93	1.95	2.04	1.81
CNS Cancer																
SF-268	1.79	1.92	1.77	2.07	1.82	1.90	1.74	1.93	1.77	1.94	2.51	1.97	2.61	1.91	1.78	2.83
SF-295	1.77	1.63	1.69	1.66	1.69	1.81	1.64	1.71	1.68	1.74	1.58	1.81	1.70	12.3	1.71	1.77
SF-539	1.78	1.75	1.65	1.77	1.75	1.80	1.68	1.85	1.52	1.63	1.79	1.79	1.64	1.90	1.72	2.14
SNB-19	1.80	1.76	1.85	2.26	1.80	1.73	1.83	1.82	1.77	1.95	2.18	2.07	1.97	1.79	1.77	3.67
SNB-75	1.29	4.08	1.52	14.7	1.23	1.28	1.26	1.40	1.22	1.50	10.3	12.9	6.96	15.3	1.22	1.47
U251	1.90	1.86	1.87	1.85	1.69	1.78	1.80	1.80	1.69	1.87	1.93	1.95	1.91	1.91	1.77	1.99
Melanoma																
MALME-3M	1.68	2.01	1.74	2.02	1.80	1.95	1.57	1.97	1.82	1.93	1.65	1.94	2.00	2.11	2.14	2.23
M14	1.74	1.51	1.78	1.70	1.81	1.45	1.79	1.72	1.64	1.74	1.70	1.84	1.83	1.75	1.83	1.87
MDA-MB-435	1.79	1.77	1.59	1.59	1.70	1.76	1.64	1.67	1.81	1.85	1.75	1.87	1.68	1.71	1.66	1.78
SK-MEL-2	1.80	2.00	1.84	1.76	2.00	1.93	1.92	1.79	1.91	1.87	2.09	2.10	2.05	15.8	1.92	2.58
SK-MEL-28	1.71	1.77	1.63	1.71	1.78	1.85	1.63	1.79	1.90	1.86	1.84	1.80	1.94	1.79	1.73	1.70
SK-MEL-5	1.74	1.69	1.65	1.52	1.60	1.70	1.65	1.66	1.63	1.65	1.60	1.76	1.65	1.64	1.61	1.88
UACC-257	1.96	1.94	1.68	1.90	2.00	1.95	1.96	1.80	1.91	1.96	1.80	2.00	1.93	16.7	1.92	2.12
UACC-62	1.69	1.72	1.82	2.09	1.79	1.72	1.71	1.74	1.72	1.83	1.67	1.82	1.78	18.5	1.79	1.81
Ovarian Cancer																
IGROV1	1.37	1.61	1.91	1.92	1.63	1.76	1.86	1.96	1.41	1.59	1.33	1.73	1.93	1.93	1.69	2.27
OVCAR-3	1.69	2.16	1.88	1.99	1.90	1.89	1.94	1.95	1.80	1.83	1.98	1.96	2.18	1.85	1.91	2.08
OVCAR-4	1.24	1.46	1.89	2.10	1.82	1.68	1.82	1.70	1.61	1.60	2.96	2.30	2.94	2.14	1.70	2.35
OVCAR-5	1.76	1.77	1.64	1.81	1.81	1.78	1.68	1.68	1.93	1.91	2.59	2.62	2.37	2.00	1.79	2.22
OVCAR-8	1.91	2.68	1.99	2.01	1.93	1.90	2.11	2.02	1.91	1.95	1.97	2.03	2.37	2.19	2.13	1.92
NCI/ADR-RES	1.99	1.83	1.76	1.81	1.87	2.07	1.93	2.03	1.91	1.98	3.20	2.40	2.48	2.06	1.90	2.09
SK-OV-3	1.59	2.52	1.88	2.52	1.84	1.99	1.92	2.03	1.65	1.73	2.62	1.90	13.7	19.4	1.65	2.18
Renal Cancer																
786-0	1.93	1.95	1.70	1.60	1.78	1.41	1.69	1.51	1.98	1.85	1.89	1.90	1.84	1.54	1.81	1.63

Table 2. Continued

Cell lines	GI_{50}[a]														
	1c	**1d**	**1g**		**1k**	**1l**	**1m**	**1n**	**1o**	**1p**	**1q**	**1r**	**1s**	**1t**	**1u**	**1v**
A498	1.86	2.06	1.65	6.59	1.89	1.78	1.80	1.62	1.98	1.87	10.0	1.89	4.91	8.86	1.81	12.6
ACHN	1.60	1.80	1.77	1.73	1.72	1.97	1.74	1.84	1.61	1.74	1.72	1.93	1.66	1.82	1.77	2.01
CAKI-1	1.48	2.58	1.64	1.80	1.63	1.77	1.65	1.77	1.59	1.65	1.98	2.08	2.86	1.84	1.60	2.02
RXF 393	1.62	1.70	1.49	1.71	1.47	1.70	1.57	1.61	1.48	1.78	1.55	1.63	1.74	1.83	1.49	1.47
SN12C	1.76	1.66	1.69	1.85	1.56	1.53	1.68	1.70	1.52	1.72	1.67	1.74	1.83	1.64	1.79	1.75
TK-10	1.97	2.25	1.88	1.49	2.19	1.71	2.11	1.56	2.30	2.22	2.76	2.74	2.59	1.48	2.33	1.97
UO-31	1.38	1.47	1.58	1.58	1.57	1.63	1.57	1.64	1.33	1.42	1.21	1.64	1.75	1.80	1.47	1.89
Prostate Cancer																
PC-3	1.45	1.47	1.60	1.89	1.64	1.55	1.63	1.71	1.47	1.69	1.84	2.40	2.13	1.98	1.58	2.02
DU-145	1.74	2.13	1.75	1.78	1.82	1.74	1.71	1.74	1.69	1.80	3.36	2.24	2.73	1.70	1.68	2.25
Breast Cancer																
MCF7	0.30	0.32	1.47	1.70	1.33	1.78	1.23	1.93	1.48	1.27	1.43	1.22	1.66	1.81	1.53	1.77
MDA-MB-231/ATCC	1.56	1.47	1.45	1.83	1.41	1.66	1.55	1.75	1.27	1.46	1.06	1.67	1.65	1.87	1.52	2.34
HS 578T	1.93	2.16	2.03	2.21	1.94	2.23	2.21	2.36	1.71	2.26	2.00	2.21	2.15	14.7	2.23	2.47
BT-549	9.00	1.68	1.81	1.80	1.93	1.61	1.80	1.71	1.65	1.63	8.82	1.78	8.96	1.79	1.86	26.3
MDA-MB-468	0.40	0.27	0.44	1.62	1.38	1.79	1.40	1.86	1.51	1.45	0.23	nd	1.78	1.97	1.77	1.68

[a] The molar concentration that inhibits 50% net cell growth.
nd : not determined

Conclusions

A new series of thiazole nortopsentin analogues of type **1,** in which the imidazole moiety of nortopsentins A-C was replaced by a thiazole core and one indole unit by a 5-azaindole ring, was efficiently synthesized in good to excellent yields. The new nortopsentin derivatives **1c,d,g,h,k-v** were active against the totality of the about 55 human tumor cell lines of NCI full panel, showing good antiproliferative activity in the micro-submicromolar range (GI_{50} 0.18-26.3 μM). Thiazoles **1k**, **1l** and **1v** were particularly efficacious against leukemia sub-panel (GI_{50} in the range 0.24-1.71 μM, 0.24-1.57 μM and 0.35-2.13 μM, respectively). Compound **1d** proved to be the most active against breast cancer sub-panel (GI_{50} in the range 0.27-2.16 μM). Furthermore, analogues **1d** and **1l** showed a good selectivity against HCT-116 cell line of the colon cancer sub-panel (GI_{50} of 0.93 μM and 0.18 μM, respectively). The encouraging biological results found for this new series confirmed the advantageous influence of the thiazole central core, in comparison with the other five-membered heterocycles, on the antiproliferative activity of this class of compounds. The reason of this improved activity could be attributed to low lying C−S σ* orbitals that, conferring small regions of low electron density on sulfur (σ-holes), may play an important role in the interaction with the biological target.[24]

Experimental Section

General. All melting point were taken on a Büchi-Tottoly capillary apparatus and are uncorrected. IR spectra were determined in bromoform with a Shimadzu FT/IR 8400S spectrophotometer. ^{1}H and ^{13}C NMR spectra were measured at 200 and 50.0 MHz, respectively, in DMSO-*d₆* solution, using a Bruker Avance II series 200 MHz spectrometer. Thiazoles **1c,d,g,h,k-v** were characterized only by ^{1}H NMR spectra, as due to their poor solubility t^{13}C NMR spectroscopy was not perfomed. Column chromatography was performed with Merk silica gel 230-400 mesh ASTM or with Büchi Sepacor chromatography module (prepacked cartridge system). Elemental analyses (C, H, N) were within ± 0.4% of theoretical values and were performed with a VARIO EL III elemental analyzer.

General procedures, analytical and spectroscopic data for intermediates **2d,3a-d,4a-c,5d,6a-d** and **7a-c** were previously reported.[18]

Synthesis of 1-methyl-1*H*-pyrrolo[3,2-*c*]pyridine (8b). To a suspension of 1*H*-pyrrolo[3,2-*c*]pyridine **8a** (0.50 g, 4.2 mmol) in toluene (30 mL), potassium *tert*-butoxide (0.64 g, 5.7 mmol) and tris[2-(2-methoxyethoxy)ethyl]amine (TDA-1) (1-2 drops) were added at 0 °C. The reaction mixture was stirred at room temperature for 4 h, and then iodomethane (0.3 mL, 4.2 mmol) was added at 0 °C. TLC analysis (DCM/MeOH 9/1) revealed that methylation was completed after 16 h at room temperature. The solvent was evaporated under reduced pressure. The residue was treated with H_2O (10 mL), extracted with EtOAc (3x10 mL), dried (Na_2SO_4), evaporated, and purified by column chromatography using DCM/MeOH (98/2) as eluent to give the desired compound as yellow oil; yield: 60%; ^{1}H NMR (200 MHz, DMSO-*d₆*) δ: 3.80 (s, 3H, CH_3), 6.58 (dd, 1H, *J* 3.2, 0.9 Hz, H-3), 7.42 (d, 1H, *J* 3.2 Hz, H-2), 7.46 (d, 1H, *J* 5.9 Hz, H-7), 8.22 (d, 1H, *J* 5.9 Hz, H-6), 8.83 (s, 1H, H-4). ^{13}C NMR (50 MHz, DMSO-*d₆*) δ: 32.4 (q), 99.9 (d), 105.2 (d), 124.9 (s), 130.8 (d), 139.5 (s), 140.0 (d), 143.0 (d). Anal. Calcd for $C_8H_8N_2$: C, 72.70; H, 6.10; N, 21.20. Found: C, 72.54; H, 5.87; N, 21.11.

General synthesis of 2-bromo-1-(1*H*-pyrrolo[3,2-*c*]pyridin-3-yl)-ethanones (9a,b). To a solution of the appropriate 5-azaindoles **8a,b** (4.2 mmol) in dry DCM (20 mL), anhydrous aluminum chloride (2.0 g, 14.8 mmol) was slowly added. The reaction mixture was heated under reflux and a solution of bromoacetyl bromide (0.37 mL, 4.2 mmol) in anhydrous DCM (2 mL) was added dropwise. The resulting solution was allowed to stir under reflux for 40 min (for derivative **9a**) or 15 min (for derivative **9b**). After cooling, water/ice were slowly added and the obtained precipitate was filtered off to give the pure desired compounds **(9a,b)**.

2-Bromo-1-(1*H*-pyrrolo[3,2-c]pyridin-3-yl)-ethanone (9a). White solid; yield: 90%; mp 285 °C ; IR (cm^{-1}) 3553, 1679; ^{1}H NMR (200 MHz, DMSO-*d₆*) δ: 5.12 (s, 2H, CH_2), 8.16 (d, 1H, *J* 6.6 Hz, H-7), 8.64 (d, 1H, *J* 6.6 Hz, H-6), 9.01 (s, 1H, H-2), 9.50 (s, 1H, H-4), 13.74 (bs, 1H, NH). ^{13}C NMR (50 MHz, DMSO-*d₆*) δ: 46.8 (t), 110.8 (d), 115.0 (s), 121.7 (s), 133.5 (d), 136.5 (d), 140.2 (d), 143.3 (s), 186.5 (s). Anal. Calcd for $C_9H_7BrN_2O$: C, 45.22; H, 2.95; N, 11.72. Found: C, 45.36; H, 2.87; N, 11.57.

2-Bromo-1-(1-methyl-1*H*-pyrrolo[3,2-c]pyridin-3-yl)-ethanone (9b). White solid; yield: 93%; mp 120-121 °C; IR (cm^{-1}) 1659; ^{1}H NMR (200 MHz, DMSO-*d₆*) δ: 4.08 (s, 3H, CH_3), 5.06 (s, 2H, CH_2), 8.34 (d, 1H, *J* 6.7 Hz, H-7), 8.74 (d, 1H, *J* 6.7 Hz, H-6), 9.07 (s, 1H, H-2), 9.48 (s, 1H, H-4). ^{13}C NMR (50 MHz, DMSO-*d₆*) δ: 34.3 (q), 46.6 (t), 109.6 (d), 114.1 (s), 121.7 (s), 133.5 (d), 136.3 (d), 143.6 (d), 143.7 (s), 186.1 (s). Anal. Calcd for $C_{10}H_9BrN_2O$: C, 47.46; H, 3.58; N, 11.07. Found: C, 47.35; H, 3.74; N, 11.25.

General procedure for the synthesis of thiazoles (1a-p). A suspension of the proper thioamides **5d,6a-d,7a-c** (2.5 mmol) and α-bromoacetyl derivatives **9a,b** (2.5 mmol) in ethanol (10 mL) was heated under reflux for 1 h. After cooling, the precipitate obtained, was filtered off and dried. Thiazoles **1c,d,g,h,k-p** were recrystallized from ethanol to give the pure compounds as hydrobromide salts. Thiazoles **1a,b,e,f,i,j** were very unstable and were immediately used for the next step without purification and characterization.

3-[2-(1-Methyl-1*H*-indol-3-yl)-1,3-thiazol-4-yl]-1*H*-pyrrolo[3,2-*c*]pyridine hydrobromide (1c). Yellow solid; yield: 84%, mp 273-274°C; IR (cm^{-1}) 3416, 3170; ^1H NMR (200 MHz, DMSO-d_6) δ: 3.92 (s, 3H, CH_3), 7.30-7.37 (m, 2H, Ar), 7.57-7.62 (m, 1H, Ar), 8.03-8.11 (m, 2H, Ar), 8.28-8.34 (m, 2H, Ar), 8.49-8.69 (m, 2H, Ar), 9.78 (s, 1H, H-4'), 13.25 (bs, 1H, NH), 15.22 (bs, 1H, NH^+). Anal. Calcd for $C_{19}H_{15}BrN_4S$: C, 55.48; H, 3.68; N, 13.62. Found: C, 55.36; H, 3.78; N, 13.53.

1-Methyl-3-[2-(1-methyl-1*H*-indol-3-yl)-1,3-thiazol-4-yl]-1*H*-pyrrolo[3,2-*c*]pyridine hydrobromide (1d). Yellow solid; yield: 52%, mp 251-252°C; IR (cm^{-1}) 3381; ^1H NMR (200 MHz, DMSO-d_6) δ: 3.91 (s, 3H, CH_3), 4.08 (s, 3H, CH_3), 7.30-7.38 (m, 2H, Ar), 7.57-7.62 (m, 1H, Ar), 8.01 (s, 1H, Ar), 8.21-8.35 (m, 3H, Ar), 8.57-8.61 (m, 2H, Ar) 9.76 (s, 1H, H-4'), 15.30 (bs, 1H, NH^+). Anal. Calcd for $C_{20}H_{17}BrN_4S$: C, 56.48; H, 4.03; N, 13.17. Found: C, 56.62; H, 3.87; N, 13.39.

3-[2-(5-Methoxy-1-methyl-1*H*-indol-3-yl)-1,3-thiazol-4-yl]-1*H*-pyrrolo[3,2-*c*]pyridine hydrobromide (1g). Yellow solid; yield: 70%, mp 264-265°C; IR (cm^{-1}) 3422, 3164; ^1H NMR (200 MHz, DMSO-d_6) δ: 3.89 (s, 6H, CH_3, OCH_3), 6.96 (dd, 1H, *J* 8.9, 2.5 Hz, H-6), 7.50 (d, 1H, *J* 8.9 Hz, H-7), 7.77 (d, 1H, *J* 2.5 Hz, H-4), 8.00 (s, 1H, Ar), 8.07 (d, 1H, *J* 6.6 Hz, H-7'), 8.20 (m, 1H, Ar), 8.52-8.56 (m, 2H, Ar), 9.76 (s, 1H, Ar), 13.20 (bs, 1H, NH), 15.15 (bs, 1H, NH^+). Anal. Calcd for $C_{20}H_{17}BrN_4OS$: C, 54.43; H, 3.88; N, 12.69. Found: C, 54.69; H, 3.77; N, 12.46.

3-[2-(5-Methoxy-1-methyl-1*H*-indol-3-yl)-1,3-thiazol-4-yl]-1-methyl-1*H*-pyrrolo[3,2-*c*]pyridine hydrobromide (1h). Yellow solid; yield: 53%, mp 277-278°C; IR (cm^{-1}) 3377; ^1H NMR (200 MHz, DMSO-d_6) δ: 3.88 (s, 3H, CH_3), 3.89 (s, 3H, CH_3), 4.08 (s, 3H, OCH_3), 6.96 (dd, 1H, *J* 8.9, 2.5 Hz, H-6), 7.50 (d, 1H, *J* 8.9 Hz, H-7), 7.76 (d, 1H, *J* 2.5 Hz, H-4), 7.96 (s, 1H, Ar), 8.18 (s, 1H, Ar), 8.23 (d, 1H, *J* 6.8 Hz, H-7'), 8.52 (s, 1H, Ar), 8.58 (d, 1H, *J* 6.8 Hz, H-6'), 9.73 (s, 1H, H-4'), 15.12 (bs, 1H, NH^+). Anal. Calcd for $C_{21}H_{19}BrN_4OS$: C, 55.39; H, 4.21; N, 12.30. Found: C, 55.23; H, 4.38; N, 12.46.

3-[2-(5-Bromo-1-methyl-1*H*-indol-3-yl)-1,3-thiazol-4-yl]-1*H*-pyrrolo[3,2-*c*]pyridine hydrobromide (1k). Yellow solid; yield: 80%, mp 309-310°C; IR (cm^{-1}) 3610, 3496; ^1H NMR (200 MHz, DMSO-d_6) δ: 3.92 (s, 3H, CH_3), 7.45 (dd, 1H, *J* 8.7, 1.9 Hz, H-6), 7.61 (d, 1H, *J* 8.7 Hz, H-7), 8.06 (s, 1H, Ar), 8.08 (d, 1H, *J* 7.4 Hz, H-7'), 8.34 (s, 1H, Ar), 8.40 (d, 1H, *J* 1.9 Hz, H-4), 8.45-8.53 (m, 2H, Ar), 9.72 (s, 1H, H-4'), 13.17 (bs, 1H, NH), 15.13 (bs, 1H, NH^+). Anal. Calcd for $C_{19}H_{14}Br_2N_4S$: C, 46.55; H, 2.88; N, 11.43. Found: C, 46.27; H, 2.71; N, 11.70.

3-[2-(5-Bromo-1-methyl-1*H*-indol-3-yl)-1,3-thiazol-4-yl]-1-methyl-1*H*-pyrrolo[3,2-*c*]pyridine hydrobromide (1l). Yellow solid; yield: 66%, mp 321-322°C; IR (cm^{-1}) 3490; ^1H NMR (200 MHz, DMSO-d_6) δ: 3.92 (s, 3H, CH_3), 4.10 (s, 3H, CH_3), 7.46 (dd, 1H, *J* 8.7, 1.9 Hz, H-6), 7.61 (d, 1H, *J* 8.7 Hz, H-7), 8.04 (s, 1H, Ar), 8.25 (d, 1H, *J* 6.8 Hz, H-7'), 8.33 (s, 1H, Ar), 8.40 (d, 1H, *J* 1.9 Hz, H-4), 8.54 (s, 1H, Ar), 8.60 (d, 1H, *J* 6.8 Hz, H-6'), 9.69 (s, 1H, H-4'), 15.16 (bs, 1H, NH^+). Anal. Calcd for $C_{20}H_{16}Br_2N_4S$: C, 47.64; H, 3.20; N, 11.11. Found: C, 47.39; H, 3.11; N, 11.24.

3-[2-(5-Fluoro-1-methyl-1*H*-indol-3-yl)-1,3-thiazol-4-yl]-1*H*-pyrrolo[3,2-*c*]pyridine hydrobromide (1m). Yellow solid; yield: 56%, mp 309°C; IR (cm^{-1}) 3604, 3428; ^1H NMR (200 MHz, DMSO-d_6) δ: 3.92 (s, 3H, CH_3), 7.19 (td, 1H, *J* 9.2, 7.9, 2.6 Hz, H-6), 7.63 (dd, 1H, *J* 7.9, 4.5 Hz, H-7), 7.99 (dd, 1H, *J* 9.2, 2.6 Hz, H-4), 8.04 (s, 1H, Ar), 8.07 (d, 1H, *J* 6.6 Hz, H-7'), 8.34 (s, 1H, Ar), 8.51 (d, 1H, *J* 6.6 Hz, H-6'), 8.58 (d, 1H, *J* 2.6 Hz, H-2'), 9.73 (s, 1H, H-4'), 13.21 (bs, 1H, NH), 15.15 (bs, 1H, NH^+). Anal. Calcd for $C_{19}H_{14}BrFN_4S$: C, 53.16; H, 3.29; N, 13.05. Found: C, 53.37; H, 3.16; N, 12.92.

3-[2-(5-Fluoro-1-methyl-1*H*-indol-3-yl)-1,3-thiazol-4-yl]-1-methyl-1*H*-pyrrolo[3,2-*c*]pyridine hydrobromide (1n). Yellow solid; yield: 70%, mp 305°C; IR (cm^{-1}) 3604; ^{1}H NMR (200 MHz, DMSO-d_6) δ: 3.92 (s, 3H, CH$_3$), 4.10 (s, 3H, CH$_3$), 7.20 (td, 1H, *J* 9.3, 7.9, 2.7 Hz, H-6), 7.64 (dd, 1H, *J* 7.9, 4.5 Hz, H-7), 8.02 (s, 1H, Ar), 8.06 (d, 1H, *J* 9.3, 2.7 Hz, H-4), 8.25 (d, 1H, *J* 6.8 Hz, H-7’), 8.34 (s, 1H, Ar), 8.59 (s, 1H, Ar), 8.60 (d, 1H, *J* 6.8 Hz, H-6’), 9.71 (s, 1H, H-4’), 15.05 (bs, 1H, NH$^+$). Anal. Calcd for $C_{20}H_{16}BrFN_4S$: C, 54.18; H, 3.64; N, 12.64. Found: C, 53.90; H, 3.56; N, 12.72.

3-[2-(5-Fluoro-1*H*-indol-3-yl)-1,3-thiazol-4-yl]-1*H*-pyrrolo[3,2-*c*]pyridine hydrobromide (1o). Yellow solid; yield: 58%, mp 254°C; IR (cm^{-1}) 3610, 3559, 3399; ^{1}H NMR (200 MHz, DMSO-d_6) δ: 7.12 (td, 1H, *J* 9.2, 7.9, 2.6 Hz, H-6), 7.55 (dd, 1H, *J* 7.9, 4.6 Hz, H-7), 7.98 (dd, 1H, *J* 9.2, 2.6 Hz, H-4), 8.05 (s, 1H, Ar), 8.07 (d, 1H, *J* 6.3 Hz, H-7’), 8.33 (d, 1H, *J* 2.9 Hz, H-2), 8.51 (d, 1H, *J* 6.3 Hz, H-6’), 8.59 (d, 1H, *J* 2.4 Hz, H-2’), 9.76 (s, 1H, H-4’), 12.06 (d, 1H, *J* 2.9 Hz, NH), 13.21 (d, 1H, *J* 2.4 Hz, NH), 15.13 (bs, 1H, NH$^+$). Anal. Calcd for $C_{18}H_{12}BrFN_4S$: C, 52.06; H, 2.91; N, 13.49. Found: C, 51.88; H, 2.67; N, 13.70.

3-[2-(5-Fluoro-1*H*-indol-3-yl)-1,3-thiazol-4-yl]-1-methyl-1*H*-pyrrolo[3,2-*c*]pyridine hydrobromide (1p). Yellow solid; yield: 67%, mp 263°C; IR (cm^{-1}) 3616, 3387; ^{1}H NMR (200 MHz, DMSO-d_6) δ

General procedure for the synthesis of thiazoles (1q-v). To a suspension of appropriate thiazole **1a,b,e,f,i,j** (0.38 mmol) in dichloromethane (10 mL), trifluoacetic acid (0.5 mL) was added. The reaction was heated at reflux for 24 h. The solvent was dried (Na_2SO_4), evaporated under reduced pressure and the residue recrystallized with ethanol to afford the desired thiazoles **1q-v**.

3-[2-(1*H*-Indol-3-yl)-1,3-thiazol-4-yl]-1*H*-pyrrolo[3,2-*c*]pyridine hydrobromide (1q). Yellow solid; yield: 55%, mp 380-381°C; IR (cm^{-1}) 3393, 3113, 3228. ^{1}H NMR (200 MHz, DMSO-d_6) δ:7.25-7.31 (m, 2H, Ar), 7.52-7.57 (m, 1H, Ar), 8.02 (s, 1H, Ar), 8.07 (d, 1H, *J* 6.6 Hz, H-7’), 8.25-8.32 (m, 2H, Ar), 8.52 (d, 1H, *J* 6.6 Hz, H-6’), 8.58 (d, 1H, *J* 2.4 Hz, H-2’), 9.80 (s, 1H, H-4’), 11.88 (d, 1H, *J* 2.4 Hz, NH), 13.06 (bs, 1H, NH), 14.82 (bs, 1H, NH$^+$). Anal. Calcd for $C_{18}H_{13}BrN_4S$: C, 54.42; H, 3.30; N, 14.10. Found: C, 54.21; H, 3.18; N, 14.32.

3-[2-(1*H*-Indol-3-yl)-1,3-thiazol-4-yl]-1-methyl-1*H*-pyrrolo[3,2-*c*]pyridine hydrobromide (1r). Yellow solid; yield: 69%, mp 194°C; IR (cm^{-1}) 3610, 3553; ^{1}H NMR (200 MHz, DMSO-d_6) δ: 4.09 (s, 3H, CH$_3$), 7.25-7.29 (m, 2H, Ar), 7.52-7.58 (m, 1H, Ar), 7.99 (s, 1H, Ar), 8.21-8.33 (m, 3H, Ar), 8.57-8.62 (m, 2H, Ar), 9.78 (s, 1H, H-4’), 11.91 (bs, 1H, NH), 15.03 (bs, 1H, NH$^+$). Anal. Calcd for $C_{19}H_{15}BrN_4S$: C, 55.48; H, 3.68; N, 13.62. Found: C, 55.63; H, 3.77; N, 13.85.

3-[2-(5-Methoxy-1*H*-indol-3-yl)-1,3-thiazol-4-yl]-1*H*-pyrrolo[3,2-*c*]pyridine hydrobromide (1s). Yellow solid; yield: 88%, mp 147°C; IR (cm^{-1}) 3359, 3216, 3125; ^{1}H NMR (200 MHz, DMSO-d_6) δ: 3.87 (s, 3H, OCH$_3$), 6.91 (dd, 1H, *J* 8.8, 2.5 Hz, H-6), 7.43 (d, 1H, *J* 8.8 Hz, H-7), 7.76 (d, 1H, *J* 2.5 Hz, H-4),7.99 (s, 1H, Ar), 8.07 (d, 1H, *J* 6.6 Hz, H-7’), 8.19 (d, 1H, *J* 2.9 Hz, H-2), 8.51 (d, 1H, *J* 6.6 Hz, H-6’), 8.56 (d, 1H, *J* 2.4 Hz, H-2’), 9.76 (s, 1H, H-4’), 11.76 (bs, 1H, NH), 13.08 (bs, 1H, NH), 14.88 (bs, 1H, NH$^+$). Anal. Calcd for $C_{19}H_{15}BrN_4OS$: C, 53.40; H, 3.54; N, 13.11. Found: C, 53.65; H, 3.80; N, 13.38.

3-[2-(5-Methoxy-1*H*-indol-3-yl)-1,3-thiazol-4-yl]-1-methyl-1*H*-pyrrolo[3,2-*c*]pyridine hydrobromide (1t). Yellow solid; yield: 72%, mp 241°C; IR (cm^{-1}) 3422, 3199; ^{1}H NMR (200 MHz, DMSO-d_6) δ: 3.87 (s, 3H, CH$_3$), 4.08 (s, 3H, OCH$_3$), 6.91 (dd, 1H, *J* 8.8, 2.5 Hz, H-6), 7.43 (d, 1H, *J* 8.8 Hz, H-7), 7.75 (d, 1H, *J* 2.5 Hz, H-4), 7.95 (s, 1H, Ar), 8.18 (d, 1H, *J* 2.8 Hz, H-2), 8.23 (d, 1H, *J* 6.8 Hz, H-7’), 8.53 (s, 1H, Ar), 8.59 (d, 1H, *J* 6.8 Hz, H-6’), 9.77 (s, 1H, H-4’), 13.06 (bs, 1H, NH), 15.07 (bs, 1H, NH$^+$). Anal. Calcd for $C_{20}H_{17}BrN_4OS$: C, 54.43; H, 3.88; N, 12.69. Found: C, 54.28; H, 3.69; N, 12.51.

3-[2-(5-Bromo-1*H*-indol-3-yl)-1,3-thiazol-4-yl]-1*H*-pyrrolo[3,2-*c*]pyridine hydrobromide (1u). Yellow solid; yield: 62%, mp 198°C; IR (cm^{-1}) 3684, 3604, 3559; ^{1}H NMR (200 MHz, DMSO-d_6) δ: 7.37-7.54 (m, 2H, Ar), 8.04-8.10 (m, 2H, Ar), 8.32-8.39 (m, 2H, Ar), 8.50-8.55 (m, 2H, Ar), 9.75 (s, 1H, H-4'), 12.10 (bs, 1H, NH), 13.07 (bs, 1H, NH), 14.92 (bs, 1H, NH$^+$). Anal. Calcd for $C_{18}H_{12}Br_2N_4S$: C, 45.40; H, 2.54; N, 11.77. Found: C, 45.21; H, 2.47; N, 12.06.

3-[2-(5-Bromo-1*H*-indol-3-yl)-1,3-thiazol-4-yl]-1-methyl-1*H*-pyrrolo[3,2-*c*]pyridine hydrobromide (1v). Yellow solid; yield: 93%, mp 241°C; IR (cm^{-1}) 3678, 3604; ^{1}H NMR (200 MHz, DMSO-d_6) δ: 4.08 (s, 3H, CH_3), 7.38 (dd, 1H, *J* 8.6, 1.9 Hz, H-6), 7.51 (d, 1H, *J* 8.6 Hz, H-7), 8.00 (s, 1H, Ar), 8.22 (d, 1H, *J* 6.8 Hz, H-7'), 8.30 (d, 1H, *J* 2.9 Hz, H-2), 8.36 (d, 1H, *J* 1.9 Hz, H-4), 8.51 (s, 1H, Ar), 8.59 (d, 1H, *J* 6.8 Hz, H-6'), 9.71 (s, 1H, H-4'), 12.11 (d, 1H, *J* 2.9 Hz, NH), 15.22 (bs, 1H, NH$^+$). Anal. Calcd for $C_{19}H_{14}Br_2N_4S$: C, 46.55; H, 2.88; N, 11.43. Found: C, 46.76; H, 2.72; N, 11.24.

Acknowledgements

This research was funded by PRIN2017, Prot.No.2017E84AA4, in favour to Patrizia Diana.

Supplementary Material

Copies of ^{1}H NMR spectra of thiazoles **1c,d,g,h,k-v** are available.

References

1. Carroll, A. R.; Copp, B. R.; Davis, R. A.; Keyzers, R. A.; Prinsep M. R.; *Nat. Prod. Rep.,* **2021**, *38*, 362-413. https://doi.org/10.1039/D0NP00089B
2. Le, H. M; Newman, D. J.; Glaser K. B.; Mayer A. M. *FASEB J.* **2020**, 34. https://doi.org/10.1096/fasebj.2020.34.s1.01808
3. Saeed, A.F.U.H.; Su, J.; Ouyang, S. *Biomed. Pharmacother.* **2021**, *134*, 111091. https://doi.org/10.1016/j.biopha.2020.111091
4. Netz, N.; Opatz, T. Mar. Drugs **2015**, *13*, 4814-4914. http://dx.doi.org/10.3390/md13084814
5. Bao, B.; Sun, Q.; Yao, X.; Hong, J.; Lee, C.; Sim, C.J.; Jung, J.H. *J. Nat. Prod.* **2005**, *68*, 711–715. https://doi.org/10.1021/np049577a.
6. Souza, C.R.M., Bezerra W.P., Souto J-T. *Marine Drugs* **2020**, *18*(3), 147. https://doi.org/10.3390/md18030147
7. Oh K.B.; Mar, W.; Kim, S.; Kim, J.Y.; Lee, T.H.; Kim, J.G.; Shin, D.; Sim, C.J., Shin, *Biol. Pharm. Bull.* **2006**, *29*(3), 570-573. https://doi.org/10.1248/bpb.29.570
8. Zhang, M-Z.; Chen, Q.; Yang; G.-F. *Eur. J. Med. Chem.* **2015**, *89*, 421-441. https://doi.org/10.1016/j.ejmech.2014.10.065
9. Sakemi, S.; Sun, H.H.; *J. Org. Chem.* **1991**, *56*, 4304–4307. http://dx.doi.org/10.1021/jo00013a044

10. Ji, X.; Guo, J.; Liu, Y.; Lu, A.; Z. Wang, Li, Y.; Yang, S., Wang, Q. *J. Agric. Food Chem*. **2018**, *66*, 4062-4072. http://dx.doi.org/10.1021/acs.jafc.8b00507
11. Cascioferro, S.; Attanzio, A.; Di Sarno, V.; Musella, S.; Tesoriere, L.; Cirrincione, G.; Diana, P.; Parrino, B. *Marine Drugs* **2019**, *17*, 35.
http://dx.doi.10.3390/md17010035
12. Carbone, D.; Parrino, B.; Cascioferro, S.; Pecoraro, C.; Giovannetti, E.; Di Sarno, V.; Musella, S.; Auriemma, G.; Cirrincione, G.; Diana, P. *ChemMedChem* **2021**, *16*, 537–554.
https://doi.org/10.1002/cmdc.202000752
13. Abo-Salem, H.M.; Abd El Salam, H.A.; Abdel-Aziem, A.M.; Abdel-Aziz, M.S.; El-Sawy, E.R. *Molecules* 2021, *26*, 4112.
https://doi.org/10.3390/molecules26144112
14. Carbone, A.; Cascioferro, S.; Parrino, B.; Carbone, D.; Pecoraro, C.; Schillaci, D.; Cusimano, M.G.; Cirrincione, G.; Diana, P. *Molecules* **2021**, *26*, 81.
https://dx.doi.org/10.3390/molecules26010081
15. Parrino, B.; Carbone, D.; Cascioferro, S.; Pecoraro, C.; Giovannetti, E.; Deng, D.; Di Sarno, V.; Musella, S.; Auriemma, G.; Cusimano, M.G.; Schillaci, D.; Cirrincione, G.; Diana P. *Eur. J. Med. Chem.* **2021**, *209*, 112892. https://doi.org/10.1016/j.ejmech.2020.112892
16. Jiang, B.; Gu, X-H. *Bioorg. Med. Chem.* **2000**, *8*, 363-371.
https://doi.org/10.1016/S0968-0896(99)00290-4
17. Kumar, D.; Kumar, N.M.; Chang, K-H.; Gupta, R.; Shah, K. *Bioorg. Med. Chem. Lett*. **2011**, *21*, 5897-5900. http://dx.doi.org/10.1016/j.bmcl.2011.07.089
18. Carbone, A.; Pennati, M.; Parrino, B.; Lopergolo, A.; Barraja, P.; Montalbano, A.; Spanò, V.; Sbarra, S.; Doldi, V.; De Cesare, M.; Cirrincione, G.; Diana, P.; Zaffaroni. *J. Med. Chem.* **2013**, *56*, 7060-7072. https://doi.org/10.1021/jm400842x
19. Di Franco, S.; Parrino, B.; Gaggianesi, M.; Pantina, V.D.; Bianca, P.; Nicotra, A.; Mangiapane, L.R.; Lo Iacono, M.; Ganduscio, G.; Veschi, V.; Brancato, O.R.; Glaviano, A.; Turdo, A.; Pillitteri, I.; Colarossi, L.; Cascioferro, S.; Carbone, D.; Pecoraro, C.; Fiori, M.E.; De Maria, R.; Todaro, M.; Screpanti, I.; Cirrincione, G.; Diana, P.; Stassi, G. *iScience,* **2021**, *24*(6), 102664.
https://doi.org/10.1016/j.isci.2021.102664
20. El-Gamal, M.I., Abdel-Maksoud, M.S., El-Din, M.M.G., Yoo, K.H., Baek, D. and Oh, C.-H. *Arch. Pharm. Chem. Life Sci*., **2014**, *347*, 635-641.
https://doi.org/10.1002/ardp.201400051
21. El-Gamal, M.I.; Oh, C.H. *J. Enzyme Inhib. Med. Chem.* **2018,** *33*, 1160–1166. https://doi.org/10.1080/14756366.2018.1491563
22. Cascioferro, S.; Li Petri, G.; Parrino, B.; Carbone, D.; Funel, N.; Bergonzini, C.; Mantini, G.; Dekker, H.; Geerke, D.; Peters, G.J.; Cirrincione, G.; Giovannetti, E.; Diana, P. *Eur. J. Med. Chem.* **2020**, *189*, 112088. https://doi.org/10.1016/j.ejmech.2020.112088
23. Cascioferro, S.; Li Petri, G.; Parrino, B.; El Hassouni, B.; Carbone, D.; Arizza, V.; Perricone, U.; Padova, A.; Funel, N.; Peters, G.J.; Cirrincione, G.; Giovannetti, E.; Diana, P. *Molecules* **2020**, *25*, 329.
https://doi:10.3390/molecules25020329
24. Cascioferro, S.; Parrino, B.; Carbone, D.; Schillaci, D.; Giovannetti, E.; Cirrincione, G.; Diana, P. *J. Med. Chem*. **2020**, *63*, 7923−7956.
https://dx.doi.org/10.1021/acs.jmedchem.9b01245

This paper is an open access article distributed under the terms of the Creative Commons Attribution (CC BY) license (_______________________________________)

Supplementary Material

Synthesis and cytotoxic activity of 3-[2-(1*H*-Indol-3-yl)-1,3-thiazol-4-yl]-1*H*-pyrrolo[3,2-*c*]pyridine hydrobromides, analogues of the marine alkaloid nortopsentin

Camilla Pecoraro,[a] Daniela Carbone,[a] Daniele Aiello,[a] and Anna Carbone*[a,b]

[a]*Dipartimento di Scienze e Tecnologie Biologiche Chimiche e Farmaceutiche (STEBICEF), Università degli Studi di Palermo, Via Archirafi 32, 90123 Palermo, Italy*
[b]*Dipartimento di Farmacia, Università degli Studi di Genova, Viale Benedetto XV 3, 16132 Genova, Italy*
Email: carbone@difar.unige.it

Figure S1. ^{1}H NMR spectra of 3-[2-(1-methyl-1*H*-indol-3-yl)-1,3-thiazol-4-yl]-1*H*-pyrrolo[3,2-*c*]pyridine hydrobromide (**1c**) S3
Figure S2. ^{1}H NMR spectra of 1-methyl-3-[2-(1-methyl-1*H*-indol-3-yl)-1,3-thiazol-4-yl]-1*H*-pyrrolo[3,2-*c*]pyridine hydrobromide (**1d**) S3
Figure S3. ^{1}H NMR spectra of 3-[2-(5-methoxy-1-methyl-1*H*-indol-3-yl)-1,3-thiazol-4-yl]-1*H*-pyrrolo[3,2-*c*]pyridine hydrobromide (**1g**) S4
Figure S4. ^{1}H NMR spectra of 3-[2-(5-methoxy-1-methyl-1*H*-indol-3-yl)-1,3-thiazol-4-yl]-1-methyl-1*H*-pyrrolo[3,2-*c*]pyridine hydrobromide (**1h**) S4
Figure S5. ^{1}H NMR spectra of 3-[2-(5-bromo-1-methyl-1*H*-indol-3-yl)-1,3-thiazol-4-yl]-1*H*-pyrrolo[3,2-*c*]pyridine hydrobromide (**1k**) S5
Figure S6. ^{1}H NMR spectra of 3-[2-(5-bromo-1-methyl-1*H*-indol-3-yl)-1,3-thiazol-4-yl]-1-methyl-1*H*-pyrrolo[3,2-*c*]pyridine hydrobromide (**1l**) S5
Figure S7. ^{1}H NMR spectra of 3-[2-(5-fluoro-1-methyl-1*H*-indol-3-yl)-1,3-thiazol-4-yl]-1*H*-pyrrolo[3,2-*c*]pyridine hydrobromide (**1m**) S6
Figure S8. ^{1}H NMR spectra of 3-[2-(5-fluoro-1-methyl-1*H*-indol-3-yl)-1,3-thiazol-4-yl]-1-methyl-1*H*-pyrrolo[3,2-*c*]pyridine hydrobromide (**1n**) S6
Figure S9. ^{1}H NMR spectra of 3-[2-(5-fluoro-1*H*-indol-3-yl)-1,3-thiazol-4-yl]-1*H*-pyrrolo[3,2-*c*]pyridine hydrobromide (**1o**) S7
Figure S10. ^{1}H NMR spectra of 3-[2-(5-fluoro-1*H*-indol-3-yl)-1,3-thiazol-4-yl]-1-methyl-1*H*-pyrrolo[3,2-*c*]pyridine hydrobromide (**1p**) S7
Figure S11. ^{1}H NMR spectra of 3-[2-(1*H*-indol-3-yl)-1,3-thiazol-4-yl]-1*H*-pyrrolo[3,2-*c*]pyridine hydrobromide (**1q**) S8
Figure S12. ^{1}H NMR spectra of 3-[2-(1*H*-indol-3-yl)-1,3-thiazol-4-yl]-1-methyl-1*H*-pyrrolo[3,2-*c*]pyridine hydrobromide (**1r**) S8
Figure S13. ^{1}H NMR spectra of 3-[2-(5-methoxy-1*H*-indol-3-yl)-1,3-thiazol-4-yl]-1*H*-pyrrolo[3,2-*c*]pyridine hydrobromide (**1s**) S9

Figure S14. ^{1}H NMR spectra of 3-[2-(5-methoxy-1*H*-indol-3-yl)-1,3-thiazol-4-yl]-1-methyl-1*H*-pyrrolo[3,2-*c*]pyridine hydrobromide (**1t**) S9
Figure S15. ^{1}H NMR spectra of 3-[2-(5-bromo-1*H*-indol-3-yl)-1,3-thiazol-4-yl]-1*H*-pyrrolo[3,2-*c*]pyridine hydrobromide (**1u**)..S10
Figure S16. ^{1}H NMR spectra of 3-[2-(5-bromo-1*H*-indol-3-yl)-1,3-thiazol-4-yl]-1-methyl-1*H*-pyrrolo[3,2-*c*]pyridine hydrobromide (**1v**)..S10

Figure S1. ^1H **NMR spectra of 3-[2-(1-methyl-1*H*-indol-3-yl)-1,3-thiazol-4-yl]-1*H*-pyrrolo[3,2-*c*]pyridine hydrobromide (1c)**

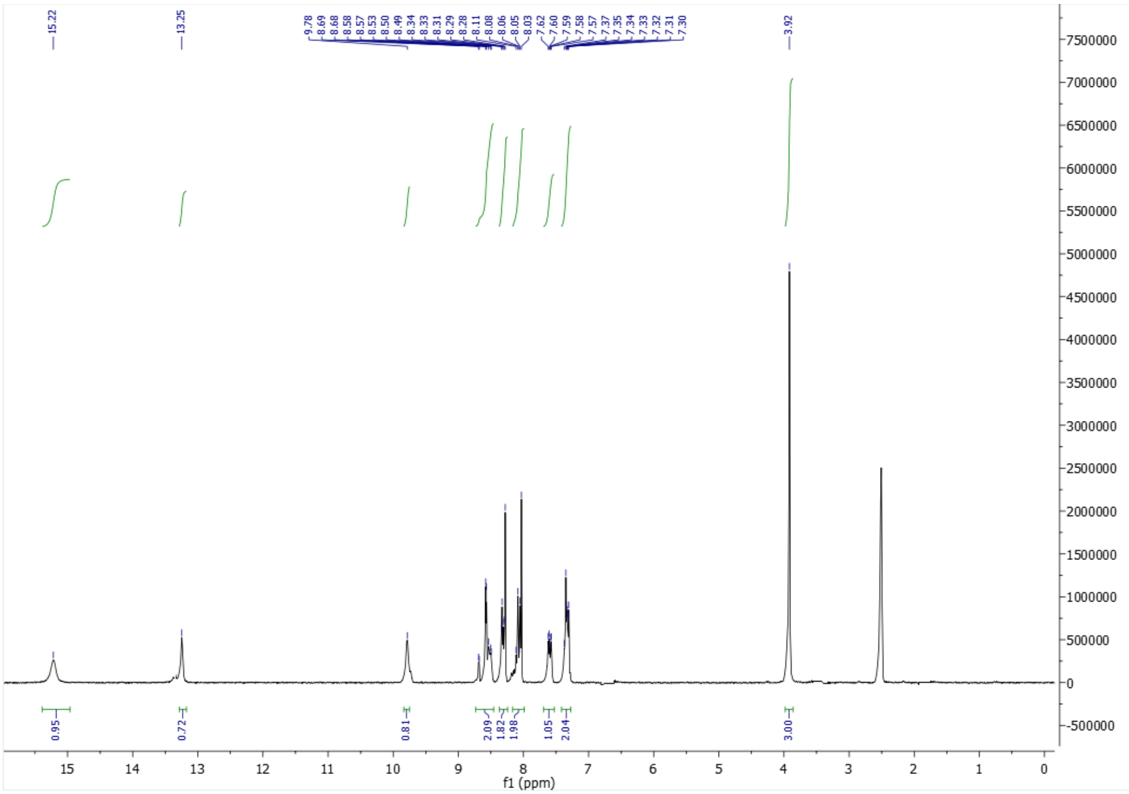

Figure S2. ^1H **NMR spectra of 1-methyl-3-[2-(1-methyl-1*H*-indol-3-yl)-1,3-thiazol-4-yl]-1*H*-pyrrolo[3,2-*c*]pyridine hydrobromide (1d)**

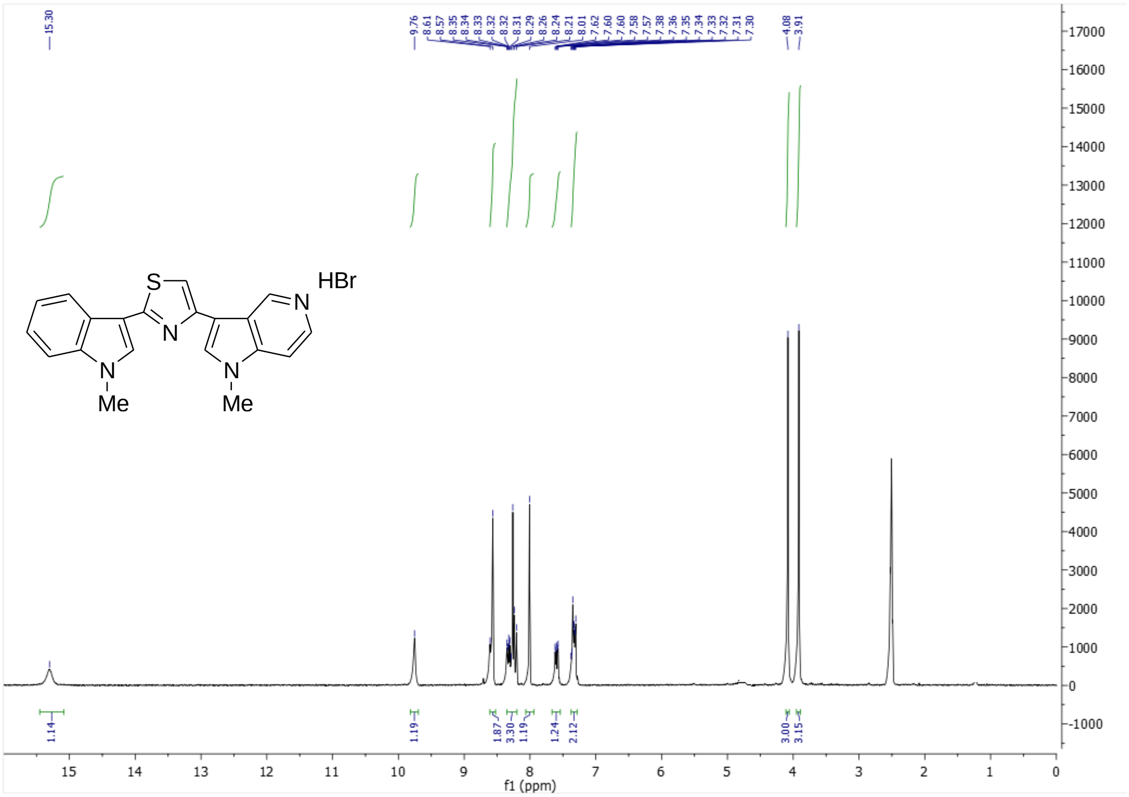

Figure S3. ^{1}H NMR spectra of 3-[2-(5-methoxy-1-methyl-1*H*-indol-3-yl)-1,3-thiazol-4-yl]-1*H*-pyrrolo[3,2-*c*]pyridine hydrobromide (1g)

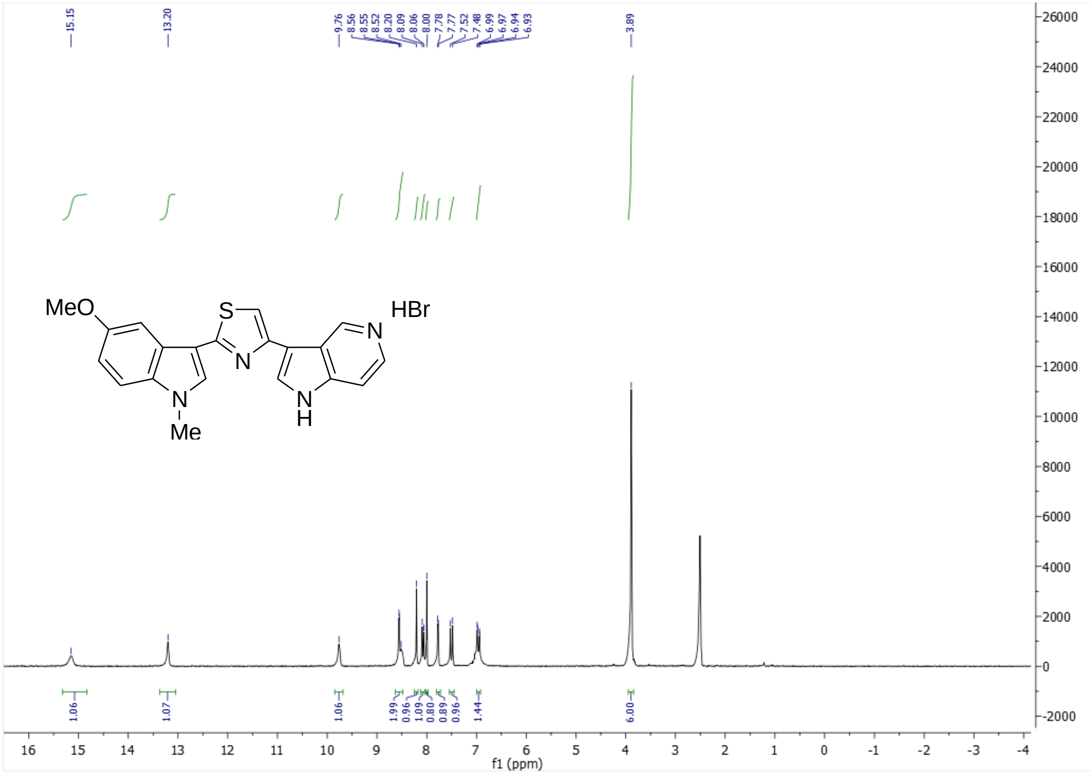

Figure S4. ^{1}H NMR spectra of 3-[2-(5-methoxy-1-methyl-1*H*-indol-3-yl)-1,3-thiazol-4-yl]-1-methyl-1*H*-pyrrolo[3,2-*c*]pyridine hydrobromide (1h)

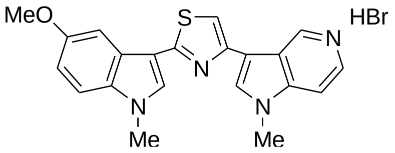

Figure S5. ^{1}H NMR spectra of 3-[2-(5-bromo-1-methyl-1*H*-indol-3-yl)-1,3-thiazol-4-yl]-1*H*-pyrrolo[3,2-*c*]pyridine hydrobromide (1k)

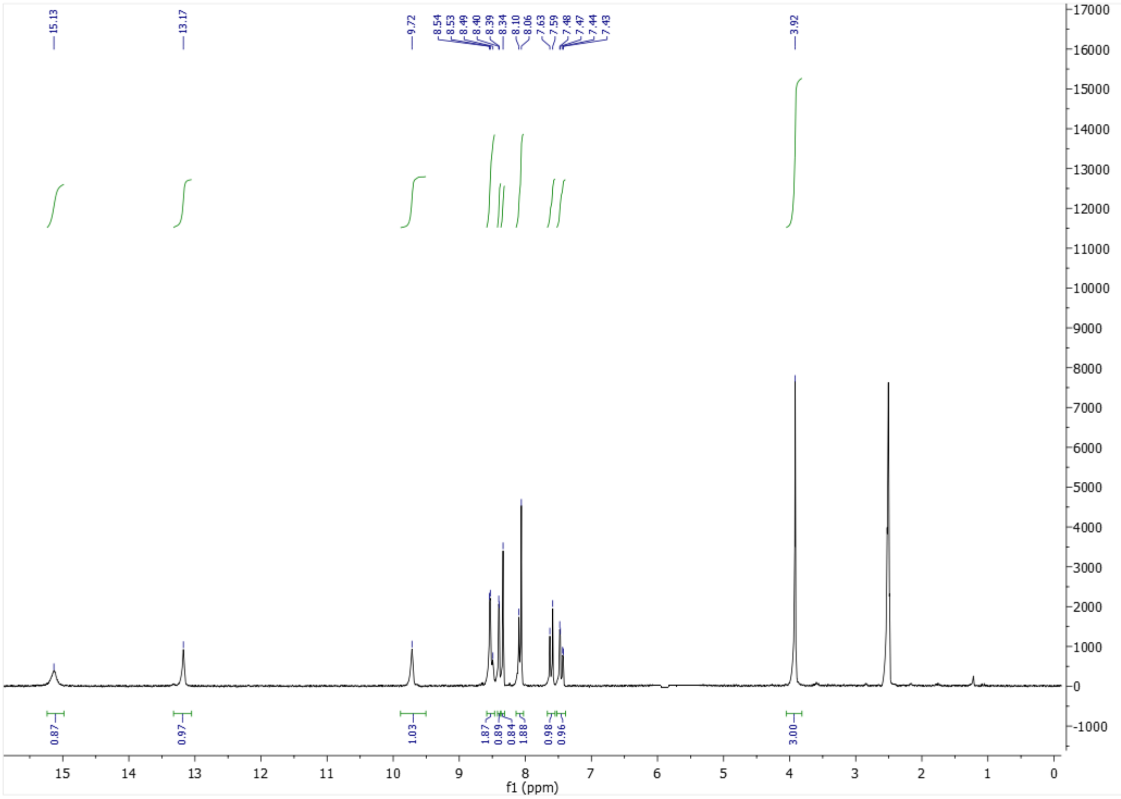

Figure S6. ^{1}H NMR spectra of 3-[2-(5-bromo-1-methyl-1*H*-indol-3-yl)-1,3-thiazol-4-yl]-1-methyl-1*H*-pyrrolo[3,2-*c*]pyridine hydrobromide (1l)

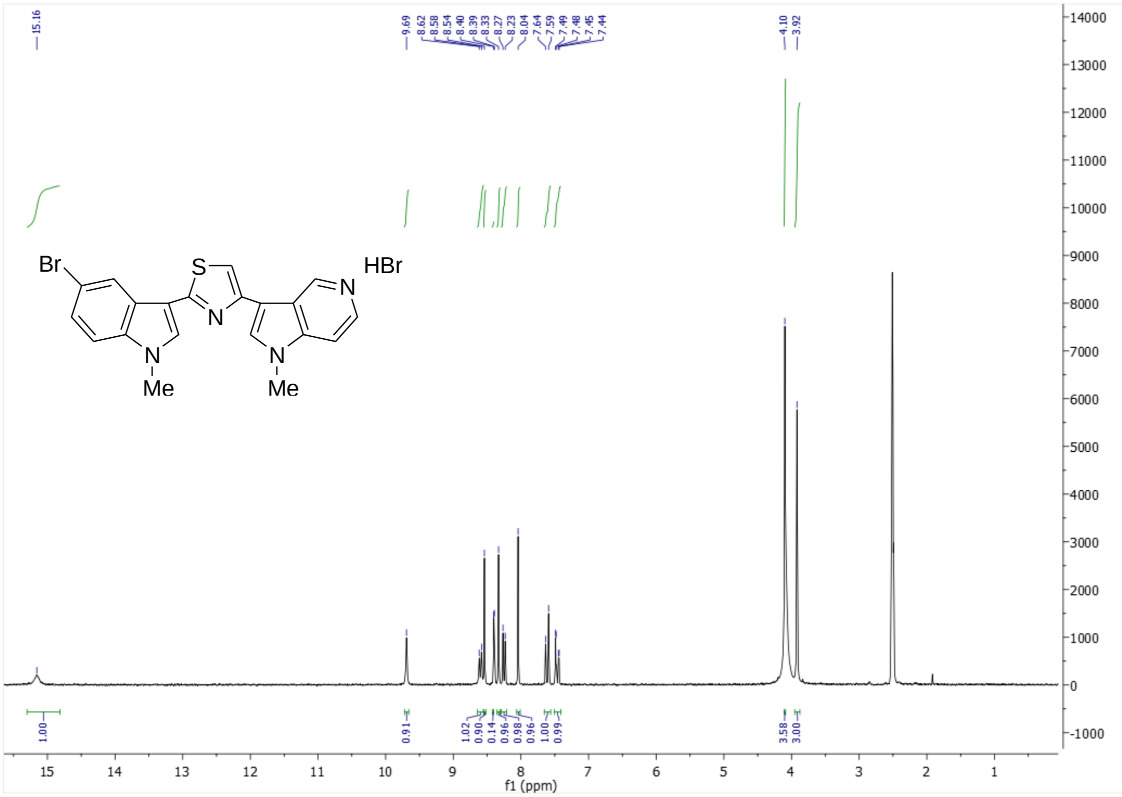

Figure S7. ^{1}**H NMR spectra of 3-[2-(5-fluoro-1-methyl-1*H*-indol-3-yl)-1,3-thiazol-4-yl]-1*H*-pyrrolo[3,2-*c*]pyridine hydrobromide (1m)**

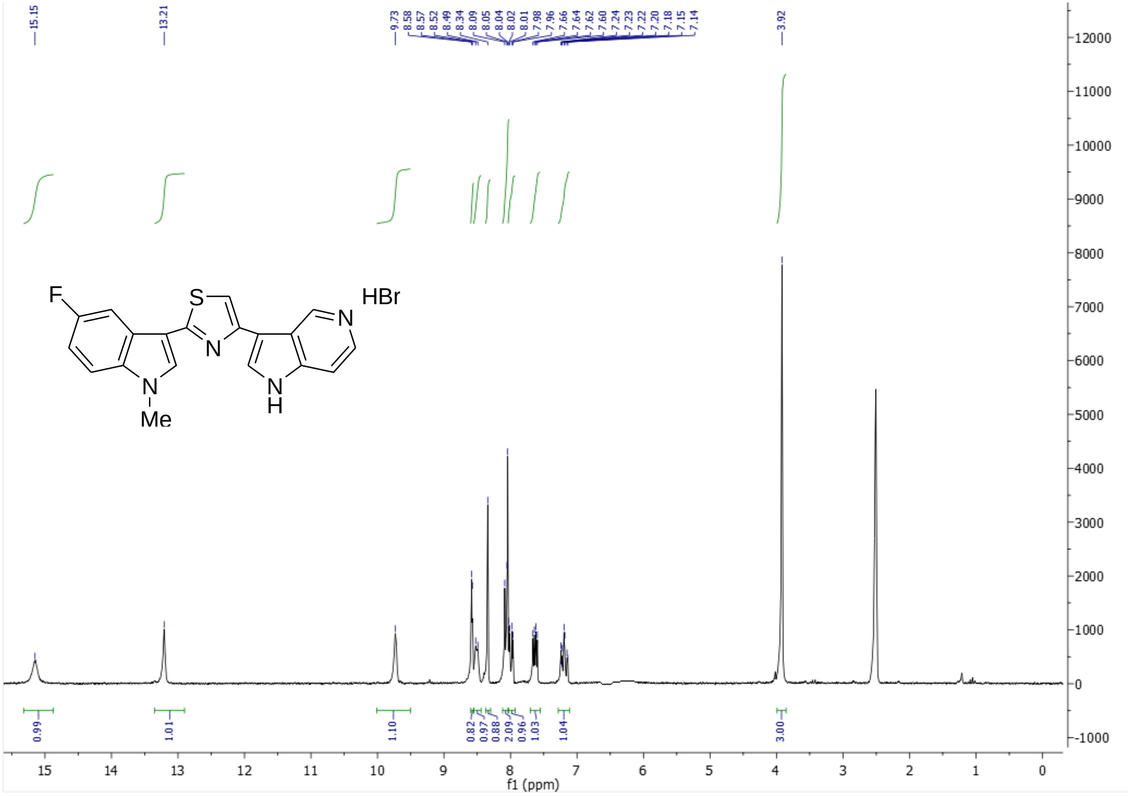

Figure S8. ^{1}**H NMR spectra of 3-[2-(5-fluoro-1-methyl-1*H*-indol-3-yl)-1,3-thiazol-4-yl]-1-methyl-1*H*-pyrrolo[3,2-*c*]pyridine hydrobromide (1n)**

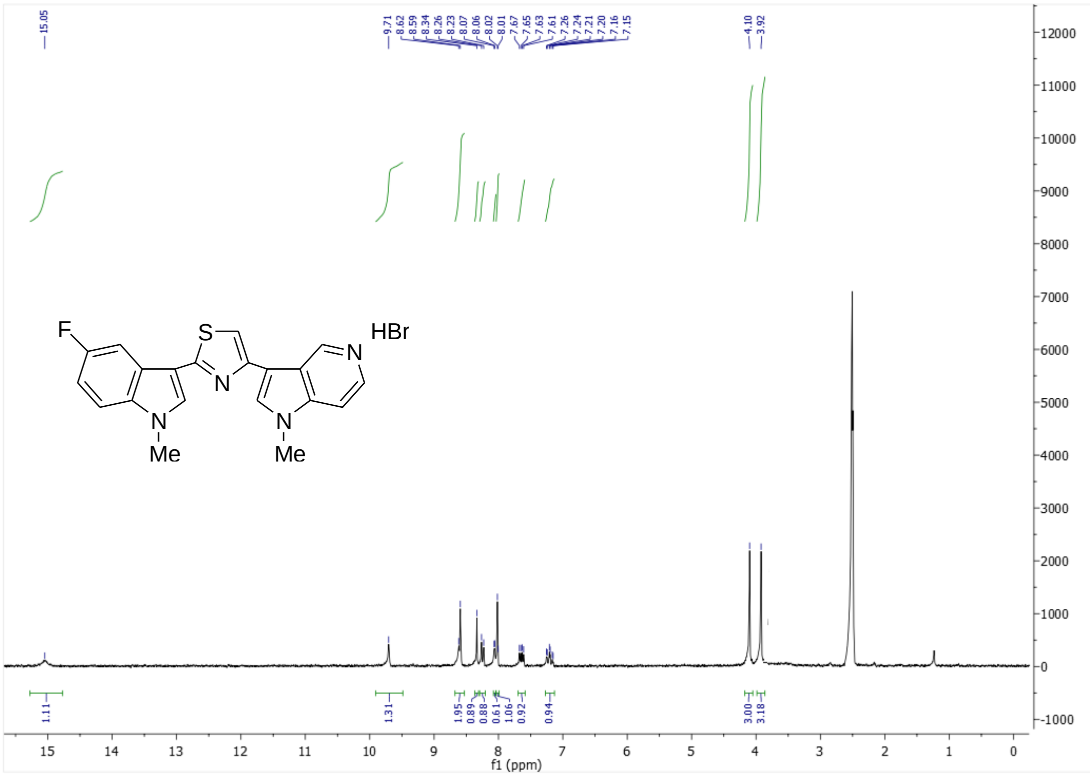

Figure S9. ^{1}H NMR spectra of 3-[2-(5-fluoro-1*H*-indol-3-yl)-1,3-thiazol-4-yl]-1*H*-pyrrolo[3,2-*c*]pyridine hydrobromide (1o)

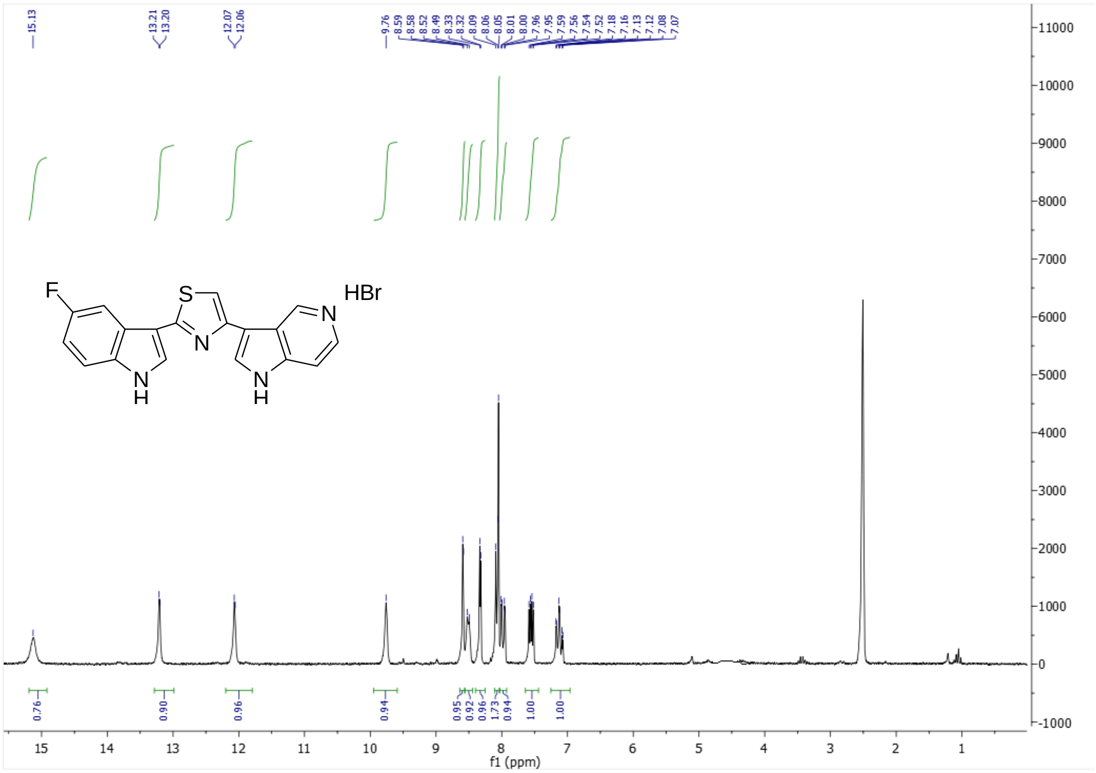

Figure S10. ^{1}H NMR spectra of 3-[2-(5-fluoro-1*H*-indol-3-yl)-1,3-thiazol-4-yl]-1-methyl-1*H*-pyrrolo[3,2-*c*]pyridine hydrobromide (1p)

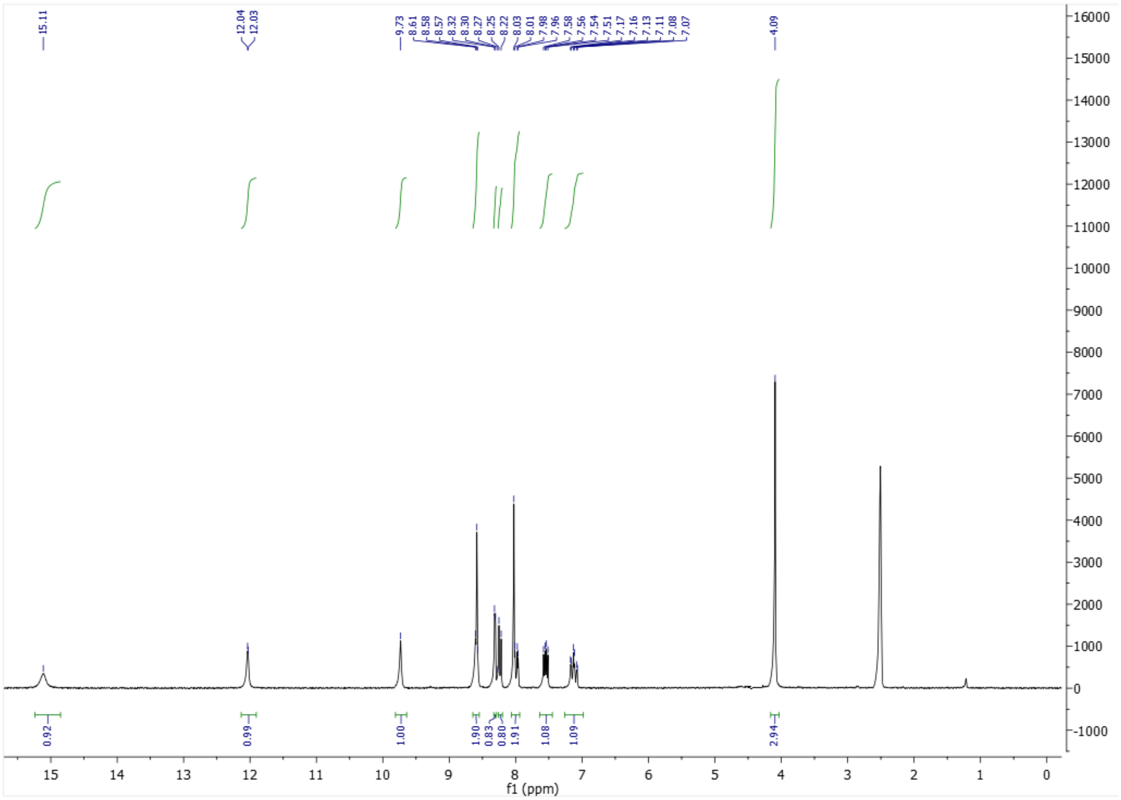

Figure S11. ^{1}H NMR spectra of 3-[2-(1*H*-indol-3-yl)-1,3-thiazol-4-yl]-1*H*-pyrrolo[3,2-*c*]pyridine hydrobromide (1q)

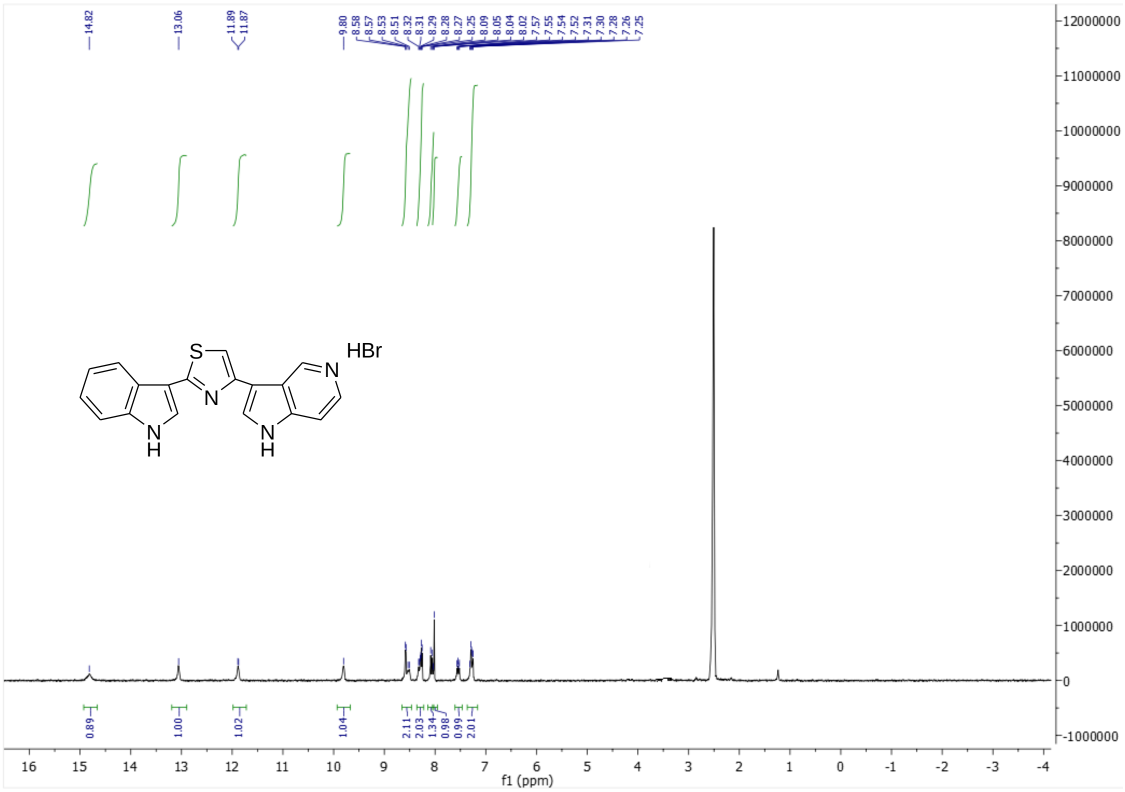

Figure S12. ^{1}H NMR spectra of 3-[2-(1*H*-indol-3-yl)-1,3-thiazol-4-yl]-1-methyl-1*H*-pyrrolo[3,2-*c*]pyridine hydrobromide (1r)

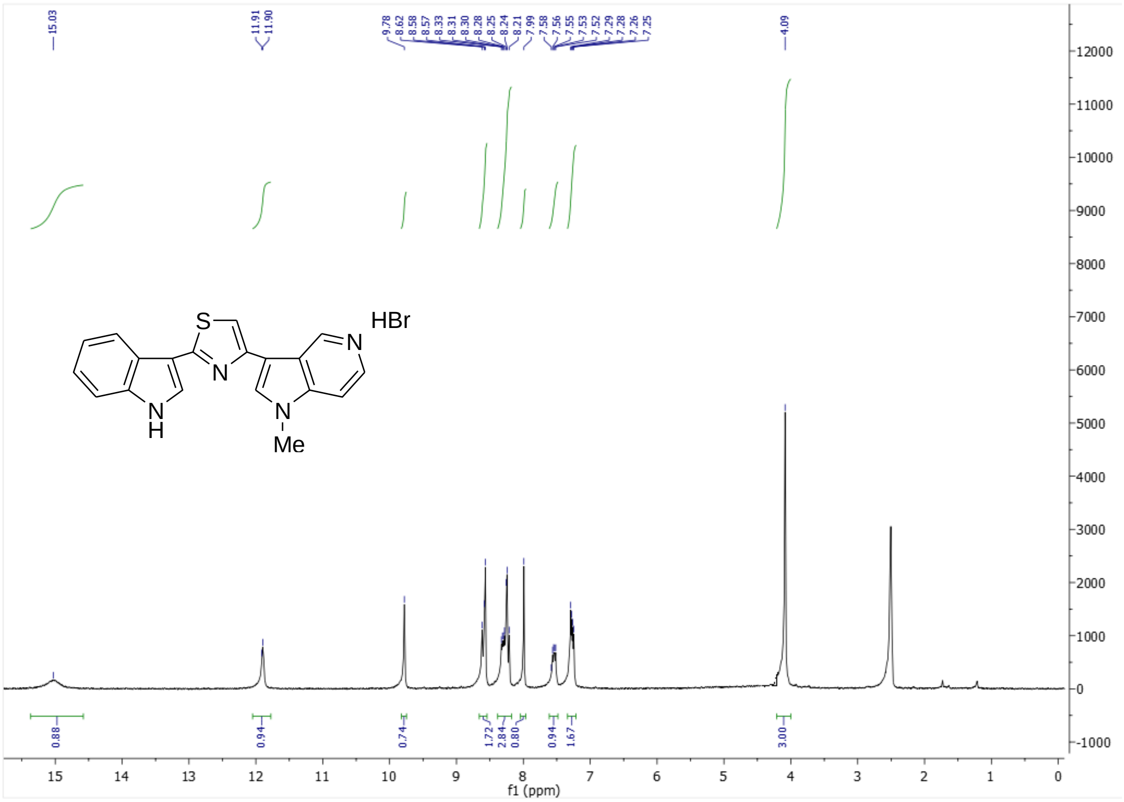

Figure S13. ^{1}H NMR spectra of 3-[2-(5-methoxy-1*H*-indol-3-yl)-1,3-thiazol-4-yl]-1*H*-pyrrolo[3,2-*c*]pyridine hydrobromide (1s)

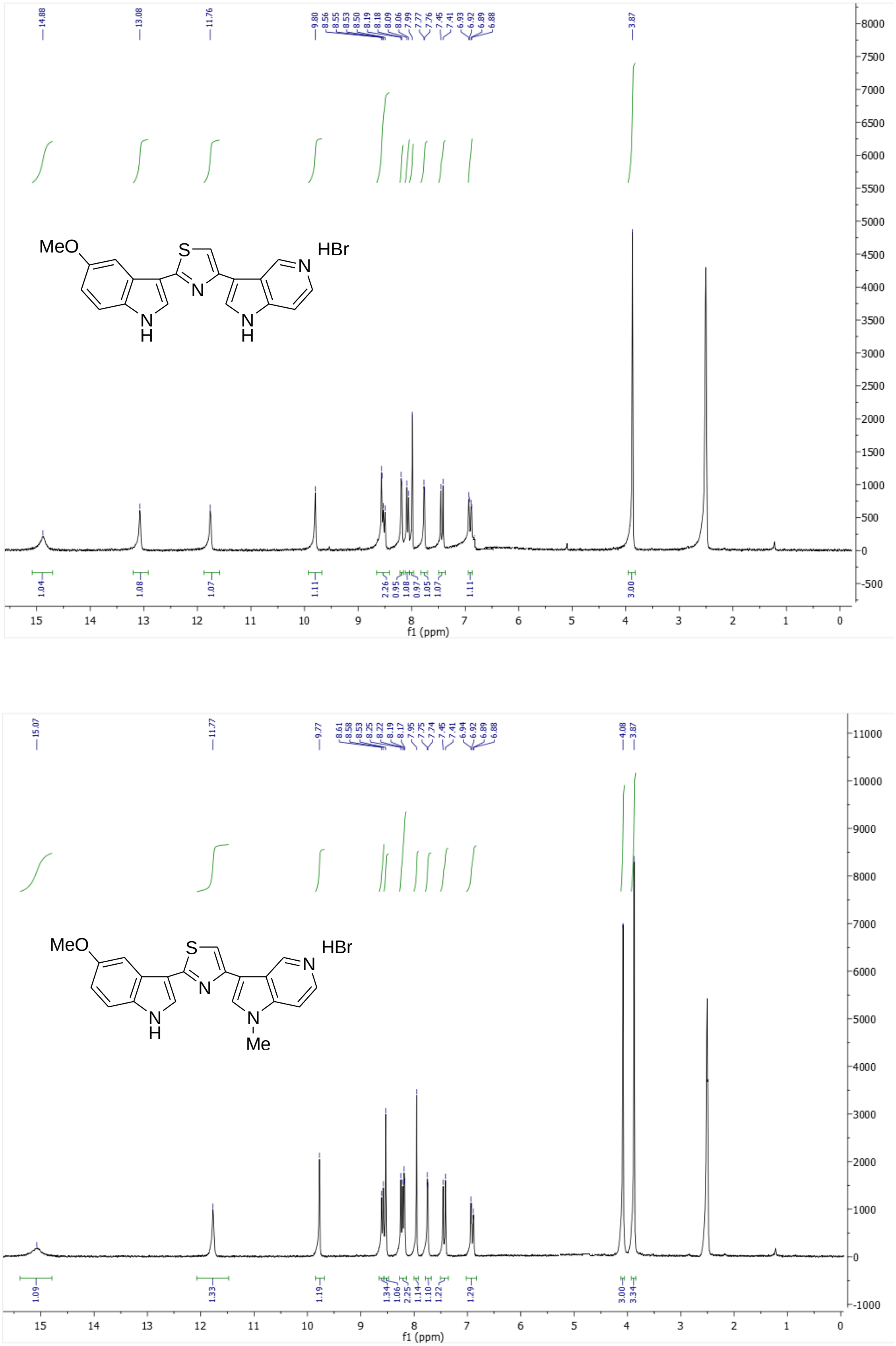

Figure S15. ^{1}H NMR spectra of 3-[2-(5-bromo-1*H*-indol-3-yl)-1,3-thiazol-4-yl]-1*H*-pyrrolo[3,2-*c*]pyridine hydrobromide (1u)

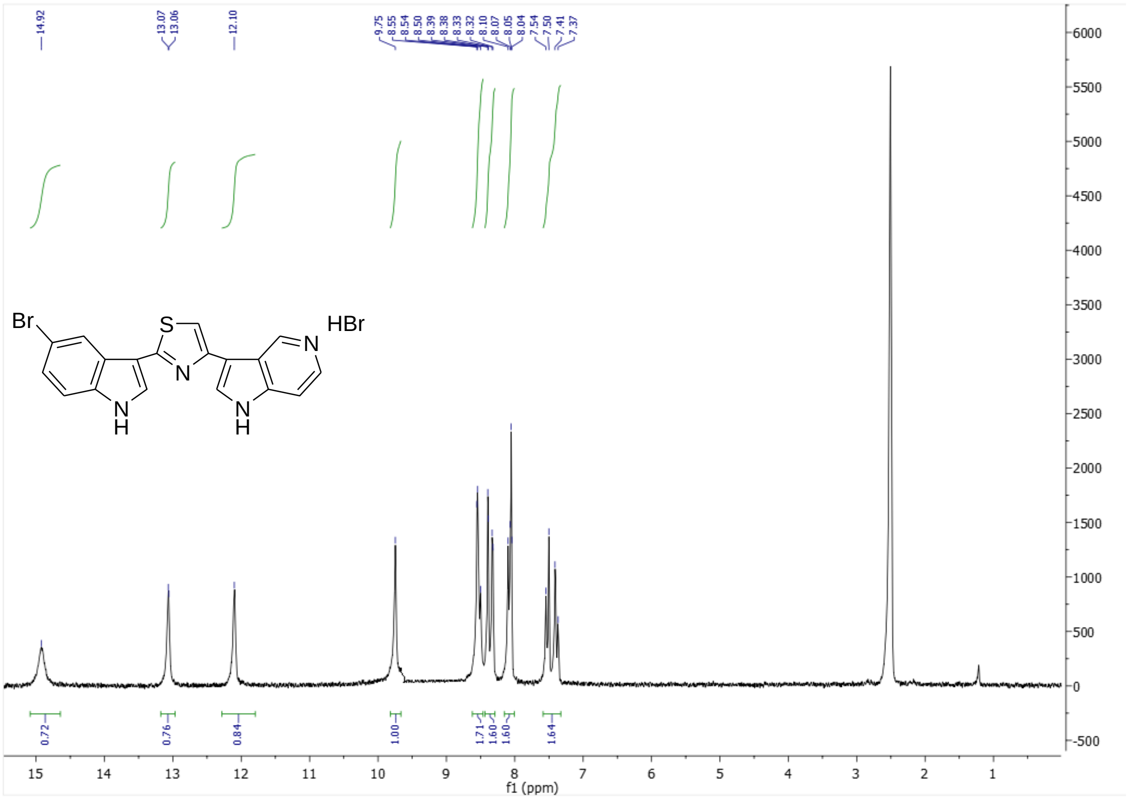

Figure S16. ^{1}H NMR spectra of 3-[2-(5-bromo-1*H*-indol-3-yl)-1,3-thiazol-4-yl]-1-methyl-1*H*-pyrrolo[3,2-*c*]pyridine hydrobromide (1v)

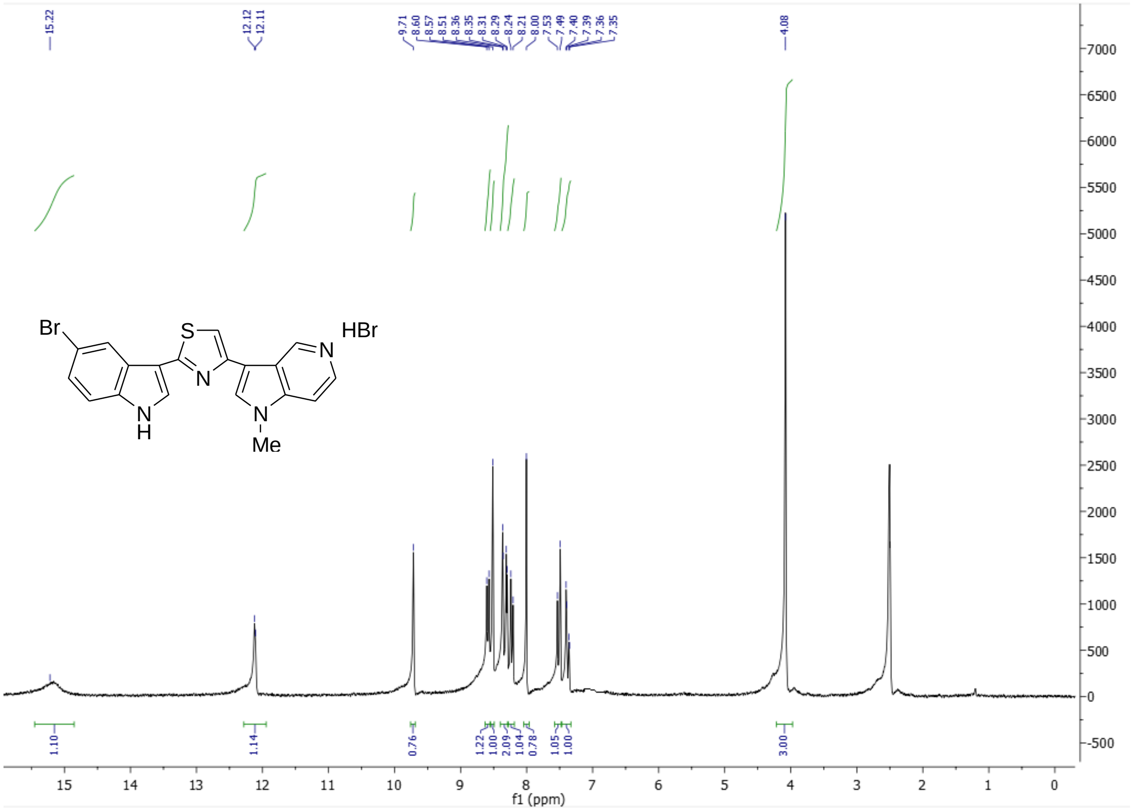

Part II

New therapeutic approaches against malignant mesothelioma

(Chapter 7,8)

Chapter 7

Splicing deregulation, microRNA and Notch aberrations: fighting the three-headed dog to overcome drug resistance in malignant mesothelioma

Dario P. Anobile,* Giulia Montenovo,* Camilla Pecoraro,*
Marika Franczak, Widad Ait Iddouch, Godefridus J. Peters,
Chiara Riganti, Elisa Giovannetti

Submitted to Expert Review of Clinical Pharmacology

* These Authors contributed equally to this study.

Splicing deregulation, microRNA and Notch aberrations: fighting the three-headed dog to overcome drug resistance in malignant mesothelioma

Dario P. Anobile,[1,2,*] Giulia Montenovo,[1,3,*] Camilla Pecoraro,[1,4,*] Marika Franczak,[1,5] Widad Ait Iddouch,[1] Godefridus J Peters,[1,5] Chiara Riganti,[2] Elisa Giovannetti[1,6]

[1]*Department of Medical Oncology, VU University Medical Center, Cancer Center Amsterdam, 1081HV Amsterdam, Netherlands;*
[2]*Department of Oncology, University of Torino, 10043 Orbassano, Italy;*
[3] *Department of Medicine and Surgery, University of Parma, 43126 Parma, Italy;*
[4]*Dipartimento Di Scienze E Tecnologie Biologiche Chimiche E Farmaceutiche (STEBICEF), Università degli Studi di Palermo, Palermo, Italy;*
[5]*Department of Biochemistry, Medical University of Gdansk, 80-210 Gdansk, Poland;*
[6]*Fondazione Pisana per la Scienza Pisa, 56100 Pisa, Italy.*

*equally contributed

ABSTRACT

Introduction. Malignant mesothelioma (MMe) is an aggressive rare cancer of the mesothelium, associated with asbestos exposure. MMe is currently an incurable disease at all stages mainly due to resistance to treatments. It is therefore necessary to elucidate key mechanisms underlying chemoresistance, in an effort to exploit them as novel therapeutic targets.

Areas covered. Chemoresistance is frequently elicited by microRNA (miRNA) alterations and splicing deregulations. Indeed, several miRNAs, such as miR-29c, have been shown to exert oncogenic or oncosuppressive activity. Alterations in the splicing machinery might also be involved in chemoresistance. Moreover, Notch signaling pathway, often deregulated in MMe, plays a key role in cancer stem cells formation and self-renewal, leading to drug resistance and relapses.

Expert opinion. The prognosis of MMe patients varies among different tumors and patient characteristics, and novel biomarkers and therapies are warranted. This work aims at giving an overview of MMe, with a special focus on state-of-the-art treatments and new therapeutic strategies against vulnerabilities emerging from studies on epigenetics factors. Besides, this review is also the first to discuss the interplay between miRNAs and alternative splicing as well as the role of Notch as new promising frontiers to overcome drug resistance in MMe.

Keywords

Chemoresistance, malignant mesothelioma, microRNA, splicing deregulation, Notch, cancer stem cells, targeted therapy.

Article highlights

- Malignant mesothelioma is a rare and aggressive cancer, characterized by a dismal prognosis and therapeutic options are limited. Therefore, it is mandatory to identify novel biomarkers and therapeutic targets, to improve prognosis and quality of life.
- Patients treated with the current chemotherapeutic regimen, based on pemetrexed and cisplatin, often develop resistance to treatment.
- Increasing evidence shows the pivotal role that microRNAs and spliceosome deregulation play in tumorigenesis and chemoresistance. Promising results from preclinical and clinical studies point into the direction of novel therapeutic agents targeting this interplay as a way to overcome chemoresistance.
- Similarly, overexpression of Notch signaling pathway has been associated to MMe chemoresistance and cancer stem cells (CSCs) formation, suggesting that Notch inhibition could represent a novel promising targeted therapy.

1. INTRODUCTION

Malignant mesothelioma (MMe) is an aggressive rare cancer of the mesothelium, a thin layer of tissue that covers the internal organs [1]. According to Globocan the number of new cases and deaths in 2020 were 30870 and 26 278, respectively [2]. The incidence rates among men are higher than women. This is typically attributed to the fact that MMe has been associated with asbestos exposure [3], both occupational and environmental, which is more frequent in men. This has been validated in workers who were exposed to asbestos in mining industries, construction and shipbuilding [4,5]. Indeed, all forms of asbestos have been classified as carcinogenic to humans (Group 1) by IARC [6].

2. MAIN FEATURES OF MALIGNANT MESOTHELIOMA

2.1 Different types of malignant mesothelioma

MMe can be classified into four subtypes: pleural, pericardial, peritoneal, and testicular. The 5-year relative survival rates differ amongst the subtypes and for US patients are: 9.5% for MMe of the pleura (malignant pleural mesothelioma, MPM) and pericardium, 24.9% for MMe of the retroperitoneum and peritoneum [7] and 49% for testicular MMe [8].

MPM originates from the pleura and is accountable for about 80-90% of all mesothelioma cases [1], being by far the most common type. PeM originates from the peritoneum and accounts for 20% of all mesothelioma cases [9]. Pericardial mesothelioma, which originates from the pericardium, accounts for 1% of the cases [10] and testicular mesothelioma which forms in the tunica vaginalis for < 1% [11].

In addition, based on a histological classification, MMe are divided into: epithelioid, sarcomatoid and biphasic [12]. The epithelioid cell type is the most common form of mesothelioma, accounting for 50-70% of all diagnoses, and is more sensitive to chemotherapy. Conversely, the sarcomatoid cell type is the least common cellular form (10% of all mesothelioma diagnoses) and is the most aggressive form of the disease. However, several molecular mechanisms play a pivotal role in MMe behavior, as well as in determining how treatments will affect a patient's prognosis.

2.2 Molecular mechanisms of mesothelioma and biomarkers

To date, the exact mechanisms leading to the development of MMe after asbestos exposure are not fully unraveled, although some of them have already been described [13].

Animal models and human studies have shown that asbestos fiber inhalation can lead to MMe, lung cancer and pulmonary fibrosis [14]. Of note, asbestos can be classified into two groups: amphiboles and serpentine. The longer and thinner amphibolic fibers can penetrate deeper into the respiratory system [15] and increase the likelihood of neoplastic diseases [14].

There are four known mechanisms by which asbestos can lead to carcinogenesis in mesothelioma [16]. The primary mechanism inducing cellular alterations and chronic inflammation is reactive oxygen species formation, subsequent to inefficient phagocytosis of asbestos fibers by macrophages. This process leads to DNA damage. Secondly, asbestos may lead to chromosomal structural abnormalities and aneuploidy of mesothelial cells if they are engulfed, thus leading to disruption of the mitotic spindles. Additionally, asbestos fibers have the ability to absorb proteins and chemicals which can lead to accumulation and deficiency of cellular proteins for mesothelial cells. Lastly, these asbestos-exposed cells release tumor necrosis factor-alpha, interleukin-1β, transforming growth factor-β and platelet-derived growth factor which induce inflammation and tumor progression. Mesothelial cells also release high-mobility group box 1 protein and then undergo necrosis, a process leading to an inflammatory response.

All these processes lead to DNA damage and aneuploidy and will potentially give rise to cancer cells due to genomic instability and epigenetic alterations [1]. Frequently occurring mutations involve tumor suppressor genes such as *CDKN2A*, *TP53*, *NF2* and *BAP1 (BRCA-1 Associated Protein 1).* Epigenetic alterations, on the other hand, will lead to deregulation of non-coding RNA (ncRNA) and changes in methylation.

The most common alterations observed in mesothelioma are acquired and germline mutations in the tumor suppressor gene *BAP1* [1], occurring in 60% of mesothelioma cases. *BAP1* is located on the short arm of chromosome 3 at position 21.1. It contains 17 exons and the protein consists of 729 amino-acids [17].

In the nucleus BAP1 has a role in maintaining genomic stability by regulating cell proliferation via host cell factor-1 (HCF-1) deubiquitination [18]. BAP1 also interacts with histone-modifying complexes during cell division [19].

In addition, BAP1 exerts functions in the cytosol, where it modulates calcium release through binding and deubiquitination of the type 3 inositol-1,4,5-triphosphate receptor (IP3R3) in the endoplasmic reticulum (ER), promoting apoptosis [1]. BAP1 is thus essential for cell proliferation, as reduced levels of the protein lead to genomic instability and decrease apoptosis, leading in turn to malignant transformation.

The molecular alterations sustaining MMe carcinogenesis could serve a diagnostic purpose to timely detect mesothelioma. Besides, there is an unmet clinical need for minimally invasive tests with high specificity and sensitivity that are able to distinguish between benign and malignant forms, and that can predict prognosis, monitor treatment response and are detectable in all biological samples [20]. Some of the current diagnostic limitations could be overcome by liquid biopsies, which are less invasive, faster and cheaper than tissue biopsies.

Despite not being yet integrated into the clinical practice, a recent study paves the way for the usage of pleural effusion and plasma as a source of circulating tumor DNA (ctDNA), offering the possibility to improve the patients' clinical management [21]. Furthermore, among all the circulating tumor-derived materials, other interesting candidates are circulating tumor RNA (ctRNA), proteins, circulating tumor cells (CTC) and extracellular vesicles (EV) [Figure 1].

A very promising biomarker candidate for MMe detection with liquid biopsies is Soluble Mesothelin Related Peptide (SMRP) [22,23] although its cutoff levels need to be further investigated [24]. Others have been recently described in an extensive review on state of the art, pitfalls, and perspectives of liquid biopsy-based studies in MMe patients [25].

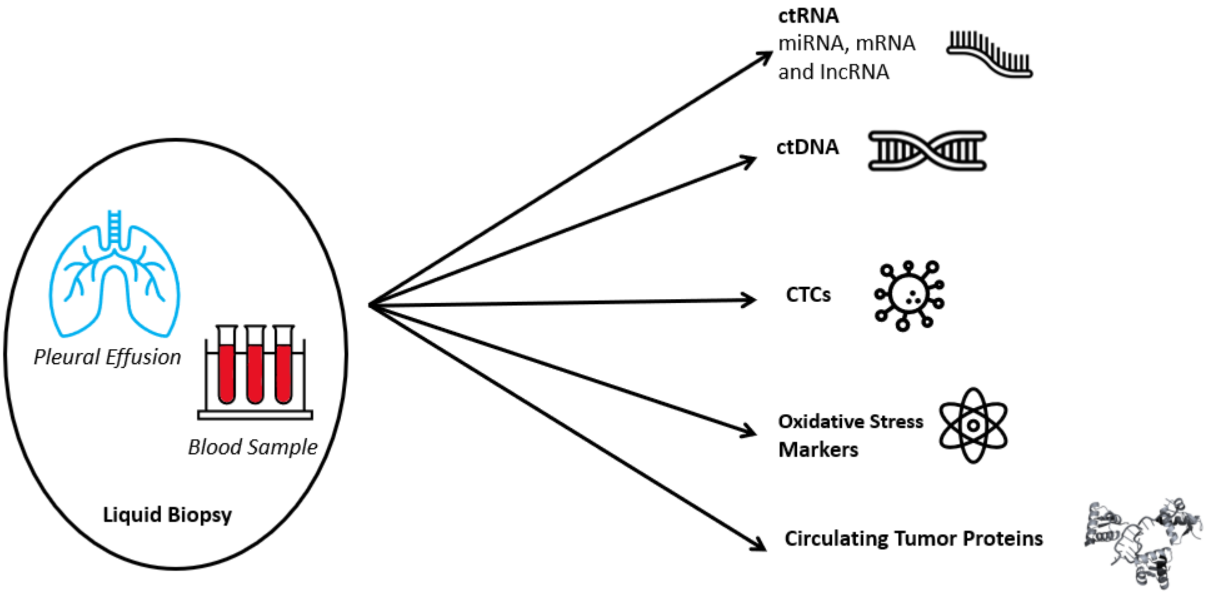

Figure 1 . Liquid biopsyies can overcome some of the current diagnostic limitations in MM. Circulating tumor-derived materials such as ctRNA, ctDNA, CTCs, Circulating Tumor Proteins and Oxidative Stress Markers could be used as diagnostic markers

3. THERAPEUTIC STRATEGIES FOR MESOTHELIOMA

3.1 Pleural mesothelioma

Available treatment options for MPM are limited and they are highly dependent on the resectability of the disease. Furthermore, primary tumors are often located near vital organs, making surgery extremely challenging. Indeed, the few available randomized trials assessing the benefit of surgery (extrapleural pneumonectomy [EPP] and video-assisted thoracoscopic partial pneumonectomy) highlight its controversial role as a valid therapeutic option, as it may be a choice for patients with stage I-III resectable disease, solely to improve clinical symptoms [26,27]. Nevertheless, the data of a randomized study suggested that EPP offers no benefit and conceivably harms patients [28].

Of note, recent evidence assessing the role of intrathoracic therapy, namely Hyperthermic intrathoracic chemoperfusion (HITHOC), state its beneficial role in improving the effects of surgery. This procedure is carried out by performing infusion of cisplatin followed by doxorubicin and mitomycin C at 41–43°C for 60–90 min. This maximizes the local effect of the chemotherapeutic agents, while decreasing systemic toxicities. On the other hand, this procedure bears a significant risk of acute kidney injury (AKI), but overall HITHOC was judged to be a safe and effective adjunct to surgery [29].

In selected patients with locally advanced disease a multidisciplinary evaluation is mandatory in order to provide them with the best treatment options according to their clinical characteristics. The role of neoadjuvant chemotherapy was recently investigated by Voigt and colleagues, who showed that

MPM patients receiving neoadjuvant chemotherapy had worse postresection survival compared to MPM patients who had undergone surgery immediately after diagnosis [30]. On the contrary adjuvant therapy does not affect surgery but may be insufficient because of poor tolerance, which can lead to dose reductions, treatment delays or even termination of therapy [26]. So far, there are no scheduled trials to compare neoadjuvant chemotherapy and resection with resection and adjuvant chemotherapy. For patients who have undergone EPP and (neo)adjuvant chemotherapy, adjuvant radiotherapy may be considered and this approach is called “trimodality therapy” [31].

As for the therapeutic agents of choice, the standard first line chemotherapy treatment in MPM has been cisplatin and pemetrexed for more than fifteen years [32], but resistance represents one of the most important challenges in MPM treatment [33]. The drug-drug interactions, cross resistance and resistance mechanisms regarding these key drugs are not well understood in MPM [34]. However, only a few studies identified potential predictors of responsiveness to chemotherapy such as increased gene expression of thymidylate synthase and reduced expression of proton-coupled folate transporter (PCFT), which can cause resistance to pemetrexed [35,36].

Patients who are ineligible for surgery are treated with palliative systemic chemotherapy. This treatment consists of four to six cycles of pemetrexed and platinum-based agents. For elderly patients, the platinum-based agent carboplatin can be used instead of cisplatin, because it is better tolerated and easier administered [37]. This replacement does not influence the progression free survival (PFS) [32].

Currently, there is no licensed chemotherapy for patients who relapsed after treatment with platinum-based chemotherapy. Thus, there is a huge unmet need for effective therapy for this class of patients, although some phase III studies have suggested potential efficacy of carboplatin/gemcitabine, or vinorelbine [38]. Despite the challenges, there are some novel randomized studies about possible alternative therapies for MPM, including radiation, antiangiogenic drugs, targeting inflammation and stem cell pathways and immunotherapy.

Unfortunately, a phase III trial exploring the possibility to exploit neurofibromin 2 (NF2) as potential therapeutic target of defactinib, a small molecule FAK inhibitor, failed to show any improvement in PFS or overall survival (OS). Nonetheless, NF2 loss has been shown to disrupt several pathways in MPM, especially Hippo-Yap-Taz, paving the way for further evaluation of mTOR inhibitors and YAP/TAZ inhibitors [27].

Another novel therapeutic target was discovered by Xu and colleagues, by performing Clustered Regularly Interspaced Short Palindromic Repeats (CRISPR) screening. They found that WEE1 contributes to pemetrexed/cisplatin resistance in MPM by deregulating G_2-M checkpoint which leads to accumulation of DNA damage and apoptosis. The inhibition of WEE1 sensitized MPM cells to the first line chemotherapy [39].

A recent multicenter, randomized, open-label phase III trial compared the use of first-line nivolumab-ipilimumab versus platinum-pemetrexed chemotherapy. The Immune Checkpoint Inhibitors (ICI) combination regimen provided significant and meaningful improvements in overall survival (OS), thus supporting its approval in the USA as of October, 2020 as a new standard of care in treatment-naive MPM patients, especially in those with non-epithelioid histology [40].

Despite these encouraging results, resistance mechanisms to ICI were observed, however, no specific underlying mechanism was identified to explain a causal connection between ICI administration and resistance.

Therefore, immunotherapy may be linked with other therapies, such as epigenetic therapy in light of the advantageous co-administration. Indeed, it has been established that histone deacetylase inhibitors (HDACi) and DNA methyltransferase exert an immunoprobing effect not only in other malignancies (i.e., melanoma and lung cancer), but also in mesothelioma preclinical studies [41–44].

Moving forward this direction, promising outcomes were also observed to the association of Notch signaling pathways inhibitors, (e.g., anti-Jagged therapies) and immune checkpoint blockade therapies (ICBT), considering the involvement of Notch pathway in the proper functioning of the immune response, the host immune system could be influenced by Notch inhibitors and consequently respond better to ICBT and achieve a synergistic effect making possible the use of even a lower dosage of ICBT and reduce toxicity [45].

Despite the significant advances in cancer immunotherapy, there still remain other outstanding questions, such as serious adverse events and hyper-progression. For instance in the DREAM trial, two MPM patients were reported as showing pseudo-progression, within the first 10–15 weeks of therapy followed by responses [46,47]. For this reason, further correlative studies are needed to provide a better and more comprehensive understanding of ICI usage in mesothelioma.

3.2 Peritoneal mesothelioma (PeM)

Although there are limited therapeutic strategies, the available options for PeM have progressed during the last few years. The therapeutic approach has indeed evolved from systemic chemotherapy and palliative surgery to aggressive cytoreductive surgery and perioperative intraperitoneal chemotherapy [48]. Cytoreduction removes all the macroscopic disease and is then followed by hyperthermic intraperitoneal chemotherapy (HIPEC), where cisplatin or mitomycin are commonly used to address any remaining microscopic disease [49]. This approach led to increased survival among preterminal patients and is now the standard practice [48]. It achieves a median survival of approximately 30 months. This treatment has to be offered to selected patients, where the prolonged survival must be weighed cautiously against the potential risk. The inclusion criteria for this treatment comprehend being fit for chemotherapy and having an absence of extra abdominal metastases and a low volume of peritoneal disease [50]. It is currently unknown which HIPEC chemotherapy regimen is the most effective as there are no clinical trials that have assessed this [51]. However, some studies have found that the administration of cisplatin leads to a more favorable survival compared to mitomycin [52,53]. The pharmacokinetic advantage of HIPEC is that high regional concentrations can be achieved because of the slow rate of movement of the drug into plasma which keeps the systemic drug levels low [49]. This can be obtained because of the peritoneal-plasma barrier, which sustains a high concentration gradient of chemotherapeutic drug between the peritoneal cavity and the plasma concentration, also leading to limited systemic cytotoxicity. Overall, the survival outcomes in PeM have been improved by cytoreduction with HIPEC. However, this procedure has a relevant morbidity rate, and chemoresistance is still an issue.

A novel minimally invasive drug delivery system [9], Pressurized Intraperitoneal Aerosol Chemotherapy (PIPAC) optimizes homogeneity of drug distribution by applying aerosols instead of a liquid solution and increased intraperitoneal hydrostatic pressure to counteract the elevated intratumoral interstitial fluid pressure. In addition, it also limits blood outflow during the drug application. Its use in palliative therapy of PeM is now being evaluated in randomized controlled trials [54,55]. Nevertheless, aerosols cannot reach some closed spaces within the peritoneal cavity, especially if there are enteroenteric and enteroparietal adhesions following surgery. This implies that PIPAC is not effective in patients who have developed a recurrence after cytoreductive surgery (CRS) and HIPEC [9], so PIPAC should be performed in the early phases of PeM instead.

Systemic chemotherapy on the other hand leads to a median survival of one year, which is comparable with a palliative approach and it is the treatment of choice for patients who are ineligible for resection [48].

The therapeutic challenges outlined so far increased the interest in identifying molecular targets to design novel efficacious therapies [51]. One of the new molecular targets identified so far is mesothelin, which is highly expressed in MMe and has a limited expression in normal human tissues. To date there are several agents targeting mesothelin: MORAb-009, a chimeric anti-mesothelin monoclonal antibody; CRS-207, a live-attenuated Listeria monocytogenes vector encoding human mesothelin; SS1P, a recombinant immunotoxin targeting mesothelin; LMB-100, a humanized anti-mesothelin Fab fragment with a newly designed PE which is less immunogenic than SS1P [22,56]. The most extensively evaluated anti-mesothelin in MMe is SS1P. One problem of this drug is the formation of antidrug antibodies, ultimately leading to inefficacy of SS1P. Nonetheless, it has been shown that one way of delaying the antibody formation is by combination with pentostatin and cyclophosphamide, a lymphocyte-depleting drug regimen [56]. In a phase I study, SS1P was given as a continuous infusion in 24 patients of which five had PeM. In one of these five patients short term resolution of ascites has been shown [57]. Other clinical studies using a bolus or continuous infusion showed no significant advantage [57]. Intraperitoneal administration of SSP1 could be potentially useful for PeM treatment, but up until now, there is no study investigating this [58]. LMB-100 is a less immunogenic alternative to SSP1. This anti-mesothelin immunotoxin was effective in different mesothelin expressing cancer cell lines and tumor xenograft models [59]. An ongoing phase I study is currently assessing the safety, pharmacokinetics and activity of LMB-100 in patients with advanced pleural or peritoneal mesothelioma that did not respond to platinum-based chemotherapy [59]. Another potential drug candidate for PeM is FTY720, an FDA-approved drug used to treat relapsing forms of multiple sclerosis [60]. FTY720 is a sphingosine analogue that, when phosphorylated, functions as an agonist for four of the five S1P receptors (S1P1, S1P3, S1P4, and S1P5) [61], inducing internalization and degradation of S1P1 [62] and ultimately leading to reduced inflammation [63,64] [Figure 2]. Nevertheless, so far, the effect of this targeted drug on the prognosis of PeM is limited, thus, other factors must play a role in the chemoresistance, including poor vascularization and increased fluid pressure of peritoneum as well as the mesothelial-mesenchymal transition during tumor progression [9].

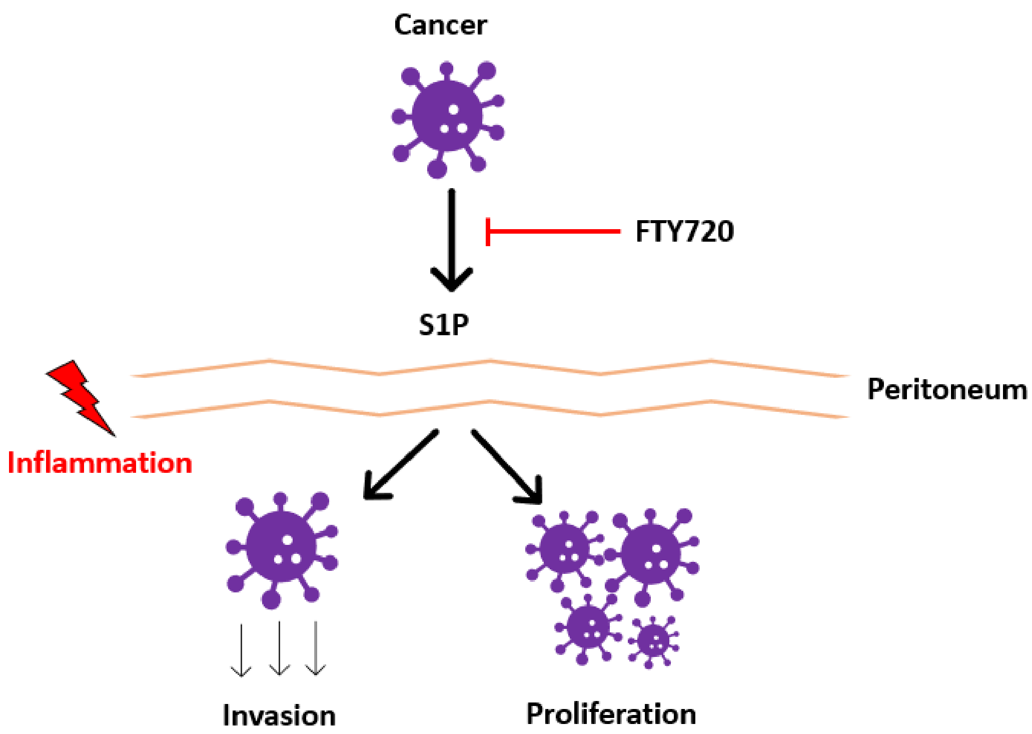

Figure 2. Targeting S1P in peritoneal mesothelioma with FTY720. S1P induces inflammation and proliferation, promoting the development of peritoneal mesothelioma. Thus, FTY720 can be a promising drug for PeM treatment

4. EPIGENETICS IN MESOTHELIOMA

High-throughput analyses, such the TCGA-MESO study, including cases with comprehensive DNA, RNA, and epigenetic profiles of 87 MPM patients, have unraveled pivotal genomic and epigenomic alterations driving MMe [65]. In addition, increasing evidence indicates that chemoresistance of MMe is due to epigenetic errors leading to aberrant gene expression in cancer cells [66].

Regarding novel epigenetic therapies, *in vivo* experiments performed by LaFave and colleagues using *BAP1*-mutant cell lines showed that epigenetic therapies may have a pivotal impact in treating this mutant cancer type. Indeed, they demonstrated a linkage between Enhancer Of Zeste 2 Polycomb Repressive Complex 2 Subunit (EZH2) mRNA expression and *BAP1* mutational state.

Silencing *EZH2* with the small-molecule EZH2 inhibitor EPZ011989 abrogated *in vivo* tumor formation of *BAP1*-mutant, but not of wild-type, cell lines. Thereby, the authors conclude that *EZH2* is a potential therapeutic target in *BAP1*-mutant cancer cells [67].

4.1 DNA methylation

The nucleosome consists of 147 base pairs of DNA wrapped twice around an octamer of H2A, H2B, H3 and H4 core histones. Covalent modifications of this region can regulate gene expression and include: acetylation, methylation, ubiquitination, phosphorylation and SUMOylation.

The most important epigenetic mechanism is DNA methylation. This process occurs almost exclusively in CpG sites and is carried out by the DNA methyltransferase enzymes (DNMT), mainly DNMT1, DNMT3A and DNMT3B, that mediate the transfer of a methyl group at the 5-carbon of the cytosine ring of DNA.

Epigenetic modifications are often observed in cancer cells and can have an impact on several aspects, such as intratumoral heterogeneity and resistance to therapy.

Kim et al. evaluated the epigenetic mechanisms involved in the tumor cell heterogeneity using side population (SP) and non-SP cells isolated from MS-1, a human malignant mesothelioma cell line [68]. The cancer cells were analyzed by methylated DNA immunoprecipitation combined with high-throughput sequencing (MeDIP-seq) and RNA-seq methodology. They identified changes in DNA methylation in 122 genes, of which 118 genes were hypermethylated and thus downregulated and 4 genes were hypomethylated and thus upregulated.

DNA methylation can indeed impact on patients' survival and prognosis, as found by Fischer and colleagues, who showed an association between OS and methylation of nine gene specific promoters in serum DNA of 43 patients with MMe, including pleural and peritoneal subtypes [69]. The combination of the hypermethylated tumor suppressors *RAR beta*, *DAPK* and *RASSF1A* was associated with shorter overall OS compared to patients who had only one or no gene methylated.

Furthermore, preclinical studies on H28, MSTO-211, H2452 and H2052 MPM cells suggested that targeting PCFT-promoter methylation through 5-aza-2′-deoxycytidine-mediated demethylation might eradicate pemetrexed-resistant cells characterized by low-PCFT expression [36].

4.2 Acetylation

The second most studied epigenetic mechanism is acetylation [70]. This process is carried out by histone acetyltransferase (HAT), an enzyme transferring an acetyl group from Acetyl-Coenzyme-A to histones, increasing gene expression. Histone deacetylase (HDAC), on the other hand, is involved in deacetylation, a process consisting of the removal of an acetyl group and resulting in decreased gene transcription.

Novel therapeutic approaches targeting HDACs are currently being investigated. Valproic acid, an HDAC inhibitor, when combined with doxorubicin has shown promising results in patients with refractory or recurrent MMe, for which no standard therapy was available [71].

Recently, Sphingosine kinase 1/sphingosine-1-phosphate (SphK1/S1P) has been shown to play an essential role in growth and development of both the epithelial and sarcomatoid subtypes of MMe, supporting its potential as a new therapeutic target [72]. SphK1 is a lipid kinase which generates S1P by phosphorylating sphingosine.

Intracellularly S1P is involved in epigenetic regulation of NF-kB signaling, by regulating its target proteins: HDACs and the E3 ubiquitin ligase tumor-necrosis factor receptor-associated factor 2 (TRAF2) [51]. S1P is also involved in calcium homeostasis, suppression of apoptosis, cell motility and cell growth [72]. On the other side, ABC transporters and Sphingolipid Transporter 2 allow S1P to be exported outside the cell where it acts as ligand for five G protein coupled receptors (S1PR1-5). In addition, S1P regulates several extracellular processes, including growth and differentiation, survival, immune defense, angiogenesis and cytoskeletal rearrangements and motility [72]. Therefore, S1P can be involved in several pathologic processes including cancer due to its role in angiogenesis, cell survival/proliferation and lymphocyte trafficking [51], as well as in metastasis through the release of the S1P receptor (S1P2) in exosomes [73].

A study by Karel and collaborators demonstrated that mesothelioma cells retain higher levels of SphK1 and SphK2 mRNA as well as higher levels of SphK1 protein and that cell proliferation is regulated by SphK1 through H3 and H4 histones acetylation signal transduction [72]. Furthermore, they showed that the exposure of mice peritoneum to multi walled carbon nanotubes, mesothelioma inducing agents, led to a higher percentage of inflammation and granulomatous nodules in WT mice compared to SphK1-null mice, thus suggesting an *in vivo* role of SphK1 in the promotion of MMe. Using the SphK1 inhibitor, SphK-I2, or gene silencing, S1P production and cell proliferation are reduced in MMe cells, and further studies evaluate FTY720 which is mainly phosphorylated in vivo by SphK2 and then target both inflammation and S1P signaling [Figure 2].

4.3 MicroRNAs

MicroRNAs (MiRNAs) consist of 18-22 nucleotides and belong to the non-coding transcriptome. They play a role in gene expression by binding to the 3'untranslated RNAs region [74]. Perfect binding to mRNA leads to deadenylation and degradation of mRNA while imperfect binding leads to translational inhibition with different biological consequences. An example of a downregulated miRNA in MPM is miR-223 whose overexpression reduces stathmin levels and inhibits cell motility [75]. Similarly, an increase in cellular levels of miR-214 leads to anti-proliferative and anti-migratory effects [76].

MiRNAs are commonly dysregulated in various cancer types, including MMe [1] and their expression patterns are tumor-specific. This makes it possible to use them as (early) diagnostic, prognostic and therapeutic tools. In addition, they can also serve as a tool to determine the severe side-effects that occur during and after cisplatin therapy, as elevated levels of miR-21, miR200c and miR-423 were detected in AKI in cisplatin-treated MPM patients [77].

The role of miRNAs as predictive biomarkers has already been investigated in different types of aggressive cancers, such as pancreatic ductal adenocarcinoma. For example, overexpression of the oncomir miR-21 has been associated with worse outcome after gemcitabine treatment, leading to shortened OS and disease-free survival, as reviewed by Capula and collaborators [78].

Table 1 gives an overview of the microRNAs identified in MMe which could be implemented in the clinic for diagnostic and prognostic purposes [1]. Of note, miRNAs can be isolated from tissues and body fluids, including blood, urine and saliva [79].

One of the most promising prognostic biomarkers is miR-29c, since it has the ability to differentiate from patients with poor prognosis and patients with good prognosis, irrespective of histology [98].

The appeal for miRNA implementation as a therapeutic option descends from their ability to target multiple genes and thus influence multiple pathways [98]. For instance, miR-34 b/c is a tumor suppressor miRNA investigated in various cancers and it is downregulated in MPM because of methylation of the promoter. This has been demonstrated by *in vitro* studies where methylation of this miRNA was detected in 85.1% of the MPM samples [99]. After re-expression of this miRNA a decrease in proliferation, motility, migration and invasion suppression could be detected. The antitumor effect has also been demonstrated *in vivo* where an adenovirus-mediated miR-34b/c gene therapy in BALB/C mice has shown a statistically significant growth inhibition of the tumor volume [100].

Similar results were observed *in vitro* after the re-expression of miRNA-1 which is also found to be downregulated in MPM [101]. Furthermore, miR-16 and miR-193a-3p restoration both *in vitro* and *in vivo* showed similar tumor suppressor effects [102,103].

Another finding supporting the possibility to therapeutically employ miRNAs comes from the use of Onconase (Ranpirnase), an enzyme which degrades RNA and has therapeutical properties. The anti-tumor effect achieved in MPM cell lines treated with this drug is mediated by the upregulation of miR-17 and the downregulation of miR-30 [104].

EphrinA1 treatment achieves inhibition of tumor growth and proliferation in MPM cell lines through a similar mechanism, upregulating the tumor suppressor miRNA let-7 and subsequently leading to the downregulation of *RAS* oncogene [105].

However, the implementation of these promising miRNAs in the clinical setting is challenging [2], [98]. The first problem is the scarcity of validation studies on the specific role of miRNAs in this malignancy due to its low incidence rate [98].

Additionally, the usage of different sample size and sources, including Formalin-Fixed Paraffin-Embedded specimens, fresh frozen tissues, cell lines, serum and plasma can also lead to conflicting results, as they are biologically not similar to one another [98] and the miRNAs found in one sample are not necessarily found in the others.

Moreover, the use of different techniques, including RNA-sequencing, Real time Quantitative PCR (RT-qPCR) and microarray yield different results as they differ in sensitivity and specificity [2]. Standardization is required to overcome these limitations.

Furthermore, the effective drug delivery has to be improved to circumvent the poor miRNA stability and the poor uptake by its targets [2]. A potential solution is the development of extracellular vesicles (EVs) containing miRNAs because EVs are non-immunogenic and their half-life of in the circulation is greater than that of liposomes due to their endogenous origin and peculiar surface composition [106]. This also enables them to specifically bind to recipient cell receptors, providing the possibility to generate EVs that specifically target a specific cell type. Several ongoing studies are evaluating the role of EVs for the development of cancer therapeutics with miRNA and hopefully, will provide another weapon to the armory for treatment of many cancers, including MMe.

Table 1 . Overview of the main miRNAs identified as (early) diagnostic and prognostic biomarkers in MM

Biomarker	Sample type	miRNA	Analysis*	References
Early diagnosis	*Serum*	↓miR-126	Its downregulation has the ability to differentiate between healthy subjects and MPM patients and correlates with worse prognosis	[74]
	Plasma/ Serum	↑miR-625-3p	Upregulated in MM patients	[75]
	Plasma	↑miR-29c ↑miR-92a ↑miR-196b	Upregulated in MM patients	[75]
	Plasma and Tissue	↓miR-16 ↓miR-17 ↓miR-486	Downregulated in MPM patients and asbestos-exposed patients	[76]
Diagnosis	*Tissue*	↓miR-141 ↓miR-200a ↓miR-200b ↓miR-200c ↓miR-203 ↓miR-205 ↓miR-429	Differentiate MPM from lung adenocarcinoma	[77], [78]
		↓miR-192 ↓miR-200c ↑miR-193a-3p	Distinguish MPM from other malignancies, including lung adenocarcinomas, renal cell carcinomas and gastrointestinal tract adenocarcinomas	[77]
		↓miR-126 ↓miR-143 ↓miR-145 ↓miR-652	Differentiate MPM from non-malignant pleural disease	[79]
	Peripheral blood	↓miR-103	Differentiate MM patients from previously asbestos-exposed patients	[54]
	Plasmatic extracellular vesicles	miR-103a-3p miR-30e-3p	These miRNAs have the ability to differentiate MM patients from previously asbestos-exposed patients	[80]
	Plasma	↓miR-132-3p	Low levels of circulating miR-132-3p have the ability to differentiate MM patients from previously asbestos-exposed patients	[81]
	Serum	↑miR-34-b/c methylation	miRNA-34-b/c DNA promoter is more methylated in MPM patients compared to patients with benign asbestosis and healthy controls	[82]
		↑miR-197-3p ↑miR-1281 ↑miR-32-3p	Increased circulating levels detected in MPM patients	[83]
	Tissue, cytologic specimens and cell lines	↑miR-21 ↓miR-126	Differentiate MM from non-malignant samples	[84]
Prognosis	*Tissue and cell lines*	↑miR-29c	Higher levels associated with the epithelial subtype and better prognosis.	[85]
		↓miR-17-5p ↓miR-30c	Low levels of miR-17-5p and miR-30c correlate with better outcome in patients with sarcomatoid subtype	[86]
	Tissue	↑Let-7 c-5p ↑miR-151a-5p	High levels of these miRNAs correlate with better prognosis	[87]
		↓miR-17-5p ↓miR-19b-3p ↓miR-625-5p	Low levels of these miRNAs correlate with better prognosis in MPM patients	[88]
		↑↓miR-31	Low levels of miR-31 have the ability to differentiate between MPM and reactive mesothelial proliferations. Yet, elevated levels correlate with a worse prognosis and were found in sarcomatoid mesothelioma cases	[23]
		↓miR-15b ↓miR-16 ↓miR-193a-3p ↓miR-195 ↓miR-200c	Low levels are associated with increased expression of PD-L1, a marker of poor prognosis	[89]
	Cell lines	↑↓miR-31	Low levels are associated with a worse prognosis and correlate with tumor recurrence in a short period. However, elevated levels are associated with chemoresistance by means of intranuclear and intracellular accumulation of low levels of platinum drugs	[90], [91]

5. DRUG RESISTANCE IN MESOTHELIOMA

5.1 miRNAs and drug resistance

5.1.1 Pemetrexed and miRNAs involved in drug resistance

Pemetrexed is one of the drugs administered in the upfront standard chemotherapy of MPM. Interestingly, its mechanism of action involves the upregulation of tumor suppressors miRNAs, including let-7c, miR-451 and miR-486-5p and oncomir miR-210 [107]. On the other hand, some miRNAs could be responsible for the development of drug resistance to pemetrexed [Figure 3A].

For instance, restoring the expression of several key downregulated miRNAs in MPM increased the sensitivity to pemetrexed. This process has been described for the following miRNAs: miR-16 [107], miR-145 [108,109] miR-379 and miR-411 [98].

A pivotal gene associated with drug sensitivity of MPM cells is *IL-18*, which is upregulated in mesothelioma and might be a potential therapeutic target, since its expression could be downregulated by miR-379 and miR-411[110].

Sensitivity to pemetrexed can also be restored by suppressing the overexpressed miR-21 [89]. Indeed, a promising new approach involves the delivery of pemetrexed together with anti-miR-21 in solid lipid nanoparticles (SLNs) [111].

Last but not least, another strategy to overcome pemetrexed resistance is by combining it with synergistic ncRNA modulating drugs [112]. One of these drugs, as discussed further along, is cisplatin, because pemetrexed is administered in combination with cisplatin as a first line treatment in MPM patients [107].

5.1.2 Cisplatin and miRNAs involved in drug resistance

Cisplatin itself suppresses the oncomir miR-21 and induces the expression of tumor suppressors let-7c, miR-34a, miR-145 and miR-451 [77,107].

However, several miRNAs are playing a role in regulating the sensitivity to cisplatin [Figure 3B] [77]. For example, loss of miR-31 restores chemosensitivity [97], while downregulation of the expression of miR-15a, mir-16a and miR-34a is associated with acquired chemoresistance to cisplatin [113]. Mimics of these tumor suppressor miRNAs demonstrated that restoring their expression could increase drug sensitivity by targeting multiple genes that play a role in the apoptotic pathways [113]. Remarkably, miR-16 mimic has already been tested in a phase I clinical trial and promising results have been reported in MPM patients [114].

The suppressed expression of miR-34a, exerting antiproliferative effects, was correlated with a poor response to chemotherapy in diffuse PeM [108]. Restoring the expression of miR-34a should therefore be further tested as a novel therapeutic option, in light of the encouraging results obtained in other types of cancers, including bladder and lung cancer, where it enhanced cisplatin activity [115,116].

Increasing evidence is pointing in the direction of a combined therapy with cisplatin and other classes of drugs, such as phenolic compounds, organosulfur compounds, terpenoids, polyunsaturated fatty acids, HDAC inhibitors and alkaloids [78]. These combined approaches would possibly lead to or downregulation of oncomirs or higher expression of tumor suppressor miRNAs which could in turn enhance cisplatin activity.

Finally, Uematsu and colleagues demonstrated an alternative method to overcome cisplatin resistance in MPM cell lines, through siRNA inhibition of Dishevelled, an intermediate of Wnt signaling, an important player in tumorigenesis [117].

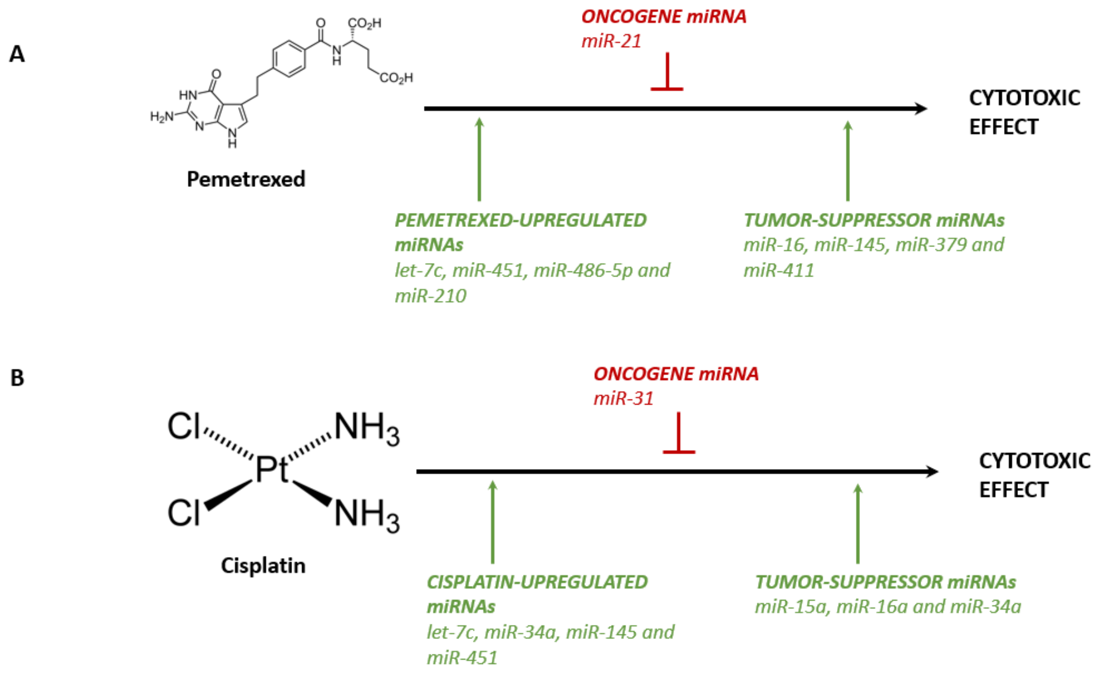
A
ONCOGENE miRNA
miR-21
Pemetrexed
CYTOTOXIC EFFECT
PEMETREXED-UPREGULATED miRNAs
let-7c, miR-451, miR-486-5p and miR-210
TUMOR-SUPPRESSOR miRNAs
miR-16, miR-145, miR-379 and miR-411
B
ONCOGENE miRNA
miR-31
Cisplatin
CYTOTOXIC EFFECT
CISPLATIN-UPREGULATED miRNAs
let-7c, miR-34a, miR-145 and miR-451
TUMOR-SUPPRESSOR miRNAs
miR-15a, miR-16a and miR-34a

Figure 3 Overview of miRNAs regulating pemetrexed (A) and cisplatin (B) activity in mesothelioma. Inhibition or restoration of the expression of some of these miRNAs can be used as a way to overcome chemoresistance

5.2 Alternative splicing and drug resistance

Pre-mRNA is only functional for protein synthesis after the removal of introns and when the exons are spliced together. The spliceosome is responsible for splicing out introns from pre-transcribed mRNA [Figure 4]. The splicing process is essential for the regulation of gene expression in eukaryotes. Mutations or differentially expressed splicing factors (SF) that form the spliceosome are common in cancer and lead to splicing deregulation such as exon skipping, intron retention and alternative splicing sites. This results in the production of aberrant mRNA splicing patterns. which affect biological processes related to chemoresistance, including decreased transport of the anticancer drugs into the intracellular space, impaired conversion to an active metabolite, altered regulation of target gene transcription and apoptosis [118]. Moreover, alternative splicing leads the formation of cancer-specific splicing isoforms which produce transcriptome changes relevant for many processes underlying tumor biology [119]. For instance, an incorrect splicing of BAP1 mRNA can impair correct protein formation, as described by Morrison and colleagues, who identified a novel homozygous substitution mutation, *BAP1* c.2054 A&T (p.Glu685Val). This causes aberrant splicing and premature truncation of the BAP1 protein, resulting in genomic instability [18].

Because of the important role in many hallmarks of cancer, alternative splicing represents a novel frontier to explore in cancer therapy.

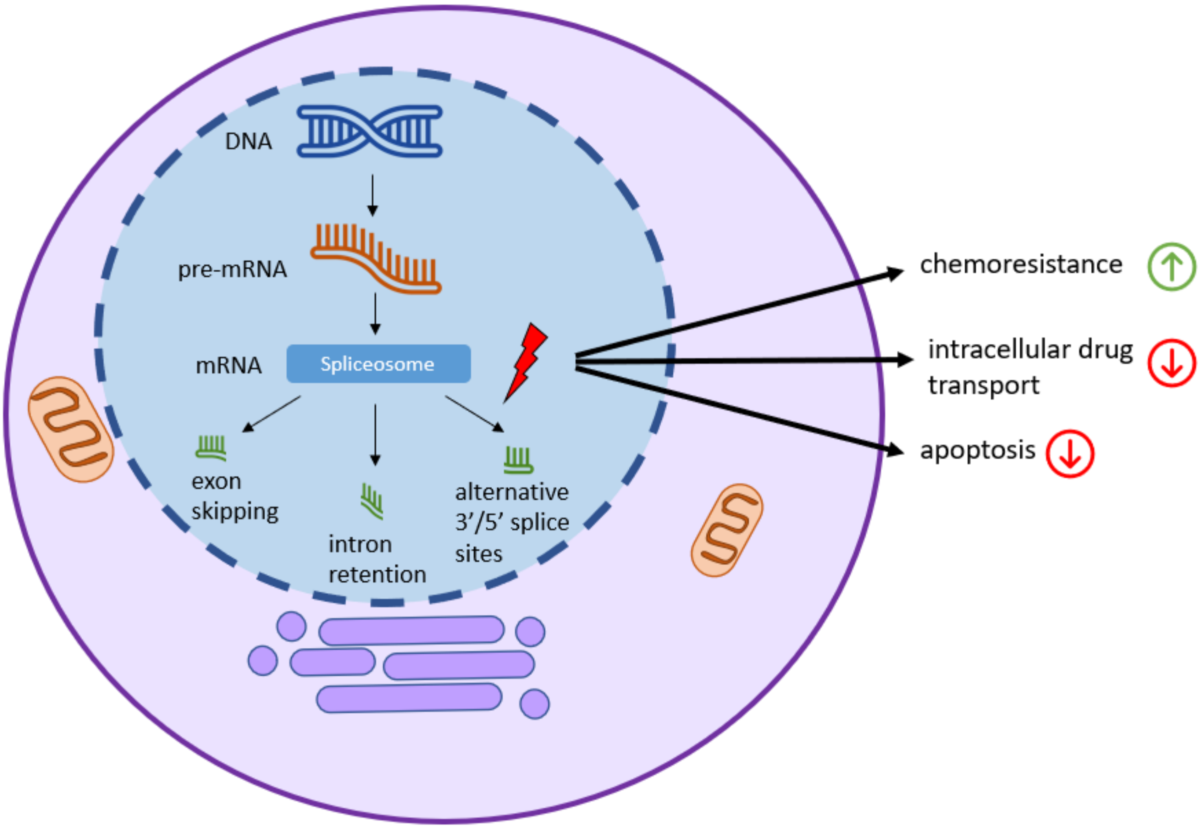

Figure 4. Spliceosome complex and splicing factors mutations are common in cancer. Those mutations result in splicing deregulation, which can alter apoptosis and intracellular drug transport, thus leading to chemoresistance.

5.2.1 Splicing deregulation and new potential targets

Bueno and collaborators demonstrated that epigenetic and splicing deregulations are crucial for MM pathogenesis and could therefore be identified as novel antitumor targets. Indeed, they performed exome sequencing analysis of MPM and described, besides the most commonly known genomic alterations, mutations in splicing factor 3b subunit 1 (SF3B1), an essential component of the spliceosome [120]. In addition, they detected recurrent gene fusions and splice alterations that are responsible for inactivation of *NF2*, *BAP1* and *SETD2*. They also reported alterations in histone methyltransferase SETD2 and the DEAD-box RNA helicases DDX51 and DDX3X, involved in both RNA processing and splicing.

Moreover, the SF3b complex has been identified as a target for a novel class of compounds, exhibiting anti-tumor activity, including meayamycins, spliceostatins and sudemycins [121–123].

Sciarrillo and collaborators were the first to investigate splicing deregulation as a potential novel therapeutic target in PeM and correlated SF3B1 expression with patient's prognosis.

They demonstrated that splicing factors and SF3b complex are upregulated in primary cell cultures (MesoII and STO) [124] and tested the effects of three modulators of this complex, namely Pladienolide-B (PB), E7107 and Meayamycin-B both *in vitro* and *in vivo*. Remarkably, the primary cell cultures were extremely sensitive to these modulators, with IC50 values in the low nanomolar range. Furthermore, splicing modulation *in vitro* perturbed the global splicing landscape of PeM cells affecting genes with tumorigenic functions in MMe. This led to reduced migration, and modulation of cell-cell interaction and cell cycle progression, ultimately leading to apoptosis.

The *in vivo* studies on diffuse malignant peritoneal (DMPM) xenografts demonstrated anti-tumor activity of E7107 and RT-PCR analysis revealed that tumor samples from treated mice exhibited splicing profile alterations similar to those observed *in vitro* after PB and E7107 exposure. Eventually Kaplan-Meier analysis showed an increase in survival rate of the E7107-treated group compared to the untreated group.

Of note, modulation of the spliceosome machinery is different in specific subtypes of cancers. Indeed, Hsu and colleagues discovered that *MYC*-driven tumors are potentially more vulnerable to modulators because of the abundant transcript activity [122] and interestingly *MYC* was found to be overexpressed in 64% of DMPM cases [124], potentially providing an explanation for the aforementioned findings.

Splice-switching oligonucleotides and RNA interference provide alternative tools to target splicing deregulation. Nonetheless, despite the encouraging *in vitro* and *in vivo* results, translating this approach to the clinical setting is still difficult due to limited intracellular uptake and stability of these modulators in plasma.

5.3 Interplay of miRNAs and alternative splicing

In light of the above-mentioned evidence, miRNAs and alternative splicing play a pivotal role in the pathogenesis of MMe, since they are both involved in gene regulation and can lead to differentially expressed genes. Furthermore, alternative splicing and miRNAs can influence each other.

MiRNAs can have a major effect on gene regulatory networks, including splicing-involved proteins [125]. For example, miR-148 has been shown to regulate specific DNMT protein isoforms, providing evidence that the relative abundance of different splice variants can be subjected to miRNA regulation [126].

Another way through which miRNAs can affect the splicing process is by targeting factors involved in this process. For instance, miR-124 is a neuron-specific miRNA which targets splicing factor PTBP1, a repressor of alternative pre-mRNA splicing [127] .

In addition, it has been demonstrated that the mRNA of splicing factor SRSF1 is a target for several miRNAs [128,129].

As a matter of fact, the other way around is also possible. This was demonstrated in a study conducted in myelodysplastic syndrome, a malignancy with frequent spliceosome mutations. Here Aslan and colleagues have demonstrated that mutations in SF3B1 affect the expression of tumor suppressor miRNAs, including several let-7 family members, miR-423, miR-103a, by downregulating them and consequently playing a role in tumorigenesis [130].

Both alternative splicing events and miRNAs regulatory effects can deeply impact the tumor cells' behavior, especially in terms of drug resistance. At the time of writing, the evidence regarding MMe is scarce, but offers promising and compelling perspectives for future studies.

5.4 Notch signaling pathway and cancer stem cells in chemotherapy resistance

Beyond epigenetic factors, it has been hypothesized that MMe relapse may be associated with the drug resistance of cancer stem cells (CSCs). CSCs have indeed been implicated in resistance of MMe cells to both cisplatin and pemetrexed [131,132]. Stem cells constitute a small subpopulation of all tumor cells, but have an endless replicative potential and exhibit high expression of pluripotency genes, leading to tumor relapse after initial response to chemotherapy [133]. Several putative markers are used to identify the presence of CSCs, including overexpression of CD24, CD133, Bmi-1, uPAR, and ABCG2, and increased activity of the enzyme aldehyde dehydrogenase [132,134,135]. A subpopulation of cells with stemness properties was also detected in MPeM. The MPeM stem cells (MPeMSCs) express a high level of stem cell biomarkers including c-MYC, NES, and VEGFR2, and are able to form a colony in presence of a matrix component [136].

However, three developmental signaling pathways (Notch, Hedgehog, and Wnt) have been found to play an essential role in the maintenance of a CSC phenotype. In particular, the Notch pathway is an important evolutionary conserved pathway that plays a key role in many several cellular processes, such as inflammation [137,138], angiogenesis [139], epithelial to mesenchymal transition (EMT), metastases [140], and cancer stem cells (CSCs) self-renewal [141]. Notch receptors are large single-pass type-I transmembrane proteins, containing 29-36 epidermal growth factor (EGF)-like tandem repeats, which mediate the interaction with Notch ligand. Notch receptors not only act as signal transducers but function also as transcription regulators [142]. The mechanism that governs the activation of the Notch pathway starts with the binding of Notch receptors with its ligands. In humans, four Notch receptors have been identified: Notch 1-4 that are expressed on the surface of the cell membrane and five ligands: three Delta-like families (Dll-1, Dll-3, Dll-4) and two Serrate-Like (Jagged-1 and Jagged-2) ligands [143]. After activation, Notch receptors are proteolytically cleaved by a metalloprotease of the ADAM family and γ-secretase, followed by the release of Notch intracellular domain (NICD), which is subsequently translocated into the nucleus where interacts with transcription factors, such as CBF-1 in mammals, which allows the release of transcriptional corepressor including CIR and histone deacetylase and the recruitment of transcriptional coactivators such as SKIP and histone acetyltransferase. Therefore, the binding of Notch with CFB1 promotes the conversion of the gene transcriptional repressor into the gene transcriptional activator [144]. Moreover, the binding of NICD with CFB1 supports the expression of Notch target genes [145,146]. Several Notch targets genes have been identified, including Cyclin D1, c-myc, nuclear factor-Kb (NF-Kb) [147], phosphatidylinositol 3-kinase, AKT [148].

Dysregulation of the Notch pathway potentially contributes to the initiation and progression of several types of cancer, including MPM [145,149]. Remarkably, previous studies reported that the Notch signaling pathway supports cells survival, with a high level of expression of Notch in MPM cells compared with the normal human mesothelial cells [144]. In addition, MPM is characterized by a hypoxic microenvironment which further strengthens the connection between Notch pathway overexpression and CSCs. Supporting studies indeed demonstrated that hypoxia-inducible factors (HIFs) are CSCs markers, and the hypoxic tumor microenvironment plays a key role in CSCs-self renewal [150,151]. Hypoxia activates the expression of Notch promoter HIFs, stabilizing them from degradation. Conversely, HIFs sustain the Notch transcriptional activity [152,153].

Interestingly, it was reported that the Notch signaling pathway has an opposite role in MPM cells. Notch1 is overexpressed and seems to upregulate the activity of the phosphoinositide 3-kinase (PI3K) pathway, by decreasing the level of phosphatase and tensin homolog (PTEN) mRNA, leading to a deregulation of the PI3K/Akt/mTOR pathway, which supports survival and invasiveness of tumor cells, also through EMT. During EMT cells acquire a mesenchymal phenotype, which allows them to invade secondary tissues, increasing tumor invasiveness, causing metastases and resistance to apoptosis [137,154]. On the other hand, Notch2 seems to be reduced or suppressed in MPM cells and is considered to have a suppressive role in the development and progression of MPM [144]. Notch2 restores the normal expression level of phosphatase PTEN and consequently equilibrates the activation of PI3K/Akt pathway. The increased expression of Notch1 and its involvement in deregulation of PI3K/Akt signaling pathway in MPM specimens was confirmed by short hairpin RNA sh(RNA) silencing of Notch1 gene expression or by γ-secretase inhibition. Artificial inhibition of Notch1 signaling by tetracycline-inducible lentiviral system, that upon doxycycline administration induces the expression of shRNA targeting Notch1, led to MPM cells death under normoxia and hypoxia conditions. These results were further supported by experiments using the γ-secretase inhibitor MRK-003, which led to MPM cell death, and this effect is more pronounced under hypoxia [144].

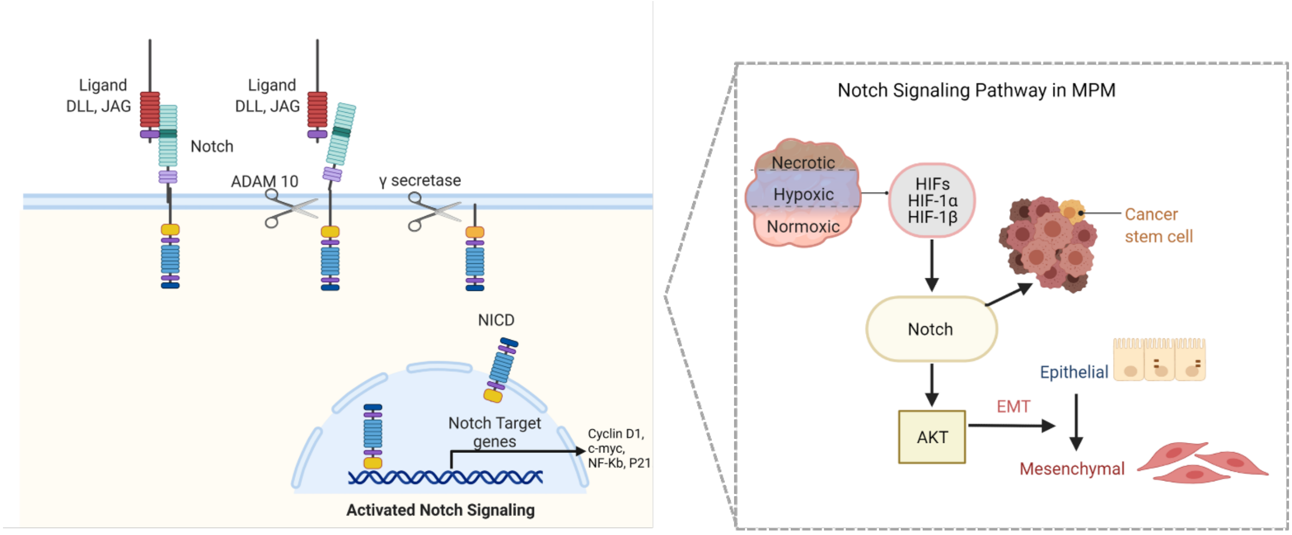
Ligand
DLL, JAG
Ligand
DLL, JAG
Notch
ADAM 10
γ secretase
NICD
Notch Target genes
Cyclin D1, c-myc, NF-Kb, P21
Activated Notch Signaling
Notch Signaling Pathway in MPM
Necrotic
Hypoxic
Normoxic
HIFs
HIF-1α
HIF-1β
Cancer stem cell
Notch
Epithelial
EMT
AKT
Mesenchymal

Figure 5 Notch signaling pathway in malignant pleural mesothelioma (MPM).
A) Notch receptor interacts with its ligands such as, Jagged-1/2 or Delta-like ligand (DLL-1/3/4) and subsequently is cleaved by protease ADAM and γ-secretase. Once released, Notch intracellular domain (NICD) translocates into the nucleus where it allows the expression of several transcription factors involved in cancer progression.
B) Hypoxia inducible factors (HIFs) lead to the overexpression of Notch signaling pathway in mesothelioma specimens, resulting in CSCs formation and EMT.

5.5 Hypoxia metabolism and miRNA

Hypoxia is a common feature of the tumor microenvironment (TME). Hypoxic tumors are distinguished by poor prognosis and chemoresistance to standard therapeutic drugs. Moreover, the hypoxic tumor cells become resistant to radiation therapy and this low oxygen tension tends to enrich the tumors of CSCs. A key role of control of hypoxic mechanisms is played by HIFs, which arrange the expression of several critical genes involved in activation of related tumor hypoxia signaling pathways [155]. Under normoxic conditions HIF proteins are hydroxylated by prolyl hydroxylases proteins (PHDs), which once hydroxylated promote the activation of von-Hippel-Lindau E3. However, under hypoxic conditions, considering that PDHs use oxygen as a co-substrate are inhibited, and are not able to hydroxylate HIF proteins, thus, cannot be ubiquitinated staying stable and not undergoing proteasomal degradation [156]. The potential role of the tumor hypoxic microenvironment in driving mesothelioma progression has been recently studied and scientific evidence confirms the presence of mesothelioma hypoxic tumor cells [157]. Not only hypoxia is a cause for metabolic derangement but it could also be regulated by miRNAs. Indeed, as shown by De Santi et al [93] Let-7c-5p belonging to the so-called "HypoxiamiRs" family, is an hypoxia regulator and together with miR-151a-5p constitutes a good prognostic tool: high levels of these miRNAs were associated with worse survival in patients with MMe. On the other hand, miR-151a-5p plays a crucial role in the energetic balance of the cell, provided that its overexpression leads to mitochondrial dysfunction, which could in turn lead to hypoxic TME and subsequent tumor progression and maintenance. The metabolic alterations induced by hypoxia are particularly evident in chemoresistant tumor cells. These cells preferentially utilize glycolysis rather than mitochondrial oxidation, for energy production, a metabolic switch known as the Warburg effect. These phenomena make them vulnerable to novel therapeutic approaches targeting hypoxic pathways and pyruvate biosynthesis enzymes [158].

A successful and promising example of this approach comes from targeting LDH-A in MPM and DMPM [159]. In this work the authors describe a novel hypoxia/PCFT-dependent chemoresistance mechanism linking LDH-A overexpression with low PCFT levels in hypoxic cells. Indeed LDH-A emerged as a new prognostic factor in both MPM and DMPM, with high levels of the enzyme linked to shorter survival of patients. Novel LDH-A inhibitors demonstrated to be a valid therapeutic strategy to overcome chemoresistance in MMe and in particular they showed synergistic effects with pemetrexed in MPM and gemcitabine in DMPM cells.

5.6 Targeted therapies against Notch

Several strategies have been studied in order to block the Notch signaling pathway [Figure 5], including small molecules inhibiting the proteolytic cleavage of receptors and neutralizing monoclonal antibodies (mAbs) inhibiting the interaction between ligand and receptors [160]. Notch inhibition showed promising results in decreasing the number of CSCs in different clinical models [161]. The first Notch inhibitors (e.g. RO4929097 and LY3039478) are small molecule γ-secretase inhibitors (GSIs), which were initially synthesized for the treatment of Alzheimer's disease and subsequently repurposed as anticancer drugs [162].

The mechanism of action of GSIs occurs trough the inhibition of proteolytic cleavage of the Notch receptors and the failure of the release of NICD which causes the lack of activation of the Notch signaling pathway [163]. GSIs inhibit all four isoforms of the Notch receptors, preventing drug resistance and relapses due to redundancy and increased expression of other isoforms that may be able to restore the Notch signaling pathway activity. However, as reported by Graziani and collaborators, the various isoforms of Notch receptors assume different roles in MPM progression, in fact Notch1 showed pro-oncogenic role, leading to the suppression of PTEN phosphatase. On the other hand, Notch2 seems to act as tumor suppressor, restoring the function of PTEN [144]. This would suggest that intermittent rather than continuous administration of GSIs could be associated with a high level of therapeutic success in MPM.

Notch receptors are not the only substrates of γ-secretase, they are nonselective drugs and their use sometimes results in the development of side effects, including secretory diarrhea. Since the latter is thought to be due to intestinal stem cell inhibition, the recommended therapeutic regimen should be alternated with days of suspension to limit adverse effects [162].

Several GSIs have reached the clinical stage; the main inhibitors include: RO4929097 and LY3039478, small molecule γ-secretase inhibitors characterized by the presence of dibenzoazepine moiety. RO4929097 was initially developed for the treatment of Alzheimer's disease but given its efficacy in inhibiting γ-secretase activity it has been repurposed for the treatment of different cancer types. The efficacy of RO4929097 was investigated against different cancer types, such as, metastatic melanoma, glioblastoma, colorectal cancer, triple negative breast cancer and ovarian cancer, however, despite the proven efficacy in the inhibition of Notch and its downstream mediators, no significant improvement in OS and PFS was observed. Therefore, it has been withdrawn following the poor results from the clinical trials [164–168]. LY3039478, also known as crenigacestat, structurally related to RO4929097, has shown potent activity in the nanomolar range in several cell lines from solid and hematological malignancies [169,170]. A recent study reported positive results of the combination of crenigacestat and prednisone in advanced or metastatic cancer, the latter compound is given to limit the gastrointestinal toxicity without affecting its pharmacokinetic properties and antitumor activity [171].

Other GSIs include PF-03084014, also known as nirogacestat, a potent small molecule, which showed promising anticancer activity in different tumor types and seems to be able to inhibit the capacity of the cells to invade secondary tissue, showing antimigratory and antimetastatic activity. In this context it was recently reported that PF-03084014 is able to inhibit the self-renewal and proliferation of CSCs through reduction of Stat3 activation and Akt phosphorylation [172]. Moreover, PF-03084014 demonstrated synergistic effects with standard chemotherapeutic drugs such as docetaxel or small molecule kinase inhibitors (SMKIs) in different cancer models [173–175].

Some evidence suggests that the simultaneous administration of Notch GSIs with SMKIs such as Akt inhibitors result in antimetastatic activity, because of the positive role on Notch GSIs in limiting drug resistance through the inhibition of EMT [176].

In addition to small molecules, other strategies for silencing the Notch signaling pathway include monoclonal antibodies (mAbs) that neutralize the interaction between the ligand and the receptor, such as Dll-4 ligand target antibody. Dll-4 plays a particularly important role in angiogenesis of cancer cells, and its inhibition has shown a positive role in tumor growth inhibition and reduction of angiogenesis, resulting in necrosis of cancer cells [177].

A different strategy involves the use of antibodies directed against Notch receptors, which inhibit the cleavage of the Notch extracellular domain causing the silencing of the Notch signaling pathway [178]. Tarextumab mAb selectively targets both Notch2 and Notch3 receptors, showing good results in different solid tumors [179]. These findings should prompt the development of new strategies for Notch inhibition to expand the therapeutic arsenal against MMe and this therapeutic strategy could be tailored to patients with MMe specimens harboring CSCs and Notch overexpression.

6. CONCLUSION

MMe is currently an incurable disease at all stages. Diagnosis is often late and therapeutic options are limited and hampered by chemoresistance. Therefore, novel, more effective therapies are urgently needed.

According to Greek mythology, Cerberus was a three-headed dog that guarded the gates of the underworld to prevent the dead from leaving. The three heads were symbolic of the past, the present, and the future and personify uncontrollable appetite. However, using his lion-skin, Hercules was able to grab this beast by the throat and wrestled him to the ground.

In the present review we described three malignant features of MMe, i.e., deregulation of miRNAs, splicing and CSCs. All these features play a key role in MMe's aggressive and chemoresistant behavior. However, improved knowledge of the associated molecular mechanisms can hopefully provide novel therapeutic targets to successfully fight MMe.

7. EXPERT OPINION

The present review summarizes the most up-to-date information on novel tools that could significantly impact MMe's (early) diagnosis, therapy and prognosis. Indeed, if successfully implemented in the clinical setting, we believe that miRNAs could dramatically change the current diagnostic landscape for a tumor where patients are often diagnosed in the advanced stages, thus shortening the gap between the disease development and its detection [74,92]. Along with miRNAs, that could also offer interesting therapeutic solutions, targeting spliceosome [120,124] and CSCs via Notch signaling showed promising results in both pre-clinical and clinical studies, paving the way for full implementation as drugs of choice [98,150].

In this regard, increasing scientific evidence has proven the efficacy of inhibition of the frequently mutated spliceosome protein SF3b1 through meayamycins, spliceostatins and sudemycins which act by inhibiting pre-mRNA splicing [121–123]. Furthermore, MMe is characterized by a hypoxic microenvironment which further sustains Notch pathway overexpression and CSCs self-renewal [144,152]. Therefore, the inhibition of Notch signaling via small molecule γ-secretase inhibitors or monoclonal antibodies (mAbs) has been evaluated positively in eradicating CSCs [160].

In addition to these three deregulated primary pathways in MMe, we reviewed the latest findings about the use of alternative promising therapeutic approaches, including the inhibition of epigenetic regulators [67], tyrosine kinase [27], cell cycle checkpoint [39] and immune checkpoint [40], whose deregulation is considered among the main causes of the failure of the standard chemotherapy. These new therapeutic strategies, along with miRNA, spliceosome and Notch inhibitors could represent a step forward compared to standard chemotherapy based on cisplatin and pemetrexed and could try to counteract the drug resistance and relapses that characterize MMe [132]. This problem is particularly significant in the sarcomatoid histotype. Patients diagnosed with it have a dismal prognosis and frequently experience chemoresistance. However, due to the intrinsic clinical characteristics of these patients, there is an underrepresentation of studies investigating the molecular circuitries responsible for this particular resistance. On that count, the mechanisms of resistance here described can be deemed as valid also for the sarcomatoid subtype, based on the examined evidence. Nonetheless, we believe that there is an urgent need for larger sarcomatoid-specific trials, in order to further elucidate the patients' response to different therapeutic strategies and to better tailor them according to the peculiar biological characteristics of this histotype.

Therefore, there are a series of new approaches to treat MMe and to overcome the dramatic problem of drug resistance. From this point of view, we believe that these therapies could either increase the efficacy of the current regimens or could replace them completely as new therapeutic standards.

When further validated miRNA, spliceosome and Notch inhibitors could constitute a novel tool to fight mesothelioma and to increase PFS and OS, and improve the Quality of Life in this aggressive and incurable tumor. Moreover, another advantage could be the possibility to better stratify patients to make an evidence-based choice for the most aggressive treatments, and subsequently decrease the morbidity rate associated for example with radical surgery. New approaches, such as the use of liquid biopsies, including the study of EV released from mesothelioma cells can reveal important information about the molecules and signaling pathways involved in the progression and resistance of the tumor [180].

Advances in new therapeutics and liquid biopsies have not yet been adopted into clinical practice, because of the limited sample size of patients who are enrolled in clinical trials, as well as lack of clinical and technological validation. However, implementation of the techniques and new design of clinical trials will hopefully positively impact the clinical outcome of MMe patients in the next 5-10 years. A good number of studies in different tumor types has proven efficacy of new therapeutic approaches, but the lack of reproducibility of certain patterns of molecular deregulation in specific cancers constitutes a major obstacle for the full validation of these tools both as diagnostic and therapeutic alternatives. Therefore, a common investigational approach is needed that uses standardized techniques on the same sample types in order to obtain reproducible and solid results. Indeed, this area of research has witnessed a huge increase in interest, thanks to the introduction of new techniques, such as silencing or reconstituting the expression of a certain miRNAs or being able to precisely target a component of the spliceosome as well as CSCs. Currently, we are still in the early phase of what we hope will be a new era of personalized medicine and targeted therapy for mesothelioma patients, marked by efficacious options for therapy and an early diagnosis.

REFERENCES

Papers of special note have been highlighted as:
* of interest
** of considerable interest

[1] Sage A, Martinez V, Minatel B, et al. Genomics and Epigenetics of Malignant Mesothelioma. High-Throughput. 2018;7(3):1-23.

[2] Globocan Observatory W. Cancer Today - World. Int Agency Res Cancer [Internet]. Lyon: IARC; 2021 [cited 2021 Aug 15] Available from: https://gco.iarc.fr/today/data/factsheets/cancers/18-Mesothelioma-fact-sheet.pdf

[3] McDonald JC, McDonald AD. The epidemiology of mesothelioma in historical context. Eur Respir J. 1996;9:1932–1942.

[4] Blyth KG, Murphy DJ. Progress and challenges in Mesothelioma: From bench to bedside. Respir Med. 2018;134:31–41.

[5] Cavone D, Caputi A, De Maria L, et al. Epidemiology of Mesothelioma. Environments. 2019;6:76.

[6] International Agency for Research on Cancer. IARC Monographs on the evaluation of carcinogenic risk to humans: Asbestos. Volume 14. Lyon: IARC; 1977.

[7] Sirri E, Kieschke J, Vohmann C, et al. Survival of malignant mesothelioma and other rare thoracic cancers in Germany and the United States: A population-based study. Int J Cancer. 2020;147:1548–1558.

[8] Nazemi A, Nassiri N, Pearce S, et al. Testicular Mesothelioma: An Analysis of Epidemiology, Patient Outcomes, and Prognostic Factors. Urology. 2019;126:140–144.

[9] Nadiradze G, Horvath P, Sautkin Y, et al. Overcoming Drug Resistance by Taking Advantage of Physical Principles: Pressurized Intraperitoneal Aerosol Chemotherapy (PIPAC). Cancers. 2019;12:34.

[10] Motamedi MR, Shishineh P. Primary Malignant Pericardial Mesothelioma. Med J Islam

Repub Iran 1997; 11(2): 163–167.

[11] Brimo F, Illei PB, Epstein JI. Mesothelioma of the tunica vaginalis: a series of eight cases with uncertain malignant potential. Mod Pathol. 2010;23:1165–1172.

[12] van Zandwijk N, Clarke C, Henderson D, et al. Guidelines for the diagnosis and treatment of malignant pleural mesothelioma. J Thorac Dis. 2013;5:54. *** of interest for the overview on diagnostic and therapeutic guidelines in MPM.**

[13] Yang H, Testa JR, Carbone M. Mesothelioma Epidemiology, Carcinogenesis, and Pathogenesis. Curr Treat Options in Oncol. 2008;9:147–157.

[14] Mesaros C, Worth AJ, Snyder NW, et al. Bioanalytical techniques for detecting biomarkers of response to human asbestos exposure. Bioanalysis. 2015;7:1157–1173.

[15] Valavanidis A, Fiotakis K, Vlachogianni T. Airborne Particulate Matter and Human Health: Toxicological Assessment and Importance of Size and Composition of Particles for Oxidative Damage and Carcinogenic Mechanisms. J Environ Sci Health, Part C Environ Carcinog Ecotoxicol Rev. 2008;26:339–362.

[16] Sekido Y. Molecular pathogenesis of malignant mesothelioma. Carcinogenesis. 2013;34:1413–1419.

[17] Morrison A, Chekaluk Y, Bacares R, et al. BAP1 Missense Mutation c.2054 A>T (p.E685V) Completely Disrupts Normal Splicing through Creation of a Novel 5' Splice Site in a Human Mesothelioma Cell Line. Buratti E, editor. PLoS ONE. 2015;10(4) :1-11

[18] Machida YJ, Machida Y, Vashisht AA, et al. The Deubiquitinating Enzyme BAP1 Regulates Cell Growth via Interaction with HCF-1. J Biol Chem. 2009;284:34179–34188. ***article of interest for the description of the molecular mechanism of action of BAP1**

[19] Misaghi S, Ottosen S, Izrael-Tomasevic A, et al. Association of C-Terminal Ubiquitin Hydrolase BRCA1-Associated Protein 1 with Cell Cycle Regulator Host Cell Factor 1. Mol Cell Biol. 2009;29:2181–2192.

[20] Pantazopoulos I, Boura P, Xanthos T, et al. Effectiveness of mesothelin family proteins and osteopontin for malignant mesothelioma. Eur Respir J. 2013;41:706–715.

[21] Moretti G, Aretini P, Lessi F, et al. Liquid Biopsies from Pleural Effusions and Plasma from Patients with Malignant Pleural Mesothelioma: A Feasibility Study. Cancers. 2021;13:2445.

[22] Hassan R, Ho M. Mesothelin targeted cancer immunotherapy. Eur J Cancer. 2008;44:46–53.

[23] Robinson BW, Creaney J, Lake R, et al. Mesothelin-family proteins and diagnosis of mesothelioma. Lancet. 2003;362:1612–1616.

[24] Matsumoto S, Nabeshima K, Hamasaki M, et al. Upregulation of microRNA-31 associates with a poor prognosis of malignant pleural mesothelioma with sarcomatoid component. Med Oncol. 2014;31:303.

[25] Cavallari I, Urso L, Sharova E, et al. Liquid Biopsy in Malignant Pleural Mesothelioma: State of the Art, Pitfalls, and Perspectives. Front Oncol. 2019;9:740. ***review of interest for the recent overview of studies with liquid biopsies for mesothelioma**

[26] Mutti L, Peikert T, Robinson BWS, et al. Scientific Advances and New Frontiers in Mesothelioma Therapeutics. J Thorac Oncol. 2018;13:1269–1283.

[27] Cui W, Popat S. Pleural mesothelioma (PM) – The status of systemic therapy. Cancer Treat Rev. 2021;100:102265.

[28] Treasure T, Lang-Lazdunski L, Waller D, et al. Extra-pleural pneumonectomy versus no extra-pleural pneumonectomy for patients with malignant pleural mesothelioma: clinical outcomes of the Mesothelioma and Radical Surgery (MARS) randomised feasibility study. Lancet Oncol. 2011;12:763–772.

[29] Järvinen T, Paajanen J, Ilonen I, et al. Hyperthermic Intrathoracic Chemoperfusion for Malignant Pleural Mesothelioma: Systematic Review and Meta-Analysis. Cancers. 2021;13:3637.

[30] Voigt SL, Raman V, Jawitz OK, et al. The Role of Neoadjuvant Chemotherapy in Patients With Resectable Malignant Pleural Mesothelioma—An Institutional and National Analysis. J Natl Cancer Instit. 2020;112:1118–1127.

[31] Cao C, Tian D, Manganas C, et al. Systematic review of trimodality therapy for patients with malignant pleural mesothelioma. Ann cardiothorac surg. 2012;1:10.

[32] de Gooijer CJ, Baas P, Burgers JA. Current chemotherapy strategies in malignant pleural mesothelioma. Transl Lung Cancer Res. 2018;7:574–583.

[33] Guazzelli A, Meysami P, Bakker E, et al. BAP1 Status Determines the Sensitivity of Malignant Mesothelioma Cells to Gemcitabine Treatment. Int J Mol Sci. 2019;20:429.

[34] Takiguchi Y. Interaction and cross-resistance of cisplatin and pemetrexed in malignant pleural mesothelioma cell lines. Oncol Rep. 2012; 28(1): 33–40.

[35] Tanino R, Tsubata Y, Harashima N, et al. Novel drug-resistance mechanisms of pemetrexed-treated non-small cell lung cancer. Oncotarget. 2018;9:16807–16821.

[36] Giovannetti E, Zucali PA, Assaraf YG, et al. Role of proton-coupled folate transporter in pemetrexed resistance of mesothelioma: clinical evidence and new pharmacological tools. Ann Oncol. 2017;28:2725–2732. ***article of interest for the identification of biomarkers of resistance to pemetrexed in MMe**

[37] Ceresoli GL, Zucali PA, Favaretto AG, et al. Phase II Study of Pemetrexed Plus Carboplatin in Malignant Pleural Mesothelioma. J Clin Oncol. 2006;24:1443–1448.

[38] Popat S, Curioni-Fontecedro A, Polydoropoulou V, et al. A multicentre randomized phase III trial comparing pembrolizumab (P) vs single agent chemotherapy (CT) for advanced pre-treated malignant pleural mesothelioma (MPM): Results from the European Thoracic Oncology Platform (ETOP 9-15) PROMISE-meso trial. Ann Oncol. 2019;30:v931.

[39] Xu D, Liang S-Q, Yang H, et al. CRISPR Screening Identifies WEE1 as a Combination Target for Standard Chemotherapy in Malignant Pleural Mesothelioma. Mol Cancer Ther. 2020;19:661–672.

[40] Baas P, Scherpereel A, Nowak AK, et al. First-line nivolumab plus ipilimumab in unresectable malignant pleural mesothelioma (CheckMate 743): a multicentre, randomised, open-label, phase 3 trial. Lancet. 2021;397:375–386.

[41] Woods DM, Sodré AL, Villagra A, et al. HDAC Inhibition Upregulates PD-1 Ligands in Melanoma and Augments Immunotherapy with PD-1 Blockade. Cancer Immunol Res. 2015;3:1375–1385.

[42] Stone ML, Chiappinelli KB, Li H, et al. Epigenetic therapy activates type I interferon signaling in murine ovarian cancer to reduce immunosuppression and tumor burden. Proc Natl Acad Sci USA. 2017;114:E10981–E10990.

[43] Topper MJ, Vaz M, Chiappinelli KB, et al. Epigenetic Therapy Ties MYC Depletion to Reversing Immune Evasion and Treating Lung Cancer. Cell. 2017;171:1284-1300.e21.

[44] Bensaid D, Blondy T, Deshayes S, et al. Assessment of new HDAC inhibitors for immunotherapy of malignant pleural mesothelioma. Clin Epigenet. 2018;10:79.

[45] Goruganthu MUL, Shanker A, Dikov MM, et al. Specific Targeting of Notch Ligand-Receptor Interactions to Modulate Immune Responses: A Review of Clinical and Preclinical Findings. Front Immunol. 2020;11:1958.

[46] Nowak AK, Lesterhuis WJ, Kok P-S, et al. Durvalumab with first-line chemotherapy in previously untreated malignant pleural mesothelioma (DREAM): a multicentre, single-arm, phase 2 trial with a safety run-in. Lancet Oncol. 2020;21:1213–1223.

[47] Gray SG, Mutti L. Immunotherapy for mesothelioma: a critical review of current clinical trials and future perspectives. Transl Lung Cancer Res. 2020;9:S100–S119.

[48] Chua TC, Yan TD. Peritoneal mesothelioma: current understanding and management. Can J Surg. 2009;52:6.

[49] González-Moreno S. Hyperthermic intraperitoneal chemotherapy: Rationale and technique. World J of Gastrointest Oncol. 2010;2:68.

[50] Yan TD, Sim J, Morris DL. Selection of Patients with Colorectal Peritoneal Carcinomatosis for Cytoreductive Surgery and Perioperative Intraperitoneal Chemotherapy. Ann Surg Oncol. 2007;14:1807–1817.

[51] Raza A. Advances in the management of peritoneal mesothelioma. World J Gastroenterol. 2014;20:11700.

[52] Alexander HR, Bartlett DL, Pingpank JF, et al. Treatment factors associated with long-term survival after cytoreductive surgery and regional chemotherapy for patients with malignant peritoneal mesothelioma. Surgery. 2013;153:779–786.

[53] Blackham AU, Shen P, Stewart JH, et al. Cytoreductive Surgery with Intraperitoneal Hyperthermic Chemotherapy for Malignant Peritoneal Mesothelioma: Mitomycin Versus Cisplatin. Ann Surg Oncol. 2010;17:2720–2727.

[54] Hübner M. In search of evidence – PIPAC on the fast lane. Pleura and Peritoneum 2018; 3(2):2-5.

[55] Bakrin N, Tempfer C, Scambia G, et al. PIPAC-OV3: A multicenter, open-label, randomized, two-arm phase III trial of the effect on progression-free survival of cisplatin and doxorubicin as Pressurized Intra-Peritoneal Aerosol Chemotherapy (PIPAC) vs. chemotherapy alone in patients with platinum-resistant recurrent epithelial ovarian, fallopian tube or primary peritoneal cancer. Pleura and Peritoneum 2018; 3(3): 1–12.

[56] Hassan R, Thomas A, Alewine C, et al. Mesothelin Immunotherapy for Cancer: Ready for Prime T? Clin Oncol. 2016;34:4171–4179.

[57] Kreitman RJ, Hassan R, FitzGerald DJ, et al. Phase I Trial of Continuous Infusion Anti-Mesothelin Recombinant Immunotoxin SS1P. Clin Cancer Res. 2009;15:5274–5279.

[58] Hassan R, Bullock S, Premkumar A, et al. Phase I Study of SS1P, a Recombinant Anti-Mesothelin Immunotoxin Given as a Bolus I.V. Infusion to Patients with Mesothelin-Expressing Mesothelioma, Ovarian, and Pancreatic Cancers. Clin Cancer Res. 2007;13:5144–5149.

[59] Hassan R. Mesothelin-Targeted Immunotoxin LMB-100 in People With Malignant Mesothelioma Identifier NCT02798536 [Internet]. [cited 2021 Aug 19]. Available from: https://clinicaltrials.gov/ct2/show/study/NCT02798536.

[60] Weber DG, Johnen G, Bryk O, et al. Identification of miRNA-103 in the Cellular Fraction of Human Peripheral Blood as a Potential Biomarker for Malignant Mesothelioma – A Pilot Study. Deb S, editor. PLoS ONE. 2012;7(1): 1-9.

[61] Allende ML, Sasaki T, Kawai H, et al. Mice Deficient in Sphingosine Kinase 1 Are Rendered Lymphopenic by FTY720. J Biol Chem. 2004;279:52487–52492.

[62] Brinkmann V, Cyster JG, Hla T. FTY720: Sphingosine 1-Phosphate Receptor-1 in the Control of Lymphocyte Egress and Endothelial Barrier Function. Am J Transplant. 2004;4:1019–1025.

[63] White C, Alshaker H, Cooper C, et al. The emerging role of FTY720 (Fingolimod) in cancer treatment. Oncotarget. 2016;7:23106–23127.

[64] Kreitzburg KM, Fehling SC, Landen CN, et al. FTY720 enhances the anti-tumor activity of carboplatin and tamoxifen in a patient-derived xenograft model of ovarian cancer. Cancer Lett. 2018;436:75–86.

[65] Weinstein JN, Collisson EA, Mills GB, et al. The Cancer Genome Atlas Pan-Cancer Analysis Project. Nat Genet. 2013; 45(10): 1113–1120.

[66] Vandermeers F, Neelature Sriramareddy S, Costa C, et al. The role of epigenetics in malignant pleural mesothelioma. Lung Cancer. 2013;81:311–318.

[67] LaFave LM, Béguelin W, Koche R, et al. Loss of BAP1 function leads to EZH2-dependent transformation. Nat Med. 2015;21:1344–1349.

[68] Kim M-C, Kim N-Y, Seo Y-R, et al. An Integrated Analysis of the Genome-Wide Profiles of DNA Methylation and mRNA Expression Defining the Side Population of a Human Malignant Mesothelioma Cell Line. J Cancer. 2016;7:1668–1679.

[69] Fischer JR, Ohnmacht U, Rieger N, et al. Promoter methylation of RASSF1A, RARβ and DAPK predict poor prognosis of patients with malignant mesothelioma. Lung Cancer. 2006;54:109–116.

[70] McLoughlin KC, Kaufman AS, Schrump DS. Targeting the epigenome in malignant pleural mesothelioma. Transl Lung Cancer Res. 2017;6:350–365.

[71] Scherpereel A, Berghmans T, Lafitte JJ, et al. Valproate-doxorubicin: promising therapy for progressing mesothelioma. A phase II study. Eur Respir J. 2011;37:129–135.

[72] Kalari S, Moolky N, Pendyala S, et al. Sphingosine Kinase 1 Is Required for Mesothelioma Cell Proliferation: Role of Histone Acetylation. Vij N, editor. PLoS ONE. 2012;7(9): 1-14.

[73] Pyne NJ, El Buri A, Adams DR, et al. Sphingosine 1-phosphate and cancer. Adv Biol

Regu. 2018;68:97–106.

[74] O'Brien J, Hayder H, Zayed Y, et al. Overview of MicroRNA Biogenesis, Mechanisms of Actions, and Circulation. Front Endocrinol. 2018;9:402. ***Article of interest because it provides a summary of the dynamics of miRNA actions and of secretion, transfer and uptake of extracellular miRNAs.**

[75] Birnie KA, Yip YY, Ng DCH, et al. Loss of miR-223 and JNK Signaling Contribute to Elevated Stathmin in Malignant Pleural Mesothelioma. Mol Cancer Res. 2015;13:1106–1118.

[76] Amatya VJ, Mawas AS, Kushitani K, et al. Differential microRNA expression profiling of mesothelioma and expression analysis of miR-1 and miR-214 in mesothelioma. Int J Onc. 2016;48:1599–1607.

[77] Biersack B. Relations between approved platinum drugs and non-coding RNAs in mesothelioma. Non-coding RNA Res. 2018;3:161–173.

[78] Capula M, Mantini G, Funel N, et al. New avenues in pancreatic cancer: exploiting microRNAs as predictive biomarkers and new approaches to target aberrant metabolism. Expert Rev Clin Pharmaco. 2019;12:1081–1090.

[79] Zununi Vahed S, Barzegari A, Rahbar Saadat Y, et al. A microRNA isolation method from clinical samples. Bioimpacts. 2016;6:25–31.

[80] Santarelli L, Strafella E, Staffolani S, et al. Association of MiR-126 with Soluble Mesothelin-Related Peptides, a Marker for Malignant Mesothelioma. Pandey S, editor. PLoS ONE. 2011;6(4):1-9.

[81] Kirschner MB, Cheng YY, Badrian B, et al. Increased Circulating miR-625-3p: A Potential Biomarker for Patients With Malignant Pleural Mesothelioma. J Thorac Oncol. 2012;7:1184–1191.

[82] Mozzoni P, Ampollini L, Goldoni M, et al. MicroRNA Expression in Malignant Pleural Mesothelioma and Asbestosis: A Pilot Study. Dis Markers. 2017;2017:1–10.

[83] Benjamin H, Lebanony D, Rosenwald S, et al. A Diagnostic Assay Based on MicroRNA Expression Accurately Identifies Malignant Pleural Mesothelioma. J Mol Diagn. 2010;12:771–779.

[84] Gee GV, Koestler DC, Christensen BC, et al. Downregulated microRNAs in the differential diagnosis of malignant pleural mesothelioma. Int J Cancer. 2010;127:2859–2869.

[85] Andersen M, Grauslund M, Ravn J, et al. Diagnostic Potential of miR-126, miR-143, miR-145, and miR-652 in Malignant Pleural Mesothelioma. J Mol Diagn. 2014;16:418–430.

[86] Cavalleri T, Angelici L, Favero C, et al. Plasmatic extracellular vesicle microRNAs in malignant pleural mesothelioma and asbestos-exposed subjects suggest a 2-miRNA signature as potential biomarker of disease. Artero R, editor. PLoS ONE. 2017;12(5):1-16.

[87] Weber DG, Gawrych K, Casjens S, et al. Circulating miR-132-3p as a Candidate Diagnostic Biomarker for Malignant Mesothelioma. Dis Markers. 2017;2017:1–15.

[88] Muraoka T, Soh J, Toyooka S, et al. The degree of microRNA-34b/c methylation in serum-circulating DNA is associated with malignant pleural mesothelioma. Lung Cancer. 2013;82:485–490.

[89] Bononi I, Comar M, Puozzo A, et al. Circulating microRNAs found dysregulated in ex-exposed asbestos workers and pleural mesothelioma patients as potential new biomarkers. Oncotarget. 2016;7:82700–82711.

[90] Cappellesso R, Nicolè L, Caroccia B, et al. Young investigator challenge: MicroRNA-21/MicroRNA-126 profiling as a novel tool for the diagnosis of malignant mesothelioma in pleural effusion cytology: miRNA Profiling in Pleural Effusions. Cancer Cytopathol. 2016;124:28–37.

[91] Pass HI, Goparaju C, Ivanov S, et al. hsa-miR-29c* Is Linked to the Prognosis of Malignant Pleural Mesothelioma. Cancer Res. 2010;70:1916–1924.

[92] Busacca S, Germano S, De Cecco L, et al. MicroRNA Signature of Malignant Mesothelioma with Potential Diagnostic and Prognostic Implications. Am J Respir Cell Mol Biol. 2010;42:312–319. ****Article of considerable interest because it describes many differentially**

expressed miRNAs in MMe and it describes their potential as diagnostic and prognostic factors.

[93] De Santi C, Melaiu O, Bonotti A, et al. Deregulation of miRNAs in malignant pleural mesothelioma is associated with prognosis and suggests an alteration of cell metabolism. Sci Rep. 2017;7:3140.

[94] Kirschner MB, Cheng YY, Armstrong NJ, et al. MiR-Score: A novel 6-microRNA signature that predicts survival outcomes in patients with malignant pleural mesothelioma. Mol Oncol. 2015;9:715–726.

[95] Kao SC, Cheng YY, Williams M, et al. Tumor Suppressor microRNAs Contribute to the Regulation of PD-L1 Expression in Malignant Pleural Mesothelioma. J Thorac Oncol. 2017;12:1421–1433.

[96] Ivanov SV, Goparaju CMV, Lopez P, et al. Pro-tumorigenic Effects of miR-31 Loss in Mesothelioma. J Biol Chem. 2010;285:22809–22817.

[97] Moody HL, Lind MJ, Maher SG. MicroRNA-31 Regulates Chemosensitivity in Malignant Pleural Mesothelioma. Mol Ther Nucleic Acids. 2017;8:317–329.

[98] Truini A, Coco S, Genova C, et al. Prognostic and Therapeutic Implications of MicroRNA in Malignant Pleural Mesothelioma. MicroRNA. 2016;5:12–18.

[99] Kubo T, Toyooka S, Tsukuda K, et al. Epigenetic Silencing of MicroRNA-34b/c Plays an Important Role in the Pathogenesis of Malignant Pleural Mesothelioma. Clin Cancer Res. 2011;17:4965–4974.

[100] Ueno T, Toyooka S, Fukazawa T, et al. Preclinical Evaluation of MicroRNA-34b/c Delivery for Malignant Pleural Mesothelioma. Acta Med Okayama. 68:4.

[101] Xu Y, Zheng M, Merritt RE, et al. miR-1 Induces Growth Arrest and Apoptosis in Malignant Mesothelioma. Chest. 2013;144:1632–1643.

[102] Reid G, Johnson TG, van Zandwijk N. Manipulating microRNAs for the Treatment of Malignant Pleural Mesothelioma: Past, Present and Future. Front Oncol. 2020;10:105.

[103] Williams M, Kirschner MB, Cheng YY, et al. miR-193a-3p is a potential tumor suppressor in malignant pleural mesothelioma. Oncotarget. 2015;6:23480–23495.

[104] Goparaju CM, Blasberg JD, Volinia S, et al. Onconase mediated NFKβ downregulation in malignant pleural mesothelioma. Oncogene. 2011;30:2767–2777.

[105] Khodayari N, Mohammed KA, Goldberg EP, et al. EphrinA1 inhibits malignant mesothelioma tumor growth via let-7 microRNA-mediated repression of the RAS oncogene. Cancer Gene Ther. 2011;18:806–816.

[106] Xu R, Rai A, Chen M, et al. Extracellular vesicles in cancer — implications for future improvements in cancer care. Nat Rev Clin Oncol. 2018;15:617–638.

[107] Biersack B. Interplay of non-coding RNAs and approved antimetabolites such as gemcitabine and pemetrexed in mesothelioma. Non-coding RNA Res. 2018;3:213–225.

[108] El Bezawy R, De Cesare M, Pennati M, et al. Antitumor activity of miR-34a in peritoneal mesothelioma relies on c-MET and AXL inhibition: persistent activation of ERK and AKT signaling as a possible cytoprotective mechanism. J Hematol Oncol. 2017;10:19.

[109] Chen J, Li X, Wei S. Critical appraisal of pemetrexed in the treatment of NSCLC and metastatic pulmonary nodules. Onco Targets Ther. 2014;937.

[110] Yamamoto K, Seike M, Takeuchi S, et al. miR-379/411 cluster regulates IL-18 and contributes to drug resistance in malignant pleural mesothelioma. Oncol Rep. 2014;32:2365–2372.

[111] Küçüktürkmen B, Bozkır A. Development and characterization of cationic solid lipid nanoparticles for co-delivery of pemetrexed and miR-21 antisense oligonucleotide to glioblastoma cells. Drug Dev Ind Pharm. 2018;44:306–315.

[112] van Beijnum JR, Giovannetti E, Poel D, et al. miRNAs: micro-managers of anticancer combination therapies. Angiogenesis. 2017;20:269–285.

[113] Williams M, Cheng YY, Phimmachanh M, et al. Tumour suppressor microRNAs contribute to drug resistance in malignant pleural mesothelioma by targeting anti-apoptotic pathways. Cancer Drug Resist. 2019; 2(4): 1193–1206.

[114] van Zandwijk N, Pavlakis N, Kao SC, et al. Safety and activity of microRNA-loaded minicells in patients with recurrent malignant pleural mesothelioma: a first-in-man, phase 1, open-label, dose-escalation study. Lancet Oncol. 2017;18:1386–1396. ***article of interest for the new therapeutic approach using miRNAs in MPM**

[115] Xue W, Dahlman JE, Tammela T, et al. Small RNA combination therapy for lung cancer. Proc Natl Acad Sci U S A. 2014; 111(34): 3553–3561.

[116] Li H, Yu G, Shi R, et al. Cisplatin-induced epigenetic activation of miR-34a sensitizes bladder cancer cells to chemotherapy. Mol Cancer. 2014;13:8.

[117] Uematsu K, Seki N, Seto T, et al. Targeting the Wnt Signaling Pathway with Dishevelled and Cisplatin Synergistically Suppresses Mesothelioma Cell Growth. Anticancer Res. 2007;27(6):4239-4242.

[118] Wojtuszkiewicz A, Assaraf YG, Maas MJ, et al. Pre-mRNA splicing in cancer: the relevance in oncogenesis, treatment and drug resistance. Expert Opin Drug Metab Toxicol. 2015;11:673–689.

[119] Bonnal SC, López-Oreja I, Valcárcel J. Roles and mechanisms of alternative splicing in cancer — implications for care. Nat Rev Clin Oncol. 2020;17:457–474.

[120] Bueno R, Stawiski EW, Goldstein LD, et al. Comprehensive genomic analysis of malignant pleural mesothelioma identifies recurrent mutations, gene fusions and splicing alterations. Nat Genet. 2016;48:407–416. ****Manuscript of special interest, providing a comprehensive genomic profile of MMe**

[121] Effenberger KA, Anderson DD, Bray WM, et al. Coherence between Cellular Responses and in Vitro Splicing Inhibition for the Anti-tumor Drug Pladienolide B and Its Analogs. J Biol Chem. 2014;289:1938–1947.

[122] Hsu TY-T, Simon LM, Neill NJ, et al. The spliceosome is a therapeutic vulnerability in MYC-driven cancer. Nature. 2015;525:384–388.

[123] Salton M, Misteli T. Small Molecule Modulators of Pre-mRNA Splicing in Cancer Therapy. Trends Mol Med. 2016;22:28–37.

[124] Sciarrillo R, Wojtuszkiewicz A, El Hassouni B, et al. Splicing modulation as novel therapeutic strategy against diffuse malignant peritoneal mesothelioma. EBioMedicine. 2019;39:215–225. ***Article of interest for the overview on splicing modulators as therapeutic tools for MMe and focus on SF3B1 as a novel potential prognostic factor in DMPM**

[125] Passetti F, Ferreira CG, Costa FF. The impact of microRNAs and alternative splicing in pharmacogenomics. Pharmacogenomics J. 2009;9:1–13.

[126] Duursma AM, Kedde M, Schrier M, et al. miR-148 targets human DNMT3b protein coding region. RNA. 2008;14:872–877.

[127] Makeyev EV, Zhang J, Carrasco MA, et al. The MicroRNA miR-124 Promotes Neuronal Differentiation by Triggering Brain-Specific Alternative Pre-mRNA Splicing. Mol Cell. 2007;27:435–448.

[128] Verduci L, Simili M, Rizzo M, et al. MicroRNA (miRNA)-mediated Interaction between Leukemia/Lymphoma-related Factor (LRF) and Alternative Splicing Factor/Splicing Factor 2 (ASF/SF2) Affects Mouse Embryonic Fibroblast Senescence and Apoptosis. J Biol Chem. 2010;285:39551–39563.

[129] Meseguer S, Mudduluru G, Escamilla JM, et al. MicroRNAs-10a and -10b Contribute to Retinoic Acid-induced Differentiation of Neuroblastoma Cells and Target the Alternative Splicing Regulatory Factor SFRS1 (SF2/ASF). J Biol Chem. 2011;286:4150–4164.

[130] Aslan D, Garde C, Nygaard MK, et al. Tumor suppressor microRNAs are downregulated in myelodysplastic syndrome with spliceosome mutations. Oncotarget. 2016;7:9951–9963.

[131] Cortes-Dericks L, Froment L, Boesch R, et al. Cisplatin-resistant cells in malignant pleural mesothelioma cell lines show ALDHhighCD44+ phenotype and sphere-forming capacity. BMC Cancer. 2014;14:304. ****Article of considerable importance because it evaluated the mRNA levels of CSC markers, such as aldehyde dehydrogenase (ALDH) and CD44 in H28, H2052**

and Meso4 MPM cell lines, demonstrating their involvement in CSCs self-renewal and chemoresistance.

[132] Cortes-Deriks L, Giovanni L. Carboni, Ralph A. Schmid, et al. Putative cancer stem cells in malignant pleural mesothelioma show resistance to cisplatin and pemetrexed. Int J Oncol. 2010;37(2):437-444. ***Article that evaluated the upregulation of CSC markers (CD133, Bmi-1, uPAR and ABCG2) in MPM cell lines, demonstrating the close connection between CSCs and resistance to standard chemotherapy drugs such as cisplatin or pemetrexed.**

[133] Panyam J. Cancer stem cells. Drug Deliv and Transl Res. 2013;3:111–112.

[134] Pasdar EA, Smits M, Stapelberg M, et al. Characterisation of Mesothelioma-Initiating Cells and Their Susceptibility to Anti-Cancer Agents. Zhang L, editor. PLoS ONE. 2015;11(5):e0156012.

[135] Ghani FI, Yamazaki H, Iwata S, et al. Identification of cancer stem cell markers in human malignant mesothelioma cells. Biochem Biophys Res Commun. 2011;404:735–742.

[136] Varghese S, Whipple R, Martin SS, et al. Multipotent Cancer Stem Cells Derived from Human Malignant Peritoneal Mesothelioma Promote Tumorigenesis. Najbauer J, editor. PLoS ONE. 2012;7(12): e52825.

[137] Huang Y, Lin L, Shanker A, et al. Resuscitating Cancer Immunosurveillance: Selective Stimulation of DLL1-Notch Signaling in T cells Rescues T-cell Function and Inhibits Tumor Growth. Cancer Res. 2011;71:6122–6131.

[138] Fazio C, Ricciardiello L. Inflammation and Notch signaling: a crosstalk with opposite effects on tumorigenesis. Cell Death Dis. 2016;7:e2515–e2515.

[139] Garcia A, Kandel JJ. Notch: A key regulator of tumor angiogenesis and metastasis. Histol

Histopathol. 2012;9.

[140] Zavadil J, Cermak L, Soto-Nieves N, et al. Integration of TGF-β/Smad and Jagged1/Notch signalling in epithelial-to-mesenchymal transition. EMBO J. 2004;23:1155–1165.

[141] Pannuti A, Foreman K, Rizzo P, et al. Targeting Notch to Target Cancer Stem Cells. Clin Cancer Res. 2010;16:3141–3152.

[142] Kopan R, Ilagan MaXG. The Canonical Notch Signaling Pathway: Unfolding the Activation Mechanism. Cell. 2009;137:216–233.

[143] Miele L. Notch signaling. Clin Cancer Res. 2006;12:1074–1079.

[144] Graziani I, Eliasz S, De Marco MA, et al. Opposite Effects of Notch-1 and Notch-2 on Mesothelioma Cell Survival under Hypoxia Are Exerted through the Akt Pathway. Cancer Res. 2008;68:9678–9685. ****Article of considerable interest because it explains the involvement of Notch signaling pathway in MPM, tumor characterized by hypoxic microenvironment which in turn sustains the expression of Notch receptors and drug resistance.**

[145] Yin L, Velazquez OC, Liu Z-J. Notch signaling: Emerging molecular targets for cancer therapy. Biochem Pharmacol. 2010;80:690–701.

[146] Wolfe MS. Substrate recognition and processing by γ-secretase. Biochim Biophys Acta Biomembr. 2020;1862:183016.

[147] Wang Z, Li Y, Banerjee S, et al. Exploitation of the Notch Signaling Pathway as a Novel Target for Cancer Therapy. Anticancer Res. 2008;10.

[148] Liu L, Zhang L, Zhao S, et al. Non-canonical Notch Signaling Regulates Actin Remodeling in Cell Migration by Activating PI3K/AKT/Cdc42 Pathway. Front Pharmacol. 2019;10:370.

[149] Aster JC, Pear WS, Blacklow SC. The Varied Roles of Notch in Cancer. Annu Rev Pathol Mech Dis. 2017;12:245–275.

[150] Venkatesh V, Nataraj R, Thangaraj GS, et al. Targeting Notch signalling pathway of cancer stem cells. Stem Cell Investig. 2018;5:5–5.

[151] Klabatsa A, Sheaff MT, Steele JPC, et al. Expression and prognostic significance of hypoxia-inducible factor 1α (HIF-1α) in malignant pleural mesothelioma (MPM). Lung Cancer. 2006;51:53–59.

[152] Gustafsson MV, Zheng X, Pereira T, et al. Hypoxia Requires Notch Signaling to Maintain the Undifferentiated Cell State. Dev Cell. 2005;9:617–628.

[153] Triner D, Shah YM. Hypoxia-inducible factors: a central link between inflammation and cancer. J Clin Invest. 2016;126:3689–3698.

[154] Mamuya FA, Duncan MK. aV integrins and TGF-β-induced EMT: a circle of regulation. J Cell Mol Med. 2012;16:445–455.

[155] Dengler VL, Galbraith MD, Espinosa JM. Transcriptional regulation by hypoxia inducible factors. Crit Rev Biochem Mol Biol. 2014;49:1–15.

[156] Petrova V, Annicchiarico-Petruzzelli M, Melino G, et al. The hypoxic tumour microenvironment. Oncogenesis. 2018;7:10.

[157] Kim M-C, Hwang S-H, Kim N-Y, et al. Hypoxia promotes acquisition of aggressive phenotypes in human malignant mesothelioma. BMC Cancer. 2018;18:819.

[158] Urso L, Cavallari I, Sharova E, et al. Metabolic rewiring and redox alterations in malignant pleural mesothelioma. Br J Cancer. 2020;122:52–61.

[159] Li Petri G, El Hassouni B, Sciarrillo R, et al. Impact of hypoxia on chemoresistance of mesothelioma mediated by the proton-coupled folate transporter, and preclinical activity of new anti-LDH-A compounds. Br J Cancer. 2020;123:644–656.

[160] Moore G, Annett S, McClements L, et al. Top Notch Targeting Strategies in Cancer: A Detailed Overview of Recent Insights and Current Perspectives. Cells. 2020;9:1503.

[161] Takebe N, Miele L, Harris PJ, et al. Targeting Notch, Hedgehog, and Wnt pathways in cancer stem cells: clinical update. Nat Rev Clin Oncol. 2015;12:445–464.

[162] Kopan R, Ilagan MXG. γ-Secretase: proteasome of the membrane? Nat Rev Mol Cell Biol. 2004;5:499–504.

[163] McCaw TR, Inga E, Chen H, et al. Gamma Secretase Inhibitors in Cancer: A Current Perspective on Clinical Performance. Oncologist. 2021;26:e608–e621.

[164] Strosberg JR, Yeatman T, Weber J, et al. A phase II study of RO4929097 in metastatic colorectal cancer. Eur J Cancer. 2012;48:997–1003.

[165] Sardesai S, Badawi M, Mrozek E, et al. A phase I study of an oral selective gamma secretase (GS) inhibitor RO4929097 in combination with neoadjuvant paclitaxel and carboplatin in triple negative breast cancer. Invest New Drugs. 2020;38:1400–1410.

[166] Lee SM, Moon J, Redman BG, et al. Phase 2 study of RO4929097, a gamma-secretase inhibitor, in metastatic melanoma: SWOG 0933: RO4929097 in Melanoma: SWOG 0933. Cancer. 2015;121:432–440.

[167] Diaz-Padilla I, Wilson MK, Clarke BA, et al. A phase II study of single-agent RO4929097, a gamma-secretase inhibitor of Notch signaling, in patients with recurrent platinum-resistant epithelial ovarian cancer: A study of the Princess Margaret, Chicago and California phase II consortia. Gynecol Oncol. 2015;137:216–222.

[168] Peereboom DM, Ye X, Mikkelsen T, et al. A Phase II and Pharmacodynamic Trial of RO4929097 for Patients With Recurrent/Progressive Glioblastoma. Neurosurg. 2021;88:246–251.

[169] Borthakur G, Martinelli G, Raffoux E, et al. Phase 1 study to evaluate Crenigacestat (LY3039478) in combination with dexamethasone in patients with T-cell acute lymphoblastic leukemia and lymphoma. Cancer. 2021;127:372–380.

[170] Azaro A, Massard C, Tap WD, et al. A phase 1b study of the Notch inhibitor crenigacestat (LY3039478) in combination with other anticancer target agents (taladegib, LY3023414, or abemaciclib) in patients with advanced or metastatic solid tumors. Invest New Drugs. 2021;39:1089–1098.

[171] Azaro A, Baldini C, Rodon J, et al. Phase 1 study of 2 high dose intensity schedules of the pan-Notch inhibitor crenigacestat (LY3039478) in combination with prednisone in patients with advanced or metastatic cancer. Invest New Drugs. 2021;39:193–201.

[172] Wu CX, Xu A, Zhang CC, et al. Notch Inhibitor PF-03084014 Inhibits Hepatocellular Carcinoma Growth and Metastasis via Suppression of Cancer Stemness due to Reduced Activation of Notch1–Stat3. Mol Cancer Ther. 2017;16:1531–1543.

[173] Yang X, Xia W, Chen L, et al. Synergistic antitumor effect of a γ-secretase inhibitor PF-03084014 and sorafenib in hepatocellular carcinoma. Oncotarget. 2018;9:34996–35007.

[174] Cui D, Dai J, Keller JM, et al. Notch Pathway Inhibition Using PF-03084014, a γ-Secretase Inhibitor (GSI), Enhances the Antitumor Effect of Docetaxel in Prostate Cancer. Clin Cancer Res. 2015;21:4619–4629.

[175] Zhang CC, Yan Z, Zong Q, et al. Synergistic Effect of the γ-Secretase Inhibitor PF-03084014 and Docetaxel in Breast Cancer Models. Stem Cells Transl Med. 2013;2:233–242.

[176] Palomero T, Sulis ML, Cortina M, et al. Mutational loss of PTEN induces resistance to NOTCH1 inhibition in T-cell leukemia. Nat Med. 2007;13:1203–1210.

[177] Liu Z, Fan F, Wang A, et al. Dll4-Notch signaling in regulation of tumor angiogenesis. J Cancer Res Clin Oncol. 2014;140:525–536.

[178] Li K, Li Y, Wu W, et al. Modulation of Notch Signaling by Antibodies Specific for the Extracellular Negative Regulatory Region of NOTCH3. J Biol Chem. 2008;283:8046–8054.

[179] Smith DC, Chugh R, Patnaik A, et al. A phase 1 dose escalation and expansion study of Tarextumab (OMP-59R5) in patients with solid tumors. Invest New Drugs. 2019;37:722–730.

[180] Ahmadzada T, Kao S, Reid G, et al. Extracellular vesicles as biomarkers in malignant pleural mesothelioma: A review. Crit Rev Oncol Hematol. 2020;150:102949.

Chapter 8

New imidazo[2,1-*b*][1,3,4]thiadiazole derivatives inhibit FAK phosphorylation and potentiate the antiproliferative effects of gemcitabine through modulation of the human equilibrative nucleoside transporter-1 in peritoneal mesothelioma.

Li Petri, G*.; Pecoraro, C*.; Randazzo, O*.; Zoppi, S.; Cascioferro, S.; Parrino, B.; Carbone, D.; El Hassouni, B.; Cavazzoni, A.; Zaffaroni, N.; Cirrincione, G.; Diana, P.; Peters, G.J.; Giovannetti, E.

Anticancer Research (2020), 40(9), 4913-4919.

* These Authors contributed equally to this study.

ANTICANCER RESEARCH *40*: 4913-4919 (2020)
doi:10.21873/anticanres.14494

New Imidazo[2,1-*b*][1,3,4]Thiadiazole Derivatives Inhibit FAK Phosphorylation and Potentiate the Antiproliferative Effects of Gemcitabine Through Modulation of the Human Equilibrative Nucleoside Transporter-1 in Peritoneal Mesothelioma

GIOVANNA LI PETRI[1,2*], CAMILLA PECORARO[1,2*], ORNELLA RANDAZZO[1,2*], SILVIA ZOPPI[1,3],
STELLA MARIA CASCIOFERRO[2], BARBARA PARRINO[2], DANIELA CARBONE[1,2],
BTISSAME EL HASSOUNI[1], ANDREA CAVAZZONI[3], NADIA ZAFFARONI[4], GIROLAMO CIRRINCIONE[2],
PATRIZIA DIANA[2], GODEFRIDUS J. PETERS[1,5] and ELISA GIOVANNETTI[1,6]

[1]*Department of Medical Oncology, Amsterdam UMC, Cancer Center Amsterdam,*
VU University Medical Center, Amsterdam, the Netherlands;
[2]*Dipartimento di Scienze e Tecnologie Biologiche Chimiche e Farmaceutiche (STEBICEF),*
Università degli Studi di Palermo, Palermo, Italy;
[3]*Department of Medicine and Surgery, University of Parma, Parma, Italy;*
[4]*Molecular Pharmacology Unit, Fondazione IRCCS Istituto Nazionale dei Tumori, Milan, Italy;*
[5]*Department of Biochemistry, Medical University of Gdansk, Gdansk, Poland;*
[6]*Cancer Pharmacology Lab, Fondazione Pisana per la Scienza, Pisa, Italy*

Abstract. *Background/Aim: A new class of imidazo[2,1-b][1,3,4]thiadiazole compounds have recently been evaluated as inhibitors of phosphorylation of focal adhesion kinase (FAK) in pancreatic cancer. FAK is overexpressed in mesothelioma and has recently emerged as an interesting target for the treatment of this disease. Materials and Methods: Ten imidazo[2,1-b][1,3,4]thiadiazole compounds characterized by indole bicycle and a thiophene ring, were evaluated for their cytotoxic activity in two primary cell cultures of peritoneal mesothelioma, MesoII and STO cells. Results: Compounds 1a and 1b showed promising antitumor activity with* IC_{50} *values in the range of 0.59 to 2.81 μM in both cell lines growing as monolayers or as spheroids. Their antiproliferative and antimigratory activity was associated with inhibition of phospho-FAK, as detected by a specific ELISA assay in STO cells. Interestingly, these compounds potentiated the antiproliferative activity of gemcitabine, and these results might be explained by the increase in the mRNA expression of the key gemcitabine transporter human equilibrative nucleoside transporter-1 (hENT-1). Conclusion: These promising results support further studies on new imidazo[2,1-b][1,3,4]thiadiazole compounds as well as on the role of both FAK and hENT-1 modulation in order to develop new drug combinations for peritoneal mesothelioma.*

Malignant mesothelioma refers to a rare but aggressive tumor derived from mesothelial cells. They form a monolayer that covers the body's serous cavities and whose main function is to provide a protective membrane for the lung (pleural), the intestine (peritoneum), the heart (pericardium) and the *tunica vaginalis*. The thorax and abdominal cavity are the primary sites for the development of cancer, with a rate of 80-90% and 10-15%, respectively (1).

Diffuse malignant peritoneal mesothelioma (DMPM) is difficult to diagnose, both clinically and histologically, and is characterized by a dismal prognosis. Most patients benefit from a multimodal treatment that includes the combination of surgery and chemotherapy. In particular, the standard of care consists in cytoreductive surgery (CRS) combined with hyperthermic intraperitoneal chemotherapy (HIPEC) (2-4). However, many patients still suffer from disease recurrence, and new therapeutic options to implement in the current surgical and HIPEC procedures are warranted.

---

*These Authors contributed equally to this study.

Correspondence to: Prof Dr. Godefridus J. Peters, Department Medical Oncology, Amsterdam UMC, VU University Medical Center, Cancer Center Amsterdam, De Boelelaan 1117, 1081 HV Amsterdam, the Netherlands. Tel: +31 204442633, Fax: +31 20 4443844, e-mail: gj.peters@amsterdamumc.nl

Key Words: Mesothelioma, imidazo[2,1-*b*][1,3,4]thiadiazole compounds, FAK, gemcitabine, human equilibrative nucleoside transporter-1.

Though all mesotheliomas originate in serous membranes, the efficacy of conventional chemotherapy varies per location (5). Like many other solid tumors, mesotheliomas develop as a result of different molecular aberrations. To understand these events, research is directed towards: first, to identify new molecules with antitumor activity and second, to assess the activity of compounds already known for their mechanism of action and used for the treatment of various diseases alone or in combination with other drugs. Recently, we reported the antitumor activity of a new class of imidazo[2,1-*b*][1,3,4]thiadiazole compounds on pancreatic ductal adenocarcinoma, highlighting their ability to reduce FAK phosphorylation on tyrosine residue (Y-397) (6). Moreover, we previously observed good results with combinations of new drugs with the antimetabolite gemcitabine in preclinical models of DMPM (7). Encouraged by these findings as well as by studies supporting 'drug repositioning' in drug discovery (8), we studied the antitumor activity of ten imidazo[2,1-*b*][1,3,4]thiadiazole compounds (Figure 1) on two primary cultures of DMPM cells, growing as monolayers or spheroids and evaluated the potential mechanisms underlying the pharmacological interaction with gemcitabine.

Materials and Methods

Drugs and chemicals. The imidazo[2,1-*b*][1,3,4]thiadiazole compounds were synthesized, and dissolved in DMSO, as described previously (6). Dulbecco's Modified Eagle Medium: Nutrient Mixture F-12 (DMEM/F-12), fetal bovine serum (FBS), penicillin (50 IU/ml) and streptomycin (50 μg/ml) were from Gibco (Gaithersburg, MD, USA). All other chemicals were from Sigma (Zwijndrecht, the Netherlands). Gemcitabine was a gift from Eli-Lilly.

Cell cultures. Human DMPM primary cultures (STO and MesoII) were derived from patients who underwent surgery (9). The cells were maintained in F-12 for less than 20 passages, supplemented with 10% heat-inactivated-FBS, 1% penicillin/ streptomycin, and routinely tested for mycoplasma.

Inhibition of cell growth. The cell growth inhibitory effect of imidazo[2,1-*b*][1,3,4]thiadiazoles was evaluated by the Sulforhodamine-B (SRB) assay, as described previously (10). Cells were seeded into 96-well flat-bottom plates (5×10^3 cells in 100 μl/well). After 24 h, cells were treated with eight different concentrations of the compounds (from 0.3 to 40 μM) for 72 h. Thereafter, cells were fixed with 25 μl of 50% cold trichloroacetic acid and kept for at least 60 minutes at 4˚C. The plates were washed gently with deionized water, dried at room temperature (RT) overnight and stained with 50 μl of 0.4% SRB solution in 1% acetic acid for 15 minutes at RT. The excess of SRB was removed on dry tissues and the plates were washed with a 1% acetic acid solution and dried at RT overnight. Finally, the SRB was dissolved in 150 μl of tris(hydroxymethyl)aminomethane solution pH 8.8 (TRIS base), and the optical density (OD) was measured at wavelenghts of 490 nm and 540 nm. The cell growth inhibition was calculated as the percentage of the OD drug-treated cells *versus* the OD of vehicle-treated cells ("negative control") (corrected for OD before drug addiction, "day-0").

Half maximal inhibitory concentration (IC_{50}) values were calculated with GraphPad Prism 7 (GraphPad, San Diego, CA, USA). In the combination studies with gemcitabine, we used the most promising compounds at their IC_{50} concentrations and gemcitabine at its IC_{25} concentration.

Wound healing assay. The *in vitro* wound-healing assay was performed as previously described (11). MesoII and STO cells were seeded in 96-well flat-bottom plates at the density of 5×10^4 cells/well and the confluent layer was scratched with a pin-tool. Thereafter, the medium was replaced in the control wells with only medium or with medium containing the compounds of interest. Wound closure was monitored by phase-contrast microscopy using the Leica-DMI300B microscope and pictures were captured immediately after scratch (T=0), and after 4, 8 and 20 h. Results were analyzed with the Scratch-Assay 6.2 software (Digital Cell Imaging Labs, Keerbergen, Belgium).

Spheroids assay. MesoII and STO spheroids were created as reported previously (12). Cells were seeded at a density of 7×10^4 cells/well for MesoII and 5×10^4 cells/well for STO, in cell repellent U-bottom plates (Greiner, Kremsmünster, Austria). After three days the spheroids were treated with **1a** and **1b** at IC_{50} and 5× IC_{50} concentrations. Pictures were taken every two days after replacing the medium of the control wells or adding medium with compounds to the experimental wells, and the experiment lasted seventeen days. The reduction in size of spheroids was monitored by phase-contrast microscopy and pictures were analysed with ImageJ (NIH, Bethesda, MD, USA), as described previously (13).

Enzyme-linked immunosorbent assay (ELISA) to evaluate FAK. To investigate whether our imidazothiadiazole compounds were able to reduce FAK phosphorylation at tyrosine residue 397 (FAK [pY397]) in the DMPM, we performed a quantitative analysis using a specific ELISA, as described (6). This assay was carried out on lysates of cells treated with compounds **1a** and **1b** at 5× IC_{50}s concentrations for 2 h.

Quantitative-PCR. Total RNA was extracted and reverse transcribed from cells treated with **1a** and **1b** at 5× IC_{50} concentrations for 24 h. The resulting cDNA was amplified by quantitative-PCR with the ABIPRISM-7500 instrument (Applied Biosystems, Foster City, CA, USA) using specific hENT-1 and primers, as previously described (12).

Statistics. All experiments were performed in triplicate and repeated at least three times. Data were expressed as mean values±SEM and were analysed by Student's *t*-test or ANOVA followed by the Tukey's multiple comparison, setting the level of significance at $p<0.05$.

Results

Antiproliferative activity. The effect of ten imidazo[2,1-*b*][1,3,4]thiadiazole compounds was evaluated on MesoII and STO cells, by the SRB assay. Only four out of the ten compounds (**1a, b, g** and **h**), showed more than 50% inhibition of growth at 10 μM and were explored in more

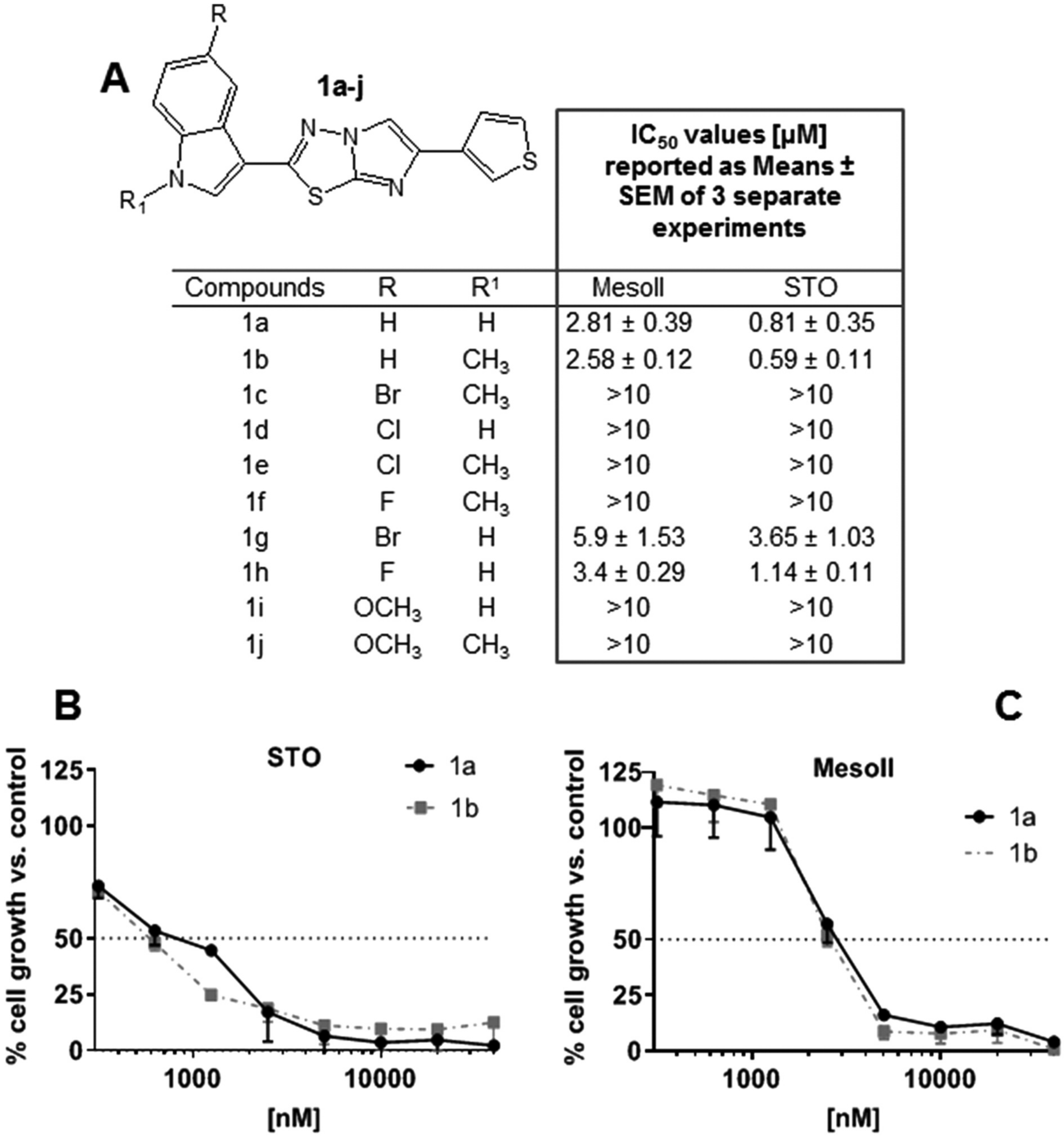

Compounds	R	R^1	MesoII	STO
			IC_{50} values [μM] reported as Means ± SEM of 3 separate experiments	
1a	H	H	2.81 ± 0.39	0.81 ± 0.35
1b	H	CH_3	2.58 ± 0.12	0.59 ± 0.11
1c	Br	CH_3	>10	>10
1d	Cl	H	>10	>10
1e	Cl	CH_3	>10	>10
1f	F	CH_3	>10	>10
1g	Br	H	5.9 ± 1.53	3.65 ± 1.03
1h	F	H	3.4 ± 0.29	1.14 ± 0.11
1i	OCH_3	H	>10	>10
1j	OCH_3	CH_3	>10	>10

Figure 1. *Antiproliferative activity of compounds 1a-j against diffuse malignant peritoneal mesothelioma cells, MesoII and STO. (A) Chemical backbone structure of compounds 1a-j with the list of the chemical structure of the R and R1 substituents for each compound and the IC_{50} values in μM of each compound against the DMPM cell lines. (B, C) Representative growth curves of STO (B) and MesoII (C) cells after 72 h of exposure to 1a or 1b. Points, mean values obtained from one representative experiment; bars, SEM.*

detail. Figure 1A summarizes their IC_{50} values, ranging from 0.59 to 5.9 μM, with the lowest IC_{50} in STO cells (Figure 1B), while in MesoII cells these compounds were less effective (Figure 1C). The results obtained with the compounds **1a** and **1b**, prompted us to investigate their cytotoxic activity on three-dimensional (3D) models.

Volume reduction of MesoII- and STO-derived tumor spheres. Earlier studies reported that the drug activity found in the two-dimensional monolayers is different from that in 3D cell cultures (14), as the 3D model offers a more realistic representation of the tumor microenvironment, including the physical and mechanical properties, oxygen,

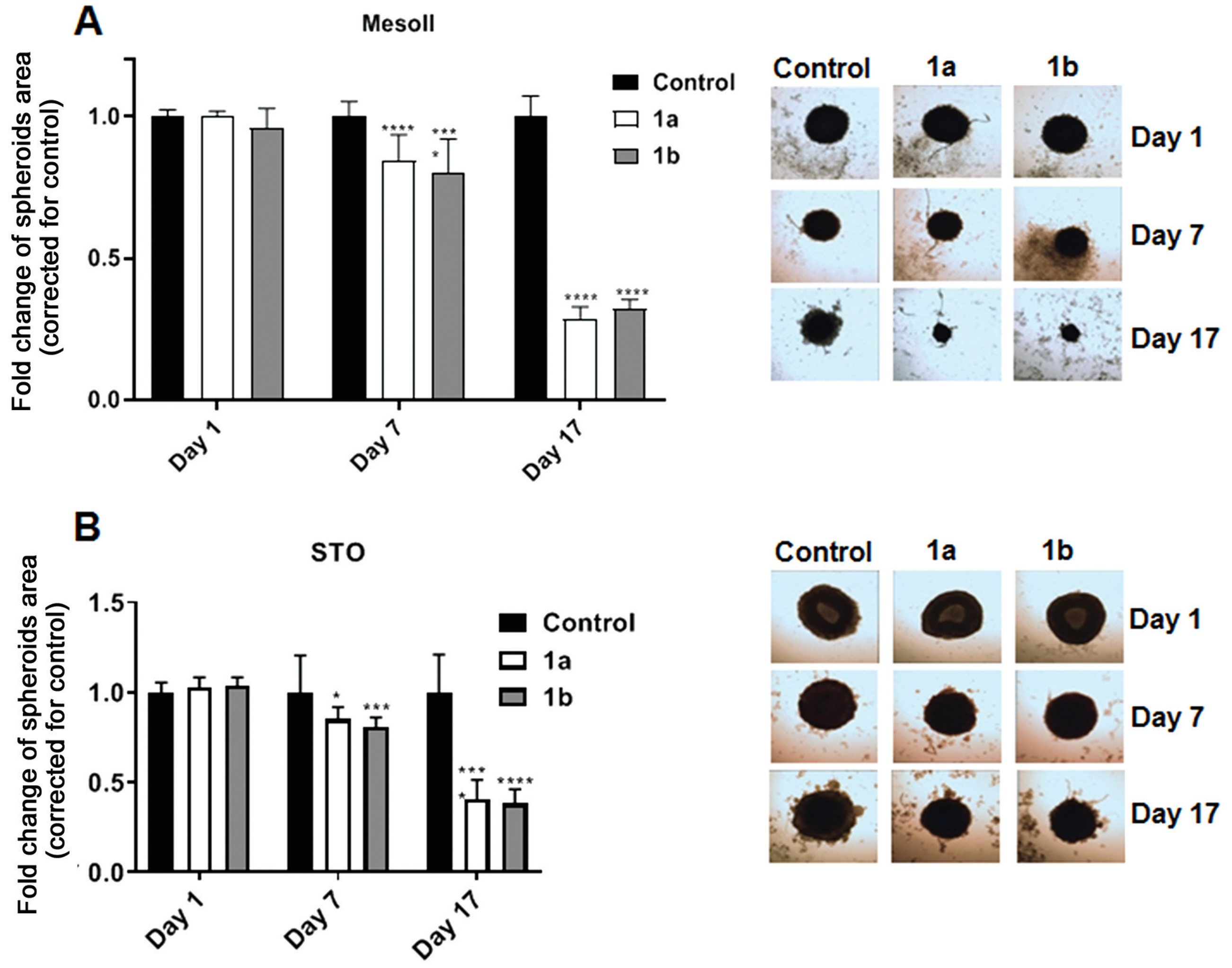

Figure 2. *Size reduction of (A) MesoII and (B) STO spheroids treated with compounds 1a or 1b at 5× IC_{50} concentrations. (Left plot) Fold-change compared to control, on day 1, 7 and 17. (Right pictures) representative images of spheroids, taken with an automated phase-contrast microscope on day 1 of treatment (Original magnification 5×), and after 7 and 17 days. All p-values were determined by Two-way ANOVA followed by Tukey's multiple comparisons test, *$p<0.05$, ***$p<0.001$, ****$p<0.0001$. These values were obtained by taking the mean value of at least ten different spheroids into account.*

pH and nutrients gradients, as well as drug transport (15). Therefore, we evaluated the ability of compounds **1a** and **1b** to affect the size of spheroids of MesoII and STO cells. As shown in Figure 2, the spheroids decreased significantly in size over time in both cell lines. Notably, after 17 days of treatment, we found about 2-fold reduction, compared to the untreated spheroids.

*Compounds **1a** and **1b** inhibited cell migration and phospho-FAK in STO cells*. Secondary lesions that originate from DMPM primary site are very uncommon. However, localized and/or regional metastasis with the involvement of lymph nodes have been observed (16-18). Furthermore, the spread of tumor cells to form new metastatic *loci* on distant organs has been reported; particularly, the pancreas and the kidneys are the main organs involved, whereas the lung, the heart and the brain are less commonly affected (19, 20). The interesting antiproliferative activity of compounds **1a** and **1b**, prompted us to investigate their anti-migratory activity by wound-healing assay in the STO cells, which were selected because of their higher sensitivity and a replication time well-above 24 h. In these cells, we observed a reduction of migration rates by 25.8% and 20%, after 20 h from the treatment, compared to control (set at 100%) (Figure 3A). Statistical analyses revealed that the reduction of migration in STO cells

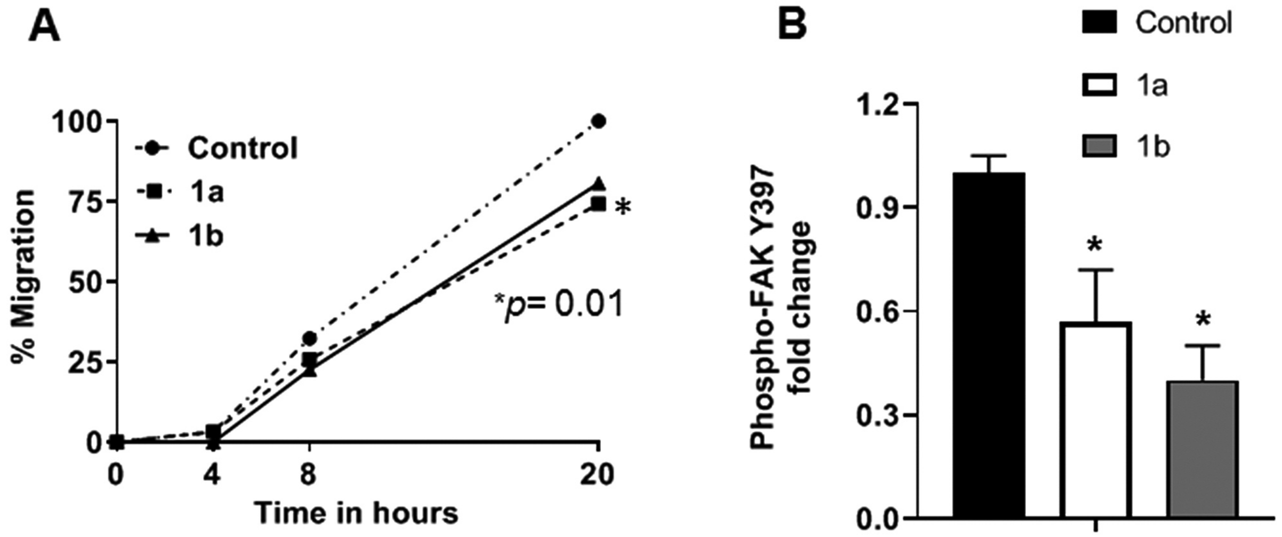

Figure 3. *(A) Modulation of the migration rate of STO cells treated for the indicated times with the compounds 1a and 1b at concentrations of 5× IC_{50}. Mean values were obtained from the means of at least six different scratch areas. SEM were always below 10%. (B) Inhibition of FAK phosphorylation at tyrosine residue 397 by compounds 1a and 1b. *p<0.05.*

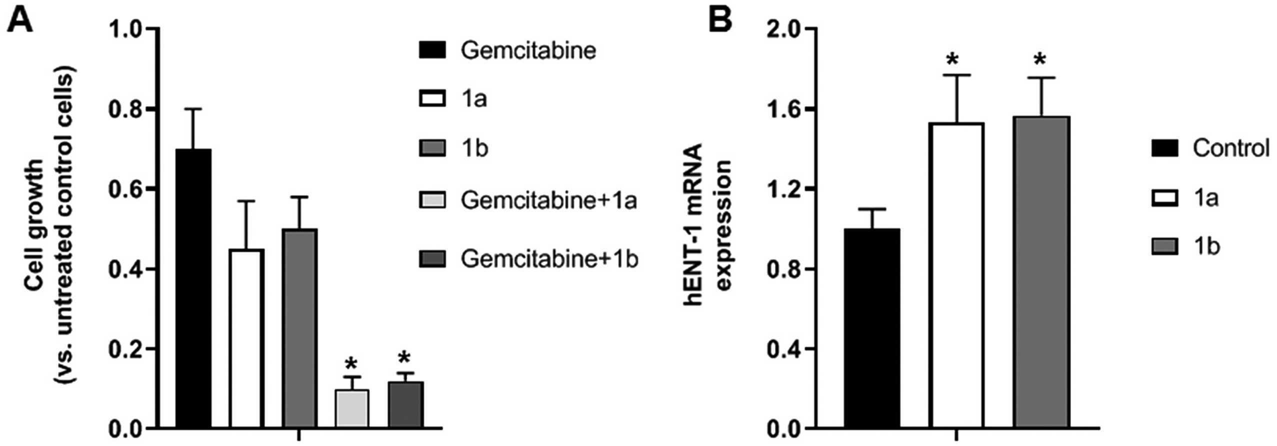

Figure 4. *The combination of compounds 1a and 1b with gemcitabine led to a significant reduction in cell growth and increased hENT-1 expression. (A) Effect of the combination of gemcitabine, at its IC_{25} concentration, with the compounds 1a or 1b, at their IC_{50} concentrations, on the growth of STO cells. (B) Modulation of hENT-1 mRNA levels in STO cells. Expression was determined with quantitative-PCR by normalization with the GAPDH housekeeping gene, and the values are expressed in arbitrary units, as described previously (12); Columns, mean values obtained from triplicate experiments. Bars, SEM; *p<0.05.*

treated with compound **1a** was significant, compared to the untreated control cells. Parallel ELISA studies revealed that both compounds **1a** and **1b** significantly reduced the phosphorylation of FAK (Figure 3B).

*Compounds **1a** and **1b** increased hENT-1 expression and gemcitabine cytotoxicity.* Since previous data showed synergistic effects of gemcitabine with the new anticancer agents in mesothelioma cells (7, 21) we tested whether the addition of compounds **1a** and **1b** at their IC_{50} concentrations would increase the antiproliferative effects of gemcitabine. These experiments were performed in STO cells because of the strongest antiproliferative and antimigratory effects. Interestingly, the combination of both compounds **1a** and **1b** at their IC_{50} concentration with gemcitabine at its IC_{25} concentration led to a significant reduction in cell growth, which reached values around 10% compared to untreated cells (Figure 4A).

Finally, to investigate the molecular mechanisms underlying the interaction of gemcitabine with compounds **1a** and **1b**, we measured the modulation of the gene expression of hENT-1, which is a key determinant of gemcitabine transport. Both compounds increased hENT-1 expression significantly (Figure 4B), suggesting its potential role in the increased activity of gemcitabine in combination with compounds **1a** and **1b**.

Discussion

Multimodal treatment including the combination of surgery and chemotherapy represents the standard of care for the treatment of patients with peritoneal mesothelioma; indeed, unlike radiotherapy, palliative surgery combined with chemotherapy showed a longer survival rate of patients, as demonstrated in a retrospective study conducted on Finnish patients with DMPM between 1 January 2000 and 31 December 2012 (22).

Ten imidazo[2,1-*b*][1,3,4]thiadiazole compounds, which inhibited FAK protein expression in the treatment of pancreatic cancer (6), were tested for their antiproliferative activity on two primary cell cultures of diffuse malignant peritoneal mesothelioma, namely MesoII and STO. Four compounds **1a, b, g** and **h** showed promising antitumor activity with IC_{50}s in the range from 0.59 to 5.9 μM. In particular, the compounds **1a** and **1b** showed the lowest IC_{50} in both cell lines. Similar results were observed in spheroids, inhibiting their area by approximately 2-fold compared to the controls. These are very interesting results since spheroids of mesothelioma cells are resistant to different treatments, including conventional chemotherapeutic drugs.

Moreover, the lowest IC_{50} values were also associated with the ability of compounds **1a** and **1b** to reduce cell migration of STO cells by 25.8% and 20%, respectively. These results gave more insight in the mechanism of action and led us to investigate the ability of these compounds to inhibit FAK phosphorylation, as reported previously (7). Remarkably, both compounds were able to reduce the phosphorylation of FAK, which is a potential target in mesothelioma (23).

Moreover, these compounds potentiated the activity of gemcitabine and we might hypothesize that this effect is due to the increased mRNA expression of hENT-1, which has been associated with gemcitabine activity in different cancer cell types (24). Of note, a previous study showed that inhibition of hENT-1-mediated transport may result from p42/44 MAPK activation in HUVEC cells after short periods of hypoxia (25). Therefore, we hypothesize that the inhibition of FAK might cause an inhibition of its downstream target MAPK and this might in turn lead to an increase in the expression of hENT-1.

In conclusion, our novel findings should prompt further studies on imidazo[2,1-*b*][1,3,4]thiadiazole compounds as well as on the role of the modulation of FAK and hENT-1 for the rational development of new drug combinations in DMPM.

Conflicts of Interest

The Authors have no conflicts of interest to disclose in relation to this study.

Authors' Contributions

GLP, OR and CP performed chemical synthesis, experimental work and wrote the manuscript. SZ, SMC, DC, BP, and BEH, assisted with experimental work. AC, NZ, and GC provided essential material and helped to revise the manuscript. PD, GJP and EG were responsible for experimental design and helped to write the manuscript.

Acknowledgements

This work was partially supported by grants to Elisa Giovannetti from "The Law Offices of Peter G. Angelos Grant" of the Mesothelioma Applied Research Foundation (E.G), CCA grant 2018, AIRC Start-Up grant, Dutch Cancer Society grants (KWF project#11957), and Polish National Science Center project 2018/31/B/NZ7/02909 (G.J.P, E.G).

Notes

Preliminary results of this study were presented at the 40th EORTC-PAMM Winter Meeting, February 2019, Verona, Italy.

References

1 Carbone M, Adusumilli PS, Alexander HR, Baas P, Bardelli F, Bononi A, Bueno R, Felley-Bosco E, Galateau-Salle F, Jablons D, Mansfield AS, Minaai M, Perrot M, Pesavento P, Rusch V, Severson DT, Taioli E, Tsao A, Woodard G, Yang H, Zauderer MG and Pass HI: Mesothelioma: Scientific clues for prevention, diagnosis, and therapy. CA Cancer J Clin *69(5)*: 402-429, 2019. PMID: 31283845. DOI: 10.3322/caac.21572

2 Kim J, Bhagwandin S and Labow DM: Malignant peritoneal mesothelioma: A review. Ann Transl Med *5(11)*, 2017. PMID: 28706904. DOI: 10.21037/atm.2017.03.96

3 Archer MA and Bueno R: Surgery for malignant pleural mesothelioma. Lung Cancer Manag *4(5)*: 231-241, 2015. DOI: 10.2217/lmt.15.26

4 Batirel HF, Metintas M, Caglar HB, Yildizeli B, Lacin T, Bostanci K, Akgul AG, Evman S and Yuksel M: Trimodality treatment of malignant pleural mesothelioma. J Thorac Oncol *3(5)*: 499-504, 2008. PMID: 18449002. DOI: 10.1097/JTO.0b013e31816fca1b

5 Garcia-Carbonero R and Paz-Ares L: Systemic chemotherapy in the management of malignant peritoneal mesothelioma. Eur J Surg Oncol *32(6)*: 676-681, 2006. DOI: 10.1016/j.ejso.2006.03.009

6 Cascioferro S, Petri GL, Parrino B, Carbone D, Funel N, Bergonzini C, Mantini G, Dekker H, Geerke D, Peters GJ, Cirrincione G, Giovannetti E and Diana P: Imidazo[2,1-b] [1,3,4]thiadiazoles with

antiproliferative activity against primary and gemcitabine-resistant pancreatic cancer cells. Eur J Med Chem *189*: 112088, 2020. PMID: 32007666. DOI: 10.1016/j.ejmech.2020.112088

7 Li Petri G, El Hassouni B, Sciarrillo R, Funel N, Mantini G, Zeeuw van der Laan EA, Cascioferro S, Avan A, Zucali PA, Zaffaroni N, Lagerweij T, Parrino B, Smid K, Deraco M, Granchi C, Braczko A, Smolenski RT, Matherly LH, Jansen G, Assaraf YG, Diana P, Cloos J, Peters GJ, Minutolo F and Giovannetti E: Impact of hypoxia on chemoresistance of mesothelioma mediated by the proton-coupled folate transporter, and preclinical activity of new anti-LDH-A compounds. Br J Cancer, 2020. DOI: 10.1038/s41416-020-0912-9

8 Xue H, Li J, Xie H and Wang Y: Review of drug repositioning approaches and resources. Int J Biol Sci *14(10)*: 1232-1244, 2018. PMID: 30123072. DOI: 10.7150/ijbs.24612

9 De Cesare M, Cominetti D, Doldi V, Lopergolo A, Deraco M, Gandellini P, Friedlander S, Landesman Y, Kauffman MG, Shacham S, Pennati M and Zaffaroni N: Anti-tumor activity of selective inhibitors of XPO1/CRM1-mediated nuclear export in diffuse malignant peritoneal mesothelioma: the role of survivin. Oncotarget *6(15)*: 13119-13132, 2015. PMID: 25948791. DOI: 10.18632/oncotarget.3761

10 Sciarrillo R, Wojtuszkiewicz A, Kooi IE, Gómez VE, Boggi U, Jansen G, Kaspers GJ, Cloos J and Giovannetti E: Using RNA-sequencing to detect novel splice variants related to drug resistance in in vitro cancer models. J Vis Exp (*118)*: 54714, 2016. PMID: 28060337. DOI: 10.3791/54714

11 Massihnia D, Avan A, Funel N, Maftouh M, Van Krieken A, Granchi C, Raktoe R, Boggi U, Aicher B, Minutolo F, Russo A, Leon LG, Peters GJ and Giovannetti E: Phospho-Akt overexpression is prognostic and can be used to tailor the synergistic interaction of Akt inhibitors with gemcitabine in pancreatic cancer. J Hematol Oncol *10(1)*: 9, 2017. PMID: 28061880. DOI: 10.1186/s13045-016-0371-1

12 Maftouh M, Avan A, Sciarrillo R, Granchi C, Leon LG, Rani R, Funel N, Smid K, Honeywell R, Boggi U, Minutolo F, Peters GJ and Giovannetti E: Synergistic interaction of novel lactate dehydrogenase inhibitors with gemcitabine against pancreatic cancer cells in hypoxia. Br J Cancer *110*: 172-182, 2014. PMID: 24178759. DOI: 10.1038/bjc.2013.681

13 Sciarrillo R, Wojtuszkiewicz A, El Hassouni B, Funel N, Gandellini P, Lagerweij T, Buonamici S, Blijlevens M, Zeeuw van der Laan EA, Zaffaroni N, Deraco M, Kusamura S, Würdinger T, Peters GJ, Molthoff CFM, Jansen G, Kaspers GJL, Cloos J and Giovannetti E: Splicing modulation as novel therapeutic strategy against diffuse malignant peritoneal mesothelioma. EBioMedicine *39*: 215-225, 2019. PMID: 30581150. DOI: 10.1016/j.ebiom.2018.12.025

14 Riedl A, Schlederer M, Pudelko K, Stadler M, Walter S, Unterleuthner D, Unger C, Kramer N, Hengstschläger M, Kenner L, Pfeiffer D, Krupitza G and Dolznig H: comparison of cancer cells in 2D vs 3D culture reveals differences in AKT-mTOR-S6K signaling and drug responses. J Cell Sci *130(1)*: 203-218, 2017. PMID: 27663511. DOI: 10.1242/jcs.188102

15 Langhans SA: Three-dimensional in vitro cell culture models in drug discovery and drug repositioning. Front Pharmacol *9*: 6, 2018. PMID: 29410625. DOI: 10.3389/fphar.2018.00006

16 Boussios S, Moschetta M, Karathanasi A, Tsiouris AK, Kanellos FS, Tatsi K, Katsanos KH and Christodoulou DK: Malignant peritoneal mesothelioma: clinical aspects, and therapeutic perspectives. Ann Gastroenterol *31(6)*: 659-669, 2018. PMID: 30386115. DOI: 10.20524/aog.2018.0305

17 Yan TD, Deraco M, Elias D, Glehen O, Levine EA, Moran BJ, Morris DL, Chua TC, Piso P and Sugarbaker PH: A novel tumor-node-metastasis (TNM) staging system of diffuse malignant peritoneal mesothelioma using outcome analysis of a multi-institutional database. Cancer *117(9)*: 1855-1863, 2011. PMID: 21509762. DOI: 10.1002/cncr.25640

18 Sugarbaker PH: Intra-abdominal manifestations of pleural mesothelioma. Ann Transl Med, 2017. PMID: 28706899. DOI: 10.21037/atm.2016.11.44

19 Tertemiz KC, Ozgen Alpaydin A, Gurel D, Savas R, Gulcu A and Akkoclu A: Multiple distant metastases in a case of malignant pleural mesothelioma. Respir Med Case Reports *13*: 16-18, 2014. PMID: 26029551. DOI: 10.1016/j.rmcr.2014.07.003

20 Finn RS, Brims FJH, Gandhi A, Olsen N, Musk AW, Maskell NA and Lee YCG: Postmortem findings of malignant pleural mesothelioma: A two-center study of 318 patients. Chest *142(5)*: 1267-1273, 2012. PMID: 22576637. DOI: 10.1378/chest.11-3204

21 Giovannetti E, Leon LG, Gómez VE, Zucali PA, Minutolo F and Peters GJ: A specific inhibitor of lactate dehydrogenase overcame the resistance toward gemcitabine in hypoxic mesothelioma cells, and modulated the expression of the human equilibrative transporter-1. Nucleosides Nucleotides Nucleic Acids *35*: 643-651, 2016. PMID: 27906635. DOI: 10.1080/15257770.2016.1149193

22 Salo SAS, Ilonen I, Laaksonen S, Myllärniemi M, Salo JA and Rantanen T: Malignant peritoneal mesothelioma: Treatment options and survival. Anticancer Res *39(2)*: 839-845, 2019. PMID: 30711965. 2019. DOI: 10.21873/anticanres.13183

23 Kanteti R, Mirzapoiazova T, Riehm JJ, Dhanasingh I, Mambetsariev B, Wang J, Kulkarni P, Kaushik G, Seshacharyulu P, Ponnusamy MP, Kindler HL, Nasser MW, Batra SK and Salgia R: Focal adhesion kinase a potential therapeutic target for pancreatic cancer and malignant pleural mesothelioma. Cancer Biol Ther *19(4)*: 316-327, 2018. PMID: 29303405. DOI: 10.1080/15384047.2017.1416937

24 El Hassouni B, Li Petri G, Liu DSK, Cascioferro S, Parrino B, Hassan W, Diana P, Ali A, Frampton AE and Giovannetti E: Pharmacogenetics of treatments for pancreatic cancer. Expert Opin Drug Metab Toxicol *15(6)*: 437-447, 2019. PMID: 31100206. DOI: 10.1080/17425255.2019.1620731

25 Casanello P, Torres A, Sanhueza F, González M, Farías M, Gallardo V, Pastor-Anglada M, San Martín R and Sobrevia L: Equilibrative nucleoside transporter 1 expression is downregulated by hypoxia in human umbilical vein endothelium. Circ Res *97(1)*: 16-24, 2005. PMID: 15933265. DOI: 10.1161/01.RES.0000172568.49367.f8

Received June 9, 2020
Revised July 8, 2020
Accepted July 9, 2020

Part III

Biological evaluation of novel compounds analogues of the marine alkaloids topsentin and nortopsentin as bacterial biofilm inhibitors

(*Chapter 9-12*)

Chapter 9

Biofilm formation as valuable target to fight severe chronic infections.

Pecoraro, C.*; Carbone, D.*, Deng, D.; Cascioferro, S.;
Diana, P.#; Giovannetti, E.#

Editorial submitted to Current Medicinal Chemistry

*These Authors contributed equally to this study.

EDITORIAL:
Biofilm formation as valuable target to fight severe chronic infections

Camilla Pecoraro,[1,2,*] Daniela Carbone,[1*] Dongmei Deng ,[3] Stella Cascioferro,[1]
Patrizia Diana,[1,#] Elisa Giovannetti[2,4,#]

[1]Department of Biological, Chemical and Pharmaceutical Sciences and Technologies (STEBICEF) University of Palermo, 90123 Palermo (Italy); [2]Department of Medical Oncology, Cancer Center Amsterdam, Amsterdam UMC, VU University Medical Center (VUmc), 1081 HV Amsterdam, The Netherlands; [3]Department of Preventive Dentistry, Academic Centre for Dentistry Amsterdam (ACTA), University of Amsterdam and VU University Amsterdam, 1081 HV Amsterdam, The Netherlands The Netherlands; [4]Cancer Pharmacology Lab, AIRC Start Up Unit, Fondazione Pisana per la Scienza, 56124 Pisa, Italy.

**Equally contributed*
#Shared last authorship

Corresponding author:
Dr. Elisa Giovannetti, Associate Professor, Department of Medical Oncology, Cancer Center Amsterdam, VU University Medical Center, De Boelelaan 1117, 1081 HV Amsterdam, The Netherlands; Phone: +31 20 444 22 67
E-mail: e.giovannetti@amsterdamumc.nl

As most countries in the world are struggling to control the COVID-19 pandemic, scientists should warn that other infective disease are inevitable, and antibiotic resistance to bacterial infections is a growing threat to public health. Thus, in this editorial we describe how the development of biofilm targeting agents is prompting an innovative research field, offering promising therapeutics for infections that are currently refractory to conventional antibiotics.

Biofilm formation significantly contributes to microbial survival in hostile environments, and it is currently considered a key virulence factor for pathogens responsible for serious chronic infections resistant to conventional antibiotic therapy. It is estimated that more than 80% of nosocomial infections are biofilm-mediated, and recent studies described the key role of biofilm in chronic inflammatory diseases, such as Crohn's disease, as well as in acute infections [1, 2].

Some evidence reports the contribution of biofilm to the growth of *P. aeruginosa, S. aureus, S. epidermidis, and E. coli* in bone and heart valves, causing severe chronic osteomyelitis and endocarditis [2, 3]. Biofilms can also sustain the progression of chronic diseases, through the release of individual cells and toxins from the original biofilm, which can invade new sites and generate new infections areas [4]. In addition, *S. aureus* biofilm is playing a specific role in the immunopathogenesis of chronic rhinosinusitis because it secretes a number of toxins that may contribute to its persistence and relapses [5, 6].

Bacterial biofilms confer to bacterial cells both resistance to antibiotics and a higher invasiveness capability, and many efforts have been made to identify new classes of small molecules endowed with biofilm inhibitory activity in clinically relevant Gram-positive and Gram-negative pathogens [7-9].

Anti-biofilm compounds act as anti-virulence agents, interfering with bacterial adhesion to host surfaces [10]. The current available strategies to fight biofilm include indeed two different approaches, the prevention of biofilm formation and the disruption of mature biofilm architecture, which often act on the same targets, such as quorum sensing system or the nucleotide second messenger signalling systems [7]. These strategies seem to be particularly advantageous to reduce the selective pressure which promotes the development of antibiotic resistance mechanisms [11].

Dispersal agents could be used in combination with antimicrobial agents in order to obtain a synergistic effect (Figure 1). *In vitro* results of such combinations are promising, but this therapeutic approach might be limited by difficulties in reachingthe simultaneous presence of both agents at the target site at biologically-active concentrations. Several important drawbacks of drug co-administration treatments, such as complex treatment schedules, increased risk of adverse effects, increased treatment costs, and antagonism, might also limit the development of this strategy [12].

Both the inhibition of biofilm formation and the dispersion of preformed biofilm showed some clinical effects for the prophylaxis of implant surgery or the use for the treatment of biofilm-associated infections in combination with conventional antibiotics. However, these approaches cannot constitute a direct eradication strategy for establishing biofilms.

Against this background, stand-alone treatments, such as biofilm eradication agents, are becoming an attractive option. In particular, the identification of novel therapeutic strategies capable of eradicating biofilm by counteracting the persister cells in the deepest layers, could be extremely advantageous in the treatment of chronic infections [13].

Persister are indeed phenotypic dormant variants of regular cells that form stochastically in microbial populations and play a key role in the relapse and recalcitrance of chronic infections, because they are highly resistant to antibiotics [14]. Moreover, the occurrence of persister cells within a biofilm confers protection from elimination by the immune system, increasing their resistance to conventional antibiotics.

The presence of persister cells acts as a nucleation point to rebuild the biofilm, causing the relapse of biofilm infection. However, the persister state can be considered as a phenotypic variant rather than a mutation, since the majority of newly generated biofilm cells exhibit no additional antimicrobial resistance compared to the original eradicated biofilm cells [15], and this should further simulate research against these cells.

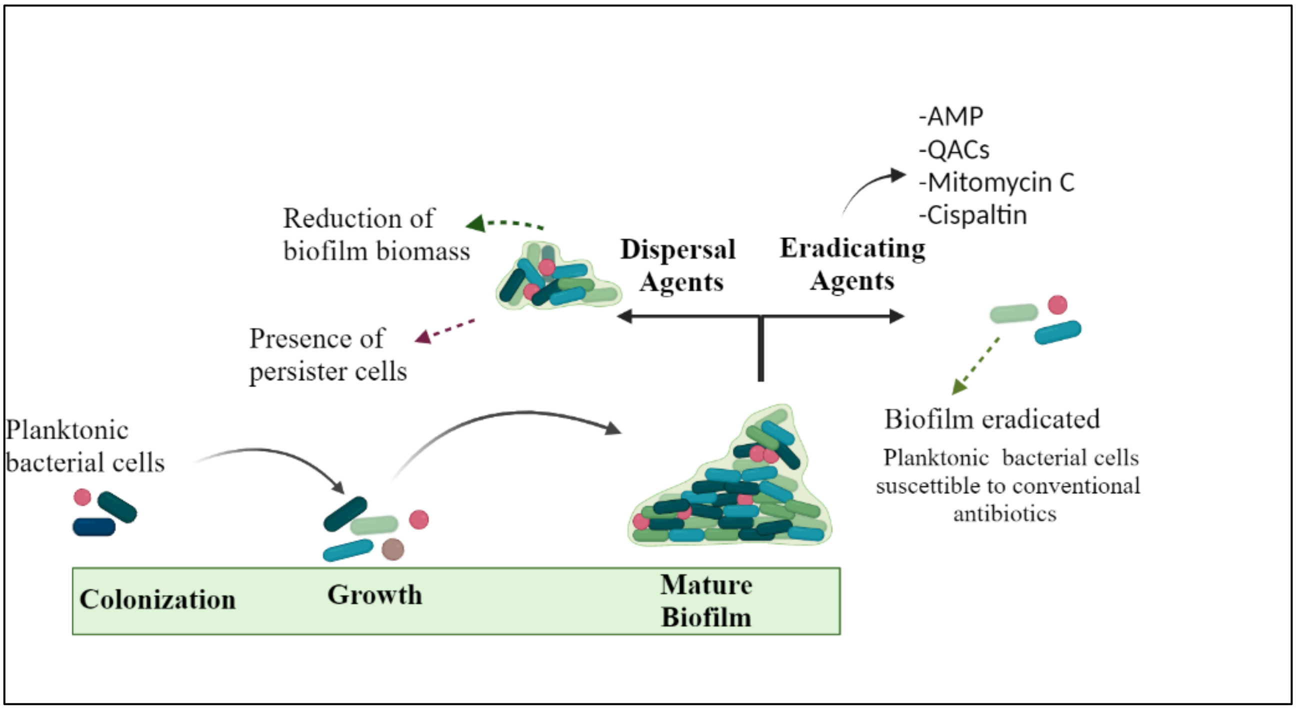
-AMP
-QACs
-Mitomycin C
-Cispaltin
Reduction of biofilm biomass
Dispersal Agents
Eradicating Agents
Presence of persister cells
Planktonic bacterial cells
Biofilm eradicated
Planktonic bacterial cells suscettible to conventional antibiotics
Colonization
Growth
Mature Biofilm

Figure 1. Biofilm formation and main strategies to counteract biofilm infections.

Considering the inefficacy of most conventional antibiotics, a variety of promising eradicating biofilm compounds have already been developed in the past years, including antimicrobial peptides (AMPs), quaternary ammonium compounds (QACs), and antimicrobial lipids. as well as anticancer drugs such as Mitomycin C and cisplatin (Figure 1) [16, 17].

Among these agents, AMPs represent the most well-studied class. Even if their mechanism of action is still not fully understood, their activity seems to be due to cytoplasmic membrane disruption and inhibition of protein folding [18].

QACs are commonly used as antiseptics, disinfectants, and preservatives, but have only recently been described for their biofilm eradication properties. Interestingly, the dicationic porphyrin QAC XF-73 is able to completely eradicate pre-formed *S. aureus* biofilms at the concentration of 2.6 μM, demonstrating also a remarkably low propensity in inducing bacterial resistance. Therefore, this compound has been evaluated in a phase 1 clinical trial, which showed rapid reduction of *Staphylococcus aureus* and minimal side effects, supporting further studies [19].

The well-known anticancer drugs Mitomycin C and cisplatin have also an encouraging biofilm eradication activity, of, but their clinical toxicity (e.g., bone marrow damage, lung fibrosis, renal failure, and haemolytic anemia) strongly limit their development for systemic treatment of biofilm-related infection[20]. However, these drugs might be used for the topical treatment of biofilm related infections within skin burns or chronic wounds, such as diabetic foot ulcers.

In conclusion, eradicating and dispersal agents are two promising approaches in the war against biofilm infections, reducing the biofilm biomass and eradicating the persister cells, respectively. However, further efforts should be made in order to understand the mechanisms of biofilm antimicrobial tolerance, in order to better design and develop new therapeutic strategies for biofilm-associated infections. Anti-virulence strategies aiming to fight biofilms represent indeed important tools to counteract the global threat of antibiotic resistance.

Financial Support: This work was supported by grants from the Cancer Center Amsterdam Foundation (to EG, DD). Associazione Italiana per la Ricerca sul Cancro (to EG) PON grant from the Italian Ministry of Education, University and Research (C.P., E.G.), and PRIN2017, Prot.No.2017E84AA4 (Patrizia Diana).

Conflicts of interest.

The authors declare no conflicts of interest.

Acknowledgment

None.

References

[1] Cascioferro, S.; Parrino, B.; Carbone, D.; Schillaci, D.; Giovannetti, E.; Cirrincione, G.; Diana, P. Thiazoles, Their Benzofused Systems, and Thiazolidinone Derivatives: Versatile and Promising Tools to Combat Antibiotic Resistance. J. Med. Chem., **2020**, 63, 7923–7956. https://doi.org/10.1021/acs.jmedchem.9b01245.

[2] Parsek, M. R., & Singh, P. K. Bacterial biofilms: an emerging link to disease pathogenesis. Annu Rev Microbiol. **2003**, 57, 677–701. https://doi.org/10.1146/annurev.micro.57.030502.090720

[3] Chatterjee, S., Maiti, P., Dey, R., Kundu, A., & Dey, R. Biofilms on indwelling urologic devices: microbes and antimicrobial management prospect. Annals of medical and health sciences research, **2014**, 4(1), 100–104. https://doi.org/10.4103/2141-9248.126612

[4] Costerton, J. W., Stewart, P. S., & Greenberg, E. P. Bacterial biofilms: a common cause of persistent infections. Science, **1999**, *284* (5418), 1318–1322. https://doi.org/10.1126/science.284.5418.1318

[5] Poddighe, D., & Vangelista, L. *Staphylococcus aureus* Infection and Persistence in Chronic Rhinosinusitis: Focus on Leukocidin ED. Toxins, **2020**, 12(11), 678. https://doi.org/10.3390/toxins12110678

[6] Ramakrishnan, Y., Shields, R. C., Elbadawey, M. R., & Wilson, J. A. (2015). Biofilms in chronic rhinosinusitis: what is new and where next?. J Laryngol Otol, 129(8), 744–751. https://doi.org/10.1017/S0022215115001620

[7] Parrino, B.; Schillaci, D.; Carnevale, I.; Giovannetti, E.; Diana, P.; Cirrincione, G.; Cascioferro, S. Synthetic small molecules as anti-biofilm agents in the struggle against antibiotic resistance. Eur. J. Med. Chem., **2019**, 161, 154–178. https://doi.org/10.1016/j.ejmech.2018.10.036

[8] Parrino, B.; Carbone, D.; Cascioferro, S.; Pecoraro, C.; Giovannetti, E.; Deng, D.; Di Sarno, V.; Musella, S.; Auriemma, G.; Cusimano, M.G.; Schillaci, D.; Cirrincione, G.; Diana, P. 1,2,4-Oxadiazole topsentin analogs as staphylococcal biofilm inhibitors targeting the bacterial transpeptidase sortase A. Eur. J. Med. Chem., **2021**, 209, 112892. https://doi.org/10.1016/j.ejmech.2020.112892

[9] Cascioferro, S.; Parrino, B.; Petri, G.L.; Cusimano, M.G.; Schillaci, D.; Di Sarno, V.; Musella, S.; Giovannetti, E.; Cirrincione, G.; Diana, P. 2,6-Disubstituted imidazo[2,1-b][1,3,4]thiadiazole derivatives as potent staphylococcal biofilm inhibitors. Eur. J. Med. Chem., **2019**, 167, 200–210. https://doi.org/10.1016/j.ejmech.2019.02.007

[10] Cascioferro, S.; Parrino, B.; Carbone, D.; Pecoraro, C.; Diana, P. Novel strategies in the war against antibiotic resistance, Fut. Med. Chem., **2021**, 13, 529–531. https://doi.org/10.4155/fmc-2021-0009

[11] Parrino, B.; Carbone, D.; Cirrincione, G.; Diana, P.; Cascioferro, S. Inhibitors of antibiotic resistance mechanisms: clinical applications and future perspectives, Fut. Med. Chem., **2020**, 12, 357–359. https://doi.org/10.4155/fmc-2019-0326

[12] Tamma, P.D.; Cosgrove, S.E.; Maragakis, L.L.Combination therapy for treatment of infections with gram-negative bacteria. Clin. Microbiol. Rev., **2012**, 25, 450–470. https://doi.org/10.1128/CMR.05041-11

[13] Žiemytė, M.; Carda-Diéguez, M.; Rodríguez-Díaz, J.C.; Ventero-Martín, M.P.; Mira, A.; Ferrer, M.D. Real-time monitoring of Pseudomonas aeruginosa biofilm growth dynamics and persister cells' eradication: P. aeruginosa persisters in biofilms. Emerg. Microbes Infect., **2021**, in press. https://doi.org/10.1080/22221751.2021.1994355

[14] Miyaue, S.; Suzuki, E.; Komiyama, Y.; Kondo, Y.; Morikawa, M.; Maeda, S. Bacterial Memory of Persisters: Bacterial Persister Cells Can Retain Their Phenotype for Days or Weeks After Withdrawal from Colony-Biofilm Culture. Front. Microbiol., **2018**, 9, 1396. https://doi.org/10.3389/fmicb.2018.01396

[15] Verderosa, A.D.; Totsika, M.; Fairfull-Smith, K.E. Bacterial Biofilm Eradication Agents: A Current Review. *Front. Chem.*, **2019**, 7, 824. https://doi.org/10.3389/fchem.2019.00824

[16] Wood, T.K.; Knabel, S.J.; Kwan, B.W. Bacterial persister cell formation and dormancy. *Appl. Environ. Microbiol*., **2013**, 79, 7116–7121. https://doi.org/10.1128/AEM.02636-13

[17] Verderosa, A.D., Totsika, M., Fairfull-Smith, K.E. Bacterial Biofilm Eradication Agents: A Current Review. *Front Chem.* 2019 Nov 28;7:824. doi: 10.3389/fchem.2019.00824.

[18] Bechinger, B.; Gorr, S.-U. Antimicrobial Peptides: Mechanisms of Action and Resistance. *J. Dent. Res.*, **2017**, 96, 254–260. https://doi.org/10.1177/0022034516679973

[19] Yendewa, G.A.; Griffiss, J.M.; Jacobs, M.R.; Fulton, S.A.; O'Riordan, M.A.; Gray, W.A.; Proskin, H.M.; Winkle, P.; Salata, R.A. A two-part phase 1 study to establish and compare the safety and local tolerability of two nasal formulations of XF-73 for decolonisation of Staphylococcus aureus: A previously investigated 0.5mg/g viscosified gel formulation versus a modified formulation. *J. Glob. Antimicrob. Resist.*, **2020**, 21, 171–180. https://doi.org/10.1016/j.jgar.2019.09.017

[20] Yuan, M.; Chua, S.L.; Liu, Y.; Drautz-Moses, D.I.; Yam, J.K.H.; Aung, T.T.; Beuerman, R.W.; Salido, M.M.S.; Schuster, S.C.; Tan, C.-H.; Givskov, M.; Yang, L.; Nielsen, T.E. Repurposing the anticancer drug cisplatin with the aim of developing novel Pseudomonas aeruginosa

infection control agents. *Beilstein J. Org. Chem.,* **2018**, 14, 3059–3069. https://doi.org/10.3762/bjoc.14.284

Chapter 10

Therapeutic Strategies to Counteract Antibiotic Resistance in MRSA Biofilm-Associated Infections.

Cascioferro, S.; Carbone, D.; Parrino, B.; **Pecoraro, C.**;
Giovannetti, E.; Cirrincione, G.; Diana, P.

ChemMedChem (2021), 16(1), 65-80.

Check for updates

ChemMedChem

Reviews
doi.org/10.1002/cmdc.202000677

Chemistry Europe
European Chemical Societies Publishing

Therapeutic Strategies To Counteract Antibiotic Resistance in MRSA Biofilm-Associated Infections

Stella Cascioferro+,[a] Daniela Carbone+,[a] Barbara Parrino,[a] Camilla Pecoraro,[a]
Elisa Giovannetti,[b, c] Girolamo Cirrincione,[a] and Patrizia Diana*[a]

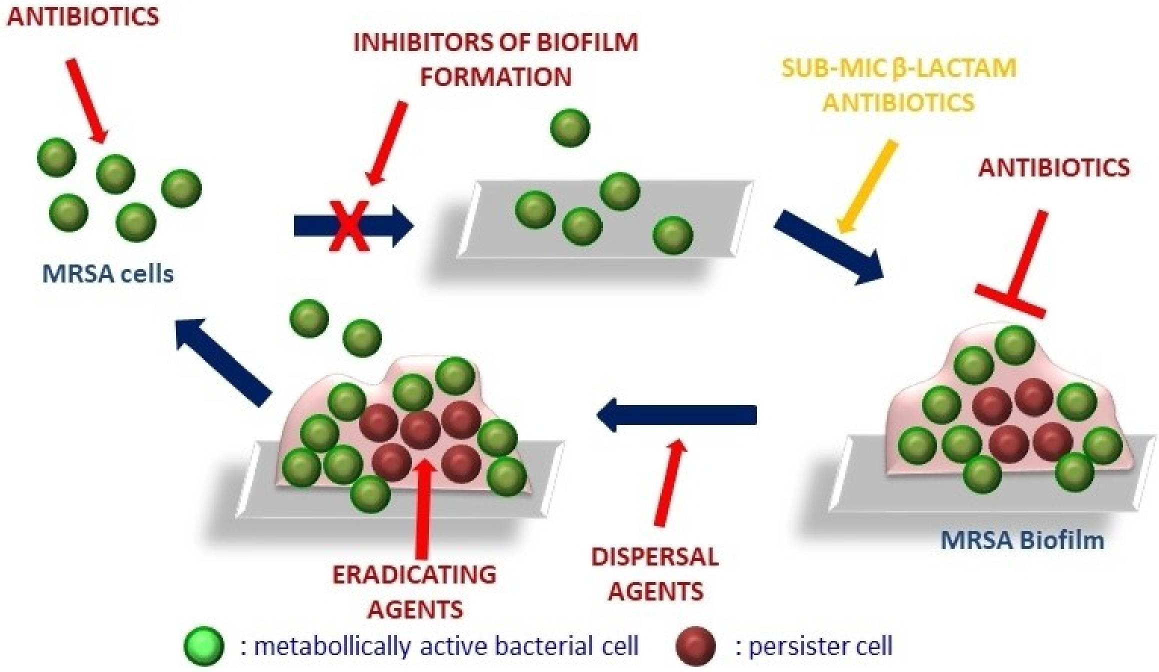
ANTIBIOTICS
INHIBITORS OF BIOFILM FORMATION
SUB-MIC β-LACTAM ANTIBIOTICS
ANTIBIOTICS
MRSA cells
MRSA Biofilm
ERADICATING AGENTS
DISPERSAL AGENTS
: metabollically active bacterial cell
: persister cell

© 2020 Wiley-VCH GmbH

Methicillin-resistant *Staphylococcus aureus* (MRSA) has emerged as one of the leading causes of persistent human infections. This pathogen is widespread and is able to colonize asymptomatically about a third of the population, causing moderate to severe infections. It is currently considered the most common cause of nosocomial infections and one of the main causes of death in hospitalized patients. Due to its high morbidity and mortality rate and its ability to resist most antibiotics on the market, it has been termed a "superbug". Its ability to form biofilms on biotic and abiotic surfaces seems to be the primarily means of MRSA antibiotic resistance and pervasiveness. Importantly, more than 80% of bacterial infections are biofilm-mediated. Biofilm formation on indwelling catheters, prosthetic devices and implants is recognized as the cause of serious chronic infections in hospital environments. In this review we discuss the most relevant literature of the last five years concerning the development of synthetic small molecules able to inhibit biofilm formation or to eradicate or disperse preformed biofilms in the fight against MRSA diseases. The aim is to provide guidelines for the development of new anti-virulence strategies based on the knowledge so far acquired, and, to identify the main flaws of this research field, which have hindered the generation of new market-approved anti-MRSA drugs that are able to act against biofilm-associated infections

1. Introduction

Antibiotic-resistance (AMR) is among the most relevant health problems of this century. There is urgent need for new therapeutic strategies which are able to overcome the main bacterial resistance mechanisms.[1,2]

Staphylococcus aureus belongs to the ESKAPE family, which includes the nosocomial relevant pathogens *Enterococcus faecalis*, *Klebsiella pneumoniae*, *Acinetobacter baumannii*, *Pseudomonas aeruginosa* and Enterobacter sp.

Methicillin-resistant *Staphylococcus aureus* (MRSA) is one of the main causes of persistent human infections. Since MRSA is responsible for severe morbidity and mortality worldwide, in 2017 it has been categorized as a high priority multi-drug resistant (MDR) pathogen by the World Health Organization (WHO).

MRSA causes serious infections resistant to conventional antibiotic therapy, such as skin and soft tissue infections, bacteremia, infective endocarditis, osteomyelitis, and pneumonia. Moreover, MRSA is often responsible of indwelling catheter infections, prosthetic devices and implant associated infections.[3,4] An important gene that confers to MRSA the capability to growth undisturbed in presence of penicillin-like antibiotics, is *mecA* gene, that is found in all MRSA strains and encodes the penicillin binding protein 2a (PBP2a).[5] PBPs are membrane-bound enzymes, which play essential roles in cell wall biosynthesis catalysing the reactions involved in the synthesis of cross-linked peptidoglycan from lipid intermediates and allowing the removal of D-alanine residue from the precursor of peptidoglycan.[6] The functionality of these enzymes, which is crucial for bacterial growth, cell division and cellular structure, was compromised by β-lactam antibiotics that cause irreparable damage to the bacterial cell wall and, consequently, the bacterial death.[7]

In *S. aureus* four PBPs named PBP1, PBP2, PBP3, and PBP4 were found. MRSA, instead, showed an additional PBP, the PBP2a, that is the unique PBP that, despite shares the structural features to the other PBPs, is not inhibited by β-lactam antibiotics.[8]

The major cause of the MRSA antibiotic resistance and pervasiveness is to be found in its ability to form biofilm on biotic and abiotic surfaces. Many factors are involved in MRSA biofilm resistance: first of all, the limitation of the antibiotic entrance due to the presence of the polymerizable mucopolysaccharide on the biofilm surface; moreover, the existence in the deepest layers of metabolically inactive cells, intrinsically resistant to antibiotics. Additionally the accumulation of bacterial cells within the biofilm facilitates the horizontal genetic transfer of the genes responsible for resistance.

Bacterial cells within the biofilm are extremely more resistant to antibiotics, as well as to host immune response, compared to the planktonic form of life.

In the last decade, many efforts have been made to identify new agents able to interfere with the staphylococcal biofilm life cycle, and many compounds showed interesting anti-biofilm activities, although none has reached the clinic.[9-15] This is mainly due to very limited *in vivo* studies capable of confirming its activity.

Anti-biofilm compounds acting as anti-virulence agents, have the advantage over conventional antibiotics, to not affect bacterial growth and then, to impose a low selective pressure on the onset of antibiotic resistance mechanisms.[16]

Anti-biofilm agents can interfere with different steps of the development process, which leads from the planktonic form to the sessile phenotype. They can inhibit the biofilm formation, mainly interfering with the bacterial adhesion, or they can disrupt preformed biofilms dissolving matrix architecture. Additionally, some anti-biofilm agents are able to kill the persister cells of the deepest layers of the biofilm, eradicating it.

---

[a] *Dr. S. Cascioferro,⁺ Dr. D. Carbone,⁺ Dr. B. Parrino, C. Pecoraro,*
Prof. G. Cirrincione, Prof. P. Diana
Department of Biological, Chemical and Pharmaceutical Sciences and Technologies (STEBICEF)
University of Palermo
Via Archirafi 32
90123, Palermo (Italy)
E-mail: patrizia.diana@unipa.it
[b] *Prof. E. Giovannetti*
Department of Medical Oncology
Cancer Center Amsterdam
VU University Medical Center (VUmc)
De Boelelaan 1117
1081HV, Amsterdam (The Netherlands)
[c] *Prof. E. Giovannetti*
Cancer Pharmacology Lab, AIRC Start Up
Fondazione Pisana per la Scienza
Via Ferruccio Giovannini 13
56017, San Giuliano Terme, Pisa (Italy)

[+] *These authors contributed equally to this work.*

© 2020 Wiley-VCH GmbH

Many bacterial processes can be considered valid targets for the development of new anti-biofilm agents such, for example, the quorum sensing (QS) system, which regulates the bacterial cell-to-cell signalling and the nucleotide second messenger signalling systems. It is recognized the key role of QS system in the coordination of the bacterial attachment and biofilm formation, as well as, in biofilm dispersion in response to changes in environmental conditions.[17]

Contrary to what is observed in other bacteria, in *S. aureus* QS system inhibits the biofilm formation through the production of matrix degrading enzymes such as protease, nuclease and lipase. This different role of QS system was confirmed by the robust biofilm production observed in a *S. aureus* strain deficient in the regulator gene *agr*, which encodes the two component regulatory system, TCRS.[18]

One of the biggest difficulties in finding valuable therapeutic strategy to treat MRSA biofilm associated infections is the existence of different staphylococcal biofilm phenotypes.[19]

While staphylococcal strains methicillin susceptible (MSSA) produce biofilms with a mechanism *ica* operon-mediated which involves *icaADBC* genes in the production of polysaccharide intercellular adhesin (PIA) or polymeric N-acetyl-glucosamine (PNAG), MRSA expresses a *ica*-independent biofilm formation

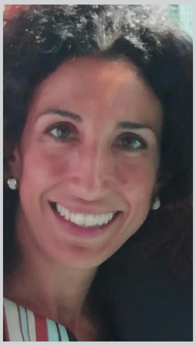

Stella Cascioferro graduated in Pharmacy with honors in 1999, and she got her Ph.D. in Medicinal Chemistry in 2004 at the University of Palermo. Her research interests include the design and the development of new heterocyclic compounds as antitumoral and anti-infective agents. Currently, she is researcher at the University of Palermo, Italy. She is the author of 66 scientific papers published in peer reviewed international journals of medicinal chemistry.

Daniela Carbone holds a master's degree in Pharmacy (full marks with honors) from the University of Palermo in 2015. From July to November 2018, she was a Ph.D. visiting student at VU University Medical Center of Amsterdam, and she earned her Ph.D. in Molecular and Biomolecular Sciences, with additional certification of Doctor Europaeus, in February 2019. Her current research interests are focused on the medicinal chemistry field, particularly the design, synthesis, and biological evaluation of heterocyclic compounds, analogues of natural marine alkaloids, with antitumor and anti-infective properties.

Barbara Parrino graduated in Medicinal Chemistry and Technology at the University of Palermo with full marks with honors in 2007. She got her Ph.D. in Pharmaceutical Sciences in March 2012. She received the "Doctor Europaeus" label. On September 2012, she was awarded the P. Ehrlich MedChem Euro-PhD Network Certificate. In 2015 she was recipient of the Medicinal Chemistry Division of the Italian Chemical Society Prize. Currently, she is researcher at the University of Palermo and author of 62 papers and one Italian patent.

Camilla Pecoraro obtained her master degree in Chemistry and Pharmaceutical Technology with full marks and honors from the University of Palermo in 2018. She is currently working toward her Ph.D. degree in Molecular and Biomolecular Sciences. Her doctoral research is focused on design and synthesis of new heterocyclic compounds with antitumor activity. Her current research interests are in the field of medicinal chemistry with a special focus on analogs of natural marine alkaloids with antitumor and antibacterial activity.

Elisa Giovannetti is associate Professor of Pharmacology at the VU University Medical Center, Amsterdam, and Principal Investigator at the Cancer Pharmacology Lab (University of Pisa). She is member of the Steering Committee of the Pharmacology and Molecular Mechanisms (PAMM) group of the EORTC, and her studies are funded by grants from Italian Association for Research against Cancer (AIRC), Netherlands Organization for Scientific Research (NWO), Cancer Center Amsterdam (CCA) Foundation, and Dutch Cancer Society (KWF).

Girolamo Cirrincione is Emeritus Professor of Medicinal Chemistry at the University of Palermo. He is a member of the Drug Discovery Committee of the Pharmacology and Molecular Mechanisms (PAMM) Group of the European Organization for Research and Treatment of Cancer, the Italian Chemical Society, where he has been President of the Medicinal Chemistry Division, and the International Society of Heterocyclic Chemistry, where he served as vice president for 2004–2005. He was Pro-rector for Research of the University of Palermo for 2015–2018.

Patrizia Diana is full Professor of Medicinal Chemistry at the University of Palermo. She is currently coordinator of the Medicinal and Biological Section of the Department of Science and Technology: Chemical, Biological and Pharmaceutical (STEBICEF) of the University of Palermo. She is a member of the Italian Chemical Society and International Society of Heterocyclic Chemistry and of the PAMM group of the ORTC.

© 2020 Wiley-VCH GmbH

process contingent on the fibronectin binding proteins, FnBPA and FnBPB, and the major autolysin, Atl.[20,21]

In this review we focused on the recent development (2014-2020) of synthetic small molecules able to prevent biofilm formation or to interfere with pre-existing biofilms of the clinically relevant Gram-positive pathogen MRSA.

The understanding of the mechanisms of action, when reported, and of the SAR of the known anti-biofilm compounds can be a valuable guide for the development of new more potent anti-virulence agents able to counteract serious chronic MRSA biofilm-associated infections.

2. MRSA biofilm development

The bacterial adhesion to host tissue represents the first step of the biofilm formation as well as of the bacterial pathogenesis.[22] In Gram-positive bacteria, the adhesion is mainly due to a class of surface proteins known as "microbial surface components recognizing adhesive matrix molecules" (MSCRAMMs).[23] These proteins are structurally characterized by the presence of the common motif LPXTG (leucine, proline, any amino acid, threonine and glycine) which is recognized by the transpeptidase sortase A (SrtA). SrtA catalyses the anchoring of the MSCRAMMs to lipid II of the peptidoglycan through two consecutive reactions of thioesterification and transpeptidation.[24] MSCRAMMs play key roles, in addition to adhesion, also in colonization and evasion of innate immune defences. Representative MSCRAMMs in *S. aureus* are the protein A Spa, the fibronectin binding proteins FnbpA and FnbpB, the clumping factors ClfA and ClfB, the collagen-binding protein Cna, and the three serine aspartate repeat proteins SdrC, SdrD, and SdrE.[25]

After the primary attachment process to biotic or abiotic surfaces, bacterial cells start to proliferate and form microcolonies. Subsequently, an extracellular matrix is produced.[26] It was found that *S. aureus*, as well as numerous Gram-positive pathogens, release extracellular polymeric substances (EPS), including extracellular proteins, lipids, extracellular DNA (eDNA) and polysaccharides, into the external environment during this phase of the biofilm formation. Among the polysaccharides, the PIA significantly contributes to the stability of the matrix structure of Gram-positive biofilms. In MRSA, differently from MSSA which showed a PIA-dependent biofilm formation, the most important mechanism of autoaggregation was the intracellular adhesion mediated by the eDNA derived from the autolysis of sessile and planktonic cells.[27]

During the last stage, known as maturation stage, microbial cells within the biofilm were released returning in planktonic state (Figure 1). All phases in the biofilm development process were regulated by the cell-to-cell communication system QS.[28] In particular, in MRSA the *agr* operon has been found fundamental in the modulation of biofilm formation, downregulating genes involved in host colonization including those encoding for the MSCRAMMs, FnBPAB and Spa, and upregulating those encoding for some proteins involved in tissue damage and autolysis.[29]

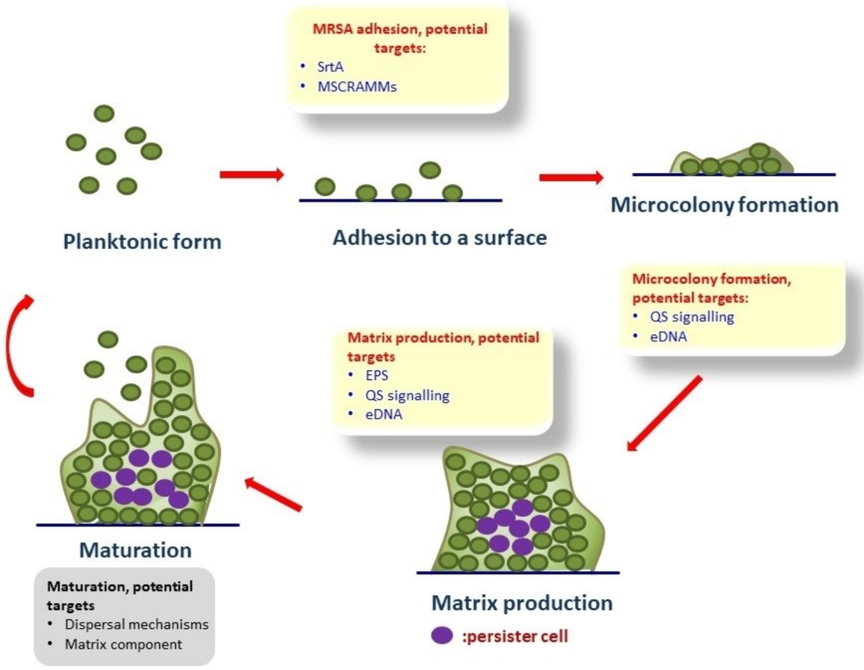

Figure 1. MRSA biofilm development.

2.1. Effects of β-lactam antibiotics on biofilm formation in MRSA

It was demonstrated that the exposure of bacterial cells to sub-MIC concentrations of β-lactam antibiotics induced biofilm formation in many *S. aureus* strains.[30] This has a great impact on the development of resistant strains since antibiotics are widely used as growth promoters in agriculture and then they can contaminate human and animal food in concentrations able to stimulate biofilm formation.[31] The effect of some β-lactam antibiotics, including methicillin, ampicillin, amoxicillin, and cloxacillin was evaluated, at the sub-MIC concentrations ranging from 0 to 10 μg/mL, on the biofilm formation in the MRSA strains 1149, Mu50 and FPR3757 (Figure 2).

All tested antibiotics showed a significant induction of biofilm formation in at least one MRSA strain and, most of them, elicited two different responses toward the biofilm in a concentration-dependent manner: biofilm stimulation at concentrations lower than the MIC values and biofilm inhibition at higher doses. Sub-MICs of methicillin promoted biofilm formation in all three MRSA strains assayed, showing the highest effect at concentrations ranging from 1 to 7 μg/mL. Additionally, it was found that biofilm promotion, induced by methicillin exposure, was mainly observed in staphylococcal strains characterized by a low basal level of biofilm production.

Further studies elucidated the mechanism of β-lactam biofilm induction, which involved an increase in eDNA levels as consequence of upregulation of the autolytic enzyme AltA. The stimulating effect of the cell wall active antibiotics was, in fact, importantly reduced in *S. aureus alt* mutant strain (KB4051) and in presence of an inhibitor of autolysis such as polyanethole sulfonate. Additionally, the eDNA role in methicillin-induced biofilms was confirmed treating the strains 11490 and FRP3757 with sub-MIC concentrations of the β-lactam antibiotic in presence and in absence of the human Dnase I, rhDNase. It was observed that rhDNase strongly inhibited methicillin induced biofilm formation.

On the contrary, the antibiotic biofilm induction proved to be independent by the *agr* quorum-sensing system as previously reported by Subrt et al.[32]

This finding suggested as low level of antibiotics may contribute to the growing development of antibiotic resistance and should be avoided in agriculture and farm animals.

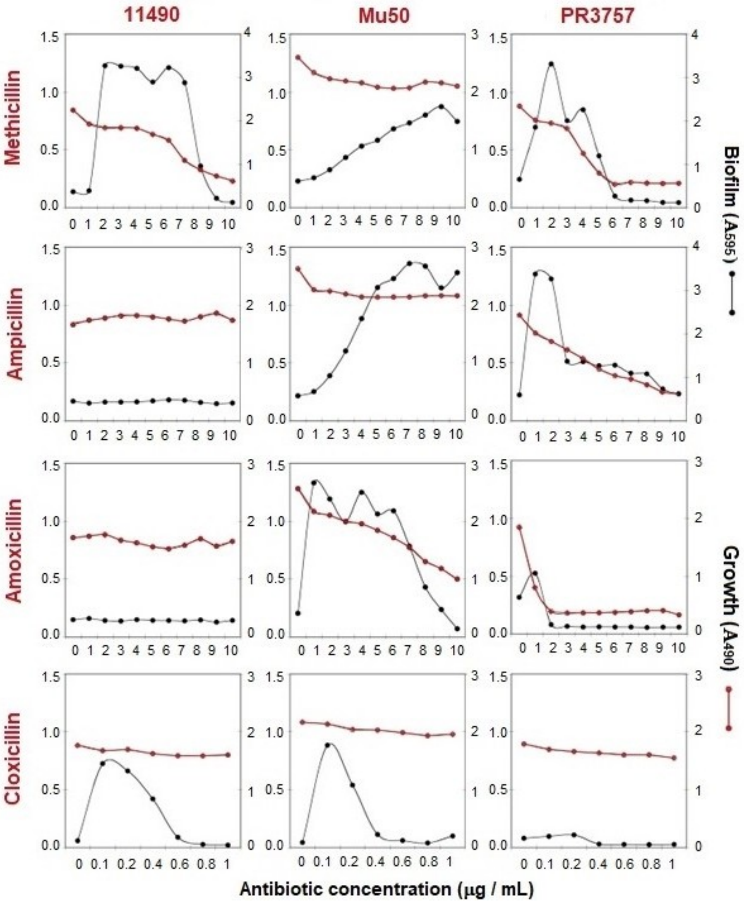

Figure 2. Effects of the β-lactam antibiotics methicillin, ampicillin, amoxicillin, and cloxacillin at the sub-MIC concentrations ranging from 0 to 10 μg/mL on cell growth and biofilm formation in the MRSA strains 1149, Mu50 and FPR3757.

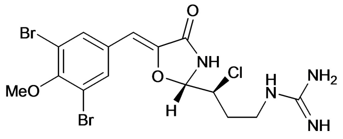

Synoxazolidinone A

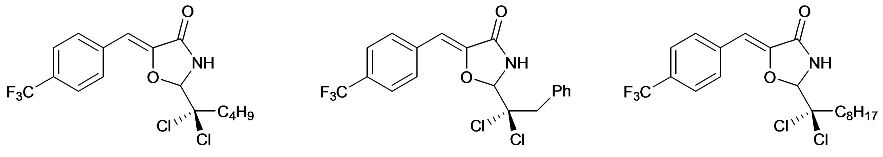

1a **1b** **1c**

Figure 3. Chemical structures of synoxazolidinone A and its derivative compounds **1 a–c**.

2.2. Inhibitors of MRSA biofilm formation and dispersal agents

An important contribute to the development of biofilm formation inhibitors against MRSA was given by Melander and collaborators who synthesized several series of 2-aminoimidazole derivatives able to potently inhibit or disperse bacterial biofilms[33–35] and it was previously discussed.[13] Few new scaffolds were reported in past five years, including oxazolidinones, lactones and quinolines.

2.2.1. Oxazolidinones

Edwards et al., on the basis of the antibacterial and anti-biofilm activity described for the natural product synoxazolidinone A, (Figure 3)[36] synthesized a series of 5-benzylidene-4-oxazolidinone derivatives, which were investigated for their ability in inhibiting biofilm-formation in MRSA strains (MRSA ATCC BAA-44, 43 300, 1685 and 1770).[37]

Among the new compounds, 4-oxazolidinones **1 a,b** (Figure 3) showed the highest potency especially against MRSA ATCC BAA-44, exhibiting BIC_{50} values of 0.78 and 1.2 μM, respectively. Compound **1 c** (Figure 3) was slightly less active in the biofilm-formation inhibition assay, eliciting 68 % of inhibition at 5 μM vs 89 % and 82 % of **1 a** and **1 b** at the same concentration, but it showed a good anti-virulence profile since it did not interfere with the bacterial growth of the tested strain (MIC >300 μM). With the aim to identify new anti-virulence strategies, the lack of activity toward the vital processes of the bacteria is considered advantageous because is associated to a lower tendency to generate antibiotic-resistance. Concerning the antibacterial activity of **1 a** and **1 b** against the planktonic form of MRSA, even if they exhibited greater activity compared to **1 c**, the growth inhibition of planktonic cells observed at the optimal biofilm inhibition concentration was very low, demonstrating a good selectivity towards biofilm form of life.

The new 4-oxazolidinones **1 a-c** also showed a good dispersal activity against MRSA ATCC BAA-44, eliciting, in the case of the most potent derivative **1 a** an IC_{50} value of 4.7 μM.

SAR studies on these derivatives revealed some important structural features required for the MRSA anti-biofilm activity. The presence of small aliphatic substituents on the aminal carbon of the 4-oxazolidinone scaffold was advantageous for the anti-biofilm properties of this class of compounds, the activity proved inversely proportional to the length of the chain. Additionally, the replacement of the trifluoromethyl group with a hydrogen atom or an electron-donating methoxy substituent was detrimental for the activity indicating the importance of electron-withdrawing substituents in the aromatic ring. Finally, the replacement of chlorine atoms in the dichloromethylene moiety with hydrogen atoms or methyl groups caused a serious drop of the activity.

A great discrepancy in the anti-biofilm activity of derivatives **1a-c** among the different MRSA strains tested was observed. These compounds, in fact, showed significantly lower potency against MRSA ATCC 43 300, 1685 and 1770 than MRSA ATCC BAA-44. This so different behaviour deserved further investigation. The lack of studies on the mechanism of action is the main drawback of this class of compounds.

2.2.2. Lactones

Valliamai et al. recently reported the anti-biofilm activity of the lactone 5- dodecanolide **2** (Figure 4) in different MRSA strains (ATCC 33591, MRSA 395, MRSA 410 and MRSA44).[38]

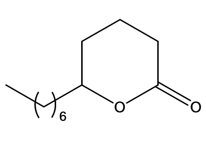

2

Figure 4. Chemical structure of compound **2**.

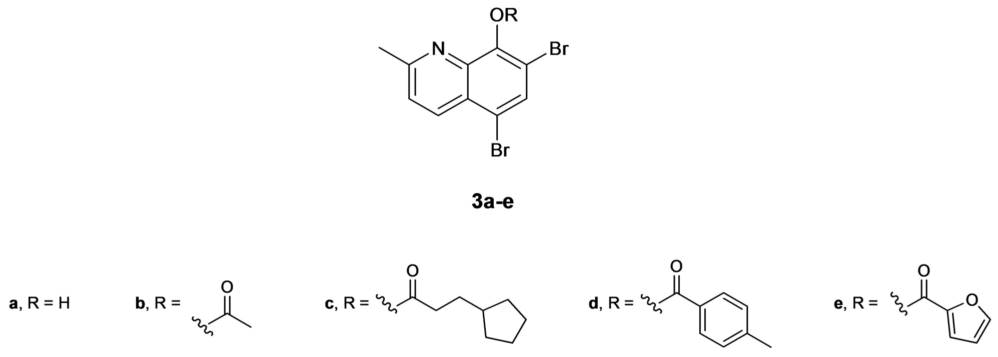

Figure 5. Chemical structures of compounds **3 a**–**e**.

Despite the compound **2** proved to be only moderately active as MRSA biofilm inhibitors, eliciting a BIC_{50} value against the ATCC 33591 of 125 μM, the in-depth studies conducted on the mechanism of action and on its *in vivo* efficacy provided the basis for the development of new more potent anti-biofilm agents. The anti-biofilm potential of **2** was first confirmed at the concentration of BIC_{90} (225 μM) employing light microscopic and confocal laser scanning microscopic analysis (CLSM), which showed a significant decrease in the surface covered as well as in the thickness of biofilm structure.

SEM analysis showed a marked arrest of MRSA biofilm formation on Titanium surface after treatment with derivative **2**. Importantly, the compound was able to inhibit biofilm formation also on titanium surface coated with host plasma protein.

Additionally, agarose gel electrophoresis and visual test tube settling assay demonstrated a significant reduction in eDNA synthesis and in the MRSA ability of autoaggregation in a dose dependent manner. It is known, in fact, that eDNA plays a key role in intracellular adhesion and in autoaggregation in MRSA.[30] The effect of compound **2** on MRSA growth and metabolism was evaluated in order to exclude an antibacterial nature of the derivative, and no growth reduction was observed in the growth curve analysis, as well as, no change in MRSA metabolism was found in Almar blue assay. These data highlighted the anti-virulence potential of this compound.

Gene expression analysis was carried out with the aim to understand the molecular mechanism of the antibiofilm activity of compound **2**, which was found due to an up regulation of *agr* gene and to a down regulation of *sarA*, *fnbA* and *fnbB*.

It is reported that *agr* system hinders the biofilm development interfering with the production of important adhesion proteins and stimulating the expression of many enzymes involved in the disruption of the biofilm matrix, including proteases, nucleases and lipases.[39] The quorum regulator SarA is responsible of the expression of many virulence factors in *S. aureus*, exercising a fundamental role in biofilm formation, bacterial pathogenesis and evasion of the host immune response. Therefore, downregulation of *sarA* leads to a significant decrease in biofilm formation and in virulence factors.[40] Moreover, FnbA and FnbB are important MSCRAMMs crucial for bacterial adhesion and tissue colonization.[41] Mutant strains with a deletion of the *fnbA* and *fnbB* genes did not show the fibronectin-binding proteins FnBPA and FnBPB and were no longer able to adhere to fibronectin or to form biofilm.

The anti-biofilm efficacy of the lactone **2** was confirmed in the MRSA *in vivo* infection model *Caenorhabditis elegans*. The CLSM micrographs of *C. elegans* treated with compound **2** at BIC_{50} concentration showed a significant decrease in biofilm formation compared to untreated nematodes.

2.2.3. Quinolines

Quinoline derivatives constitute a class of promising compounds for the treatment of MRSA infections. In addition to their significant antibacterial and eradicating activity (see section of Biofilm-eradicating agents) different quinolines were described for their potent dispersal activity. Quinolines **3 a**-**e** (Figure 5) proved to be very potent in dispersing MRSA-2 preformed biofilm showing EC_{50} values ranging from 2.06 to 2.74 μM (Table 1).[42] The potency of the derivatives **3 a**-**e** as dispersal agents was evaluated also in terms of EC_{90} values and all compounds showed EC_{90} values against established MRSA-2 biofilms lower than 30 μM. In particular, compound **3 c**, substituted at the 8-position of the quinoline scaffold with a 3-cyclopentylpropanoate and **3 d** bearing at the same position a 4-methylbenzoate moiety, exhibited the highest potency with EC_{90} of 16.6 and 17.4 μM, respectively. Compounds **3 a**-**e** showed potent antibacterial activity also against the planktonic form of *S. aureus* ATCC 29213 eliciting MIC values in the range 0.39-1.56 μM (Table 1) but no data were reported on their activity on the free form of MRSA.

Table 1. Antibacterial and biofilm dispersion activities of select quinolones **3 a**–**e** against *S. aureus.*

Compound	*S. aureus* ATCC 29213 MIC [μM]	MRSA-2 biofilm dispersion EC_{50} [μM]	MRSA-2 biofilm dispersion EC_{90} [μM]
3 a	0.39	2.60	22.9
3 b	0.39-0.78	2.55	22.9
3 c	0.78-1.56	2.09	16.6
3 d	1.56	2.06	17.4
3 e	0.39	2.74	24.0

2.2.4. Thiazole derivatives

Thiazole ring is widely recognized as scaffold of great value for obtaining molecules endowed with potent antibacterial and anti-biofilm properties.[15,43] Recently, the 5-acetyl-4-methyl-2-(3-pyridyl) thiazole **4** (Figure 6) was found able to interfere with the QS system as well as with the production of virulence factors including biofilm formation.[44] The antivirulence effects were evaluated on the clinical isolates MRSA–C18 and MRSA–C91, which are known for their multidrug-resistance and their strong biofilm forming capacity. Thiazole **4** was more active than vancomycin and teichoplanin in inhibiting MRSA growth in the planktonic form, additionally, it proved to significantly reduce biofilm formation at subinhibitory concentrations. The compound acted in the first stage of the MRSA biofilm formation showing no activity in preformed biofilm of the same strains. With the aim to investigate the anti-virulence mechanism of action of thiazole **4**, the effect on the MRSA production of haemolysin and protease was evaluated, and a reduced activity in both enzymes was observed after treatment with the thiazole derivative. The results are in agreement with an anti-QS mechanism targeting the Agr QS system.

2.2.5. Coumarin derivatives

During a study aiming to identify novel small molecules with antibacterial activity against MRSA, Qu et al. synthesized and evaluated for their antimicrobial properties, new 667 derivatives bearing to 26 different classes of compounds, including coumarin, hydroquinoline, diludine, hydropyran, and acridine derivatives.[45] Among these compounds 3,3′-(3,4-dichlorobenzylidene)-bis-(4-hydroxycoumarin) 5 showed potent inhibitory effects on the growth and the biofilm formation of the MRSA strains ATCC 70699, USA 300 and XJ 75302. Compound **5** (Figure 7) exhibited a marked selectivity against MRSA, showing no activity against Gram-negative pathogens such as *E. coli*, *K. pneumoniae*, *A. baumannii*, *Salmonella typhimurium*, and *P. aeruginosa. In vitro* experiments showed MRSA growth inhibition at concentration of 4 or 8 μg/ml. Importantly, the therapeutic effect against the MRSA infections was also evaluated *in vivo* in mice infected with MRSA USA 300, and coumarin derivative **5**, intraperitoneally administered at concentrations of 2.5 and 5 mg/kg, proved to be able to improve the survival rate to 56 and 67 %, respectively.

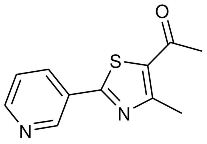

4

Figure 6. Chemical structure of the thiazole derivative **4**.

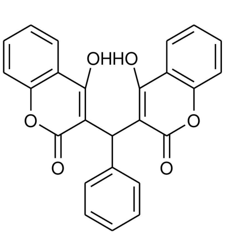

5

Figure 7. Chemical structure of the coumarin derivative **5**.

Noteworthy, the antibiofilm activity against the MRSA strains of compound **5** was assayed *in vivo* for evaluating the effect on MRSA adhesion to a catheter surface inserted in the rat bladder. These results are particular relevant since one of the major cause of the absence of antibiofilm agents in clinic was due to the lack of *in vivo* studies. Compound **5** administered at doses of 5 and 10 mg/kg inhibited MRSA USA 300 adhesion and biofilm formation on the surface of the catheter. Additionally, it was also able to inhibit the diffusion of the pathogen from the catheter to the liver, lung, kidney and spleen.

Quantitative real-time polymerase chain reaction (PCR) elucidated a mechanism of action involving the inhibition of the expression levels of the genes *srtA*, *altE*, *aap*, *icaA* and *arc* gene cluster transcription. In particular compound **5** proved to be able to interfere with the arginine catabolic pathway by competitively binding to the arginine repressor ArgR.

The toxicity of the coumarin derivative 5 was evaluated both *in vitro*, against human umbilical vein endothelial cells (HUVECs) and cells from human embryonic myocardial tissue (CC-HHM-2), and *in vivo*, in mice and rats after oral administration. Results highlighted a low toxicity of the compound, which showed a therapeutic index in mouse of 37.56. Additionally, treatment with 2×, 4× and 8× MIC **5** did not induce resistance in treated bacterial strains. On the basis of the obtained results, compound **5** can be considered an ideal lead compound for development of new therapeutic approaches to fight MRSA infections.

2.3. Biofilm-eradicating agents

Biofilm eradicating agents, differently from biofilm inhibitors and biofilm dispersal agents, act killing persister cells within the biofilm. This distinct mechanism of action confers them the potential to be employed as standalone antibiofilm therapy. Antimicrobial peptides (AMP), which cause bacterial cell lysis through the crushing of the bacterial membrane, are the most well known biofilm eradicating agents.[46,47] The main obstacle for their development in clinical use is the difficulty to obtain AMP which are able to target selectively bacterial cell membrane. Therefore, it should be useful in this field to identify new agents able to kill dormant cells through alternative mechanisms of action, for which a higher selectivity is feasible.

© 2020 Wiley-VCH GmbH

2.3.1. Phenazines

Diverse classes of phenazines were described as MRSA biofilm-eradicating agents, which are able, unlike the inhibitors of biofilm formation and the dispersal agents, to kill persister cells. Since conventional antibiotics, affecting life processes of the bacterium, are not efficacious against the non-replicating dormant cells, these are often the main cause of the resistance of the biofilm-associated infections.

On the basis of the potent antibacterial activity observed for the marine phenazine antibiotic **6** (Figure 8) Garrison and co-workers synthesized a series of halogenated phenazines (HPs) with the aim to enhance their antimicrobial potency and in order to obtain compounds which were also capable of inhibiting persistent cells.[48–50] The influence of the substitutions at the positions 2-, 4-, 7-, and 8- of the phenazine scaffold, on both antibacterial and biofilm eradicating activity, was widely studied providing pivotal information on the structural features required for the activity.[48] Among the tested compounds derivative (2-bromo-7,8-dichloro-4-iodo-1-hydroxyphenazine) **7** (Figure 8) showed, in the Calgary biofilm device (CDB) assay,[51] the highest activity against MRSA biofilms (MRSA-2, MRSA BAA-1707, MRSA BAA-44) eliciting minimum biofilm eradication concentration (MBEC) values ranging from 6.25 to 9.38 μM (Table 2). The viable biofilm cell count at the MBEC value highlighted the almost total eradication of the persister cells within the biofilm.

Since the antibiotics normally used in the treatment of MRSA infections, including vancomycin, daptomycin and linezolid, were ineffective against MRSA biofilms and persister cells at concentration higher than 2000 μM, the results obtained for compound **7** are very encouraging. Additionally, compound **7** was compared to known biofilm- or persister-eradicating agents such as the AMP mimic membrane lysing agent QAC-10 (quaternary ammonium cation-10), the membrane-active ionophore CCCP (carbonyl cyanide *m*-chlorophenyl hydrazine), the antioxidant NAC (N-acetylcysteine), and persister cells eradicator pyrazinamide. All the known anti-biofilm compounds proved to be 12 to 200-fold less active in eradicating MRSA biofilms than the HP **7**. With the aim to investigate a possible membrane-lysing mechanism of action the hemolysis activity against human red blood cells was evaluated at the screening concentration of 200 μM and, as observed generally for phenazine analogs, also in this case no significant hemolysis was found (<3%). These results suggested a different mechanism of action with respect to the prevalent class of biofilm-eradicating agents described to date, which is constituted by the AMPs.[47,52] A non-hemolytic mechanism of action may be beneficial to achieve lower human toxicity, which is one of the main impediments to obtaining therapeutically valid AMPs that should specifically target bacterial membranes over mammalian cell membranes.[53] The low toxicity of the phenazine analogs synthesized, was also confirmed in a lactate dehydrogenase (LDH) release assay against HeLa cells highlighting the promising therapeutic profile of this class of compounds to be developed into a new class of antimicrobial agents to treat serious MRSA infections.

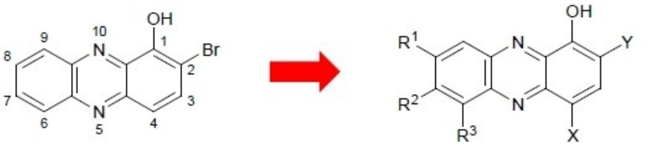

6

7, $R^1=R^2=Cl$, $R^3=H$, $Y=Br$, $X=I$
8, $R^1=R^2=H$, $R^3=CH_3$, $X=Y=Br$
9, $R^1=R^2=H$, $R^3=C_2H_5$, $X=Y=Br$

Figure 8. Chemical structures of compounds **6**–**9**.

Preliminary mechanistic investigations elucidated a metal (II)-dependent eradicating mechanism of action. The co-treatment of phenazine **7**, at the MIC concentration, with 200 μM of copper(II), iron(II) and magnesium(II) resulted in a significant reduction in antibacterial activity, up to 48 times in the case of copper(II).

Based on the interesting results, new HP were synthesized in order to obtain more potent biofilm-eradicating agents against MRSA.[54]

The Wohl-Aue reaction was employed to lead a small library of HPs bearing different substituents at the 6-, 7-, 8- and 9-positions. Among the new compounds 2,4-dibromo-HP analogs **8** and **9** (Figure 8) showed the highest antibacterial activity against both the planktonic and the biofilm form of MRSA BAA-1707. HP **8** and **9** proved to be equipotent against the planktonic form eliciting a MBC value of 6.25 μM (Table 2). Additionally, they showed potent biofilm-eradicating activity with MBEC values of 6.25 and 4.69 μM, respectively. At the MIC concentration, the new HP analogs **8** and **9** demonstrated an important reduction (99.9%) in viable MRSA BAA-1707 biofilm cells.

Similarly to HP **7**, compounds **8** and **9** showed a metal (II) chelating mechanism of action and a lack of red blood cell hemolysis and HeLa cytotoxicity. Among biofilm-eradicating agents effective against MRSA, HP analogs showed interesting features to be developed into innovative treatments of chronic biofilm-associated MRSA infections. 1-Hydroxyl group and 2-bromine atom on the phenazine scaffold were recognized key structural features for the antimicrobial activity of this class of

Table 2. Antibacterial and biofilm eradication activity of compounds **7**–**9** (μM).

	MRSA-2			MRSA BAA 17–07			MRSA BAA-44		
Compound	MIC	MBC	MBEC	MIC	MBC	MBEC	MIC	MBC	MBEC
7	3.13	3.13	9.38	0.30	4.69	6.25	3.13	12.5	9.38
8	0.30	–	–	0.30	6.25	6.25	0.39	–	–
9	0.39	–	–	0.10	6.25	4.69	0.59	-	–

compounds. The presence of an additional bromine atom at 4-position as well as a methyl or ethyl group at 6-position was advantageous for both antibacterial and biofilm eradicating activity. Furthermore, two chlorine atoms at 7- and 8- positions proved to be relevant for the eradication potency against MRSA-2, MRSA BAA-1707 and MRSA BAA-44 strains. On the contrary, the replacement of the two chlorine atoms at the same positions with two bromine atoms as well as removing the halogen from position 4 led to a significant loss of activity.

2.3.2. Quinolines

With the aim to identify novel potent antibiofilm compounds to counteract MRSA infections a series of halogenated quinolines (HQs), structurally related to HPs, were investigated *in vitro* in antibacterial and biofilm eradication assays.[45,55] Among the new quinolines, several derivatives showed potent antibacterial activity, with MICs in some cases lower than 1 μM, and biofilm dispersal action against methicillin-resistant *S. aureus* clinical isolate MRSA-2, with EC_{50} in the low micromolar range (See the section 4). Conversely, regarding MRSA biofilm eradication, the replacement of the HP scaffold with the HQ nucleus was detrimental for the activity. HQ analogs were inactive or only weakly active. The first HQ that showed a weak biofilm eradicating activity with a metal(II)-dependent mechanism against MRSA (MBEC = 250 μM) was the quinoline **10** (Figure 9).[55]

Basak et al. during a study aimed to investigate structural modifications at the 2-position of the HQ scaffold, which was recognized crucial for the antibacterial activity, identified compound **11** (Figure 9), which was slightly more active than **10** but significantly less active than the HP analogues, showing a MBEC value against MRSA-2 of 125 μM.

Abouelhassan et al. described the potentiating effect of the plant derived phytochemical gallic acid **12** (Figure 9) on the antibacterial and eradicating activity of the HQ **10**.[56] The combination therapy (HQ **10** at MIC concentration + **12** 1 mM) was 11800-fold more potent against *S. aureus* 29213 with a MIC value of 0.05 nM, and, interestingly, was 4-fold more effective in the biofilm-eradication assays, showing a MBEC value of 62.5 μM vs 250 μM of HQ **10** used alone.

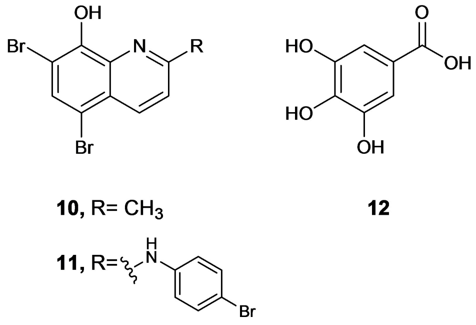

10, R= CH_3

12

11, R=

Figure 9. Chemical structures of compounds **10**–**12**.

2.3.3. Quinones

Quinone derivatives are a class of synthetic and natural compounds endowed with different pharmacological activities, including antiviral, antifungal, antibacterial and anti-biofilm properties.[57] Structurally they are characterized by a common pattern constituted by an *ortho* or a *para* substituted dione conjugated to an aromatic cycle such as in the benzoquinones, or to polycyclic aromatic system, such as in anthraquinones, naphtoquinones and anthracyclinones. Recently, three furanoquinones **13**, **14 a** and **14 b** (Figure 10) were described for their interesting activity against MRSA.[58,59]

The naphtho[1,2-*b*]furan-4,5-dione **13**, tested against MRSA ATCC 33591 and the two MRSA clinical isolates KM-1 and KM-2, proved to be significantly more potent than oxacillin (MIC = 160 - 630 μM) used as reference compound, eliciting MIC values in the range 4.9–9.8 μM. (Table 3).[58] Studies on MRSA morphology carried out through a transmission electron microscopy (TEM) before and after treatment with **13** highlighted the ability of the compound to cause a bacterial surface damage. The presence of depressions on the cell surface suggested the loss of intracellular material due to an osmotic alteration of the bacterial membrane. A proteomic assay, employed to deepen the mechanism of action of compound **13**, suggested strong interferences with crucial bacterial metabolic pathways, including translocase elongation factor G (EF–G), phosphoenolpyruvate carboxykinase (PEPCK), citrate synthase and arginine deiminase. In particular, the profiling assay of MRSA proteins revealed that furanoquinone potently inhibited staphylococcal EF–G, which plays a key role in bacterial protein synthesis, catalysing the translocation of transfer RNA (tRNA) and messenger RNA (mRNA) through the ribosome. The consequent inhibition of protein synthesis in MRSA led to bacterial death.

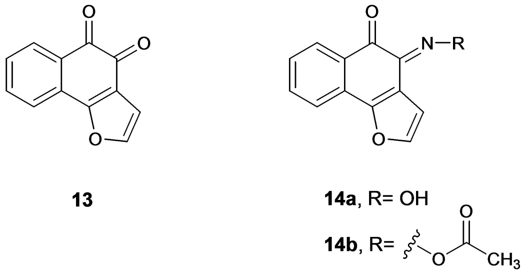

13

14a, R= OH

14b, R=

Figure 10. Chemical structures of compounds **13** and **14 a,b**.

Table 3. MIC and MBC values of derivatives **13** and **14 a,b** against MRSA KM-1, MRSA KM-2, MRSA KM-5 and MRSA ATCC 33591 (μM).

Compound	MRSA KM-1		MRSA KM-2		MRSA KM-5		MRSA ATCC 33591	
	MIC	MBC	MIC	MBC	MIC	MBC	MIC	MBC
13	4.9	4.9-9.8	4.9–9.8	4.9–19	–	–	4.9–9.8	9.8–39
14 a	45.5-91.5	91.5-183.0	–	–	11.7-91.5	91.5-731.7	45.5–91.5	91.5
14 b	76.4	76.4-152.8	–	–	9.4-76.4	76.4-152.8	9.4–38.0	76.4

© 2020 Wiley-VCH GmbH

An important downregulation in bacterial PEPCK expression was found as a consequence of the exposure to derivative **13**. Being PEPCK an enzyme involved in the gluconeogenesis, its inhibition led to the bacterial death because of the absence of glucose, which is fundamental for the microbial growth. Derivative **13** proved to be active also in inhibiting citrate synthase, which catalyzes the last steps of Krebs cycle and finally, it interfered with the arginine metabolism, hindering the enzyme arginine deiminase which is well known as important virulence factor responsible of the MRSA invasion and growth in host cells.

Compound **13** was found able to reduce biofilm thickness from 24 to 16 μm and to kill bacterial cells inside the immune cells THP-1 (human myelomonocytic cell line), showing low toxicity toward macrophages at the biocidal dose.

Subsequently, two furanoquinone derivatives containing imine moiety, **14 a** and **14 b**, were found able to eradicate MRSA biofilm causing, at concentrations ranging from 391 to 469 μM, a 1000-fold reduction of the bacterial cells inside the biofilm with a biofilm thickness reduction from 30 to 17.2 μm for the most active compound **14 a**.[59] Considering the high morbidity and mortality due to colonization of cutaneous wounds by MRSA biofilms the *in vivo* efficacy of the two compounds in treating skin infection was also assayed in mice subcutaneously inoculated with MRSA. Topical application of the two compounds led to a significant reduction of MRSA-infected abscess after two days treatment, causing only a very slight skin irritation on intact mouse skin. Compounds **14 a** and **14 b** proved to be active also against the planktonic form of MRSA ATCC 33591 (Table 3) eliciting a bactericidal effect as their MBC values are no higher than 4xMIC values. Even if structurally very similar to compound **13**, for furanoquinones **14 a** and **14 b** no bacterial membrane damage was observed by scanning electron microscopy (SEM). In order to clarify the mechanism of action, the total amount of DNA, RNA and proteins were quantified in MRSA cells treated with the furanoquinones **14 a** and **14 b** and a significant decrease in DNA content was observed. The inhibitory activity of the compounds against DNA polymerase, topoisomerase I and gyrase was evaluated in polymerase chain reaction analysis (PCR) and in a wrapping assay. Derivatives **14 a** and **14 b**, at concentrations ranging from 0.3 to 9 μM, were inactive against topoisomerase I whereas they interfered with DNA polymerase and gyrase.

2.4. Aryl-alkyl-lysines

Another class of compounds described for its promising antibacterial activity against the persister cells is constituted by the membrane active aryl-alkyl-lysines of type **15** (Figure 11).[60]

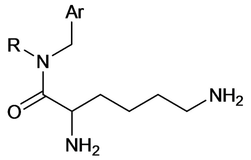

15a, R = C_8H_{17}, Ar = $C_{10}H_7$
15b, R = $C_{10}H_{21}$, Ar = $C_{10}H_7$
15c, R = $C_{10}H_{21}$, Ar = C_6H_5
15d, R = $C_{12}H_{25}$, Ar = C_6H_5

Figure 11. Chemical structures of compounds **15 a–d**.

Table 4. Activity of compounds **15 a–d** against Staphylococcal planktonic cells (including clinical isolates).

Compound	Minimum Inhibitory Concentration [μM]			
	S. aureus MTCC 737	MRSA ATCC 33591	MRSA R3889	MRSA R3890
15 a	10.8 ± 1.7	8.8 ± 2.6	10.8 ± 1.7	7.9 ± 1.0
15 b	5.7 ± 0.5	4.1 ± 0.1	4.4 ± 0.3	4.8 ± 0.3
15 c	10.9 ± 0.1	25.5 ± 0.2	11.3 ± 1.4	10.2 ± 0.4
15 d	5.5 ± 1.1	5.1 ± 0.6	4.5 ± 0.3	± 1.1

All the four compounds **15 a-d** showed antibacterial good activity against the planktonic form of three MRSA strains, including ATCC 33591, R3889 and R3890, with MIC value ranging from 4.1 to 25.5 μM (Table 4). Importantly, they elicited no propensity to induce resistance in Gram-positive strains, since they maintained unchanged the MIC value toward *S. aureus* MTCC 737 after 20 treatments at the highest concentration of half of MIC, whereas the MIC of norfloxacin, used as reference compound, increased by 800 fold. Derivative **15 b** was chosen as representative compound of the series for further studies in order to evaluate the anti-biofilm properties and the mechanism of action of this class of compounds. Naphthalene derivative **15 b** was able to remove the *S. aureus* persister cells completely at the concentration of 5xMIC, which is a very interesting result considering that ampicillin was ineffective against persister cells at concentrations higher than 500xMIC. This effect on the dormant cells seemed to be due to the membrane active properties of the compound, which proved to be able of strongly depolarizing the membrane within the first minute of exposure.

At 10xMIC **15 b** significantly reduced pre-formed MRSA (ATCC 33591) biofilm leading to a biofilm thickness reduction from 23 to 2 μm. Since skin infections represent one of the most relevant problems caused by MRSA in hospital, efficacy of **15 b** was confirmed in an *in vivo* mice model of skin infection. The results indicated higher potency in treating infections compared to fusidic acid used as reference drug.

2.5. Antibiotics

The susceptibility of the planktonic and the biofilm forms of MRSA to conventional antibiotics was investigated with the aim to identify an efficacious combination therapy to treat chronic biofilm-associated infections. Vancomycin is a glycopeptide antibiotic extensively used as first-line treatment for serious MRSA infections, including endocarditis, meningitis, bacteremia and osteomyelitis. Unfortunately, its extensive use together with the need to use increasing dosages in an attempt to

© 2020 Wiley-VCH GmbH

penetrate the MRSA biofilm, over time, have led to a significant increase in the MIC of this antibiotic.[61]

Chopra et al. studied the anti-biofilm properties of clindamycin, vancomycin and minocycline (Figure 12) against two different strains of MRSA: ATCC 33591 and ATCC 43 300.[62]

The choice of the two strains was made in order to evaluate the influence of the presence of the intercellular adhesion (*ica)*-locus on the bacterial susceptibility to the antibiotics, MRSA ATCC 33591 is, in fact, an *ica*-locus positive strain whereas ATCC 43 300 is an *ica*-locus negative strain. Both are well-known biofilm producer strains but the composition of the biofilm matrix is very different.

Ica-locus is involved in the production of the polysaccharide intercellular adhesin (PIA), which is composed of linear glucosaminoglycans and plays a key role in the intercellular adhesion during the biofilm formation.[63] Therefore, the biofilm matrix of the *ica*-locus positive strain MRSA ATCC 33591 was mainly made of PIA. Instead, the main component of the biofilm matrix in *ica*-locus negative strain ATCC 43 300 is eDNA. The biofilm eradication activity of vancomycin and minocycline was evaluated in both strains in order to compare their effectiveness.

All the three antibiotics proved to be active against the tested MRSA strains in planktonic growth with similar potency against the two strains (Table 5), substantial differences were indeed observed regarding the anti-biofilm effect against the two strains. In particular, vancomycin showed a good biofilm-eradicating activity against the *ica*-locus negative strain on mature biofilm with MIC and MBC values of 11-22 μM, respectively. On the contrary, the same antibiotic showed no effect in eradicating *ica*-positive MRSA biofilm eliciting MBC value higher than 700 μM. These so different results were probably due to the different composition of the biofilm matrix in the two strains: the presence of PIA in the matrix confers a greater density to the biofilm structure, which becomes difficult the penetration of the vancomycin.

Differently, the tetracycline minocycline proved to be quite active in eradicating both *ica*-negative and *ica*-positive MRSA mature biofilm with MBC values of 4.3 and 34 μM, respectively.

Moreover, only minocycline showed also a significant inhibition of biofilm formation in the two strains. Probably, the effect against *ica*-negative biofilm was due to the suppression of Alt (major autolysin), which is involved in the initial bacterial adhesion to the surface and in the lysis of bacterial cells that determines the eDNA release in the biofilm matrix.[64] The results highlighted the correlation between the anti-biofilm efficacy of vancomycin and minocyclin with the biochemical composition of MRSA biofilm.

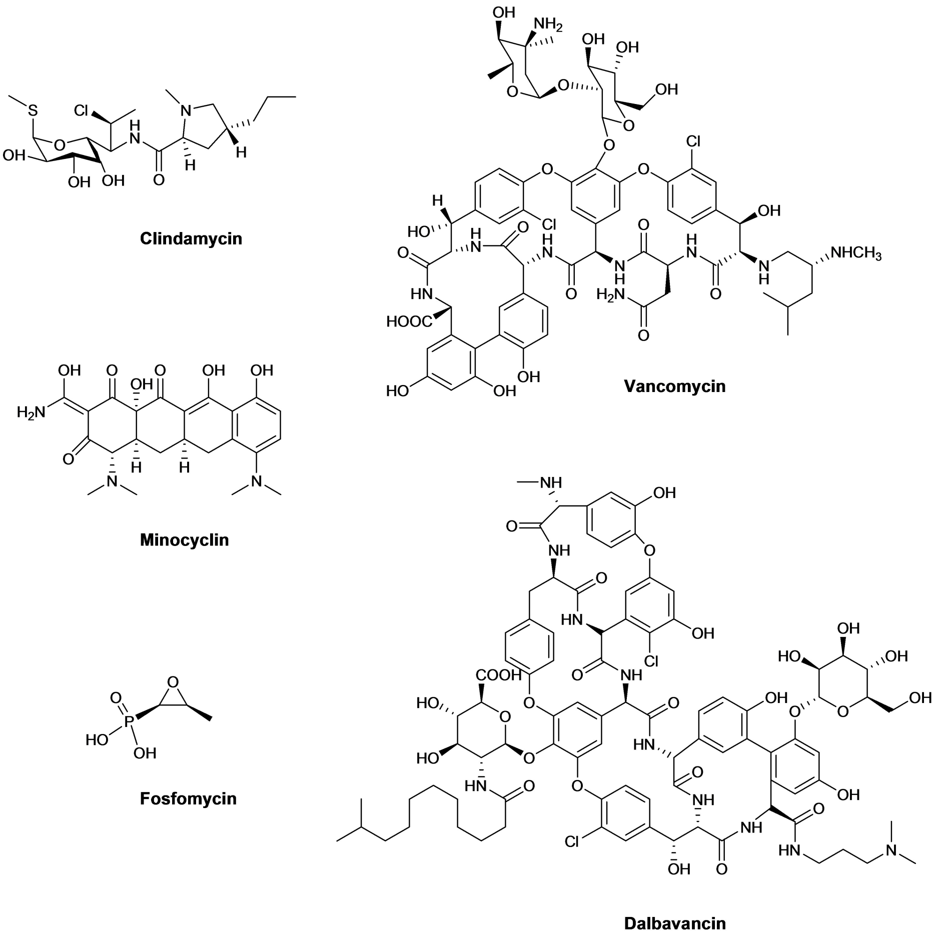

Figure 12. Chemical structure of clindamycin, vancomycin, minocycline, fosfomycin and dalbavacin.

Table 5. Antibiotic susceptibility of three antibiotics against MRSA biofilms in different phases of biofilm formation.

		Clindamycin [µM]		Vancomycin [µM]		Minocyclin [µM]	
Mode of growth	Initial bacterial density [CFU mL^{-1}]	MIC	MBC	MIC	MBC	MIC	MBC
ica-negative MRSA							
Log planktonic	1.2×10^{5}	150	301	5.5	11	0.5	2.1
Stationary planktonic	1.1×10^{7}	–	>2409	–	11	–	8.7
Mature biofilm	1.3×10^{-7}	>2409	>2409	11	22	1	4.3
ica-positive MRSA							
Log planktonic	3.4×10^{5}	301	602	5.5	44	1	4.3
Stationary planktonic	3.5×10^{8}	–	1204	–	176	–	17
Mature biofilm	3.2×10^{8}	>2409	>2409	353	>706	17	34

Considering the genetic heterogeneity of the resistant bacterial cells inside the biofilm and the growing loss of activity of vancomycin toward MRSA infections, the effectiveness of combinations of vancomycin with other antibiotics in inhibiting MRSA biofilm were evaluated.

Shi et al. reported an *in vivo* study on the synergistic bactericidal effect of the association vancomycin-fosfomycin on chronic biofilm-associated MRSA infection.[65] The *in vitro* efficacy of this antibiotics combination against planktonic and biofilm forms of *S. aureus* and different MRSA strains were previously described.[66,67]

Vancomycin and fosfomycin elicited, when used alone, MIC values against MRSA KZ306 and ATCC43300 of 1.3 and 14.5 µM, respectively, but bacterial regrowth was observed after 24 h. Lasting and long-term bactericidal effect on MRSA was recorded in presence of higher concentrations, approximately 8-fold the MIC value. Combination therapy of the two antibiotics provided better results, showing a complete antibacterial effectiveness at significant lower concentrations (MIC vancomycin $+\,^{1}/_{2}$ MIC fosfomycin).

The synergistic antibacterial activity of the two antibiotics was also evaluated against the biofilm. It is known that the association of antibiotics with different mechanisms of action can give good results in biofilm eradication for the theory of the mutant selection window.[68] For this theory, in fact, the simultaneous use of antibiotics with different bactericidal effect, prevent mutant selection and decrease the side effects. In the case of the association vancomycin-fosfomycin, for example, a significant reduction of the renal toxicity of vancomycin was observed, thus providing an important advantage for antibacterial therapy in patients with renal failure.

Furthermore, the synergistic effect of the two antibiotics was evaluated *in vivo* in a carboxymethyl cellulose (CMC)-pouch biofilm model in rats. The CMC pouch was made through an injection, in the animals, of a mixture of 5 mL of CMC and 5 mL of 1×10^{7} CFU/mL of MRSA KZ306 or ATCC43300.

Nine days after the inoculation of the bacteria, which is the time required to obtain a mature biofilm, vancomycin and fosfomycin were administered intraperitoneally, alone or in combination, at the dosage of 100 mg/Kg and 200 mg/Kg, respectively.

For both strains the combination therapy proved to be significantly more potent than the mono-administration in eradicating mature biofilm. The *in vivo* model was employed not only to evaluate the ability of the antibiotics in killing bacterial inside the biofilm, but also to study the structural modification and the inflammatory response of the biofilm. The histological analysis of MRSA biofilm tissue showed a marked loss of the biofilm structure and a notable reduction of the necrosis process. After 9 days of treatment with the combination therapy, the animals elicited a remarkable decrease in white blood cells, in C-reactive protein in blood samples and in exudate colonies. Results confirmed *in vivo* the synergic bactericidal activity of vancomycin and fosfomycin in the treatment of chronic MRSA infections.

Recently, the *in vitro* efficacy of the novel lipoglycopeptide dalbavancin against MRSA-biofilm associated infections was investigated.[69] Compared to vancomycin, dalbavancin proved to be more advantageous in terms of both dosage, which was weekly, and efficacy in patients with catheter-related bloodstream infections.[70] Dalbavancin was able to reduce biofilm with MBC values in the range 1-4 mg/mL (0.5-2.2 µM) in ten MRSA isolates.

2.5.1. Human kinase inhibitors

The strategy to repurpose drugs, which have been discovered for the treatment of a particular disorder, to counteract another disease, can be extremely advantageous since their safety profiles are well known and they can be easily obtained for clinical trials.[71]

A screening of a library of commercial kinase inhibitors for their antibacterial activity against *S. aureus* and MRSA led to the identification of the anticancer drug sorafenib **17** (Figure 13) as a potent antimicrobial compound effective against MSSA (methicillin-sensitive *S. aureus*).[72]

Derivative **17** was able to inhibit the bacterial growth of *S. aureus* NCTC 8325 and ATCC 12598 with MIC values of 7.6 µM, eliciting, indeed, no effect on MRSA tested strains ATCC 33592, ATCC 49476 and SCCmec VT.

In order to obtain more potent antibacterial compounds, effective also against MRSA, a library of analogs of compound **16** (Figure 13) was synthesized and tested *in vitro* and *in vivo* against *S. aureus* and MRSA infections. Among the new compounds, two derivatives **17** and **18** (Figure 13) showed increased potency against MRSA compared to the lead **16**.[72,73]

Compounds **17** and **18** showed against the tested 100 clinical MRSA isolates MIC values in the low micromolar range.

Results highlighted the importance of the 4-chloro-3-(trifluoromethyl) phenyl moiety for the antibacterial activity, in

© 2020 Wiley-VCH GmbH

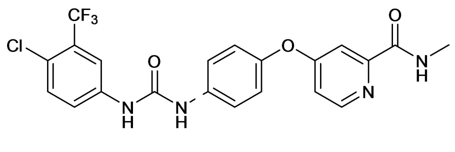

16

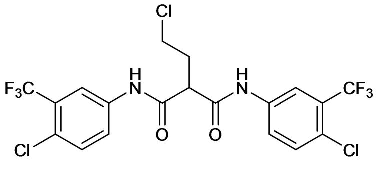

17

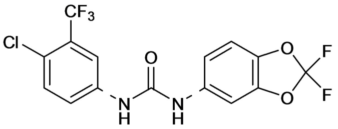

18

Figure 13. Chemical structure of compounds **16**–**18**.

fact, its replacement with different aliphatic or aromatic groups led to inactive compounds. On the contrary, the aryl heteroaryl ether group was found the portion of the molecule that can be optimized to enhance the antibacterial properties of this class of compounds. In particular, its replacement with the 2,2-difluoro-1,3-benzodioxole gave derivative **16** with significantly enhanced MRSA potency (MIC = 3 μM). This nucleus proved to play a key role in the anti-MRSA activity, as small structural modifications, including the removal of the fluorine atoms or opening the acetal group, caused the complete loss of the activity. Importantly, compound **16** showed potent biofilm-eradicating activity against the staphylococcal strains killing the persister cells in a concentration- and time-dependent manner eliciting a BEC_{50} against pre-formed *S. aureus* ATCC 29213 biofilm of 3.13 μM (Figure 14).

The tendency of **18** to induce bacterial antibiotic resistance was also assayed treating the bacterial cells with different compound concentrations, ranging from 0.25 to 4-fold MIC, for 27 days. Interestingly, unlike from compound **16** and ofloxacin used as reference antibiotic, which showed rapidly a significant decrease of the activity, compound **18** maintained the same antibacterial activity during all the treatment. In order to identify the mechanism of action, chemical proteomics studies for the identification of the target were carried out and demethylmenaquinone methyltransferase (MenG), which catalyses the synthesis of the vitamin menaquinone, was recognized as the strongest hit. Inhibition of menaquinone determined the bacterial death since it is involved in the bacterial respiration and energy metabolism.

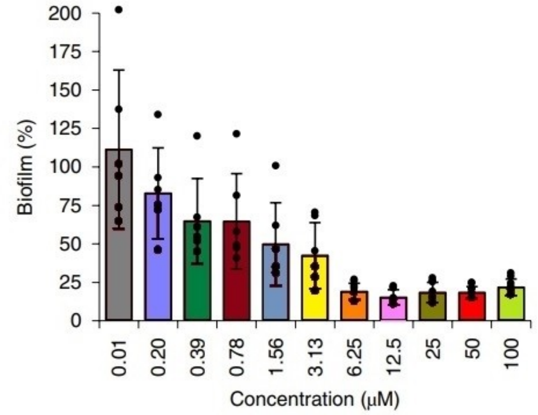

Figure 14. Eradication of *S. aureus* ATCC 29213 biofilm after treatment (24 h) with different concentrations of compound **18**.

Based on the high potency and the absence of resistance development, the pharmaceutical profile of derivative **18** was deepened in *in vivo* studies. To identify the therapeutic window for the *in vivo* treatment of MRSA infection, was first calculated the ratio between the cytotoxicity against human cell lines (IC_{50}) and the antibacterial activity (MIC), which it was found between 23 to 52 μM. Additionally, **18** did not induce haemolysis of red blood cells and showed excellent plasma stability.

The *in vivo* antibacterial efficacy was evaluated in neutropenic mouse model infected with MRSA strain ATCC33591 and treated with 20 mg/Kg of **18** orally administered. A significant reduction in colony-forming unit (c.f.u./g), up to ten-fold, was observed in comparison the vehicle-treated mice. No toxic effects were revealed for orally and intravenously administrations at dosages of 20 mg/Kg and 10 mg/Kg, respectively. Moreover, an oral bioavailability of 63% was found for derivative **18**.

3. Conclusions

It was established that more than 80% of the bacterial infections are biofilm-mediated.

The growing knowledge of the staphylococcal biofilm genetics has certainly helped us in the understanding of the complex process of biofilm formation, and have also pointed to potential new therapeutic strategies for serious device-associated infection.[74]

However, despite important progresses have been made in this field, many gaps in knowledge are till uncovered due, principally, to the lack of *in vivo* studies and explanations on the mechanisms of action. The individuation of the bacterial target responsible of the anti-biofilm properties of a class of compounds, as well as their validation in a valid *in vivo* model, were crucial steps for the development of new valuable therapeutic strategies in the struggle against MRSA chronic infections.

The applications of the various anti-biofilm agents change according to the biofilm formation phase on which they interfere. Compounds able to interfere with the biofilm formation should be useful in the prophylaxis to avoid skin or implants biofilm-associated infections caused by MRSA contamination. Dispersal agents could be administered, instead, in association with an antibiotic since they act disrupting the biofilm architecture and then freeing the bacterial cells in their planktonic form.

Eradicating agents represent a valuable strategy to treat established biofilm-associated infections; therefore, they have the potential to become the first-line treatment of chronic MRSA diseases.

Key roles in MRSA biofilm formation were recognized for MSCRAMMs, the major autolysin and eDNA.

Since eDNA is the most common component in MRSA biofilms, whereas PIA is important for a small number of isolates, eDNA can be considered one of the primary target for developing eradication strategies against MRSA biofilms.

Many compounds with interesting anti-biofilm properties and good toxicity profiles were described in the last decade. Nevertheless, the identification of new synthetic small molecules able to eradicate mature MRSA biofilm and to kill persister cells without affecting mammalian cell growth remains an important challenge.

Among them, HPs showed in many cases potent eradication activity against pre-formed MRSA associated with a low toxicity against human cells. HP **7-9** proved to be able to eradicate MRSA biofilms through a non-hemolytic metal(II)-dependent eradicating mechanism of action which demonstrated to be selective towards bacterial cells over mammalian cells. For these features HP scaffold deserves further studies in order to identify the bacterial target and to confirm the anti-biofilm properties in *in vivo* models.

Noteworthy, the 1-[4-chloro-3-(trifluoromethyl)phenyl]-3-(2,2-difluoro-1,3-benzodioxol-5-yl)urea **18** exhibited very interesting results against both planktonic and biofilm forms of MRSA. Interestingly its antibacterial efficacy and its low toxicity were confirmed in *in vivo* assays. Additionally, compound **18** is one of the few anti-MRSA biofilm agents for which the mechanism of action has been identified.

Since there are no approved drugs specifically effective against MRSA biofilms in clinical trials to date, further efforts should be made to identify more efficient therapeutic approaches that hopefully target MRSA communities and to deepen the main mechanisms of action as well as the *in vivo* efficacy.

Conflict of Interest

The authors declare no conflict of interest.

Keywords: MRSA · biofilms · antibiotic resistance · antivirulence · eradicating agents

[1] D. Schillaci, V. Spanò, B. Parrino, A. Carbone, A. Montalbano, P. Barraja, P. Diana, G. Cirrincione, S. Cascioferro, *J. Med. Chem.* **2017**, *60*, 8268–8297.
[2] B. Parrino, D. Carbone, G. Cirrincione, P. Diana, S. Cascioferro, *Fut. Med. Chem.* **2020**, *12*, 357–359.
[3] A. Hassoun, P. K. Linden, B. Friedman, *Critical Care.* **2017**, *21*, 211.
[4] A. S. Lee, H. de Lencastre, J. Garau, J. Kluytmans, S. Malhotra-Kumar, A. Peschel, S. Harbarth, *Nat Rev Dis Primers.* **2018**, *4*, 1–23.
[5] J. Fishovitz, J. A. Hermoso, M. Chang, S. Mobashery, *IUBMB Life.* **2014**, *66*, 572–577.
[6] D. L. Popham, K. D. Young, *Curr. Opin. Microbiol.* **2003**, *6*, 594–599.
[7] K.-F. Kong, L. Schneper, K. Mathee, *APMIS.* **2010**, *118*, 1–36.
[8] D. Lim, N. C. J. Strynadka, *Nat. Struct. Biol.* **2002**, 9, 870–876.
[9] S. Cascioferro, B. Parrino, G. L. Petri, M. G. Cusimano, D. Schillaci, V. Di Sarno, S. Musella, E. Giovannetti, G. Cirrincione, P. Diana, *Eur. J. Med. Chem.* **2019**, *167*, 200–210.
[10] R. Sommer, K. Rox, S. Wagner, D. Hauck, S. S. Henrikus, S. Newsad, T. Arnold, T. Ryckmans, M. Brönstrup, A. Imberty, A. Varrot, R. W. Hartmann, A. Titz, *J. Med. Chem.* **2019**, *62*, 9201–9216.
[11] A. Carbone, B. Parrino, M. G. Cusimano, V. Spanò, A. Montalbano, P. Barraja, D. Schillaci, G. Cirrincione, P. Diana, S. Cascioferro, *Mar. Drugs* **2018**, *16*, 274.
[12] A. R. Kayumov, E. N. Khakimullina, I. S. Sharafutdinov, E. Y. Trizna, L. Z. Latypova, H. Thi Lien, A. B. Margulis, M. I. Bogachev, A. R. Kurbangalieva, *The J. Antibiot.* **2015**, *68*, 297–301.
[13] B. Parrino, D. Schillaci, I. Carnevale, E. Giovannetti, P. Diana, G. Cirrincione, S. Cascioferro, *Eur. J. Med. Chem.* **2019**, *161*, 154–178.
[14] H.-S. Kim, S.-H. Lee, Y. Byun, H.-D. Park, *Sci. Rep.* **2015**, *5*, 8656.
[15] S. Cascioferro, B. Parrino, D. Carbone, D. Schillaci, E. Giovannetti, G. Cirrincione, P. Diana, *J. Med. Chem.* **2020**, *63*, 7923–7956.
[16] B. Parrino, P. Diana, G. Cirrincione, S. Cascioferro, *Open J. Med. Chem.* **2018**, *12*, 84-87.
[17] F. Fitzpatrick, H. Humphreys, J. P. O'Gara, *Clin. Microbiol. Infect.* **2005**, *11*, 967–973.
[18] J. A. Geoghegan, R. M. Corrigan, D. T. Gruszka, P. Speziale, J. P. O'Gara, J. R. Potts, T. J. Foster, *J. Bacteriol.* **2010**, *192*, 5663–5673.
[19] C. Pozzi, E. M. Waters, J. K. Rudkin, C. R. Schaeffer, A. J. Lohan, P. Tong, B. J. Loftus, G. B. Pier, P. D. Fey, R. C. Massey, J. P. O'Gara, *PLoS Pathog.* **2012**, *8*, e1002626.
[20] E. O'Neill, C. Pozzi, P. Houston, H. Humphreys, D. A. Robinson, A. Loughman, T. J. Foster, J. P. O'Gara, *J. Bacteriol.* **2008**, *190*, 3835–3850.
[21] P. Houston, S. E. Rowe, C. Pozzi, E. M. Waters, J. P. O'Gara, *Infect. Immun.* **2011**, *79*, 1153–1165.
[22] S. Cascioferro, M. G. Cusimano, D. Schillaci, *Fut. Microbiol.* **2014**, *9*, 1209–1220.
[23] T. J. Foster, J. A. Geoghegan, V. K. Ganesh, M. Höök, *Nat Rev Micro.* **2014**, *12*, 49–62.
[24] S. Cascioferro, M. Totsika, D. Schillaci, *Microb. Pathog.* 2014, 77 C, 105–112.
[25] R. Nandakumar, M. P. Nandakumar, M. R. Marten, J. M. Ross, *J. Proteome Res.* **2005**, *4*, 250–257.
[26] L. Foulston, A. K. W. Elsholz, A. S. DeFrancesco, R. Losick, *mBio* **2014**, *5*, e01667-14.
[27] S. Sugimoto, F. Sato, R. Miyakawa, A. Chiba, S. Onodera, S. Hori, Y. Mizunoe, *Sci. Rep.* **2018**, *8*, 2254.
[28] J. M. Yarwood, D. J. Bartels, E. M. Volper, E. P. Greenberg, *J. Bacteriol.* **2004**, *186*, 1838–1850.
[29] C. O. Beltrame, M. F. Côrtes, R. R. Bonelli, A. B. de A. Côrrea, A. M. N. Botelho, M. A. Américo, S. E. L. Fracalanzza, A. M. S. Figueiredo, *PLoS One.* **2015**, *10*, e0138924.
[30] J. B. Kaplan, E. A. Izano, P. Gopal, M. T. Karwacki, S. Kim, J. L. Bose, K. W. Bayles, A. R. Horswill, *mBio* **2012**, *3*, e00198-12.
[31] D. L. Smith, A. D. Harris, J. A. Johnson, E. K. Silbergeld, J. G. Morris, *Proc. Natl. Acad. Sci. USA* **2002**, *99*, 6434–6439.

© 2020 Wiley-VCH GmbH

[32] N. Subrt, L. R. Mesak, J. Davies, *J. Antimicrob. Chemother.* **2011**, *66*, 979–984.
[33] R. E. Furlani, A. A. Yeagley, C. Melander, *Eur. J. Med. Chem.* **2013**, *62*, 59–70.
[34] T. E. Ballard, J. J. Richards, A. Aquino, C. S. Reed, C. Melander, *J. Org. Chem.* **2009**, *74*, 1755–1758.
[35] S. A. Rogers, R. W. Huigens, J. Cavanagh, C. Melander, *Antimicrob. Agents Chemother.* **2010**, *54*, 2112–2118.
[36] M. Tadesse, M. B. Strøm, J. Svenson, M. Jaspars, B. F. Milne, V. Tørfoss, J. H. Andersen, E. Hansen, K. Stensvåg, T. Haug, *Org. Lett.* **2010**, *12*, 4752–4755.
[37] G. A. Edwards, N. V. Shymanska, J. G. Pierce, *Chem. Commun. (Camb.).* **2017**, *53*, 7353–7356.
[38] A. Valliammai, S. Sethupathy, A. Priya, A. Selvaraj, J. P. Bhaskar, V. Krishnan, S. K. Pandian, *Sci. Rep.* **2019**, *9*, 13744.
[39] B. R. Boles, A. R. Horswill, *PLoS Pathog.* **2008**, *4*, e1000052.
[40] P. Balamurugan, V. Praveen Krishna, D. Bharath, R. Lavanya, P. Vairaprakash, S. Adline Princy, *Front. Microbiol.* **2017**, *8*, 1290.
[41] J. McCourt, D. P. O'Halloran, H. McCarthy, J. P. O'Gara, J. A. Geoghegan, *FEMS Microbiol. Lett.* **2014**, *353*, 157–164.
[42] Y. Abouelhassan, A. T. Garrison, G. M. Burch, W. Wong, V. M. Norwood, R. W. Huigens, *Bioorg. Med. Chem. Lett.* **2014**, *24*, 5076–5080.
[43] H. Mohammad, A. S. Mayhoub, M. Cushman, M. N. Seleem, *J Antib.* **2015**, *68*, 259–266.
[44] Y. M. Ibrahim, A. M. Abouwarda, T. Nasr, F. A. Omar, S. Bondock, *Microb. Pathog.* **2020**, *149*, 104500.
[45] D. Qu, Z. Hou, J. Li, L. Luo, S. Su, Z. Ye, Y. Bai, X. Zhang, G. Chen, Z. Li, Y. Wang, X. Xue, X. Luo, M. Li, *Sci. Adv.* **2020**, *6*, eaay9597.
[46] H.-K. Kang, C. Kim, C. H. Seo, Y. Park, *J. Microbiol.* **2017**, *55*, 1–12.
[47] M. G. Cusimano, A. Spinello, G. Barone, D. Schillaci, S. Cascioferro, A. Magistrato, B. Parrino, V. Arizza, M. Vitale, *Mar. Drugs* **2019**, *17*, 159.
[48] A. T. Garrison, Y. Abouelhassan, V. M. Norwood, D. Kallifidas, F. Bai, M. T. Nguyen, M. Rolfe, G. M. Burch, S. Jin, H. Luesch, R. W. Huigens, *J. Med. Chem.* **2016**, *59*, 3808–3825.
[49] A. T. Garrison, Y. Abouelhassan, D. Kallifidas, F. Bai, M. Ukhanova, V. Mai, S. Jin, H. Luesch, R. W. Huigens, *Angew. Chem. Int. Ed. Engl.* **2015**, *54*, 14819–14823.
[50] A. T. Garrison, F. Bai, Y. Abouelhassan, N. G. Paciaroni, S. Jin, R. W. H. Iii, *RSC Adv.* **2014**, *5*, 1120–1124.
[51] J. J. Harrison, R. J. Turner, D. A. Joo, M. A. Stan, C. S. Chan, N. D. Allan, H. A. Vrionis, M. E. Olson, H. Ceri, *Antimicrob. Agents Chemother.* **2008**, *52*, 2870–2881.
[52] D. Schillaci, A. Spinello, M. G. Cusimano, S. Cascioferro, G. Barone, M. Vitale, V. Arizza, *World J. Microbiol. Biotechnol.* **2016**, *32*, 124.
[53] G. H. De Zoysa, A. J. Cameron, V. V. Hegde, S. Raghothama, V. Sarojini, *J. Med. Chem.* **2015**, *58*, 625–639.
[54] H. Yang, Y. Abouelhassan, G. M. Burch, D. Kallifidas, G. Huang, H. Yousaf, S. Jin, H. Luesch, R. W. Huigens, *Sci. Rep.* **2017**, *7*, 2003.
[55] A. Basak, Y. Abouelhassan, R. W. Huigens, *Org. Biomol. Chem.* **2015**, *13*, 10290–10294.
[56] Y. Abouelhassan, A. T. Garrison, F. Bai, V. M. Norwood, M. T. Nguyen, S. Jin, R. W. Huigens, *ChemMedChem.* **2015**, *10*, 1157–1162.
[57] N. El-Najjar, H. Gali-Muhtasib, R. A. Ketola, P. Vuorela, A. Urtti, H. Vuorela, *Phytochem. Rev.* **2011**, *10*, 353.
[58] S.-C. Yang, F.-L. Yen, P.-W. Wang, I. A. Aljuffali, Y.-H. Weng, C.-H. Tseng, J.-Y. Fang, *Future Microbiol.* **2017**, *12*, 1059–1073.
[59] S.-C. Yang, K.-W. Tang, C.-H. Lin, A. Alalaiwe, C.-H. Tseng, J.-Y. Fang, *Front. Microbiol.* **2019**, *10*, 1197.
[60] C. Ghosh, G. B. Manjunath, M. M. Konai, D. S. S. M. Uppu, J. Hoque, K. Paramanandham, B. R. Shome, J. Haldar, *PLoS One* **2015**. *10*, e0144094.
[61] W. E. Rose, P. T. Poppens, *J. Antimicrob. Chemother.* **2009**, *63*, 485–488.
[62] S. Chopra, K. Harjai, S. Chhibber, *J. Antibiot.* **2015**, 68, 15–22.
[63] S. E. Cramton, C. Gerke, N. F. Schnell, W. W. Nichols, F. Götz, *Infect. Immun.* **1999**, *67*, 5427–5433.
[64] Z. Qin, Y. Ou, L. Yang, Y. Zhu, T. Tolker-Nielsen, S. Molin, D. Qu, *Microbiol.* **2007**, *153*, 2083–2092.
[65] J. Shi, N.-F. Mao, L. Wang, H.-B. Zhang, Q. Chen, H. Liu, X. Tang, T. Jin, C.-T. Zhu, F.-B. Li, L.-H. Sun, X.-M. Xu, Y.-Q. Xu, *PLoS One* **2014**, *9*, e113133.
[66] M. E. Pachón-Ibáñez, S. Ribes, M. A. Domínguez, R. Fernández, F. Tubau, J. Ariza, F. Gudiol, C. Cabellos, *Eur. J. Clin. Microbiol. Infect. Dis.* **2011**, *30*, 89–95.
[67] H.-J. Tang, C.-C. Chen, W.-C. Ko, W.-L. Yu, S.-R. Chiang, Y.-C. Chuang, *Int. J. Antimicrob. Agents.* **2011**, *38*, 46–51.
[68] J. Perlroth, M. Kuo, J. Tan, A. S. Bayer, L. G. Miller, *Arch. Intern. Med.* **2008**, *168*, 805–819.
[69] D. Knafl, S. Tobudic, S. C. Cheng, D. R. Bellamy, F. Thalhammer, *Eur. J. Clin. Microbiol. Infect. Dis.* **2017**, *36*, 677–680.
[70] I. Raad, R. Darouiche, J. Vazquez, A. Lentnek, R. Hachem, H. Hanna, B. Goldstein, T. Henkel, E. Seltzer, *Clin. Infect. Dis.* **2005**, *40*, 374–380.
[71] N. Nosengo, *Nature News.* **2016**, *534*, 314.
[72] H.-C. Chang, Y.-T. Huang, C.-S. Chen, Y.-W. Chen, Y.-T. Huang, J.-C. Su, L.-J. Teng, C.-W. Shiau, H.-C. Chiu, *J. Antimicrob. Chemother.* **2016**, *71*, 449–459.
[73] P. Le, E. Kunold, R. Macsics, K. Rox, M. C. Jennings, I. Ugur, M. Reinecke, D. Chaves-Moreno, M. W. Hackl, C. Fetzer, F. A. M. Mandl, J. Lehmann, V. S. Korotkov, S. M. Hacker, B. Kuster, I. Antes, D. H. Pieper, M. Rohde, W. M. Wuest, E. Medina, S. A. Sieber, *Nat. Chem.* **2020**, *12*, 145–158.
[74] E. M. Hetrick, M. H. Schoenfisch, *Chem. Soc. Rev.* **2006**, *35*, 780–789.

Manuscript received: August 30, 2020
Revised manuscript received: October 5, 2020
Accepted manuscript online: October 14, 2020
Version of record online: November 6, 2020

© 2020 Wiley-VCH GmbH

Chapter 11

Thiazole analogues of the marine alkaloid nortopsentin as inhibitors of bacterial biofilm formation.

Carbone, A.; Cascioferro, S.; Parrino, B.; Carbone, D.; **Pecoraro, C.**; Schillaci, D.; Cusimano, M. G.; Cirrincione, G.; Diana, P.

Molecules (2021), 26(1), 81.

molecules

Article

Thiazole Analogues of the Marine Alkaloid Nortopsentin as Inhibitors of Bacterial Biofilm Formation

Anna Carbone †,‡, Stella Cascioferro †, Barbara Parrino, Daniela Carbone, Camilla Pecoraro, Domenico Schillaci, Maria Grazia Cusimano, Girolamo Cirrincione and Patrizia Diana *

Dipartimento di Scienze e Tecnologie Biologiche Chimiche e Farmaceutiche (STEBICEF), Università degli Studi di Palermo, Via Archirafi 32, 90123 Palermo, Italy; anna.carbone@unipa.it (A.C.); stellamaria.cascioferro@unipa.it (S.C.); barbara.parrino@unipa.it (B.P.); daniela.carbone@unipa.it (D.C.); camilla.pecoraro@unipa.it (C.P.); domenico.schillaci@unipa.it (D.S.); mariagrazia.cusimano@unipa.it (M.G.C.); girolamo.cirrincione@unipa.it (G.C.)

* Correspondence: patrizia.diana@unipa.it

† Present address: Dipartimento di Farmacia, Università degli Studi di Genova, Viale Benedetto XV 3, 16132 Genova, Italy.

‡ These authors contributed equally to this work.

Abstract: Anti-virulence strategy is currently considered a promising approach to overcome the global threat of the antibiotic resistance. Among different bacterial virulence factors, the biofilm formation is recognized as one of the most relevant. Considering the high and growing percentage of multi-drug resistant infections that are biofilm-mediated, new therapeutic agents capable of counteracting the formation of biofilms are urgently required. In this scenario, a new series of 18 thiazole derivatives was efficiently synthesized and evaluated for its ability to inhibit biofilm formation against the Gram-positive bacterial reference strains *Staphylococcus aureus* ATCC 25923 and *S. aureus* ATCC 6538 and the Gram-negative strain *Pseudomonas aeruginosa* ATCC 15442. Most of the new compounds showed a marked selectivity against the Gram-positive strains. Remarkably, five compounds exhibited BIC_{50} values against *S. aureus* ATCC 25923 ranging from 1.0 to 9.1 µM. The new compounds, affecting the biofilm formation without any interference on microbial growth, can be considered promising lead compounds for the development of a new class of anti-virulence agents.

Keywords: antibiofilm agents; antibiotic resistance; thiazole derivatives; marine alkaloids analogues; nortopsentin

Citation: Carbone, A.; Cascioferro, S.; Parrino, B.; Carbone, D.; Pecoraro, C.; Schillaci, D.; Cusimano, M.G.; Cirrincione, G.; Diana, P. Thiazole Analogues of the Marine Alkaloid Nortopsentin as Inhibitors of Bacterial Biofilm Formation. *Molecules* **2021**, *26*, 81. https://dx.doi.org/10.3390/molecules26010081

Academic Editor: Manuel Simões
Received: 30 October 2020
Accepted: 23 December 2020
Published: 27 December 2020

Publisher's Note: MDPI stays neutral with regard to jurisdictional claims in published maps and institutional affiliations.

Copyright: © 2020 by the authors. Licensee MDPI, Basel, Switzerland. This article is an open access article distributed under the terms and conditions of the Creative Commons Attribution (CC BY) license (https://creativecommons.org/licenses/by/4.0/).

1. Introduction

The development of synthetic small molecules able to counteract antibiotic resistance (AMR) mechanisms is urgently needed [1]. In fact, most antibiotics used to date to treat the most common infections are becoming ineffective. Many bacteria, including the well-known ESKAPE pathogens (*Enterococcus faecium*, *Staphylococcus aureus*, *Klebsiella pneumoniae*, *Acinetobacter baumannii*, *Pseudomonas aeruginosa*, and *Enterobacter* species) evolved in highly resistant forms through different mechanisms that include the inactivation of the antibiotic, chemical modification of the antibiotic target, alteration of cell permeability, and biofilm formation [2]. In particular, bacterial biofilm is currently considered one of the most relevant virulence factors, which is capable of making pathogens up to 1000 times more resistant than their planktonic form [3]. It was estimated that more than 80% of chronic infections are caused by biofilm formation on indwelling medical devices or host tissues [4].

Biofilm is a complex multicellular structure in which bacterial cells are embedded in a matrix constituted of extracellular polymeric substance (EPS), which is mainly formed by polysaccharides, proteins, lipids, extracellular DNA (e-DNA), and molecules originating from the host including mucus and DNA [5]. In the past decade, many efforts have been made for identifying new therapeutic strategy able to eradicate biofilm-associated infections, [6] and, despite numerous compounds being described as potent anti-biofilm agents, no new derivative has reached the clinic. The lack of approved anti-biofilm drugs together with the increase in the spread of chronic biofilm-related nosocomial infections make the research in this field particularly relevant.

Among the bioactive scaffolds recently described for their interesting anti-biofilm properties, thiazole derivatives are considered among the most promising compounds [7].

Sulfur-containing heterocycles are often involved in attractive nonbonding interactions that play an important role in the control of molecular conformation. In comparison with other five-membered heterocycles, the thiazole nucleus has unique features due to the presence of the low-lying C –S σ* orbitals. The small regions of low electron density present on the sulfur atom, known as σ-holes, are often involved in drug–target interactions, thus improving the affinity toward the biological receptor [8].

Many thiazole compounds were reported in the last decade as potent anti-biofilm agents. The 4-(*o*-methoxyphenyl)-2-aminothiazoles **1a,b** (Figure 1) were found to be able to significantly inhibit *P. aeruginosa* biofilm formation at concentrations in the low micromolar range, interfering with the quorum sensing (QS) system [9]. The thiazole derivatives **2a,b** (Figure 1) showed potent anti-biofilm activity against eight methicillin-resistant (MRSE) and two reference (ATCC 12228, ATCC 35984) strains of *Staphylococcus epidermidis* eliciting BIC_{50} values ranging from 0.35 to 7.32 μg/mL [10].

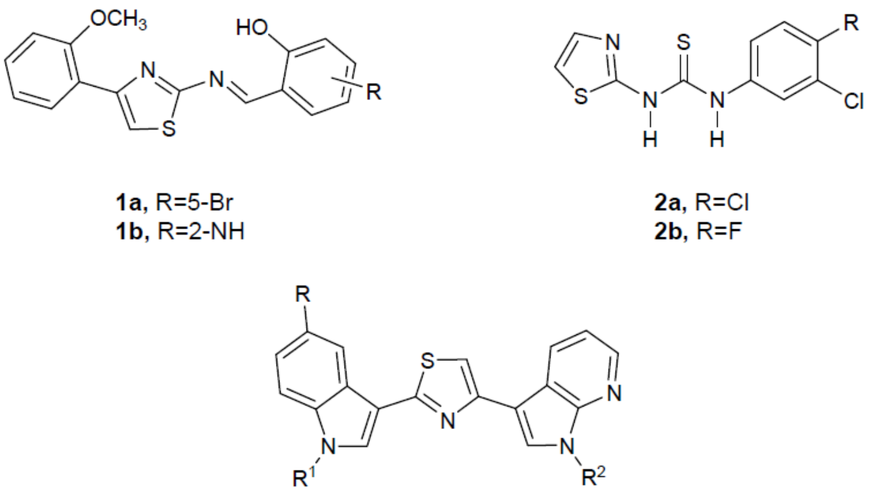

1a, R=5-Br
1b, R=2-NH

2a, R=Cl
2b, R=F

3

Figure 1. Chemical structures of the thiazole compounds **1a,b**; **2a,b**; and **3**.

On the basis of the interesting anti-biofilm properties described for the thiazole scaffold and continuing our search for new nortopsentin alkaloid analogues with promising biological activity [11–13], we recently reported the synthesis and the anti-biofilm activity of the new nortopsentin analogues of type **3**, in which the imidazole nucleus of the natural compound was replaced by the thiazole ring, and the indole moiety in position 4 was replaced by 7-azaindole (Figure 1) [14]. The thiazole derivatives **3** were tested against *S. aureus* ATCC 25923, *S. aureus* ATCC 6538, and *P. aeuruginosa* ATCC 15442 in order to evaluate their ability to inhibit biofilm formation and microbial growth. Most of the new thiazole nortopsentin analogues proved to be active as inhibitors of biofilm formation exhibiting marked selectivity toward staphylococcal biofilms, showing BIC_{50} values in the low micromolar range. Compounds of type **3** showed a typical anti-virulence profile, fighting bacterial virulence factors, such as biofilm formation, without interfering with the bacterial growth, thus imposing a low selective pressure for the onset of antibiotic resistance mechanisms.

With the aim to obtain more potent anti-biofilm agents that could be effective in the treatment of staphylococcal infections that are biofilm-mediated, herein, we report the synthesis of a new series of thiazole derivatives, structurally related to the nortopsentin analogues **3**, in which the 7-azaindole nucleus in position 4 of the thiazole ring was replaced by a thiophene (**1a–q**) or a pyridine ring (**2a–q**), and the aromatic bicyclic system in position 2 of the thiazole nucleus can be either an indole or a 7-azaindole moiety.

In fact, thiophene and pyridine moieties are recognized as valuable scaffolds in the development of potent anti-biofilm derivatives [15,16]. Additionally, the thiophene ring was recently discovered as a key nucleus in a series of compounds able to potently inhibit the virulence of relevant Gram-negative pathogens interfering with bacterial Disulfide bond enzyme A (DsbA) enzymes, which catalyzes disulfide bond formation in secreted and outer membrane proteins with virulence functions [17]. Therefore, since the so-far synthesized thiazole nortopsentin analogues have shown a strong selectivity toward the Gram-positive pathogens, we investigated whether the introduction of the thiophene ring could improve the anti-biofilm activity against the Gram-negative bacteria.

2. Results and Discussion

2.1. Chemistry

The new substituted thiazoles **1** and **2** (Scheme 1, Tables 1 and 2) were efficiently synthesized by Hantzsch reaction between an appropriate thioamide of type **3–8**, previously obtained [18], and a suitable α-bromoacetyl derivative **11,12**.

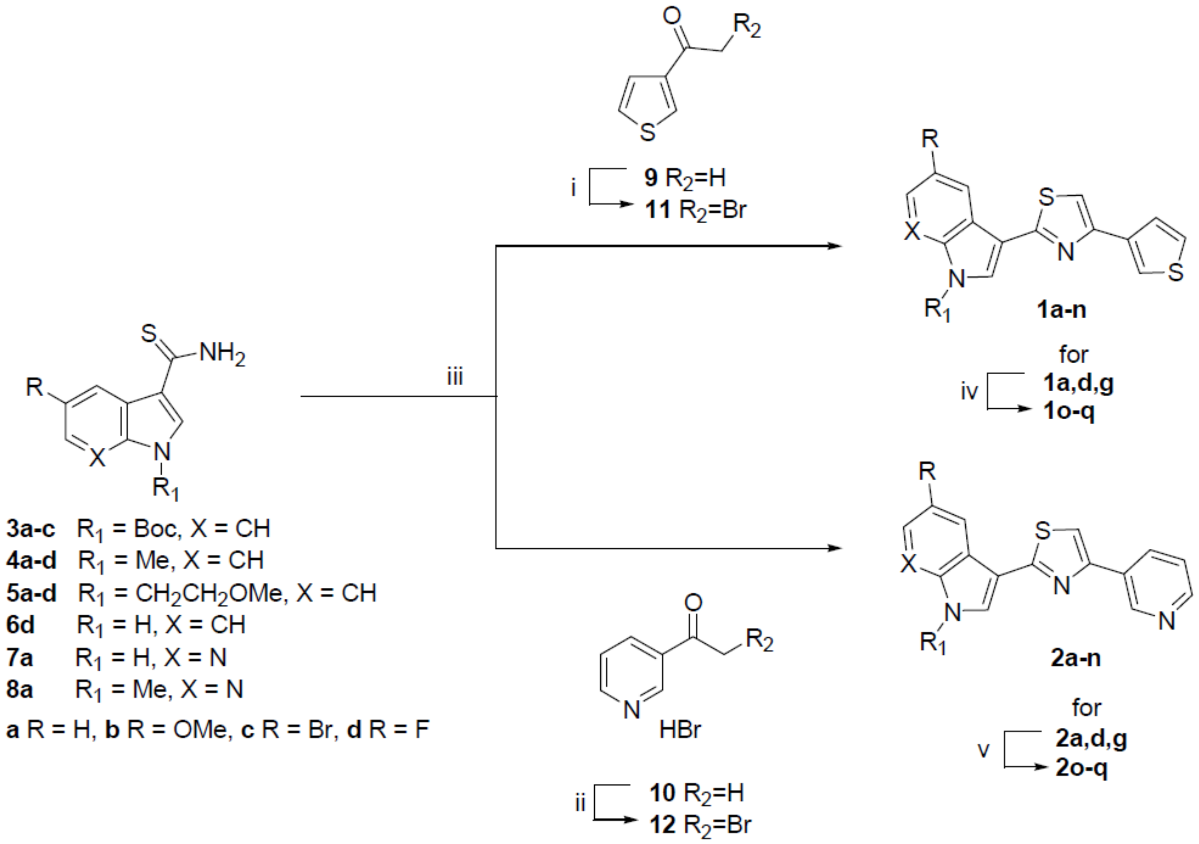

Scheme 1. Synthesis of new thiazole derivatives of type **1a–q** and **2a–q**. Reagents: (i) (a) Br_2, DCM, r.t., 1 h; (b) aq. $NaHCO_3$, 80%; (ii) (a) 48% HBr, r.t. then 80 ˚C, Br_2, 2 h; (b) acetone, 0 ˚C, 90%; (iii) EtOH, reflux, 30 min, 74–98% for **1a–n** and 73–99% for **2a–n**; (iv) (a) TFA, DCM, reflux, 24 h; (b) aq $NaHCO_3$, 72–98%; (v) TFA, DCM, reflux, 24 h, 77–95%.

The key intermediates **11,12** were prepared from the corresponding ethanones **9,10**. In particular, 1-thiophene-3-yl-ethanone **9** was converted into 2-bromo-1-thiophen-3-yl-ethanone **11** (80%), using bromine in dichloromethane [19]; while 1-pyridin-3-yl-ethanone **10** was turned into 2-bromo-1-pyridin-3-yl-ethanone hydrobromide **12** (90%) by reaction with 48% hydrobromic acid and bromine [20].

The reaction of thioamides **3a–c**, **4a–d**, **5a–d**, **6d**, **7a**, and **8a** with 2-bromo-1-heteroaryl-3-yl-ethanones **11** and **12** provided the desired 3-[4-(thiophen-3-yl)-1,3-thiazol-2-yl]-1*H*-indoles **1a–n** and 3-[4-(pyridin-3-yl)-1,3-thiazol-2-yl]-1*H*-indole hydrobromides **2a–n** in good to excellent yields (74–98% and 73–99%, respectively). The subsequent deprotection of *N*-tert-butylcarboxylate derivatives **1a**,**d**,**g** and **2a**,**d**,**g** using trifluoroacetic acid in dichloromethane under reflux, after neutralization with aqueous hydrogen carbonate solution, gave the thiazoles **1o–q** (72–98%), whereas thiazoles **2o–q** were directly isolated without neutralization (72–95%).

Table 1. Substituted 3-[4-(thiophen-3-yl)-1,3-thiazol-2-yl]-1*H*-indoles **1a–q**.

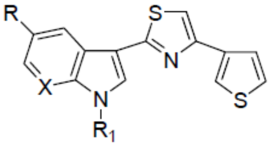

Compd	R	R1	X	Compd	R	R1	X
1a	H	Boc	CH	1j	F	H	CH
1b	H	Me	CH	1k	F	Me	CH
1c	H	CH_2CH_2OMe	CH	1l	F	CH_2CH_2OMe	CH
1d	OMe	Boc	CH	1m	H	H	N
1e	OMe	Me	CH	1n	H	Me	N
1f	OMe	CH_2CH_2OMe	CH	1o	H	H	CH
1g	Br	Boc	CH	1p	OMe	H	CH
1h	Br	Me	CH	1q	Br	H	CH
1i	Br	CH_2CH_2OMe	CH				

Table 2. Substituted 3-[4-(pyridin-3-yl)-1,3-thiazol-2-yl]-1*H*-indole hydrobromides **2a–q**.

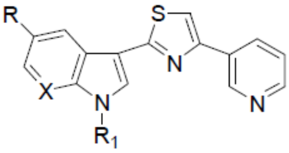

Compd	R	R1	X	Compd	R	R1	X
2a	H	Boc	CH	2j	F	H	CH
2b	H	Me	CH	2k	F	Me	CH
2c	H	CH_2CH_2OMe	CH	2l	F	CH_2CH_2OMe	CH
2d	OMe	Boc	CH	2m	H	H	N
2e	OMe	Me	CH	2n	H	Me	N
2f	OMe	CH_2CH_2OMe	CH	2o	H	H	CH
2g	Br	Boc	CH	2p	OMe	H	CH
2h	Br	Me	CH	2q	Br	H	CH
2i	Br	CH_2CH_2OMe	CH				

2.2. Biological Studies

All the new compounds were first tested for evaluating the antibacterial activity against the planktonic form of the Gram-positive *S. aureus* ATCC 25923, *S. aureus* ATCC 6538, and of the Gram-negative pathogen *P. aeruginosa* ATCC 15442. All the new thiazole derivatives, analogously to the precursors **3**, did not affect the microbial growth, showing Minimum Inhibitory Concentration (MIC) values greater than 100 μg/mL. This result is in agreement with the desired anti-virulence profile.

Inhibition of biofilm formation of the same bacterial strains was evaluated for all the new derivatives **1a–q** and **2a–q** at sub-MIC concentrations, and BIC_{50} values (the concentration of compound needed to inhibit biofilm formation by 50%) were determined for the compounds that showed a percentage of biofilm inhibition greater than 20% at the screening concentration of 10 μg/mL at least against one bacterial strain (Table 3).

Table 3. Inhibition of biofilm formation, BIC_{50}, µg/mL and µM.

Comp	*S.aureus* **ATCC 25923**		*S. aureus* **ATCC 6538**		*P. aeruginosa* **ATCC 15442**	
	µg/mL	**µM**	**µg/mL**	**µM**	**µg/mL**	**µM**
1a	n.s.	n.s.	14.5 ± 0.9	37.9	5.7 ± 0.5	14.9
1b	n.s.	n.s.	n.s.	n.s.	14.7 ± 1.2	49.5
1c	5.7 ± 0.7	16.7	6.6 ± 0.5	19.3	n.s.	n.s.
1d	n.s.	n.s.	5.7 ± 0.3	13.8	25.7 ± 1.7	62.2
1e	n.s.	n.s.	38.1 ± 1.8	116.7	11.2 ± 0.8	34.3
1f	18.5 ± 0.9	49.9	n.s.	n.s.	n.s.	n.s.
1g	8.1 ± 0.4	17.5	12.7 ± 0.9	27.5	10.6 ± 0.9	22.9
1h	10.1 ± 0.1	26.9	n.s.	n.s.	n.s.	n.s.
1i	11.2 ± 0.8	26.7	2.04 ± 0.07	4.8	n.s.	n.s.
1j	n.s.	n.s.	19.1 ± 0.9	63.5	35.6 ± 1.3	118.5
1k	n.s.	n.s.	3.9 ± 0.1	12.4	n.s.	n.s.
1l	1.4 ± 0.09	3.9	4.6 ± 0.2	12.8	n.s.	n.s.
1m	n.s.	n.s.	3.7 ± 0.08	13.0	n.s.	n.s.
1o	n.s.	n.s.	21.8 ± 1.3	77.1	12.6 ± 0.7	44.6
1p	n.s.	n.s.	n.s.	n.s.	13.6 ± 1.1	43.5
1q	n.s.	n.s.	16.4 ± 1.2	45.4	8.1 ± 0.6	22.4
2b	2.6 ± 0.1	6.9	12.9 ± 0.9	34.6	n.s.	n.s.
2c	3.8 ± 0.2	9.1	14.4 ± 1.1	34.5	13.3 ± 0.5	31.9
2e	n.s.	n.s.	4.8 ± 0.2	11.9	n.s.	n.s.
2h	n.s.	n.s.	17.1 ± 0.9	37.9	n.s.	n.s.
2i	0.5 ± 0.008	1.0	10.4 ± 0.8	20.1	n.s.	n.s.
2j	5.6 ± 0.4	14.8	9.2 ± 0.7	24.4	n.s.	n.s.
2k	3.2 ± 0.2	8.1	3.0 ± 0.01	7.6	n.s.	n.s.
2l	6.9 ± 0.4	15.8	n.s.	n.s.	12.5 ± 1.5	28.7
2m	n.s.	n.s.	n.s.	n.s.	0.2 ± 0.007	5.5
2o	15.2 ± 1.2	42.4	6.9 ± 0.5	19.2	n.s.	n.s.
2p	n.s.	n.s.	9.8 ± 0.3	25.2	n.s.	n.s.

n.s.: not significant because lower than 20% of inhibition percentage at the screening concentration of 100 µg/mL. The averages from at least three independent experiments are reported with standard deviation (SD).

All derivatives **1** and most of the compounds **2** showed antibiofilm activity, eliciting, as previously observed for the nortopsentin analogues of type **3**, a marked selectivity against the Gram-positive pathogens, in particular toward *S. aureus* ATCC 25923. Compounds **1l**, **2b**, **2c**, **2i**, and **2k** exhibited the highest potency with BIC_{50} values ranging from 1.0 to 9.1 µM. The replacement of the indole ring with the 7-azaindole moiety, as well as its substitution at position 5 with a halogen atom or a methoxy group, does not entail advantages in terms of the biofilm inhibition. Instead, the presence of a methoxyethyl group on the indole nitrogen generally led to an improvement of the antibiofilm activity against the staphylococcal strains. Compounds **1l**, **2b**, **2c**, **2i**, and **2k** were also tested by using viable plate count, and the activity of inhibition of staphylococcal biofilm formation was reported in terms of log reduction. By using such a method, compound **2i** was the most effective compound in interfering with biofilm formation, since it causes the greatest log reduction ranging from 2.62 to 1.73 at concentrations between 10 and 0.1 µg/mL (see Figure 2).

Most of the new thiazole derivatives **1** and **2** were inactive or weakly active against the Gram-negative strain. Only compounds **1a** and **2m** showed a significant inhibition of *P. aeruginosa* biofilm formation, eliciting BIC_{50} values of 14.9 and 5.5 µM, respectively.

Additionally, the most active compounds, for every bacterial strain, were selected and tested at the screening concentration of 100 µg/mL, for evaluating their dispersal activity against the 24 h preformed biofilm. No derivatives was able to interfere with the biofilm architecture; only compound **2m** showed weak dispersal activity eliciting a percentage of inhibition of 36% against *P. aeruginosa* at the screening concentration. Biological results highlighted the ability of the new compounds to interfere with the first stage of the biofilm life cycle, which consists in the bacterial adhesion to surfaces [21]. Anti-adhesion agents represent a valuable alternative to antibiotics, since they deprive the bacterium of its pathogenicity by preventing its adhesion to the host cells.

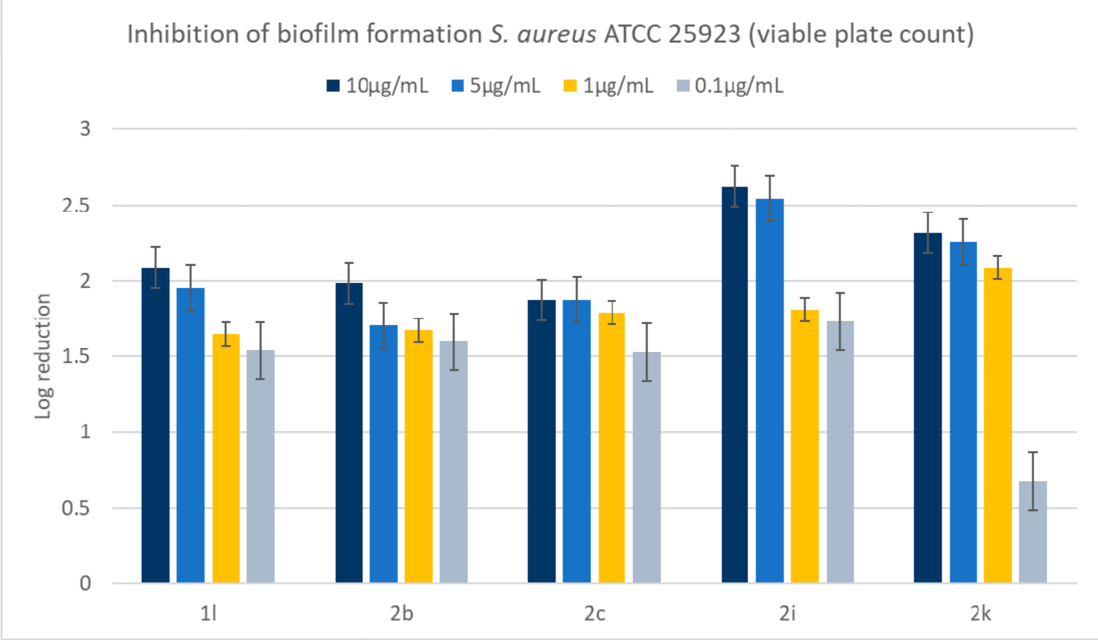

Figure 2. Inhibition of staphylococcal biofilm formation (viable plate count). Activity expressed in terms of log reduction. Each value is the average (reported with the SD values and error bars) from at least two independent experiments, $p < 0.05$.

3. Materials and Methods

3.1. Chemistry

3.1.1.General

All melting points were taken on a Büchi-Tottoly capillary apparatus (Büchi, Cornaredo, Italy) and are uncorrected. IR spectra were determined in bromoform with a Shimadzu FT/IR 8400S spectrophotometer (Shimadzu Corporation, Milan, Italy). ^{1}H and ^{13}C NMR spectra were measured at 200 and 50.0 MHz, respectively, in DMSO-d_6 solution, using a Bruker Avance II series 200 MHz spectrometer (Bruker, Milan, Italy). Column chromatography was performed with Merk silica gel 230–400 mesh ASTM or with Büchi Sepacor chromatography module (prepacked cartridge system). Elemental analyses (C, H, and N) were within ± 0.4% of theoretical values. The purity of all the tested compounds was greater than 95%, as determined by HPLC (Agilent 1100 Series).

3.1.2. General Procedures for the Synthesis of Thioamides **3a–c**, **4a–d**, **5a–d**, **6d**, **7a**, and **8a**

These compounds were prepared using procedures previously reported [17,18]. Analytical and spectroscopic data are in agreement with those previously reported.

3.1.3. General Procedures for the Synthesis of 3-bromoacetyl compounds **11** and **12**

These compounds were prepared using known procedures (80–90%). Analytical and spectroscopic data are compatible with those previously reported [19,20].

3.1.4. General Procedure for the Synthesis of Thiazole Derivatives (**1a–n**) and (**2a–n**)

A suspension of the proper thioamides **3a–c**, **4a–d**, **5a–d**, **6d**, **7a**, **8a** (2 mmol) and bromoacetyl derivatives **11, 12** (2 mmol) in anhydrous ethanol (8 mL) was refluxed for 30 min. After cooling, the obtained precipitate was filtered off, dried, and recrystallized from ethanol to give the desired thiazoles **1a–n** and **2a–n**.

Tert-Butyl-3-[4-(Thiophen-3-yl)-1,3-Thiazol-2-yl]-1H-Indole-1-Carboxylate (**1a**)

Yellow solid; yield: 79%; mp: 219–220 °C; IR cm^{-1}: 1750 (CO); ^{1}H NMR (200 MHz, DMSO-d_6) δ: 1.68 (s, 9H, 3 x CH$_3$), 7.40–7.53 (m, 2H, H-5′ and H-6′), 7.66–7.74 (m, 2H, H-4′′ and H-5′′), 8.00 (s, 1H, H-5), 8.10 (dd, 1H, *J* = 2.8, 1.3 Hz, H-2′′), 8.16–8.20 (m, 1H, H-7′), 8.33 (s, 1H, H-2′), 8.47–8.52 (m, 1H, H-4′); ^{13}C (50 MHz, DMSO-d_6) δ: 27.6 (3 x q), 84.8 (s), 112.2 (d), 114.9 (d), 121.5 (d), 122.5 (d), 123.8 (d), 125.5 (d), 125.6 (d), 126.3 (d), 126.6 (s), 126.8 (s), 127.1 (d), 135.0 (s), 136.2 (s), 148.6 (s), 150.9 (s), 160.2 (s). Anal. Calcd for $C_{20}H_{18}N_2O_2S_2$: C, 62.80; H, 4.74; N, 7.32%. Found: C, 62.59; H, 4.56; N, 7.21%.

1-Methyl-3-[4-(Thiophen-3-yl)-1,3-Thiazol-2-yl]-1H-Indole (**1b**)

Yellow solid; yield: 98%; mp: 248–249 °C; ^{1}H NMR (200 MHz, DMSO-d_6) δ: 3.89 (s, 3H, CH$_3$), 7.23–7.36 (m, 2H, H-5′ and H-6′), 7.55–7.72 (m, 3H, H-4′′, H-5′′ and H-7′), 7.79 (s, 1H, H-5), 8.03 (dd, 1H, *J* = 2.8, 1.3 Hz, H-2′′), 8.19 (s, 1H, H-2′), 8.31–8.35 (m, 1H, H-4′); ^{13}C (50 MHz, DMSO-d_6) δ: 32.9 (q), 109.1 (s), 110.0 (d), 110.6 (d), 120.6 (d), 121.1 (d), 122.2 (d), 122.5 (d), 124.5 (s), 126.3 (d), 127.0 (d), 130.8 (d), 136.2 (s), 137.0 (s), 149.8 (s), 162.5 (s). Anal. Calcd for $C_{16}H_{12}N_2S_2$: C, 64.83; H, 4.08; N, 9.45%. Found: C, 65.11; H, 3.91; N, 9.59%.

1-(2-Methoxyethyl)-3-[4-(Thiophen-3-yl)-1,3-Thiazol-2-yl]-1H-Indole (**1c**)

Orange solid; yield: 80%; mp: 169–170 °C; ^{1}H NMR (200 MHz, DMSO-d_6) δ: 3.24 (s, 3H, CH$_3$), 3.72 (t, 2H, *J* = 5.1 Hz, CH$_2$), 4.46 (t, 2H, *J* = 5.1 Hz, CH$_2$), 7.23–7.33 (m, 2H, H-5′ and H-6′), 7.62–7.81 (m, 3H, H-4′′, H-5′′ and H-7′), 7.81 (s, 1H, H-5), 8.04 (dd, 1H, *J* = 2.8, 1.4 Hz, H-2′′), 8.17 (s, 1H, H-2′), 8.30–8.34 (m, 1H, H-4′); ^{13}C (50 MHz, DMSO-d_6) δ: 45.7 (t), 58.1 (q), 70.6 (t), 109.3 (s), 110.1 (d), 110.9 (d), 120.5 (d), 121.1 (d), 122.3 (d), 122.5 (d), 124.6 (s), 126.3 (d), 127.0 (d), 130.3 (d), 136.1 (s), 136.5 (s), 149.7 (s), 162.4 (s). Anal. Calcd for $C_{18}H_{16}N_2OS_2$: C, 63.50; H, 4.74; N, 8.23%. Found: C, 63.26; H, 4.90; N, 8.02%.

Tert-Butyl 5-Methoxy-3-[4-(Thiophen-3-yl)-1,3-Thiazol-2-yl]-1H-Indole-1-Carboxylate (**1d**)

Pink solid; yield: 89%; mp: 185–186 °C; IR cm^{-1}: 1733 (CO); ^{1}H NMR (200 MHz, DMSO-d_6) δ: 1.67 (s, 9H, 3 x CH$_3$), 3.90 (s, 3H, CH$_3$), 7.09 (dd, 1H, *J* = 9.0, 2.6 Hz, H-6′), 7.66–7.73 (m, 2H, H-4′′ and H-7′), 7.98 (s, 1H, H-5), 8.04–8.07 (m, 3H, H-2′′, H-4′ and H-5′′), 8.29 (s, 1H, H-2′); ^{13}C (50 MHz, DMSO-d_6) δ: 27.6 (3 x q), 55.3 (q), 84.7 (s), 103.8 (d), 112.2 (d), 114.2 (d), 114.7 (s), 115.8 (d), 122.4 (d), 126.1 (d), 126.2 (d), 127.2 (d), 127.6 (s), 129.6 (s), 136.2 (s), 148.6 (s), 150.8 (s), 156.2 (s), 160.4 (s). Anal. Calcd for $C_{21}H_{20}N_2O_3S_2$: C, 61.14; H, 4.89; N, 6.79%. Found: C, 60.89; H, 5.03; N, 6.56%.

5-Methoxy-1-Methyl-3-[4-(Thiophen-3-yl)-1,3-Thiazol-2-yl]-1H-Indole (**1e**)

Orange solid; yield: 98%; mp: 232–233 °C; ^{1}H NMR (200 MHz, DMSO-d_6) δ: 3.86 (s, 3H, CH$_3$), 3.87 (s, 3H, CH$_3$), 6.95 (dd, 1H, *J* = 8.9, 2.5 Hz, H-6′), 7.48 (d, 1H, *J* = 8.9 Hz, H-7′), 7.66–7.69 (m, 2H, H-4′′ and H-5′′), 7.77 (s, 1H, H-5), 7.83 (d, 1H, *J* = 2.5 Hz, H-4′), 8.00 (dd, 1H, *J* = 2.7, 1.5 Hz, H-2′′), 8.13 (s, 1H, H-2′); ^{13}C (50 MHz, DMSO-d_6) δ: 33.1 (q), 55.3 (q), 102.3 (d), 108.5 (s), 109.8 (d), 111.5 (d), 112.4 (d), 122.2 (d), 125.1 (s), 126.2 (d), 127.1 (d), 131.2 (d), 132.2 (s), 136.0 (s), 149.5 (s), 155.0 (s), 162.7 (s). Anal. Calcd for $C_{17}H_{14}N_2OS_2$: C, 62.55; H, 4.32; N, 8.58%. Found: C, 62.31; H, 4.15; N, 8.32%.

5-Methoxy-1-(2-Methoxyethyl)-3-[4-(Thiophen-3-yl)-1,3-Thiazol-2-yl]-1H-Indole (**1f**)

Yellow solid; yield: 91%; mp: 213–214 °C; ^{1}H NMR (200 MHz, DMSO-d_6) δ: 3.24 (s, 3H, CH$_3$), 3.69 (t, 2H, *J* = 5.1 Hz, CH$_2$), 3.87 (s, 3H, CH$_3$), 4.41 (t, 2H, *J* = 5.1 Hz, CH$_2$), 6.93 (dd, 1H, *J* = 8.9, 2.5 Hz, H-6′), 7.55 (d, 1H, *J* = 8.9 Hz, H-7′), 7.64–7.71 (m, 2H, H-4′′ and H-5′′), 7.78 (s, 1H, H-5), 7.83 (d, 1H, *J* = 2.5 Hz, H-4′), 8.00 (dd, 1H, *J* = 2.7, 1.5 Hz, H-2′′), 8.10 (s, 1H, H-2′); ^{13}C (50 MHz, DMSO-d_6) δ: 45.9 (t), 55.3 (q), 58.1 (q), 70.7 (t), 102.3 (d), 108.8 (s), 109.8 (d), 111.8 (d), 112.3 (d), 121.2 (d), 125.1 (s), 126.2 (d), 127.1 (d), 130.6 (d), 131.6 (s), 136.1 (s), 149.5 (s), 154.9 (s), 162.6 (s). Anal. Calcd for $C_{19}H_{18}N_2O_2S_2$: C, 61.60; H, 4.90; N, 7.56%. Found: C, 61.45; H, 4.79; N, 7.39%.

Tert-Butyl 5-Bromo-3-[4-(Thiophen-3-yl)-1,3-Thiazol-2-yl]-1H-Indole-1-Carboxylate (**1g**)

Pink solid; yield: 85%; mp: 174–175 °C; IR cm$-^1$: 1739 (CO); ^{1}H NMR (200 MHz, DMSO-d_6) δ: 1.68 (s, 9H, 3 x CH$_3$), 7.64 (dd, 1H, *J* = 8.9, 2.0 Hz, H-6′), 7.70–7.71 (m, 2H, H-4″ and H-5″), 8.01 (s, 1H, H-5), 8.04 (dd, 1H, J = 2.1, 1.3 Hz, H-2″), 8.11 (d, 1H, J = 8.9 Hz, H-7′), 8.38 (s, 1H, H-2′), 8.61 (d, 1H, J = 2.0 Hz, H-4′); ^{13}C (50 MHz, DMSO-d_6) δ: 27.6 (3 x q), 85.4 (s), 112.6 (d), 116.4 (s), 116.9 (d), 119.3 (d), 122.4 (d), 123.8 (d), 126.2 (d), 127.0 (d), 127.3 (s), 128.1 (d), 128.4 (s), 133.9 (s), 136.1 (s), 148.3 (s), 150.9 (s), 159.8 (s). Anal. Calcd for $C_{20}H_{17}BrN_2O_2S_2$: C, 52.06; H, 3.71; N, 6.07%. Found: C, 51.85; H, 3.94; N, 6.22%.

5-Bromo-1-Methyl-3-[4-(Thiophen-3-yl)-1,3-Thiazol-2-yl]-1H-Indole (**1h**)

Orange solid; yield: 90%; mp: 250–251 °C; ^{1}H NMR (200 MHz, DMSO-d_6) δ: 3.89 (s, 3H, CH_3), 7.44 (dd, 1H, J = 8.7, 1.9 Hz, H-6′), 7.58 (d, 1H, J = 8.7 Hz, H-7′), 7.67–7.68 (m, 2H, H-4″ and H-5″), 7.81 (s, 1H, H-5), 7.99 (dd, 1H, J = 2.1, 1.3 Hz, H-2″), 8.24 (s, 1H, H-2′), 8.47 (d, 1H, J = 1.9 Hz, H-4′); ^{13}C (50 MHz, DMSO-d_6) δ: 33.1 (q), 108.8 (s), 110.3 (d), 112.8 (d), 113.8 (s), 122.1 (d), 122.8 (d), 125.0 (d), 126.1 (s), 126.2 (d), 127.1 (d), 132.0 (d), 135.8 (s), 136.4 (s), 150.3 (s), 161.8 (s). Anal. Calcd for $C_{16}H_{11}BrN_2S_2$: C, 51.20; H, 2.95; N, 7.46%. Found: C, 50.93; H, 2.90; N, 7.18%.

5-Bromo-1-(2-Methoxyethyl)-3-[4-(Thiophen-3-yl)-1,3-Thiazol-2-yl]-1H-Indole (**1i**)

Yellow solid; yield: 92%; mp: 226–227 °C; ^{1}H NMR (200 MHz, DMSO-d_6) δ: 3.24 (s, 3H, CH_3), 3.72 (t, 2H, J = 5.0 Hz, CH_2), 4.46 (t, 2H, J = 5.0 Hz, CH_2), 7.42 (dd, 1H, J = 8.8, 2.0 Hz, H-6′), 7.65 (d, 1H, J = 8.8 Hz, H-7′), 7.63–7.68 (m, 2H, H-4″ and H-5″), 7.81 (s, 1H, H-5), 7.99 (dd, 1H, J = 2.1, 1.3 Hz, H-2″), 8.22 (s, 1H, H-2′), 8.46 (d, 1H, J = 2.0 Hz, H-4′); ^{13}C (50 MHz, DMSO-d_6) δ: 46.0 (t), 58.1 (q), 70.6 (t), 109.0 (s), 110.4 (d), 113.1 (d), 113.8 (s), 122.1 (d), 122.7 (d), 125.0 (d), 126.1 (s), 126.2 (d), 127.1 (d), 131.5 (d), 135.4 (s), 136.3 (s), 150.2 (s), 161.8 (s). Anal. Calcd for $C_{18}H_{15}BrN_2OS_2$: C, 51.55; H, 3.61; N, 6.68%. Found: C, 51.27; H, 3.77; N, 6.81%.

5-Fluoro-3-[4-(Thiophen-3-yl)-1,3-Thiazol-2-yl]-1H-Indole (**1j**)

Yellow solid; yield: 74%; mp: 209–210 °C; IR cm^{-1}: 3270 (NH); ^{1}H NMR (200 MHz, DMSO-d_6) δ: 7.10 (td, 1H, J = 11.6, 9.2, 2.6 Hz, H-6′), 7.51 (dd, 1H, J = 11.6, 4.6 Hz, H-7′), 7.64–7.71 (m, 2H, H-4″ and H-5″), 7.79 (s, 1H, H-5), 8.01–8.08 (m, 2H, H-2″ and H-4′), 8.23 (d, 1H, J = 2.9 Hz, H-2′); 11.90 (bs, 1H, NH); ^{13}C (50 MHz, DMSO-d_6) δ: 105.3 (d, $J_{C6'\text{-}F}$ = 24.4 Hz), 110.0 (d), 110.4 (d, $J_{C7'a\text{-}F}$ = 4.6 Hz), 110.2 (d, $J_{C4'F}$ = 26.0 Hz), 113.4 (d, $J_{C7'\text{-}F}$ = 9.6 Hz), 122.2 (d), 124.5 (d, $J_{C3'a\text{-}F}$ = 10.8 Hz), 126.2 (d), 127.0 (d), 128.7 (d), 133.2 (s), 134.3 (s), 136.4 (s), 150.1 (s), 157.9 (d, $J_{C5'\text{-}F}$ = 235 Hz). Anal. Calcd for $C_{15}H_9FN_2S_2$: C, 59.98; H, 3.02; N, 9.33%. Found: C, 59.67; H, 2.93; N, 9.18%.

5-Fluoro-1-Methyl-3-[4-(Thiophen-3-yl)-1,3-Thiazol-2-yl]-1H-Indole (**1k**)

Yellow solid; yield: 95%; mp: 231–232 °C; ^{1}H NMR (200 MHz, DMSO-d_6) δ: 3.90 (s, 3H, CH_3), 7.18 (td, 1H, J = 11.7, 9.2, 2.6 Hz, H-6′), 7.57–7.71 (m, 3H, H-4″, H-5″ and H-7′), 7.78 (s, 1H, H-5), 8.02–8.08 (m, 2H, H-2″ and H-4′), 8.25 (s, 1H, H-2′); ^{13}C (50 MHz, DMSO-d_6) δ: 33.2 (q), 105.5 (d, $J_{C6'\text{-}F}$ = 24.4 Hz), 109.3 (d, $J_{C7'a\text{-}F}$ = 4.6 Hz), 110.0 (d), 110.7 (d, $J_{C4'F}$ = 26.3 Hz), 113.5 (d, $J_{C7'\text{-}F}$ = 9.7 Hz), 122.6 (d), 124.8 (d, $J_{C3'a\text{-}F}$ = 10.8 Hz), 126.2 (d), 127.0 (d), 132.4 (d), 133.8 (s), 136.3 (s), 150.2 (s), 157.2 (d, $J_{C5'\text{-}F}$ = 234 Hz), 162.1 (s). Anal. Calcd for $C_{16}H_{11}FN_2S_2$: C, 61.12; H, 3.53; N, 8.91%. Found: C, 60.88; H, 3.47; N, 8.74%.

5-Fluoro-1-(2-Methoxyethyl)-3-[4-(Thiophen-3-yl)-1,3-Thiazol-2-yl]-1H-Indole (**1l**)

Yellow solid; yield: 88%; mp: 200–201 °C; ^{1}H NMR (200 MHz, DMSO-d_6) δ: 3.25 (s, 3H, CH_3), 3.72 (t, 2H, J = 5.0 Hz, CH_2), 4.46 (t, 2H, J = 5.0 Hz, CH_2), 7.16 (td, 1H, J = 11.8, 9.2, 2.6 Hz, H-6′), 7.64–7.71 (m, 3H, H-4″, H-5″ and H-7′), 7.80 (s, 1H, H-5), 8.01–8.07 (m, 2H, H-2″ and H-4′), 8.23 (s, 1H, H-2′); ^{13}C (50 MHz, DMSO-d_6) δ: 46.0 (t), 58.1 (q), 70.7 (t), 105.5 (d, $J_{C6'\text{-}F}$ = 25.0 Hz), 109.5 (d, $J_{C7'a\text{-}F}$ = 4.6 Hz), 110.1 (d), 110.7 (d, $J_{C4'F}$ = 26.1 Hz), 117.3 (d, $J_{C7'\text{-}F}$ = 9.8 Hz), 122.3 (d), 124.9 (d, $J_{C3'a\text{-}F}$ = 10.7 Hz), 126.2 (d), 127.0 (d), 131.8 (d), 133.3 (s), 136.3 (s), 150.2 (s), 158.1 (d, $J_{C5'\text{-}F}$ = 234 Hz), 162.0 (s). Anal. Calcd for $C_{18}H_{15}FN_2OS_2$: C, 60.31; H, 4.22; N, 7.82%. Found: C, 60.03; H, 4.05; N, 7.64%.

3-[4-(Thiophen-3-yl)-1,3-Thiazol-2-yl]-1H-Pyrrolo[2,3-b]Pyridine (**1m**)

Yellow solid; yield: 93%; mp: 268–269 °C; IR cm^{-1}: 3273 (NH); ^{1}H NMR (200 MHz, DMSO-d_6) δ: 7.37 (dd, 1H, J = 7.9, 4.9 Hz, H-5′), 7.64–7.73 (m, 2H, H-4″ and H-5″), 7.84 (s, 1H, H-5), 8.09 (dd, 1H, J = 2.8, 1.3 Hz, H-2″), 8.34 (d, 1H, J = 2.0 Hz, H-2′), 8.41 (dd, 1H, *J* = 4.9, 1.5 Hz, H-6′), 8.80 (dd, 1H, *J* = 7.9, 1.5 Hz, H-4′), 12.50 (bs, 1H, NH); ^{13}C (50 MHz, DMSO-d_6) δ: 111.0 (s), 112.1 (d), 118.2 (d), 120.2 (s), 123.4 (d), 127.2 (d), 128.0 (d), 129.2 (d), 134.4 (d), 137.2 (s), 141.0 (d), 145.2 (s), 151.4 (s), 162.1 (s). Anal. Calcd for $C_{14}H_9N_3S_2$: C, 59.34; H, 3.20; N, 14.83%. Found: C, 59.03; H, 3.44; N, 15.06%.

1-Methyl-3-[4-(Thiophen-3-yl)-1,3-Thiazol-2-yl]-1H-Pyrrolo[2,3-b]Pyridine (**1n**)

Yellow solid; yield: 96%; mp: 254–255 °C; ^{1}H NMR (200 MHz, DMSO-d_6) δ: 3.92 (s, 3H, CH_3), 7.34 (dd, 1H, *J* = 7.9, 4.7 Hz, H-5′), 7.64–7.73 (m, 2H, H-4″ and H-5″), 7.83 (s, 1H, H-5), 8.07 (dd, 1H, *J* = 2.8, 1.3 Hz, H-2″), 8.38 (s, 1H, H-2′), 8.42 (dd, 1H, *J* = 4.7, 1.6 Hz, H-6′), 8.72 (dd, 1H, *J* = 7.9, 1.6 Hz, H-4′); ^{13}C (50 MHz, DMSO-d_6) δ: 31.7 (q), 108.3 (s), 110.7 (d), 117.3 (d), 118.0 (s), 122.4 (d), 126.3 (d), 127.0 (d), 131.1 (2 x d), 136.3 (s), 142.2 (d), 146.0 (s), 150.4 (s), 161.3 (s). Anal. Calcd for $C_{15}H_{11}N_3S_2$: C, 60.58; H, 3.73; N, 14.13%. Found: C, C, 60.33; H, 3.59; N, 13.89%.

Tert-Butyl 3-[4-(Pyridin-3-yl)-1,3-Thiazol-2-yl]-1H-Indole-1-Carboxylate Hydrobromide (**2a**)

Pink solid; yield: 90%; mp: 171–172 °C; IR cm^{-1}: 1737 (CO), 3420 (NH$^+$); ^{1}H NMR (200 MHz, DMSO-d_6) δ: 1.69 (s, 9H, 3 x CH_3), 7.43–7.54 (m, 2H, H-5′ and H-6′), 8.09 (dd, 1H, *J* = 8.1, 5.4 Hz, H-5″), 8.14–8.23 (m, 1H, H-7′), 8.44 (s, 1H, H-2′), 8.49–8.53 (m, 1H, H-4′), 8.62 (s, 1H, H-5), 8.88 (d, 1H, *J* = 5.4 Hz, H-6″), 9.08 (d, 1H, *J* = 8.1 Hz, H-4″), 9.53 (s, 1H, H-2″); ^{13}C (50 MHz, DMSO-d_6) δ: 27.6 (3xq), 85.0 (s), 114.3 (s), 115.0 (d), 118.1 (d), 121.5 (d), 124.0 (d), 125.6 (d), 126.3 (d), 126.5 (s), 127.2 (d), 132.4 (s), 134.9 (s), 140.1 (d), 141.3 (d), 141.6 (d), 148.4 (s), 148.5 (s), 161.8 (s). Anal. Calcd for $C_{21}H_{20}BrN_3O_2S$: C, 55.03; H, 4.40; N, 9.17%. Found: C, 54.78; H, 4.57; N, 8.98%.

1-Methyl-3-[4-(Pyridin-3-yl)-1,3-Thiazol-2-yl]-1H-Indole Hydrobromide (**2b**)

Orange solid; yield: 79%; mp: 266–267 °C; IR cm^{-1} 3423 (NH$^+$); ^{1}H NMR (200 MHz, DMSO-d_6) δ: 3.91 (s, 3H, CH_3), 7.25–7.38 (m, 2H, H-5′ and H-6′), 7.57–7.61 (m, 1H, H-7′), 8.21 (dd, 1H, *J* = 8.2, 5.7 Hz, H-5″), 8.29 (s, 1H, H-2′), 8.35–8.40 (m, 1H, H-4′), 8.52 (s, 1H, H-5), 8.94 (d, 1H, *J* = 5.7 Hz, H-6″), 9.21 (d, 1H, *J* = 8.2 Hz, H-4″), 9.55 (d, 1H, *J* = 1.7 Hz, H-2″); ^{13}C (50 MHz, DMSO-d_6) δ: 32.9 (q); 108.8 (s), 110.7 (d), 116.2 (d), 120.6 (d), 121.3 (d), 122.7 (d), 124.4 (s), 127.5 (d), 131.4 (d), 133.1 (s), 137.0 (s), 139.0 (d), 140.3 (d), 142.1 (d), 147.5 (s), 163.9 (s). Anal. Calcd for: $C_{17}H_{14}BrN_3S$: C, 54.85; H, 3.79; N, 11.29%. Found: C, 54.64; H, 4.00; N, 11.47%.

1-(2-Methoxyethyl)-3-[4-(Pyridin-3-yl)-1,3-Thiazol-2-yl]-1H-Indole Hydrobromide (**2c**)

Orange solid; yield: 73%; mp: 190–191 °C; IR cm^{-1} 3425 (NH$^+$); ^{1}H NMR (200 MHz, DMSO-d_6) δ: 3.24 (s, 3H, CH_3), 3.73 (t, 2H, *J* = 5.0 Hz, CH_2), 4.47 (t, 2H, *J* = 5.0 Hz, CH_2), 7.25–7.35 (m, 2H, H-5′ and H-6′), 7.64–7.68 (m, 1H, H-7′), 8.23 (dd, 1H, *J* = 8.2, 5.8 Hz, H-5″), 8.27 (s, 1H, H-2′), 8.33–8.37 (m, 1H, H-4′), 8.56 (s, 1H, H-5), 8.82 (d, 1H, *J* = 5.8 Hz, H-6″), 9.24 (d, 1H, *J* = 8.2 Hz, H-4″), 9.58 (d, 1H, *J* = 1.5 Hz, H-2″); ^{13}C (50 MHz, DMSO-d_6) δ: 45.8 (t), 50.1 (q), 70.6 (t), 109.1 (s), 111.0 (d), 116.3 (d), 120.6 (d), 121.3 (d), 122.7 (d), 124.5 (s), 127.6 (d), 131.0 (d), 133.1 (s), 136.6 (s), 139.1 (d), 140.4 (d), 142.3 (d), 147.5 (s), 163.9 (s). Anal. Calcd for: $C_{19}H_{18}BrN_3OS$: C, 54.81; H, 4.36; N, 10.09%. Found: C, 54.60; H, 4.21; N, 9.92%.

Tert-Butyl 5-Methoxy-3-[4-(Pyridin-3-yl)-1,3-Thiazol-2-yl]-1H-Indole-1-Carboxylate Hydrobromide (**2d**)

Orange solid; yield: 88%; mp: 154–155 °C; IR cm^{-1}: 1734 (CO), 3422 (NH$^+$); ^{1}H NMR (200 MHz, DMSO-d_6) δ: 1.68 (s, 9H, 3 x CH_3), 3.91 (s, 3H, CH_3), 7.11 (dd, 1H, *J* = 9.1, 2.6 Hz, H-6′), 7.82 (d, 1H, *J* = 2.6 Hz, H-4′), 8.05 (d, 1H, *J* = 9.1 Hz, H-7′), 8.13 (dd, 1H, *J* = 8.2, 5.6 Hz, H-5″), 8.38 (s, 1H, H-2′), 8.63 (s, 1H, H-5), 8.91 (d, 1H, *J* = 5.6 Hz, H-6″), 9.07 (d, 1H, *J* = 8.2 Hz, H-4″), 9.50 (d, 1H, *J* = 2.0 Hz, H-2″); ^{13}C (50 MHz, DMSO-d_6) δ: 27.6 (3 x q), 55.4 (q), 84.9 (s), 103.8 (d), 114.0 (d), 115.8 (d), 118.0 (d), 126.9 (d), 127.2 (d), 129.5 (s), 132.4 (s), 140.0 (d), 141.2 (d), 141.3 (s), 141.5 (d), 148.2 (s), 148.5 (s), 149.7 (s), 156.2 (s), 161.9 (s). Anal. Calcd for: $C_{22}H_{22}BrN_3O_3S$: C, 54.10; H, 4.54; N, 8.60%. Found: C, 54.35; H, 4.30; N, 8.46%.

5-Methoxy-1-Methyl-3-[4-(Pyridin-3-yl)-1,3-Thiazol-2-yl]-1H-Indole Hydrobromide (**2e**)

Orange solid; yield: 96%; mp: 210–211 °C; IR cm^{-1} 3429 (NH$^+$); ^{1}H NMR (200 MHz, DMSO-d_6) δ: 3.87 (s, 3H, CH_3), 3.90 (s, 3H, CH_3), 6.99 (dd, 1H, *J* = 8.9, 2.4 Hz, H-6′), 7.63 (d, 1H, *J* = 8.9 Hz, H-7′), 7.83 (d, 1H, *J* = 2.4 Hz, H-4′), 8.19–8.25 (m, 2H, H-2′ and H-5″), 8.50 (s, 1H, H-5), 8.94 (d, 1H, *J* = 5.3 Hz, H-6″), 9.20 (d, 1H, *J* = 8.3 Hz, H-4″), 9.51 (s, 1H, H-2″); ^{13}C (50 MHz, DMSO-d_6) δ: 33.1 (q), 55.4 (q), 102.5 (d), 108.4 (s), 111.6 (d), 112.3 (d), 115.9 (d), 125.0 (s), 127.5 (d), 131.7 (d), 132.2 (s), 133.1 (s), 139.1 (d), 140.4 (d), 141.9 (d), 147.4 (s), 155.1 (s), 164.2 (s). Anal. Calcd for: $C_{18}H_{16}BrN_3OS$: C, 53.74; H, 4.01; N, 10.44%. Found: C, 53.50; H, 3.83; N, 10.70%.

5-Methoxy-1-(2-Methoxyethyl)-3-[4-(Pyridin-3-yl)-1,3-Thiazol-2-yl]-1H-Indole Hydrobromide (**2f**)

Orange solid; yield: 89%; mp: 122–123 °C; IR cm^{-1} 3426 (NH$^+$); ^{1}H NMR (200 MHz, DMSO-d$_6$) δ: 3.24 (s, 3H, CH$_3$), 3.71 (t, 2H, *J* = 5.0 Hz, CH$_2$), 3.89 (s, 3H, CH$_3$), 4.42 (t, 2H, *J* = 5.0 Hz, CH$_2$), 6.95 (dd, 1H, *J* = 8.9, 2.5 Hz, H-6′), 7.56 (d, 1H, *J* = 8.9 Hz, H-7′), 7.81 (d, 1H, *J* = 2.5 Hz, H-4′), 8.18–8.22 (m, 2H, H-2′ and H-5″), 8.50 (s, 1H, H-5), 8.93 (d, 1H, *J* = 5.2 Hz, H-6″), 9.15 (d, 1H, *J* = 8.4 Hz, H-4″), 9.51 (d, 1H, *J* = 1.3 Hz, H-2″); ^{13}C (50 MHz, DMSO-d$_6$) δ: 46.0 (t), 55.4 (q), 58.1 (q), 70.6 (t), 102.5 (d), 108.7 (s), 111.9 (d), 112.2 (d), 115.8 (d), 125.1 (s), 127.3 (d), 131.1 (d), 131.7 (s), 133.0 (s), 139.5 (d), 140.8 (d), 141.6 (d), 147.6 (s), 155.0 (s), 164.1 (s). Anal. Calcd for: $C_{20}H_{20}BrN_3O_2S$: C, 53.82; H, 4.52; N, 9.41%. Found: C, 53.65; H, 4.47; N, 9.66%.

Tert-Butyl 5-Bromo-3-[4-(Pyridin-3-yl)-1,3-Thiazol-2-yl]-1H-Indole-1-Carboxylate Hydrobromide (**2g**)

Yellow solid; yield: 78%; mp: 185–186 °C; IR cm^{-1}: 1749 (CO), 3421 (NH$^+$); ^{1}H NMR (200 MHz, DMSO-d_6) δ: 1.68 (s, 9H, CH$_3$); 7.63 (dd, 1H, *J* = 8.9, 2.0 Hz, H-6′), 8.01–8.13 (m, 2H, H-5″ and H-7′), 8.45 (s, 1H, 2′), 8.57 (d, 1H, *J* = 2.0 Hz, H-4′), 8.60 (s, 1H, H-5), 8.89 (d, 1H, *J* = 5.5 Hz, H-6″), 8.99 (d, 1H, *J* = 8.3 Hz, H-4″), 9.46 (d, 1H, *J* = 1.8 Hz, H-2″); ^{13}C (50 MHz, DMSO-d_6) δ: 27.6 (3 x q), 85.5 (s), 113.4 (s), 116.5 (d), 116.8 (s), 118.2 (d), 123.5 (d), 127.1 (d), 127.6 (d), 128.0 (s), 128.1 (d), 132.2 (s), 133.7 (s), 140.3 (d), 140.9 (d), 141.9 (d), 148.1 (s), 148.5 (s), 161.3 (s). Anal. Calcd for: $C_{21}H_{19}Br_2N_3O_2S$: C, 46.95; H, 3.56; N, 7.82%. Found: C, 47.18; H, 3.41; N, 7.56%.

5-Bromo-1-Methyl-3-[4-(Pyridin-3-yl)-1,3-Thiazol-2-yl]-1H-Indole Hydrobromide (**2h**)

Orange solid; yield: 94%; mp: 279–280 °C; IR cm^{-1}: 3420 (NH$^+$); ^{1}H NMR (200 MHz, DMSO-d_6) δ: 3.89 (s, 3H, CH$_3$), 7.41 (dd, 1H, *J* = 8.7, 1.9 Hz, H-6′), 7.56 (d, 1H, *J* = 8.7 Hz, H-7′), 8.18 (dd, 1H, *J* = 8.2, 5.6 Hz, H-5″), 8.31 (s, 1H, H-2′), 8.43 (d, 1H, *J* = 1.9 Hz, H-4′), 8.49 (s, 1H, H-5), 8.92 (d, 1H, *J* = 5.6 Hz, H-6″), 9.09 (d, 1H, *J* = 8.2 Hz, H-4″), 9.47 (d, 1H, *J* = 1.8 Hz, H-2″); ^{13}C (50 MHz, DMSO-d_6) δ: 33.2 (q), 108.4 (s), 112.9 (d), 114.1 (s), 116.2 (d), 122.7 (d), 125.2 (d), 125.9 (s), 127.3 (d), 132.7 (d), 132.8 (s), 135.8 (s), 139.6 (d), 141.0 (d), 141.4 (d), 147.8 (s), 163.4 (s). Anal. Calcd for: $C_{17}H_{13}Br_2N_3S$: C, 45.26; H, 2.90; N, 9.31%. Found: C, 45.44; H, 2.65; N, 9.47%.

5-Bromo-1-(2-Methoxyethyl)-3-[4-(Pyridin-3-yl)-1,3-Thiazol-2-yl]-1H-Indole Hydrobromide (**2i**)

Red solid; yield: 87%; mp: 196–197 °C; IR cm^{-1}: 3427 (NH$^+$); ^{1}H NMR (200 MHz, DMSO-d_6) δ: 3.23 (s, 3H, CH$_3$), 3.72 (t, 2H, *J* = 5.0 Hz, CH$_2$), 4.46 (t, 2H, *J* = 5.0 Hz, CH$_2$), 7.42 (dd, 1H, *J* = 8.8, 2.0 Hz, H-6′), 7.65 (d, 1H, *J* = 8.8 Hz, H-7′), 8.18 (dd, 1H, *J* = 8.2, 5.6 Hz, H-5″), 8.32 (s, 1H, H-2′), 8.44 (d, 1H, *J* = 2.0 Hz, H-4′), 8.51 (s, 1H, H-5), 8.92 (d, 1H, *J* = 5.6 Hz, H-6″), 9.10 (d, 1H, *J* = 8.2 Hz, H-4″), 9.49 (d, 1H, *J* = 1.7 Hz, H-2″); ^{13}C (50 MHz, DMSO-d_6) δ: 46.0 (t), 58.1 (q), 70.6 (t), 108.7 (s), 113.2 (d), 114.0 (s), 116.3 (d), 122.7 (d), 125.2 (d), 126.0 (s), 127.2 (d), 132.2 (d), 132.7 (s), 135.5 (s), 139.8 (d), 141.2 (d), 141.3 (d), 148.0 (s), 163.3 (s). Anal. Calcd for: $C_{19}H_{17}Br_2N_3OS$: C, 46.08; H, 3.46; N, 8.48%. Found: C, 46.33; H, 3.60; N, 8.66%.

5-Fluoro-3-[4-(Pyridin-3-yl)-1,3-Thiazol-2-yl]-1H-Indole Hydrobromide (**2j**)

Yellow solid; yield: 90%; mp: 284–285 °C; IR cm^{-1}: 3159 (NH), 3428 (NH$^+$); ^{1}H NMR (200 MHz, DMSO-d_6) δ: 7.13 (td, 1H, *J* = 11.6, 9.3, 2.5 Hz, H-6′), 7.54 (dd, 1H, *J* = 9.3, 4.6 Hz, H-7′), 8.06–9.19 (m, 2H, H-4′ and H-5″), 8.34 (d, 1H, *J* = 2.9 Hz, H-2′), 8.48 (s, 1H, H-5), 8.90 (d, 1H, *J* = 4.8 Hz, H-6″), 9.14 (d, 1H, *J* = 8.4 Hz, H-4″), 9.54 (d, 1H, *J* = 1.7 Hz, H-2″), 12.02

(bs, 1H, NH); ^{13}C (50 MHz, DMSO-d_6): 105.4 (d, $J_{C6'-F}$ = 24.2 Hz), 110.0 (d, $J_{C'7a-F}$ = 4.6 Hz), 110.9 (d, $J_{C4'-F}$ = 26.2 Hz), 113.5 (d, $J_{C7'-F}$ = 10.2 Hz), 116.2 (d), 124.4 (d, $J_{C3'a-F}$ = 10.9 Hz), 127.4 (d), 129.4 (d), 133.0 (s), 133.2 (s), 139.4 (d), 140.6 (d), 141.9 (d), 147.6 (s), 158.1 (d, $J_{C5'-F}$ = 234 Hz), 164.1 (s). Anal. Calcd for: $C_{16}H_{11}BrFN_3S$: C, 51.08; H, 2.95; N, 11.17%. Found: C, 51.36; H, 3.09; N, 11.41%.

5-Fluoro-1-Methyl-3-[4-(Pyridin-3-yl)-1,3-Thiazol-2-yl]-1H-Indole Hydrobromide (**2k**)

Orange solid; yield: 92%; mp: 277–278 °C; IR cm^{-1}: 3420 (NH$^+$); ^{1}H NMR (200 MHz, DMSO-d_6) δ: 3.89 (s, 3H, CH$_3$), 7.13 (td, 1H, *J* = 11.7, 9.2, 2.6 Hz, H-6′), 7.60 (dd, 1H, *J* = 9.2, 4.4 Hz, H-7′), 8.05 (dd, 1H, *J* = 11.7, 2.6 Hz, H-4′), 8.16 (dd, 1H, *J* = 8.2, 5.6 Hz, H-5″), 8.32 (s, 1H, H-2′), 8.48 (s, 1H, H-5), 8.91 (d, 1H, *J* = 5.6 Hz, H-6″), 9.19 (d, 1H, *J* = 8.2 Hz, H-4″), 9.52 (d, 1H, *J* = 1.6 Hz, H-2″); ^{13}C (50 MHz, DMSO-d_6): 33.2 (q), 105.6 (d, $J_{C6'-F}$ = 24.9 Hz), 110.0 (d, $J_{C'7a-F}$ = 4.6 Hz), 110.9 (d, $J_{C4'-F}$ = 25.7 Hz), 112.1 (d, $J_{C7'-F}$ = 10.3 Hz), 115.9 (d), 124.7 (d, $J_{C3'a-F}$ = 11.0 Hz), 127.2 (d), 132.8 (s), 133.0 (d), 133.8 (s), 139.7 (d), 141.0 (d), 141.5 (d), 147.8 (s), 158.3 (d, $J_{C5'-F}$ = 236 Hz), 163.6 (s). Anal. Calcd for: $C_{17}H_{13}BrFN_3S$: C, 52.32; H, 3.36; N, 10.77%. Found: C, 52.14; H, 3.48; N, 10.53%.

5-Fluoro-1-(2-Methoxyethyl)-3-[4-(Pyridin-3-yl)-1,3-Thiazol-2-yl]-1H-Indole Hydrobromide (**2l**)

Orange solid; yield: 88%; mp: 202 °C; IR cm^{-1}: 3421 (NH$^+$); ^{1}H NMR (200 MHz, DMSO-d_6) δ: 3.24 (s, 3H, CH$_3$), 3.72 (t, 2H, *J* = 5.1 Hz, CH$_2$), 4.46 (t, 2H, *J* = 5.1 Hz, CH$_2$), 7.17 (td, 1H, *J* = 11.7, 9.2, 2.6 Hz, H-6′), 7.69 (dd, 1H, *J* = 9.2, 4.5 Hz, H-7′), 8.07 (dd, 1H, *J* = 11.7, 2.6 Hz, H-4′), 8.16 (dd, 1H, *J* = 8.2, 5.6 Hz, H-5″), 8.33 (s, 1H, H-2′), 8.50 (s, 1H, H-5), 8.91 (d, 1H, *J* = 5.6 Hz, H-6″), 9.14 (d, 1H, *J* = 8.2 Hz, H-4″), 9.54 (d, 1H, *J* = 1.7 Hz, H-2″); ^{13}C (50 MHz, DMSO-d_6): 46.1 (t), 58.1 (q), 70.6 (t), 105.6 (d, $J_{C6'-F}$ = 25.0 Hz), 109.2 (d, $J_{C'7a-F}$ = 4.7 Hz), 110.9 (d, $J_{C4'-F}$ = 26.3 Hz), 112.4 (d, $J_{C7'-F}$ = 9.8 Hz), 116.0 (d), 124.8 (d, $J_{C3'a-F}$ = 10.8 Hz), 127.2 (d), 132.5 (d), 132.8 (s), 133.4 (s), 139.9 (d), 141.2 (d), 141.4 (d), 147.9 (s), 162.1 (d, $J_{C5'-F}$ = 234 Hz), 163.6 (s). Anal. Calcd for: $C_{19}H_{17}BrFN_3OS$: C, 52.54; H, 3.95; N, 9.67. Found: C, 52.23; H, 3.77; N, 9.81.

3-[4-(Pyridin-3-yl)-1,3-Thiazol-2-yl]-1H-Pyrrolo[2,3-b]Pyridine Hydrobromide (**2m**)

Yellow solid; yield: 95%; mp: 324–325 °C; IR cm^{-1}: 3227 (NH), 3423 (NH$^+$); ^{1}H NMR (200 MHz, DMSO-d_6) δ: 7.46 (dd, 1H, *J* = 7.9, 5.1 Hz, H-5′), 8.23 (dd, *J* = 8.2, 5.7 Hz, 1H, H-5″), 8.47–8.49 (m, 2H, H-2′ and H-6′), 8.63 (s, 1H, H-5), 8.94–8.95 (m, 2H, H-4′ and H-6″), 9.27 (d, 1H, *J* = 8.2 Hz, H-4″), 9.63 (d, 1H, *J* = 1.4 Hz, H-2″), 12.50 (bs, 1H, NH); ^{13}C (50 MHz, DMSO-d_6): 109.3 (s), 117.3 (2 x d), 118.4 (s), 127.5 (d), 128.8 (d), 132.3 (d), 132.9 (s), 139.2 (d), 140.5 (d), 141.3 (d), 142.4 (d), 145.4 (s), 147.7 (s), 165.0 (s). Anal. Calcd for: $C_{15}H_{11}BrN_4S$: C, 50.15; H, 3.09; N, 15.60%. Found: C, 50.42; H, 3.20; N, 15.83%.

1-Methyl-3-[4-(Pyridin-3-yl)-1,3-Thiazol-2-yl]-1H-Pyrrolo[2,3-b]Pyridine Hydrobromide (**2n**)

Yellow solid; yield: 99%; mp: 280–282 °C; IR cm^{-1}: 3425 (NH$^+$); ^{1}H NMR (200 MHz, DMSO-d_6) δ: 3.92 (s, 3H, CH$_3$), 7.37 (dd, 1H, *J* = 7.9, 4.8 Hz, H-5′), 8.21 (dd, *J* = 8.2, 5.7 Hz, 1H, H-5″), 8.44 (dd, 1H, *J* = 4.8, 1.5 Hz, H-6′), 8.49 (s, 1H, H-2′), 8.58 (s, 1H, H-5), 8.78 (dd, 1H, *J* = 7.9, 1.5 Hz, H-4′), 8.95 (d, 1H, *J* = 5.7 Hz, H-6″), 9.23 (d, 1H, *J* = 8.2 Hz, H-4″), 9.59 (d, 1H, *J* = 1.7 Hz, H-2”); ^{13}C (50 MHz, DMSO-d_6): 31.6 (q), 107.6 (s), 116.9 (d), 117.3 (s), 117.5 (d), 127.5 (d), 130.2 (d), 131.6 (d), 132.9 (s), 139.1 (d), 140.4 (d), 142.3 (d), 143.2 (d), 146.8 (s), 147.6 (s), and 163.2 (s). Anal. Calcd for: $C_{16}H_{13}BrN_4S$: C, 51.48; H, 3.51; N, 15.01%. Found: C, 51.76; H, 3.72; N, 14.92%.

3.1.5. General Procedure for the Synthesis of Thiazole Compounds (**1o–q**)

To a suspension of appropriate thiazole **1a,d,g** (0.38 mL) in DCM (5 mL) trifluoroacetic acid (7.0 mmol, 0.54 mL) was added, and the mixture was heated under reflux for 24 h. After cooling, the mixture was neutralized with saturated aqueous sodium hydrogen carbonate solution and extracted with dichloromethane (3 x 20 mL). The organic phases were dried (Na_2SO_4), evaporated under reduced pressure, and the obtained residue was recrystallized with ethanol to afford the desidered thiazoles **1o–q**.

3-[4-(Thiophen-3-yl)-1,3-Thiazol-2-yl]-1H-indole (**1o**)

Yellow solid; yield: 95%; mp: 181–182 °C; IR cm^{-1}: 3216 (NH); ^{1}H NMR (200 MHz, DMSO-d_6) δ: 7.22–7.27 (m, 2H, H-5′ and H-6′), 7.50–7.54 (m, 1H, H-7′), 7.64–7.72 (m, 2H, H-4″ and H-5″), 7.81 (s, 1H, H-5), 8.06 (dd, 1H, *J* = 2.8, 1.4 Hz, H-2″), 8.19 (d, 1H, *J* = 2.9 Hz, H-2′), 8.29–8.33 (-1H, H-4′); 11.86 (bs, 1H, NH); ^{13}C (50 MHz, DMSO-d_6) δ: 109.8 (s), 110.1 (d), 112.3 (d), 120.3 (d), 121.0 (d), 122.4 (d), 122.5 (d), 124.2 (s), 126.3 (d), 127.1 (d), 127.2 (d), 135.9 (s), 136.5 (s), 149.4 (s), 163.0 (s). Anal. Calcd for $C_{15}H_{10}N_2S_2$: C, 63.80; H, 3.57; N, 9.92%. Found: C, 63.57; H, 3.45; N, 10.22%.

5-Methoxy-3-[4-(Thiophen-3-yl)-1,3-THIAZOL-2-yl]-1H-indole (**1p**)

Orange solid; yield: 98%; mp: 183–184 °C; IR cm^{-1}: 3264 (NH); ^{1}H NMR (200 MHz, DMSO-d_6) δ: 3.87 (s, 3H, CH$_3$), 6.89 (dd, 1H, *J* = 8.8, 2.5 Hz, H-6′), 7.40 (d, 1H, *J* = 8.8 Hz, H-7′), 7.63–7.75 (m, 2H, H-4″ and H-5″), 7.75 (s, 1H, H-5), 7.84 (d, 1H, *J* = 2.5 Hz, H-4′), 8.00 (dd, 1H, *J* = 2.8, 1.4 Hz, H-2″), 8.07 (d, 1H, *J* = 2.9 Hz, H-2′), 11.63 (bs, 1H, NH); ^{13}C (50 MHz, DMSO-d_6) δ: 55.2 (q), 102.1 (d), 109.6 (d), 110.1 (s), 112.4 (d), 112.9 (d), 122.0 (d), 124.8 (s), 126.2 (d), 127.0 (d), 127.2 (d), 131.5 (s), 135.5 (s), 150.0 (s), 154.6 (s), 163.0 (s). Anal. Calcd for $C_{16}H_{12}N_2OS_2$: C, 61.51; H, 3.87; N, 8.97%. Found: C, 61.30; H, 3.68; N, 9.15%.

5-Bromo-3-[4-(Thiophen-3-yl)-1,3-Thiazol-2-yl]-1H-Indole (**1q**)

Yellow solid; yield: 72%; mp: 164–165 °C; IR cm^{-1}: 3269 (NH); ^{1}H NMR (200 MHz, DMSO-d_6) δ: 7.37 (dd, 1H, *J* = 8.9, 1.9 Hz, H-6′), 7.49 (d, 1H, *J* = 8.9 Hz, H-7′), 7.68–7.69 (m, 2H, H-4″ and H-5″), 7.80 (s, 1H, H-5), 8.00 (t, 1H, *J* = 2.1 Hz, H-2″), 8.22 (d, 1H, *J* = 2.8 Hz, H-2′), 8.61 (d, 1H, *J* = 1.9 Hz, H-4′), 11.99 (bs, 1H, NH); ^{13}C (50 MHz, DMSO-d_6) δ: 110.0 (s), 110.2 (d), 113.4 (s), 114.2 (d), 122.0 (d), 122.7 (d), 125.0 (d), 126.0 (s), 126.2 (d), 127.1 (d), 128.2 (d), 135.3 (s), 136.5 (s), 150.3 (s), 162.2 (s). Anal. Calcd for $C_{15}H_9BrN_2S_2$: C, 49.87; H, 2.51; N, 7.75%. Found: C, 49.66; H, 2.42; N, 7.57%.

3.1.6. General Procedure for the Synthesis of Thiazole Derivatives (**2o–q**)

To a suspension of appropriate thiazole **2a,d,g** (0.38 mL) in DCM (5 mL), trifluoroacetic acid (7.0 mmol, 0.54 mL) was added, and the mixture was heated under reflux for 24 h. After cooling, the solvent was evaporated under reduced pressure, and the obtained residue was recrystallized with ethanol to afford the desidered thiazoles **2-q**.

3-[4-(Pyridin-3-yl)-1,3-Thiazol-2-yl]-1H-Indole Hydrobromide (**2o**)

Yellow solid; yield: 72%; mp: 204–205 °C; IR cm^{-1}: 3558 (NH), 3426 (NH$^+$); ^{1}H NMR (200 MHz, DMSO-d_6) δ: 7.24–7.31 (m, 2H, H-5′ and H-6′), 7.49–7.57 (m, 1H, H-7′), 8.05 (dd, 1H, *J* = 8.1, 5.4 Hz, H-5″), 8.25 (d, 1H, *J* = 2.9 Hz, H-2′), 8.35–8.39 (m, 1H, H-4′), 8.41 (s, 1H, H-5), 8.85 (dd, 1H, *J* = 5.4, 1.8 Hz, H-6″), 8.99–9.05 (m, 1H, H-4″), 9.49 (d, 1H, *J* = 1.8 Hz, H-2″), 11.90 (bs, 1H, NH); ^{13}C (50 MHz, DMSO-d_6) δ: 109.9 (s), 112.3 (d), 115.8 (d), 120.5 (d), 121.0 (d), 122.6 (d), 124.1 (s), 127.2 (d), 127.6 (d), 132.9 (s), 136.6 (s), 139.9 (d), 141.1 (d), 141.4 (d), 147.8 (s), 164.4 (s). Anal. Calcd for: $C_{16}H_{12}BrN_3S$: C, 53.64; H, 3.38; N, 11.73%. Found: C, 53.43; H, 3.24; N, 11.96%.

5-Methoxy-3-[4-(Pyridin-3-yl)-1,3-Thiazol-2-yl]-1H-Indole Hydrobromide (**2p**)

Orange solid; yield: 95%; mp: 228–229 °C; IR cm^{-1}: 3313 (NH), 3421 (NH$^+$); ^{1}H NMR (200 MHz, DMSO-d_6) δ: 3.89 (s, 3H, CH$_3$), 6.72 (dd, 1H, *J* = 8.8, 2.5 Hz, H-6′), 7.43 (d, 1H, *J* = 8.8 Hz, H-7′), 7.84 (d, 1H, *J* = 2.5 Hz, H-4′), 8.09 (dd, 1H, *J* = 8.1, 5.5 Hz, H-5″), 8.19 (d, 1H, *J* = 2.9 Hz, H-2′), 8.42 (s, 1H, H-5), 8.87 (d, 1H, *J* = 5.5 Hz, H-6″), 9.06 (d, 1H, *J* = 8.1 Hz, H-4″), 9.50 (d, 1H, *J* = 2.0 Hz, H-2″), 11.79 (d, 1H, *J* = 2.9 Hz, NH); ^{13}C (50 MHz, DMSO-d_6) δ: 55.3 (q), 102.3 (d), 109.7 (s), 112.4 (d), 113.0 (d), 115.1 (d), 124.7 (s), 126.9 (d), 127.9 (d), 131.6 (s), 132.6 (s), 140.4 (d), 140.6 (d), 141.9 (d), 148.0 (s), 154.8 (s), 164.5 (s). Anal. Calcd for: $C_{17}H_{14}BrN_3OS$: C, 52.59; H, 3.63; N, 10.82%. Found: C, 52.35; H, 3.51; N, 11.08%.

5-Bromo-3-[4-(Pyridin-3-yl)-1,3-Thiazol-2-yl]-1H-Indole Hydrobromide (**2q**)

Yellow solid; yield: 86%; mp: 245–246 °C; IR cm^{-1}: 3193 (NH), 3422 (NH$^+$); ^{1}H NMR (200MHz, DMSO-d_6) δ: 7.40 (dd, 1H, *J* = 8.6, 2.0 Hz, H-6′), 7.51 (d, 1H, *J* = 8.6 Hz, H-7′), 8.00 (dd, 1H, *J* = 8.1, 5.4 Hz, H-5″), 8.31 (d, 1H, *J* = 2.9 Hz, H-2′), 8.39 (s, 1H, H-5), 8.49 (d, 1H, *J* = 2.0 Hz, H-4′), 8.82 (d, 1H, *J* = 5.4 Hz, H-6′′), 8.91 (d, 1H, *J* = 8.1 Hz, H-4′′), 9.44 (d, 1H, *J* = 1.6 Hz, H-2′′), 12.09 (bs, 1H, NH); ^{13}C (50 MHz, DMSO-d_6) δ: 109.5 (s), 113.6 (s), 114.4 (d), 115.6 (d), 122.6 (d), 125.2 (d), 125.8 (s), 126.7 (d), 129.0 (d), 132.4 (s), 135.3 (s), 140.1 (d), 140.9 (d), 142.3 (d), 148.4 (s), 163.7 (s). Anal. Calcd for: $C_{16}H_{11}Br_2N_3S$: C, 43.96; H, 2.54; N, 9.61%. Found: C, 43.68; H, 2.68; N, 9.42%.

3.2. Biology

3.2.1. Minimum Inhibitory Concentrations (MICs) Determination

MICs were determined by using a microdilution method as recommended by CLSI for bacteria that grow aerobically (CLSI) (Clinical and Laboratory Standards Institute. Methods for Dilution Antimicrobial Susceptibility Tests for Bacteria That Grow Aerobically; Approved Standard—Ninth Edition. CLSI document M07-A9 (ISBN 1-56238-783-9 [Print]; ISBN 1-56238-784-7 [Electronic])) and Tryptic Soy Broth (TSB) (VWR International, Leuven, Belgium) as medium. It starts with the preparation of the bacterial suspension by diluting the bacteria grown at 37 °C for 24 h on Tryptic Soy Agar (TSA) (VWR International, LLC, Leuven, Belgium) in 5 mL of 0.9% NaCl to obtain a culture suspension whose optical density (O.D.) at 570 nm is of about 0.190 (corresponding to 10^6 colony-forming units CFU/mL); a further dilution 1:20 is always carried out in physiological solution. Serial dilutions 1:2 of the substance to be tested are performed, starting from the highest concentration, in culture medium (TSB); then, 10 µL of the prepared inoculum was added to each well containing substance solution. A positive growth control (test bacterial strain in the medium without inhibitor), a substance control (only the substance solution without inoculum), and a negative control (only the medium without inoculum), to check respectively the bacterial growth, the absorbance of substance at the highest concentration, and the sterility of medium, were also included in the assay. Thus, the plate prepared is incubated at 37 °C for 24 h, MICs were read by a microplate spectrophotometer (GloMax®-Multi Detection System, Promega Italia s.r.l, Milan, Italy) as the lowest concentration of sample whose O.D. at 570 nm is comparable to O.D. values of negative control wells.

3.2.2. Inhibition of Biofilm Formation (Crystal Violet Method)

Bacterial strains were incubated in test tubes with TSB (5 mL) containing 2% *w/v* glucose at 37 °C for 24 h. After that, the bacterial suspensions were diluted to achieve a turbidity equivalent to a 0.5 McFarland standard. The diluted suspension (2.5 µL) was added to each well of a single cell culture polystyrene sterile, flat-bottom 96-well plate filled with TSB (200 µL) with 2% *w/v* glucose. Sub-MIC concentration values of all compounds were directly added to the wells to reach concentrations ranging from 100 to 0.1 µM to assess BIC_{50} values—that is, the concentration at which the percentage of inhibition of biofilm formation is equal to 50%. Plates were incubated at 37 °C for 24 h. After biofilm growth, the content of each well was removed, wells were washed twice with sterile NaCl 0.9% and stained with 200 µL of 0.1% *w/v* crystal violet solution for 15 min at 37 °C. Excess solution was removed, and the plate was washed twice, using tap water. A volume of 200 µL of ethanol was added to each stained well to solubilize the dye. Optical density (O.D.) was read at 600 nm using a microplate reader (GloMax®-Multi Detection System, Promega Italia s.r.l, Milan, Italy).

The experiments were run at least in triplicates, and three independent experiments were performed.

The percentage of inhibition was calculated through the formula:

$$\% \text{ Inhibition} = (\text{OD growth} - \text{OD sample}/\text{OD growth control}) \times 100. \quad (1)$$

3.2.3. Antibiofilm Activity Against Pre-Formed Biofilm

A suspension of bacteria (0.5 McFarland standard) was obtained using the procedure described above for the inhibition of biofilm formation test. First, 2.5 mL of suspension was added to each well of a 96-well plate containing TSB (200 µL) with 2% *w/v* glucose. After the growth of a biofilm (24 h old), the content of each well was removed; then, wells were washed up twice with sterile PBS (Phosphate Buffered Saline) and filled with fresh TSB medium (200 µL). After that, different concentrations of compounds were added starting from a concentration equal or greater than the MIC obtained against the planktonic form of tested strains using TSB as the medium. The microtiter plate was sealed and incubated at 37 °C for further 24 h. The content of each well was removed, wells were washed twice with sterile PBS (100 mL to each well) and the 96-well plate was placed at 37 °C for 1 h before staining with a 0.1% *w/v* crystal violet solution. After 30 min, plates were washed with tap water to remove any excess stain.

Biofilm formation was determined by solubilizing crystal violet as above described, and the absorbance was read at 540 nm using a microplate reader (Glomax Multidetection System Promega, Promega Italia s.r.l, Milan, Italy). The percentages of inhibition were calculated with the above-reported. Each assay was performed in triplicate and repeated at least twice.

3.2.4. Inhibition of Biofilm Formation (Viable Plate Count)

Compounds **1l**, **2b**, **2c**, **2i**, and **2k**, which exhibited the highest potency in inhibiting *S.aureus* ATCC 25923 biofilm formation by the crystal violet method, were tested against the same strain by using a viable plate counts method [22]. Briefly, a suspension of the tested strain was obtained as described in Section 3.2.2. Polystyrene flat-bottom 24-well plates were filled with 2 mL of TSB with 2% *w/v* glucose; then, we added 25 µL of bacterial suspension and sub-MIC concentrations (10; 5; 1; 0.1 µg/mL) of the above-mentioned compounds and incubated them for 24 h at 37 °C. After that time, the wells were washed 3 times with 1 mL of sterile NaCl (0.9% *v/v* solution), and the surface of each well was scraped 3 times. The inocula were put in test tubes with 10 mL of NaCl (0.9% *v/v* solution) and sonicated (ultrasonic nominal power equal to 215 kHz) for 2 min. Eight serial dilutions 1:10 were prepared and 100 µL aliquots of each dilution were plated onto tryptic soy agar (TSA). Then, petri dishes were incubated at 37 °C and CFU/mL were counted after 24 h. Each assay was performed in triplicate and repeated at least twice. Activity was expressed as log reduction with respect to the not treated growth control.

3.2.5. Statistical Analysis

Mean values, standard deviation (SD), and significance testing (*p*-value) were calculated on a PC with the computer program, Microsoft Excel 2019 (Microsoft Corporation, Redmond, WA, USA).

4. Conclusions

With the aim to identify novel therapeutic approaches targeting antibiotic resistance mechanisms, two new series of 3-[4-(thiophen-3-yl)-1,3-thiazol-2-yl]-1*H*-indoles **1a–n** and 3-[4-(pyridin-3-yl)-1,3-thiazol-2-yl]-1*H*-indole hydrobromides 2a-n were efficiently synthesized and evaluated for their anti-biofilm activity. For almost all the new compounds, a marked selectivity toward the staphylococcal strains has been observed. In particular, compounds **1l** and **2i** showed the highest potency against *S. aureus* ATCC 25923, eliciting BIC_{50} values of 3.9 and 1.0 µM, respectively. Whereas, the 3-[4-(thiophen-3-yl)-1,3-thiazol-2-yl]-1*H*-indole **1a** and 3-[4-(pyridin-3-yl)-1,3-thiazol-2-yl]-1*H*-indole **2m** proved to be good inhibitors of *P. aeruginosa* biofilm formation with BIC_{50} values of 14.9 and 5.5 µM, respectively.

Among the novel approaches evaluated in response to the emergence of the antibiotic resistance, the anti-virulence strategy is considered one of the most encouraging [23]. Disarming the bacteria from their pathogenicity tools, as the biofilm formation, was found to be more beneficial than interfering with their growth. In this scenario, the new thiazole derivatives **1l**, **2b**, **2c**, **2i**, and **2m**, which proved to be able to interfere with the biofilm formation, without affecting the microbial vital processes, can be considered promising lead compounds for the development of new anti-virulence agents usable for the treatment of biofilm-associated infections or for the prophylaxis of implant surgery.

Author Contributions: A.C., S.C., B.P., D.C., and C.P. performed chemical research and analyzed the data; D.S. and M.G.C. performed biological research and analyzed the data; P.D. and G.C. participated in the design of the research and the writing of the manuscript. All authors have read and agreed to the published version of the manuscript.

Funding: This research was funded by European Union 2014–2020 PON Ricerca e Innovazione grant from the Italian Ministry of Education, University and Research, entitled "PROGEMA—Processi Green per l'Estrazione di Principi Attivi e la Depurazione di Matrici di Scarto e Non" (ARS01_00432) to P.D.

Conflicts of Interest: The authors declare no conflict of interest. The funders had no role in the design of the study; in the collection, analyses, or interpretation of data; in the writing of the manuscript, or in the decision to publish the results.

Sample Availability: Samples of the compounds are available from the authors.

References

1. Parrino, B.; Schillaci, D.; Carnevale, I.; Giovannetti, E.; Diana, P.; Cirrincione, G.; Cascioferro, S. Synthetic small molecules as anti-biofilm agents in the struggle against antibiotic resistance. *Eur. J. Med. Chem.* **2019**, *161*, 154–178. [CrossRef] [PubMed]
2. Cascioferro, S.; Carbone, D.; Parrino, B.; Pecoraro, C.; Giovannetti, E.; Cirrincione, G.; Diana, P. Therapeutic strategies to counteract antibiotic resistance in MRSA biofilm-associated infections. *ChemMedChem* **2020**, *15*, 1–17. [CrossRef]
3. Potera, C. ANTIBIOTIC RESISTANCE: Biofilm Dispersing Agent Rejuvenates Older Antibiotics. *Environ. Heal. Perspect.* **2010**, *118*, A288. [CrossRef]
4. Sun, F.; Qu, F.; Ling, Y.; Mao, P.; Xia, P.; Chen, H.; Zhou, D. Biofilm-associated infections: Antibiotic resistance and novel therapeutic strategies. *Futur. Microbiol.* **2013**, *8*, 877–886. [CrossRef]
5. Parrino, B.; Diana, P.; Cirrincione, G.; Cascioferro, S. Bacterial Biofilm Inhibition in the Development of Effective Anti-Virulence Strategy. *Open Med. Chem. J.* **2018**, *12*, 84–87. [CrossRef]
6. Parrino, B.; Carbone, D.; Cascioferro, S.; Pecoraro, C.; Giovannetti, E.; Deng, D.; Di Sarno, V.; Musella, S.; Auriemma, G.; Cusimano, M.G.; et al. 1,2,4-Oxadiazole topsentin analogs as staphylococcal biofilm inhibitors targeting the bacterial transpeptidase sortase A. *Eur. J. Med. Chem.* **2021**, *209*, 112892. [CrossRef]
7. Cascioferro, S.; Parrino, B.; Carbone, D.; Schillaci, D.; Giovannetti, E.; Cirrincione, G.; Diana, P. Thiazoles, Their Benzofused Systems, and Thiazolidinone Derivatives: Versatile and Promising Tools to Combat Antibiotic Resistance. *J. Med. Chem.* **2020**, *63*, 7923–7956. [CrossRef]
8. Beno, B.R.; Yeung, K.-S.; Bartberger, M.D.; Pennington, L.D.; Meanwell, N.A. A Survey of the Role of Noncovalent Sulfur Interactions in Drug Design. *J. Med. Chem.* **2015**, *58*, 4383–4438. [CrossRef]
9. More, P.G.; Karale, N.N.; Lawand, A.S.; Narang, N.; Patil, R.H. Synthesis and anti-biofilm activity of thiazole Schiff bases. *Med. Chem. Res.* **2014**, *23*, 790–799. [CrossRef]
10. Stefanska, J.; Nowicka, G.; Struga, M.; Szulczyk, D.; Koziol, A.E.; Augustynowicz-Kopec, E.; Napiorkowska, A.; Bielenica, A.; Filipowski, W.; Filipowska, A.; et al. Antimicrobial and anti-biofilm activity of thiourea derivatives incorporating a 2-aminothiazole scaffold. *Chem. Pharm. Bull.* **2015**, *63*, 225–236. [CrossRef]
11. Cascioferro, S.; Attanzio, A.; Di Sarno, V.; Musella, S.; Tesoriere, L.; Cirrincione, G.; Diana, P.; Parrino, B. New 1,2,4-Oxadiazole Nortopsentin Derivatives with Cytotoxic Activity. *Mar. Drugs* **2019**, *17*, 35. [CrossRef] [PubMed]
12. Parrino, B.; Attanzio, A.; Spanò, V.; Cascioferro, S.; Montalbano, A.; Barraja, P.; Tesoriere, L.; Diana, P.; Cirrincione, G.; Carbone, A. Synthesis, antitumor activity and CDK1 inhibiton of new thiazole nortopsentin analogues. *Eur. J. Med. Chem.* **2017**, *138*, 371–383. [CrossRef] [PubMed]
13. Spanò, V.; Attanzio, A.; Cascioferro, S.; Carbone, A.; Montalbano, A.; Barraja, P.; Tesoriere, L.; Cirrincione, G.; Diana, P.; Parrino, B. Synthesis and Antitumor Activity of New Thiazole Nortopsentin Analogs. *Mar. Drugs* **2016**, *14*, 226. [CrossRef] [PubMed]
14. Carbone, A.; Parrino, B.; Cusimano, M.G.; Spanò, V.; Montalbano, A.; Barraja, P.; Schillaci, D.; Cirrincione, G.; Diana, P.; Cascioferro, S. New Thiazole Nortopsentin Analogues Inhibit Bacterial Biofilm Formation. *Mar. Drugs* **2018**, *16*, 274. [CrossRef]
15. Sommer, R.; Rox, K.; Wagner, S.; Hauck, D.; Henrikus, S.S.; Newsad, S.; Arnold, T.; Ryckmans, T.; Brönstrup, M.; Imberty, A.; et al. Anti-biofilm Agents against Pseudomonas aeruginosa: A Structure-Activity Relationship Study of C-Glycosidic LecB Inhibitors. *J. Med. Chem.* **2019**, *62*, 9201–9216. [CrossRef]
16. Nagender, P.; Reddy, G.M.; Kumar, R.N.; Poornachandra, Y.; Kumar, C.G.; Narsaiah, B. Synthesis, cytotoxicity, antimicrobial and anti-biofilm activities of novel pyrazolo[3,4-b]pyridine and pyrimidine functionalized 1,2,3-triazole derivatives. *Bioorg. Med. Chem. Lett.* **2014**, *24*, 2905–2908. [CrossRef]
17. Totsika, M.; Vagenas, D.; Paxman, J.J.; Wang, G.; Dhouib, R.; Sharma, P.; Martin, J.L.; Scanlon, M.J.; Heras, B. Inhibition of Diverse DsbA Enzymes in Multi-DsbA Encoding Pathogens. *Antioxid Redox Signal* **2018**, *29*, 653–666. [CrossRef]

18. Carbone, A.; Parrino, B.; Di Vita, G.; Attanzio, A.; Spanò, V.; Montalbano, A.; Barraja, P.; Tesoriere, L.; Livrea, M.A.; Diana, P.; et al. Synthesis and antiproliferative activity of thiazolyl-bis-pyrrolo[2,3-b]pyridines and indolyl-thiazolyl-pyrrolo[2,3-c]pyridines, nortopsentin analogues. *Mar. Drugs* **2015**, *13*, 460–492. [CrossRef]
19. La Regina, G.; Bai, R.; Rensen, W.; Coluccia, A.; Piscitelli, F.; Gatti, V.; Bolognesi, A.; Lavecchia, A.; Granata, I.; Porta, A.; et al. Design and Synthesis of 2-Heterocyclyl-3-arylthio-1H-indoles as Potent Tubulin Polymerization and Cell Growth Inhibitors with Improved Metabolic Stability. *J. Med. Chem.* **2011**, *54*, 8394–8406. [CrossRef]
20. Wang, H.-Y.; Huang, K.; De Jesús, M.; Espinosa, S.; Piñero-Santiago, L.E.; Barnes, C.L.; Ortiz-Marciales, M. Synthesis of enantiopure 1,2-azido and 1,2-amino alcohols via regio- and stereoselective ring-opening of enantiopure epoxides by sodium azide in hot water. *Tetrahedron Asymmetry* **2016**, *27*, 91–100. [CrossRef]
21. Cascioferro, S.; Cusimano, M.G.; Schillaci, D. Antiadhesion agents against Gram-positive pathogens. *Futur. Microbiol.* **2014**, *9*, 1209–1220. [CrossRef] [PubMed]
22. Di Stefano, V.; Pitonzo, R.; Schillaci, D. Phytochemical and anti-staphylococcal biofilm assessment of Dracaena draco L. Spp. draco resin. *Pharmacogn. Mag.* **2014**, *10*, S434–S440.
23. Parrino, B.; Carbone, D.; Cirrincione, G.; Diana, P.; Cascioferro, S. Inhibitors of antibiotic resistance mechanisms: Clinical applications and future perspectives. *Futur. Med. Chem.* **2020**, *12*, 357–359. [CrossRef] [PubMed]

Chapter 12

1,2,4-Oxadiazole topsentin analogs as staphylococcal biofilm inhibitors targeting the bacterial transpeptidase sortase

A.Parrino, B.; Carbone, D.; Cascioferro, S.; **Pecoraro, C.**; Giovannetti, E.; Deng, D.; Di Sarno, V.; Musella, S.; Auriemma, G.; Cusimano, M. G.; Schillaci, D.; Cirrincione, G.; Diana, P.

European Journal of Medicinal Chemistry (2021), 209, 112892.

European Journal of Medicinal Chemistry 209 (2021) 112892

Contents lists available at ScienceDirect

European Journal of Medicinal Chemistry

journal homepage: http://www.elsevier.com/locate/ejmech

Research paper

1,2,4-Oxadiazole topsentin analogs as staphylococcal biofilm inhibitors targeting the bacterial transpeptidase sortase A

Barbara Parrino [a, 1], Daniela Carbone [a, 1], Stella Cascioferro [a], Camilla Pecoraro [a], Elisa Giovannetti [b, c], Dongmei Deng [d], Veronica Di Sarno [e], Simona Musella [e], Giulia Auriemma [e], Maria Grazia Cusimano [a], Domenico Schillaci [a], Girolamo Cirrincione [a], Patrizia Diana [a, *]

[a] *Department of Biological, Chemical and Pharmaceutical Sciences and Technologies (STEBICEF), University of Palermo, Via Archirafi 32, 90123, Palermo, Italy*

[b] *Department of Medical Oncology, VU University Medical Center, Amsterdam, the Netherlands*

[c] *Fondazione Pisana per La Scienza, Pisa, Italy*

[d] *Department of Preventive Dentistry, Academic Centre for Dentistry Amsterdam (ACTA), University of Amsterdam and VU University Amsterdam, Amsterdam, the Netherlands*

[e] *Department of Pharmacy, University of Salerno, Via G. Paolo II 132, Fisciano, 84084, Italy*

ARTICLE INFO

Article history:
Received 21 June 2020
Received in revised form
19 September 2020
Accepted 24 September 2020
Available online 29 September 2020

Keywords:
1,2,4-Oxadiazoles
Antibiofilm activity
Sortase A inhibitors
Anti-virulence agents
Marine alkaloids
Topsentin analogs

ABSTRACT

The inhibition or prevention of biofilm formation represents an emerging strategy in the war against antibiotic resistance, interfering with key players in bacterial virulence. This approach includes the inhibition of the catalytic activity of transpeptidase sortase A (Srt A), a membrane enzyme responsible for covalently attaching a wide variety of adhesive matrix molecules to the peptidoglycan cell wall in Gram-positive strains. A new series of seventeen 1,2,4-oxadiazole derivatives was efficiently synthesized and screened as potential new anti-virulence agents. The ability of inhibiting biofilm formation was evaluated against both Gram-positive and Gram-negative pathogens. Remarkably, all these compounds inhibited *S. aureus* and/or *P. aeruginosa* biofilm formation in a dose dependent manner, with 50% biofilm inhibitory concentrations (BIC_{50s}) below 10 μM for the most active compounds. Inhibition of SrtA was validated as one of the possible mechanisms of action of these new 1,2,4-oxadiazole derivatives, in the tested Gram-positive pathogen, using a specific enzymatic assay for a recombinant *S. aureus* SrtA. The three most active compounds, eliciting BIC_{50} values for *S. aureus* ATCC 25923 between 0.7 and 9.7 μM, showed a good activity toward the enzyme eliciting IC_{50} values ranging from 2.2 to 10.4 μM.

© 2020 Elsevier Masson SAS. All rights reserved.

1. Introduction

Every year in the world hundreds of thousands of people die because of drug-resistant infections, and the growing spread of multidrug-resistant (MDR) bacterial strains makes the search for new therapeutic strategies extremely urgent [1–3].

In the battle against antibiotic resistance, a strategy of great interest focuses on the search for anti-virulence molecules, which are able to “disarm” the pathogens, by fighting their virulence factors, without killing or inhibiting the growth of microorganisms. It was indeed observed that the lack of activity toward bacterial viability is an advantageous property in terms of selectivity pressure avoiding the development of MDR bacterial strains. Among the bacterial virulence factors, biofilm is considered one of the most relevant. Bacterial cells within biofilms are up to thousand times more resistant than their free form. This antibiotic resistance is due to the sum of the common resistance mechanisms of each single bacterial cell, which are conserved inside the biofilm, and to some specific features related to the growth as a sessile community [4].

Within biofilms the bacterial cells are embedded in a matrix consisting of a self-synthesized layer of extracellular polymeric substance known as EPS, which is mainly composed by polysaccharides, proteins, lipids and extracellular DNA (e-DNA) together with molecules originating from the host, such as mucus

---

* Corresponding author.
E-mail address: patrizia.diana@unipa.it (P. Diana).

[1] These authors contributed equally.

https://doi.org/10.1016/j.ejmech.2020.112892

0223-5234/© 2020 Elsevier Masson SAS. All rights reserved.

and DNA. In addition to the physical limitation to the penetration of drugs into the biofilm, the presence in the deepest layers of metabolically inactive cells, the “dormant cells”, confers a level of resistance that is difficult to overcome with common antibiotics. Most of the chronic and severe hospital-acquired infections, such as pneumonia in cystic fibrosis patients, chronic wound infections, osteomyelitis and otitis, are biofilm-mediated infections. Against this background, biofilm was identified as an attractive target and medicinal chemists have developed many strategies to 1) inhibit the biofilm formation or 2) to disrupt preformed biofilm [5,6].

An efficient approach to interfere with the biofilm formation consists in inhibiting the bacterial adhesion to the host tissue [7]. An important mechanism of adhesion in Gram-positive pathogens involves surface proteins known as microbial surface components recognizing adhesive matrix molecules (MSCRAMMs).

These proteins, which are structurally characterized by the presence of a C-terminal LPXTG motif, include indispensable *Staphylococcus aureus* virulence factors such as protein A (Spa), two fibronectin binding proteins (FnbpA and FnbpB), two clumping factors (ClfA and ClfB), a collagen-binding protein (Cna), two serine-aspartate glycosyltransferases (SdgA and SdgB) and three serine-aspartate repeat proteins (SdrC, SdrD, and SdrE) [8,9]. Of note, the covalent binding of MSCRAMMs to the peptidoglycan is catalyzed by the transpeptidase sortase A (SrtA), and overexpression of SrtA resulted in increased levels of biofilm formation in several staphylococcal strains [10].

The key role of SrtA in the pathogenicity of many relevant Gram-positive pathogens, including staphylococci, streptococci, enterococci and *Listeria monocytogenes,* was widely demonstrated using *in vitro* and *in vivo* studies. Gene knockout mutants of SrtA in *S. aureus*, resulting in defective surface expression of various MSCRAMMs, were unable to adhere to host surface and to cause renal abscesses and acute infection in mice [11,12]. Importantly, it was also demonstrated that SrtA contributes to *S. aureus* survival inside macrophages following phagocytosis [13].

These observations, along with 1) the consideration that SrtA is not involved in microbial viability processes and 2) the fact that, as a membrane enzyme, SrtA is more easily accessible by inhibitors than intracellular bacterial targets, make this enzyme an extremely appealing target for the development of new classes of anti-virulence compounds [14]. Additionally, since eukaryotic cells do not have sortase homologues, SrtA inhibitors should have a good selectivity and low toxicity.

In the past decade many natural and synthetic compounds were reported for their activity against SrtA [15]. In particular, natural compounds belonging to the topsentin class, isolated from the marine sponge *Spongosorites* sp., emerged as potential SrtA inhibitors. Among these bis(indolyl) alkaloids, deoxytopsentin **1,** bromodeoxytopsentin **2** and bromotopsentin **3** (Fig. 1) showed a good activity toward SrtA eliciting IC_{50} values of 15.67, 19.44 and 16.70 μM, respectively. *In vivo* studies, performed on *S. aureus* cell adhesion assays, confirmed the ability of these compounds to inhibit bacterial adhesion to fibronectin-coated surfaces in a dose dependent manner [16].

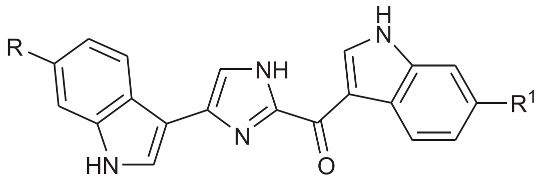

1 R=R^1=H
2 R=Br; R^1=H
3 R=Br; R^1=OH

Fig. 1. Chemical structures of deoxytopsentin **1**, bromodeoxytopsentin **2** and bromotopsentin **3**.

Additionally, several nitrogenous heterocycles, including imidazoles, pyrazoles, thiadiazoles, thiazoles, triazoles, purine and oxadiazoles were reported in the past decade for their interesting antibiofilm properties [17–23]. Concerning oxadiazole derivatives, it was demonstrated that the presence of the –N=C–*O*- sequence is advantageous for both antibacterial and anti-biofilm activity in *S. aureus,* since it may react with the nucleophilic centers of potential microbial targets. In particular, oxadiazole derivatives may interfere with the transcription of biofilm related genes, including *sarA*, *icaA*, *spa*, *fnbA* and *fnbB*, which play a key role in bacterial biofilm formation [24]. Keeping with the previous evidence of SrtA inhibitors activity for the topsentin analogs as well as for the oxadiazole scaffold, we decided to continue our studies on heterocyclic derivatives of pharmaceutical interest [25–35], with a special focus on marine alkaloid analogs endowed with antibacterial or anticancer activities [36–44]. Therefore, in the present study, we synthesized a new series of 1,2,4-oxadiazole topsentin analogs in order to obtain new anti-virulence compounds targeting biofilm formation. For comparative reasons, the ability of these new compounds in inhibiting biofilm formation was also evaluated against two important Gram-negative strains, *Pseudomonas aeruginosa* and *Escherichia coli*, that do not have the investigated target transpeptidase SrtA.

2. Chemistry

The synthesis of 1,2,4-oxadiazoles **3a-q** (Scheme 1) starts from 1-methyl-1*H*-indoles of type **4**, prepared from their corresponding indoles, as previously reported [45–47].

The acylation reaction of compounds **4a-d**, performed with an excess of oxalyl chloride in diethyl ether at 0 °C, under nitrogen atmosphere, led to the corresponding indolyl-oxo-acetyl chlorides 5**a-d** in excellent yields (89–96%). In the attempt to obtain 1,2,4-oxadiazoles **3** or their precursors carboximidamide **8**, compounds **5** were first reacted with carboxamidines of type **7**. In spite of several reaction conditions employed, in no case, the expected compounds were isolated in acceptable yields, due to the extreme reactivity of the indolyl-oxo-acetyl chlorides in the complex reaction mixture. Thus, indolyl-oxo-acetyl chlorides **5** were quickly converted into the corresponding (1-methyl-1*H*-indol-3-yl)-oxo-acetic acids **6a-d**, using an excess of an aqueous solution of sodium hydroxide (2 M) at room temperature (78–95%).

The latter were then subjected to a coupling reaction with carboxamidines **7a-e**, synthesized from the corresponding 1-methyl-1*H*-indoles, converted to their carbonitriles and successive reaction with hydroxylamine hydrochloride [48]. The coupling reaction was performed in anhydrous dimethylformamide (DMF) and in the presence of trimethylamine (Et_3N), *N*-ethyl-*N*′-(3-dimethylaminopropyl)carbodiimide hydrochloride (EDC·HCl) and 1-hydroxybenzotriazole hydrate (HOBt) as the coupling reagents, giving the carboximidamides **8a-n** (84–98%) that precipitated from the reaction mixture. Once isolated, the latter were subjected to base-catalyzed cyclodehydration reaction, performed at room temperature, leading to the synthesis of derivatives **3a-n** in good yields (77–90%) (Table 1). However, in the attempt to obtain 1,2,4-oxadiazoles **3o-q**, it was not possible to isolate the carboximidamides **8** from the reaction mixture. Potential explanations include the high-energy, highly reactivity and short-lifetime of these intermediates. In fact, monitoring the progress of reaction by

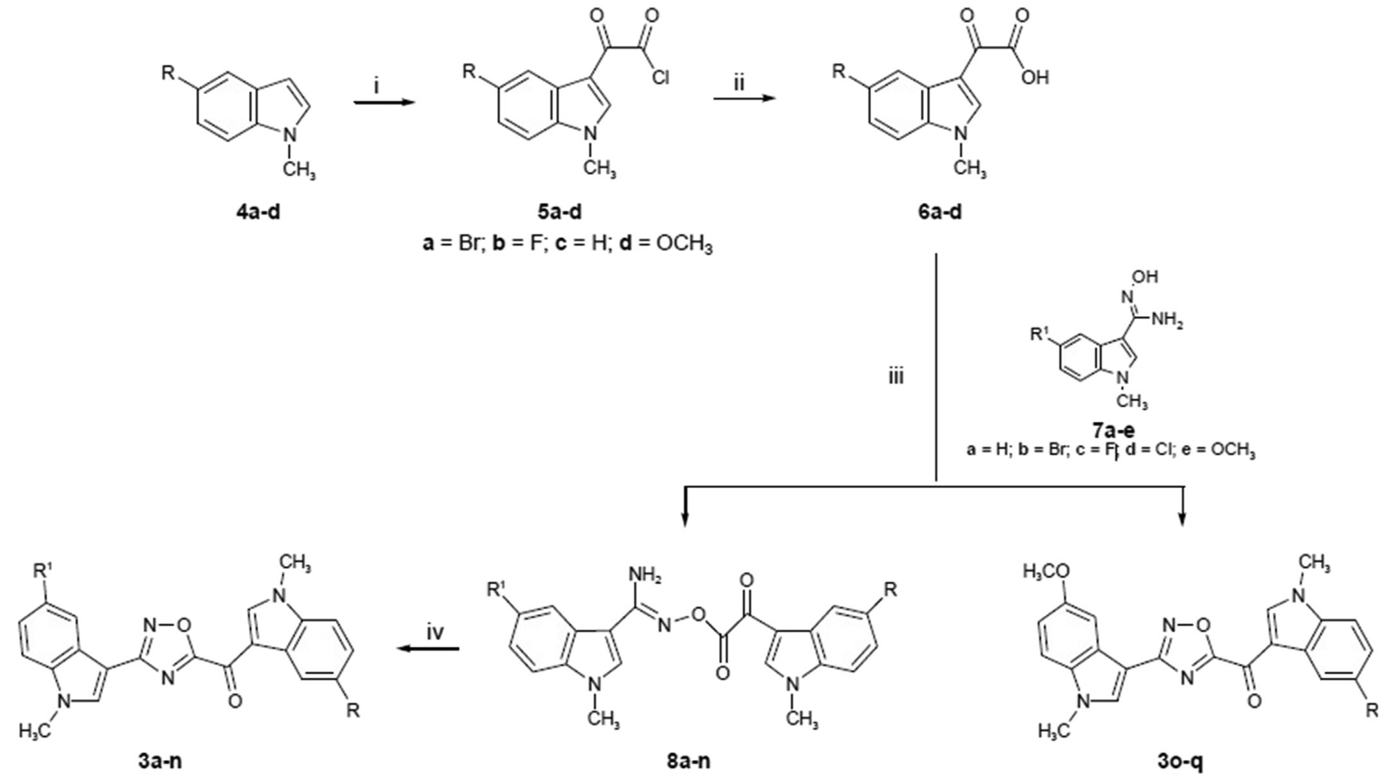
4a-d
5a-d
6a-d
a = Br; b = F; c = H; d = OCH3
i
ii
iii
iv
7a-e
a = H; b = Br; c = F; d = Cl; e = OCH3
3a-n
8a-n
3o-q

Scheme 1. Synthesis of new 1,2,4-oxadiazoles 3. Reagents: (i) ClCOCOCl, diethyl ether, 0 °C, N_2 atmosphere, 89–96%; (ii) aq NaOH (2 M), THF, rt, overnight, 78–95%; (iii) HOBt, EDC, Et_3N, DMF, 0 °C, 84–98% (for compounds 8a-n) and 78–81% (for compounds 3o-q); (iv) aq NaOH (2 M), acetone, rt, 77–90%.

Table 1
(1-Methyl-1*H*-indol-3-yl)[3-(1-methyl-1*H*-indol-3-yl)-1,2,4-oxadiazol-5-yl]methanones **3a-q**.

Compound	R	R^1	Yield (%)
3a	OCH_3	H	82%
3b	Br	H	78%
3c	H	H	77%
3d	F	Br	81%
3e	H	Br	80%
3f	OCH_3	Br	88%
3g	H	F	80%
3h	F	F	82%
3i	Br	F	82%
3j	OCH_3	F	90%
3k	Br	Cl	79%
3l	OCH_3	Cl	81%
3m	H	Cl	84%
3n	OCH_3	OCH_3	79%
3o	Br	OCH_3	78%
3p	F	OCH_3	80%
3q	H	OCH_3	81%

thin layer chromatography (TLC), once the corresponding derivatives **8** have been formed, they spontaneously convert into more stable derivatives through *in situ* cyclodehydration, giving the desired oxadiazole derivatives **3o-q** in yields ranging from 78 to 81% (Table 1).

3. Result and discussion

All the synthesized 1,2,4-oxadiazole compounds **3a-q** were initially submitted to an antibacterial screening test, in order to evaluate their *in vitro* antimicrobial activity against the planktonic form of the Gram-positive bacterial reference strains *S. aureus* ATCC 25923 and *S. aureus* ATCC 6538, and of the Gram-negative strains *P. aeruginosa* ATCC 15442 and *E. coli* ATCC 25922. The minimum inhibitory concentrations (MIC) of the tested compounds were evaluated in all these models. This analysis revealed that all compounds did not interfere with the planktonic bacterial growth (MIC >100 μg/mL). The lack of activity on the bacterial viability is consistent with the desired anti-virulence profile.

All the derivatives were then assayed for their *in vitro* anti-biofilm activity against the same four bacterial strains and the lowest concentration that showed 50% inhibition of the biofilm formation (BIC_{50}s) are reported in Table 2.

Most of compounds **3a-q** resulted especially active in inhibiting the formation of biofilm of the Gram-positive pathogen *S. aureus* ATCC 25923, showing BIC_{50} values between 0.7 and 40.0 μM. In particular, the derivatives **3d**, **3h** and **3n** were able to inhibit the biofilm formation with BIC_{50} values of 9.7, 0.7 and 2.2 μM, respectively. Some of the new topsentin derivatives proved to be active also against the Gram-negative pathogen *P. aeruginosa* ATCC 15442, eliciting in the case of the most active compounds, **3g** and **3j**, BIC_{50} values of 24.0 and 11.6 μM, respectively.

An evaluation of the BIC_{50}s observed for the most sensitive strain, *S. aureus* ATCC 25923, allows to hypothesize the SAR of the series of the 1,2,4-oxadiazoles tested. Starting from the unsubstituted derivative **3c** ($BIC_{50} = 14$ μM), the introduction of a halogen in the indole moiety bound to the position 3 of the oxadiazole (R^1) is detrimental for the activity and the increase of the size of the halogen makes the activity even worse (compare **3g**, **3m** and **3e**). Also, the replacement of the hydrogen with the methoxy group in the 3-carbonyl indole moiety (R) decreases the activity and the introduction of a halogen in R^1 of this compound leads to a further decrease of the activity (compare **3a**, **3f**, **3j** and **3l**). Additionally, replacement of the hydrogen of the 3-carbonyl indole moiety (R)

Table 2
Biofilm inhibitory concentrations (BIC$_{50}$s) of compounds **3a-q**.

Compound	BIC$_{50}$, μg/mL (μM)			
	S. aureus ATCC 25923	*S. aureus* ATCC 6538	*P. aeruginosa* ATCC 15442	*E. coli* ATCC 25922
3a	12.8 (33.1)	n.s	11.6 (30.0)	21.4 (55.4)
3b	17.2 (39.5)	n.s	17.1 (39.3)	17.1 (39.3)
3c	5.0 (14.0)	19.1 (53.6)	13.1 (36.7)	25.7 (72.1)
3d	4.4 (9.7)	n.s	n.s	n.s
3e	n.s	n.s	34.2 (78.6)	n.s
3f	19.1 (41.0)	n.s	n.s	n.s
3g	11.4 (30.4)	n.s	9.0 (24.0)	n.s
3h	0.27 (0.7)	n.s	19.5 (49.7)	n.s
3i	13.4 (29.6)	n.s	n.s	20.7 (45.7)
3j	16.0 (39.6)	n.s	4.7 (11.6)	n.s
3k	13.0 (27.7)	n.s	25.3 (53.9)	n.s
3l	n.s	n.s	n.s	n.s
3m	18.6 (47.6)	n.s	20.9 (53.5)	23.3 (59.6)
3n	0.9 (2.2)	n.s	31.1 (74.7)	n.s
3o	8.9 (19.1)	n.s	13.1 (28.1)	n.s
3p	6.0 (14.8)	n.s	21.1 (52.1)	n.s
3q	n.s	n.s	18.3 (47.4)	n.s

n.s. not significant because lower than 15% of inhibition percentage at the screening concentration of 100 μg/mL.

with a bromine leads to a lower activity but the introduction of a further halogen in R^1 restores, at least in part, the activity (compare **3b**, **3i** and **3k**). Symmetrical substitution of R and R^1 leads to the most active compounds (**3h** and **3n**). With the replacement of the methoxy group in the 3-carbonyl indole moiety (R) by halogen atoms, we obtained additional interesting derivatives (**3o** and **3p**), even if their BIC$_{50}$ were higher than the symmetrical OCH$_3$-substituted compound **3n**. However, when the fluorine in R^1 of **3h** is replaced by a bromine the activity decreases by one order of magnitude.

The new compounds did not interfere with microbial growth but were able to inhibit biofilm formation showing the highest activity toward the Gram-positive pathogen *S. aureus* ATCC 25923. The biological results obtained in our studies clearly support the mechanism of action based on the SrtA inhibition. In order to confirm this hypothesis, the three most promising compounds (**3d**, **3h**, **3n**) were further tested in order to evaluate their ability in inhibiting recombinant *S.aureus* SrtA. Interestingly, all three compounds proved to be potent SrtA inhibitors, eliciting IC$_{50}$ values of 2.2, 10.4 and 2.2 μM, respectively. Remarkably, the compounds **3d**, **3h**, **3n,** were significantly more potent against the enzyme than the lead compound deoxytopsentin **1.**

To evaluate potential harmful effects of the most active compounds **3d**, **3h** and **3n** on normal cells, we assessed the cell viability of human normal skin fibroblast Hs27 after treatment with different concentrations of each compound, ranging from 0.1 to 10 μM. As shown in Fig. 2, all these derivatives were relatively non-toxic to normal fibroblast cells. We found only 10–20% growth inhibition of Hs27 cells after 72 h exposure at the highest concentration tested (10 μM). The non-toxicity of these derivatives was confirmed on Hs27 cells treated with the other concentrations (0.1 and 1 μM), which showed a cell growth rates comparable to untreated cells.

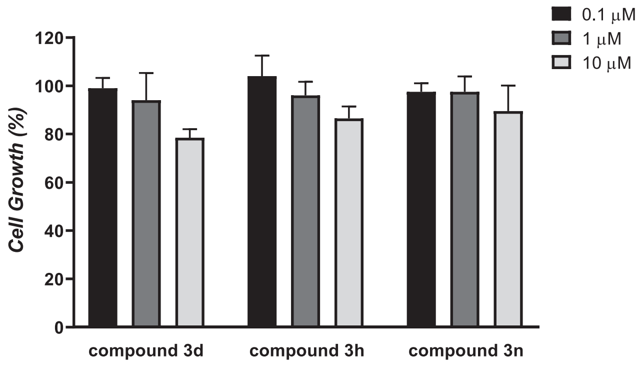

Fig. 2. Assessment of toxicity of compounds **3d**, **3h** and **3n** (at three different concentrations) against human skin fibroblast Hs27 compared to untreated cells.

4. Conclusion

New strategies to combat antibiotic resistant pathogens are warranted. To this goal we synthesized a new series of compounds with anti-virulence and anti-biofilm features. Transpeptidase SrtA, a membrane enzyme not involved in microbial viability processes, whose overexpression is related to increased levels of biofilm formation in numerous staphylococcal strains, represents an excellent target for the development of such new classes of compounds. It is also noteworthy that SrtA is a bacterial enzyme, not present in the eukaryotic cells; thereby, its inhibition is not going to induce toxicity in human cells or drug resistance in the bacteria [49].

Considering the interesting SrtA inhibitory activity of natural compounds belonging to topsentin class, we focused our studies on the synthesis of a new series of 1,2,4-oxadiazole topsentin analogs.

The new compounds were tested in order to evaluate their ability in inhibiting biofilm formation of the Gram-positive pathogens *S. aureus* ATCC 25923 and *S. aureus* ATCC 6538 and of the Gram-negative *E. coli* ATCC 25922 and *P. aeruginosa* ATCC 15442. All synthesized compounds inhibited *S. aureus ATCC 25923* and/or *P. aeruginosa* ATCC 15442 biofilm formation in a dose dependent manner, showing, in most cases, BIC$_{50}$ lower than 10 μM. Remarkably, compounds **3d**, **3h** and **3n** inhibited the formation of *S. aureus* ATCC 25923 biofilm with BIC$_{50}$ ranging from 0.7 to 9.7 μM. Moreover, the biofilm inhibitory concentrations of the three most active compounds against *S. aureus* were found to be non-toxic for human skin fibroblast Hs27, proving the absence of cytotoxicity in human normal cells. We then decided to further evaluate these promising antibiofilm agents for the specific inhibition of SrtA, as possible mechanism of action toward *S. aureus* ATCC 25923. The results of these experiments showed that the three most active compounds had excellent activity against SrtA, eliciting IC$_{50}$ values ranging from 2.2 to 10.4 μM. These data are extremely promising since previous studies demonstrated that a similar inhibition of

SrtA caused a significant decrease in bacterial virulence, since SrtA is involved in bacterial biofilm formation, bacterial adhesion, invasion to the host tissue, as well as in the bacterial resistance to the human immunity defense [50]. Conversely, as *P. aeruginosa* does not possess the transpetidase SrtA, the mechanism of action based on interference with the activity of this enzyme cannot be evoked, and further studies should focus on other targets. In conclusion, our data are opening new avenues for the control of polymicrobial infections caused by bacterial *S. aureus* and *P. aeruginosa* biofilm formation, and will prompt further studies in this important scientific and clinical topic [51].

5. Experimental section

5.1. Chemistry

The anhydrous solvents used for organic synthesis (acetonitrile, dimethylformamide and diethyl ether) and the reagents were purchased from Sigma-Aldrich Co, Alfa Aesar, VWR International and Acros Organics. Other solvents were purified and dried using standard method: toluene was distilled from calcium hydride, ethanol and methanol from iodine and magnesium. All anhydrous solvents were stored over 4 Å molecular sieves. All air- or moisture-sensitive reactions were performed using oven-dried glassware under an inert dry nitrogen atmosphere. Analytical thin layer chromatography (TLC) was performed on silica gel 60 F254 plates (0.25 mm thickness) and the develop plates were examined under ultraviolet (UV) light. All melting points were taken on a Buchi-Tottoly capillary apparatus and were uncorrected. IR spectra were determined in bromoform with a Shimadzu FT/IR 8400S spectrophotometer and peaks were reported in wavenumber (cm^{-1}). ^{1}H and ^{13}C NMR spectra were measured at 200 and 50 MHz, respectively, on DMSO-d_6 solution, using a Bruker Avance II series 200 MHz spectrometer. Chemical shifts were described in parts per million (δ), coupling constants (J) are expressed in Hertz (Hz), and splitting patterns were reported as singlet (s), doublet (d), triplet (t), quartet (q), multiplet (m), doublet of doublets (dd) and triplet of doublets (td). Chromatography column was performed with MERK silica gel 230–400 mesh ASTM or FLASH40i Biotage chromatography or with Buchi Sepacor chromatography module (prepacked cartridge reference). Elementary analyses (C, H, N) were within ±0.4% of the theoretical values.

Compounds **8a-n, 3a,b, 3d-f, 3h-q,** were characterized only by ^{1}H NMR spectra, for their poor solubility.

5.1.1. General procedure for the synthesis of (1-methyl-1H-indol-3-yl)-oxo-acetyl chlorides (**5a-d**)

To a solution of the opportune methyl-indole of the type **4** (10 mmol) in anhydrous diethyl ether (20 mL), oxalyl chloride (11.16 mmol, 0.95 mL) was added dropwise at 0 °C. The reaction mixture was left to stir at 0 °C for 3 h and then brought to room temperature for 1 h. The resulting solid product was collected by *vacuum* filtration and recrystallized from diethyl ether.

*5.1.1.1. (5-Bromo-1-methyl-1H-indol-3-yl)-oxo-acetyl chloride (**5a**).* Yellow solid; yield: 91%; mp: 134.4 °C; IR (cm^{-1}): 1772 (CO), 1613 (CO); ^{1}H NMR (200 MHz, DMSO-d_6) δ: 3.92 (3H, s, CH_3), 7.50 (1H, dd, J = 8.7, 1.9 Hz, H-6), 7.61 (1H, d, J = 8.7 Hz, H-7), 8.31 (1H, d, J = 1.9 Hz, H-4), 8.55 (1H, s, H-2); ^{13}C NMR (50 MHz, DMSO-d_6) δ: 33.6 (q), 110.6 (s), 113.4 (d), 115.9 (s), 123.3 (d), 126.2 (d), 127.7 (s), 136.2 (s), 142.2 (d), 164.6 (s), 179.9 (s); *Anal.* Calculated for $C_{11}H_7BrClNO_2$ (MW: 300.54): C, 43.96; H, 2.35; N, 4.66%. Found: C, 44.14; H, 2.29; N, 4.78%.

*5.1.1.2. (5-Fluoro-1-methyl-1H-indol-3-yl)-oxo-acetyl chloride (**5b**).* Yellow solid; yield: 96%; mp: 148.6 °C; IR (cm^{-1}): 1743 (CO), 1642 (CO);^{1}H NMR (200 MHz, DMSO-d_6) δ: 3.93 (3H, s, CH_3), 7.22 (1H, td, J = 9.6, 9.2, 2.6 Hz, H-6), 7.64 (1H, dd, J = 9.2, 4.4 Hz, H-7), 7.86 (1H, dd, J = 9.6, 2.6 Hz, H-4), 8.55 (1H, s, H-2); ^{13}C NMR (50 MHz, DMSO-d_6) δ: 33.7 (q), 106.2 (d, J_{C4-F} = 24.8 Hz), 111.1 (s, J_{C7a-F} = 4.4 Hz), 111.7 (d, J_{C6-F} = 25.7 Hz), 112.7 (d, J_{C7-F} = 9.8 Hz), 126.7 (s, J_{C3a-F} = 11.2 Hz), 134.0 (s), 142.4 (d), 159.3 (s, J_{C5-F} = 234.3 Hz), 166.4 (s), 181.2 (s). *Anal.* Calculated for $C_{11}H_7ClFNO_2$ (MW: 239.63): C, 55.13; H, 2.94; N, 5.85%. Found: C, 54.98; H, 3.01; N, 5.69%.

*5.1.1.3. (1-Methyl-1H-indol-3-yl)-oxo-acetyl chloride (**5c**).* Yellow solid; yield: 89%; mp: 156.4 °C; IR (cm^{-1}): 1735 (CO); 1604 (CO); ^{1}H NMR (200 MHz, DMSO-d_6) δ: 3.93 (3H, s, CH_3), 7.28–7.41 (2H, m, H-5 and H-6), 7.59–7.64 (1H, m, H-7), 8.18–8.23 (1H, m, H-4), 8.50 (1H, s, H-2); ^{13}C NMR (50 MHz, DMSO-d_6) δ: 33.4 (q), 111.1 (s), 111.2 (d), 121.2 (d), 123.1 (d), 123.7 (d), 126.0 (s), 137.35 (s), 141.3 (d), 165.1 (s), 180.0 (s); *Anal.* Calculated for $C_{11}H_8ClNO_2$ (MW: 221,64): C, 59.61; H, 3.64; N, 6.32%. Found: C, 59.69; H, 3.70; N, 6.18%.

*5.1.1.4. (5-Methoxy-1-methyl-1H-indol-3-yl)-oxo-acetyl chloride (**5d**).* Orange solid; yield: 90%, mp: 132.2 °C; IR (cm^{-1}): 1779 (CO); 1625 (CO); ^{1}H NMR (200 MHz, DMSO-d_6) δ: 3.82 (3H, s, CH_3), 3.89 (3H, s, OCH_3), 6.98 (1H, dd, J = 8.9, 2.5 Hz, H-6), 7.52 (1H, d, J = 8.9 Hz, H-7), 7.70 (1H, d, J = 2.5 Hz, H-4), 8.42 (1H, s, H-2); ^{13}C NMR (50 MHz, DMSO-d_6) δ: 33.5 (q), 55.3 (q), 103.2 (d), 110.9 (s), 112.0 (d), 113.1 (d), 127.0 (s), 132.2 (s), 141.0 (d), 156.4 (s), 165.3 (s), 180.0 (s). *Anal.* Calculated for $C_{12}H_{10}ClNO_3$ (MW: 251.67): C, 57.27; H, 4.01; N, 5.57%. Found: C, 57.19; H, 4.12; N, 5.37%.

5.1.2. General procedure for the synthesis of (1-methyl-1H-indol-3-yl)-oxo-acetic acids (**6a-d**)

To a solution of the suitable acylchloride of the type **5** (10 mmol) in anhydrous THF (20 mL), 15 mL of a aqueous solution of sodium hydroxide (NaOH) 2 M were added dropwise, until complete alkalization (pH = 14). The reaction mixture was stirred at room temperature overnight. Hydrochloric acid (HCl) 6 M (10 mL) was added up to pH = 1. The resulting solid precipitate was collected by *vacuum* filtration, washed with H_2O, dried under *vacuum* for 24 h and purified by column chromatography using ethyl acetate as eluent to give the desired oxo-acetic acids **6a-d**.

*5.1.2.1. (5-Bromo-1-methyl-1H-indol-3-yl)-oxo-acetic acid (**6a**).* Yellow solid; yield: 87%; mp: 256.6 °C; IR (cm^{-1}): 3273 (OH), 1760 (CO), 1628 (CO); ^{1}H NMR (200 MHz, DMSO-d_6) δ: 3.93 (3H, s, CH_3), 7.50 (1H, dd, J = 8.7, 1.5 Hz, H-6), 7.62 (1H, d, J = 8.7, H-7), 8.31 (1H, d, J = 1.5, H-4), 8.55 (1H, s, H-2), 14.03 (1H, s, OH); ^{13}C NMR (50 MHz, DMSO-d_6) δ: 33.6 (q), 110.6 (s), 113.4 (d), 116.0 (s), 123.3 (d), 126.2 (d), 127.7 (s), 136.2 (s), 142.2 (d), 164.7 (s), 180.0 (s); *Anal.* Calculated for $C_{11}H_8BrNO_3$ (MW: 282.09): C, 46.84; H, 2.86; N, 4.97%. Found: C, 46.54; H, 2.98; N, 5.14%.

*5.1.2.2. (5-Fluoro-1-methyl-1H-indol-3-yl)-oxo-acetic acid (**6b**).* Yellow solid; yield: 95%; mp: 194.5 °C; IR (cm^{-1}): 3216 (OH), 1760 (CO), 1623 (CO); ^{1}H NMR (200 MHz, DMSO-d_6) δ: 3.93 (3H, s, CH_3), 7.23 (1H, td, J = 9.2, 9.1, 2.6 Hz, H-6), 7.66 (1H, dd, J = 9.1, 4.5 Hz, H-7), 7.86 (1H, dd, J = 9.2, 2.6 Hz, H-4), 8.56 (1H, s, H-2), 13.94 (1H, s, OH); ^{13}C NMR (50 MHz, DMSO-d_6) δ: 33.7 (q), 106.2 (d, J_{C4-F} = 24.8 Hz), 111.1 (s, J_{C7a-F} = 4.4 Hz), 111.7 (d, J_{C6-F} = 25.7 Hz), 112.8 (d, J_{C7-F} = 9.8 Hz), 126.8 (s, J_{C3a-F} = 11.2 Hz), 134.0 (s), 142.4 (d), 159.3 (s, J_{C5-F} = 234.3 Hz), 164.8 (s), 179.9 (s); *Anal.* Calculated for $C_{11}H_8FNO_3$ (MW: 221.18): C, 59.73; H, 3.65; N, 6.33%. Found: C, 60.01; H, 3.81; N, 6.53%.

*5.1.2.3. (1-Methyl-1H-indol-3-yl)-oxo-acetic acid (**6c**).* Yellow solid; yield: 78%; mp: 150.6 °C; IR (cm^{-1}): 3261 (OH), 1748 (CO), 1623 (CO); ^{1}H NMR (200 MHz, DMSO-d_6) δ: 3.93 (3H, s, CH_3), 7.28–7.41 (2H, m, H-5 and H-6), 7.62 (1H, m, H-7), 8.20 (1H, m, H-4), 8.49 (1H, s, H-2), 13.88 (1H, s, OH); ^{13}C NMR (50 MHz, DMSO-d_6) δ: 33.4 (q), 111.1 (s), 111.2 (d), 121.2 (d), 123.1 (d), 123.7 (d), 126.0 (s), 137.3 (s), 141.3 (d), 165.2 (s), 180.2 (s); *Anal.* Calculated for $C_{11}H_9NO_3$ (MW: 203.19): C, 65.02; H, 4.46; N, 6.89%. Found: C, 65.28; H, 4.26; N, 6.74%.

*5.1.2.4. (5-Methoxy-1-methyl-1H-indol-3-yl)-oxo-acetic acid (**6d**).* Yellow solid; yield: 86%; mp: 196.2 °C; IR (cm^{-1}): 3216 (OH), 1765 (CO), 1628 (CO); ^{1}H NMR (200 MHz, DMSO-d_6) δ: 3.82 (3H, s, CH_3), 3.89 (3H, s, OCH_3), 6.98 (1H, dd, *J* = 8.9, 2.5 Hz, H-6), 7.52 (1H, d, *J* = 8.9 Hz, H-7), 7.7 (1H, d, *J* = 2.5 Hz, H-4), 8.41 (1H, s, H-2), 13.89 (1H, s, OH); ^{13}C NMR (50 MHz, DMSO-d_6) δ: 33.5 (q), 55.3 (q), 103.2 (d), 110.9 (s), 112.0 (d), 113.1 (d), 127.0 (s), 132.2 (s), 141.0 (d), 156.4 (s), 165.3 (s), 180.0 (s); *Anal.* Calculated for $C_{12}H_{11}NO_4$ (MW: 233.22): C, 61.80; H, 4.75; N, 6.01%. Found: C, 61.58; H, 4.55; N, 6.23%.

*5.1.3. General procedure for the synthesis of 1-methyl-N'-{[(1-methyl-1H-indol-3-yl)(oxo)acetyl]oxy}-1H-indole-3-carboximidamides (**8a-n**) and (1-methyl-1H-indol-3-yl)[3-(5-methoxy-1-methyl-1H-indol-3-yl)-1,2,4-oxadiazol-5-yl]methanone (**3o-q**)*

To a solution of the proper 5-substituted (1-methyl-1*H*-indol-3-yl)-oxo-acetic acid **6a-d** (1.42 mmol) and 1-hydroxybenzotriazole hydrate (HOBt) (230 mg, 1.70 mmol) in anhydrous dimethylformamide (DMF) (2 mL) at 0 °C, *N*-ethyl-*N*′-(3-dimethylaminopropyl)carbodiimide hydrochloride (EDC·HCl) (326 mg, 1.70 mmol) was added in portions. After 15 min, a DMF (1 mL) solution of trimethylamine (Et_3N) (0.2 mL, 1.42 mmol) and appropriate 1-methyl-1*H*-indole-3-carboxamidine **7a-e** (0.71 mmol) was added dropwise at 0 °C. The reaction mixture was stirred at 0 °C for 15 min. The mixture was poured into water and ice and the obtained precipitate was filtered off and dried, to give the desired derivatives **8a-n** and **3o-q**, which were recrystallized from ethanol (for compounds **8a-n**) or purified by column chromatography (for compounds **3o-q**) using dichloromethane as eluent.

*5.1.3.1. N'-{[(5-methoxy-1-methyl-1H-indol-3-yl)(oxo)acetyl]oxy}-1-methyl-1H-indole-3-carboximidamide (**8a**). Workup:* Yellow solid; yield: 85%; mp: 101.5 °C; IR (cm^{-1}): 1612 (CO), 1740 (CO), 3324, 3360 (NH_2); ^{1}H NMR (200 MHz, DMSO-d_6) δ: 3.82 (3H, s, CH_3), 3.84 (3H, s, CH_3), 3.90 (3H, s, OCH_3), 6.69 (2H, s, NH_2), 6.97–7.03 (2H, m, H-5 and H-6′), 7.15–7.23 (1H, m, H-6), 7.45–7.57 (2H, m, H-7′ and H-4), 7.73 (1H, d, *J* = 2.4 Hz, H-4′), 7.98–8.02 (2H, m, H-4 and H-2), 8.38 (1H, s, H-2'); *Anal.* Calculated for $C_{22}H_{20}N_4O_4$ (MW: 404.42): C, 65.34; H, 4.98; N, 13.85%. Found: C, 65.02; H, 5.06; N, 13.62%.

*5.1.3.2. N'-{[(5-bromo-1-methyl-1H-indol-3-yl)(oxo)acetyl]oxy}-1-methyl-1H-indole-3-carboximidamide (**8b**).* Yellow solid; yield: 84%; mp: 143.6 °C; IR (cm^{-1}): 1624 (CO), 1740 (CO), 3334, 3406 (NH_2); ^{1}H NMR (200 MHz, DMSO-d_6) δ: 3.82 (3H, s, CH_3), 3.93 (3H, s, CH_3), 6.72 (2H, s, NH_2), 6.91–7.00 (1H, m, H-5), 7.15–7.23 (1H, m, H-6), 7.44–7.49 (1H, m, H-7), 7.54 (1H, dd, *J* = 8.7, 1.9 Hz, H-6′), 7.65 (1H, d, *J* = 8.7 Hz, H-7′), 7.92–7.98 (2H, m, H-4 and H-2), 8.36 (1H, d, *J* = 1.9 Hz, H-4′), 8.52 (1H, s, H-2'); *Anal.* Calculated for $C_{21}H_{17}BrN_4O_3$ (MW: 453.29): C, 55.64; H, 3.78; N, 12.36%. Found: C, 55.92; H, 3.60; N, 12.12%.

*5.1.3.3. 1-Methyl-N'-{[(1-methyl-1H-indol-3-yl)(oxo)acetyl]oxy}-1H-indole-3-carboximidamide (**8c**).* Yellow solid; yield: 95%; mp: 121.6 °C; IR (cm^{-1}): 1623 (CO), 1748 (CO), 3381, 3495 (NH_2); ^{1}H NMR (200 MHz, DMSO-d_6) δ: 3.81 (3H, s, CH_3), 3.93 (3H, s, CH_3), 6.70 (2H, s, NH_2), 6.95 (1H, t, *J* = 7.4 Hz, H-5), 7.18 (1H, t, *J* = 7.6 Hz, H-5′), 7.36–7.48 (3H, m, H-6, H-6′ and H-7), 7.61–7.66 (1H, m, H-7′), 7.96–8.00 (2H, m, H-4 and H-2), 8.22–8.30 (1H, m, H-4), 8.46 (1H, s, H-2'); *Anal.* Calculated for $C_{21}H_{18}N_4O_3$ (MW: 374.39): C, 67.37; H, 4.85; N, 14.96%. Found: C, 67.65; H, 4.97; N, 15.11%.

*5.1.3.4. 5-Bromo-N'-{[(5-fluoro-1-methyl-1H-indol-3-yl)(oxo)acetyl]oxy}-1-methyl-1H-indole-3-carboximidamide (**8d**).* Yellow solid; yield: 90%; mp: 135.8 °C; IR (cm^{-1}): 1612 (CO), 1740 (CO), 3374, 3475 (NH_2); ^{1}H NMR (200 MHz, DMSO-d_6) δ: 3.82 (3H, s, CH_3), 3.95 (3H, s, CH_3), 6.79 (2H, s, NH_2), 7.19–7.34 (2H, m, H-6 and H-6′), 7.47 (1H, d, *J* = 8.7 Hz, H-7), 7.68 (1H, dd, *J* = 9.0, 4.4 Hz, H-7′), 7.90 (1H, dd, *J* = 9.6, 2.5 Hz, H-4′), 8.04 (1H, s, H-2), 8.21 (1H, m, H-4), 9.09 (1H, s, H-2'); *Anal.* Calculated for $C_{21}H_{16}BrFN_4O_3$ (MW: 471.28): C, 53.52; H, 3.42; N, 11.89%. Found: C, 53.70; H, 3.51; N, 11.62%.

*5.1.3.5. 5-Bromo-1-methyl-N'-{[(1-methyl-1H-indol-3-yl)(oxo)acetyl]oxy}-1H-indole-3-carboximidamide (**8e**).* Yellow solid; yield: 89%; mp: 139.8 °C; IR (cm^{-1}): 1621 (CO), 1740 (CO), 3330, 3480 (NH_2); ^{1}H NMR (200 MHz, DMSO-d_6) δ: 3.82 (3H, s, CH_3), 3.94 (3H, s, CH_3), 6.77 (2H, s, NH_2), 7.29–7.39 (3H, m, H-5′, H-6′ and H-6), 7.48 (1H, d, *J* = 8.8 Hz, H-7), 7.61–7.65 (1H, m, H-7′), 8.04 (1H, s, H-2), 8.19–8.28 (2H, m, H-4 and H-4′), 8.49 (1H, s, H-2'); *Anal.* Calculated for $C_{21}H_{17}BrN_4O_3$ (MW: 453.29): C, 55.64; H, 3.78; N, 12.36%. Found: C, 55.85; H, 3.58; N, 12.28%.

*5.1.3.6. 5-Bromo-N'-{[(5-methoxy-1-methyl-1H-indol-3-yl)(oxo)acetyl]oxy}-1-methyl-1H-indole-3-carboximidamide (**8f**).* Yellow solid; yield: 95%; mp: 133.1 °C; IR (cm^{-1}): 1622 (CO), 1740 (CO), 3324, 3470 (NH_2); ^{1}H NMR (200 MHz, DMSO-d_6) δ: 3.83 (6H, bs, CH_3 x 2), 3.90 (3H, s, OCH_3), 6.78 (2H, s, NH_2), 6.99 (1H, dd, *J* = 8.9, 2.4 Hz, H-6′), 7.32 (1H, dd, *J* = 8.8, 1.8 Hz, H-6), 7.42–7.56 (2H, m, H-7 and H-7′), 7.72 (1H, d, *J* = 2.4 Hz, H-4′), 8.45 (1H, s, H-2), 8.20–8.27 (1H, m, H-4), 8.41 (1H, s, H-2'); *Anal.* Calculated for $C_{22}H_{19}BrN_4O_4$ (MW: 483.31): C, 54.67; H, 3.96; N, 11.59%. Found: C, 54.92; H, 3.88; N, 11.88%.

*5.1.3.7. 5-Fluoro-1-methyl-N'-{[(1-methyl-1H-indol-3-yl)(oxo)acetyl]oxy}-1H-indole-3-carboximidamide (**8g**).* Yellow solid; yield: 98%; mp: 101.1 °C; IR (cm^{-1}): 1637 (CO), 1725 (CO), 3392, 3520 (NH_2); ^{1}H NMR (200 MHz, DMSO-d_6) δ: 3.83 (3H, s, CH_3), 3.94 (3H, s, CH_3), 6.74 (2H, s, NH_2), 7.05 (1H, td, *J* = 9.1, 9.1, 2.6 Hz, H-6), 7.34–7.39 (2H, m, H-5′ and H-6′), 7.50 (1H, dd, *J* = 9.1, 4.5 Hz, H-7), 7.61–7.65 (1H, m, H-7′), 7.75 (1H, m, H-4), 8.06 (1H, s, H-2), 8.21–8.25 (1H, m, H-4′), 8.47 (1H, m, H-2'); *Anal.* Calculated for $C_{21}H_{17}FN_4O_3$ (MW: 392.38): C, 64.28; H, 4.37; N, 14.28%. Found: C, 64.55; H, 4.48; N, 14.48%.

*5.1.3.8. 5-Fluoro-N'-{[(5-fluoro-1-methyl-1H-indol-3-yl)(oxo)acetyl]oxy}-1-methyl-1H-indole-3-carboximidamide (**8h**).* Yellow solid; yield: 91%; mp: 146.3 °C; IR (cm^{-1}): 1628 (CO), 1736 (CO), 3353, 3450 (NH_2); ^{1}H NMR (200 MHz, DMSO-d_6) δ: 3.82 (3H, s, CH_3), 3.94 (3H, s, CH_3), 6.75 (2H, s, NH_2), 7.05 (1H, td, *J* = 9.3, 9.2, 2.5 Hz, H-6), 7.25 (1H, td, *J* = 9.2, 9.1, 2.4 Hz, H-6′), 7.50 (1H, dd, *J* = 9.1, 4.5 Hz, H-7′), 7.64–7.71 (2H, m, H-7 and H-4′), 7.90 (1H, dd, *J* = 9.6, 2.5 Hz, H-4), 8.05 (1H, s, H-2), 8.53 (1H, s, H-2'); *Anal.* Calculated for $C_{21}H_{16}F_2N_4O_3$ (MW: 410.37): C, 61.46; H, 3.93; N, 13.65%. Found: C, 61.59; H, 4.10; N, 13.82%.

*5.1.3.9. N'-{[(5-bromo-1-methyl-1H-indol-3-yl)(oxo)acetyl]oxy}-5-fluoro-1-methyl-1H-indole-3-carboximidamide (**8i**).* Yellow solid; yield: 85%; mp: 168.8 °C; IR (cm^{-1}): 1623 (CO), 1735 (CO), 3353, 3410 (NH_2); ^{1}H NMR (200 MHz, DMSO-d_6) δ: 3.82 (3H, s, CH_3), 3.93

(3H, s, CH_3), 6.78 (2H, s, NH_2), 7.05 (1H, td, *J* = 9.1, 9.1, 2.5 Hz, H-6), 7.46–7.55 (2H, m, H-6′ and H-7′), 7.61–7.71 (2H, m, H-7 and H-4), 8.06 (1H, s, H-2), 8.35 (1H, d, *J* = 1.7 Hz, H-4′), 8.53 (1H, s, H-2’); *Anal.* Calculated for $C_{21}H_{16}BrFN_4O_3$ (MW: 471.28): C, 53.52; H, 3.42; N, 11.89%. Found: C, 53.72; H, 3.27; N, 11.80%.

*5.1.3.10. 5-Fluoro-N’-{[(5-methoxy-1-methyl-1H-indol-3-yl)(oxo)acetyl]oxy}-1-methyl-1H-indole-3-carboximidamide (**8j**).* Yellow solid; yield: 84%; mp: 114.8 °C; IR (cm^{-1}): 1637 (CO), 1736 (CO), 3243, 3374 (NH_2); ^1H NMR (200 MHz, DMSO-d_6) δ: 3.82–3.83 (6H, m, CH_3 x 2), 3.90 (3H, s, OCH_3), 6.75 (2H, s, NH_2), 6.96–7.11 (2H, m, H-6 and H-6′), 7.45–7.55 (2H, m, H-7 and H-7′), 7.72–7.78 (2H, m, H-4 and H-4′), 8.05 (1H, s, H-2), 8.35 (1H, s, H-2’); *Anal.* Calculated for $C_{22}H_{19}FN_4O_4$ (MW: 422.41): C, 62.55; H, 4.53; N, 13.26%. Found: C, 62.80; H, 4.41; N, 13.39%.

*5.1.3.11. N’-{[(5-bromo-1-methyl-1H-indol-3-yl)(oxo)acetyl]oxy}-5-chloro-1-methyl-1H-indole-3-carboximidamide (**8k**).* Yellow solid; yield: 95%; mp: 131.3 °C; IR (cm^{-1}): 1628 (CO), 1748 (CO), 3330, 3347 (NH_2); ^1H NMR (200 MHz, DMSO-d_6) δ: 3.82 (3H, s, CH_3), 3.93 (3H, s, CH_3), 6.81 (2H, s, NH_2), 7.18 (1H, dd, *J* = 8.6, 1.9 Hz, H-6′), 7.49–7.54 (2H, m, H-6 and H-7), 7.63 (1H, d, *J* = 8.6 Hz, H-7′), 7.94–7.95 (1H, m, H-4), 8.05 (1H, s, H-2), 8.36 (1H, d, *J* = 1.9 Hz, H-4′), 8.53 (1H, s, H-2’); *Anal.* Calculated for $C_{21}H_{16}BrClN_4O_3$ (MW: 487.73): C, 51.71; H, 3.31; N, 11.49%. Found: C, 51.90; H, 3.45; N, 11.60%.

*5.1.3.12. 5-Chloro-N’-{[(5-methoxy-1-methyl-1H-indol-3-yl)(oxo)acetyl]oxy}-1-methyl-1H-indole-3-carboximidamide (**8l**).* Yellow solid; yield: 88%; mp: 112.2 °C; IR (cm^{-1}): 1629 (CO), 1726 (CO), 3347, 3450 (NH_2); ^1H NMR (200 MHz, DMSO-d_6) δ: 3.83 (6H, s, CH_3 x 2), 3.90 (3H, s, OCH_3), 6.77 (2H, s, NH_2), 6.99 (1H, dd, *J* = 8.9, 2.5 Hz, H-6′), 7.21 (1H, dd, *J* = 8.8, 2.1 Hz, H-6), 7.51–7.55 (2H, m, H-7 and H-7′), 7.73 (1H, d, *J* = 2.5 Hz, H-4′), 8.04–8.06 (2H, m, H-4 and H-2), 8.40 (1H, s, H-2’); *Anal.* Calculated for $C_{22}H_{19}ClN_4O_4$ (MW: 438.86): C, 60.21; H, 4.36; N, 12.77%. Found: C, 60.38; H, 4.49; N, 12.62%.

*5.1.3.13. 5-Chloro-1-methyl-N’-{[(1-methyl-1H-indol-3-yl)(oxo)acetyl]oxy}-1-methyl-1H-indole-3-carboximidamide (**8m**).* Yellow solid; yield: 90%; mp: 137.3 °C; IR (cm^{-1}): 1625 (CO), 1744 (CO), 3336, 3490 (NH_2); ^1H NMR (200 MHz, DMSO-d_6) δ: 3.82 (3H, s, CH_3), 3.94 (3H, s, CH_3), 6.77 (2H, s, NH_2), 7.20 (1H, dd, *J* = 8.7, 2.1 Hz, H-6), 7.33–7.39 (2H, m, H-5′ and H-6′), 7.52 (1H, d, *J* = 8.7 Hz, H-7), 7.61–7.65 (1H, m, H-7′), 8.03–8.06 (2H, m, H-4 and H-2), 8.21–8.27 (1H, m, H-4′), 8.48 (1H, s, H-2’); *Anal.* Calculated for $C_{21}H_{17}ClN_4O_3$ (MW: 408.84): C, 61.69; H, 4.19; N, 13.70%. Found: C, 61.78; H, 4.33; N, 13.76%.

*5.1.3.14. 5-Methoxy-N’-{[(5-methoxy-1-methyl-1H-indol-3-yl)(oxo)acetyl]oxy}-1-methyl-1H-indole-3-carboximidamide (**8n**).* Yellow solid; yield: 86%; mp: 134.3 °C; IR (cm^{-1}): 1624 (CO), 1740 (CO), 3330, 3450 (NH_2); ^1H NMR (200 MHz, DMSO-d_6) δ: 3.80 (6H, bs, CH_3 x 2), 3.87 (6H, bs, OCH_3 x 2), 6.91–7.07 (3H, m, NH_2 and H-6), 7.24–7.63 (5H, m, H-6′, H-7′, H-7, H-4′ and H-4), 7.69–7.86 (1H, m, H-2′), 8.24–8.33 (1H, m, H-2’); *Anal.* Calculated for $C_{23}H_{22}N_4O_5$ (MW: 434.16): C, 63.59; H, 5.10; N, 12.90%. Found: C, 63.70; H, 5.35; N, 13.04%.

*5.1.3.15. (5-Bromo-1-methyl-1H-indol-3-yl)[3-(5-methoxy-1-methyl-1H-indol-3-yl)-1,2,4-oxadiazol-5-yl]methanone (**3o**).* Yellow solid; yield: 78%; mp: 218 °C (dec.); IR (cm^{-1}): 1632 (CO); ^1H NMR (200 MHz, DMSO-d_6) δ: 3.86 (3H, s, CH_3), 3.93 (3H, s, CH_3), 4.03 (3H, s, OCH_3), 6.98 (1H, dd, *J* = 9.1, 2.4 Hz, H-6′), 7.52–7.60 (3H, m, H-6, H-7 and H-7′), 7.67–7.73 (1H, m, H-4′), 8.34 (1H, s, H-2’), 8.46 (1H, d, *J* = 1.8 Hz, H-4), 9.10 (1H, s, H-2); *Anal.* Calculated for $C_{22}H_{17}BrN_4O_3$ (MW: 465.30): C, 56.79; H, 3.68; N, 12.04%. Found: C, 56.99; H, 3.51; N, 12.34%.

*5.1.3.16. (5-Fluoro-1-methyl-1H-indol-3-yl)[3-(5-methoxy-1-methyl-1H-indol-3-yl)-1,2,4-oxadiazol-5-yl]methanone (**3p**).* Yellow solid; yield: 80%; mp: 227 °C (dec.); IR (cm^{-1}): 1629 (CO); ^1H NMR (200 MHz, DMSO-d_6) δ: 3.86 (3H, s, CH_3), 3.92 (3H, s, CH_3), 4.04 (3H, s, OCH_3), 6.98 (1H, dd, *J* = 8.9, 2.4 Hz, H-6′), 7.30 (1H, td, *J* = 9.3, 9.1, 2.5 Hz, H-6), 7.52–7.56 (2H, m, H-7′ and H-4′), 7.74 (1H, dd, *J* = 9.1, 4.4 Hz, H-7), 8.00 (1H, dd, *J* = 9.3, 2.5 Hz, H-4), 8.34 (1H, s, H-2’), 9.11 (1H, s, H-2); *Anal.* Calculated for $C_{22}H_{17}FN_4O_3$ (MW: 404.39): C, 65.34; H, 4.25; N, 13.85%. Found: C, 65.49; H, 4.38; N, 13.64%.

*5.1.3.17. [3-(5-Methoxy-1-methyl-1H-indol-3-yl)-1,2,4-oxadiazol-5-yl](1-methyl-1H-indol-3-yl)methanone (**3q**).* Yellow solid; yield: 81%; mp: 252 °C (dec.); IR (cm^{-1}): 1628 (CO); ^1H NMR (200 MHz, DMSO-d_6) δ: 3.87 (3H, s, CH_3), 3.93 (3H, s, CH_3), 4.03 (3H, s, OCH_3), 6.98 (1H, dd, *J* = 9.1, 2.7 Hz, H-6′), 7.39–7.47 (2H, m, H-5 and H-6), 7.53–7.57 (2H, m, H-7 and H-7′), 7.68–7.73 (1H, m, H-4′), 8.32–8.37 (2H, m, H-4 and H-2’), 9.07 (1H, s, H-2); *Anal.* Calculated for $C_{22}H_{18}N_4O_3$ (MW: 386.40): C, 68.35; H, 4.70; N, 14.50%. Found: C, 68.49; H, 4.58; N, 14.64%.

*5.1.4. General procedure for the synthesis of (1-methyl-1H-indol-3-yl)[3-(1-methyl-1H-indol-3-yl)-1,2,4-oxadiazol-5-yl]methanones (**3a-n**)*

To a solution of **8a-n** (0.19 mmol) in acetone (15 mL), an aqueous solution of sodium hydroxide (0.1 mL, 2 M) was added and stirred at room temperature for 30–60 min. The precipitated solid was filtered off, washed with water and dried under high *vacuum*. The product was purified by column chromatography using dichloromethane as eluent.

*5.1.4.1. (5-Methoxy-1-methyl-1H-indol-3-yl)[3-(1-methyl-1H-indol-3-yl)-1,2,4-oxadiazol-5-yl]methanone (**3a**).* Conditions: 30 min at room temperature; cream-white solid; yield: 82%; mp: 265 °C (dec.); IR (cm^{-1}): 1611 (CO); ^1H NMR (200 MHz, DMSO-d_6) δ: 3.86 (3H, s, CH_3), 3.96 (3H, s, CH_3), 4.01 (3H, s, OCH_3), 7.04 (1H, dd, *J* = 8.9, 2.5 Hz, H-6), 7.25–7.40 (2H, m, H-5′ and H-6′), 7.63 (2H, m, H-7 and H-7′), 7.84 (1H, d, *J* = 2.5 Hz, H-4), 8.11 (1H, m, H-4′), 8.40 (1H, s, H-2’), 8.97 (1H, s, H-2); *Anal.* Calculated for $C_{22}H_{18}N_4O_3$ (MW: 386.40): C, 68.38; H, 4.70; N, 14.50%. Found: C, 68.48; H, 4.57; N, 14.38%.

*5.1.4.2. (5-Bromo-1-methyl-1H-indol-3-yl)[3-(1-methyl-1H-indol-3-yl)-1,2,4-oxadiazol-5-yl]methanone (**3b**).* Conditions: 30 min at room temperature; light yellow solid; yield: 78%; mp: 238 °C (dec.); IR (cm^{-1}): 1623 (CO); ^1H NMR (200 MHz, DMSO-d_6) δ: 3.96 (3H, s, CH_3), 4.04 (3H, s, CH_3), 7.27–7.39 (2H, m, H-5′ and H-6′), 7.54–7.72 (3H, m, H-6, H-7 and H-7′), 8.02–8.12 (1H, m, H-4′), 8.41–8.46 (2H, m, H-4 and H-2’), 9.09 (1H, s, H-2); *Anal.* Calculated for $C_{21}H_{15}BrN_4O_2$ (MW: 435.27): C, 57.95; H, 3.47; N, 12.87%. Found: C, 57.75; H, 3.32; N, 12.66%.

*5.1.4.3. (1-Methyl-1H-indol-3-yl)[3-(1-methyl-1H-indol-3-yl)-1,2,4-oxadiazol-5-yl]methanone (**3c**).* Conditions: 30 min at room temperature; yellow solid; yield: 77%; mp: 246 °C (dec.); IR (cm^{-1}): 1634 (CO); ^1H NMR (200 MHz, DMSO-d_6) δ: 3.96 (3H, s, CH_3), 4.04 (3H, s, CH_3), 7.27–7.47 (4H, m, H-5, H-5′, H-6 and H-6′), 7.62–7.72 (2H, m, H-7 and H-7′), 8.07–8.13 (1H, m, H-4′), 8.32–8.37 (1H, m, H-4), 8.42 (1H, s, H-2’), 9.06 (1H, s, H-2); ^{13}C NMR (50 MHz, DMSO-d_6) δ: 33.0 (q), 33.7 (q), 100.9 (s), 110.9 (d), 111.5 (d), 112.7 (s), 120.7 (d), 121.4 (d), 121.5 (d), 122.8 (d), 123.6 (d), 124.2 (d), 124.5 (s), 126.3 (s), 133.4 (d), 137.4 (s), 137.5 (s), 142.3 (d), 165.0 (s), 169.7 (s), 170.4 (s); *Anal.* Calculated for $C_{21}H_{16}N_4O_2$ (MW: 356.38): C, 70.77; H, 4.53; N, 15.72%. Found: C, 70.99; H, 4.58; N, 15.54%.

*5.1.4.4. [3-(5-Bromo-1-methyl-1H-indol-3-yl)-1,2,4-oxadiazol-5-yl](5-fluoro-1-methyl-1H-indol-3-yl)methanone (**3d**).* Conditions: 1 h at room temperature; light yellow solid; yield: 81%; mp: 256 °C (dec.); IR (cm^{-1}): 1610 (CO); ^{1}H NMR (200 MHz, DMSO-d_6) δ: 3.96 (3H, s, CH_3), 4.04 (3H, s, CH_3), 7.29 (1H, td, J = 9.2, 9.1, 2.6 Hz, H-6), 7.48 (1H, dd, J = 8.8, 1.9 Hz, H-6′), 7.64 (1H, d, J = 8.8 Hz, H-7′), 7.74 (1H, dd, J = 9.1, 4.4 Hz, H-7), 7.99 (1H, dd, J = 9.5, 2.6 Hz, H-4), 8.21 (1H, d, J = 1.9 Hz, H-4′), 8.45 (1H, s, H-2’), 9.09 (1H, s, H-2); *Anal.* Calculated for $C_{21}H_{14}BrFN_4O_2$ (MW: 453.26): C, 55.65; H, 3.11; N, 12.36%. Found: C, 55.55; H, 3.31; N, 12.53%.

*5.1.4.5. [3-(5-Bromo-1-methyl-1H-indol-3-yl)-1,2,4-oxadiazol-5-yl](1-methyl-1H-indol-3-yl)methanone (**3e**).* Conditions: 30 min at room temperature; light yellow solid; yield: 80%; mp: 250 °C (dec.); IR (cm^{-1}): 1628 (CO); ^{1}H NMR (200 MHz, DMSO-d_6) δ: 3.97 (3H, s, CH_3), 4.04 (3H, s, CH_3), 7.40–7.52 (3H, m, H-5, H-6 and H-7), 7.64–7.73 (2H, m, H-6′ and H-7′), 8.23 (1H, d, J = 1.8 Hz, H-4′), 8.32–8.36 (1H, m, H-4), 8.47 (1H, s, H-2’), 9.05 (1H, s, H-2); *Anal.* Calculated for $C_{21}H_{15}BrN_4O_2$ (MW: 435.27): C, 57.95; H, 3.47; N, 12.87%. Found: C, 57.77; H, 3.55; N, 12.69%.

*5.1.4.6. [3-(5-Bromo-1-methyl-1H-indol-3-yl)-1,2,4-oxadiazol-5-yl](5-methoxy-1-methyl-1H-indol-3-yl)methanone (**3f**).* Conditions: 30 min at room temperature; yellow solid; yield: 88%; mp: 255 °C (dec.); IR (cm^{-1}): 1623 (CO); ^{1}H NMR (200 MHz, DMSO-d_6) δ: 3.86 (3H, s, CH_3), 3.96 (3H, s, CH_3), 4.00 (3H, s, OCH_3), 7.04 (1H, dd, J = 8.9, 2.5 Hz, H-6), 7.49 (1H, dd, J = 8.8, 1.9 Hz, H-6′), 7.58–7.67 (2H, m, H-7′ and H-7), 7.83 (1H, d, J = 2.5 Hz, H-4), 8.22 (1H, d, J = 1.9 Hz, H-4′), 8.45 (1H, s, H-2’), 8.95 (1H, s, H-2); *Anal.* Calculated for $C_{22}H_{17}BrN_4O_3$ (MW: 465.30): C, 56.79; H, 3.68; N, 12.04%. Found: C, 56.95; H, 3.78; N, 12.11%.

*5.1.4.7. [3-(5-Fluoro-1-methyl-1H-indol-3-yl)-1,2,4-oxadiazol-5-yl](1-methyl-1H-indol-3-yl)methanone (**3g**).* Conditions: 1 h at room temperature; yellow solid; yield: 80%; mp: 242 °C (dec.); IR (cm^{-1}): 1634 (CO); ^{1}H NMR (200 MHz, DMSO-d_6) δ: 3.97 (3H, s, CH_3), 4.03 (3H, s, CH_3), 7.22 (1H, td, J = 9.3, 9.2, 2.6 Hz, H-6′), 7.36–7.47 (2H, m, H-5 and H-6), 7.64–7.78 (3H, m, H-7, H-7′ and H-4′), 8.32–8.36 (1H, m, H-4), 8.47 (1H, s, H-2’), 9.04 (1H, m, H-2); ^{13}C NMR (50 MHz, DMSO-d_6) δ: 33.4 (q), 33.7 (q), 101.0 (s, J_{C7a-F} = 4.2 Hz), 105.5 (d, J_{C4-F} = 24.4 Hz), 111.0 (d, J_{C6-F} = 26.0 Hz), 111.5 (d), 112.4 (d, J_{C7-F} = 9.9 Hz), 112.7 (s), 121.5 (d), 123.6 (d), 124.1 (d), 124.9 (s, J_{C3a-F} = 10.8 Hz), 126.3 (s), 134.1 (s), 134.9 (d), 137.5 (s), 142.3 (d), 158.2 (s, J_{C5-F} = 254.9 Hz), 164.7 (s), 169.8 (s), 170.3 (s); *Anal.* Calculated for $C_{21}H_{15}FN_4O_2$ (MW: 374.37): C, 67.37; H, 4.04; N, 14.97%. Found: C, 67.51; H, 3.88; N, 15.11%.

*5.1.4.8. (5-Fluoro-1-methyl-1H-indol-3-yl)[3-(5-fluoro-1-methyl-1H-indol-3-yl)-1,2,4-oxadiazol-5-yl]methanone (**3h**).*
Conditions: 30 min at room temperature; cream-white solid; yield: 82%; mp: 265 °C (dec.); IR (cm^{-1}): 1629 (CO); ^{1}H NMR (200 MHz, DMSO-d_6) δ: 3.97 (3H, s, CH_3), 4.04 (3H, s, CH_3), 7.17–7.35 (2H, m, H-6 and H-6′), 7.65–7.78 (3H, m, H-7, H-7′ and H-4′), 8.00 (1H, dd, J = 9.6, 2.6 Hz, H-4), 8.47 (1H, s, H-2’), 9.09 (1H, s, H-2); *Anal.* Calculated for $C_{21}H_{14}F_2N_4O_2$ (MW: 392.36): C, 64.28; H, 3.60; N, 14.28%. Found: C, 64.43; H, 3.70; N, 14.47%.

*5.1.4.9. (5-Bromo-1-methyl-1H-indol-3-yl)[3-(5-fluoro-1-methyl-1H-indol-3-yl)-1,2,4-oxadiazol-5-yl]methanone (**3i**).*
Conditions: 30 min at room temperature; light yellow solid; yield: 82%; mp: 270 °C (dec.); IR (cm^{-1}): 1634 (CO); ^{1}H NMR (200 MHz, DMSO-d_6) δ: 3.97 (3H, s, CH_3), 4.04 (3H, s, CH_3), 7.22 (1H, td, J = 9.4, 9.3, 2.6 Hz, H-6′), 7.58 (1H, dd, J = 8.6, 1.9 Hz, H-6), 7.65–7.69 (1H, m, H-7), 7.72–7.78 (2H, m, H-7’and H-4′), 8.45 (1H, d, J = 1.9 Hz, H-4), 8.48 (1H, s, H-2′), 9.08 (1H, s, H-2); *Anal.* Calculated for $C_{21}H_{14}BrFN_4O_2$ (MW: 453.26): C, 55.65; H, 3.11; N, 12.36%. Found: C, 55.84; H, 3.26; N, 12.53%.

*5.1.4.10. [3-(5-Fluoro-1-methyl-1H-indol-3-yl)-1,2,4-oxadiazol-5-yl](5-methoxy-1-methyl-1H-indol-3-yl)methanone (**3j**).*
Conditions: 1 h at room temperature; yellow solid; yield: 90%; mp: 250 °C (dec.); IR (cm^{-1}): 1617 (CO); ^{1}H NMR (200 MHz, DMSO-d_6) δ: 3.86 (3H, s, CH_3), 3.97–4.00 (6H, m, CH_3 and OCH_3), 7.02–7.07 (1H, m, H-6′), 7.17–7.27 (1H, m, H-6), 7.58–7.84 (4H, m, H-7, H-7′, H-4 and H-4′), 8.47 (1H, s, H-2’), 8.96 (1H, s, H-2); *Anal.* Calculated for $C_{22}H_{17}FN_4O_3$ (MW: 404.39): C, 65.34; H, 4.24; N, 13.85%. Found: C, 65.55; H, 4.36; N, 13.56%.

*5.1.4.11. (5-Bromo-1-methyl-1H-indol-3-yl)[3-(5-chloro-1-methyl-1H-indol-3-yl)-1,2,4-oxadiazol-5-yl]methanone (**3k**).*
Conditions: 1 h at room temperature; light yellow solid; yield: 79%; mp: 273 °C (dec.); IR (cm^{-1}): 1623 (CO); ^{1}H NMR (200 MHz, DMSO-d_6) δ: 3.97 (3H, s, CH_3), 4.04 (3H, s, CH_3), 7.35–7.40 (1H, m, H-6′), 7.55–7.60 (1H, m, H-6), 7.70 (2H, m, H-7′ and H-7), 8.06 (1H, s, H-4), 8.45 (1H, s, H-4′), 8.48 (1H, s, H-2’), 9.08 (1H, s, H-2); *Anal.* Calculated for $C_{21}H_{14}BrClN_4O_2$ (MW: 469.72): C, 53.70; H, 3.00; N, 11.93%. Found: C, 53.92; H, 3.17; N, 12.09%.

*5.1.4.12. [3-(5-Chloro-1-methyl-1H-indol-3-yl)-1,2,4-oxadiazol-5-yl](5-methoxy-1-methyl-1H-indol-3-yl)methanone (**3l**).*
Conditions: 1 h at room temperature; yellow solid; yield: 81%; mp: 254 °C (dec.); IR (cm^{-1}): 1626 (CO); ^{1}H NMR (200 MHz, DMSO-d_6) δ: 3.86 (3H, s, CH_3), 3.97 (3H, s, CH_3), 4.00 (3H, s, OCH_3), 7.04 (1H, dd, J = 8.9, 2.5 Hz, H-6), 7.38 (1H, dd, J = 8.8, 2.1 Hz, H-6′), 7.61 (1H, d, J = 8.9 Hz, H-7), 7.70 (1H, d, J = 8.8 Hz, H-7′), 7.84 (1H, d, J = 2.5 Hz, H-4), 8.07 (1H, d, J = 2.1 Hz, H-4′), 8.48 (1H, s, H-2’), 8.96 (1H, s, H-2); *Anal.* Calculated for $C_{22}H_{17}ClN_4O_3$ (MW: 420.85): C, 62.79; H, 4.07; N, 13.31%. Found: C, 63.02; H, 4.17; N, 13.44%.

*5.1.4.13. [3-(5-Chloro-1-methyl-1H-indol-3-yl)-1,2,4-oxadiazol-5-yl](1-methyl-1H-indol-3-yl)methanone (**3m**).* Conditions: 30 min at room temperature; light yellow solid; yield: 84%; mp: 250 °C (dec.); IR (cm^{-1}): 1628 (CO); ^{1}H NMR (200 MHz, DMSO-d_6) δ: 3.97 (3H, s, CH_3), 4.04 (3H, s, CH_3), 7.37–7.44 (3H, m, H-5, H-6 and H-6′), 7.68–7.73 (2H, m, H-7′ and H-7), 8.06–8.07 (1H, m, H-4′), 8.31–8.37 (1H, m, H-4), 8.49 (1H, s, H-2’), 9.05 (1H, s, H-2); *Anal.* Calculated for $C_{21}H_{15}ClN_4O_2$ (MW: 390.82): C, 64.54; H, 3.87; N, 14.34%. Found: C, 64.86; H, 3.69; N, 14.21%.

*5.1.4.14. (5-Methoxy-1-methyl-1H-indol-3-yl)[3-(5-methoxy-1-methyl-1H-indol-3-yl)-1,2,4-oxadiazol-5-yl]methanone (**3n**).*
Conditions: 30 min at room temperature; light yellow solid; yield: 79%; mp: 218 °C (dec.); IR (cm^{-1}): 1617 (CO); ^{1}H NMR (200 MHz, DMSO-d_6) δ: 3.86 (6H, m, CH_3 x 2), 3.93 (3H, s, OCH_3), 4.00 (3H, s, OCH_3), 6.95–7.07 (2H, m, H-6 and H-6′), 7.52–7.63 (3H, m, H-7, H-7′ and H-4′), 7.84 (1H, d, J = 2.4 Hz, H-4), 8.33 (1H, s, H-2’), 8.98 (1H, s, H-2); *Anal.* Calculated for $C_{23}H_{20}N_4O_4$ (MW: 416.43): C, 66.34; H, 4.84; N, 13.45%. Found: C, 66.55; H, 4.96; N, 13.22%.

5.2. Biology

5.2.1. Minimum inhibitory concentrations (MICs) determination

MICs were determined by using a microdilution method as recommended by CLSI for bacteria that grow aerobically (CLSI) [Clinical and Laboratory Standards Institute. Methods for Dilution Antimicrobial Susceptibility Tests for Bacteria That Grow

Aerobically; Approved Standard—Ninth Edition. CLSI document M07-A9 (ISBN 1-56238-783-9 [Print]; ISBN 1-56238-784-7 [Electronic]) and Tryptic Soy Broth (TBS) (VWR International, Leuven) as medium. It starts with the preparation of the bacterial suspension by diluting the bacteria grown at 37 °C for 24 h on Tryptic Soy Agar (TSA) in 5 mL of 0.9% NaCl, to obtain a culture suspension whose optical density (O.D.) at 570 nm is of about 0.190 (corresponding to 10^6 CFU/mL), a further dilution 1:20 is always carried out in physiological solution. Serial dilutions 1: 2 of the substance to be tested are performed, starting from the highest concentration, in culture medium (TSB), then 10 μL of the prepared inoculum was added to each well containing substance solution. A positive growth control (test bacterial strain in the medium without inhibitor), a substance control (only the substance solution without inoculum) and a negative control (only the medium without inoculum), to check respectively the bacterial growth, the absorbance of substance at the highest concentration and the sterility of medium, were also included in the assay. The plate thus prepared is incubated at 37 °C for 24 h, MICs were read by a microplate spectrophotometer (GloMax®-Multi Detection System, Promega Italia s.r.l, Milan, Italy) as the lowest concentration of sample whose OD at 570 nm is comparable to OD values of negative control wells.

5.2.2. Inhibition of biofilm formation (crystal violet method)

Bacterial strains were incubated in test tubes with TSB (5 mL) containing 2% w/v glucose at 37 °C for 24 h. After that, the bacterial suspensions were diluted to achieve a turbidity equivalent to a 0.5 McFarland standard. The diluted suspension (2.5 μL) was added to each well of a single cell culture polystyrene sterile, flat-bottom 96-well plate filled with TSB (200 μL) with 2% w/v glucose. Sub-MIC concentration values of all compounds were directly added to the wells to reach concentrations ranging from 100 to 0.1 μM to assess BIC_{50} values that is the concentration at which the percentage of inhibition of biofilm formation is equal to 50%. Plates were incubated at 37 °C for 24 h. After biofilm growth, the content of each well was removed, wells were washed twice with sterile NaCl 0.9% and stained with 200 μL of 0.1% w/v crystal violet solution for 15 min at 37°C. Excess solution was removed and the plate was washed twice, using tap water. A volume of 200 μL of ethanol was added to each stained well to solubilize the dye. Optical density (OD) was read at 600 nm using a microplate reader (GloMax®-Multi Detection System).

The experiments were run at least in triplicates and three independent experiments were performed.

The percentage of inhibition was calculated through the formula: % of inhibition = [(OD growth control - OD sample) / OD growth control] x 100

5.2.3. Screening as sortase A (SrtA) inhibitors

The most promising antibiofilm compounds **3d**, **3h** and **3n** were tested at three screening concentrations (10, 1 and 0.1 μg/mL) (1% DMSO) in black 96-well plates (Greiner Bio-One) in order to evaluate their activity as SrtA inhibitors. A known SrtA inhibitor, 4-(hydroxymercuri)benzoic acid, was used as positive control. The inhibitory activity of the three compounds was evaluated by quantifying the increase in fluorescence intensity upon cleavage of the Fluorescence Resonance Energy Transfer (FRET) peptide substrate into two separate fragments resulting in the release of 5-Fam fluorescence, which can be monitored at excitation/emission ¼ 490/520 nm. A commercial kit (SensoLyte® 520 Sortase A Activity Assay Kit * Fluorimetric*) was used with slight modifications. Briefly, the reactions were performed in a volume of 100 mL containing 1X assay buffer, 2.5 mg/mL SrtA protease recombinant, 4 mM fluorescent peptide substrate, and the prescribed concentrations of the test compounds or positive control. The peptide substrate without the recombinant SrtA was incubated under the same conditions, and used as a negative control. The reactions were conducted adding both the test compounds and the diluted enzyme solution to the microplate wells. Then sortase substrate solution was added into each well. For kinetic reading, fluorescence was immediately measured, at Ex/Em ¼ 490/520 nm, and then data were registered continuously, every 5 min, for 60 min. All the results were expressed in relative fluorescence units (RFU).

5.2.4. Cytotoxicity assay

Skin fibroblasts Hs27 were obtained from the American Type Culture Collection (ATCC, Manassas, VA). Cells were cultured in RPMI-1640 medium, supplemented with 10% heat-inactivated fetal bovine serum (FBS) and 1% streptomycin/penicillin, at 37 °C, under an atmosphere of 5% CO_2. The cells were maintained in 75 cm^2 culture flasks (Greiner-Bio-One, Frickenhausen, Germany) and harvested with trypsin-EDTA (Invitrogen, Paisley, UK) in their exponentially growing phase. Cytotoxicity tests were performed using the SRB assay, as described previously [52]. Briefly, selected compounds **3d**, **3h** and **3n** were dissolved in sterile DMSO at 2 μM and stored at 20 °C, in the dark. They were diluted in sterile culture medium immediately before their use. Cells were seeded into a 96-well flat-bottom plates at 8×10^3 cells/well and incubated for 24 h at 37 °C to create a confluent monolayer. Then, the cells were treated with each compound in triplicate at three different concentrations (0.1, 1 and 10 μM); while control cells were exposed to an equivalent concentration of DMSO (0.25% v/v, negative control). At the end of drug incubation (72 h), growth inhibition was expressed as the percentage of control absorbance (corrected for absorbance before drug addition).

Declaration of competing interest

The authors declare that they have no known competing financial interests or personal relationships that could have appeared to influence the work reported in this paper.

Acknowledgments

This research was funded by European Union 2014–2020 PON Ricerca e Innovazione grant from the Italian Ministry of Education, University and Research, entitled “PROGEMA—Processi Green per l’Estrazione di Principi Attivi e la Depurazione di Matrici di Scarto e Non” (ARS01_00432) in favour of P.D.

Appendix A. Supplementary data

Supplementary data to this article can be found online at https://doi.org/10.1016/j.ejmech.2020.112892.

References

[1] D. Schillaci, V. Spano`, B. Parrino, A. Carbone, A. Montalbano, P. Barraja, P. Diana, G. Cirrincione, S. Cascioferro, Pharmaceutical approaches to target antibiotic resistance mechanisms, J. Med. Chem. 60 (2017) 8268–8297, https://doi.org/10.1021/acs.jmedchem7b00215.

[2] G.-F. Zha, S.-M. Wang, K.P. Rakesh, S.N.A. Bukhari, H.M. Manukumar, H.K. Vivek, N. Mallesha, H.-L. Qin, Discovery of novel arylethenesulfonyl fluorides as potential candidates against methicillin-resistant of Staphylococcus aureus (MRSA) for overcoming multidrug resistance of bacterial infections, Eur. J. Med. Chem. 162 (2019) 364–377, https://doi.org/10.1016/j.ejmech.2018.11.012.

[3] X. Zhang, M.H. Marichannegowda, K.P. Rakesh, H.-L. Qin, Master mechanisms of Staphylococcus aureus: consider its excellent protective mechanisms hindering vaccine development!, Microbiol. Res. 212–213 (2018) 59–66, https://doi.org/10.1016/j.micres.2018.05.002.

[4] B. Parrino, P. Diana, G. Cirrincione, S. Cascioferro, Bacterial biofilm inhibition in the development of effective anti-virulence strategy, Open J. Med. Chem. 12 (2018) 84–87, https://doi.org/10.2174/1874104501812010084.

[5] B. Parrino, D. Carbone, G. Cirrincione, P. Diana, S. Cascioferro, Inhibitors of antibiotic resistance mechanisms: clinical applications and future perspectives, Future Med. Chem. 12 (2020) 357–359, https://doi.org/10.4155/fmc-2019-0326.

[6] Y.H.E. Mohammed, H.M. Manukumar, K.P. Rakesh, C.S. Karthik, P. Mallu, H.-L. Qin, Vision for medicine: Staphylococcus aureus biofilm war and unlocking key's for anti-biofilm drug development, Microb. Pathog. 123 (2018) 339–347, https://doi.org/10.1016/j.micpath.2018.07.002.

[7] S. Cascioferro, M.G. Cusimano, D. Schillaci, Antiadhesion agents against Gram-positive pathogens, Future Microbiol. 9 (2014) 1209–1220, https://doi.org/10.2217/fmb.14.56.

[8] K.P. Rakesh, M.H. Marichannegowda, S. Srivastava, X. Chen, S. Long, C.S. Karthik, P. Mallu, H.-L. Qin, Combating a master manipulator: Staphylococcus aureus immunomodulatory molecules as targets for combinatorial drug discovery, ACS Comb. Sci. 20 (2018) 681–693, https://doi.org/10.1021/acscombsci.8b00088.

[9] X. Zhang, H.M. Manukumar, K.P. Rakesh, C.S. Karthik, H.S. Nagendra Prasad, S.N. Swamy, P. Mallu, M. Eissa, H. Yasser, H.-L. Qin, Role of BP*C@AgNPs in Bap-dependent multicellular behavior of clinically important methicillin-resistant Staphylococcus aureus (MRSA) biofilm adherence: a key virulence study, Microb. Pathog. 123 (2018) 275–284, https://doi.org/10.1016/j.micpath.2018.07.025.

[10] E. O'Neill, C. Pozzi, P. Houston, H. Humphreys, D.A. Robinson, A. Loughman, T.J. Foster, J.P. O'Gara, A novel Staphylococcus aureus biofilm phenotype mediated by the fibronectin-binding proteins, FnBPA and FnBPB. J. Bacteriol. 190 (2008) 3835–3850, https://doi.org/10.1128/JB.00167-08.

[11] S.K. Mazmanian, G. Liu, E.R. Jensen, E. Lenoy, O. Schneewind, Staphylococcus aureus sortase mutants defective in the display of surface proteins and in the pathogenesis of animal infections, Proc. Natl. Acad. Sci. U.S.A. 97 (2000) 5510–5515, https://doi.org/10.1073/pnas.080520697.

[12] W.J. Weiss, E. Lenoy, T. Murphy, L. Tardio, P. Burgio, S.J. Projan, O. Schneewind, L. Alksne, Effect of SrtA and SrtB gene expression on the virulence of Staphylococcus aureus in animal models of infection, J. Antimicrob. Chemother. 53 (2004) 480–486, https://doi.org/10.1093/jac/dkh078.

[13] M. Kubica, K. Guzik, J. Koziel, M. Zarebski, W. Richter, B. Gajkowska, A. Golda, A. Maciag-Gudowska, K. Brix, L. Shaw, T. Foster, J. Potempa, A potential new pathway for Staphylococcus aureus dissemination: the silent survival of S. aureus phagocytosed by human monocyte-derived macrophages, PloS One 3 (2008) e1409, https://doi.org/10.1371/journal.pone.0001409.

[14] S. Cascioferro, M. Totsika, D. Schillaci, Sortase A: an ideal target for anti-virulence drug development, Microb. Pathog. 77 (2014) 105–112, https://doi.org/10.1016/j.micpath.2014.10.007.

[15] S. Cascioferro, D. Raffa, B. Maggio, M.V. Raimondi, D. Schillaci, G. Daidone, Sortase A inhibitors: recent advances and future perspectives, J. Med. Chem. 58 (2015) 9108–9123, https://doi.org/10.1021/acs.jmedchem.5b00779.

[16] K.B. Oh, W. Mar, S. Kim, J.Y. Kim, M.N. Oh, J.G. Kim, D. Shin, C.J. Sim, J. Shin, Bis(indole) alkaloids as sortase A inhibitors from the sponge Spongosorites sp, Bioorg. Med. Chem. Lett 15 (2005) 4927–4931, https://doi.org/10.1016/j.bmcl.2005.08.021.

[17] S. Cascioferro, B. Parrino, D. Carbone, D. Schillaci, E. Giovannetti, G. Cirrincione, P. Diana, Thiazoles, their Benzofused Systems, and thiazolidinone derivatives: versatile and promising tools to combat antibiotic resistance, J. Med. Chem. 63 (2020) 7923–7956, https://doi.org/10.1021/acs.jmedchem.9b01245.

[18] B. Parrino, D. Schillaci, I. Carnevale, E. Giovannetti, P. Diana, G. Cirrincione, S. Cascioferro, Synthetic small molecules as anti-biofilm agents in the struggle against antibiotic resistance, Eur. J. Med. Chem. 161 (2019) 154–178, https://doi.org/10.1016/j.ejmech.2018.10.036.

[19] W.-Y. Fang, L. Ravindar, K.P. Rakesh, H.M. Manukumar, C.S. Shantharam, N.S. Alharbi, H.-L. Qin, Synthetic approaches and pharmaceutical applications of chloro-containing molecules for drug discovery: a critical review, Eur. J. Med. Chem. 173 (2019) 117–153, https://doi.org/10.1016/j.ejmech.2019.03.063.

[20] C. Zhao, K.P. Rakesh, L. Ravidar, W.-Y. Fang, H.-L. Qin, Pharmaceutical and medicinal significance of sulfur (SVI)-Containing motifs for drug discovery: a critical review, Eur. J. Med. Chem. 162 (2019) 679–734, https://doi.org/10.1016/j.ejmech.2018.11.017.

[21] H. Liu, S. Long, K.P. Rakesh, G.- F Zha, Structure-activity relationships (SAR) of triazine derivatives: promising antimicrobial agents, Eur. J. Med. Chem. 185 (2020) 111804, https://doi.org/10.1016/j.ejmech.2019.111804.

[22] M. Wang, K.P. Rakesh, J. Leng, W.-Y. Fang, L. Ravindar, D. Channe Gowda, H.-L. Qin, Amino acids/peptides conjugated heterocycles: a tool for the recent development of novel therapeutic agents, Bioorg. Chem. 76 (2018) 113–129, https://doi.org/10.1016/j.bioorg.2017.11.007.

[23] K.P. Rakesh, H.K. Vivek, H.M. Manukumar, C.S. Shantharam, S.N.A. Bukhari, H.-L. Qin, M.B. Sridhara, Promising bactericidal approach of dihydrazone analogues against bio-film forming Gram-negative bacteria and molecular mechanistic studies, RSC Adv. 8 (2018) 5473–5483, https://doi.org/10.1039/C7RA13661G.

[24] Z. Zheng, Q. Liu, W. Kim, N. Tharmalingam, B.B. Fuchs, E. Mylonakis, Antimicrobial activity of 1,3,4-oxadiazole derivatives against planktonic cells and biofilm of Staphylococcus aureus, Future Med. Chem. 10 (2018) 283–296, https://doi.org/10.4155/fmc-2017-0159.

[25] S. Cascioferro, G. Li Petri, B. Parrino, D. Carbone, N. Funel, C. Bergonzini, G. Mantini, H. Dekker, D. Geerke, G.J. Peters, G. Cirrincione, E. Giovannetti, P. Diana, Imidazo[2,1-b] [1,3,4]thiadiazoles with antiproliferative activity against primary and gemcitabine-resistant pancreatic cancer cells, Eur. J. Med. Chem. 189 (2020) 112088, https://doi.org/10.1016/j.ejmech.2020.112088.

[26] S. Cascioferro, G. Li Petri, B. Parrino, B. El Hassouni, D. Carbone, V. Arizza, U. Perricone, A. Padova, N. Funel, G.J. Peters, G. Cirrincione, E. Giovannetti, P. Diana, 3-(6-Phenylimidazo [2,1-b][1,3,4]thiadiazol-2-yl)-1H-indole derivatives as new anticancer agents in the treatment of pancreatic ductal adenocarcinoma, Molecules 25 (2020) 329, https://doi.org/10.3390/molecules25020329.

[27] B. El Hassouni, G. Li Petri, D.S.K. Liu, S. Cascioferro, B. Parrino, A. Ali, A.E. Frampton, E. Giovannetti, Pharmacogenetics of treatments for pancreatic cancer, Expet Opin. Drug Metabol. Toxicol. 15 (2019) 437–447, https://doi.org/10.1080/17425255.2019.1620731.

[28] S. Cascioferro, B. Parrino, V. Spanò, A. Carbone, A. Montalbano, P. Barraja, P. Diana, G. Cirrincione, 1,3,5-Triazines: a promising scaffold for anticancer drugs development, Eur. J. Med. Chem. 142 (2017) 523–549, https://doi.org/10.1016/j.ejmech.2017.09.035.

[29] B. Parrino, C. Ciancimino, A. Carbone, V. Spanò, A. Montalbano, P. Barraja, G. Cirrincione, P. Diana, Synthesis of isoindolo[1,4]benzoxazinone and isoindolo[1,5]benzoxazepine: two new ring systems of pharmaceutical interest, Tetrahedron 71 (2015) 7332–7338, https://doi.org/10.1016/j.tet.2015.04.083.

[30] B. Parrino, A. Carbone, V. Spanò, A. Montalbano, D. Giallombardo, P. Barraja, A. Attanzio, L. Tesoriere, M. Palumbo, C. Sissi, M. Palumbo, G. Cirrincione, P. Diana, Aza-isoindolo and isoindolo-azaquinoxaline derivatives with antiproliferative activity, Eur. J. Med. Chem. 94 (2015) 367–377, https://doi.org/10.1016/j.ejmech.2015.03.009.

[31] B. Parrino, A. Carbone, C. Ciancimino, V. Spanò, A. Montalbano, P. Barraja, G. Cirrincione, P. Diana, C. Sissi, M. Palumbo, O. Pinato, G. Beretta, M. Folini, P. Matyus, B. Balogh, N. Zaffaroni, Water-soluble isoindolo[2,1-a]quinoxalin-6-imines: in vitro antiproliferative activity and molecular mechanism(s) of action, Eur. J. Med. Chem. 94 (2015) 149–162, https://doi.org/10.1016/j.ejmech.2015.03.005.

[32] A. Montalbano, B. Parrino, P. Diana, P. Barraja, A. Carbone, V. Spanò, G. Cirrincione, Synthesis of the new oligopeptide pyrrole derivative isonetropsin and its one pyrrole unit analogue, Tetrahedron 69 (2013) 2550–2554, https://doi.org/10.1016/j.tet.2013.01.076.

[33] P. Diana, A. Stagno, P. Barraja, A. Montalbano, A. Carbone, B. Parrino, G. Cirrincione, Synthesis of the new ring system pyrrolizino[2,3-b]indol-4(5H)-one, Tetrahedron 67 (2011) 3374–3379, https://doi.org/10.1016/j.tet.2011.03.060.

[34] S. Cascioferro, B. Parrino, G.L. Petri, M.G. Cusimano, D. Schillaci, V. Di Sarno, S. Musella, E. Giovannetti, G. Cirrincione, P. Diana, 2,6-Disubstituted imidazo[2,1-b][1,3,4]thiadiazole derivatives as potent Staphylococcal biofilm inhibitors, Eur. J. Med. Chem. 167 (2019) 200–210, https://doi.org/10.1016/j.ejmech.2019.02.007.

[35] P. Diana, P. Barraja, A. Lauria, A. Montalbano, A. Almerico, G. Dattolo, G. Cirrincione, Pyrrolo[2,1-d][1,2,3,5]tetrazine-4(3H)-ones, a new class of azolotetrazines with potent antitumor activity, Biorg. Med. Chem. 11 (2003) 2371–2380, https://doi.org/10.1016/S0968-0896(03)00145-7.

[36] A. Carbone, B. Parrino, M.G. Cusimano, V. Spanò, A. Montalbano, P. Barraja, D. Schillaci, G. Cirrincione, P. Diana, S. Cascioferro, New thiazole nortopsentin analogues inhibit bacterial biofilm formation, Mar. Drugs 16 (2018) 274, https://doi.org/10.3390/md16080274.

[37] V. Spanò, A. Attanzio, S. Cascioferro, A. Carbone, A. Montalbano, P. Barraja, L. Tesoriere, G. Cirrincione, P. Diana, B. Parrino, Synthesis and antitumor activity of new thiazole nortopsentin analogs, Mar. Drugs 14 (2016) 226, https://doi.org/10.3390/md14120226.

[38] B. Parrino, A. Carbone, G. Di Vita, C. Ciancimino, A. Attanzio, V. Spanò, A. Montalbano, P. Barraja, L. Tesoriere, M.A. Livrea, P. Diana, G. Cirrincione, 3-[4-(1H-Indol-3-yl)-1,3-thiazol-2-yl]-1H-pyrrolo[2,3-b]pyridines, nortopsentin analogues with antiproliferative activity, Mar. Drugs 13 (2015) 1901–1924, https://doi.org/10.3390/md13041901.

[39] A. Carbone, B. Parrino, G. Di Vita, A. Attanzio, V. Spanò, A. Montalbano, P. Barraja, L. Tesoriere, M.A. Livrea, P. Diana, G. Cirrincione, Synthesis and antiproliferative activity of thiazolyl-bis-pyrrolo[2,3-b]pyridines and indolyl-thiazolyl-pyrrolo[2,3-c]pyridines, nortopsentin analogues, Mar. Drugs 13 (2015) 460–492, https://doi.org/10.3390/md13010460.

[40] A. Carbone, M. Pennati, P. Barraja, A. Montalbano, B. Parrino, V. Spanò, A. Lopergolo, S. Sbarra, V. Doldi, N. Zaffaroni, G. Cirrincione, P. Diana, Synthesis and antiproliferative activity of substituted 3[2-(1H-indol-3-yl)-1, 3-thiazol-4-yl]-1H-pyrrolo[3,2-b]pyridines, marine alkaloid nortopsentin analogues, Curr. Med. Chem. 21 (2014) 1654–1666, https://doi.org/10.2174/09298673113206660307.

[41] A. Carbone, B. Parrino, P. Barraja, V. Spanò, G. Cirrincione, P. Diana, A. Maier, G. Kelter, H.H. Fiebig, Synthesis and antiproliferative activity of 2,5-bis(3'-Indolyl)pyrroles, analogues of the marine alkaloid Nortopsentin, Mar. Drugs 11 (2013) 643–654, https://doi.org/10.3390/md11030643.

[42] P. Diana, A. Carbone, P. Barraja, A. Montalbano, B. Parrino, A. Lopergolo, M. Pennati, N. Zaffaroni, G. Cirrincione, Synthesis and antitumor activity of 3-(2-phenyl-1,3-thiazol-4-yl)-1H-indoles and 3-(2-phenyl-1,3-thiazol-4-yl)-1H-7-azaindoles, ChemMedChem 6 (2011) 1300–1309, https://doi.org/10.1002/cmdc.201100078.

[43] P. Diana, A. Carbone, P. Barraja, A. Martorana, O. Gia, L. DallaVia, G. Cirrincione, 3,5-Bis(3′-indolyl)pyrazoles, analogues of marine alkaloid nortopsentin: synthesis and antitumor properties, Biorg. Med. Chem. Lett. 17 (2007)

6134–6137, https://doi.org/10.1016/j.bmcl.2007.09.042.

[44] P. Diana, A. Carbone, P. Barraja, A. Montalbano, A. Martorana, G. Dattolo, O. Gia, L. DallaVia, G. Cirrincione, Synthesis and antitumor properties of 2,5-bis(3′-indolyl)thiophenes: analogues of marine alkaloid nortopsentin, Biorg. Med. Chem. Lett. 17 (2007) 2342–2346, https://doi.org/10.1016/j.bmcl.2007.01.065.

[45] P. Diana, A. Carbone, P. Barraja, G. Kelter, H.H. Fiebig, G. Cirrincione, Synthesis and antitumor activity of 2,5-bis(3'-indolyl)-furans and 3,5-bis(3'-indolyl)-isoxazoles, nortopsentin analogues, Bioorg. Med. Chem. 18 (2010) 4524–4529, https://doi.org/10.1016/j.bmc.2010.04.061.

[46] A. Carbone, M. Pennati, B. Parrino, A. Lopergolo, P. Barraja, A. Montalbano, V. Spanò, S. Sbarra, V. Doldi, M. De Cesare, G. Cirrincione, P. Diana, N. Zaffaroni, Novel 1H-Pyrrolo[2,3-b]pyridine derivative nortopsentin analogues: synthesis and antitumor activity in peritoneal mesothelioma experimental models, J. Med. Chem. 56 (2013) 7060–7072, https://doi.org/10.1021/jm400842x.

[47] B. Parrino, A. Attanzio, V. Spanò, S. Cascioferro, A. Montalbano, P. Barraja, L. Tesoriere, P. Diana, G. Cirrincione, A. Carbone, Synthesis, antitumor activity and CDK1 inhibiton of new thiazole nortopsentin analogues, Eur. J. Med. Chem. 137 (2017) 371–383, https://doi.org/10.1016/j.ejmech.2017.06.052.

[48] S. Cascioferro, A. Attanzio, V. Di Sarno, S. Musella, L. Tesoriere, G. Cirrincione, P. Diana, B. Parrino, New 1,2,4-oxadiazole nortopsentin derivatives with cytotoxic activity, Mar. Drugs 17 (2019) 35, https://doi.org/10.3390/md17010035.

[49] A.W. Maresso, O. Schneewind, Sortase as a target of anti-infective therapy, Pharmacol. Rev. 60 (2008) 128–141, https://doi.org/10.1124/pr.107.07110.

[50] S. Cascioferro, M. Totsika, D. Schillaci, Sortase A: an ideal target for anti-virulence drug development, Microb. Pathog. 77 (2014) 105–112, https://doi.org/10.1016/j.micpath.2014.10.007.

[51] R.G. Frykberg, J. Banks, Challenges in the treatment of chronic wounds, Adv. Wound Care 4 (2015) 560–582, https://doi.org/10.1089/wound.2015.0635.

[52] R. Sciarrillo, A. Wojtuszkiewicz, I.E. Kooi, V.E. Gómez, U. Boggi, G. Jansen, G.J. Kaspers, J. Cloos, E. Giovannetti, Using RNA-sequencing to detect novel splice variants related to drug resistance in in vitro cancer models, JoVE 118 (2016), e54714.

Supplementary data

1,2,4-Oxadiazole topsentin analogs as staphylococcal biofilm inhibitors targeting the bacterial transpeptidase Sortase A

Barbara Parrino[1,†], Daniela Carbone[1,†], Stella Cascioferro[1], Camilla Pecoraro[1], Elisa Giovannetti[2,3], Dongmei Deng[4], Veronica Di Sarno[5], Simona Musella[5], Giulia Auriemma[5], Maria Grazia Cusimano[1], Domenico Schillaci[1], Girolamo Cirrincione[1] and Patrizia Diana[1,*]

1. *Department of Biological, Chemical and Pharmaceutical Sciences and Technologies (STEBICEF), University of Palermo, via Archirafi 32, 90123 Palermo, Italy;*
2. *Department of Medical Oncology, VU University Medical Center, Amsterdam, The Netherlands*
3. *Fondazione Pisana per la Scienza, Pisa, Italy;*
4. *Department of Preventive Dentistry, Academic Centre for Dentistry Amsterdam (ACTA), University of Amsterdam and VU University Amsterdam, Amsterdam, The Netherlands;*
5. *Department of Pharmacy, University of Salerno, Via G. Paolo II 132, Fisciano, 84084, Italy*

† These authors contributed equally.

[*] Corresponding author.

Compound **3a** ^{1}H NMR

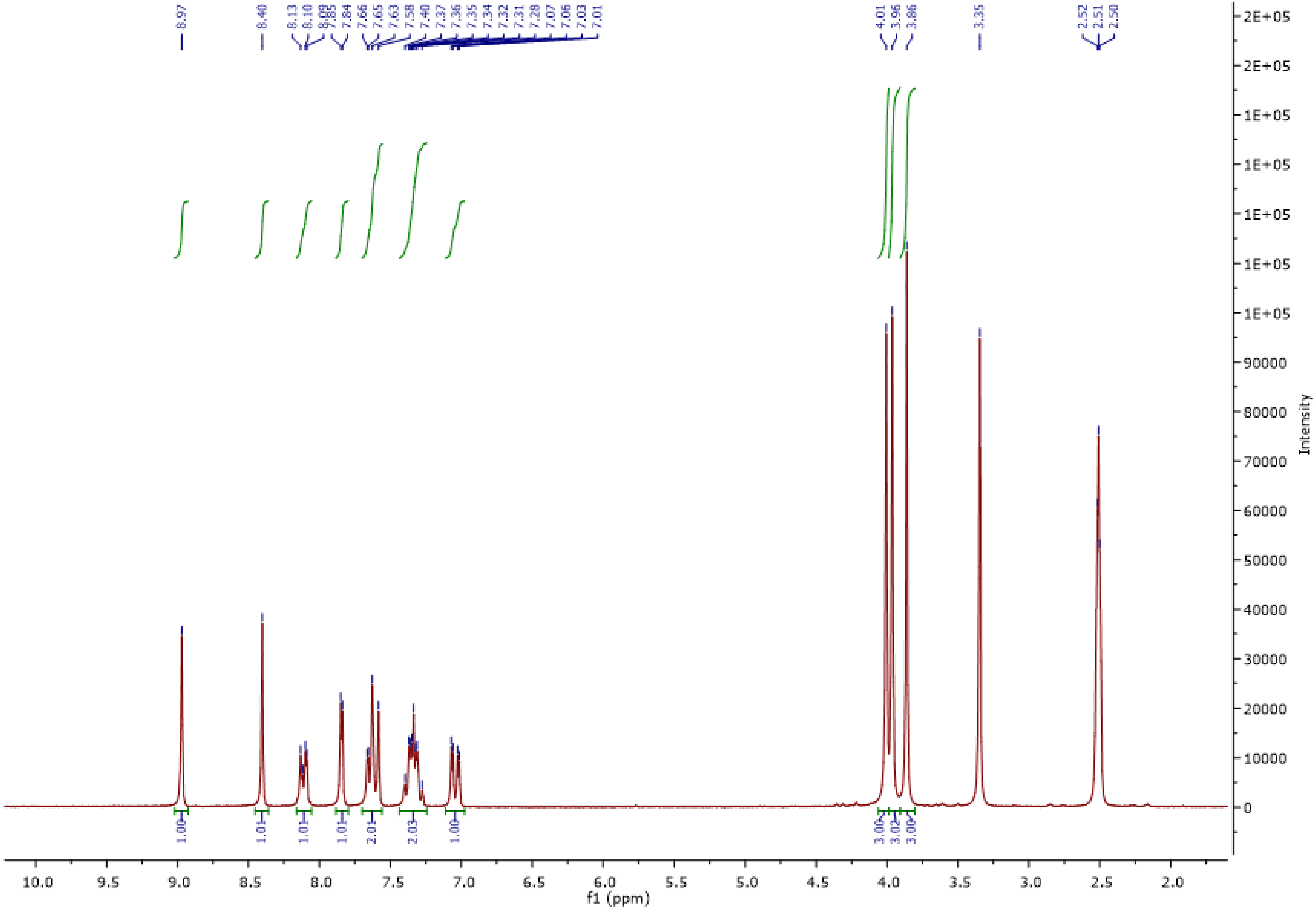

Compound **3b** ^{1}H NMR

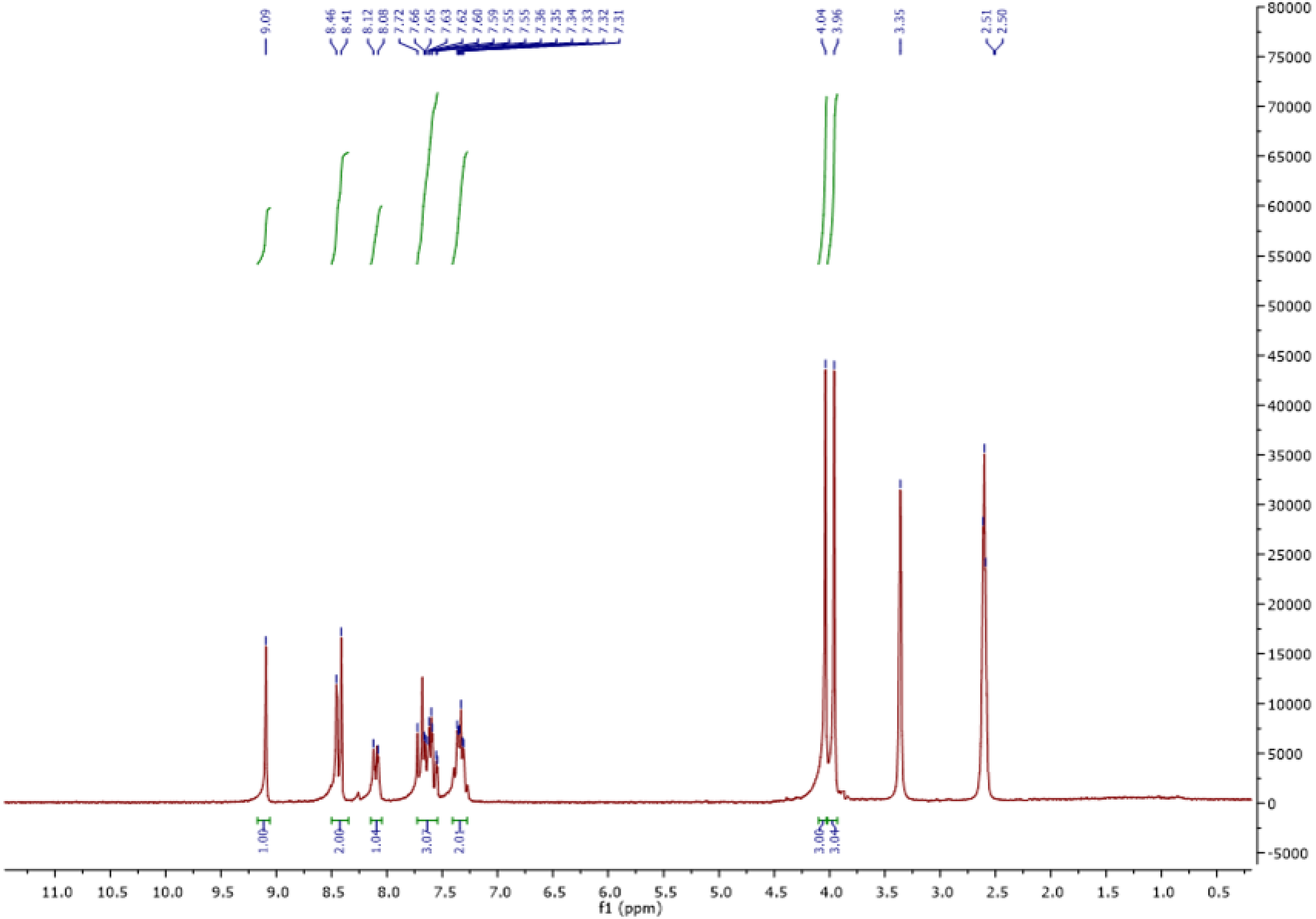

Compound **3c** ^{1}H NMR

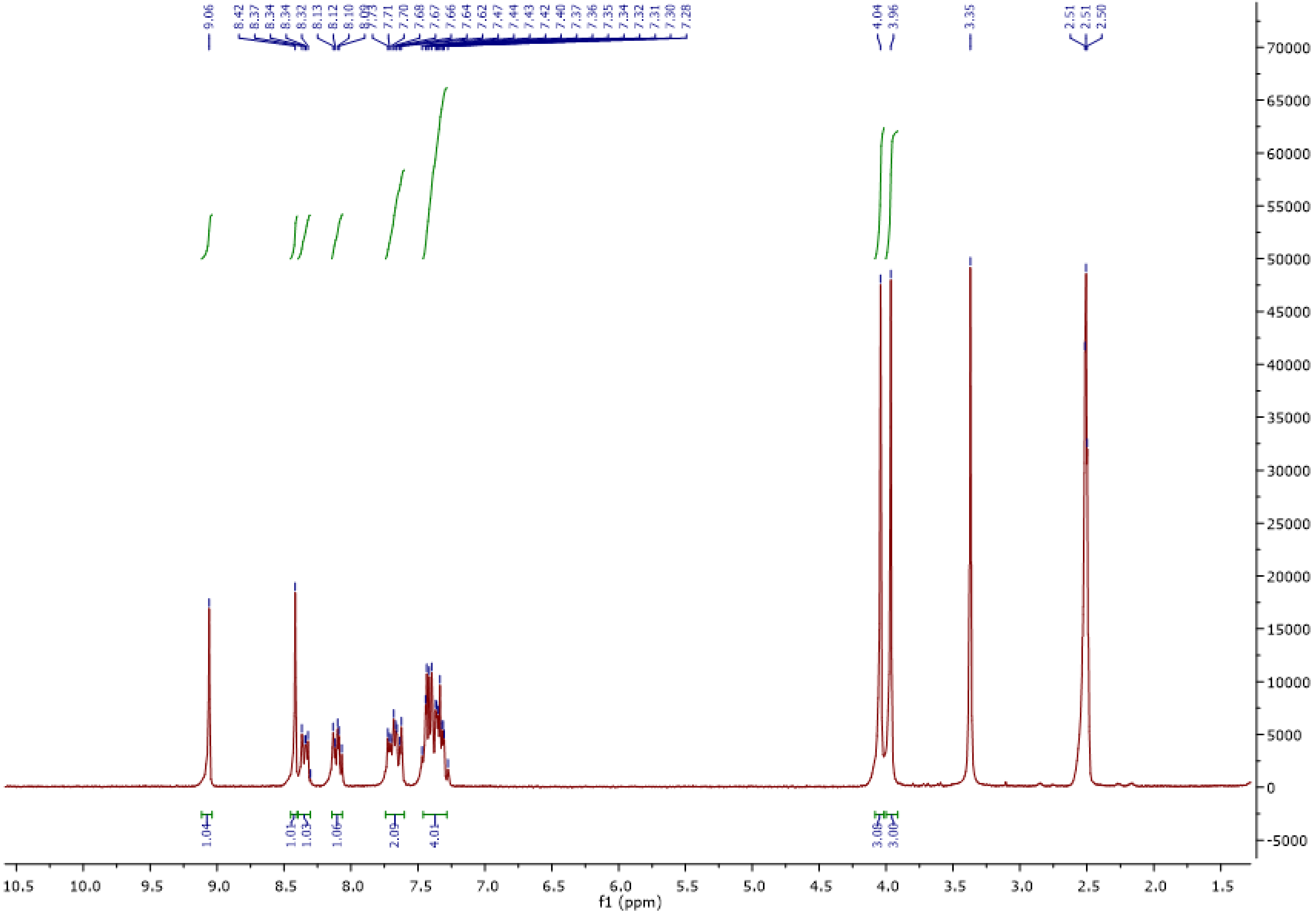

Compound **3c** ^{13}C NMR

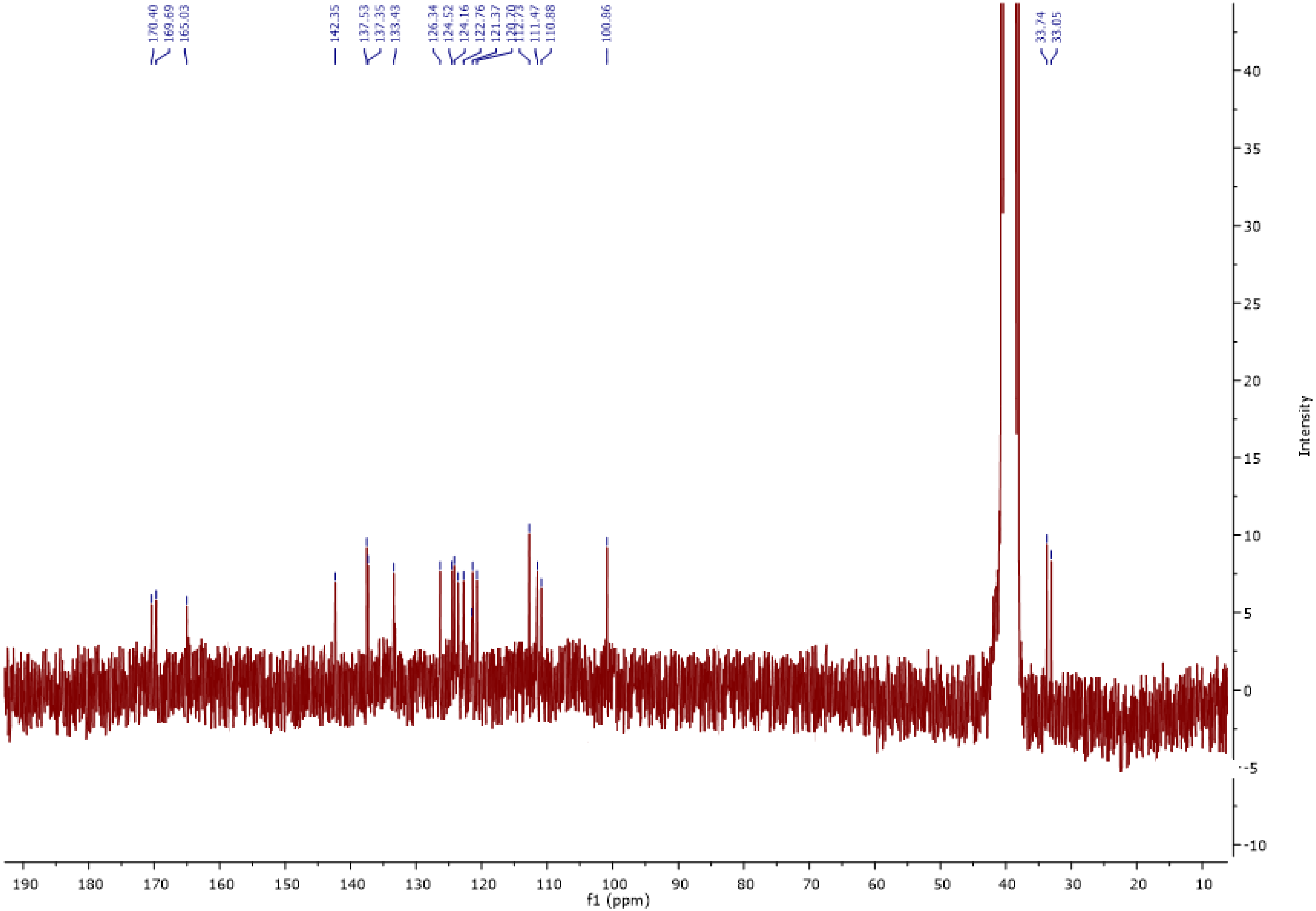

Compound **3d** ^{1}H NMR

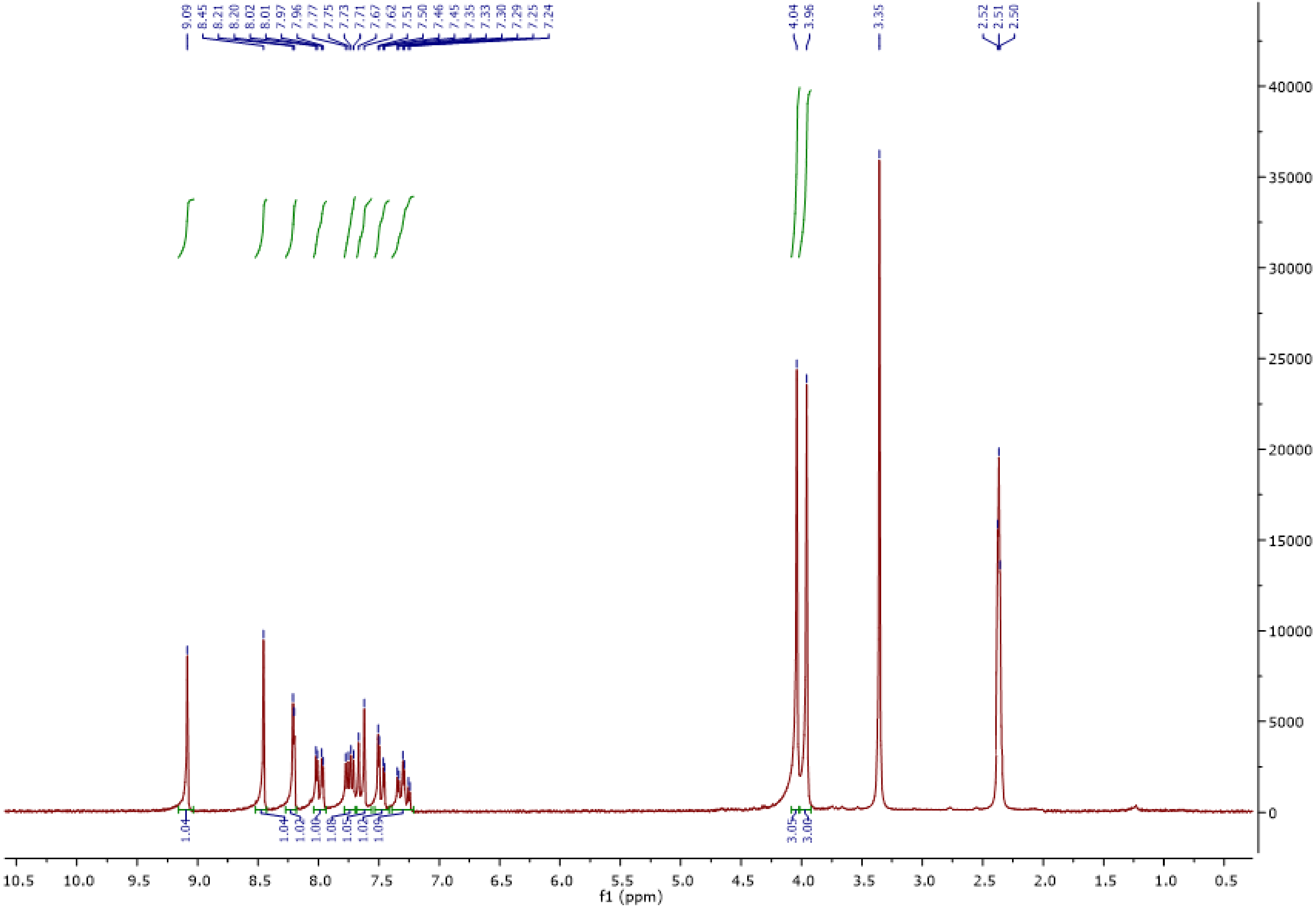

Compound **3e** ^{1}H NMR

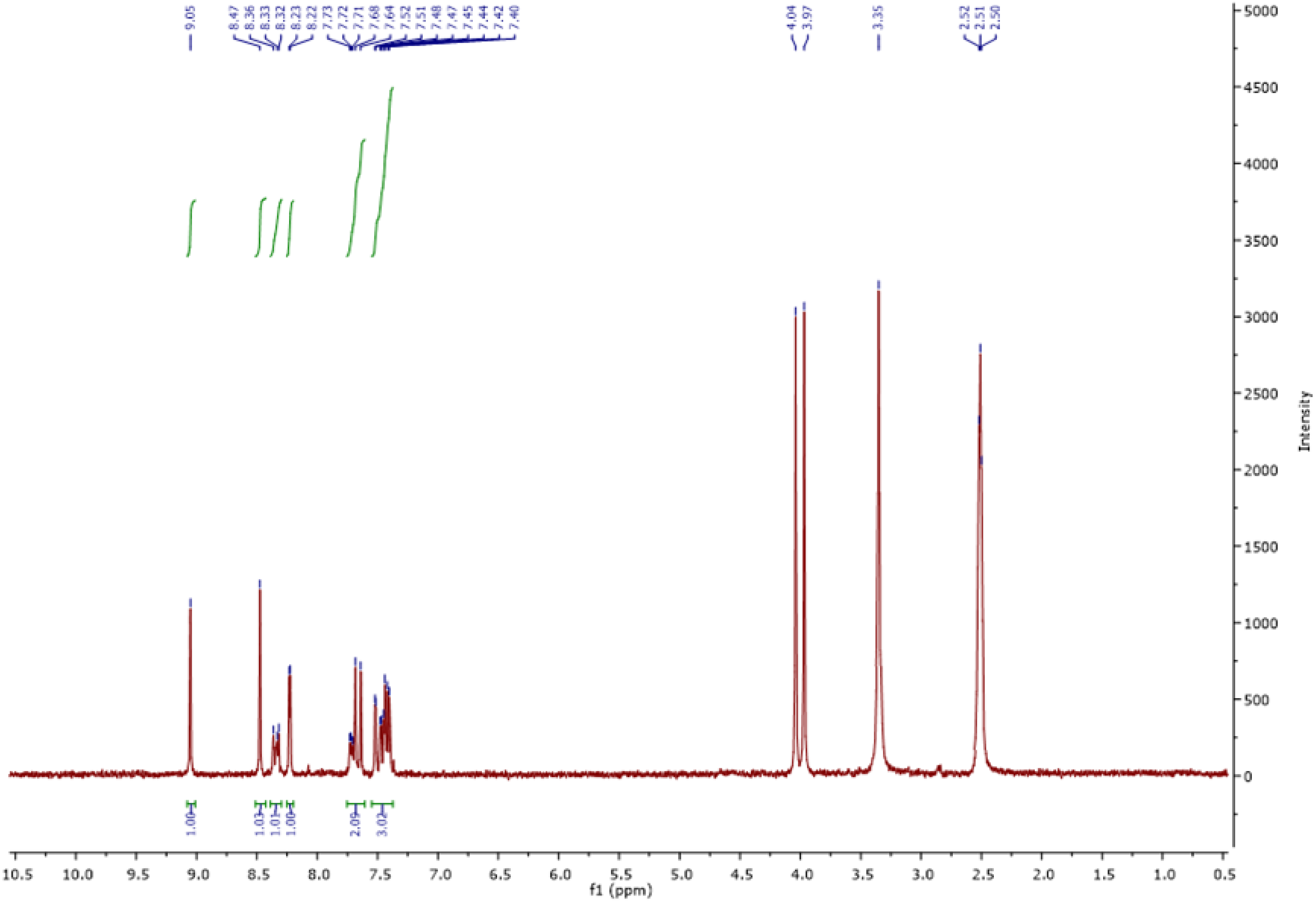

Compound **3f** ^{1}H NMR

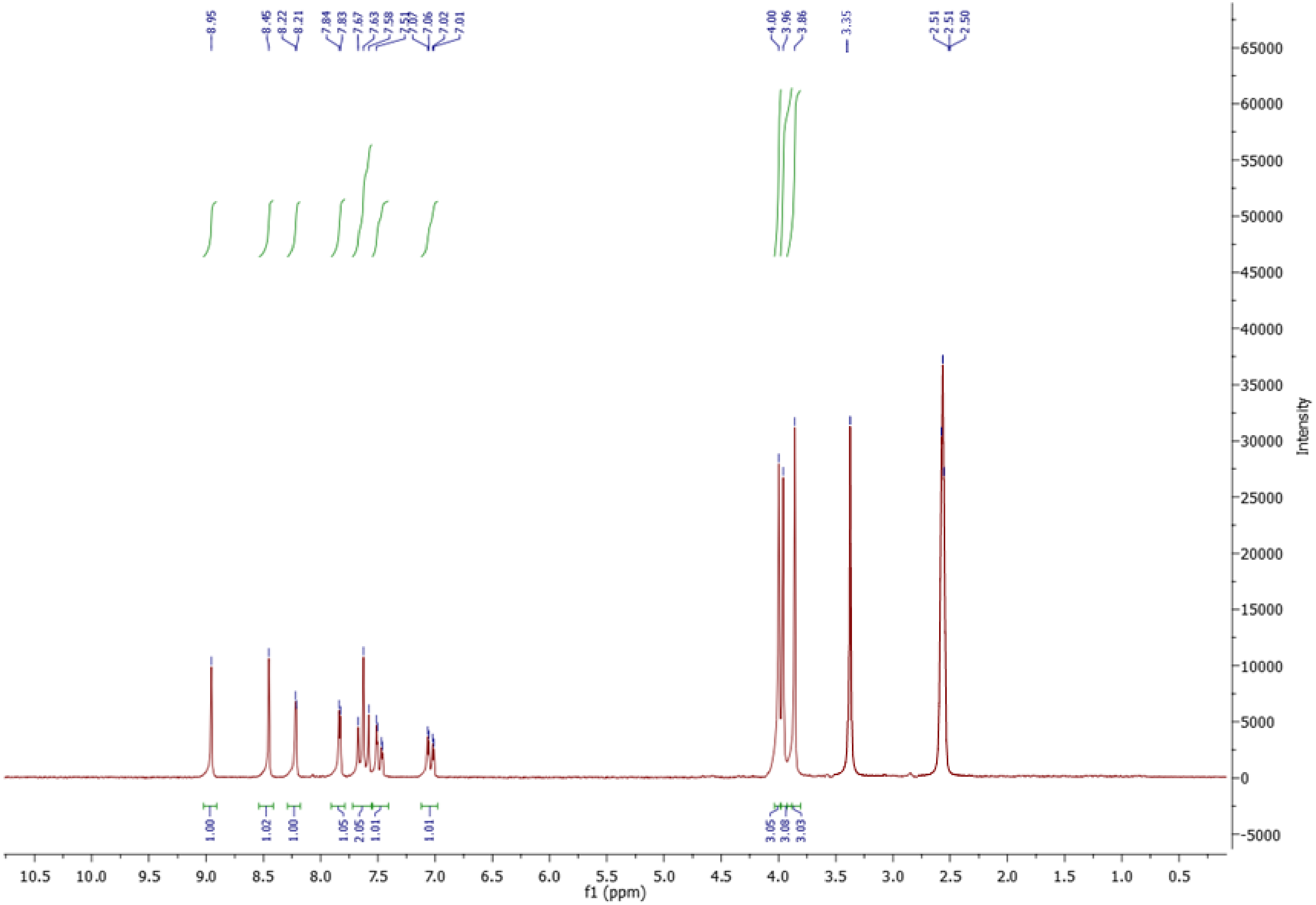

Compound **3g** ^{1}H NMR

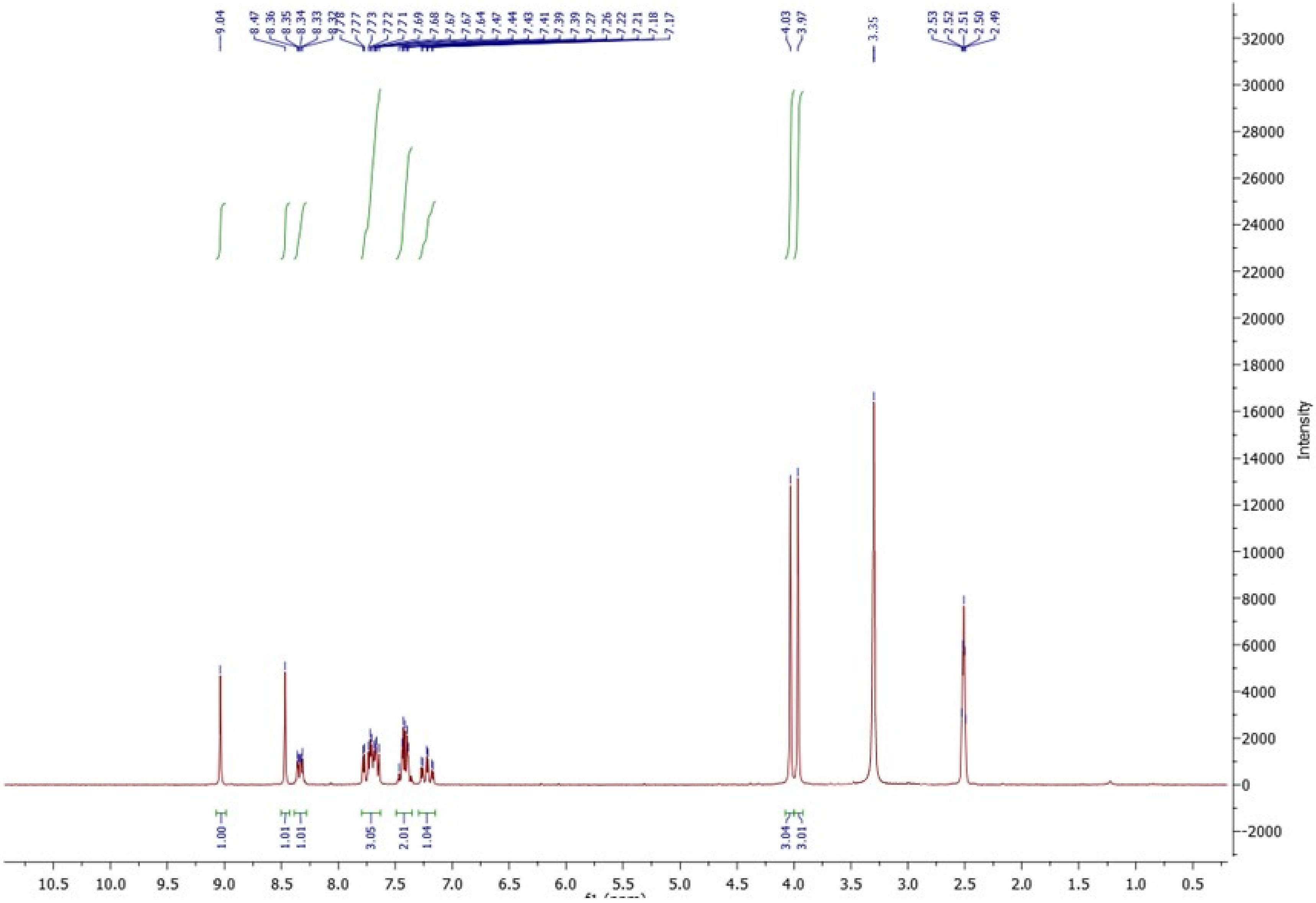

Compound **3g** ^{13}C NMR

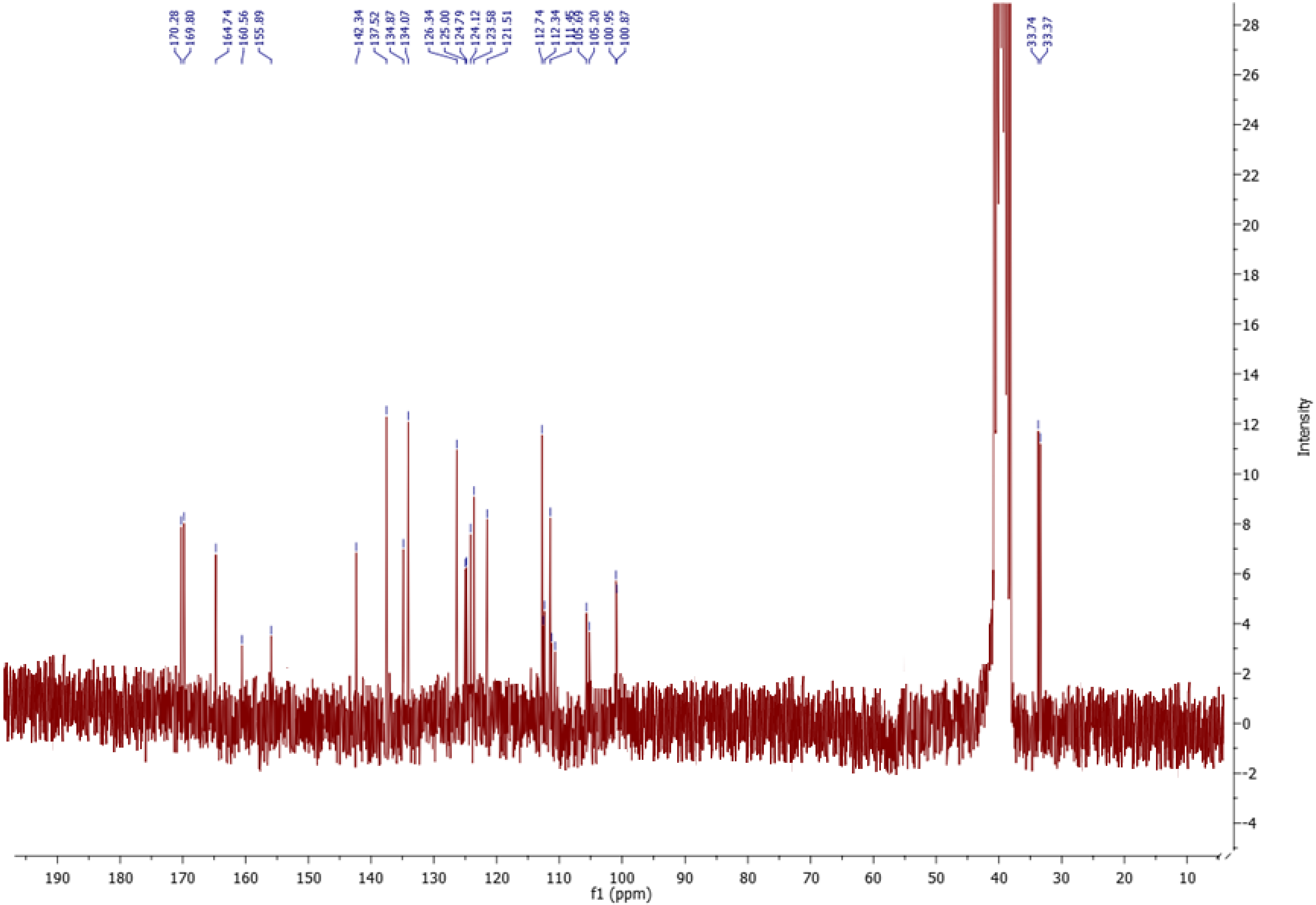

Compound **3h** ^{1}H NMR

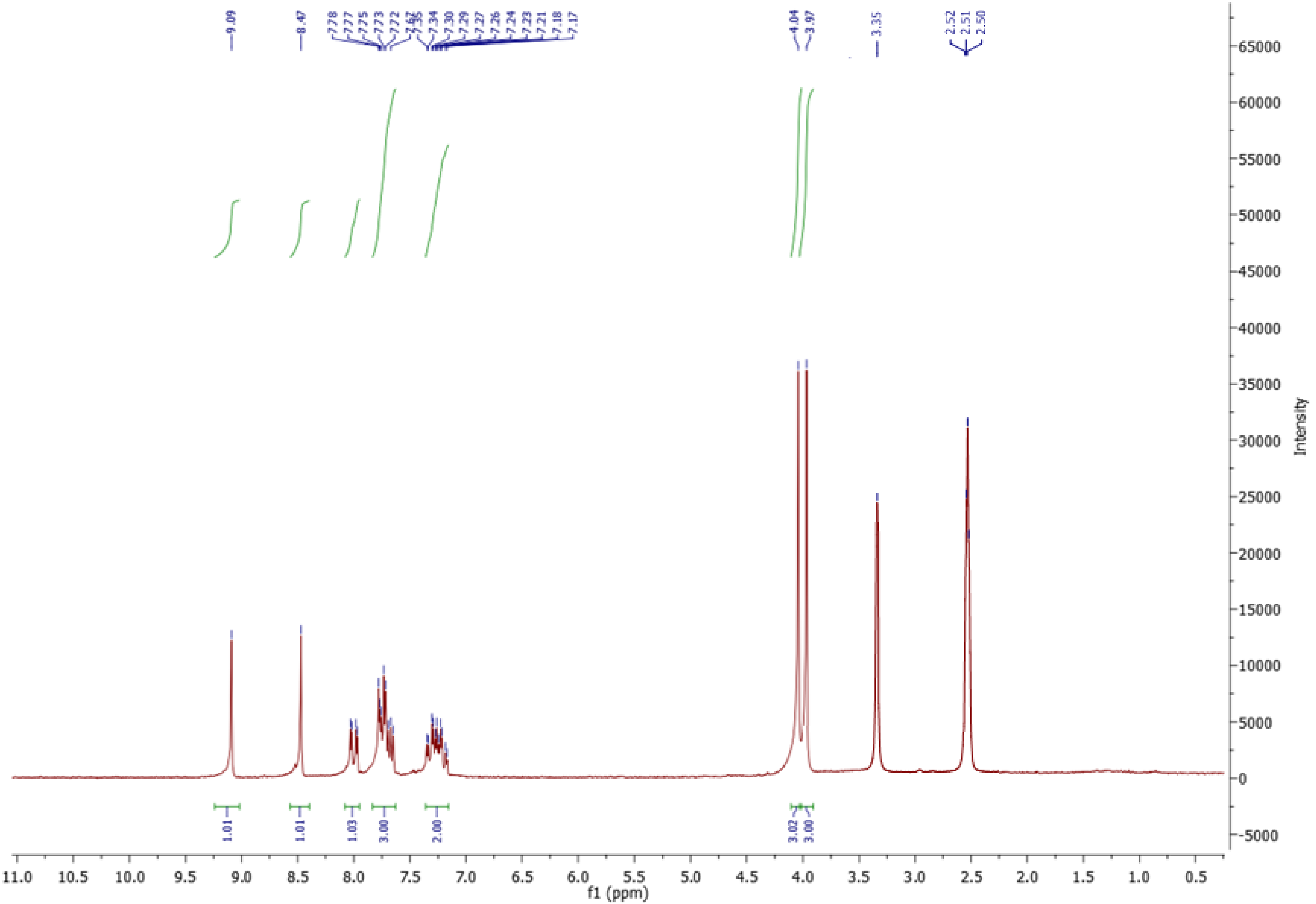

Compound **3i** ^{1}H NMR

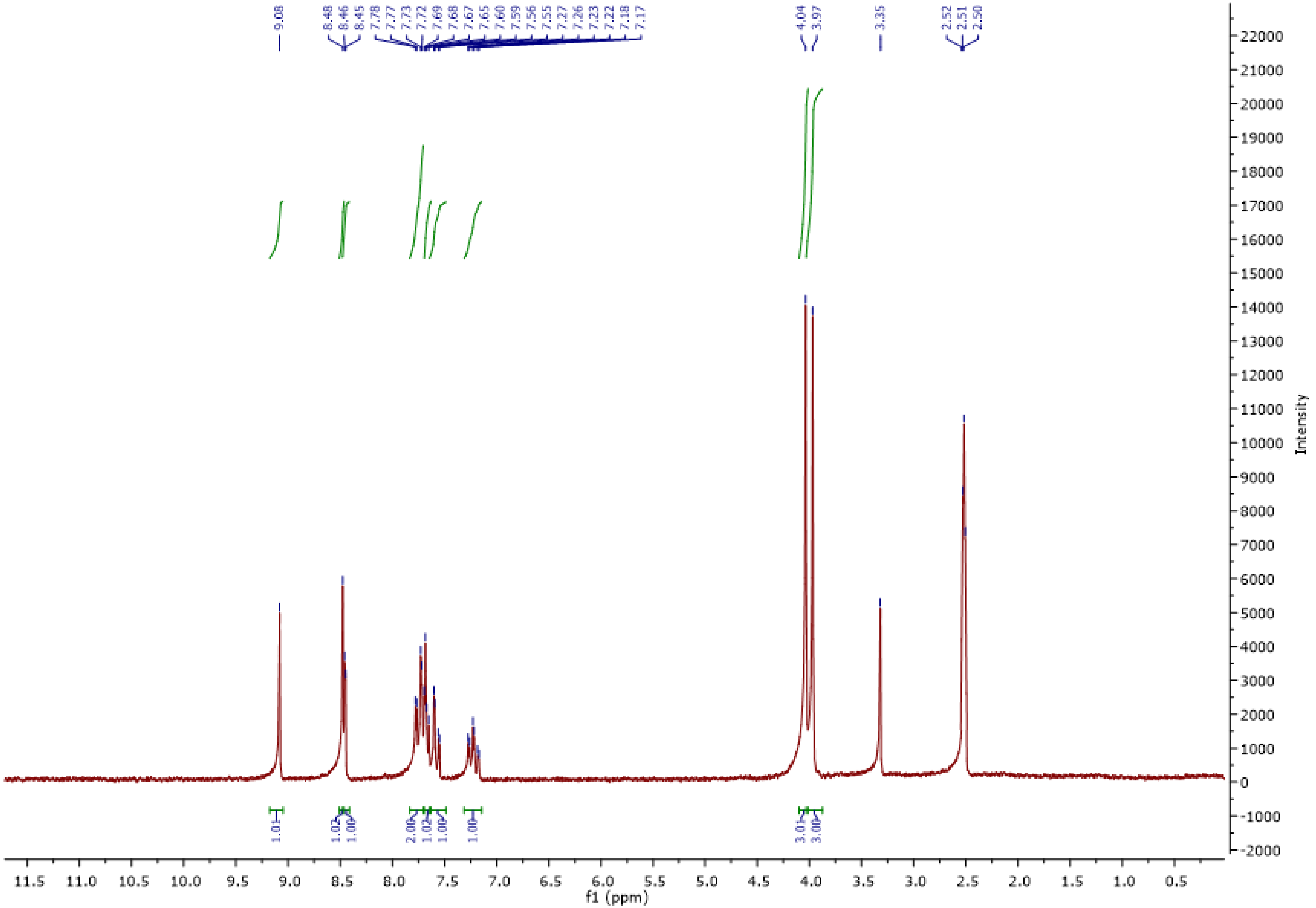

Compound **3j** ^{1}H NMR

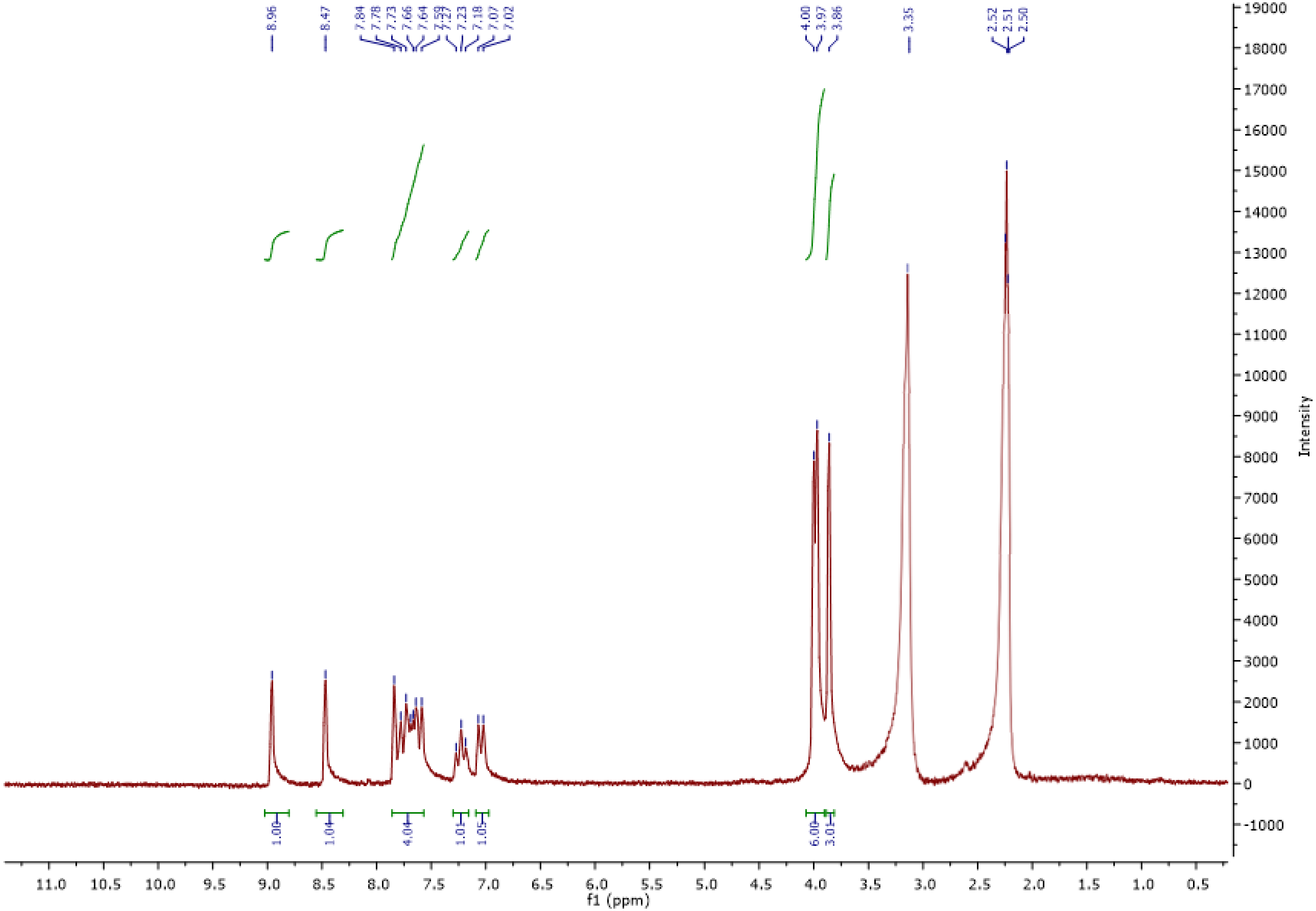

Compound **3k** ^{1}H NMR

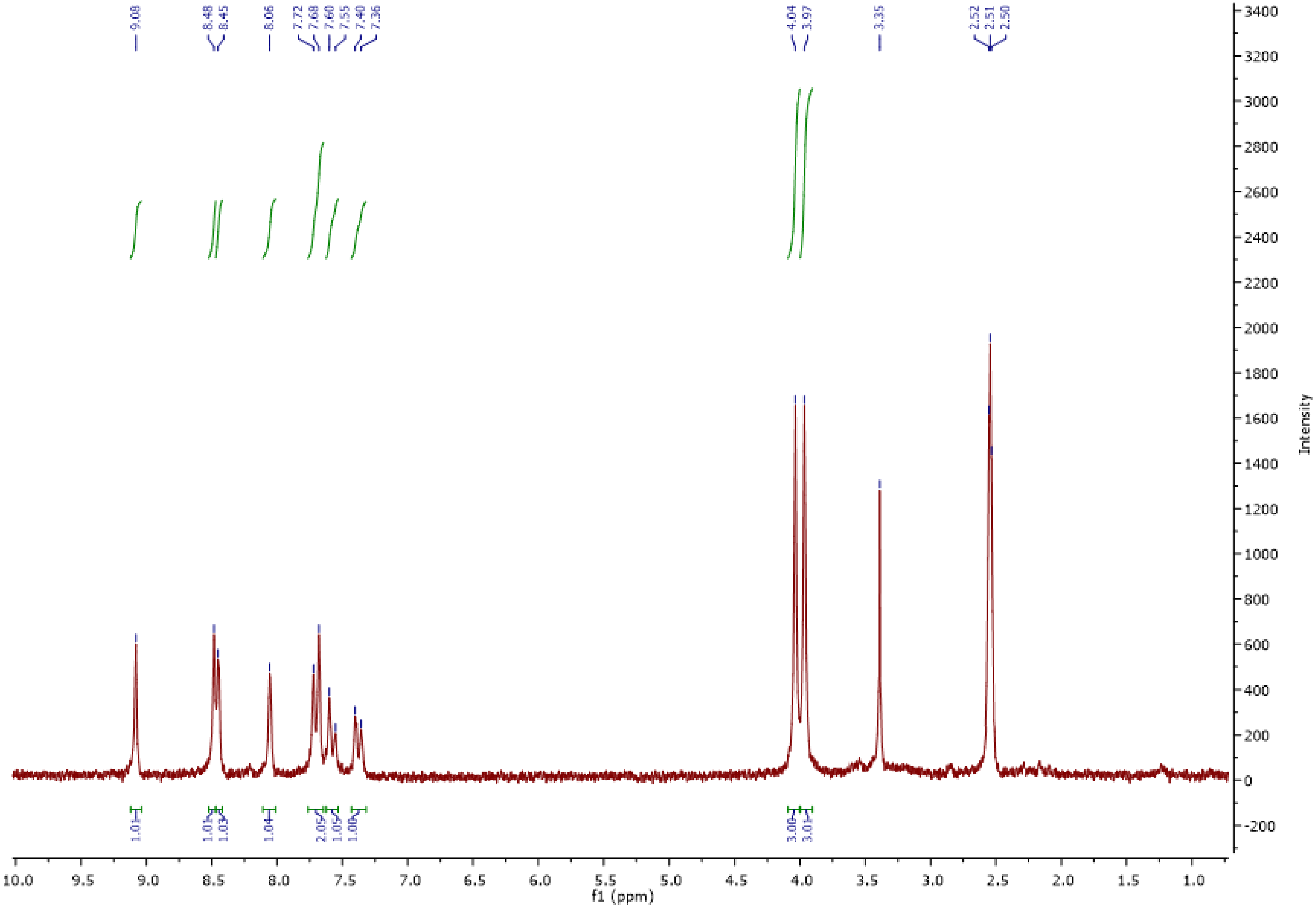

Compound **3l** ^{1}H NMR

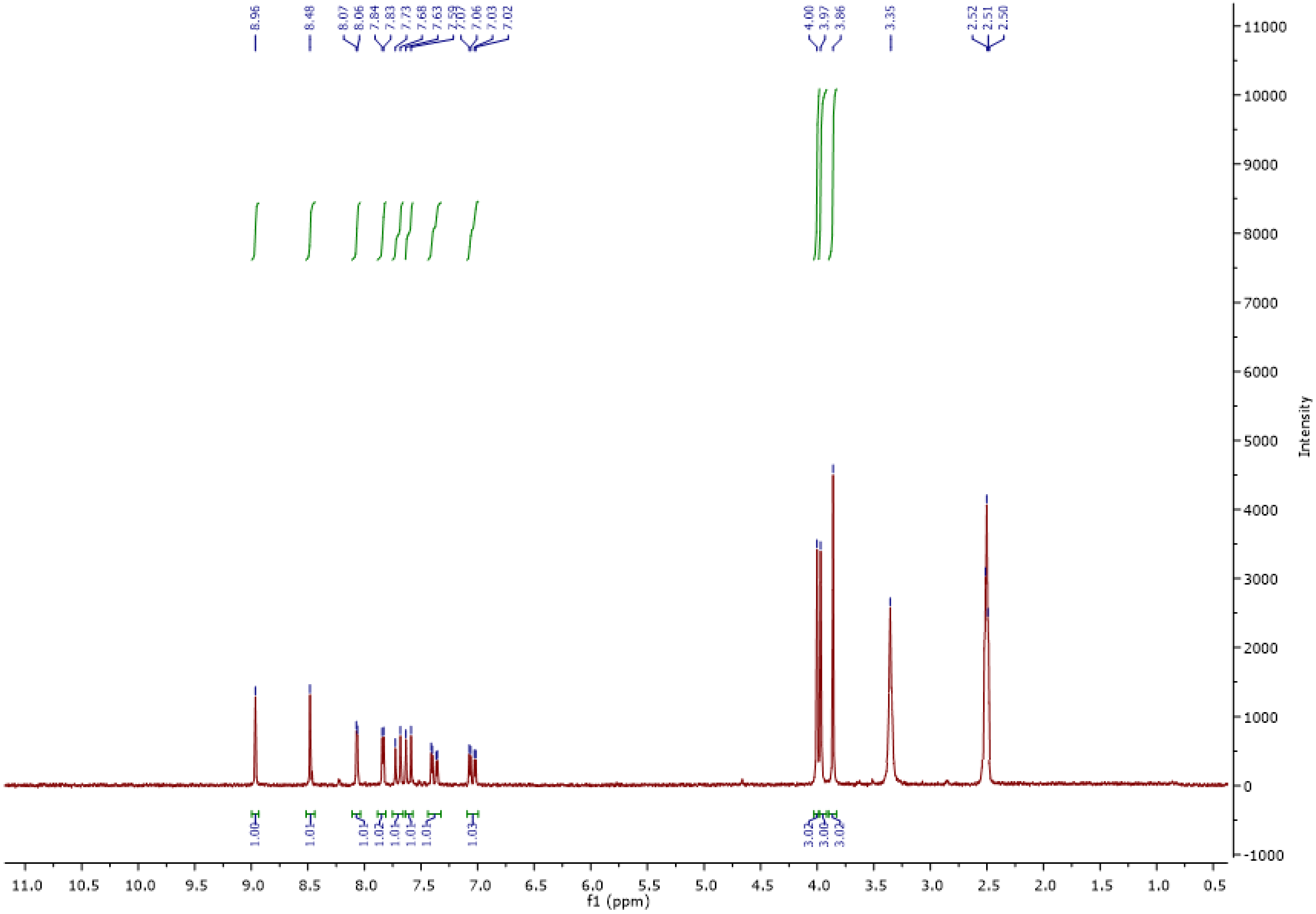

Compound **3m** ^{1}H NMR

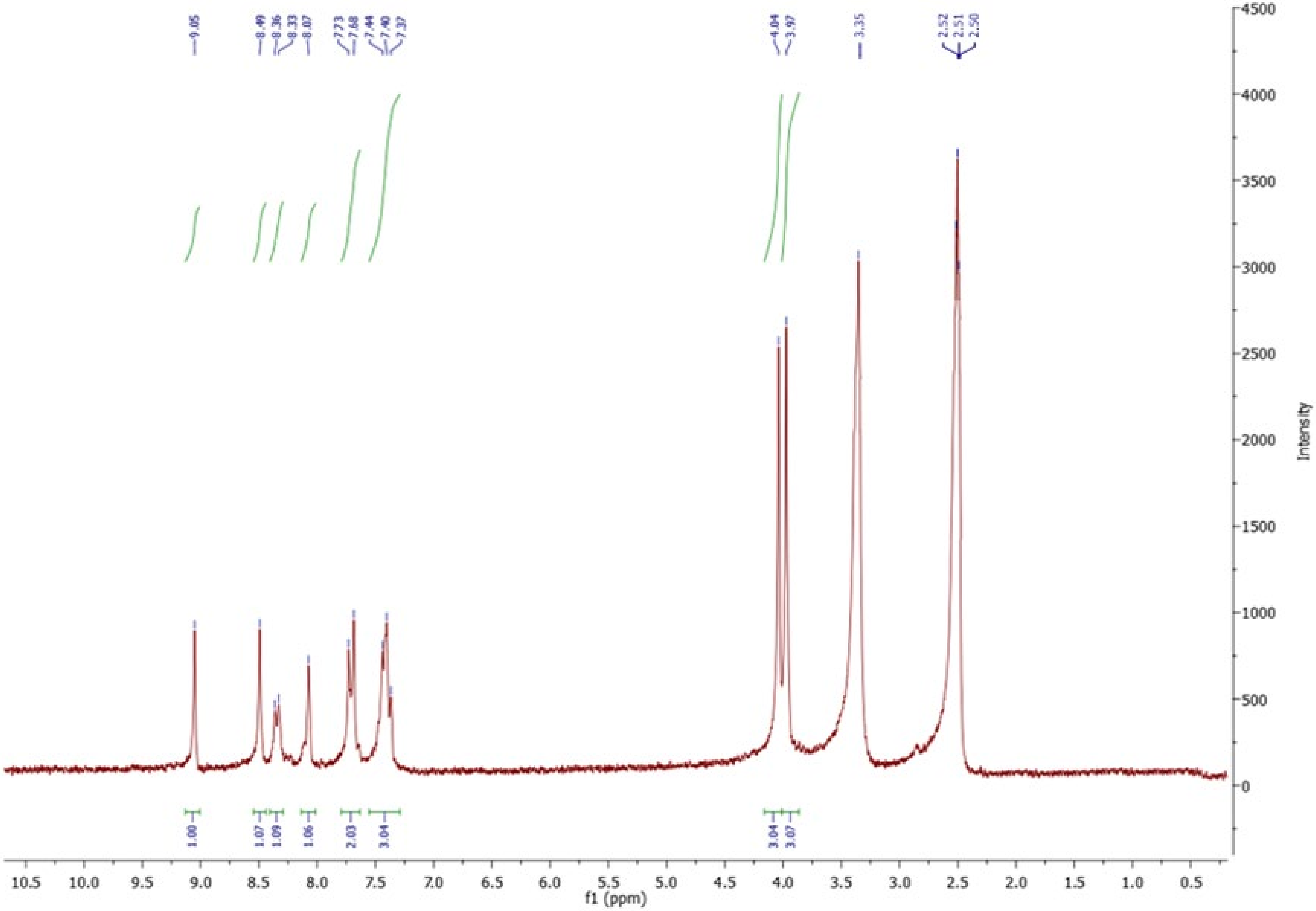

Compound **3n** ^{1}H NMR

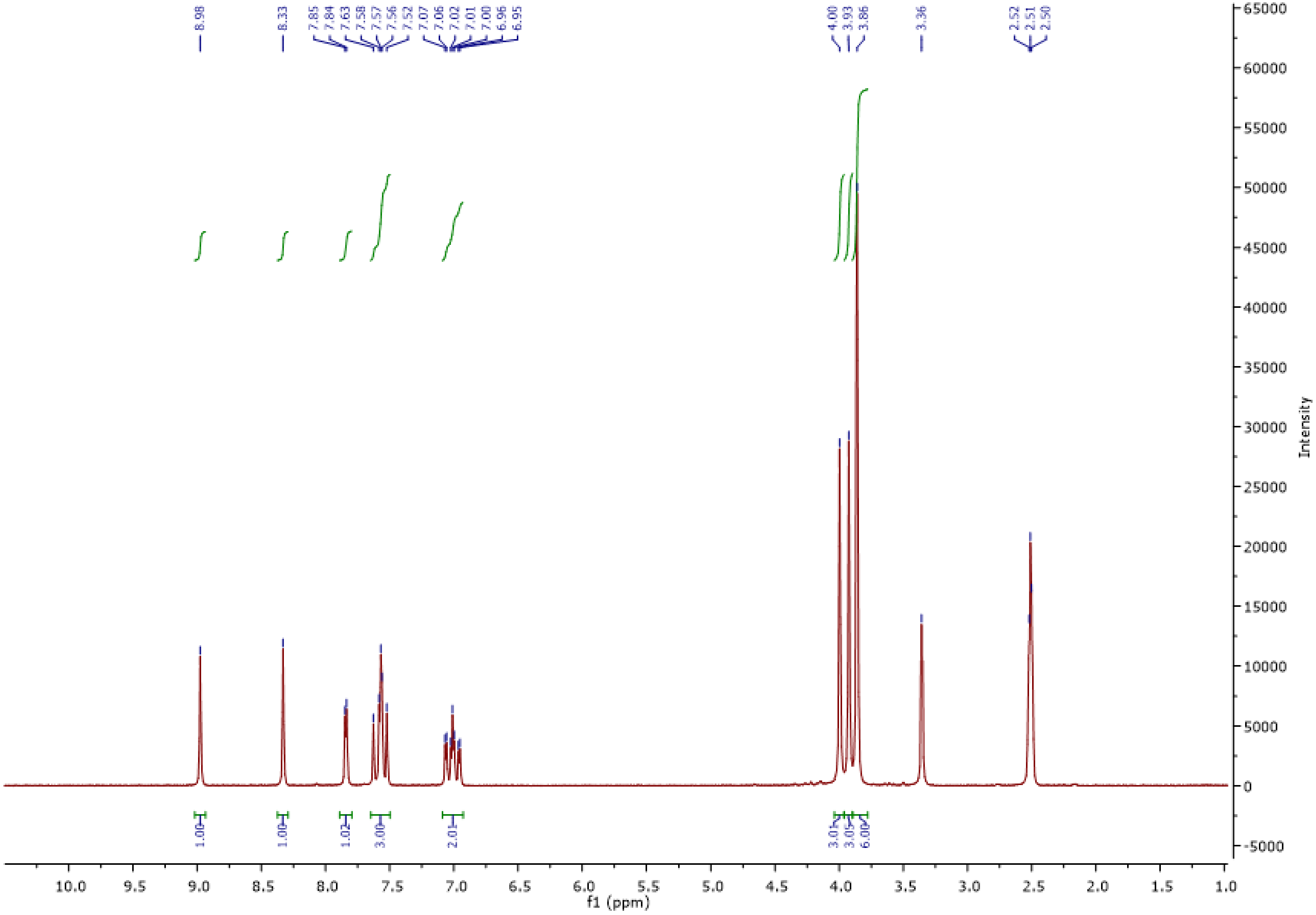

Compound **3o** ^{1}H NMR

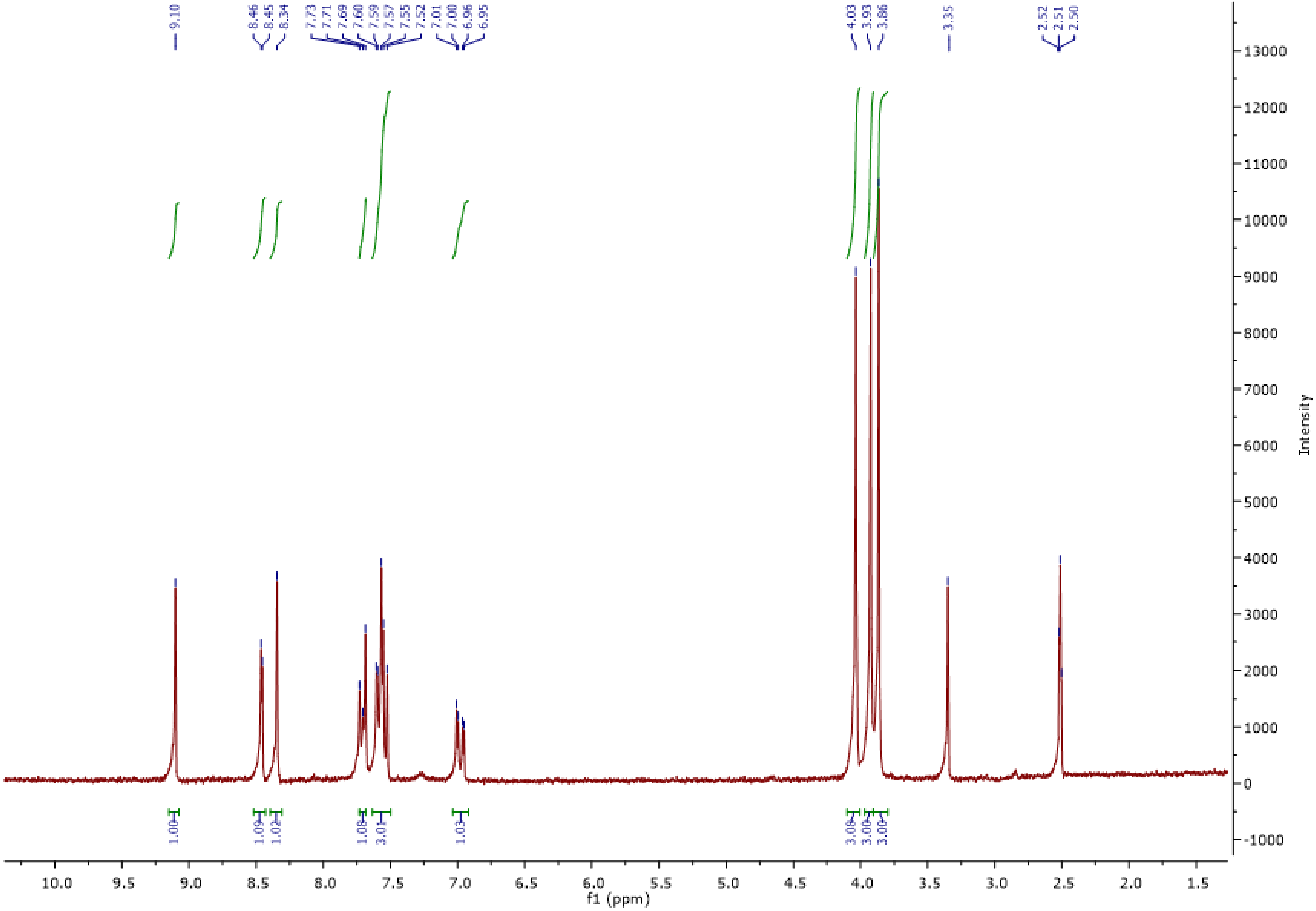

Compound **3p** ^{1}H NMR

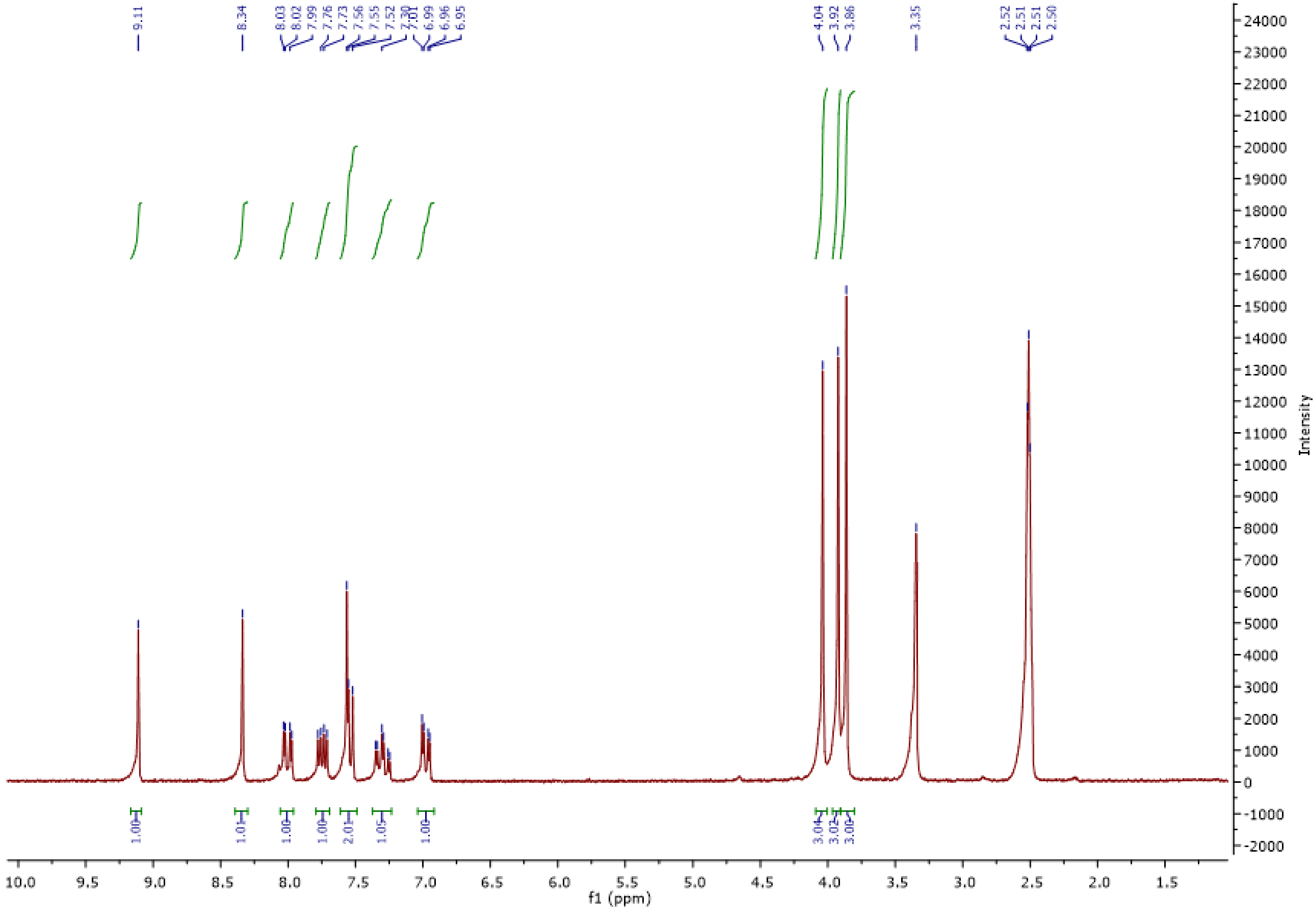

Compound **3q** ^{1}H NMR

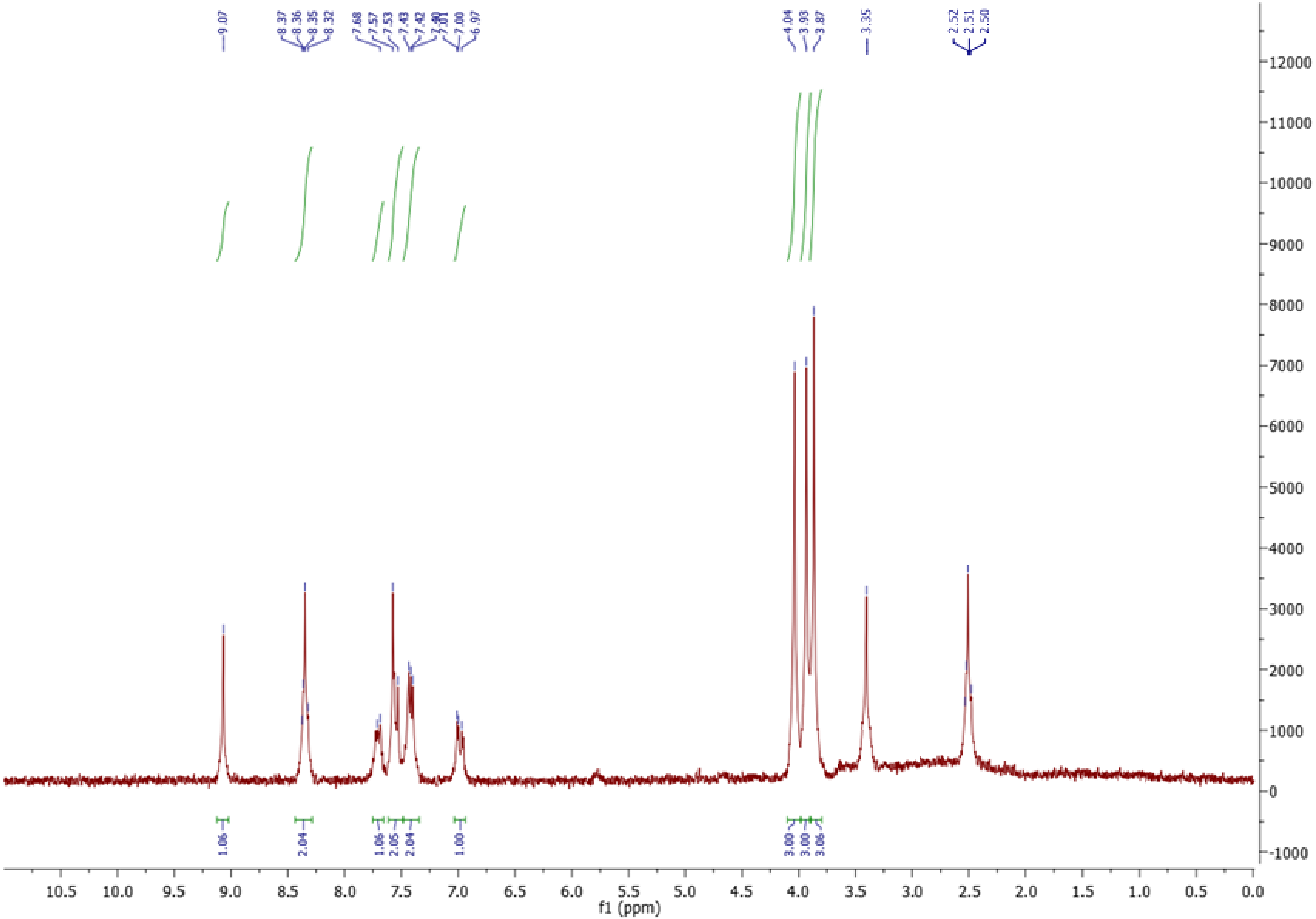

Chapter 13

Discussion & Conclusion

Discussion

In recent years, particular attention has been paid to those molecular pathways considered to be major causes of drug resistance, in order to develop alternative strategies to standard chemotherapy. Many types of cancer are characterized by late diagnosis, are not eligible for surgical resection [1] and are resistant to standard chemotherapy. Pancreatic cancer is an example of such a tumor. It is a very lethal disease with a very poor prognosis due to the late detection, drug resistance and high rate of metastasis. Surgery represents the only curative treatment but only a small percentage of PDACs are eligible for resection. Combinations of chemotherapeutics, such as FOLFIRINOX and gemcitabine plus nab-paclitaxel are now considered the standard therapy. However not all treated patients show response to these therapies [2].

Among the several biological factors, protein kinases have proven to be promising pharmacological targets and are considered as an alternative for traditional chemotherapy, given their role of control in a wide range of fundamental cellular activities such as: DNA replication, gene transcription, DNA damage repair and energy metabolism [3].

There are several factors that may explain the low efficacy of chemotherapy and the resulting poor prognosis of PDAC treated patients. These include deregulation of cell cycle, development of a subset of CSCs, EMT and metastasis, which play an important role in the survival and invasiveness of cancer cells. For these reasons, the protein kinases covered in this thesis include CDK1, which is important for maintenance of the cell cycle homeostasis, for the promotion of self-renewal of CSCs and for GSK-3-β, involved in metastases of tumor cancer cell lines [4-6].

Similar to PDAC malignant mesothelioma is a rare but aggressive disease and difficult to diagnose for the long latency period before clinical signs. The standard therapeutic approaches include surgery, platinum based chemotherapy and radiation. However, the overall median survival rate is about one year [7]. There is evidence that supports the importance of developing new biomarkers enabling an earlier detection of MM to increase prognosis and overall survival [8].

In other scenario, biofilm formation represents another main cause of drug resistance and ineffectiveness of standard antibiotics drugs. Considering that the high and growing percentage of drug resistant infections are mediated by biofilm formation, the latter was recognized as one of the most relevant cause of ineffectiveness of standard antibiotics therapies. Therefore, new therapeutic agents able to counteract the biofilm formation represent an important issue to be solved in drug discovery field [9].

The present thesis aimed to explore new therapeutic strategies and agents able to counteract drug resistance in PDAC, mesotheliomas and biofilm infections. For this purpose, new small molecules were designed and synthesized, which were characterized by the presence of five-membered nitrogen heterocycles, such as, oxadiazoles and thiazoles; and also fused bicyclic heterocycles such as indoles and imidazothiadiazoles. Scaffolds characterized by the presence of several heteroatoms such as amino groups, nitrogen atoms, hydroxy group and oxygen atoms that could form several hydrogen bonds with the kinase hinge region [3].

More specifically the oxadiazole ring is found in many molecules and shows significant biological activity, especially antitumor [10]. In a similar manner the thiazole central core, in comparison with the other five-membered heterocycles, showed promising results on antiproliferative activity. The reason of improved activity of thiazole central ring could be attributed to low lying C−S σ* orbitals that, conferring small regions of low electron density on sulfur (σ-holes), may play an important role in the interaction with the biological target [11].

In the first part of the thesis the involvement of CDK1 and GSK-3β was analyzed in PDACs onset, progression, and resistance. Considering the lack of effective therapeutic strategies to treat pancreatic cancer, alternative therapies were also evaluated to treat PDAC.

With the aim to discover new small molecules, a new series of 1,2,4-oxadiazole topsentin analogs were synthesized, of which the antiproliferative activity was evaluated against a wide range of pancreatic cancer cell lines and for their ability to inhibit the activity of CDK1 and GSK-3β. Moreover, molecular modeling was performed in order to validate the biological results and to confirm the mechanism of action of the new synthesized compounds.

Secondly, considering the observation of the wide antitumor activity of thiazole central core, in the first part of the thesis the synthesis and the biological evaluation of new thiazoles nortopsentin analogs were also reported, which were prescreened against the full panel of the National Cancer Institute (NCI) for their antiproliferative activity.

In the second part of the thesis the different types of malignant mesotheliomas were studied with particular focus on malignant pleural mesothelioma (MPM) and malignant peritoneal mesothelioma (MPeM).

The role of Notch receptors was investigated assumed to play a role in MPM progression, considering their well-known involvement in promoting the establishment of CSCs under hypoxic condition, The role of Notch signaling pathway was analyzed as new target therapy in order to overcome the drug resistance in MPM.

Moreover in this section the synthesis of a new series of imidazo[2,1-*b*][1,3,4]thiadiazole compounds was reported which could inhibit the proliferation of two primary cultures of MPeM (such as STO and Meso II) and reduce FAK phosphorylation on tyrosine residue (Tyr-397) activation site.

Lastly in the third part of the thesis the role of biofilm formation was evaluated in antibiotic resistance and new scaffolds have been synthesized characterized by the presence of oxadiazole or thiazole central core. These have been evaluated for their antibacterial capacity and their ability to inhibit the membrane enzyme sortase A (Srt A)

Part I

Role of CDK-1 and GSK-3 β in driving key hallmarks of PDAC and preclinical evaluation of novel marine alkaloids analogs (Chapter 2-6)

The role of CDK1 in pancreatic cancer progression and evaluation of CDK1 inhibition as a potential novel target to treat PDAC was reviewed in **Chapter 2**.

In this section the mechanism through which CDK1 exerts its tumorigenic effect was also evaluated including its role in the stimulation of cell cycle progression even in case of DNA damage. This research also underlined the connection between the tumor suppressor protein TP53, mutated in almost all PDACs and CDK1 aberrant expression in the progression of PDAC.

Moreover, the role of CDK1 to induce and maintain a CSCs subpopulation inside the tumor was reviewed, underlining that CDK1 inhibition could reduce the number of CSCs by altering the expression of stemness related proteins such as Nanog, OCT4 and Sox2.

We further reported the status of the multiple ongoing clinical trials of CDK1 inhibitors on PDACs and their possible use alone or in combination with other therapeutic strategies such as radiation therapy or DNA damaging chemotherapy in order to improve the efficacy of pancreatic cancer treatment and the outcome of PDACs patients.

In **Chapter 3** the synthesis and biological evaluation of a new series of 1,2,4-oxadiazole derivatives was reported. The new 1,2,4-oxadiazole topsentin analogs were obtained by the structural manipulation of topsentin, extracted from *Topsentia genitrix.*

Topsentin was characterized for the *in vitro* cytotoxic activity against P-388 murine tumor cells, with an IC_{50} of 8.8 μM and at micromolar concentrations against several human cancer cell lines, representing a promising lead compound for further chemical manipulation to obtain new promising small molecules [12].

The *in vitro* antiproliferative activity of new 7-azaindolyl oxadiazole topsentin analogs was initially evaluated on PATU-T immortalized PDAC cell lines. Among the tested compounds, (5-Bromo-1-methyl-1*H*-pyrrolo[2,3-*b*]pyridin-3-yl)-[3-(5-fluoro-1-methyl-1*H*-indol-3-yl)-[1,2,4]oxadiazol-5-yl]-methanone showed the highest potency against PATU-T pancreatic cell line. In order to extend the antiproliferative evaluation of this compound towards other pancreatic tumor cells, the inhibition of cell growth was assessed in two immortalized pancreatic cell lines including HPAF-II and Hs766T and also against the primary culture PDAC3, showing antiproliferative activity against all these three PDAC cells, with IC_{50} values ranging from 5.7 to 9.8 μM.

Moreover, the new oxadiazole agent was screened at 10 μM to assess its ability in the modulation of CDK1 expression compared to control cells, showing a great reduction of CDK1 expression level after the treatment.

To further confirm the mechanism of action of our compound its ability in the induction of apoptosis was evaluated and a significant increase in the portion of apoptotic Hs766T and PATU-T pancreatic cancer cell was demonstrated, in a similar percentage to that observed for gemcitabine.

In order to further analyze the CDK1 potential activity of this compound, molecular modeling was performed into CDK1 (PDB ID: 4YC6). The molecular docking scores of our oxadiazole derivative was found to be -6.999 Kcal/mol, indicating efficient binding to the active site of CDK1.

In **chapter 4** the role of the serine-threonine kinase GSK-3β, as promising new PDAC therapeutic target was reviewed.

GSK3β was initially known for its role in glycogen synthesis, however, it was further characterized as a master kinase involved in the regulation of activity of more than 40 substrates and in many fundamental cellular processes, therefore it was defined *multitasking* kinase [13]. Aberrant GSK3β activity has been implicated in different human disorders including bipolar depression, neurodegenerative disorders and acute myeloid leukemia.

Remarkably there isa strong connection between mutant KRAS, observed in 91% of pancreatic cancers and the overexpression of active GSK-3β. This demonstrates that this protein is involved in PDAC onset and progression and is often correlated with poorly prognosis of PDAC patients. Moreover, in the present chapter the latest GSK-3β inhibitors were reviewed subdividing them according to their mechanism of action.

In **Chapter 5** the synthesis and biological evaluation of new class of [3-(1*H*-indol-3-yl)-1,2,4-oxadiazol-5-yl](1-methyl-1*H*-indol-3-yl) methanones were reported. Among the sixteen topsentin analogues, five derivatives exhibited good antiproliferative activity against SUIT-2, Capan-1 and Panc-1 PDAC cells, with EC_{50} values ranging from micromolar to sub micromolar level. The new 1,2,4-oxadiazoles were also able to induce the apoptosis, evaluated by the externalization of phosphatidylserine, and to inhibit migration of cancer cells, assessed through wound healing assay in the metastatic Capan-1 PDAC cell lines. Moreover, the compounds can modulate the GSK-3β phosphorylation level at Tyr 216 by ELISA specific assays in Panc-1 cells.

In order to further confirm the mechanism of action, molecular modeling was performed into GSK-3β binding pocket (PDB 1UV5), showing similar interactions to the co-crystalized ligand 6-bromoindirubin, a known potent and selective bis-indolyl GSK3-3β inhibitor, confirming the ability of novel oxadiazole derivatives to inhibit GSK-3β activity.

In **chapter 6**, we aimed to exploit the marine microenvironments as an important resource of new bioactive molecules. Therefore we synthesized new 3-[2-(1*H*-Indol-3-yl)-1,3-thiazol-4-yl]-1*H*pyrrolo[3,2-c]pyridine hydrobromides obtained through the chemical manipulation of nortopsentin.

More specifically the imidazole central moiety of nortopsentin was replaced by thiazole ring and an indole portion was substituted by a 5-azaindole ring. The novel derivatives were efficiently synthesized in good to excellent yields ranging from 62 to 93%. All the synthesized compounds were prescreened according to the NCI protocol at 10^{-5} M against a panel of 55 human cancer cell lines derived from 9 human cancer cell types, including leukemia, non-small cell lung, colon, central nervous system, melanoma, ovarian, renal, prostate, and breast tumor. All tested thiazoles satisfied the criteria set by the NCI for activity and were selected for further screenings at five concentrations ranging from 10^{-4} to 10^{-8} M on the full panel.

Among the tested compounds the best results were observed in the leukemia sub-panel showing GI_{50} ranging from 0.24 to 2.13 μM; in breast cancer sub-panel with GI_{50} in the range of 0.27-2.16 μM. Furthermore, good selectivity was observed against colon cancer HCT-116 cells.

Part II

New therapeutic approaches against malignant mesothelioma (7,8)

In **Chapter 7** the different types of mesotheliomas were reviewed, as well as their current available therapeutic options, and their mechanisms responsible of chemoresistance, in an effort to exploit novel therapeutic targets.

The role of miRNAs was summarized, together with alternative splicing and the role of Notch signaling pathway as a main cause of drug resistance. Their role as new promising frontiers was analyzed in order to overcome chemoresistance in MM.

To further demonstrate a potential role of alternative splicing, miRNAs and Notch, several validated therapeutic options against these three targets were described. More specifically the inhibition of pre-mRNA splicing and inhibition of Notch signaling via small molecules γ-secretase inhibitors or monoclonal antibodies (mAbs) has been positively evaluated in eradicating CSCs. Furthermore, MM is characterized by a hypoxic microenvironment which further sustain Notch pathway overexpression and CSCs self-renewal.

In addition to these three deregulated primary pathways in MM, the latest findings were reviewed about the use of alternative promising therapeutic approaches, including the inhibition of epigenetic regulators, kinase, cell cycle checkpoint and immune checkpoint. The deregulation of the latter is considered among the main causes of the failure of the standard chemotherapy.

In **Chapter 8** the synthesis and the antitumor activity was reported for a new class of imidazo[2,1-*b*][1,3,4]thiadiazole compounds against malignant peritoneal mesothelioma cancer cell lines, highlighting their ability to reduce the cell growth in two mesothelioma cancer cell lines (MesoII and STO).

Among the ten synthesized derivatives, two compounds showed IC_{50} values of 0.81 and 0.59 μM after treatment. The other eight compounds showed only moderate cytotoxic activities; therefore we investigated the antiproliferative activity of the two best compounds using 3D models of MesoII and STO cells. In both cell lines, after seventeen days of treatment, we observed a statistically significant reduction of the size of spheroids with a fold-change of approximately 2, compared to those not treated.

In order to evaluate the antimigratory activities of the new imidazothiadiazoles their ability to inhibit migration was investigated in MesoII and STO cells by scratch wound-healing assays. After 20 hours of the treatment, a reduction of migration rates varying from 20 to 25.81% compared to control (set at 100%).
Therefore our imidazo[2,1-*b*][1,3,4]thiadiazole derivatives showed relevant *in vitro* antitumor activity but only small antimigratory effect. Further investigations were carried out for a better understanding of the mechanism of action.

For this purpose, preclinical studies on this new class of compounds demonstrated their ability to reduce FAK phosphorylation on Tyr-397, which is overexpressed in malignant mesothelioma cells and recently became an interesting target for the treatment of this disease. Additionally, the new imidazothiadiazole showed good results in combination with the antimetabolite gemcitabine in preclinical models of DMPM. Therefore, it can be stated that the imidazothiadiazole derivatives could represent a valid alternative therapeutic strategy for the treatment of mesothelioma.

Part III

Biological evaluation of novel compounds analogues of the marine alkaloids topsentin and nortopsentin as bacterial biofilm inhibitors (chapters 9-13)

In **Chapter 9**, the biofilm was introduced as a key factor in the promotion of microbial survival in hostile environments, constituting the main virulence element for pathogens responsible for resistant chronic infections.

In this chapter the antibiofilm agents were also introduced, which were divided into two main categories:

1. Eradicating agents, compounds able to interfere with the biofilm formation, used in the prophylaxis to avoid biofilm-associated infections.

2. Dispersal agents, compounds that could be administered in association with a standard antibiotic; since they act by eradicating the biofilm architecture and then counteract the bacterial cells in their planktonic form.

In **Chapter 10** the latest findings about the antibiotic resistance (AMR) were reviewed. Among the main cause of AMR the *Staphylococcus aureus* methicillin resistant (MRSA) is one of the primary reasons for persistent human infections with high rate of mortality and morbidity.

More specifically an important gene that seems to be responsible of MRSA is the penicillin-like antibiotic (*mecA* gene) that encodes for the penicillin binding protein 2a (PBP2a). PBP2a is an enzyme responsible for the synthesis of cross-linked peptidoglycan from lipid intermediates and allows the removal of D-alanine residue from the peptidoglycan precursor.

Moreover, in this chapter the development of synthetic small molecules (over the period 2014 to 2020) were summarized and which were able to prevent biofilm formation.

In **Chapter 11** the synthesis and biological evaluation of eighteen new compounds belonging to 3-[4-(thiophen-3-yl)-1,3-thiazol-2-yl]-1*H*-indoles and 3-[4-(pyridin-3-yl)-1,3-thiazol-2-yl]-1*H*-indole hydrobromides was reported.

The new thiazoles were efficiently synthesized in excellent yields ranging from 72 to 98%. All the new synthesized compounds were firstly evaluated as antibacterial agents against the planktonic form of the Gram-positive *S. aureus* ATCC 25923, *S. aureus* ATCC 6538, and of the Gram-negative *P. aeruginosa* ATCC 15442, showing no influence in the microbial growth, with Minimum Inhibitory Concentration (MIC) values greater than 100 μg/mL, confirming their anti-virulence activity.

Moreover, the capability was tested for novel thiazoles to inhibit biofilm onset and progression. For the compounds that show biofilm inhibition greater than 20% at 10 μg/mL the concentration was calculated required to inhibit biofilm formation by 50% (BIC_{50}) at least against one bacterial strain.

Notably, 5-fluoro-1-(2-methoxyethyl)-3-[4-(thiophen-3-yl)-1,3-thiazol-2-yl]-1*H*-indole and 5-bromo-1-(2-methoxyethyl)-3-[4-(pyridin-3-yl)-1,3-thiazol-2-yl]-1H-indole hydrobromide showed highest potency against *S. aureus* ATCC 25923, with BIC_{50} values of 3.9 and 1.0 µM, respectively. Whereas 3-[4-(thiophen-3-yl)-1,3-thiazol-2-yl]-1H-indole and 3-[4-(pyridin-3-yl)-1,3-thiazol-2-yl]-1*H*-indole demonstrated good inhibitory activity against *P. aeruginosa* biofilm formation with BIC_{50} values of 14.9 and 5.5 µM, respectively.

In **Chapter 12** the synthesis of novel 1,2,4-oxadiazole derivatives as new anti-virulence compounds target biofilm formation was reported. The mechanism of action of the novel 1,2,4-oxadiazoles takes place by arresting the activity of SrtA and consequently inhibiting the biofilm adhesion to the host tissue. The bacterial adhesion in Gram-positive pathogens involves that microbial surface components recognize adhesive matrix molecules (MSCRAMMs), which are recognized and covalently bound to peptidoglycan by the transpeptidase SrtA. Remarkably, it was reported that overexpression of SrtA resulted in an increased tendency to form biofilms in several *Staphylococcus s*trains.

Moreover, mice *knockout* of SrtA in *S. aureus* results in a less tendency to form biofilms, due to the absence of recruitment of matrix adhesive proteins [14, 15].

SrtA was confirmed to be a promising target for biofilm eradication, since the inhibition of SrtA do not alter the viability of the cells, avoiding multidrug-resistant (MDR) in bacteria [16].

The new series of 1,2,4-oxadiazole was efficiently synthesized in yields ranging from 78 to 81%. All synthesized compounds were initially screening against the planktonic form of the Gram-positive *S. aureus* ATCC 25923, *S. aureus* ATCC 6538 and against the Gram-negative *P. aeruginosa* ATCC 15442 and *Escherichia coli* ATCC 25922.

All compounds were not able to inhibit the planktonic bacterial growth, showing MIC value >100 µg/mL. These results were in accordance with the desired anti-virulence profile. Therefore, all compounds were screened for their antibiofilm activities against same bacterial strains. The best results were obtained in the Gram-positive *S. aureus* ATCC 25923, for which the compounds were able to inhibit the biofilm at 50%, showing a BIC_{50} value ranging from 0.7 to 47.6 μM and against the Gram-negative *P. aeruginosa* ATCC15442, with BIC_{50} values ranging from 11.6 to 78.6 μM. To further confirm the ability of the new 1,2,4-oxadiazoles to inhibit the biofilm formation, an enzymatic assay was carried out against *S. aureus* SrtA with the compounds that showed the best values of BIC_{50}, demonstrating their ability to inhibit the SrtA activity with IC_{50} valued ≤ 10.4 μM. Moreover, the most active compounds were tested against human skin fibroblast Hs27, demonstrating no activity against human normal cells.

Conclusion

In the present thesis, the main causes of drug-resistance in pancreatic carcinoma, malignant mesotheliomas and drug-resistant infections have been described. In particular, in the first part of the thesis, we describe pancreatic ductal adenocarcinoma (PDAC) as a form of cancer characterized by poor prognosis and lack of specific signs and symptoms.

The therapeutic strategies available to date for the treatment of PDAC are not able to eradicate this form of cancer and therefore its survival is estimated to be 5 years in only 8% of cases [16].

The main mutations that occur in the PDAC have been analyzed and, the KRAS activating mutation and lack of expression of TP53 are the most common ones [17, 18].

Among the main cellular effectors whose activity was influenced by KRAS and TP53 mutations, it emerged that CDK1 was overexpressed in PDAC and is responsible for an even worse prognosis. CDK1 is a protein known for its leading role in the progression of the cell cycle, and whose activity is strictly regulated by TP53, [19].

Under physiological condition, in case of DNA damage, TP53 blocks CDK1 activity, arresting the replication of faulty cells [20]. Conversely, in the case of TP53 inactivating mutations, CDK1 activity continues even in the presence of DNA damage, leading to replication of cells with DNA damage [21].

On the other hand, the KRAS activating mutation, known to be present in almost all PDACs, triggers activation of constitutively active Ras that in turn activates Raf/MEK/ERK signaling pathway with a considerable increase of GSK-3β expression. The explanation behind the increased activity of GSK-3β can be found in the fact that activated Ras/Raf/MEK/ERK pathways induced ETS2 to bind to the GSK-3β promoter which occurred in association with p300 histone acetyltransferase resulting in chromatin remodeling and GSK-3β expression [22].

Similar to pancreatic cancer, malignant mesothelioma is a form of cancer characterized by poor prognosis, late diagnosis and inefficacy of traditional chemotherapy. Therefore, new biomarkers for early detection and new therapeutic targets are urgently needed. For this purpose, three main causes of drug resistance in mesothelioma have been studied and identified, such as miRNA, alternative splicing and Notch signaling pathway and can be considered as new promising frontiers to overcome drug resistance in MM [8].

In addition, in malignant peritoneal mesothelioma (MPeM) the activity of new compounds was tested to act as potential inhibitors of focal adhesion kinase (FAK), assessing the synergy that the new imidazothiadiazole derivatives show with gemcitabine in the cell lines treated. Remarkably FAK is well known to be overexpressed in mesothelioma cells [23].

Another part of the PhD work involves the study of biofilm formation and the inefficacy of traditional antibiotic therapies. In this section the role of biofilms in antibiotic resistance was analyzed and new scaffolds have been synthesized whose antibiofilm capacity and inhibition of the membrane enzyme SrtA has been evaluated.

For the synthesis of the new compounds the marine microenvironment, has been exploited as an important resource for biologically active molecules, characterized by the presence of different nitrogen heterocycles [24]. Structural modifications on topsentin and nortopsentin marine alkaloids were carried out.

Topsentin is a marine alkaloid extracted from the sponge *Topsentia genitrix* and showed *in vitro* cytotoxic activity against P-388 murine tumor cells, with IC_{50} of 8.8 μM as well as at micromolar concentrations against several human cancer cell lines [12].

The main structural changes of topsentin involved the replacement of the imidazole central core with 1,2,4-oxadiazole ring, the methylation of one or both indole portions and the introduction of a nitrogen atom at seven positions. Notably, it has been observed that the compounds characterized by the presence of the methyl groups in both indole or 7-azaindole portions possessed marked antiproliferative activity in PDAC cancer cell lines. Therefore, considering the anti-proliferative activity of (1-methyl-1*H*-pyrrolo[2,3-*b*]pyridin-3-yl)-[3-(1-methyl-1*H*-indol-3-yl)-[1,2,4]oxadiazol-5-yl]-methanones and [3-(1*H*-indol-3-yl)-1,2,4-oxadiazol-5-yl](1-methyl-1*H*-indol-3-yl)methanones, was tested for their ability to inhibit the activity of CDK1 and GSK-3β, respectively, demonstrating the property of novel synthesized compounds to modulate CDK1 expression and GSK-3β Tyr 216 phosphorylation. Moreover, their ability to induce apoptosis and reduce migration in pancreatic cancer cell lines was assessed.

On the other hand, in the oxadiazoles characterized by free indole NH group no significant antiproliferative activity was found, however a great ability in the inhibition of biofilm formation in Gram-positive *S. aureus* and Gram-negative *P. aeruginosa and E. coli*, was observed. Remarkably, the oxadiazole ring, in addition to the antitumor properties, was also known to possess antibacterial and antibiofilm activity and the presence of the sequence -N=C-O- in the oxadiazole ring was shown to be beneficial for antibacterial activity, since it can react with nucleophilic centers of potential bacterial agents [25].

In addition to topsentin structure manipulation, nortopsentin, a bis-indolyl alkaloids, isolated from the Halichondride sponge *Spongosorites ruetzleri*, was investigated as a promising lead compound for the synthesis of new derivatives. Nortopsentin is characterized by the presence of an imidazole central core and is well known to exhibit *in vitro* cytotoxic activity against P388 leukemia cells (IC_{50}, 4.5− 20.7 μM) and antibacterial activity against *Bacillus subtilis* and *Candida albicans* [26].

The main structural manipulations in nortopsentin have involved in the replacement of the imidazole central ring with the thiazole ring. The thiazole central core is known to possess great antiproliferative activity in comparison with the other five-membered heterocycles.

In addition, other modifications of nortopsentin involved the introduction of a nitrogen atom in position 5 of an indole ring, and NH group of the indole moiety was methylated or a tert-butoxy carboxylate group was added.

All synthesized 3-[2-(1*H*-Indol-3-yl)-1,3-thiazol-4-yl]-1*H*pyrrolo[3,2-c]pyridine hydrobromides were submitted to the National Cancer Institute (NCI, Bethesda MD) in order to evaluate their antiproliferative activity.

All derivates were selected, according to the NCI protocol, for the *in vitro* disease-oriented antitumor one dose screening (10^{-5} M) against the full NCI panel comprising five leukemia cell lines, nine non-small cell lung cancer cell lines, seven colon cancer cell lines, six central nervous system cancer cell lines, eight melanoma cell lines, six ovarian cancer cell lines, eight renal cancer cell lines, two prostate cancer cell lines and breast cancer cell lines.

All tested thiazoles satisfied the criteria set by the NCI for activity and were selected for further screening at five concentrations ranging from 10^{-4} to 10^{-8} M on the full panel.

Among the cell lines of the NCI panel, the compounds elicited the best antiproliferative activity in the leukemia sub-panel, breast cancer sub-panel and colon cancer HCT-116 cell line.

Further series of nortopsentin derivatives characterized by the presence of the thiazole central core were manipulated by replacing an indole portion with a thiophene or pyridine ring, while the hydrogen of amino group of the indole moiety has been substituted by methyl, tert-butoxy carboxylate or methoxyethyl group. These compounds have distinguished themselves to act as anti-virulence agents showing antibiofilm activity.

Finally, a series of nortopsentin derivatives in which the thiazole central core was replaced with imidazothiadiazole ring was synthesized and showed activity in malignant peritoneal mesothelioma (MPeM) cell lines such as, Meso-II and STO and elicited ability to inhibit phosphorylation of the protein kinase FAK, a target known to be overexpressed in mesothelioma specimens.

References

1. Holohan, C., Van Schaeybroeck, S., Longley, D. B., & Johnston, P. G. (2013). Cancer drug resistance: an evolving paradigm. Nature reviews. Cancer, 13(10), 714–726.

2. Neoptolemos, J. P., Kleeff, J., Michl, P., Costello, E., Greenhalf, W., & Palmer, D. H. (2018). Therapeutic developments in pancreatic cancer: current and future perspectives. Nature reviews. Gastroenterology & hepatology, 15(6), 333–348.

3. Attwood, M. M., Fabbro, D., Sokolov, A. V., Knapp, S., & Schiöth, H. B. (2021). Trends in kinase drug discovery: targets, indications and inhibitor design. Nature reviews. Drug discovery, 20(11), 839–861.

4. Shibue, T., & Weinberg, R. A. (2017). EMT, CSCs, and drug resistance: the mechanistic link and clinical implications. Nature reviews. Clinical oncology, 14(10), 611–629.

5. Menon, D. R., & Fujita, M. (2019). A state of stochastic cancer stemness through the CDK1-SOX2 axis. Oncotarget, 10(27), 2583–2585.

6. Huang, Z., Shen, G., & Gao, J. (2021). CDK1 promotes the stemness of lung cancer cells through interacting with Sox2. Clinical & translational oncology : official publication of the Federation of Spanish Oncology Societies and of the National Cancer Institute of Mexico, 23(9), 1743–1751.

7. Nabavi, N., Bennewith, K. L., Churg, A., Wang, Y., Collins, C. C., & Mutti, L. (2016). Switching off malignant mesothelioma: exploiting the hypoxic microenvironment. Genes & cancer, 7(11-12), 340–354.

8. Carbone, M., Adusumilli, P.S., Alexander, H.R. Jr, Baas, P., Bardelli, F., Bononi, A., Bueno, R., Felley-Bosco, E., Galateau-Salle, F., Jablons, D., Mansfield, A.S., Minaai, M., de

Perrot, M., Pesavento, P., Rusch, V., Severson, D.T., Taioli, E., Tsao, A., Woodard, G., Yang, H., Zauderer, M.G., Pass, H.I. (2019). Mesothelioma: Scientific clues for prevention, diagnosis, and therapy. CA Cancer J Clin. 69(5):402-429.

9. Roy, R., Tiwari, M., Donelli, G., & Tiwari, V. (2018). Strategies for combating bacterial biofilms: A focus on anti-biofilm agents and their mechanisms of action. Virulence, 9(1), 522–554.

10. Benassi, A., Doria, F., & Pirota, V. (2020). Groundbreaking Anticancer Activity of Highly Diversified Oxadiazole Scaffolds. International journal of molecular sciences, 21(22), 8692.

11. Sharma, P. C., Bansal, K. K., Sharma, A., Sharma, D., & Deep, A. (2020). Thiazole-containing compounds as therapeutic targets for cancer therapy. European journal of medicinal chemistry, 188, 112016.

12. Tsujii, S., Rinehart, K.L., Gunasekera, S.P., Kashman, Y., Cross, S.S., Lui, M.S., Pomponi, S.A., Diaz, M.C. (1988). Topsentin, bromotopsentin, and dihydrodeoxybromotopsentin: antiviral and antitumor bis(indolyl)imidazoles from Caribbean deep-sea sponges of the family Halichondriidae. Structural and synthetic studies. Journal of Organic Chemistry. 53, 23, 5446–5453

13. Luo J. (2009). Glycogen synthase kinase 3beta (GSK3beta) in tumorigenesis and cancer chemotherapy. Cancer letters, 273(2), 194–200.

14. Mazmanian, S. K., Liu, G., Jensen, E. R., Lenoy, E., & Schneewind, O. (2000). Staphylococcus aureus sortase mutants defective in the display of surface proteins and in the pathogenesis of animal infections. Proceedings of the National Academy of Sciences of the United States of America, 97(10), 5510–5515.

15. Weiss, W. J., Lenoy, E., Murphy, T., Tardio, L., Burgio, P., Projan, S. J., Schneewind, O., & Alksne, L. (2004). Effect of srtA and srtB gene expression on the virulence of Staphylococcus aureus in animal models of infection. The Journal of antimicrobial chemotherapy, 53(3), 480–486.

16. McGuigan, A., Kelly, P., Turkington, R. C., Jones, C., Coleman, H. G., & McCain, R. S. (2018). Pancreatic cancer: A review of clinical diagnosis, epidemiology, treatment and outcomes. World journal of gastroenterology, 24(43), 4846–4861.

17. Lennerz, J. K., & Stenzinger, A. (2015). Allelic ratio of KRAS mutations in pancreatic cancer. The oncologist, 20(4), e8–e9.

18. Fiorini, C., Cordani, M., Padroni, C., Blandino, G., Di Agostino, S., & Donadelli, M. (2015). Mutant p53 stimulates chemoresistance of pancreatic adenocarcinoma cells to gemcitabine. Biochimica et biophysica acta, 1853(1), 89–100.

19. Dong, S., Huang, F., Zhang, H., & Chen, Q. (2019). Overexpression of BUB1B, CCNA2, CDC20, and CDK1 in tumor tissues predicts poor survival in pancreatic ductal adenocarcinoma. Bioscience reports, 39(2), BSR20182306.

20. Lacroix, M., Riscal, R., Arena, G., Linares, L. K., & Le Cam, L. (2020). Metabolic functions of the tumor suppressor p53: Implications in normal physiology, metabolic disorders, and cancer. Molecular metabolism, 33, 2–22.

21. Chen J. (2016). The Cell-Cycle Arrest and Apoptotic Functions of p53 in Tumor Initiation and Progression. Cold Spring Harbor perspectives in medicine, 6(3), a026104.

22. Fitzgerald, T. L., Lertpiriyapong, K., Cocco, L., Martelli, A. M., Libra, M., Candido, S., Montalto, G., Cervello, M., Steelman, L., Abrams, S. L., & McCubrey, J. A. (2015). Roles of EGFR and KRAS and their downstream signaling pathways in pancreatic cancer and pancreatic cancer stem cells. Advances in biological regulation, 59, 65–81.

24. Kanteti, R., Mirzapoiazova, T., Riehm, J. J., Dhanasingh, I., Mambetsariev, B., Wang, J., Kulkarni, P., Kaushik, G., Seshacharyulu, P., Ponnusamy, M. P., Kindler, H. L., Nasser, M. W., Batra, S. K., & Salgia, R. (2018). Focal adhesion kinase a potential therapeutic target for pancreatic cancer and malignant pleural mesothelioma. Cancer biology & therapy, 19(4), 316–327.

25. Kamel, M.M., Abdel-hameid, M.K., El-Nassan, H.B., El-Khouly, E.A. (2020) Recent Advances in the Synthesis and Biological Applications of Nortopsentin Analogs. Chem Heterocycl Comp 56, 499–502.

26. Zheng, Z., Liu, Q., Kim, W., Tharmalingam, N., Fuchs, B. B., & Mylonakis, E. (2018). Antimicrobial activity of 1,3,4-oxadiazole derivatives against planktonic cells and biofilm of Staphylococcus aureus. Future medicinal chemistry, 10(3), 283–296.

27. Sakemi, S.; Sun, H.H. J. Nortopsentins A, B, and C. Cytotoxic and antifungal imidazolediylbis[indoles] from the sponge Spongosorites ruetzleri. Org Chem 1991, 56, 4304–4307.

Chapter 14

Appendices

Acknowledgements

"SE DUE SISTEMI INTERAGISCONO TRA LORO PER UN CERTO PERIODO DI TEMPO E SUCCESSIVAMENTE VENGONO SEPARATI, NON POSSONO PIÙ ESSERE DESCRITTI COME DUE SISTEMI DISTINTI, MA DIVENTANO UN UNICO SISTEMA"

"IF TWO SYSTEMS INTERACT WITH EACH OTHER FOR A CERTAIN PERIOD OF TIME AND THEN ARE SEPARATED, THEY CAN NO LONGER BE DESCRIBED AS TWO SEPARATE SYSTEMS, BUT BECOME ONE SYSTEM"

Paul A.M. Dirac

Il lavoro di questi tre anni è stato ricco di sfide che mi hanno formato e temprato, è stato un cammino che mi ha profondamente arricchito mentalmente e spiritualmente. Per tutte queste ragioni che ho il dovere di ringraziare tutti i Docenti che mi hanno seguito, che considero delle incrollabili guide, tutti i "compagni di viaggio" che mi hanno sostenuto durante questo percorso ed infine la mia famiglia per avermi insegnato i veri valori della vita.

The work of these three years has been rich in challenges that have formed and hardened me, it has been a trajectory that has deeply enriched me mentally and spiritually. For all these reasons, I'd like to thank all the Professors who have followed me, who I consider to be unshakable guides, all my "travelling companions" who have supported me during this trajectory and finally my family for teaching me the true values of life.

Curriculum Vitae

Camilla Pecoraro was born on the seventh of May 1994, in Palermo, Italy. She obtained a classical education diploma at Don Bosco Ranchibile Institute, Palermo, in 2012 and then joined the faculty of Chemistry and Pharmaceutical Tecnology at the University of Palermo (UNIPA). In 2018, she achieved her master's degree (full marks and honors), with a thesis entitled: "Sintesi ed attività antitumorale di nuovi derivati della nortopsentina come potenziali inibitori di GSK-3β", under the supervision of Prof. Patrizia Diana and Prof. Barbara Parrino. In November 2018, Camilla started her PhD degree in Molecular and Biomolecular Sciences with a PhD project entitled: "Synthesis and Biological Evaluation of Novel Kinase Inhibitors Involved in Cancer Progression and Drug Resistance", coordinated by Prof. Patrizia Diana and Prof. Elisa Giovannetti. During her PhD, she had the opportunity to spend a research period at VU University Medical Center, Cancer Center of Amsterdam, under the guidance of Prof. Elisa Giovannetti and Prof. G.J. Peters. The research results of this trajectory have been reported in the present PhD thesis and in various publications. Her current research interests are in the field of medicinal chemistry with a special focus on protein kinase inhibitors.

LIST OF PUBLICATIONS

Synthesis and cytotoxic activity of 3-[2-(1*H*-Indol-3-yl)-1,3-thiazol-4-yl]-1*H*pyrrolo[3,2-*c*]pyridine hydrobromides - analogues of the marine alkaloid nortopsentin

Pecoraro, C., Carbone, D., Aiello, D., Carbone, A. *Arkivoc* **2021.**

https://doi.org/10.24820/ark.5550190.p011.640

SF3B1 modulators affect key genes in metastasis and drug influx: a new approach to fight pancreatic cancer chemoresistance.

Randazzo, O. *, Cascioferro, S.M. *, **Pecoraro, C. *,** Iddouch, W.A., Avan, A., Parrino, B., Carbone, D., Perricone, U., Peters, G.J., Diana, P., Giovannetti, E. *Cancer Drug Resist* **2021,** *4*, 904-922.

http://dx.doi.org/10.20517/cdr.2021.61

Cyclin Dependent Kinase-1 (CDK-1) Inhibition as a Novel Therapeutic Strategy against Pancreatic Ductal Adenocarcinoma (PDAC).

Wijnen, R.*, **Pecoraro, C. ***, Carbone, D., Fiuji, H., Avan, A., Peters, G. J., Giovannetti, E., Diana, P *Cancers*, **2021**, *13*(17), 4389.

http://dx.doi.org/10.3390/cancers13174389

GSK3β as a novel promising target to overcome chemoresistance in pancreatic cancer.

Pecoraro, C.*, Faggion, B.*, Balboni, B., Carbone, D., Peters, G. J., Diana, P., Assaraf, Y. G., & Giovannetti, E.. *Drug resistance updates: reviews and commentaries in antimicrobial and anticancer chemotherapy*, **2021**, *58*, 100779.

https://doi.org/10.1016/j.drup.2021.100779

Nobiletin and Xanthohumol Sensitize Colorectal Cancer Stem Cells to Standard Chemotherapy

Turdo, A., Glaviano, A., Pepe, G., Calapà, F., Raimondo, S., Fiori, M.E., Carbone, D., Basilicata, M.G., Di Sarno, V., Ostacolo, C., Parrino, B., Cascioferro, S., **Pecoraro, C.**, Di Franco, S., Bellavia, D., Gaggianesi, M., Veschi, V., Lo Iacono, M., Ganduscio, G., Pantina, V.D., Mangiapane, L.R., Bongiorno, M.R., Alessandro, R., Todaro, M., De Maria, R., Diana, P., Campiglia, P., Stassi, G. *Cancers* **2021**, 13, 3927.

https://doi.org/10.3390/cancers13163927

CHK1 inhibitor sensitizes resistant colorectal cancer stem cells to nortopsentin

Di Franco S., Parrino B., Gaggianesi M., Pantina V.D., Bianca P., Nicotra A., Mangiapane R.L., Lo Iacono M., Ganduscio G., Veschi V., Brancato O.R., Glaviano A., Turdo A., Pillitteri I., Colarossi L., Cascioferro S., Carbone D., **Pecoraro C.**, Fiori M.E., De Maria R., Todaro M., Screpanti I., Cirrincione G., Diana P., Stassi G. *iScience* **2021**, 24, 102664.

https://doi.org/10.1016/j.isci.2021.102664

Eight-membered heterocycles with two heteroatoms in a 1,3-relationship of interest in medicinal chemistry.

Parrino B., Cascioferro S., Carbone D., **Pecoraro C.**, Cirrincione G., Diana P. *Advances in Heterocyclic Chemistry* **2021**.

http://doi.org/10.1016/bs.aihch.2020.11.001

1,2,4-Oxadiazole Topsentin Analogs with Antiproliferative Activity against Pancreatic Cancer Cells, Targeting GSK3β Kinase.

Carbone, D., Parrino, B., Cascioferro, S., **Pecoraro, C.**, Giovannetti, E., Di Sarno, V., Musella, S., Auriemma, G., Cirrincione, G., Diana, P. *ChemMedChem* **2021**, 16(3), 537-554.

https://doi.org/10.1002/cmdc.202000752

1,2,4-Oxadiazole topsentin analogs as staphylococcal biofilm inhibitors targeting the bacterial transpeptidase sortase A.

Parrino, B., Carbone, D., Cascioferro, S., **Pecoraro, C.**, Giovannetti, E., Deng, D., Di Sarno, V., Musella, S., Auriemma, G., Cusimano, M.G., Schillaci, D., Cirrincione, G., Diana, P. *European Journal of Medicinal Chemistry* **2021**, 209, 112892.

https://doi.org/10.1016/j.ejmech.2020.112892

Therapeutic Strategies to Counteract Antibiotic Resistance in MRSA Biofilm-Associated Infections.

Cascioferro, S., Carbone, D., Parrino, B., **Pecoraro, C.**, Giovannetti, E., Cirrincione, G., Diana, P. *ChemMedChem* **2021**, 16(1), 65-80.

https://doi.org/10.1002/cmdc.202000677

Novel strategies in the war against antibiotic resistance.

Cascioferro, S., Parrino, B., Carbone, D., **Pecoraro, C.**, Diana, P. *Future Medicinal Chemistry* **2021**, 13(6), 529-531.

https://doi.org/10.4155/fmc-2021-0009

Thiazole analogues of the marine alkaloid nortopsentin as inhibitors of bacterial biofilm formation.

Carbone, A., Cascioferro, S., Parrino, B., Carbone, D., **Pecoraro, C.**, Schillaci, D., Cusimano, M.G., Cirrincione, G., Diana, P.. *Molecules* **2021**, 26(1), 81.

https://doi.org/10.3390/molecules26010081

New imidazo[2,1-*b*][1,3,4]thiadiazole derivatives inhibit FAK phosphorylation and potentiate the antiproliferative effects of gemcitabine through modulation of the human equilibrative nucleoside transporter-1 in peritoneal mesothelioma.

Li Petri, G.*, **Pecoraro, C.***, Randazzo, O.*, Zoppi, S., Cascioferro, S., Parrino, B., Carbone, D., El Hassouni, B., Cavazzoni, A., Zaffaroni, N., Cirrincione, G., Diana, P., Peters, G.J., Giovannetti, E. *Anticancer Research* **2020**, 40(9), 4913-4919.

https://doi.org/10.21873/anticanres.14494